Ratiometric luminescent probes

Pál, Robert

Ratiometric Luminescent Probes

Robert Pál

A thesis submitted for the degree of Doctor of Philosophy

Department of Chemistry

Durham University

2007

Declaration

The research described in this thesis was undertaken at the Department of Chemistry of Durham University between October 2004 and September 2007. All of the work is my own; no part of it has previously been submitted for a degree at this or any other university

Statement of Copyright

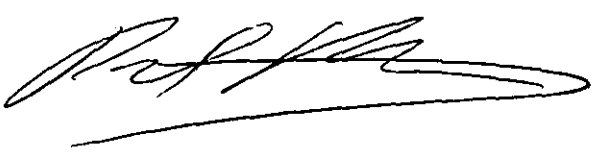

Acknowledgements

Sincere thanks to:

My supervisor Prof. David Parker for giving me this life changing opportunity to continue my work in chemistry at Durham University and for the time he has spent in giving his guidance, patience, optimism and expertise throughout these years.

My co-supervisor Dr. Ritu Kataky, Dr. Junhua Yu, Dr. Lars-Olaf Palsson, Dr. Andrew Bebby and Dr. Mark P. Lowe for their friendly help and advice.

Dr Alan Kenwright, Catherine Hefferman and Ian McKeag for their assistance with NMR spectroscopy. Dr Mike Jones, Lara Turner and Dr. Jackie A. Mosely for help with mass spectrometry and for carrying out accurate mass determination.

Dr Aileen Congreve for the time she has given to sorting my many cells by flow cytometry and Dr Chris Ottley for carrying out ICP-MS measurements.

The current and past members of the DP lab for the stimulating working environment and friendly advice throughout my time in Durham.

Everybody form the Department of Chemistry, especially from Chemistry Stores & Workshops for their friendship and help.

My beautiful fiancée Veronika, my family and my friends for their encouragement and support.

Abstract

A ratiometric, luminescent Eu probe was sought for use in measuring intracellular pH, that can be excited in the range 355-405 nm. In order to achieve this, a series of 1-azathiaxanthone based chromophores has been synthesised and studied to find the best candidate to promote Eu emission. A series of 'DO2A' derivatives was synthesised incorporating both the chosen chromophore (2-methyl-1-azathioxanthone) and a pH-dependent binding moiety (a tethered sulfonamide). Measurements were carried out in order to study and understand the properties of the complexes, especially the nature of the pH dependence. The protonation constants of the pendant pH 'switch' in each system were determined by luminescence titration. The influence on Eu emission of some endogenous anions and protein has also been examined by luminescence spectroscopy, along with calculations of their apparent binding constants in order to find the best candidate for measuring intracellular pH.

A novel bicarbonate sensor has also been synthesised and studied incorporating a 7-(methylcarbamoylmethyl)-azathioxanthone sensitiser moiety. The luminescence properties have been thoroughly studied, and the changes in the photophysical properties and the sensitivity towards anion and protein binding rationalised. The complex displayed sensitivity towards endogenous anions and protein binding, however, a suitable calibration curve was obtained in the desired 5 – 30 mM HCO_3^- range in simulated endogenous anion mixture, using intensity ratio *vs.* pH plots.

A series of ratiometric Eu(III)complexes has been synthesised incorporating an efficient sensitiser for measuring citrate concentrations in seminal and prostate fluid samples. Their luminescent properties were thoroughly studied using simulated prostate fluid as the background to find the best candidate for prostate adenocarcinoma detection. Preliminary studies have been undertaken to determine citrate levels in 'clinical' prostate and seminal fluid samples.

Cellular uptake and localisation studies have also been undertaken with each complex revealing the complex uptake profile and the time-dependent localisation behaviour within the cell. Each complex showed no significant evidence for toxicity. Images were observed using unfixed cells, appropriate for live cell imaging applications.

- Table of Contents -

Declaration i

Acknowledgement ii

Abstract iii

Table of Contents iv

Abbreviations ix

Chapter 1: General Introduction 1

1.1.1 Luminescence Properties of the Lanthanides 2

1.1.1 Lanthanide Metals 2

1.1.1.1 Lanthanide Luminescence 2

1.1.1.2 Photophysical Properties of Europium and Terbium 4

1.2 Sensitised Emission 5

1.2.1 Mechanisms of Energy transfer 7

1.2.2 Luminescence Quantum Yield and Competing De-activation Pathways 9

1.2.3 Deactivation of the Lanthanide Emissive State 10

1.3 Lanthanide Complexes and Luminescent Probes 13

1.3.1 Choice of Ligand 14

1.3.2 Choice of Sensitising Moiety 17

1.3.3 Applications of Luminescent Lanthanide Complexes 20

1.3.3.1 Ln-complexes for Luminescent Resonance Energy Transefer 21

1.3.3.2 Probes for the Study of Ionic Concentrations 22

1.3.3.3 Ln-complexes for 'In-cellulo' Imaging 24

1.4 Other Fluorescence-based Cellular Probes 27

1.4.1 Fluorescent Proteins 27

1.4.2 Organic Fluorescent Dyes 28

1.4.3 Quantum Dots as Fluorescent Labels 30

1.4.4 Transition Metal Complexes 31

1.5 Luminescence Microscopy 32

1.5.1 The Basics of Microscopy 32

1.5.2 Confocal Microscopy 34
1.5.3 Multiphoton Excitation 35
1.5.4 Time Gated Detection 36
1.5.5 Time Resolved Fluorescence Microscopy 37
1.6 Cellular Uptake and Localisation 37
1.6.1 Mechanisms of Cellular Uptake 38
1.7 References 43

Chapter 2: Synthetic Aspects: Chromophore, Ligand and Complexes 48

2.1 Outline and Direction of Work 49
2.2 Chromophore Synthetic Scheme 52
2.3 Chromophore Photophysical Data 55
2.3.1 Absorption Properties 55
2.3.2 Singlet and Triplet Energy Measurements 57
2.3.3 Summary and Comparison of Photophysical Properties 61
2.4 Ligand and Complex Synthetic Scheme 61
2.4.1 Complexes Incorporating Carboxylate Pendant Arms 62
2.4.1.1 Complex Data 66
2.4.2 Complexes Incorporating Amide Pendant Arms 69
2.4.2.1 Complex Data 73
2.5 References 75

Chapter 3: pH Probes 76

3.1 Intorduction 77
3.1.1 Measuring pH with Optical Sensors 79
3.1.1.1 Advantages of a Europium-based pH probe 82
3.1.2 Choice of pH-dependent Binding Moiety 87
3.2 Luminescence Titrations and pK_a Determinations 88
3.2.1 pK_a Determination of Eu(MS)DCP2 89
3.2.2 pK_a Determination of Eu(MS)DGP2 90

3.2.3 pK_a Determination of Eu(MS)DAdP2 92
3.2.3.1 Variation of Relaxivity with pH of Gd(MS)DAdP2 94
3.3 Effect of Added Anions on Emission Profiles 94
3.3.1 Effect of Added Anions on the EuDCP2 Emission Profile 95
3.3.2 Effect of Added Anions on the Eu(MS)DCP2 Emission Profile 97
3.3.2.1 Photophysical Response to Endogenous Anions 103
3.3.3 Effect of Added Anions on the Eu(MS)DGP2 Emission Profile 106
3.3.4.1 Photophysical Response to Endogenous Anions 111
3.3.4 Effect of Added Anions on the Eu(MS)DAdP2 Emission Profile 113
3.3.4.1 Photophysical Response to Endogenous Anions 117
3.4 Quenching Studies with Eu(MS))DADP2 119
3.5 Effect of Added Protein on the Eu(MS)DAdP2 Emission Profiles 120
3.5.1 Photophysical Response to Protein (HSA) 123
3.5.1.1 Analysis of Protein Binding Using Gd(MS)DAdP2 125
3.6 'In cellulo' Studies 126
3.6.1 Cellular Uptake Study 127
3.6.1.1 'In cellulo' pH Determination 131
3.6.2. Determination of the Intracellular Europium Concentration 132
3.7 Conclusions and Future Work 135
3.8 References 136

Chapter 4: Carbonate Sensors **138**

4.1 Introduction 139
4.1.1 Measuring $[HCO_3^-]$ 140
4.1.2 Advantages and Concept of Lanthanide-based Carbonate Sensors 142
4.2 Concept and Design of a Novel Ratiometric Carbonate Sensor 149
4.3 Effect of Added Anion on Emission Profile 152
4.3.1 ^1H NMR Studies of Anion Binding 157
4.3.2 CPL Studies 158
4.3.3 Photophysical Response to Endogenous Anions 160
4.4 Effect of Added Protein on Emission Profile 163

4.3.1 Analysis of Protein Binding Using GdDAP7A 165
4.5 Quenching Studies 167
4.6 Two Photon Absorption and Photoluminescence 167
4.7 'In cellulo' Studies 170
4.7.1 Cellular Uptake and Localisation 170
4.7.2 Determination of the Intracellular Europium Concentration 176
4.8 Conclusions and Future Work 178
4.9 References 179

Chapter 5: Citrate Sensors 182

5.1 Introduction 183
5.1.1 The Prostate Gland 183
5.1.2 Prostate Cancer 185
5.1.3 Current Screening Procedures and Diagnosis 187
5.1.4 Citric Acid and Zinc Elevation 189
5.2 General Luminescence Studies 194
5.2.1 Design, Concept and Characteristics of a Suitable Citrate Sensor 194
5.3 Luminescence Studies in Simulated Prostate Fluid 198
5.3.1 Citrate Dependence Studies 198
5.3.1.1 Citrate Binding of EuDAP2 and EuDPP2 198
5.3.1.2 Citrate Binding of EuDPPA2 and EuDAPA2 199
5.3.1.3 Citrate Binding of EuDGP2 201
5.3.2 Lactate Interference in Citrate Analysis 205
5.3.3 Protein Binding Studies 210
5.4 'In vivo' Studies in Seminal Fluid Samples 211
5.5 Prostate Fluid Analysis 213
5.6 'In cellulo' Studies 217
5.6.1 Cellular Uptake Studies of EuDPPA2 218
5.6.2 Cellular Uptake Studies of EuDGP2 219
5.6.3 Cellular Uptake Studies of EuDAPA2 221

5.6.3.1 Time-resolved Microscopy with EuDAPA2 223

5.6.3.2 Determination of the Intracellular Europium Concentration 224

5.7 Conclusions, Future Work and Comparison of Results 225

5.8 References 228

Chapter 6: Experimental and Synthetic Procedures **230**

6.1 General Experimental 231

6.1.1 Reagents and Solvents 231

6.1.2 Chromatography 231

6.1.3 Spectroscopy 231

6.1.4 pH Measurements 233

6.1.5 Lifetime Measurements 233

6.1.6 Inner Sphere Hydration Number Determination 234

6.1.7 Molar Extinction Coefficient Measurements 236

6.1.8 Triplet Energy Measurements 236

6.1.9 Quantum Yield Determination 237

6.1.10 Anion and Protein Affinity Measurements 238

6.1.11 Biological Samples: Seminal and Prostate Fluid 239

6.1.12 Microscopy 240

6.1.13 Cell Culture Work 240

6.1.14 Flow Cytometry and ICP-MS 241

6.1.15 HPLC Analysis 241

6.1.16 Single Crystal X-ray Diffraction 242

6.2 Synthetic Procedures and Characterisation 243

6.3 HPLC Data of Complexes 295

6.4 References 301

Abbreviations

x10	ten times dilution
A	absorbance
aDO2A	1,7,-bis(α-dimethyladipate)- 1,4,7,10-tetraazacyclododecane
Ac	acetate
'anion-stew'	simulated extracellular anion mixture
AMP	adenosine monophosphate
ATP	adenosine triphosphate
ATX	azathioxanthone group
BP	band-pass filter
BPH	benign prostate hyperplasia or hypertrophy
br	broad
°C	degrees Celsius
CA	carbonic anhydrase
CCD	charge coupled device (camera)
CF	cystic fibrosis
CHEF	chelation enhanced fluorescence
CHEQ	chelation enhanced quenching
CHO	Chinese hamster ovarian cells
cm^{-1}	wave number
CPL	circular polarised luminescence
CT	charge transfer / computer tomography
cyclen	1,4,7,10-tetraazacyclododecane
d	doublet
DCM	dichloromethane
dd	doublet of doublets
DIC	differential interference contrast objective
DMEM	Dulbecco's modified eagle medium
DNA	deoxyribonucleic acid
DO2A	1,7,-bis(carboxymethyl)- 1,4,7,10-tetraazacyclododecane
DO3A	1,4,7,-tris(carboxymethyl)- 1,4,7,10-tetraazacyclododecane

DOTA	1,4,7,10-tetraazacyclododecane-1,4,7,10-tetraacetic acid
DRE	digital rectal examination
DTPA	diethylene triamine pentaacetic acid
EDC	1-ethyl-3-[3-dimethylaminopropyl]carbodiimide hydrochloride
EPA	Et_2O – isopentane – EtOH (2:5:5 by volume)
$ESMS^-$	electrospray mass spectroscopy using negative ion mode
$ESMS^+$	electrospray mass spectroscopy using positive ion mode
eq.	equivalent
F12(Ham)	medium for chinese hamster ovarian cells
FLIM	fluorescence lifetime imaging
FRET	fluorescence resonance energy transfer
g, mg, μg	gram, milligram, microgram
gDO2A	1,7,-bis(α-dimethylglutarate)- 1,4,7,10-tetraazacyclododecane
GFP	green fluorescent protein
h, min, sec, ms, μs	hour, minute, second, milliseconds, microseconds
HEPES	4-(2-hydroxyethyl)-1-piperazineethanesulfonic acid
HOMO	highest energy occupied molecular orbital
HPLC	high pressure liquid chromatography
$HRMS^+$	high resolution electrospray mass spectroscopy using positive ion mode
$HRMS^-$	high resolution electrospray mass spectroscopy using negative ion mode
Hz	Hertz
IC	internal conversion
ICP-MS	indouctively coupled plasma – mass spectrometry
ISC	inter system crossing
IR	infra red (spectroscopy)
K	Kelvin
L, mL, μL	litre, millilitre, microlitre
LDH	lactate dehydrogenase

LMCT	ligand metal charge transfer
Ln	lanthanide ion
LP	long-pass filter
LRET	luminescence resonance energy transfer
$LV_{min/max}$	minimum / maximum limiting values
LUMO	lowest energy un-occupied molecular orbital
m	multiplet
M, mM, μM	molar: [mol dm^{-3}], millimolar, micromolar
m-Ac	mitochondrial aconitase enzyme
MeCN	acetonitrile
MIS	metal ion stock (solution)
MLCT	metal ligand charge transfer
mol, mmol, μmol	mole, millimole, micromole
m.p.	melting point
MS	methylsulfonyl-amino-ethyl group
MRI	magnetic resonance imaging
MRSI	magnetic resonance spectroscopy imaging
NAD	nicotinamide adenine dinucleotide
NBS	N-bromosuccinimide
NC	nano-crystals
NCS	newborn calf serum
NIH 3T3	mouse skin fibroblast cells
NIR	near infrared
nm	nanometer
NMR	nuclear magnetic resonance
p	pentet
PBS	phosphate buffered saline
PCa	prostate cancer (prostate adenocarcinoma)
PET	photoinduced electron transfer
PF	prostate fluid
Ph	phenyl
PL	photo luminescence

PMT	photomultiplier tube
ppb	parts per billion
ppm	parts per million
PSA	prostate specific antigen
q	quartet
QD	quantum dot
r	relaxivity [$M^{-1}s^{-1}$]
s	singlet
SAP	square antiprismatic
SF	seminal fluid
SPECT	single photon computer tomography
t	triplet
TFA	trifluoroacetic acid
Tf	triflate
THF	tetrahydrofuran
TLC	thin layer chromatography
TPE	two photon excitation
TR	time resolved
TSAP	twisted square antiprismatic
UV-Vis	ultraviolet and visible region
β_{as}	rocking in plane vibration
β_s	scissoring in plane vibration
γ_{as}	twisting (torsion) out of plane vibration
γ_s	wagging out of plane vibration
δ_{as}	asymmetrical bending vibration
δ_s	symmetrical bending vibration
ε	molar extinction coefficient
τ	radiative lifetime
ν_{as}	asymmetrical stretching vibration
ν_s	symmetrical stretching vibration

CHAPTER 1

General Introduction

1 General Introduction

1.1 Luminescent Properties of the Lanthanides

1.1.1 Lanthanide Metal Ions

Lanthanide metal ions have found an ever increasing use in many areas of research such as synthesis, coordination chemistry, material science and crystal engineering. Over the last three decades the interest in the chemistry of lanthanide complexes has been focused on their use as biological imaging agents and luminescent probes in the detection of chemical species.

The most stable and predominant oxidation state of the lanthanides in solution is +3 with an electronic configuration of $[Xe]\ 4f^n5d^16s^2$, with n varying from 0 (La^{3+}) to 14 (Lu^{3+}). The exceptions to this occur when the ion can attain an empty (f^0), half filled (f^7), or filled (f^{14}) subshell, such as Ce^{4+} and Eu^{2+}.

The *4f* valence electrons are not readily available for bonding, as a result of shielding from the outer *5s* and *5p* filled orbitals, and have no significant stereochemical influence on ligands surrounding the lanthanide ion centre. Instead, the geometry in usually is determined by the need to minimise the steric repulsion between the ligands that surround the lanthanide metal centre.[1,2] The coordination number, which ranges from 6-9 (max 12)[3], decreases across the series due to the lanthanide contraction.[4-6] In comparison with *dd* bands of transition metals, the ligand field splittings are typically small, with values of the order of 100 cm^{-1}. Therefore, the *ff* bands in the emission spectra do not significantly broaden or shift in wavelength upon complexation.[7,8] Whilst this may suggest that the potential role for these complexes as responsive probes is limited, changes in the fine structure of the emission bands and their relative intensities can be very informative, allowing ratiometric analysis.[9]

1.1.1.1 Lanthanide Luminescence

Luminescence occurs when an atom or molecule in an excited state emits photons and returns to the ground state. As the process involves the excitation energy being released in the form of a photon, it is described as a radiative decay process. A non-

radiative decay occurs when the energy is transferred to vibrational, rotational and translational motion of the surrounding molecules

There are lanthanides that emit in the visible region (Sm^{3+}, Eu^{3+}, Tb^{3+} and Dy^{3+}) (*Fig. 1.1*) and in the near infrared spectral range (Nd^{3+}, Ho^{3+}, Er^{3+} and Yb^{3+}), in which biological tissue is relatively transparent.[8,10] These lanthanides exhibit strong luminescence, owing to the large energy gap between the lowest excited state and the highest ground levels. Moreover, these large energy gaps make the competing non-radiative decay less likely to occur, which is necessary in order for a compound to be useful in luminescence based applications.

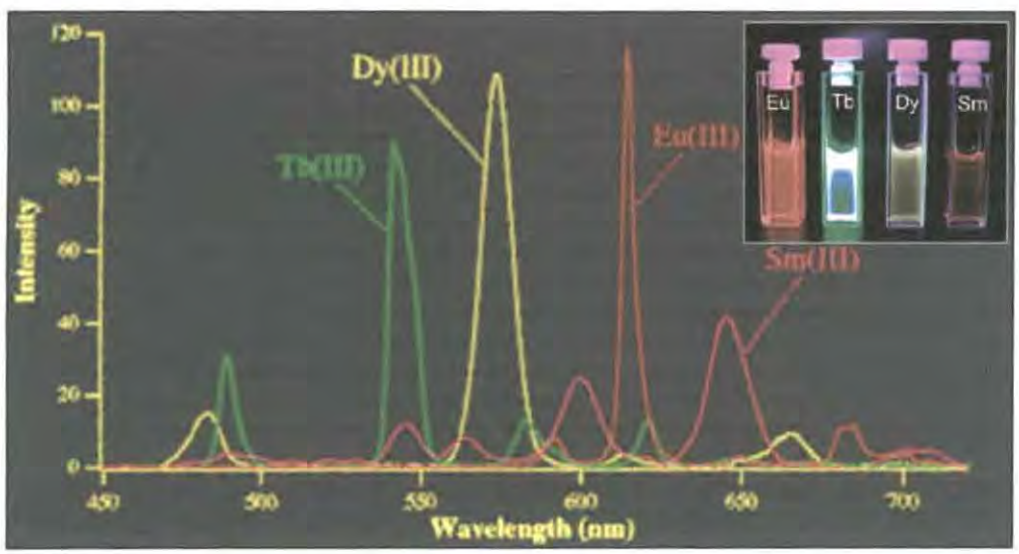

Fig. 1.1. Typical low-resolution emission spectra of luminescent lanthanide complexes containing the highlighted metal ions and an antenna chromophore, excited at 354 nm.[11]

The properties of lanthanides, such as long-lived luminescence and sharp absorption and emission lines, can be attributed to various transitions of the *f*-electrons. As noted before, the *f*-electrons are shielded from external influences by the filled *5s* and *5p* orbitals, so upon metal-ligand binding there is very little interaction between the orbitals.[6] This consequently leads to minimal mixing of the electronic excited states with asymmetric ligand vibrations, which ensures that the Laporte forbidden *ff* transitions[12] remain weak, leading to very low molar extinction coefficients (0.5 – 3 $dm^3mol^{-1}cm^{-1}$)[13] in the absorption spectra and long natural lifetimes, ranging from the order of microseconds (*e.g.* Yb, Nd) to milliseconds (*e.g.* Eu and Tb). Although this long lived emission is an attractive feature in luminescent sensors as it allows time-resolved

detection,[14] direct excitation of the ion becomes very difficult and only achievable with lasers.[15] Terbium and europium are two examples that can be excited in this manner by using an argon ion laser at 488 nm (matching the $^7F_6 \rightarrow {}^5D_4$ transition of Tb) or Rhodamine110 in a dye laser at 580 nm ($^7F_0 \rightarrow {}^5D_0$ transition of Eu).

1.1.1.2 Photophysical Properties of Europium and Terbium

Emission spectra of lanthanide ions consist of several well defined, sharp and narrow bands. The ratio of intensities and fine structure of these bands can provide valuable information about the coordination sphere of the lanthanide. The energy levels of the *4f* orbitals are not degenerate, with electronic repulsion between electrons disrupting the degeneracy to yield spectroscopic terms with separations typically of the order of 5,000 - 10,000 cm^{-1} between neighbouring terms, with[16] *J* levels of each term being separated by about 1,000 cm^{-1} within each manifold. Absorption of light can promote lanthanides to any energetically accessible state, but rapid internal conversion occurs to the lowest *J* state of the first excited spectroscopic term. This ensures that emission arises almost exclusively from this state, consisting of a series of bands to multiple *J* levels; recently interest has been shown in Sm(III) and Dy(III) complexes for the development of dual luminescent time–resolved immunoassays.[17] The two longest lived and most commonly studied-emissive lanthanide ions are Eu and Tb, which possess luminescent $^5D_0$ (17,200 cm^{-1}) and $^5D_4$ (20,400 cm^{-1}) excited states respectively.[15]

For ***Eu(III)*** complexes,[18] the strongest emissions generally arise from $^5D_0 \rightarrow {}^7F_{1,2}$ transitions at 590 and 612 nm respectively. The $^5D_0 \rightarrow {}^7F_1$ ($\Delta J = 1$) transition (*Fig 1.2*) is magnetic dipole in character and largely independent of the coordination sphere, whereas the electric dipole $^5D_0 \rightarrow {}^7F_2$ ($\Delta J = 2$) transition is extremely sensitive to the nature and symmetry of the coordination sphere. Its intensity is enhanced by distortion of the symmetry around the ion and by the presence of polarisable donor groups. The number of bands in the $\Delta J = 1$ manifold is determined by the site symmetry: two bands are observed for C_n-symmetric complexes, whereas less symmetric complexes display three bands. Similar arguments apply for the analysis of the $\Delta J = 2$ manifold. The $^5D_0 \rightarrow {}^7F_4$ transition is also relatively intense and sensitive to the ligand field, being predominantly electric dipole in character. The $^5D_0 \rightarrow {}^7F_3$ transitions are generally weak, whilst transitions in

the $\Delta J = 4$ manifold are very sensitive to the polarisability of the donor ligands atoms and are hypersensitive. The $^5D_0 \rightarrow {}^7F_0$ transition, at 580 nm, is weak but sensitive to the ligand environment and is used as a probe of Eu^{3+} coordination homogeneity. In fact, since the $^5D_0$ and $^7F_0$ states are non-degenerate, the number of absorption or emission bands observed is related to the number of chemically distinct environments of the ion.

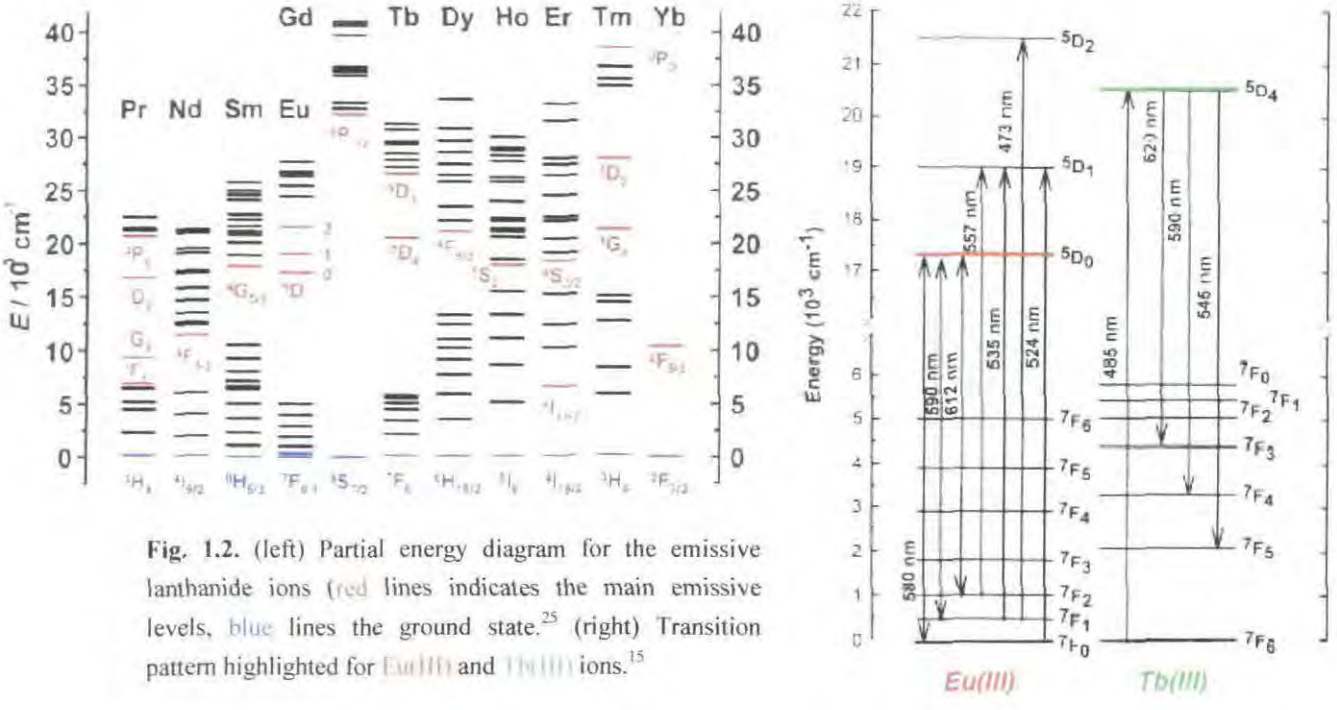

Fig. 1.2. (left) Partial energy diagram for the emissive lanthanide ions (red lines indicates the main emissive levels, blue lines the ground state.[25] (right) Transition pattern highlighted for Eu(III) and Tb(III) ions.[15]

In the case of ***Tb(III)***, all emissions arise from the $^5D_4$ level. The $^5D_4 \rightarrow {}^7F_5$ ($\Delta J = 1$) emission band, at 545 nm, is the most intense and is hypersensitive, but not as sensitive to the ion environment as the $^5D_0 \rightarrow {}^7F_2$ transition of Eu^{3+}. The analysis of the fine structure of the spectrum does not provide much information about the local symmetry of the metal ion, because emission bands normally consist of a large number of transitions, which can rarely be fully resolved. In fact, the J values of the levels involved in the transitions are high, resulting in splitting of the J levels into many sublevels.

1.2 Sensitised Emission

As stated above, the population of the lanthanide excited state is difficult to achieve *via* direct excitation. One solution to overcome this problem is to incorporate an

organic chromophore (often referred to as an 'antenna group') into the lanthanide binding ligand,[19, 20] allowing the use of lower intensity 'conventional' light sources with a greatly increased 'effective' molar absorption coefficient for the metal ion.[21] Organic chromophores are usually much better of absorbing light, thus allowing indirect excitation of the complexed lanthanide ion *via* intramolecular energy transfer (*Fig. 1.3*),[22] whereby the excited state is reached following energy transfer from the triplet level of a suitable chromophore.

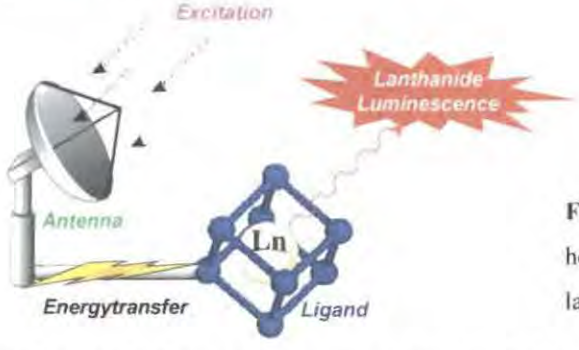

Fig. 1.3. Schematic diagram showing how organic antennas are used to aid lanthanide(III) ion luminescence.

Before excitation, the electronic configuration of the sensitising moiety is in the ground state (S_0). The sensitiser is first excited to an electronically excited level of the singlet state (S_n). There are several isoenergic vibrational states of this level that the excited fluorophore may occupy via ***internal conversion***, whereas the separation between these levels is about 1,500 cm^{-1}, which is greater than the thermal energy needed to populate these states at room temperature (~200 cm^{-1}). The excess energy of the S_1 excited state is then lost by vibrational relaxation. This excited state can then decay by ***fluorescence*** or undergo a formally forbidden ***intersystem crossing*** to populate the triplet state (T_n) of lower energy. Finally, sensitiser ***phosphorescence*** competes with ***energy transfer*** from the higher lying triplet state of the sensitising chromophore to the emissive state of the lanthanide metal ion. The excited Ln(III)ion then relaxes to its ground state via lanthanide luminescence. For efficient sensitisation, the triplet energy should be slightly higher (> 1,700 cm^{-1}) than the emissive state of the appropriate lanthanide ion. If the difference is to small, then thermally activated back energy transfer can occur leading to both a reduction in the emission intensity and lifetime.[23] For Eu(III), a photoinduced electron transfer from the chromophore to the metal centre can also take place owing to the ease of reduction to Eu(II). This process often deactivates the singlet excited state of the antenna in a non-radiative way, reducing its efficiency as a sensitiser.[15]

These reaction kinetics and emission processes can be explained using a *Jablonski diagram* (*Fig. 1.4*)[24]

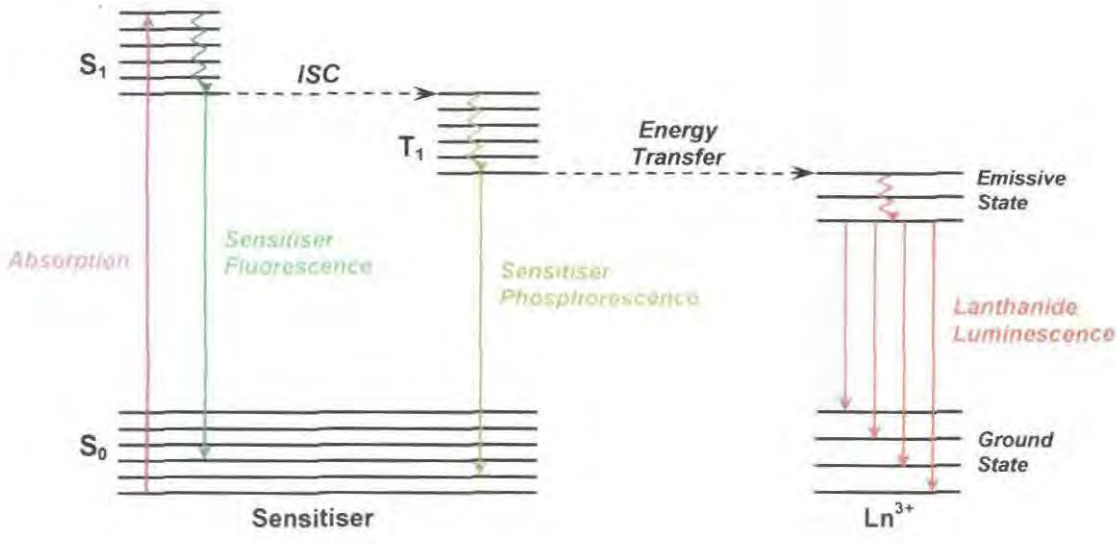

Fig. 1.4. Jablonski diagram detailing the mechanism of the above discussed energy transfer.

Several other techniques have been shown success in promoting lanthanide luminescence. Lanthanide(III) ions that are able to accept electrons more readily possess available charge transfer states, such as Sm(III), Eu(III) and Yb(III). In these cases, ligand to metal charge transfer (*LMCT*) may afford a mechanism of sensitisation. These applications involve the insertion of these complexes into organic matrices.[25] Other methods involve energy transfer from a transition metal[26] or metal-to-ligand charge transfer (*MLCT*) from transition metal complexes[27-29] which has been used to sensitise NIR emissive lanthanides. A similar approach has also been demonstrated where one lanthanide complex been used to sensitise emission from another, located nearby.[30]

1.2.1 Mechanisms of Energy Transfer[31-33]

There are two main classes of electronic energy transfer mechanism: radiative and non-radiative. Each process relies on overlap between the emission spectrum of the donor and the absorption spectrum of the acceptor.

Radiative energy transfer involves the donor emitting light that is subsequently re-absorbed by the acceptor. This mechanism is favoured where the spectral overlap is good

and the quantum yield of emission of the donor and the light absorbing properties of the acceptor are maximised.

There are number of different mechanisms that are generally accepted to occur for the non-radiative interaction. In principle, the energy transfer step may occur either from the singlet or triplet excited states of the chromophore. In most cases only the latter is significant, but examples have been postulated of direct energy transfer from the sensitiser's first singlet excited state to the lanthanide emissive state.[34] There are three mechanisms that detail energy transfer from the triplet state of the chromophore to the emissive state of lanthanide: the dipole-dipole pathway (Förster); the exchange mechanism (Dexter); and a dipole-multipole mechanism. The main mechanisms are the former two.

The ***Förster***[35] mechanism is a through-space dipole-dipole (Coulombic) interaction between the donor and acceptor and can be expressed as the rate of energy transfer (k_{ET}) which is a function of the separation of the donor and acceptor (R_{DA}) with a distance dependence of $1/R_{DA}^6$.

The ***Dexter***[36] mechanism (*Fig. 1.5*) involves mutual electron exchange between the sensitiser and acceptor, with conservation of multiplicity of the system. Such a mechanism requires effective overlap of the electronic orbitals of the donor and acceptor species.

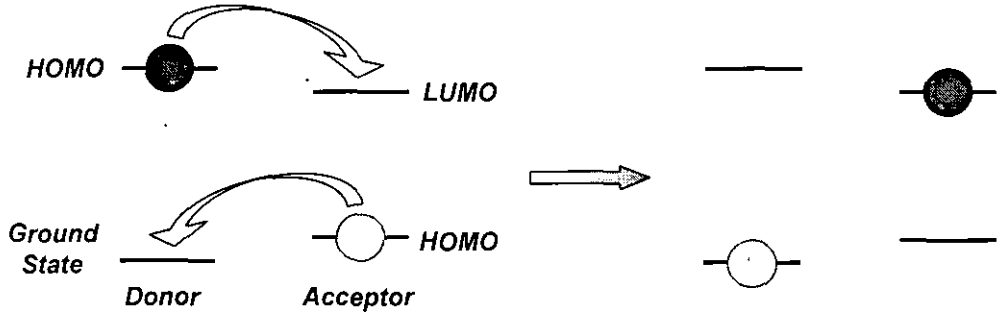

Fig. 1.5. Schematic diagramm of electron exchange between donor and acceptor.

The rate of energy transfer in each case decreases exponentially with increasing separation between the donor and acceptor, R_{DA}. This is due to the fact that electron densities usually fall off exponentially as the distance from the nucleus increases. Therefore efficient sensitisation requires as small separation as possible.

1.2.2 Luminescence Quantum Yield and Competing De-activation Pathways

In summary, effective lanthanide emission can be achieved by using an antenna group absorbing with a high molar extinction coefficient at a suitable wavelength, that possesses fast intersystem crossing and effective energy transfer. For this sensitised lanthanide emission process, the efficiency of each of the three main steps is described by the overall luminescence quantum yield. This is the product of the quantum yields of each individual energy transfer step involved in reaching the lanthanide emissive state, and can be considered as the ratio of the number of photons emitted through lanthanide luminescence to the number of photons absorbed by the sensitiser. This value (Φ_{tot}) is based on the efficiency of the sensitization (η_{sens}) and on the quantum yield of the lanthanide luminescence step (Φ_{Ln}), whereas Φ_{Ln} is defined by how the rate constant of radiative processes (k_r) compares to the rate constant of non-radiative processes (k_{nr}) *(Eq. 1.1)*[37]

$$\Phi_{tot} = \eta_{sen}\Phi_{Ln} \quad ; \text{where} \quad \Phi_{Ln} = \frac{k_r}{k_r + k_{nr}} \qquad (1.1)$$

1.2.2.1 Deactivation of the Chromophore Excited States

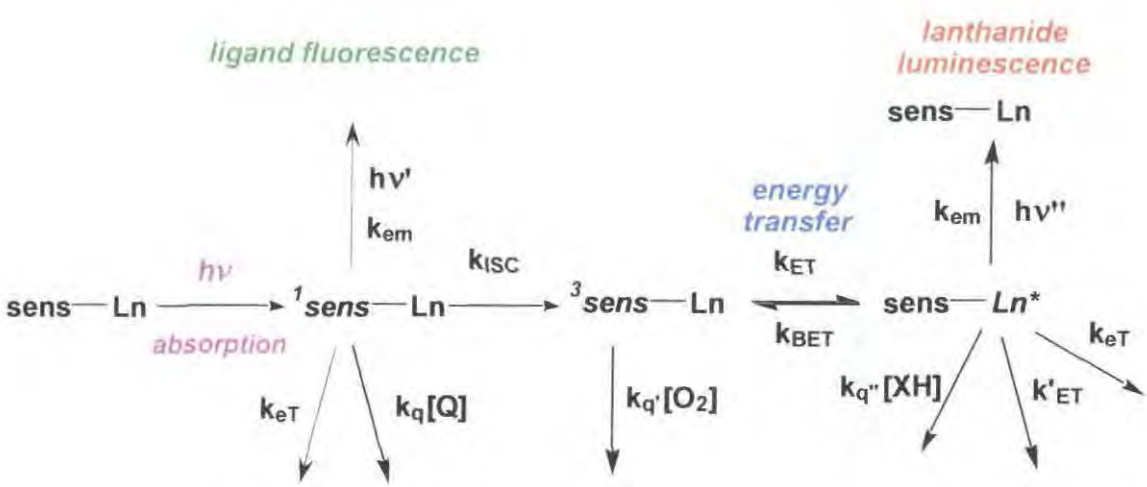

Fig. 1.6. A diagram to show the competing deactivation pathways for sensitized lanthanide emission.

The quantum yield of sensitized emission may be decreased by a number of different deactivation pathways, which can occur at any stage of the energy transfer process (*Fig. 1.6*). There are three excited states that may be perturbed: the singlet and triplet state of the sensitiser and the lanthanide emissive state. To maximize the quantum yield it is necessary to have a fast rate of intersystem crossing (ISC) and a high rate of energy transfer from the sensitiser to the metal ion. More particularly, these rates should be higher than those for competitive deactivation.

The sensitiser ***singlet excited state*** can be deactivated by fluorescence or either by electron or charge-transfer process which may be intra- or intermolecular in nature.[38,39] Such quenching pathways *e.g.* 'collisional' intermolecular interactions with halide ions could compete with the desired ISC rate, depleting the population of the triplet excited state and consequently decreasing the intensity of the lanthanide emission. Another possible mechanism can be attributed to cases where a reversible change occurs in the structure of the chromophore (*i.e.* protonation or metal binding to the chromophore) changing the energy level of the singlet (and therefore the triplet) state.[15] Consequently, by selecting an appropriate wavelength to allow selective excitation, pH-dependent luminescence occurs.

The ***triplet excited state*** of the sensitiser is susceptible to quenching by molecular oxygen, leading to relaxation of the sensitiser to the ground state and generation of singlet oxygen. Whilst this may be considered as a disadvantageous and irreversible effect, this process has been utilized in luminescent lanthanide oxygen sensors.[15] As mentioned earlier, the triplet state can also be deactivated via back intersystem crossing to the singlet excited state (although there is often a considerable thermal barrier to overcome), by phosphorescence or again by the desired route of energy transfer to the lanthanide.

1.2.2.2 Deactivation of the Lanthanide Emissive State

Deactivation of the Ln(III) emissive state can occur through ***vibrational energy transfer*** to either solvent molecules or to the bound ligand, resulting in a decrease in both the intensity and lifetime of the lanthanide emission. Radiative rate constants for the depopulation of the excited states of some Eu(III) and Tb(III) complexes have previously

been measured in H_2O and D_2O and the quenching effect of proximate OH, NH, CH and C=O[40] oscillators investigated.[41]

Amine NH and OH oscillators are the most effective quenchers in both the solid state and in solution (*Fig. 1.7*). In an aqueous medium (most relevant to applications of responsive complexes), the main quenching process involves energy transfer to O-H oscillators, whereby directly coordinated water molecules have a more substantial effect than closely diffusing water molecules. Displacement of any bound water molecule(s) by either inter- or intramolecular anion directly to the Ln(III) center can lead to both an increase in emission intensity and radiative lifetime. These processes can allow ratiometric analyses[42,43] associated with the reversible anion binding process.

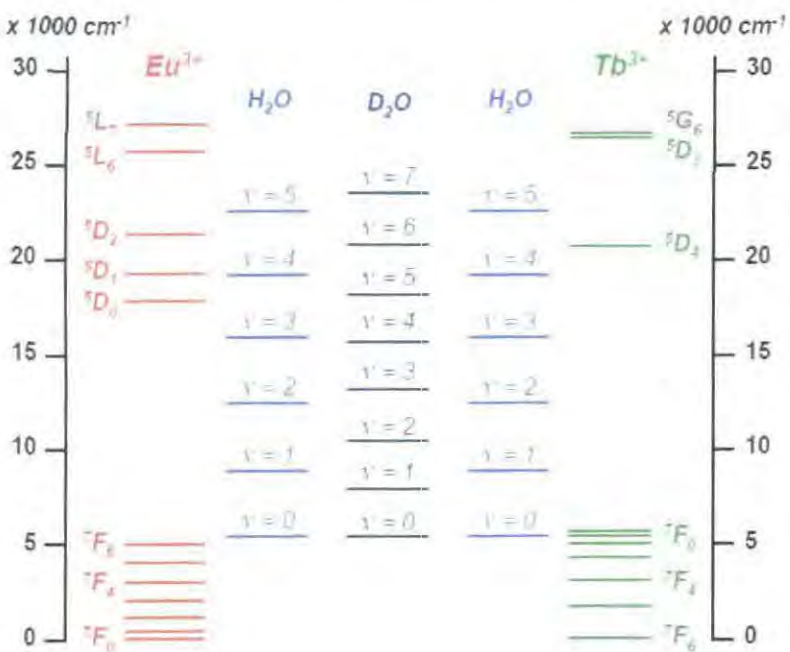

Fig. 1.7. Relative energies of OH oscillators in bound water molecules, compared to Eu^{3+} and Tb^{3+} excited state levels.

Quenching by energy matched oscillators can be attributed to the weak coupling between the *f*-electronic states of the *lanthanide ion* and the vibrational overtones of O-H and N-H oscillators, where the energy gap between the lanthanide emissive state and the highest level of the ground manifold can be bridged by these vibronic states. The energy gap for Eu(III) and Tb(III) ions are about 12,000 cm^{-1} and 15,000 cm^{-1}, equating to the

third and fourth vibrational overtone of proximate O-H oscillators respectively. The lower overtone in the former case accounts for the observation that Eu(III) complexes are more sensitive towards vibrational quenching. A given X-D oscillator (X = O, N, C) resonates at (approximately $1/\sqrt{2}$) lower energy, than its corresponding X-H equivalent. Early work by Haas and Kropp and Windsor established that the quenching of europium complexes observed in H_2O is significantly reduced in D_2O,[44] as the Franck-Condon overlap factor with the metal emissive state is less favourable.

The vibrational stretching frequencies of amide NH (ν_{NH} ~ 3,300 cm^{-1}) and methylene CH bonds (ν_{CH} ~ 2,950 cm^{-1}) are similar to those of an OH group (ν_{OH} ~ 3,400 cm^{-1}) and are therefore also capable of quenching the Eu(III) $^5D_0$ state. The effect is less pronounced for terbium. The difference in measured rate constants for depopulation of the lanthanide excited state in H_2O and D_2O is proportional to the quenching effect of exchangeable XH oscillators, allowing an estimation of the solution hydration state (*i.e.* number of bound H_2O molecules) for a given lanthanide complex.[41,42,45,46] (*For more detail on these hydration state calculations and the contributions of outer sphere water molecules and N-H oscillators see 6.1.6.*)

Electron-rich species may also quench the long-lived lanthanide excited state by ***electron*** or ***charge transfer***. This case is more likely to be prevalent in cationic complexes or with systems in which the ligand has a low-lying LUMO. The Tb and Eu excited states lie at 2.44 and 2.06 eV above the ground state[47] respectively, and this free energy can be used to 'drive' the charge transfer process in quenching by an electron-rich species. Iodide anions and low molecular weight anti-oxidants, e.g. urate and ascorbate, have recently been shown to quench the lanthanide excited state by reducing the emission intensity and lifetime. The magnitude of the second-order rate constant that defines this quenching process (10^5 to 10^6 $M^{-1}s^{-1}$ in case of iodine) is a rather low value compared to the values of $>10^9$ $M^{-1}s^{-1}$ that characterise dynamic quenching of aryl triplet states by molecular oxygen. This probably reflects the inhibition to collisional encounter on diffusion (i.e. the longer range nature of the process), associated with the relative inaccessibility of the encapsulated lanthanide to the quenching species.

The lanthanide excited state can also be quenched by intermolecular ***energy transfer*** to a proximal acceptor group of similar energy.[10,30]

1.3 Lanthanide Complexes and Luminescent Probes

Eu(III) complexes that are subject of the current work, were intended to serve as ratiometric, luminescent probes for measuring intracellular pH, p[citrate^{3-}], and p[HCO_3^-] in a complex that is preferably excited at a wavelength greater than 355 nm.

In designing such probes a number of beneficial factors need to be taken into consideration:

- their excited states possesses lifetimes in the millisecond range allowing time-gated measurements in order to overcome the problems of light scattering and background fluorescence that often compromise the analysis of biological samples;
- they are emissive in the green/red region of the visible spectrum with large Stokes' shifts between the excitation and detection wavelengths;
- the excitation spectra of such complexes permit the identification of donor groups in the metal and ligand binding sites;
- measurement of the radiative lifetimes of Eu(III) and Tb(III) in H_2O and D_2O can allow the determination of the inner sphere hydration number;
- changes in intensity and fine structure of their sharp, line-like emission spectrum can provide information on the local environment, allowing the opportunity for ratiometric analysis;
- interactions between Ln(III) and ligands are mostly electrostatic, so that modifications to the ligand frame can be performed without significantly altering the metal's photophysical properties.

With the aid of these unique photophysical properties, responsive and ratiometric probes can be engineered by careful design and selection of the appropriate ligand and sensitising moiety.

1.3.1 The Choice of Ligand[38,48]

The structure of the ligand that binds to the lanthanide ion is of key importance when determining the overall stability of the complex.[49] If the complex is to be used in a biological medium, then there are significant concentrations of potentially competitive chelating ligands to consider (*i.e.* protein, endogenous anions). When considering the potential applications of such complexes, for example, as luminescent probes or MRI contrast agents, it is critically important that the ligand should complex the appropriate lanthanide ion tightly to yield a kinetically stable and thermodynamically inert complex. 'Free' lanthanide ions in the human body are relatively toxic *in vivo* (LD_{50} ~0.1 mmol kg^{-1}) and in cells as they may replace Ca^{2+} in biological processes.[50]

Lanthanide ions have high coordination number requirements. Typically, coordination numbers are 7 – 10, and in solution the ions are fully hydrated. The low polarisability and high charge density of the Ln (III) ions accounts for their 'hard acid' like behaviour. Consequently, lanthanide ions are best accommodated by ligands offering 'hard' donor atoms, such as nitrogen and oxygen, allowing coordination *via* ionic interactions. Often, upon complexation, the enthalpy of bond formation does not fully compensate for the enthalpy of dehydration. A favourable Gibbs free energy term is still possible if there is a sufficient entropy change, this can be achived by using polydentate[51] (*e.g.* DTPA) and in particular macrocyclic[52] (*e.g.* DOTA) ligands (*Fig. 1.8*). Enhanced stability can be achieved by the incorporation of negatively charged donor atoms leading to significantly more stable complexes, as a result of charge compensation.

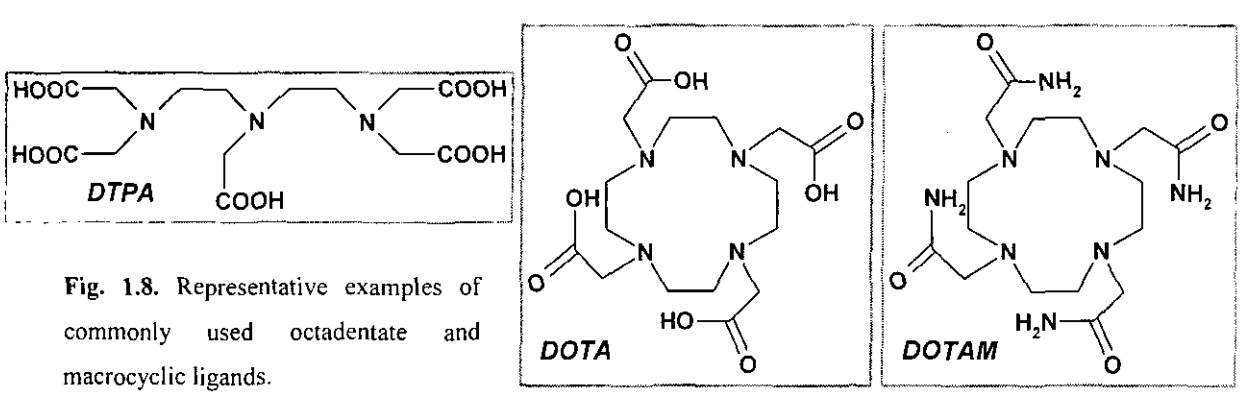

Fig. 1.8. Representative examples of commonly used octadentate and macrocyclic ligands.

Complexes based on a 1,4,7,10-tetraazacyclododecane (cyclen) skeleton satisfy many of these requirements. The addition of pendant arms, containing further donor groups, to the N of the cyclen ring such as carboxylate, phosphonate or amide groups (*e.g.* DOTAM) can participate in binding to the metal centre, forming a 'cage' like ligand, with a considerable increase in the complex stability. Upon pendant arm ligation, enhanced shielding from intermolecular ligation of chelating species, or quenching effects of the solvent water molecules may be achieved, resulting in increased metal based luminescence.[53]

Complexes based on 1,4,7,10-tetraazacyclododecane-1,4,7,10-tetraacetic acid (DOTA) framework have been shown to possess high stability constants for lanthanide ions (*Fig. 1.9*), with Eu^{3+}, Tb^{3+} and Gd^{3+} fitting the vacant cavity most efficiently.[54] It is an octadentate ligand with C_4-symmetry leaving one coordination site free for intermolecular ligation to complete the mono-capped, square antiprismatic coordination environment.[55]

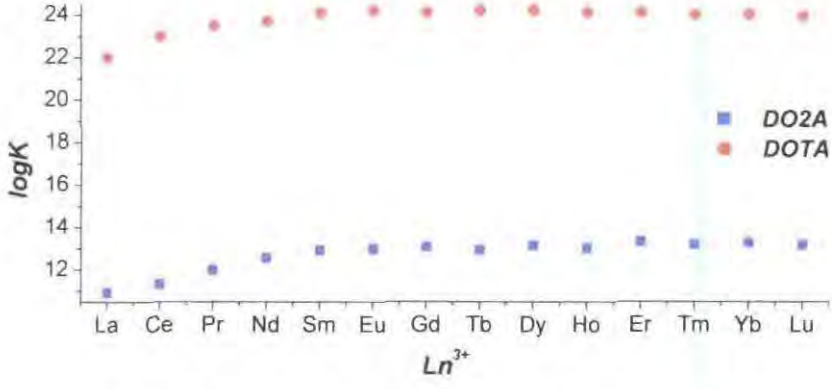

Fig. 1.9. LogK *vs.* Ln^{3+} size plot to highlight the cavity and coordination number effect in the case of DOTA[56] (●) and DO2A[57] (■) (1,4,7,10-tetraazacyclododecane-1,7-diacetic acid).

The macrocyclic lanthanide complexes can adopt a number of different isomeric configurations, the ratio of which depends on the nature of the lanthanide ion, solvent, temperature, pressure and most importantly the nature of the ligand itself.[38] Lanthanide complexes of DOTA give rise to two macrocyclic conformations $\lambda\lambda\lambda\lambda$ and $\delta\delta\delta\delta$ depending on whether the NCCN chelate ring torsion angle is positive (δ) or negative (λ). There are also two possible arrangements for the pendant arms, (Δ) arranged in a clockwise and (Λ) anticlockwise fashion (with positive and negative NCCO torsion

angles respectively).[58] This leads to a formation of four possible stereoisomers, that exist as two pairs of enantiomers (*Fig. 1.10*).

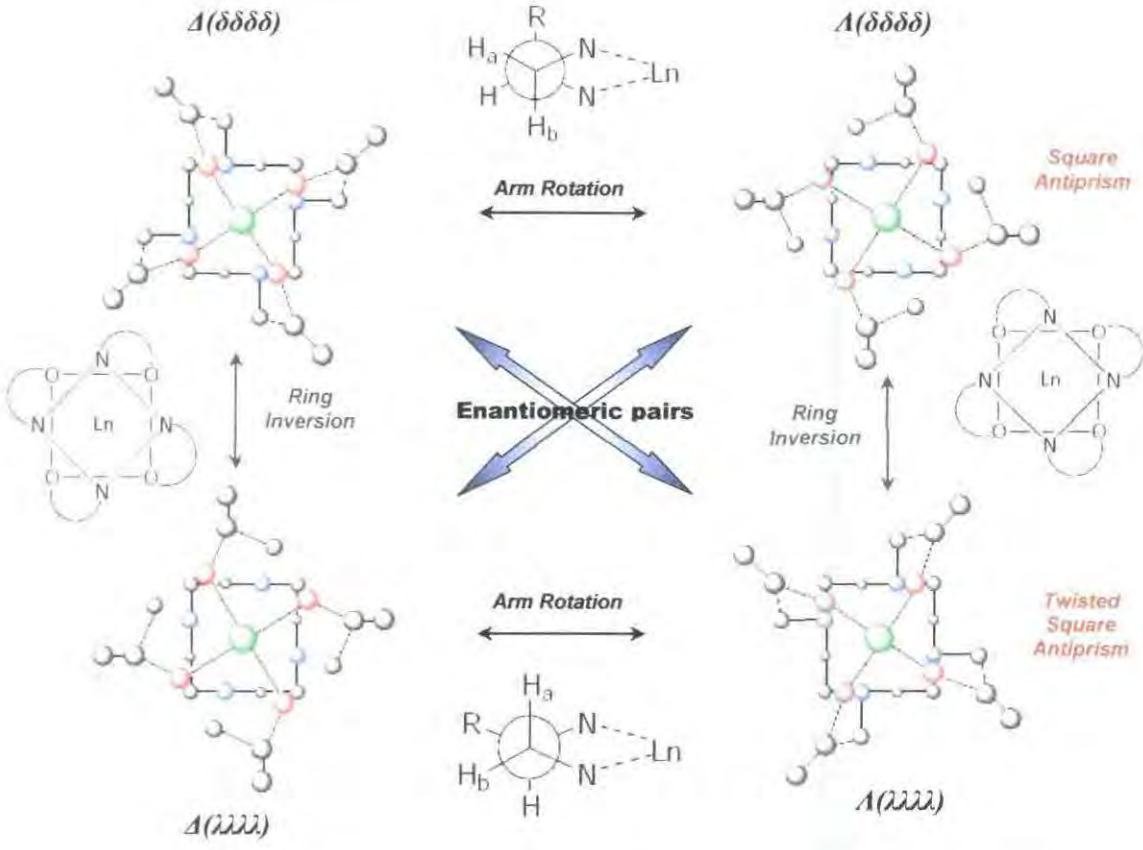

Fig. 1.10. The four stereoisomers of Ln-DOTA complexes showing the two possible orientation of the cyclen ring, and the two conformations of the pendant arms.

The stereoisomers adopt either a square antiprismatic (SAP) geometry, with a twist angle of ~40° between the O and N (*Δ* (*λλλλ*) and *Λ* (*δδδδ*)) or a twisted square antiprismatic (TSAP) geometry, with a twist angle of ~29° (*Λ* (*λλλλ*) and *Δ* (*δδδδ*)). The enantiometric pairs may interconvert between these two geometries in solution, via independent cooperative pendant arm rotation (*Λ* ↔ *Δ*) or ring inversion processes (*λλλλ* ↔ *δδδδ*). The introduction of a substituent α or *β* to one of the ring nitrogens imparts conformational rigidity. Arm rotation is sterically inhibited, and ring inversion may slow down, so that one isomer in conformation may be preferentially populated in solution.

In addition to cyclen derivatives, other systems such as cryptates,[14,59] calixarenes,[60,61] podands,[11] helicates[62] and bipyridyl-functionised[59] macrocycles have been employed as chelating ligands for lanthanide emissive compounds.

1.3.2 The Choice of Sensitising Moiety

As described previously, the attachment of an organic chromophore to the chelating ligand is crucial in the design of an efficient luminescent lanthanide complex.

Requirements for a suitable sensitiser are:

- a triplet state, with sufficient energy from which energy transfer can occur efficiently to the lanthanide excited state. Ideally to promote both Eu(III) and Tb(III) emission this equates to a triplet energy of about 22,500 cm^{-1}. Such energies favour efficient sensitization as they significantly reduce the disadvantageous thermally activated back energy transfer to the aryl triplet state. However, these values give an upper limit to the absorption wavelength (420nm and 490 nm for Eu(III) and Tb(III) respectively);
- high molar extinction coefficient for the aryl singlet state, in the range 350-420 nm thereby avoiding the need for expensive quartz optics, whilst preventing excitation of endogenous chromophores (*i.e.* proteins and nucleic acids);[63,64]
- a small singlet – triplet energy separation, minimizing ligand fluorescence and allowing efficient inter-system crossing to populate the triplet state of the sensitiser;
- the ability to coordinate to the lanthanide ion to minimize the sensitiser-Ln distance. This is not only beneficial for the desired antenna-Ln intramolecular energy transfer, but effectively shields the metal ion from intermolecular binding by maximising its coordination requirements. Furthermore, this interaction tends to inhibit the possibility of quenching by electron-transfer;
- a high reduction potential, hence avoiding electron-transfer quenching by biomolecules (such as urate and ascorbate), but with deference to the fact that the S_1 state of electron-rich aromatics can be effectively oxidized via electron transfer by a Eu(III) ion at the expense of the sensitization process.

The search for systems that operate using longer excitation wavelength has led to the development of NIR emitting lanthanide complexes (incorporating Nd(III) and Yb(III) ions).[65-67] However, these systems are restricted in their use due to the lack of instruments that can record emission above 800 nm. Thus, research in recent years has been focused on optimizing lanthanide luminescence using chromophores that can be excited at wavelengths in the range 330 - 410 nm. The next few examples of such sensitizing moieties provides a general review of commonly used chromophores and their photophysical properties, as revealed through a series of luminescent Eu(III) and Tb(III) complexes using DO3A as chelating agent.

Acridone[49, 68, 69] 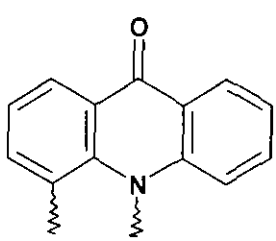 *C-linked* *N-linked*	• λ_{max}= 410 nm, ε = 5,300 $dm^3mol^{-1}cm^{-1}$ • E_T= 21,050 cm^{-1} (poor Tb^{3+} sensitization) • Non-binding group, q=2 (for Eu-complex) • Φ_{Eu} = 0.05, τ_{Eu} = 0.37 ms ⇒ Efficient Eu^{3+} sensitizing, with low quantum yield which can be attributed to high (~90%) ligand fluorescence. Also the relatively high number of quenching water molecules around the metal ion decreases the lifetime of the luminescence.
Triazophthalazine[70] 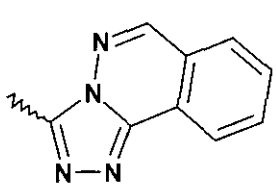	• λ_{max}= 304 nm, ε = 2,400 $dm^3mol^{-1}cm^{-1}$ • E_T= 23,600 cm^{-1} • Monodentate binding, q=1 (for Eu-complex) • τ_{Eu} = 0.62 ms ⇒ Direct binding maximises the through-bond electron exchange with pO_2 insensitive luminescence. Modest ligand fluorescence, but low excitation wavelength and molar extinction coefficient.

1,10-Phenanthroline[71] 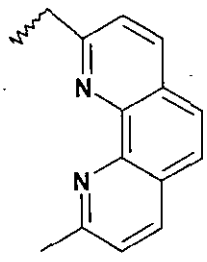	• λ_{max}= 278 nm, ε = 14,760 $dm^3mol^{-1}cm^{-1}$ • E_T= 22,100 cm^{-1} (poor Tb^{3+} sensitization) • Bidentate binding, q = 0 • Φ_{Eu} = 0.21, τ_{Eu} = 1.24 ms • Φ_{Tb} = 0.11, τ_{Tb} = 0.31 ms ⇒ Efficient for sensitising Eu^{3+} with high luminescence efficiency in water, but insufficienty low excitation wavelength and high oxygen sensitivity of the T_1 state (Φ_{Tb} = 0.55, τ_{Tb} = 1.51 ms)
Tetrazatriphenylene[64, 72, 73] 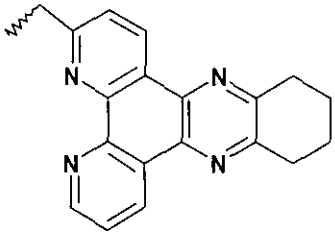	• λ_{max}= 348 nm, ε = 6,440 $dm^3mol^{-1}cm^{-1}$ • E_T= 24,000 cm^{-1} • Bidentate binding, q = 0 • Φ_{Eu} = 0.16, τ_{Eu} = 0.99 ms • Φ_{Tb} = 0.40, τ_{Tb} = 1.46 ms ⇒ High quantum yields in water, with zero ligand fluorescence, although the excitation wavelength is slightly less than the >355 nm target.
Azaxanthone[74] 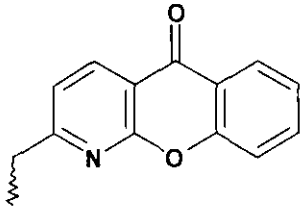	• λ_{max}= 336 nm, ε = 8,790 $dm^3mol^{-1}cm^{-1}$ • E_T= 26,100 cm^{-1} (minimised back energy transfer) • Φ_{Eu} = 0.07, τ_{Eu} = 0.57 ms • Φ_{Tb} = 0.14, τ_{Tb} = 1.82 ms • Monodentate binding, q=1 ⇒ Efficient for sensitising, with modest ligand fluorescence, but still a low excitation wavelength (can be improved by additional electron rich groups on the aromatic ring)

All τ and Φ values referring to measurements in H_2O

What these examples show is that there is a wide variety of factors that need to be balanced in order to create a luminescent lanthanide complex with the desired properties to be used in practical applications. However, it is evident from this brief overview, the most important property must be the design of the chromophore itself, its positioning, proximity, photophysical properties and the number of donor groups binding to the metal centre.

At the outset of this work, it was decided to examine systems based on the introduction of methyl-1-azathioxanthone[75,76] based chromophores (*Fig. 1.11*). These sulfur containing azaxanthone derivatives seemed to be promising candidates to promote Eu(III)-emission, owing to their attractive photophysical properties.

Both 2-methyl-1-azathioxanthone and 7- methyl-1-azathioxanthone are excellent sensitizing moieties. They absorbs at 372 nm and 381 nm and possesses triplet energies of 23,700 cm^{-1} and 22,800 cm^{-1} respectively. Such energies are sufficiently high for energy transfer to the emissive states of both Eu(III) and Tb(III). The pyridine N is a reasonably good ligand towards both lanthanide metal ion and, as a result, the distance between the donor and acceptor should be small, and hence the rate of energy transfer should be high.

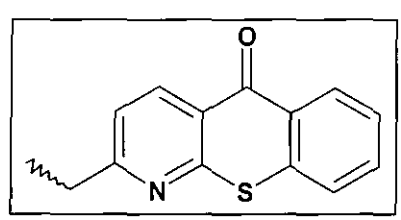

Fig. 1.11. The structure of 2-methyl-azathioxanthone.

1.3.3 Applications of Luminescent Lanthanide Complexes

A new and promising class of fluorescent probes consists of luminescent lanthanide complexes. As previously mentioned, such complexes with emission that range from visible to the near IR region of the spectrum are commonly used in the study of biological systems as fluorescent labels.[77] The long lifetime of lanthanide luminescence means that this emission can be easily distinguished from any short-lived background fluorescence from the observed biological media. Thus, a delay is set

between the pulse used to excite and the recording of the luminescence from the lanthanide complex to reduce the interference of background luminescence.[78] This is in contrast to the luminescence behavior of the organic dyes currently used as labels, which have short-lived emission, with bandwidths that frequently overlap making assignment of individual species difficult.

1.3.3.1 Ln-complexes for Luminescent Resonance Energy Transfer

Fluorescent resonance energy transfer (FRET) is a technique that is used to monitor interactions between two or more molecules, often for the purpose of studying specific protein-protein interactions, lipids, enzymes, DNA or RNA inside living cells. This technique relies on a transfer of energy from a donor to an acceptor fluorophore, with suitably matched energy levels, so that efficient energy transfer can occur between them, which lead to spectral changes. This energy transfer process occurs through a dipole-dipole mechanism and its rate constant shows distance dependence (R^{-6}). Depending on the extent of overlap between the emission spectrum of the acceptor and absorption spectrum of the donor, the quantum yield of the donor and the relative orientation of the interacting partners. The amount of energy transfer can be deduced by monitoring these changes; and in combination with a microscope, and a suitable calibrations, one can obtain both spatial information about the specific binding interaction (donor-acceptor distance) and its time-course.[79] Experimentally, this can be achieved by determination of what is normally quoted as the 'FRET efficiency'. This can be defined as the ratio of the deactivation of the donor by energy transfer over all of the deactivation pathways. The acceptor does not need to be fluorescent; its deactivation can be either by radiative or non- radiative quenching. The limitation of this technique lays in the requirement for a short donor acceptor distance (2 – 8 nm in particular).[80] The FRET technique typically used to be based around organic-based dyes, but with the ever expanding application of lanthanide complexes, the technique can use luminescent lanthanide donors to transfer energy to an (organic-based) dye, through the use of an appropriate ligand, allowing the possibility of bioconjugation (*Fig. 1.12*). This is often refered to as lanthanide-based or ***Luminescence Resonance Energy Tranfer*** (LRET).[63,81,82]

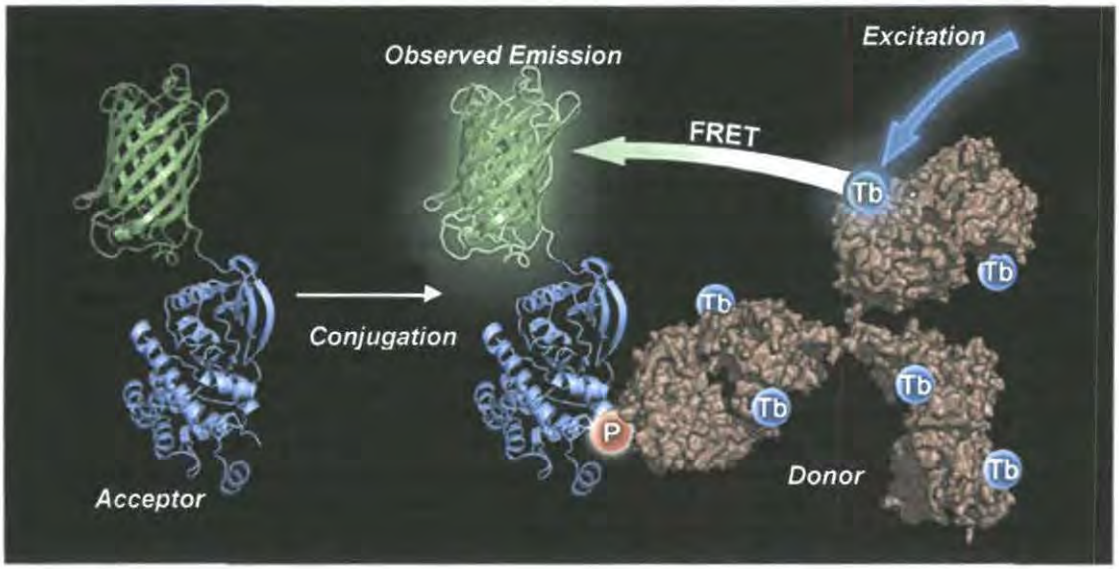

Fig. 1.12. The principle and application of FRET, more specifically LRET.[63]

Such systems (*Fig. 1.13*) often have technical advantages compared to using all-organic dyes, which include a larger measurable distance range (>100 Å), with significantly greater accuracy, improved signal to background ratio and insensitivity to incomplete probe labeling.[63]

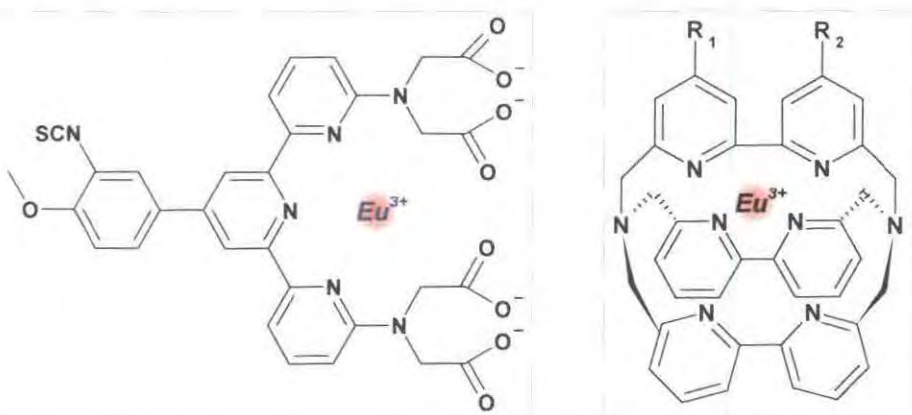

Fig. 1.13. Structures of typical lanthanide components in a TR-FRET assay: (*left*) terpyridine-bis(methylenamine)tetraacetic acid[81] *(right)* trisbipyridine cryptate.[82]

1.3.3.2 Probes for the Study of Ionic Concentrations[13]

Other applications of luminescent lanthanide complexes include their use as probes for the study of intracellular ionic concentrations[43,69] and in monitoring anion

binding.[9,83,84] The types of probes that are of interest are either for the detection or monitoring of changes in the concentration of chemical species. Ligands that do not fully saturate the coordination sphere or in which some of the donor groups can undergo exchange can be useful in detecting species capable of coordinating to the metal centre or changing the affinity of binding of a donor group on the ligand. Detection involves tracking or tagging, and monitoring is concerned with responsive systems where the properties vary as a function of the local concentration of the targeted analyte. The purpose of this section is to give a brief overview on luminescent lanthanide sensors/probes detailed introductions can be found in the individual chapters dedicated to such complexes (*section 3.1 (pH), 4.1 (Carbonate) and 5.1 (Citrate)*)

In recent years, attention has turned towards the design of pH-responsive luminescent lanthanide complexes. Such work has been stimulated by the observation that the extracellular pH of several tumors (~6.8) is more acidic than both intercellular tumor pH (~7.2) and the pH of normal extracellular tissue pH (~7.4).[85] Such luminescent lanthanide complexes[86-88] that are able to be used for this purpose must incorporate a well characterised pH switch. For example, a ligating moiety needs to be identified that can bind reversibily to the Ln(III) centre as a function of pH. This reversibile binding should cause a change in the lanthanide coordination environment, leading to differences in the intensity and structure of the emission spectrum. By studying such a change it is possible, with a use of a well defined calibration, to estimate the pH of the local environment.

In the pursuit of bioactive anion binding studies Ln(III) complexes are being more and more frequently applied. Due to the nature of this thesis, only those lanthanide complexes will be detailed here that incorporate luminescence detection of the binding anion species. It should be noted that there are numerous lanthanide complexes that have been studied for this purpose using the aid of NMR detection.[84] As it is clear from previous applications of emissive lanthanide complexes, the main aspect of these sensors is based upon the relative ease by which bound water molecules may be replaced by anions, perturbing both the intensity and lifetime of the emissive lanthanide.[9,83,84,89-91] Specific binding moieties have also been attached to luminescent lanthanide complexes, rendering them sensitive to oxygen[20,92] or to metal ions, such as Zn^{2+} ion,[135] Cu^{2+} ion,[71b] Na^{+}, K^{+} ions.[93] Recent probes for ionic concentration measurements involving the use of

Eu(III) ion. Upon replacement of a coordinated water molecule, dramatic structural changes can be observed in the metal-based emission spectra. These complexes allow the development of ratiometric analyses for measuring analyte concentration.[69,94-96] This is attractive as the measurement (*Fig. 1.14*) of emission intensity ratios is independent of probe complex concentration.

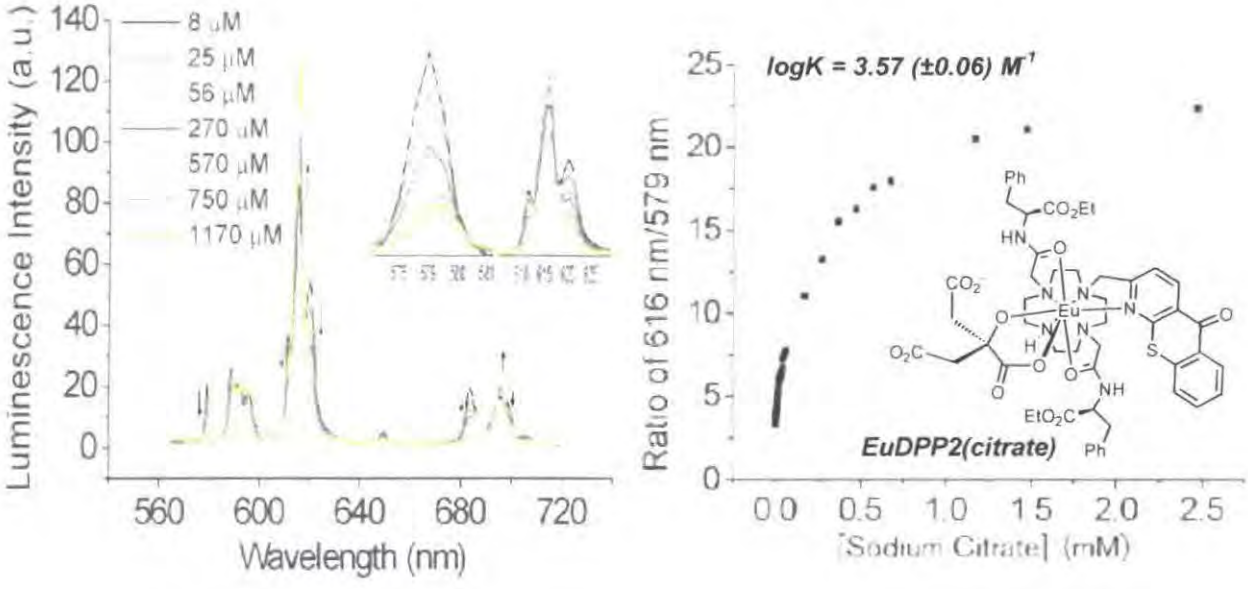

Fig. 1.14. Example of a ratiometric luminescent europium complex used as citrate sensor. (*left*) The luminescence spectra of aqueous EuDPP2 solution (10 μM) upon titration with added sodium citrate (pH = 7.4, λ_{ex} = 384 nm). (*right*) Selected intensity ratio *vs.* added citrate concentration plot for calculating the apparent binding constant (logK) for the EuDPP2(citrate) adduct.[43]

1.3.3.3 Lanthanide Complexes for 'In cellulo' Imaging

Luminescent lanthanide complexes complement the beneficial properties that are associated with fluorescent proteins, organic dyes and quantum-dots that are being used today for live-cell imaging. This may be related to their unique spectroscopic properties: they possess sharper line-like emission spectra than quantum-dots. Their broad emission range, large Stokes' shift and long emission lifetimes ranging from μs to ms, allow the use of time-gated detection methods. Despite these favourable properties, there are relatively few examples where lanthanide complexes have been specifically used for

imaging of live cells. Therefore the strategic development of suitable luminescent lanthanide probes for *in cellulo* applications is promising and worthy of study.

Recent work has shown[64,94,95,97] that some luminescent Eu(III) and Tb(III) complexes are able to cross the cell membrane in eukaryotic cells, with different, well defined compartmentalisation or localisation profiles (*representative examples: Fig. 1.15-17*). Therefore the essential features to engineer into such complexes not only incorporate all the requirements stated previously, but also requires a complex with targeted localization.[98] In order to be employed as a cellular probe, the complex must show cell permeability whether by passive diffusion or by an active transport mechanism. If the probe is to act as a tag for certain cellular species, it must contain reactive groups to allow bioconjugation. However, the mechanism by which these complexes are able to penetrate the plasma membrane is not well understood; the small number of studies that have been undertaken allow some very tentative conclusions to be drawn, which highlight certain structural features, that may be responsible for mediating the uptake, transport and localization of such complexes.[64,69,94] (*Further detail and conclusion on these studies will be interpreted at section 3.6, 4.7 and 5.6*)

Fig. 1.15. Confocal microscopy images of a Eu complex[69] incorporating a C-linked acridone sensitising moiety, co-localised with Brefeldin-A® in NIH 3T3 cells. Orange regions of the merged images correspond to areas where both stain and complex are localized confirming ***localization in the endoplasmic reticulum***. However, a more diffuse background is also apparent, corresponding to distribution throughout the cytosol.

Fig. 1.16. Confocal microscopy images of a Eu complex[99] incorporating an N-linked acridone sensitising moiety, co-localised with Lysotracker green® in NIH 3T3 cells. Orange regions of the merged images correspond to areas where both stain and complex are localized confirming ***lysosomal localization***.

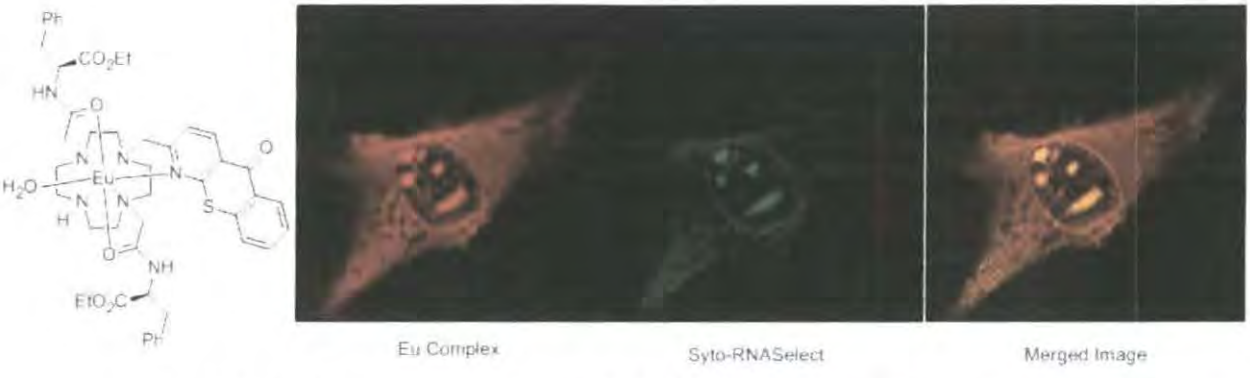

Fig. 1.17. Confocal microscopy images of EuDPP2[94] incorporating 2-methyl-azathioxnathone sensitising moiety, co-localised with Syto-RNASelect® in NIH 3T3 cells. Orange regions of the merged images correspond to areas where both stain and complex are localized confirming ***ribosomal localization,*** (highlighting strong localization in the nucleus).

The above brief overview highlights the versatility of Ln(III) complexes, where binding modes, selectivity and cellular localization can each be altered by adjustment of the central Ln(III) ion, but more importantly, structural modification of the coordinating ligand. The spectroscopic data accumulated from these complexes helps in the pursuit of designing new, better and more specific luminescent lanthanide compounds.

1.4 Other Fluorescence-based Cellular Probes[100]

Fluorescence microscopy has proven to be a useful technique and over the years a number of different classes of compounds has been used, or has been suggested to have potential application as probes for live cell imaging and/or tracking subcellular events.[101] As a non-invasive method, it is of particular use in examining living cells. In order to utilise this technique, the species of interest must be fluorescent, or labelled with a fluorescent moiety. Much of the understanding related to the structure and composition of cells and the processes that occur within them has been gained through the use of fluorescent stains probes or labels, such as mutant forms of green fluorescent protein and commercially available organic dyes. More recently, the application of quantum dots and emissive metal complexes has also shown great promise in this pursuit.

1.4.1 Fluorescent Proteins

One of the first classes of fluorescent probes arose from the molecular cloning and careful genetic engineering of Green Fluorescent Protein (GFP)[102] from the bioluminescent jellyfish *Aequorea victoria*. GFP (*Fig. 1.18*) is a 26.9 kDa protein comprised of 238 amino acids, possessing an 11-strand β-barrel structure (24Å x 42Å), with inward facing sidechains from what its 4-(*p*-hydroxybenzylidene)-imidazolid-5-one fluorophore is formed in an autocatalytic cyclisation reaction (Ser65-***Tyr66***-Gly67). It is a widely used marker for *in vivo* imaging because that it can be expressed in a wide variety of cells. It exhibits spontaneous fluorescence without requiring cofactors and rarely exhibits any phototoxicity. Its excitation wavelength is above 350 nm and it emits in the visible region, making it ideal for microscopic applications. As a protein, recombinant forms of GFP can be engineered in which it is tagged with a signaling peptide or tailored to another protein.[103] Furthermore, mutagenesis of GFP has resulted in a generation of fluorescent proteins that span the visible spectrum, such as blue (BFP), green (GFP), yellow (YFP), cyan (CFP) and red (RFP) fluorescent protein.[104,105] The primary limitations of fluorescent proteins are relate to their complicated photophysical properties,[106] high molecular weight and relatively time-consuming labeling process, meaning that for many applications simple organic dyes often have clear advantages.

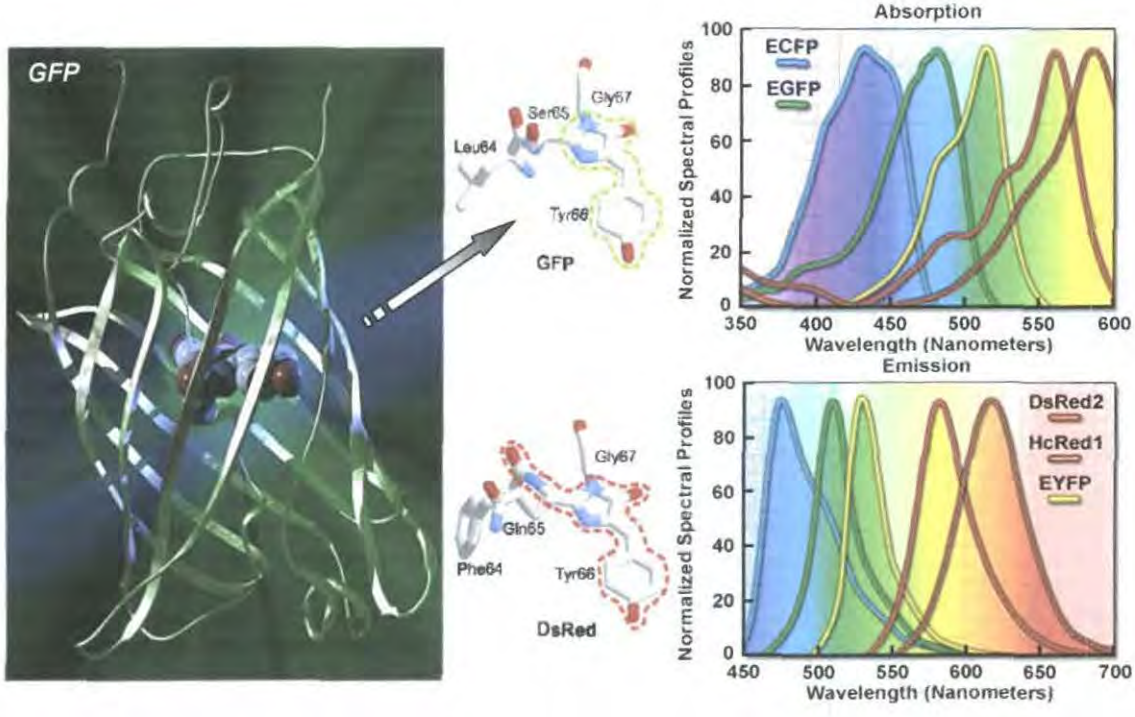

Fig. 1.18. (*left*) Structure of GFP and its fluorophore ($\lambda_{abs.}$ = 398 nm, $\lambda_{em.}$ = 508 nm and φ = 80%).[106] (*right*) Excitation and emission spectra for a range of commercially available fluorescent proteins.[105]

1.4.2 Organic Fluorescent Dyes

For many years, organic fluorescent dyes have constituted the main alternative to fluorescent proteins as cellular probes. They are highly emissive, and possess large molar absorption coefficients. Their structure and conjugation mode can be easily modified in order to suite particular applications. While synthesis of novel classes of efficient dyes remains a challenge, with slight modifications to the structure of common dyes, a wide array of dyes can be generated with vastly different fluorescence properties.[107, 108] The most common classes of fluorescent dyes are derivatives of fluorescein and rhodamine (*Fig. 1.19. left*),[109] each of which possesses relatively high molar extinction coefficients at a suitable wavelength (488 nm argon laser), excellent fluorescence quantum yield, good water solubility, and can be easily linked to other compounds through ester or amide derivatives. However, their applications are limited by their relatively high rate of photobleaching, pH-dependent fluorescence (fluorescein pK_a ~6.4) and broad emission and absorption bands, which can be quenched upon coordination to biopolymers. These

problems have been reduced to some extent by the introduction of fluorescent dyes based on BODIPY® and AlexaFluor® (*Fig. 1.19. right*), which possess high absorption coefficients and quantum yields that are often in excess of 0.5.[110]

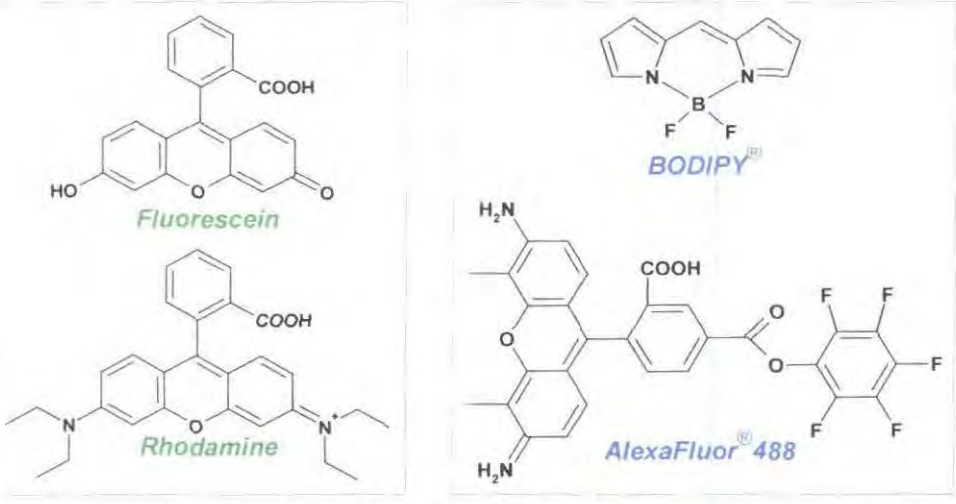

Fig. 1.19. (*left*) The structure of fluorescein and rhodamine, and (*right*) examples of organic dyes developed to overcome the limitations of the former.[109]

Both AlexaFluor® and BODIPY® dyes are available with a wide range of excitation and emission wavelengths and can span most of the visible spectrum (*Fig. 1.20*) AlexaFluor® dyes are similar in structure to fluorescein and rhodamine, while the structure of BODIPY® relies upon a totally different sub-structure, with interesting features such as neutral charge and non-polar design.

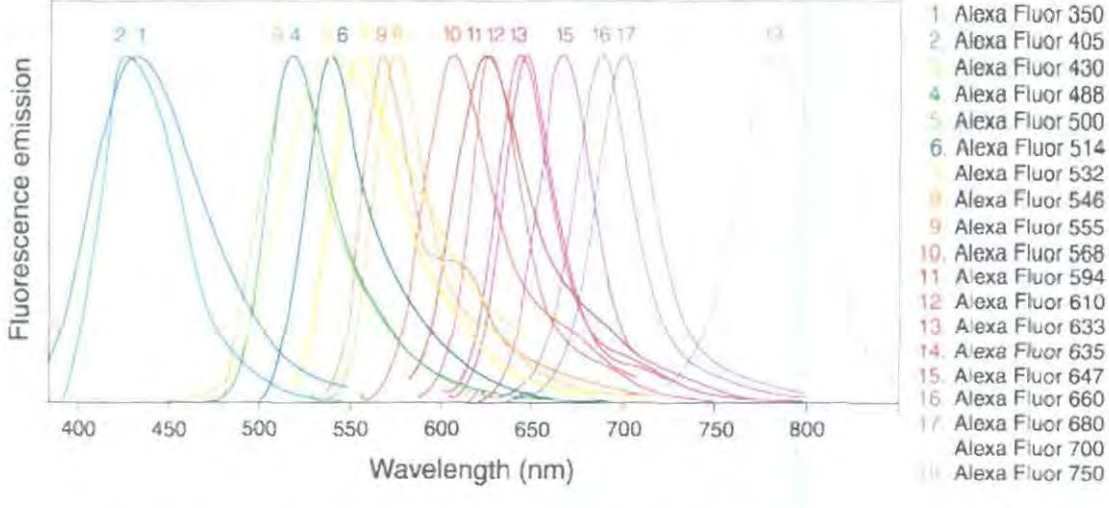

Fig. 1.20. Emission profiles for the range of AlexaFluor® dyes.[109]

The limitation of organic dyes remain the high signal to noise ratio in fluorescence microscopy due to their short emissive lifetimes, small Stokes' shifts and interference from autofluorescence of the cell; sometimes this can be overcome by the use of multiphoton excitation. Therefore, different approaches such as the use of quantum dots and metal complexes have received increasing interest over recent years in an attempt to obviate these undesirable properties.

1.4.3 Quantum Dots as Fluorescent Labels

Quantum dots are fluorescent semiconducting nanocrystals with typical diameters of 2-8 nm, generally constructed from elements from groups II and IV (*i.e.* CdSe and CdTe) or from groups III and V (InP and InAs). They have recently received interest for applications in *in vivo* (and *in cellulo*) imaging and diagnostics, due to their unique size- and composition- tunable photophysical properties.[111,112] These include high molar extinction coefficients (in the range of 10^6 $M^{-1}cm^{-1}$) and elevated quantum yields (typically 80%). They also possess relatively narrow absorption and emission bands with large Stokes' shifts (up to 400 nm) and high photostability. QDs can also be employed in combination, in which QDs of different colours and intensities are combined to encode an array of genes, proteins or small molecules. QDs have been widely used as alternatives to fluorescent proteins for labeling cellular proteins. A challenge to the use of QDs is the means of their intracellular delivery. Labeling often requires microinjection or induced endocytosis, due to their non-polar coating.[113] For cellular applications several solubilisation methods can be applied to overcome this problem. Either encapsulation by an amphiphilic polymer coating or attachment of appropriate molecules to the surface can be used to promote cellular uptake, localization via bioconjugation and low cytotoxicity[114] (*Fig. 1.21*). Other drawbacks to their use are that QDs often require multiphoton excitation due to their less favourable excitation wavelength. Moreover, they are not responsive to their local environment, and therefore can only act as fluorescent tags. This is perhaps one area where metal complexes could extend the scope of analyses in living cells.

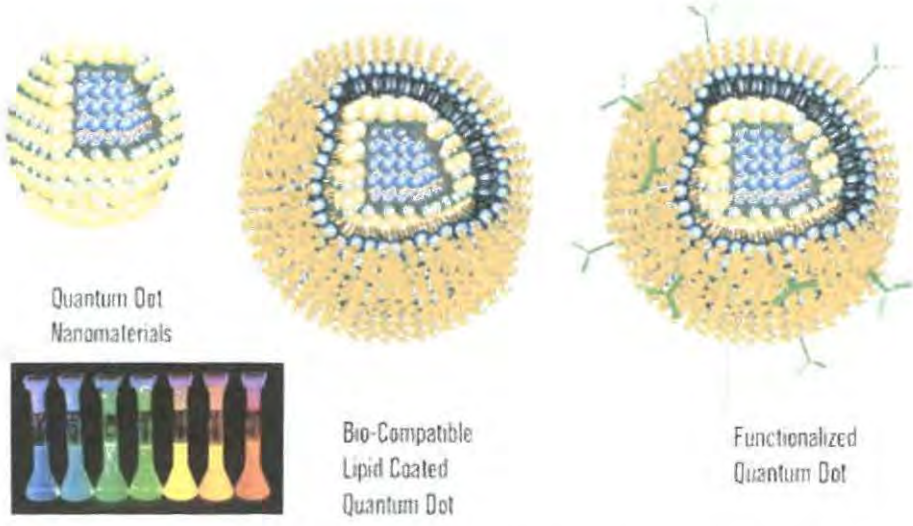

Fig. 1.21. Structures, evolution and emission range of multifunctional quantum dots.[112]

1.4.4 Transition Metal Complexes

In a number of studies over the last century, it was observed that the presence of a metal ion could alter the fluorescence of a system. Two phenomena were identified: Chelation Enhanced Fluorescence (CHEF), in which metal binding increases the fluorescence of the fluorophore (*e.g.* Al(III), Ce(III), Ga(III), La(III) and Zn(II)), and Chelation Enhanced Quenching (CHEQ), where the presence of the metal leads to decreased fluorescence (*e.g.* Hg(II)).[115] Changes in the fluorescence have also been observed with change in the oxidation state (Ni(II)/Ni(III) and Cu(I)/Cu(II)).[116]

Based on these properties, complexes of transition metal ions, and in particular those belonging to the platinum group have been studied as luminescent sensors or probes. The majority of them are designed to provide quantitative information about the presence of certain analytes in solution, either indirectly via attachment to the pendant group, or by direct coordination to the metal.[117] The response is generally observed as a change in the emission profile of the complex, often as a result of a charge (MLCT/LMCT/ILCT) or energy transfer interaction (Förster). There are a number of examples that are designed to monitor DNA intercalations,[118,119] membrane binding and micelle encapsulaion[120] (*Fig. 1.22*). However, there are few examples for *in vivo* applications, although fluorescent imaging of pO_2 in liver using ruthenium complexes has been reported[121] along with their successful application in immunobiological assays.[122]

[123] The emission lifetimes of these and similar transition metal complexes are of the order of microseconds, allowing the use of time resolved techniques, similar to those already being commercially used in lanthanide based assays.[124]

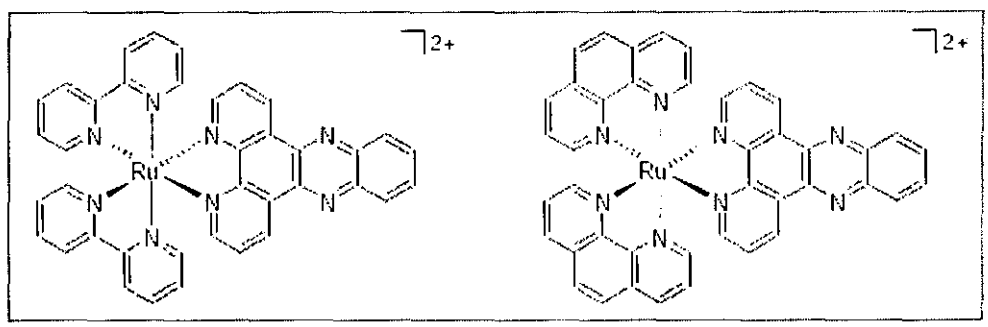

Fig. 1.22. Structures of typical ruthenium based luminescent transition metal complexes.[118]

1.5 Luminescence Microscopy[125]

Fluorescence microscopy has proved to be a useful technique in the analysis of living biological systems, in particular for the imaging of live cells and the subcellular events that occur within them.[101,102] Essential to the use of this technique is that the species of interest must be fluorescent or labelled with a fluorescent moiety (*see 1.3.3 and 1.4*). Technology has now reached a level where through the use of an appropriate tag it is possible to monitor single molecules in real time.[126] The following section will outline the evolution and key features of modern microscopy techniques.

1.5.1 The Basics of Microscopy

Fluorescence microscopes are relatively simple optical devices (*Fig. 1.23*). An external light source provides light energy that is focused through an objective lens onto the sample, where it is absorbed by the applied luminescent moiety raising this molecule to an excited state. Generally, a broad band excitation source, such as a Xe lamp is used as the light source and the excitation wavelength (or range of wavelengths) is chosen through the application of an appropriate filter. Emission from the sample is observed as its fluorescent tag relaxes back to its ground state. This light is focused by an objective either to the observer (eyes) or onto a CCD camera. Since the emitted light is of lower

energy than the absorbed photons it allows discrimination between the excitation and emission signal. Practically, this is done by introducing a dichroic mirror to the set-up; this is inclined at 45° to the direction of the excitation source. This mirror is chosen such that the excitation light is reflected; whilst the lower energy light is emitted by the sample is allowed to pass through. However, often absorption and emission spectra of fluorophores are broad resulting in spectral overlap. As a consequence, some reflected or scattered excitation light can pass through the mirror giving a lower than optimal signal to noise ratio, hence reduced sensitivity. A second filter is usually used that is appropriate for the desired emissive range of the chropmophore, allowing more specific selection of the wavelengths of interest.[126]

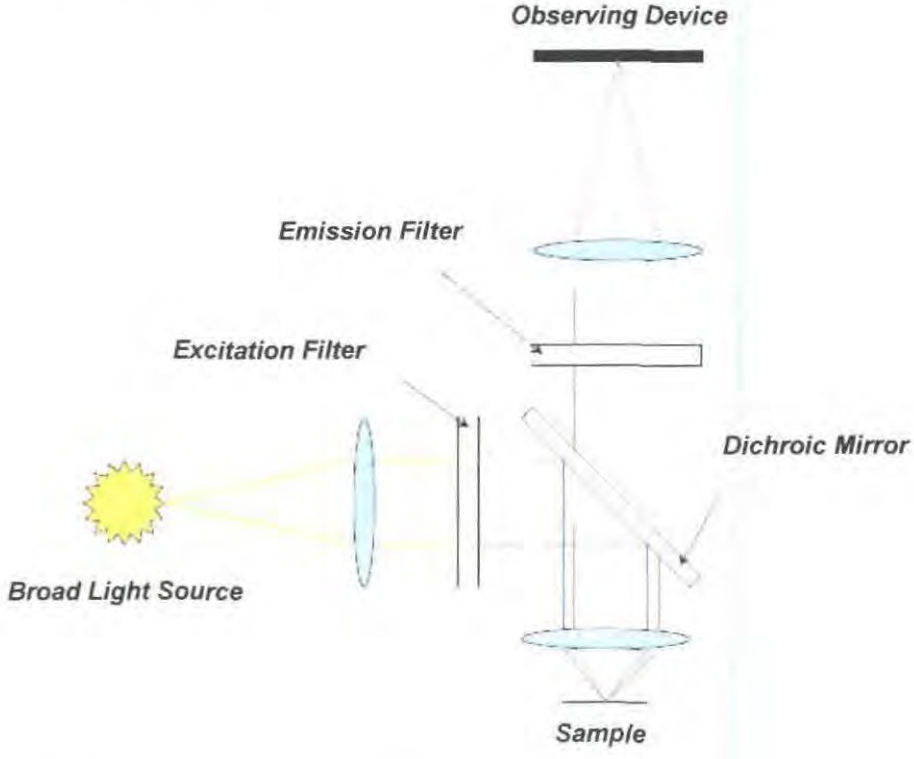

Fig. 1.23. Schematic diagram of a basic fluorescence microscope.

Modifications to this basic system allow the luminescent emission to be characterised not only by modulation in its intensity, but also by changes in its lifetime, polarization and emission wavelength. Thus, it is possible to carry out multidimensional analysis of a sample in order to gain information about the position, concentration, and environment of interaction of molecules within that system.[102,127]

1.5.2 Confocal Microscopy

One of the disadvantages of traditional fluorescence microscopy is that the images are often degraded by the presence of light that is emitted or scattered by features that are out of the plane of focus. This problem can be overcome in a number of ways: through the use of image processing and deconvolution software,[100] through the use of an apotome (a commericallly available attachment for most fluorescent microscope) or through confocal imaging.[102] In a confocal microscope (*Fig. 1.24*), both the illumination and detection systems are focused on the same focal point within the sample. Out of focus light from the areas above or below the focal plane are simply eliminated through the use of a pinhole. (The diagram illustrates how behind the objective lens, all of the light rays come together at a crossover point.) The crossover point for light from out-of-focus plane is above or below that for light from the in-focus plane. The insertion of a pinhole at the correct height allows the in-focus light to pass, but blocks nearly all of the dispersed light from planes that are higher or lower.

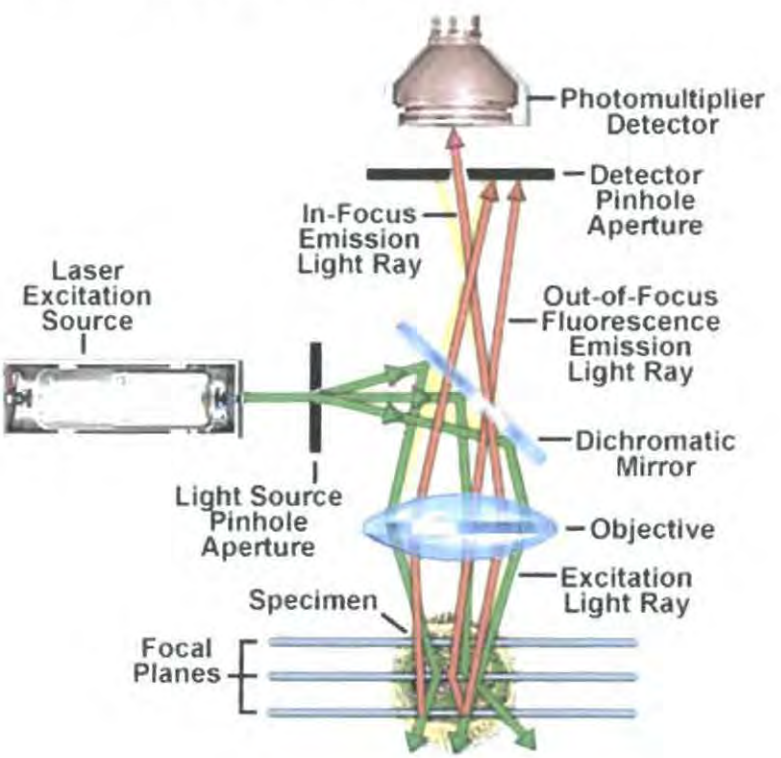

Fig. 1.24. The confocal light pathway principle and its application in microscopy.[125]

Scattered light can inevitably still pass through the pinhole and it is for this reason that the excitation light is also focused onto the focal point; if the light reaching regions above and below the focal plane is weak, then the intensity of scattered light will also be low. In confocal microscopy, the field of view is restricted to the size of the de-magnified pinhole; therefore the image must be built up by scanning over the sample until the area of interest has been covered. In association with the fact that a useful image often consists of 10^6 pixels, the time taken to record each pixel must be kept short and hence an intense source of light, such as a laser source is needed accompanied by a photomultiplier device, built-in to the detector to enhance image intensity and thereby reducing the acquisition time.[100]

Whilst the confocal microscope gives the obvious advantage of better resolution compared to traditional bright field microscopy this advantage must be evaluated against the increased cost of the instrument and the limitations associated with the availability of a laser of appropriate wavelength for the fluorophore. In addition, the light intensity at the focal point is very high (of the order of MW/cm^2) and may cause photobleaching and degeneration of the studied specimen. As a result, the light intensity should be carefully controlled, so that it is of sufficient intensity to produce a high signal to background noise intensity, but should not be too high as to degrade the fluorescent tag or sample.

1.5.3 Multiphoton Excitation

The use of multiphoton excitation causes less photobleaching and damage to the sample than single photon methods, since excitation is achieved through the use of ultrashort laser pulses (10^{-14} s). Whilst the laser energy is high, the sample is only irradiated for a very short period of time; practically, this means that a much smaller area of the fluorescent specimen is being stimulated and consequently photobleaching only occurs in the focal plane.[102] However, multiphoton excitation requires considerably higher laser intensities (about 5 - 10 times) than those used in single photon methods, with exact values depending on the absorption cross-section of the applied dye.[128]

An additional advantage of multiphoton excitation is that it allows excitation using light in the NIR region of the spectrum, whilst still observing visible emission. Biological tissue is most effectively penetrated in the 710-820 nm range of the spectrum.

This can increase the penetration depth of sensitized emission to the order of 5 to 10 mm, and therefore luminescence microscopy may allow the method to be extended to selected *in vivo* applications. Multiphoton excitation is becoming more accessible with the development of new and cheaper laser sources capable of producing ultrafast pulse sequences. Therefore, it is practicable to design probes for biological systems with the intention of using combined single and/or multiphoton excited applications. It is a promising prospect that the use of two photon excitation could facilitate the use of many Eu(III) and Tb(III) complexes already proven to be successful as sensors in the analysis of biological samples with UV excitation.[129]

1.5.4 Time Gated Detection

Because *f-f* transition are formally Laporte forbidden, the Ln(III) ions display long emissive lifetimes. For europium and terbium, these values are of the order of milliseconds, much longer than the autofluorescence from biological samples. The difference can be used to significantly enhance signal to noise and signal to background intensity ratios.

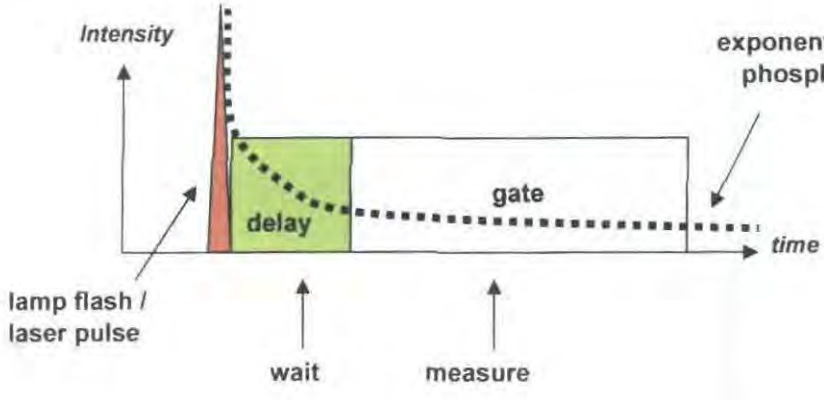

Fig. 1.25. The principle of time gated detection.

Experimentally (*Fig. 1.25*), this is done using an integrating camera and a pulse excitation source, used to excite the sample. Usually a delay of the order of 10 - 100 ns is then introduced; over this time period, all background emission intensity will decay to zero whilst the lanthanide intensity remains relatively high. The camera then detects only lanthanide related emission. Scattered light does not reach the CCD camera, since the

excitation is off whilst the signal is being acquired. The use of an integrating camera allows the application of lower intensity excitation, since a number of pulses and detection cycles can be carried out.

1.5.5 Time-Resolved Fluorescence Microscopy[80,125,127]

Two techniques that take advantage of time gated instrumental setups are Fluorescence Lifetime Imaging (FLIM) and Time-Resolved Anisotropy Imaging (TR-FIAM). They both take advantage of changes in the lifetime of emission to provide information about the environment of a chosen fluorophore that would otherwise be difficult to obtain by Fluorescence Intensity Imaging. The former provides a map of lifetimes over the sample, whereas the latter informs us about the rotational mobility of the fluorophore.

1.6 Cellular Uptake and Localisation

In order to be employed as a cellular probe (*Fig. 1.26*) a complex must exhibit a number of essential features, such as suitable excitation wavelength to avoid auto-fluorescence form the observed environment, high overall quantum yield and of key importance cell permeability and low cell toxicity. This uptake can occur either by passive diffusion or by an active transport mechanism, in which the complex avoids irreversible trafficking *via* vesicle-lysosome pathway. Furthermore compartmentalization or localization in specific regions of the cell is also a desirable feature.

Luminescent lanthanide complexes have been reported to localise to the nucleolus,[94,95] endoplasmic reticulum,[69] lysosomes,[99] nucleus[64] and in the outer mitochondrial membrane.[130] However, the number of studies focused purely onto the mechanistic aspects of cellular uptake is very limited. In order to specifically design and improve luminescent lanthanide complexes as cellular probes, a better understanding of this process needs to be gained.

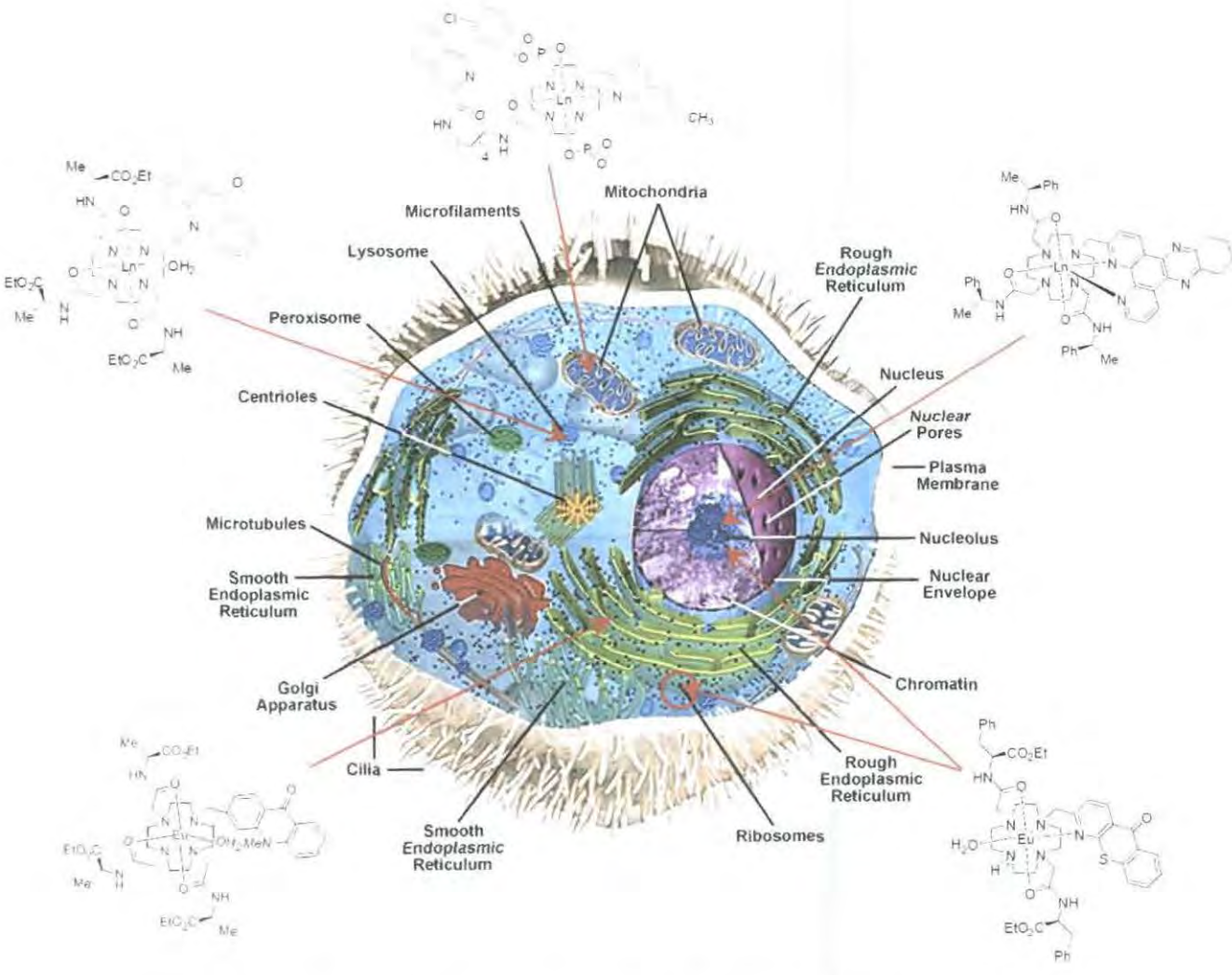

Fig. 1.26. Schematic drawing of an eukaryotic cell highlighting the subcellular organelles[131] to which various lanthanide complexes are suggested or have been found to be localized.

1.6.1 Mechanisms of Cellular Uptake

There are three major categories of mechanism by which species can be transported across the cell membrane (*Fig. 1.27*): passive transport, active transport and vesicular transport.[131]

Active transport requires the input of energy. Primary active transport involves the use of specific membrane-bound carries or channels to move species across the cell membrane. For example, the Na^+/K^+-ATPase uses the energy from ATP to simultaneously move three sodium ion out of the cell to be exchanged to two potassium

ion. In contrast, secondary active transport uses an ion gradient which has already been established by a primary pump.

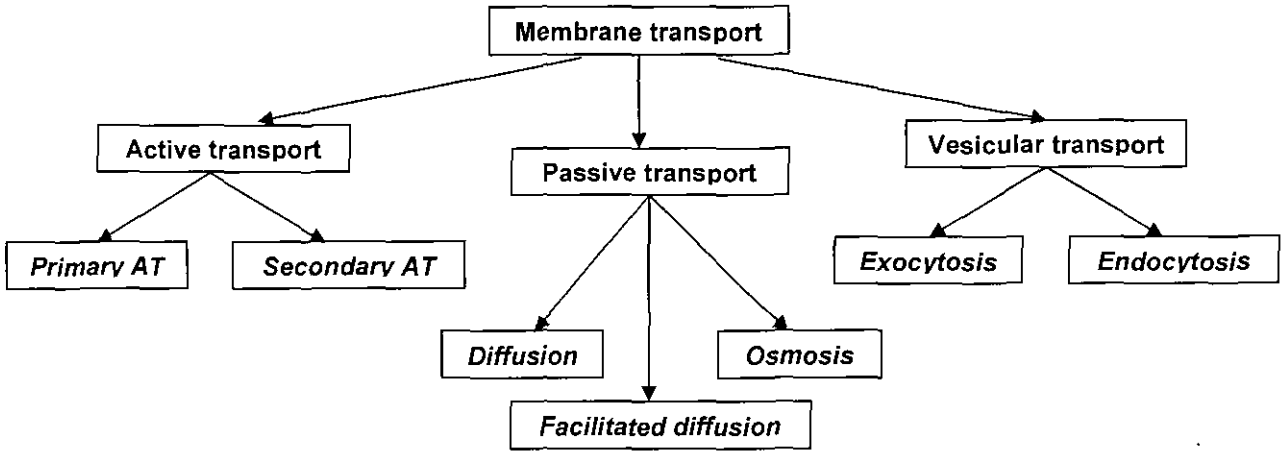

Fig. 1.27. Methods of membrane transport.

Passive transport refers to pathways, where the driving force for the transport is the concentration gradient of the transported species; therefore this transport mechanism does not requires energy. Osmosis is the movement of water from regions of low to high solute concentration, while diffusion refers to the movement of the transported ion/molecule itself by its concentration gradient. In facilitated diffusion, species move through protein channels in the cell membrane. While this process usually applies to small ions such as Na^{+}, K+, Ca^{2+} and Cl^{-}, some metal complexes have been observed to enter the cells through ion channels, such as cisplatin which is thought to enter cells through the copper transporter Ctr1.[131]

Vesicular transport involves several specific transport mechanisms (*Fig. 1.28*). It is the least understood mechanism of the membrane transport, but perhaps of the greatest interest, since the relatively large lanthanide complexes are unlikely to be transported via active or passive transport mechanisms. Endocytosis and exocytosis are essentially reverse processes, enabling the transport of species in and out of the cell respectively. In a broad sense, endocytosis describes the process by which the membrane internalizes an extracellular particle via encapsulating it in to the vesicle.

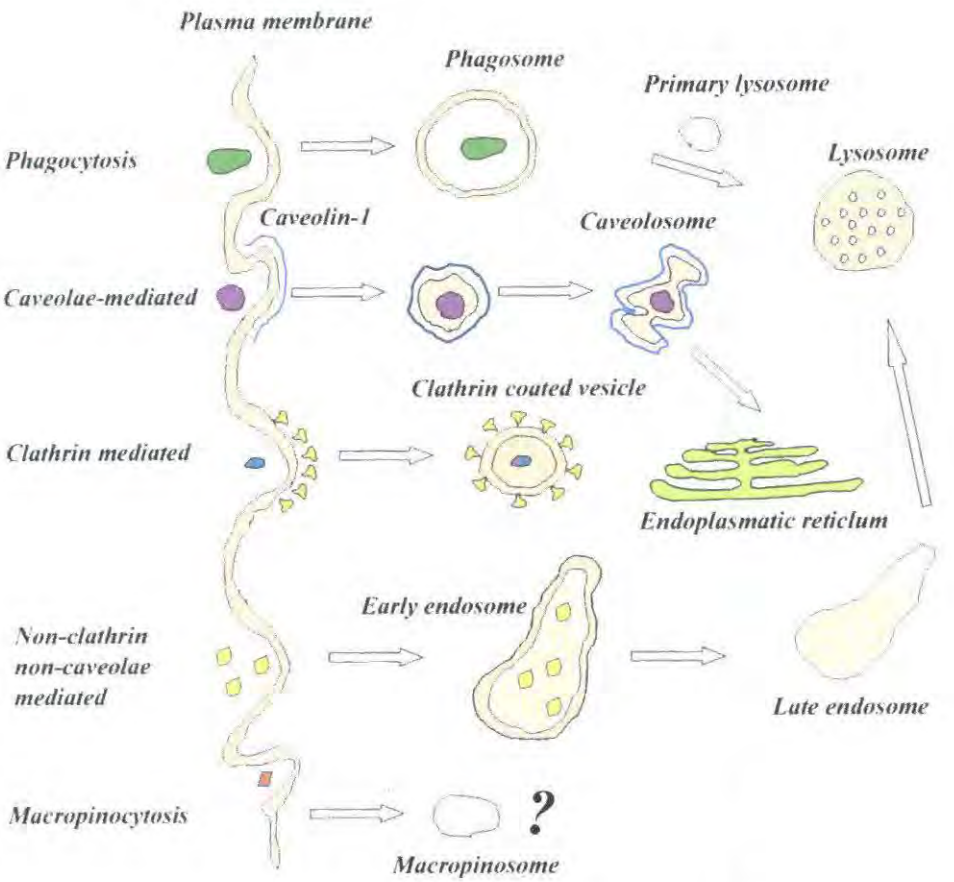

Fig. 1.28. Putative mechanisms of membrane transport by endocytosis.[132]

Endocytosis is a process by which eukaryotic cells are able to internalize both small and large molecules thorugh incorporation into membrane vesicles at the plasma membrane. It can be broken down to two major categories: phagocytosis involves the transport of large multimolecular particles (d >0.5 μm) that must bind to specific plasma membrane receptors to trigger their own uptake, while pinocytosis refers to the non-specifically bound uptake of extracellular fluid and any small particles (d <0.2 μm) it may contain.[131]

In phagocytosis, the cell membrane engulfs the solid particle forming a phagosome, which upon incorporation with a primary lysosome, forms a lysosome for degradation. The rate of these processes and the amount of membrane and extracellular fluid that may be internalized is estimated for cells, such as macrophages and fibroblasts, is more than 200% of their entire cell surface hourly. The degraded products are then

released intracellularly for further processing, or *via* exocytosis. Exocytosis is essentially the reverse of endocytosis, where the cell excretes species by the fusion of vesicles into the plasma membrane.

Pinocytosis can be further sub-categorised according to mechanism. The best understood route for endocytosis in the clathrin-mediated endocytosis, which occurs at specific regions called 'coated pits' of the cell membrane. These regions are enriched with certain proteins, such as clathrin (180 kDa) and AP-2.[133] These proteins facilitate the invagination of the cell membrane, and pinch off to form clathrin-coated vesicles. Once inside the cell the vesicles combines with an early endosome, and the membrane proteins are then recycled to form a new coated pit. Clathrin-mediated endocytosis is of particular interest as it regulates the uptake of proteins and membrane localized cell compartments.

An alternative mediated uptake mechanism occurs *via* caveolae, which are flask shaped invaginations of the cell membrane. They are coated with a number of lipids and proteins, such as caveolin, and internalize species by potocytosis. This term specifically describes the uptake and transport of small molecules through the mediated formation of a caveolosome. This organelle then may deliver its contents to various locations, such as the cytoplasm, endoplasmic reticulum, or to the cell membrane for release or repositioning of the substrate.

Endosomes act as sorting terminals: membrane and receptor molecules are returned to the cell surface by exocytosis or alternatively transferred (in)to lysosomes to be degraded. Any remaining material is transferred from early endosomes on microtubules to the perinuclear cytoplasm, where they diffuse with the late endosomes. The role of these cell compartments, as they have lysosome type characteristics, is to accumulate and concentrate internalized contents after their passage through early endosomes.

Clathrin and caveolae-dependent endocytosis rely on specific binding to signal vesicular formation. These processes allow routing of ligands to areas of the cell, such as the endoplasmic reticulum, which are not easily accessible by other endocytotic mechanisms. In contrast, macropinocytosis is a non-specific mechanism of internalization, with lateral heterogeneity in the plasma membrane. It occurs when the rim of the cell membrane forms a relatively large irregular shape vesicle, taking

extracellular fluid and macromolecules (non-specifically) inside the cell. This process is driven by actin and myosin, while the mechanism of membrane invagination is similar to that of phagocytosis. It is not well understood how the contents of macropinosomes are processed, but it is known that they can fuse with one another, and can also reassociate with the cell membrane, but they certainly do not associate with early or late endosomes.[133]

Observations of persistent endocytosis in the presence of clathrin and caveolae blocking drugs led to the hypothesis of an additional pathway called non-clathrin and non-caveolae dependent endocytosis, whose mechanism is not yet fully understood.[134] Any endocytotic material released into the cytoplasm is transported via microtubules (d = 22 μm, l = 1 μm). They are also responsible for asymmetrical cell shape, 'scaffolding' within the cell and regulation of the transport of macromolecules within the cell. Any movement of endocytotic material relies on energy from ATP hydrolysis and requires the coupling of the 'motor' proteins to the microtubule, such as kinensin and dynein. These two move in opposite direction, species destined for the cell surface associate with kinensins while those transported to the cell interior are linked to dyneins.

The exact mechanism of cellular uptake and the factors which lead to compartmentalisation of luminescent lanthanide complexs, in specific vesicles is not well understood, however these targeted complexes could help to investigate these processes.

1.7 References

1 P. W. Atkins, 'Physical Chemistry', Oxford University press, 6th ed., 1999.

2 A. D. Sherry and C. F. G. Geraldes, in 'Lanthanide Probes in Life, Chemical and Earth Science', 1989.

3 J. A. Peters, J. Huskens, and D. J. Raber, *Prog. Nucl. Magn. Reson. Spectrsc.*, 1996, 283.

4 D. F. Shriver and P. W. Atkins, 'Inorganic Chemistry', 2001.

5 N. N. Greenwood and A. Earnshaw, 'Chemistry of the Elements', 1998.

6 J. I. Bruce, M. P. Lowe, and D. Parker, 'The Chemistry of Contrast Agents, Chapter II', ed. A. Merbach and E. Toth, J. Wiley, 2001.

7 F. A. Cotton, G. G. Wilkinson, C. A. Murillo, M. Bochman, and R. Grimes, 'Advanced Inorganic Chemistry', 2000.

8 A. Døssing, *Eur. J. Inorg. Chem.*, 2005, 1425.

9 J. I. Bruce, R. S. Dickins, L. J. Govenlock, T. Gunnlaugsson, S. Aime, and M. Botta, *J. Am. Chem. Soc.*, 2000, **122**, 9674.

10 S. Faulkner, S. J. A. Pope, and B. P. Burton-Pye, *App. Spec. Rev.*, 2005, **40**, 1.

11 S. Petoud, S. M. Cohen, J.-C. G. Bunzli, and K. N. Raymond, *J. Am. Chem. Soc.*, 2003, **125**, 13324.

12 J. H. van Vleck, *J. Chem. Phys.*, 1942, **41**, 67.

13a D. Parker and J. A. G. Williams, in 'Responsive Luminescent Lanthanide Complexes', ed. A. Sigel, H. Sigel, and J. Wiley, New York, 2003.

13b T. Gunnlaugson, J . P. Leonard, *Chem. Commun.*, 2005, 3114

13c T. Gunnlaugson, J . P. Leonard, *J. Fluoresc.*, 2005, **15**, 585

14 G. Mathis, *Clin. Chem.*, 1995, **41**, 1391.

15 D. Parker, *Coord. Chem. Rev.*, 2000, **205**, 109.

16 W. T. Carnall, 'Handbook on the Physics and Chemistry of Rare Earths', ed. K. A. Gschneider and L. Eyring, Elsevier, 1998.

17 I. Hemmila and V. M. Mukkala, *Crit. Rev. Clin. Lab. Sci.*, 2001, **38**, 441.

18 S. P. Sinha, 'Europium', Springer-Verlang Berlin, 1967.

19 D. Parker and J. A. G. Williams, *J. Chem. Soc.*, 1996, **18**, 3613.

20 D. Parker and J. A. G. Williams, in 'Metal Ions in Biological Systems,' 1998.

21 S. I. Weissman, *J. Chem. Phys.*, 1942, **10**, 214.

22 N. Sabbatini, M. Guardigli, and J. M. Lehn, *Coord. Chem. Rev.*, 1993, **123**, 201.

23 A. Beeby, D. Parker, and J. A. G. Williams, *J. Chem. Soc. Perkin Trans. 2*, 1996, **8**, 1565.

24 T. Steinkamp and U. Karst, *Analytical and Bioanalytical Chemistry*, 2004, **380**, 24.

25 J.-C. G. Bünzli and C. Piguet, *Chem. Soc. Rev.*, 2005, **34**, 1048.

26 D. Imbert, M. Cantuel, J.-C. G. Bunzli, G. Bernardinelli, and C. Piguet, *J. Am. Chem. Soc.*, 2003, **125**, 15698.

27 N. M. Shavaleev, G. Accorsi, D. Virgili, Z. R. Bell, T. Lazaridies, G. Calogero, N. Amaroli, and M. D. Ward, *Inorg. Chem.*, 2005, **44**, 61.

28 S. J. Pope, B. J. Coe, S. Faulkner, and R. H. Laye, *Dalton Trans*, 2005, 1482.

29 N. M. Shavaleev, S. J. Pope, L. P. Moorcraft, Z. R. Bell, S. Faulkner, and M. D. Ward, *Chem. Eur. J.*, 2003, **9**, 5283.

30 S. Faulkner and S. J. A. Pope, *J. Am. Chem. Soc.*, 2003, **125,** 10526.

31 I. M. Clarkson, 'Energy Transfer in Lanthanide Complexes', PhD, University of Durham, Durham, 1999.

32 J. L. Kropp and M. W. Windsor, *J. Chem. Phys.*, 1963, **39**, 2769.

33 W. Siebrand, *J. Chem. Phys.*, 1967, 440.

34 G. E. Buono-Core and H. Li, *Coord. Chem. Rev.*, 1990, **90**, 55.

35 T. Förster, *Discuss. Faraday Soc.*, 1959, **27**, 7.

36 D. L. Dexter, *J. Chem. Phys.*, 1953, **21**, 836.

37 M. H. V. Werts, R. T. F. Jukes, and J. W. Verhoeven, *Phys. Chem. Chem. Phys.*, 2002, **4**, 1542.

38 D. Parker, R. S. Dickins, H. Puschmann, C. Crossland, and J. A. K. Howard, *Coord. Chem. Rev.*, 2002, **102**, 1977.

39 D. Parker, *Chem. Soc. Rev.*, 2004, **2**, 156.

40 J. L. Kropp and M. W. Windsor, *J. Chem. Phys.*, 1965, **42**, 1599.

41 A. Beeby, I. M. Clarkson, R. S. Dickins, S. Faulkner, D. Parker, L. Royle, A. S. de Sousa, J. A. G. Williams, and M. Woods, *J. Chem. Soc. Perkin trans 2.*, 1999, 493.

42 R. S. Dickins, D. Parker, A. S. de Sousa, and J. A. G. Williams, *Chem. Commun.*, 1996, 697.

43 D. Parker and J. Yu, *Chem. Commun.*, 2005, 3141.

44 Y. Haas and G. Stein, *J. Phys. Chem.*, 1972, **76**, 1093.

45 S. Faulkner, A. Beeby, M.-C. Carrie, A. Dadabhoy, A. M. Kenwright, and P. G. Sammes, *Inorg. Chem. Commun.*, 2001, 187.

46 R. M. Supkowski and W. D. Horrocks, *Inorg, Chim. Acta*, 2002, **340**, 44.

47 R. A. Poole, 'Luminescent Lanthanide Complexes for Cellular Applications', PhD, Durham University, Durham, 2006.

48 R. S. Dickins, J. A. K. Howard, C. W. Lehmann, J. Moloney, D. Parker, and R. D. Peacock, *Angew. Chem.*, 1997, **36**, 521.

49 S. Lis, M. Elbanowski, B. Makowska, and Z. Hantejko, *J. Photochem. Photobiol. A: Chem.*, 2002, **150**, 233.

50 C. H. Evans, 'Biochemistry of Lanthanides', Plenum press., 1990.

51 G. Schwarzenbach, *Helv. Cim. Acta.*, 1952, **35**, 2344.

52 D. K. Cabbiness and D. W. Margerum, *J. Am. Chem. Soc.*, 1969, **91**, 6540.

53 A. Beeby, L. M. Bushby, D. Maffeo, and J. A. G. Williams, *J. Chem. Soc., Dalton Trans.*, 2002, **1**, 48.

54 K. Kumar and M. F. Tweedle, *Pure and Applied Chem.*, 1993, **65**, 515.

55 J. I. Bruce, D. Parker, and D. J. Tozer, *Chem. Commun.*, 2001, 2250.

56 R. M. Smith, A. E. Martell, and R. J. Motekaitis, in 'Criticall Selected Stability Constants of Metal Complexes', Plenum press, 1997.

57 C. A. Chang, Y.-H. Chen, and F.-A. Shieh, *Dalton Trans*, 1998, 3243.

58 R. S. Dickins, J. A. K. Howard, C. L. Maupin, J. M. Moloney, D. Parker, R. D. Peacock, J. P. Riehl, and G. Siligardi, *New. J. Chem*, 1998, **22**, 890.

59 G. Mathis, *Clin. Chem.*, 1993, **39**, 1953.

60 N. Sabbatini, M. Guardigli, I. Manet, V. Balzani, R. Ungaro, C. Fischer, A. Casnati, R. Ziessel, and G. Ulrich, *New. J. Chem*, 1995, **19**, 137.

[61] N. Sabbatini, M. Guardigli, A. Mecati, V. Balzani, R. Ungaro, E. Ghidini, A. Casnati, and A. Pochini, *Chem Commun.*, 1990, 887.

[62] C. G. Piguet, J.-C. G. Bunzli, G. Bernardinelli, C. G. Bochet, and P. J. Froidevaux, *Dalton Trans*, 1995, 83.

[63] P. R. Selvin, J. Jancarik, M. Li, and L. Hung, *Inorg. Chem.*, 1996, **35**, 700.

[64] R. A. Poole, G. Bobba, M. J. Cann, J.-C. Frias, D. Parker, and R. D. Peacock, *Org. Biomol. Chem.*, 2005, **3**, 1013.

[65] S. I. Klink, P. O. Alink, L. Grave, G. A. Peters, J. W. Hofstaart, F. Geurts, and F.C. J. M. van Veggel, *J. Chem. Soc.*, 2001, Perkin Trans. 2, **3**, 363.

[66] M. H. V. Werts, J. W. Hofstaat, F. A. J. Geurts, and J. W. Verhoeven, *Chem. Phys. Lett.*, 1997, **276**, 196.

[67] M. H. V. Werts, J. W. Verhoeven, and J. W. Hofstraat, *J. Chem. Soc., Perkin Trans. 2*, 2000, **3**, 433.

[68] A. Dabadhoy, S. Faulkner, and P. G. Sammes, *J. Chem. Soc.*, Perkin Trans. 2, 2002, **2**, 348.

[69] Y. Bretonniere, M. J. Cann, D. Parker, and R. Slater, *Chem. Commun.*, 2002, 1930.

[70] B. P. Burton-Pye, S. L. Heath, and S. Faulkner, *Dalton Trans*, 2005, **1**, 146.

[71a] S. Quici, G. Marzanni, M. Cavazzini, P. L. Anelli, M. Botta, E. Gianolio, G. Accorsi, N. Armaroli, and F. Barigelletti, *Inorg. Chem.*, 2002, **41**, 2777.

[71b] T. Gunnlaugson, J . P. Leonard, K. Sénéchal, A. J. Harte, *Chem. Commun.*, 2004, 782.

[72] G. Bobba, J.-C. Frias, and D. Parker, *Chem. Commun.*, 2002, 890.

[73] G. Bobba, 'Interaction of chiral lanthanide complexes with nucleic acids', PhD, University of Durham, Durham, 2002.

[74] P. Atkinson, K. S. Findlay, F. Kielar, R. Pal, D. Parker, R. A. Poole, H. Puschmann, S. L. Richardson, P. A. Stenson, A. L. Thompson, and J. Yu, *Org. Biomol. Chem.*, 2006, **4**, 1707.

[75] M. G. Neumann, M. H. Gehlen, M. V. Encinas, N. S. Allen, T. Corrales, C. Peinado, and F. Catalina, *J. Chem Soc, Faraday Trans.*, 1997, **93**, 1517.

[76] X. Allonas, C. Ley, C. Bibatu, P. Jacques, and J. P. Fouassier, *Chem. Phys. Lett.*, 2000, **322**, 483.

[77] J.-C. Frias, G. Bobba, M. J. Cann, C. J. Hutchnson, and D. Parker, *Org. Biomol. Chem.*, 2003, **1**, 905.

[78] L. Charbonniere, R. Ziessel, M. Guardigli, A. Roda, N. Sabbatini, and M. Cesario, *J. Am. Chem. Soc.*, 2001, **123**, 2436.

[79] G. W. Gordon, G. Berry, X. H. Liang, B. Levine, and B. Herman, *Biophys. J.*, 1998, **74**, 2702.

[80] R. D. Goldman and D. L. Spector, 'Live Cell Imaging - A Laboratory Manual', Cold Harbor Laboratory press., 2005.

[81] S. G. Jones, D. Y. Lee, J. F. Wright, C. N. Jones, M. E. Lee, S. Y. Gregory, and D. O. Burns, *J. Fluoresc.*, 2001, **11**, 13.

[82] www.htrf-assay.com/techno/fluorescence.html

[83a] S. Aime, A. Barge, M. Botta, J. A. K. Howard, R. Kataky, M. P. Lowe, J. M. Moloney, D. Parker, and A. S. de Sousa, *Chem. Commun.*, 1999, 1047.

[83b] R. S. Dickins, S. Aime, A. S. Batsanov, A. Beeby, M. Botta, J. I. Bruce, J. A. K. Howard, C. S. Love, D. Parker, R. D. Peacock, and H. Puschmann, *J. Am. Chem. Soc.*, 2002, **124**, 12697.

[84] J . P. Leonard, C. M. G. dos Santos, S. E. Plush, T. McCabe, T. Gunnlaugson, *Chem. Commun.*, 2007, 191.

[85] R. J. Gillies, N. Raghunand, M. L. Garcia-Martin, and R. A. Gatenby, *Med. Biol. Mag.*, 2004, **23**, 57.

[86] M. P. Lowe and D. Parker, *Chem Commun.*, 2000, 707.

[87] M. P. Lowe and D. Parker, *Inorg. Chim. Acta*, 2001, **317**, 163.

[88] M. P. Lowe, D. Parker, O. Reany, S. Aime, M. Botta, G. Castellano, E. Gianolio, and R. Pagliarin, *J. Am. Chem. Soc.*, 2001, **123**, 7601.

[89] R. S. Dickins, T. Gunnlaugsson, D. Parker, and R. D. Peacock, *Chem Commun.*, 1998, 1643.

[90] P. Atkinson, Y. Bretonniere, D. Parker, and G. Muller, *Helv. Cim. Acta.*, 2005, **88**, 391.

[91] P. Atkinson, Y. Bretonniere, and D. Parker, *Chem Commun.*, 2004, 438.

[92] S. Blair, R. Kataky, and D. Parker, *New. J. Chem*, 2002, **26**, 530.

[93a] C. Li, G. L. Law, and W. T. Wong, *Org. Lett.*, 2004, **6**, 4841.

[93b] T. Gunnlaugson, J . P. Leonard, *Chem. Commun.*, 2003, 2424.

[93c] T. Gunnlaugson, J . P. Leonard, *Dalton Trans.*, 2005, 3204.

[94] J. Yu, D. Parker, R. Pal, R. A. Poole, and M. J. Cann, *J. Am. Chem. Soc.*, 2006, **128**, 2294.

[95] R. Pal and D. Parker, *Chem Commun.*, 2007, 474.

[96] J. Yu and D. Parker, *Eur. J. Org. Chem.*, 2005, 4249.

[97] R. A. Poole, C. P. Montgomery, E. J. New, A. Congreve, D. Parker, and M. Botta, *Org. Biomol. Chem.*, 2007, **5**, 2055.

[98] S. Pandya, J. Yu, and D. Parker, *Dalton Trans.*, 2006, 2757.

[99] Y. Bretonniere, M. J. Cann, D. Parker, and R. Slater, *Org. Biomol. Chem.*, 2004, **2**, 1624.

[100] J. L. Lakowicz, 'Principles of Fluorescence Spectroscopy', Academic/Plenum press., 1999.

[101] R. A. Bissel, A. P. de Silva, H. Q. N. Gunaranthe, P. L. M. Lynch, C. P. McCoy, G. E. M. Maguire, and K. R. A. S. Sandanayake, 'Fluorescent and Photochemical Probes of Dynamic Biochemical Signals inside Living Cells', ed. A. W. Czarnik, 1993.

[102] N. J. Emptage, *Curr. Opin. Pharma*, 2001, **1**, 521.

[103] R. Rizzuto, M. Brini, F. de Giorgi, R. Rossi, R. Heim, R. Y. Tsien, and T. Pozzan, *Curr. Biol.*, 1996, **6**, 183.

[104] J. Zhang, R. E. Campbell, A. Y. Ting, and R. Y. Tsien, *Nat. Rev. Mol. Cell Biol.*, 2002, **3**, 906.

[105] R. Y. Tsien, *Annu. Rev. Biochem.*, 1998, **67**, 509.

[106] M. Zimmer, *Chem. Rev.*, 2002, **102**, 759.

[107] T. Ueno, Y. Urano, K. Setsukinai, H. Takakusa, H. Kojima, K. Kikuchi, K. Ohkubo, F. Fukuzimi, and T. Nagano, *J. Am. Chem. Soc.*, 2004, **126**, 14079.

[108] Y. Urano, M. Kamiya, K. Kanda, T. Ueno, K. Hirose, and T. Nagano, *J. Am. Chem. Soc.*, 2004, **127**, 4888.

[109] R. P. Haugland, 'A Guide to Fluorescent Probes and Labeling Technologies', Molecular Probes, 2005.

[110] T. Yogo, Y. Urano, Y. Ishuitsuka, F. Maniwa, and T. Nagano, *J. Am. Chem. Soc.*, 2005, **127**, 12162.

[111] W. C. W. Chen, D. J. Maxwell, X. H. Gao, R. E. Bailey, and M. Y. Han, *Curr. Opin. Biotechnol.*, 2002, **12**, 40.

[112] M. Y. Han, X. H. Gao, J. Z. Su, and S. M. Nie, *Nat. Bioechnol.*, 2001, **19**, 631.

[113] X. Michalet, F. F. Pinaud, L. A. Bentolila, J. M. Tsay, S. Doose, J. L. Li, G. Sundaresan, A. M. Wu, S. S. Gambhir, and S. Weiss, *Science*, 2005, **307**, 538.

[114] X. Gao, L. Yang, J. A. Petros, F. F. Marshall, J. W. Simons, and S. Nie, *Curr. Opin. Biotechnol.*, 2005, **16**, 63.

[115] A. W. Czarnik, 'Supramolecular Chemistry', Fluorescence and Sensing, 1993.

[116] L. Fabbrizzi and A. Poggi, *Chem. Soc. Rev.*, 1995, 197.

[117] M. H. Keefe, K. D. Benkstein, and T. J. Hupp, *Coord. Chem. Rev.*, 2000, **205**, 201.

[118] A. E. Friedman, J. C. Chambron, J. P. Sauvage, N. J. Turro, and J. K. Barton, *J. Am. Chem. Soc.*, 1990, **112**, 4960.

[119] C. Hiort, P. Lincoln, and B. Norden, *J. Am. Chem. Soc.*, 1993, **115**, 3448.

[120] L. Li, F. N. Castellano, I. Gryczynski, and J. R. Lakowicz, *Chem. Phys. Lipids*, 1999, **1**, 99.

[121] M. Paxian, S. A. Kellar, B. Cross, T. T. Huynh, and M. G. Clemens, *Am. J. Physiol. Liver Physiol.*, 2004, **286**, 637.

[122] H. J. Youn, E. Terpetsching, H. Szmacinski, and J. R. Lakowicz, *Anal. Biochem.*, 1995, **232**, 24.

[123] X. Q. Guo, G. N. Castellano, L. Li, and J. R. Lakowicz, *Anal. Chem.*, 1998, 632.

[124] J. N. Demas and B. A. DeGraff, *Coord. Chem. Rev.*, 2001, **211**, 317.

[125] R. D. Goldman and D. L. Spector, 'Basic Methods in Microscopy', Cold Spring Harbor Press, 2006.

[126] X. Michalet, F. F. Pinaud, S. Doose, J. L. Li, A. N. Kadanipis, T. Laurence, M. Pfulghoefft, and S. Weiss, *Annu. Rev. Biophys. Biomol. Struct.*, 2003, **23**, 161.

[127] K. Suhling, P. M. W. French, and D. Philips, *Photchem. Photobiol. Sci.*, 2005, **4**, 13.

[128] M. H. V. Werts, N. Nerambourg, D. Pelegry, Y. LeGrand, and M. Blanchard, *Photochem. Photobiol. Sci.*, 2005, **4**, 531.

[129] L.-O. Palsson, R. Pal, B. Murray, D. Parker, and A. Beeby, *Dalton Trans*, 2007, 5726.

[130] H. C. Manning, T. Goebel, R. C. Thompson, R. R. Price, H. Lee, and D. J. Bornhop, *Bioconjugate Chem.*, 2004, **15**, 1488.

[131] H. Lodish, A. Berk, P. Matsudaria, C. A. Krieger, M. P. Scott, S. L. Zipursky, and J. Darnell, 'Molecular Cell Biology, 5th Ed.' W.H. Freeman Co., 2004.

[132] *Courtesy of Veronika Boczonadi, School of Biomedical Sciences, Durham University.*

[133] B. Alberts, A. Johnson, J. Lewis, M. Ragg, K. Roberts, and P. Walter, 'Molecular Biology of the Cell', Garland Science, 2002.

[134] S. Mukherjee, R. N. Gosh, and F. R. Maxfield, *Physiol. Rev.*, 1997, 77, 759.

[135] S. J. A. Pope, R. H. Laye, *Dalton Trans.*, 2006, 3108.

CHAPTER 2

Synthetic Aspects: *Chromophore, Ligand and Complexes*

2 Synthetic Aspects: *Chromophore, Ligand and Complexes*

2.1 Outline and Direction of Work

The work described in this thesis can be divided into two major categories; ***pH probes***, and ***anion sensors***. In the pursuit of designing such molecular devices, several macrocyclic compounds have been synthesised and studied to find the best candidate for each individual purpose. Thus, in this section brief explanations will be provided, with regard to defining the key design criteria for the responsive Eu(III) probes of this thesis.

As detailed previously in *Chapter 1*, the implementation of such single-component, ratiometric luminescence analysis requires Eu(III) complexes. Embedding the Eu(III) into a kinetically inert and thermodynamically stable complex is a key feature; therefore the use of functionalized macrocyclic ligands is evident. However, one of the most important features is the incorporation of an effective sensitiser, with sufficient photophysical properties to promote Eu emission in biological applications (λ_{ex}>355 nm). As found previously by past members of the Parker group, azathioxanthones fulfill these photophysical requirements[2-4] (*detailed interpretation of these properties will presented later*). Direct binding of the chromophore to the metal centre is advantageous, ensuring sufficient energy transfer form the chromophores T_1 state to the lanthanide emissive state, and discouraging vibrational energy transfer quenching by removing energy matched OH quenching oscillators from close proximity. Therefore, almost every complex in this thesis incorporates a 2-methyl-azathioxanthone sensitiser. This chromophore possesses a methyl group in the α position to the pyridyl nitrogen, and upon incorporation into the chelating framework the pyridyl N may be positioned to allow Eu(III) coordination.

Ligands for ratiometric pH sensors were synthesized by taking into account the earlier work of Lowe.[5-7] Consequently, a series of ligands, possessing the chosen chromophore, was synthesized incorporating carboxymethyl, α-glutarate and α-adipate pendant arms in 1,7-trans position on the applied tetraazacyclododecane macrocycle (*Fig. 2.1*).

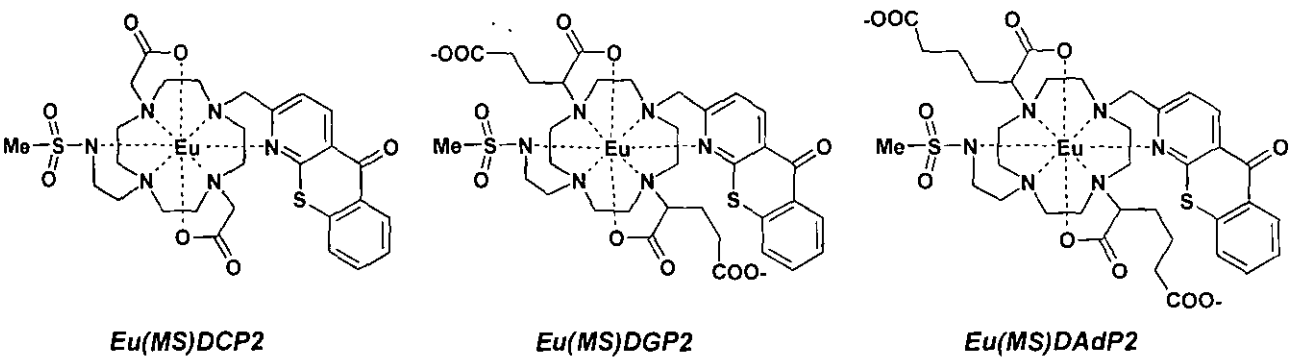

Eu(MS)DCP2 ***Eu(MS)DGP2*** ***Eu(MS)DAdP2***

Fig. 2.1. Structures of target Eu(III) complexes as pH probes incorporating carboxymethyl (***Eu(MS)DCP2***), α-glutarate (***Eu(MS)DGP2***) and α-adipate (***Eu(MS)DAdP2***) pendant arms.

Such luminescent lanthanide complexes that are able to be used for this purpose must possess a well characerised pH dependent binding moiety. Therefore, this setup leaves a nitrogen accessible on the chelating framework for the incorporation of a pH 'switch', which can coordinate to the metal center in a pH responsive manner. This reversible binding facilities ratiometric analysis by causing changes in the lifetime, and more importantly, in the fine structure of the Eu(III) emission. Considering previous attempts to make such pH-probes, this moiety was chosen to be *N*-methyl-sulfonamide group (*further justification on this choice will be provided in Chapter 3.*).[8]

As had been observed by Lowe studying Gd(III)-based pH responsive systems; complexes incorporating a carboxymethyl pendant arm were found to be sensitive towards endogenous anion binding, jeopardizing their pH mapping function in biological applications. In an attempt to overcome this problem, new ligands possessing bulky carboxylic 'side-chains' have been introduced, such as α-glutarate and α-adipate. Considering that intramolecular glutarate arm ligation may also occur in these complexes, forming a seven membered chelate competing with the desired sulfonamide binding to the Eu(III)centre,[5,6] complexes incorporating α-adipate arms were also synthesized and studied.

For ratiometric intra and extracellular anion sensing, different ligands incorporating acetamide (based on either (*S*)-alanine or (*S*)-phenyalanine) pendant arms were used (*Fig. 2.2*).

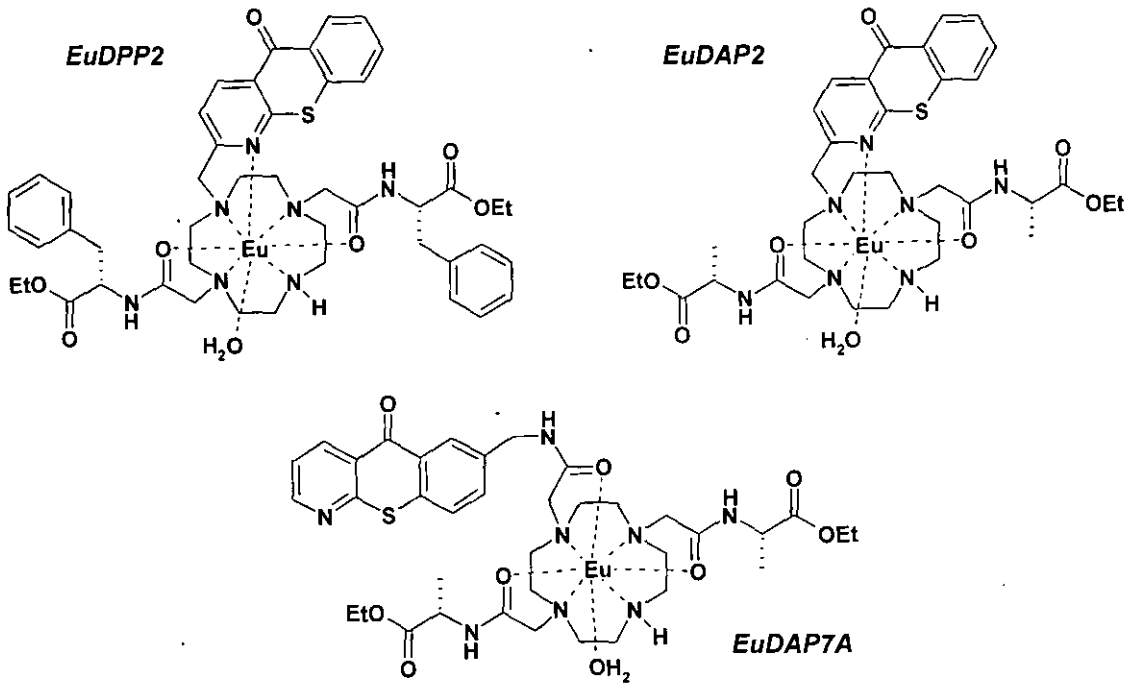

Fig. 2.2. Structures of target Eu(III) complexes as anion sensors incorporating (*S*)-phenylalanine (***EuDPP2***) and (*S*)-alanine (***EuDAP2***) pendant arms for citrate sensing; and (*S*)-alanine pendant arms (***EuDAP7A***) for carbonate sensing.

These ligands were chosen as a result of their effective binding and cellular uptake properties[9, 10]. In an attempt to gain more kinetic stability towards citrate anion binding by decreasing the overall positive charge of the 'sensor', complexes possessing the hydrolysed derivatives of the pendant arms were also prepared and studied.

2-Methyl-azathioxanthone was used as the sensitiser for citrate sensors, while this chromophore structure was modified, for the synthesis of carbonate sensors. This modification was carried out with the aim of lowering the affinity constant of the target anion,[11] as a result of enhanced steric repulsion and more effective lanthanide shielding. The aim was to 'push' the chromophore out of the lanthanide plane where it was bound *via* its pyridine nitrogen, with the predicted result of a more compact structure. This provides more flexibility for 'tighter' pendant arm binding, but preserves the sensitiser's ability of direct binding to the lanthanide centre. This was achieved by incorporating a 7-(methylcarbamoylmethyl)-azathioxanthone into the chelating framework providing the possibility of amide carbonyl oxygen ligation to the Eu(III) centre.

The synthetic aspects and photohysical properties of these Eu(III) complexes for both pH-responsive and anion-sensitive biological applications will be detailed in the following sections.

2.2 Chromophore Synthetic Scheme

Azaxanthones, previously synthesized in the Parker group[1], have been found to be efficient sensitisers for Eu(III) and Tb(III) emission. In an attempt to improve their beneficial photophysical properties even further, a modified series of compounds were considered, by exchanging the oxygen heteroatom incorporated in the bridging ring of the azaxanthone (*Fig. 2.3*). These sulfur containing azathioxanthones were postulated to possess favourable phototphysical properties as sensitizing moieties (longer λ_{ex}, lower E_T) leading to their incorporation in the complexes detailed in this thesis.

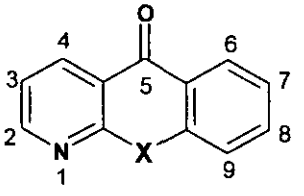

X = O → *azaxanthone*

X = S → *azathioxanthone*

Fig. 2.3. General structure of 1-azaxanthone and 1-axathioxanthone, with the numbering system used.

The azathioxanthone heterocycles were prepared by minor modifications of the existing methods[12-14], and yields for the required synthetic routes were optimized. For example, ***2-methyl-azathioxanthone***, was synthesized according to *Scheme 2.1*. 6-Methyl-2-chloronicotinic acid underwent nucleophilic aromatic substitution with thiophenol, in the presence of CuBr and K_2CO_3 to form 6-methyl-2-phenylsulfonyl nicotinic acid. The heterocyclic ring was formed by subsequent acid catalysed cyclisation in hot polyphosphoric acid. Isolation of the product was achieved by pouring the reaction mixture onto cold aqueous sodium hydroxide solution to yield the desired compound, which was purified by recrystallisation from warm ethanol. This synthetic route was then adopted for the synthesis of the 6, 7, 8 or 9- methyl-azathioxanthone chromophores from the corresponding substituted thiophenol. The final stage of the synthesis, prior to introduction of the chosen chromophore to the chelating framework, requires selective

benzylic bromination of the chromophore. This was achieved by radical bromination using NBS, benzoyl-peroxide initiator and irradiation of the reaction mixture by a 100W tungsten lamp.

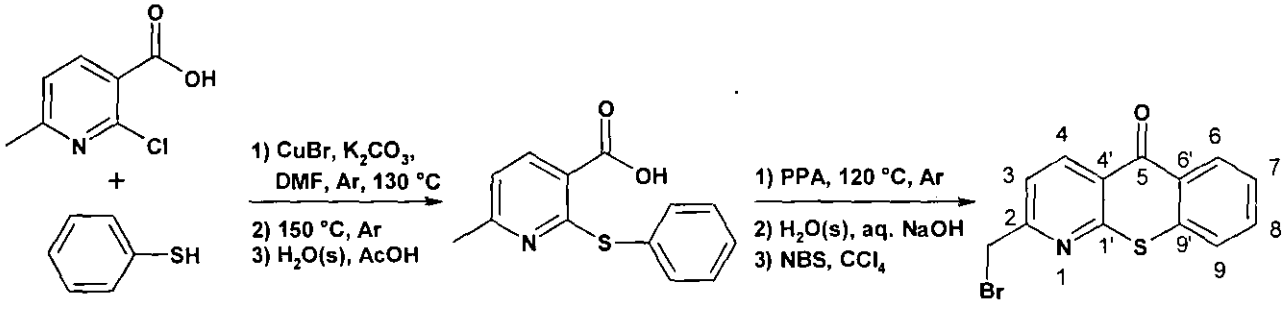

Scheme 2.1. Formation of the 2-methyl-azathioxanthone chromophore.

Having successfully synthesised and characterised the synthesized n-methyl-azathioxanthones (*Fig. 2.4*), their photophysical properties were full examined in order to understand the variation of key spectroscopic changes (*e.g.* λ_{ex}, λ_{em}, T_1) as a consequence of structural modifications.

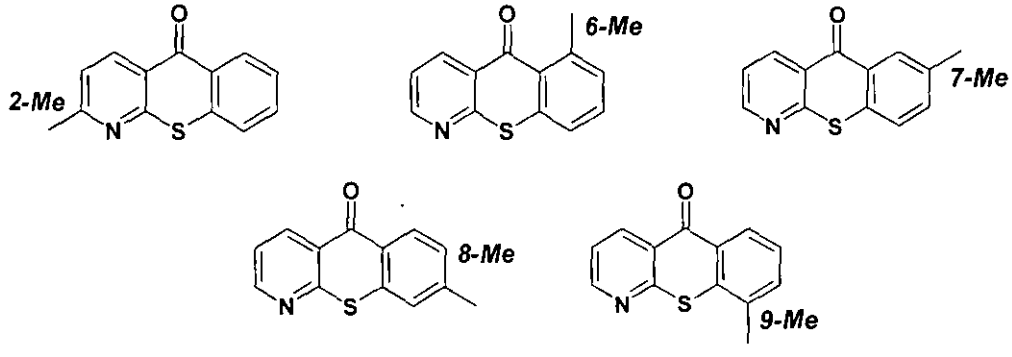

Fig. 2.4. Structures of the n-methyl-azaxanthones.

Consequently, two basic n-methyl-azathixanthone skeletons were chosen from the synthesized azathioxanthones as a result of their sufficient structural and photophysical properties. In case of the pH probes and citrate sensors direct binding of the chromophore to the metal centre was an essential feature. Therefore, the ***2-Me*** derivative was the perfect candidate to promote Eu(III) emission, as a result of its ligation *via* pyridyl nitrogen.

As discussed above, for carbonate sensors, the ***7-Me*** derivative was used as the donor sensitiser, converting its methyl group to methylcarbamoylmethyl, which still ensures ligation to the lanthanide center via the amide carbonyl group. Moreover, by the introduction of this group the chromophore sits outside of the plane providing more space for pendant arm binding without significant changes in the photophysical properties.

Several methods were considered in the attempt to prepare the target ***7-(methylcarbamoylmethyl)-azathioxanthone*** chromophore (*Scheme 2.2*)

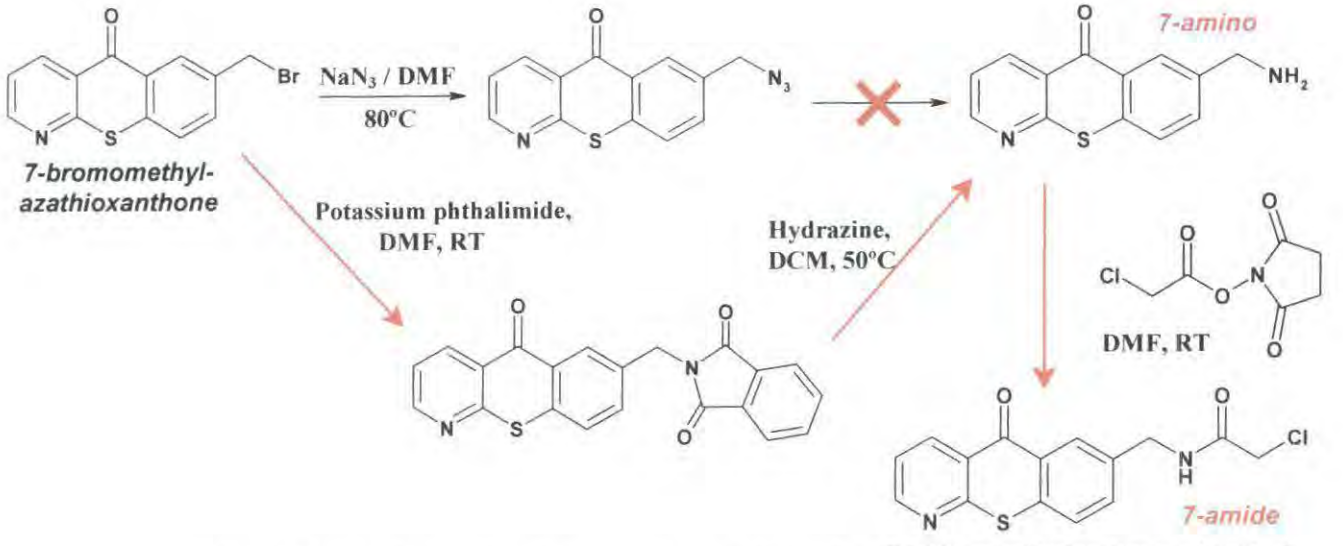

Scheme 2.2. Synthesis and applied synthetic routes for the 7-aminomethyl-azathioxanthone (***7-amino***) and 7-(chlormethyl-carbamoylmethyl)-azathioxanthone (***7-amide***) chromophore.

An initial attempt used the Staudinger reaction[15] (*Scheme 2.2. 'black'*), which is a very mild azide reduction[16], as there are a wide variety of methods for preparing azides. This reaction makes it possible to use the azido group as an $-NH_2$ precursor via the synthetic route where the reagent triphenylphosphine reacts with the applied azide to generate a phosphazide, which loses N_2 to form an iminophosphorane. Aqueous work up leads to the amine and triphenyl-phosphine oxide. The 7-azidomethyl-azathioxanthone was prepared from 7-bromomethyl-azathioxanthone using nucleophilic sutbstitution with NaN_3. However, several attempts to promote conversion to the target amine failed; in each case analysis (^{1}H-NMR, ESMS) of the crude reaction mixture showed evidence of disintegration of the heterocyclic ring. It is essential to note that the precursor 7-

bromomethyl-azathioxanthone and the 7-azidomethyl-azathioxanthone product shared identical spectroscopic values in ^{1}H-NMR and in TLC chromatography. The presence of a well defined absorption band in IR-spectroscopy at 2,100 cm^{-1} consistent with the azide group and a 20 ppm shift of the methylene carbon signal in ^{13}C-NMR allowed their identification.

An alternative route[17] (*Scheme 2.2. 'red'*) was implemented to synthesise the target ***7-amino*** derivative from 7-bromomethyl-azathioxanthone. This involved the intermediacy of a 7-phthalimidomethyl-azathioxanthone, prepared using potassium phthalimide, followed by demasking of the amine using hydrazine hydrate and subsequent addition of conc. HCl allowing the product to be cleanly obtained as its hydrochloride salt. The desired 7-(chloromethylcarbamoylmethyl)-azathioxanthone chromophore was then prepared by further reaction with the freshly synthesised N-hydroxysuccinimidyl ester of chloroacetic acid.

2.3 Chromophore Photophysical Data

2.3.1 Absorption Properties

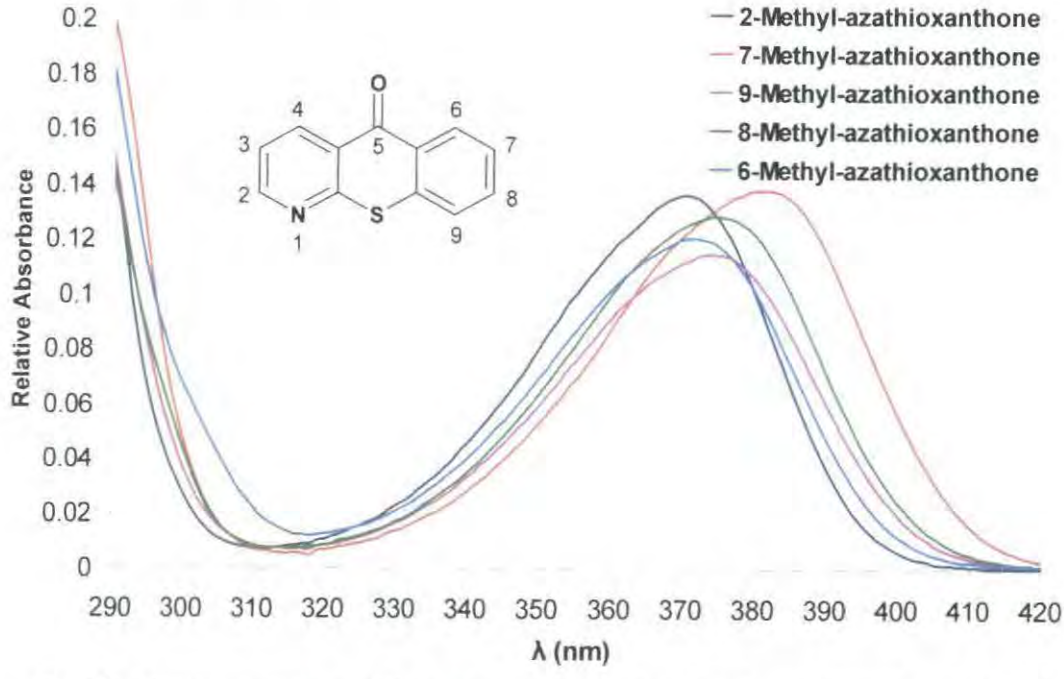

Fig. 2.5. Absorption spectrum of the synthesized methyl-azathioxanthone chromophores (MeOH, 295 K).

Having first prepared the chromophores, it was essential that their photophysical properties were thoroughly examined before further synthesis and examination of the lanthanide complexes that incorporate such sensitizing moieties could begin. The UV absorption spectra were recorded in a protic solvent (MeOH) for each of the methyl-substituted chromophores (*Fig. 2.5*). Absorption bands were observed at $\lambda_{abs.}$ 371 nm (6,770 $dm^3mol^{-1}cm^{-1}$) for ***2-Me***, 381 nm (5,350 $dm^3mol^{-1}cm^{-1}$) for ***6-Me***, 374 nm (5,760 $dm^3mol^{-1}cm^{-1}$) for ***9-Me***, 375 nm (5,450 $dm^3mol^{-1}cm^{-1}$) for ***8-Me*** and 372 nm (5,790 $dm^3mol^{-1}cm^{-1}$) for the ***7-Me*** derivative respectively.

In accordance with these values changing the position of the methyl group around the original 2-methyl-azathioxanthone structure results in small bathochromic shifts in the absorption spectra with the biggest red shift of 10 nm in case of the 6-methyl-azathioxanthone. This increase in the singlet state energy could be attributed to a weak hyperconjugative interaction of the electron donating methyl group with respect to the carbonyl group. Moreover, when studying the fluorescence properties of this derivative (***6-Me***), only very weak fluorescence was observed. This is due to vibrational deactivation of the $n\pi^*$ singlet state by the proximate methyl C-H oscillators, *i.e. via* an intermolecular C-H···O interaction.

Information on the characteristics of the singlet state of a given chromophore can be gained by examining the polarity dependence of the $n\pi^*$ singlet state. By recording the absorption spectra of the chromophore as a function of the polarity of the medium, a well defined increasing blue shift of the absorption maximum may occur as a function of solvent polarity. Such behaviour has been reported previously by Scaiano and co-workers, studying the photophysical changes of the 1-azaxanthone chromophore as a function of the solvent polarity.[18,19] However, the absorption spectrum of the 2-methyl-azathioxanthone (***2-Me***) exhibited a small red shift upon increasing solvent polarity, shifting from 368 nm (MeCN) to 371 nm and 372 nm in MeOH and H_2O respectively. Such behaviour is consistent with an increasing contribution from low-lying $\pi\pi^*$ states to the lowest energy transition that has predominantly $n\pi^*$ character. The extinction coefficient of the 372 nm band of the 2-methyl derivative in MeOH was measured in the presence of increasing amounts of water, and decreased from 6,770 cm^{-1} in pure MeOH to approaching a limiting value of 4,070 cm^{-1} in 40% water-methanol, as a result of the

reduction in the oscillator strength of the transition associated with polarity dependent change in the characteristics of the singlet state.

As expected, further alterations in the structure of the ***7-Me*** derivative (λ_{abs} = 372 nm, ε = 5,790 $dm^3mol^{-1}cm^{-1}$) to achieve the target ***7-amide*** chromophore did not result in significant changes of the absorption properties with $\lambda_{abs.}$ values of 376 nm and 380 nm for the ***7-amino*** and ***7-amide*** analogues respectively. The molar extinction coefficient values were also increased to 7,980 $dm^3mol^{-1}cm^{-1}$ and 10,730 $dm^3mol^{-1}cm^{-1}$ for the ***7-amine*** and ***7-amide*** analogues respectively (in MeOH). In accordance with these observation, the introduction of an electron withdrawing methyl-ester group in 7-position to the azathioxanthone resulted in a hypsochromic shift in the absorption maximum (369 nm) and a slight decrease in the molar extinction coefficient (5,360 $dm^3mol^{-1}cm^{-1}$)[1].

2.3.2 Singlet and Triplet Energy Measurements

As described previously (*Section 1.2*) efficient sensitized emsission requires a high quantum yield, which is achievable by suppressing non-radiative deactivating processes. Ideally, chromophores should possess both a fast rate of intersystem crossing and energy transfer to the lanthanide emissive state, with minimal quenching of this state. The relatively high molar extinction coefficient values of the azathioxanthone chromophores, especially the amine and amide derivatives indicate that they absorb light efficiently, enhancing the population of the singlet excited state of the sensitiser. A further requirement for fast ISC to the desired triplet excited state is that radiative fluorescence from this excited singlet state back to the ground state should be negligible.

Emission spectra were recorded for each azathioxanthone chromophore and were observed within the region 425-440 nm. The observed variation λ_{em} values mirrored changes found in their absorption maximum values, as a function of the nature and position of substituent on the benzenoid ring system. Each chromophore exhibited a relatively weak and broad fluorescence emission at room temperature.

Chromophore	λ_{max} (nm)[a]	ε ($dm^3mol^{-1}cm^{-1}$)[b]	λ_{em} (nm)[c]	E_T (cm^{-1})[d]
2-Me 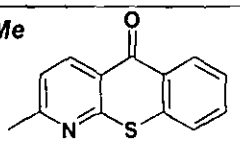	371	6,770	425 (3.3)	22,600
6-Me 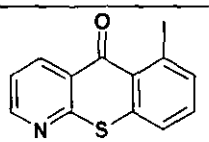	381	5,350	(440) very weak	22,400
7-Me 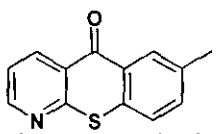	372	5,790	428 (3.6)	21,700
8-Me 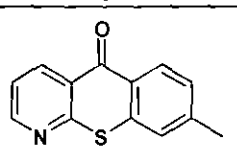	375	5,450	437 (1.0)	22,400
9-Me 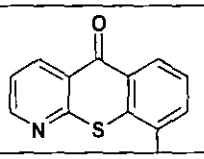	374	5,760	437 (5.1)	22,500
7-ester[1] 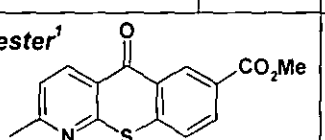	369	5,360	423 (2.8)	22,700
7-amine 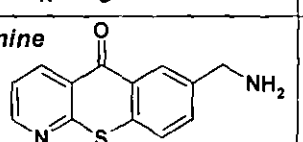	376	7,980	430 (1.7)	22,200
7-amide 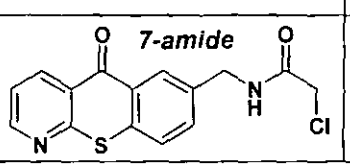	380	10,730	436 (2.3)	20,500.

a) in MeOH at RT; b) in MeOH at RT, the errors associated with these values is ± 2%; c) values in brackets the approximate relative signal intensity compared to the signal intensity of the 2-methyl-azaxanthone at 405 nm[1]; d) in EPA at 77 K (*Fig. 2.6*) the error associated with these values is ± 50 cm^{-1}

Table 2.1. Photophysical data from a range of azathioxanthone based chromophores.

The solvent dependence of the weak fluorescence emission of 2-methyl-azathioxanthone was studied to help probe the character of the singlet excited state. The emission band observed at room temperature shifted to the blue (hypsochromic shift) and become even less intense in solvents of lower polarity. Indeed, the emission band was not

observed in DCM, EtOAc, THF and toluene. Such behaviour may be related to an enhancement of the $\pi\pi^*$ character of the singlet excited state in more polar media, consequently depopulating the singlet excited state. This observation suggests that the rate constant of fluorescence is increasing with respect to the rate constant of the desired ISC step as a function of increasing solvent polarity. This undesirable photophysical property could sabotage high quantum yield lanthanide emission using this sensitizing moiety for examining biological systems.

The phosphorescence properties of the sensitizing group were measured at 77 K in an 'EPA' (Et_2O-isopropane-EtOH) frozen glass. Such experiments not only provide valuable information regarding the chromophores' triplet state energy level, but also helps distinguishing the character of this state. More importantly, they give an indication whether the studied chromophore is suitable to promote Eu(III) and Tb(III) sensitized emission.

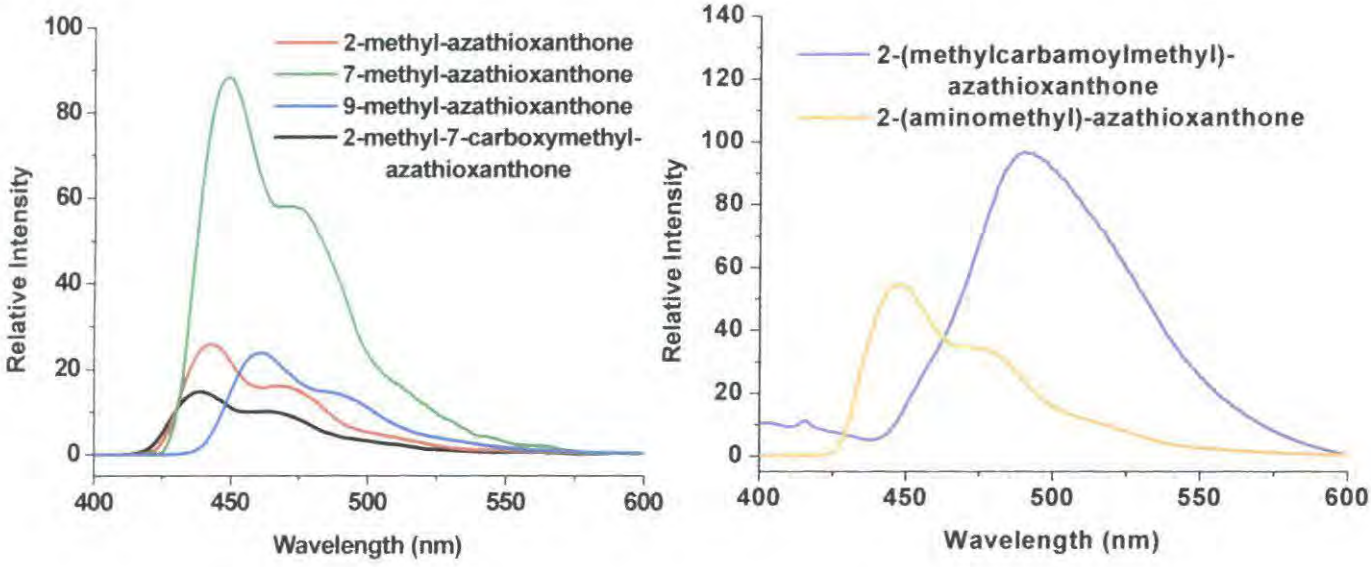

Fig. 2.6. Phosphoresence emission spectra for synthesized azathioxanthone derviatives (EPA glass, 77 K).

It is well know that aryl ketones are effective triplet sensitisers in organic photochemistry. Low temperature phosphorescence emission was strong in every case examined. The highest energy vibrational band in each spectrum (*Fig. 2.6*) belongs to the 0,0 ($T_{1,\ v=0}$) → ($S_{0,\ v=0}$) transition manifold, which corresponds to the triplet energy of the

chromophore. Triplet energy values were calculated from the maximum intensity of this band. Values were found to be 22,600 cm^{-1} (443 nm) for the ***2-Me***, 22,200 cm^{-1} (449 nm) for the ***7-Me***, 22,200 cm^{-1} (450 nm) for the ***7-amino*** and 20,500 cm^{-1} (490 nm) for the ***7-amide*** dervatves. The triplet energy levels of each azathioxanthone derivative were proven to be sufficiently high to promote Eu(III) emission, but were not uniformly high enough for Tb(III) sensitization at ambient temperature. For the ***7-amide*** derivative **a** structureless phosphorescence spectrum was recorded, resembling a more $\pi\pi^*$ character with high relative intensity and a significantly lower triplet energy level. This behaviour is consistent with some degree of mixing of the $n\pi^*$ states of the 2 carbonyl groups in this chromophore. For the other examples, fine structure in the phosphorescence spectra was observed, clearly with each spectrum exhibiting three less intense bands separated by about 1,650 cm^{-1}. This behaviour is typical of carbonyl vibrational fine structure, and is consistent with the dominant $n\pi^*$ character of the triplet states.[1] Although the distinctiveness of these bands is not as clear as found previously with some azaxanthones[1], the triplet state is predominantly $n\pi^*$ in character; any $\pi\pi^*$ contribution is likely to be favoured by the increasing polarity of the solvent.

This behaviour may be contrasted with the behaviour for the 8-amino-azaxanthone[1]. Where the lowest energy absorption band (356 nm) was more intense than the higher energy shoulder (330 nm), the triplet energy lowered with comparison to the methyl derivative with no distinct vibrational fine structure and there was also a 500-fold increase in relative fluorescence emission intensity observed at room temperature. Taken together such behaviour is consistent with conjugation of the exocyclic N lone pair, lowering the energy of the LUMO, accompanied by a switch to predominant $\pi\pi^*$ character in the singlet and triplet excited states. The above stated 356 nm and 330 nm bands presumably correspond to transitions with dominant $n\pi^*$ and $\pi\pi^*$ character. For the ***7-amino*** and ***7-amide*** this undesirable photophysical property has been eliminated with the introduction of a methyl bridging group between the hetaroaromatic ring and the nitrogen atom in the aryl moiety; therefore there is negligible conjugation between them.

2.3.3 Summary and Comparison of Photophysical Properties

Exchanging the heteroatom in the bridging ring containing the carbonyl group, caused a bathochromic shift in the absorption maximum due to the decreased electronegativity of the heteroatom, resulting in more subtle variations in singlet and triplet energies. As a result of this, all azathioxanthone absorption wavelengths are sufficiently high (>355 nm) to allow their application as an antenna group in biological media. Alkyl substitution in the 6-position produced the most significant bathochromic shift in the absorption spectrum, with a parallel increase in the fluorescence emission wavelength (very weak at 440 nm). Compared to the 2-methyl derivative, moving the methyl group around the benzenoid ring to the 7, 8 or 9-position did not perturb the observed singlet and triplet energies significantly, nor did it affect the observed emission band intensities. Modifying the structure of the ***7-Me*** derivative by attaching an amine group onto the alkyl moiety, did not perturb the photophysical properties significantly. However, conversion of this group to an amide resulted in an unexpected further decrease in the triplet energy level. In contrast with the azaxanthones, the singlet-triplet energy gap is smaller, and typically was of the order of 3,500 cm^{-1}, which should ensure a faster rate of ISC; T_1 energies examined were typically close to 23,500 cm^{-1} (±500 cm^{-1}) and dominantly $n\pi^*$ in character, with an increasing $\pi\pi^*$ contribution as a function of solvent polarity. This energy is well suited for Eu(III) ($^5D_0$ lies at 17,200 cm^{-1})sensitization, but is at the practicable limit for Tb(III) ($^5D_4$ lies at 20,400 cm^{-1}), at least for room temperature applications.

2.4 Ligand and Complex Synthetic Scheme

In the search for new potential chromophores, it was envisaged that both 2-methyl and 7-(methylcarbamoylmethyl)-azathioxanthones would bind lanthanide ions via pyridyl nitrogen and amide carbonyl oxygen atoms in a monodentate fashion. This not only ensures fixed minimized metal–ligand distance for efficient energy transfer, but also contributes towards quantum yield increase as a result of decreasing the number of water molecules in the inner-sphere. To ensure this desired binding each chromophore had to be prepared as an α-bromomethyl or N-chloromethyl analogue; 2-methyl-azathioxanthone

may undergo selective radical α-monobromination, while premeditated synthesis of 7-(chloromethyl-carbonylmethyl)-azathoixanthone had been carried out in the amide conversion step.

Having synthesized these new and promising azathioxanthone chromophores for Eu(III) sensitization, the synthesized complexes incorporating these antenna groups can be divided into two major categories with regard to the nature of their pendant arms attached to the chelating framework, possessing either *carboxyate* or *amide* pendant arms.

This section is focused purely on the synthetic aspects highlighting important observations towards any similar synthesis being carried out in the future; detailed synthetic procedures are given in *Chapter 6.* To help understanding the abbreviations used for each complex, a detailed explanation, using Eu(MS)DCP2 as a model compound can be seen below (*Fig. 2.7*)

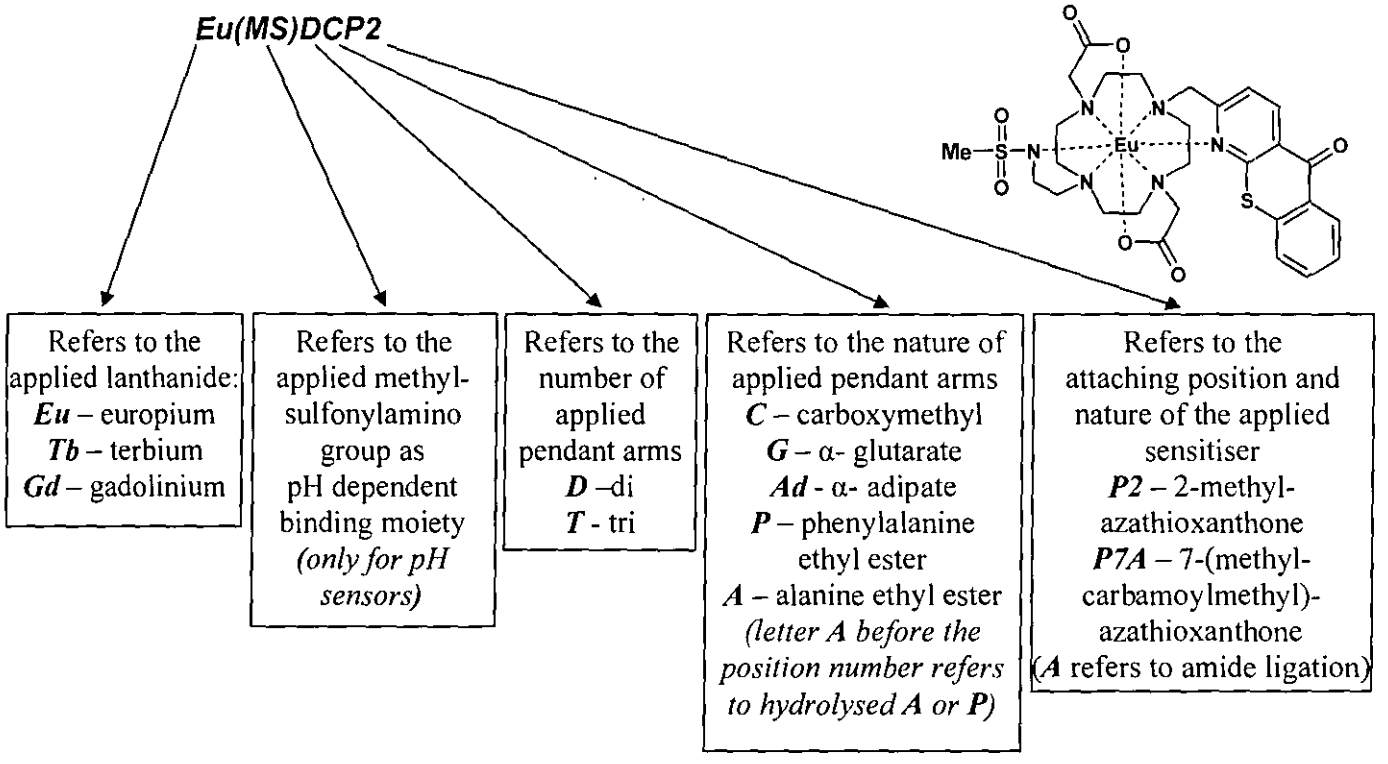

Fig. 2.7. Explanation of used complex abbreviations, using Eu(MS)DCP2 as model complex.

2.4.1 Complexes Incorporating Carboxylic Pendant Arms

In seeking a suitable Eu(III) complex for measuring intracellular pH, several macrocyclic ligands were synthesised incorporating carboxylate pendant arms (*Fig.2.8&9*).

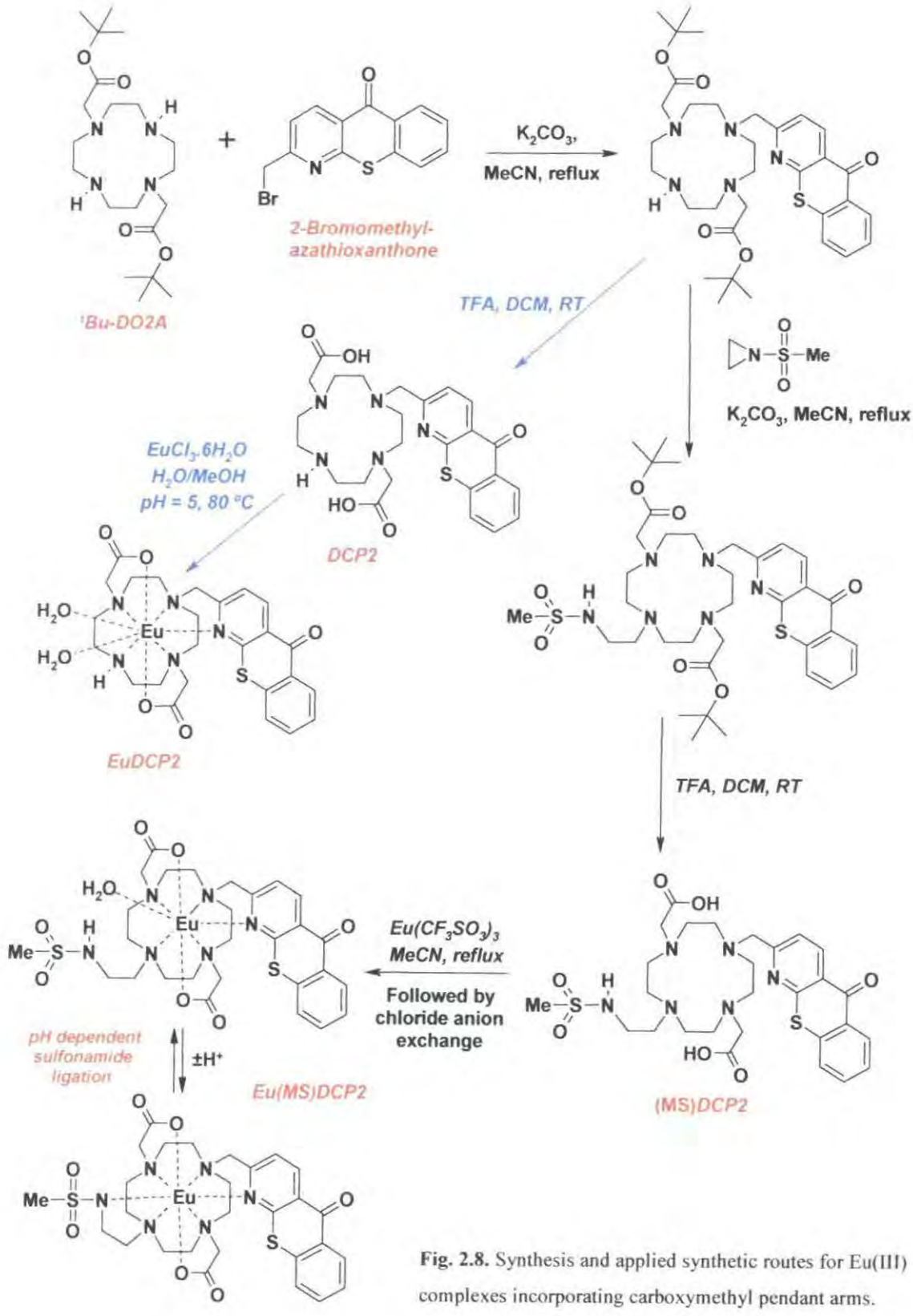

Fig. 2.8. Synthesis and applied synthetic routes for Eu(III) complexes incorporating carboxymethyl pendant arms.

These ligands were prepared from tetraazacyclododecane by selective protection of two non-adjacent nitrogens (using CBZ protection) of the macrocycle, followed by reaction with the appropriate halocarboxylate ester of the pendant arm in the presence of K_2CO_3 in hot acetonitrile. After deprotection of the macrocycle, the addition of the chosen sensitiser moiety, as 2-bromomethyl-azathioxanthone was undertaken. It is important to note here that this alkylation step always requires column chromatography purification, as a result of undesired di-alkylation. Although this purification step could not be eliminated, the ratio of the desired ligand to byproduct ratio was increased by using the more weakly basic $NaHCO_3$ at a lower reaction temperature (70 °C). The next step, in almost every case where carboxylic pendant arm bearing ligands have been synthesized, was the introduction of the chosen pH dependent binding moiety ('pH switch'). This important part of the ligand was chosen to be an N-methyl-sulfonylamino-ethyl group as a result of its suitable properties for this role (*further justification of this choice can be found in Chapter 3.*). The preparation of this tetra substituted tetrazacyclododecane took advantage of the ring opening reaction of N-methanesulfonyl-aziridine with secondary amines.[20] The final step prior to metal complexation involved deprotection of the ester groups in the pendant arm. The complexation reaction was examined using various europium salts, but in terms of water solubility and a choice of an appropriate counterion, reaction using $Eu(OAc)_3$ proved to be the most successful.

Three ligands were synthesized in the aim of selecting the be st candidate to function as a responsive Eu(III) complex for measuring intracellular pH. Complexes incorporating carboxymethyl-, α-glutarate- and α-adipate groups were synthesized.

The first ligand to be synthesised from this 'family' was DCP2 incorporating carboxymethyl pendant arms (*Fig. 2.8*); from this the ligand (MS)DCP2 was prepared by introducing the pH dependent binding moiety. Each ligand was used immediately in complexation reactions to yield ***EuDCP2*** and ***Eu(MS)DCP2*** respectively. Thorough examination of these complexes highlighted some major issues regarding their application in biological media. The complex EuDCP2 was synthesized to compare its behaviour and luminescence propeties to Eu(MS)DCP2 thereby understanding the role, advantage and nature of the pH dependent sulfonamide ligation. Very weak europium emission was observed for the former compound in aqueous media, as a result of

vibrational quenching by ligand NH, and the OH oscillators of bound water molecules. When the complex was introduced to a solution containing millimolar concentrations of biologically common anions, such as carbonate, lactate and citrate ligand exchange reactions took place. This led to complex dissociation and therefore quenched the desired sensitized lanthanide emission.

The instablility of EuDCP2 towards trans-complexation by anions meant that further investigation of this compound was terminated and attention turned towards Eu(MS)DCP2 bearing the pH dependent binding moiety.

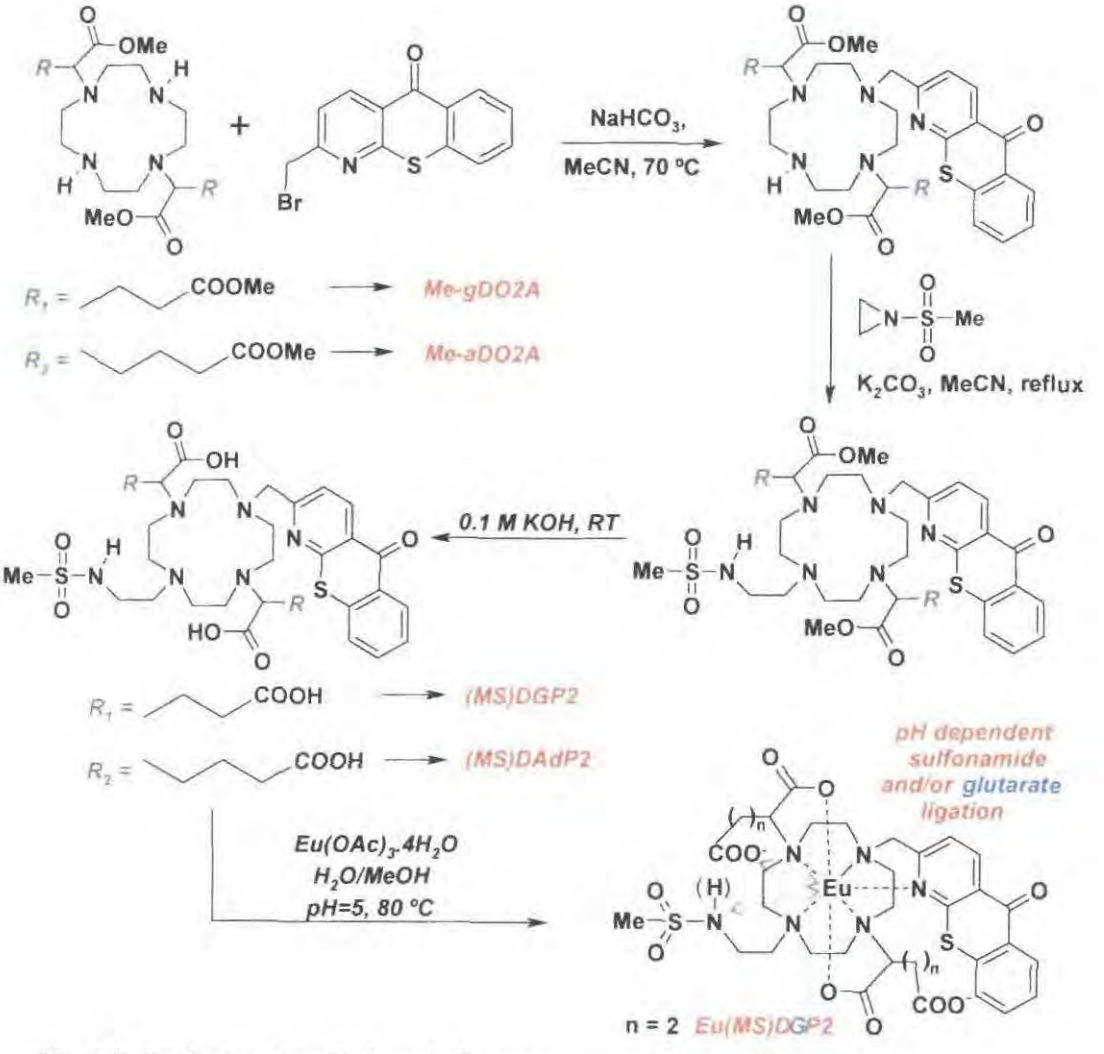

Fig. 2.9. Synthesis and applied synthetic routes for Eu(III) complexes incorporating α-glutarate or α-adipate pendant arms.

The next complexes synthesized possessed α-glutaric (***Eu(MS)DGP2***) or α-adipic (***Eu(MS)DAdP2***) acid pendant arms (*Fig. 2.9*). In the former case, as found previously[5-7], intramolecular glutarate arm ligation occurred, forming a seven membered chelate competing with sulfonamide binding to the Eu centre. However, this competitive binding mode proved to be advantageous in the subsequent design of citrate sensors (*Chapter 5.*). The synthesis of this complex (***EuDGP2***) was carried out, with the exclusion of the pH switch attaching step, following the synthetic route detailed above. For the pH sensor work this undesired intramolecular ligation mode needed to be suppressed by exchanging the pendant arms to α-adipate groups. With the introduction of a methylene spacer into the side arms intramolecular carboxylate binding is disfavoured, as a consequence of the instability of an 8-ring chelate. Each complex synthesized was confirmed for homogenety by HPLC chromatography, while HRMS and ^{1}H NMR were used for structural identification (for values see *Chapter 6.*). Proton NMR spectra of the complexes were found to be exchange broadened in aqueous solvents over the observed 200-700 MHz frequency régime. Detailed information on pH-probe related measurements and their interpretation follows in *Chapter 3.*

2.4.1.1 Complex Data

Having successfully synthesized the target complexes, it was necessary to study their photophysical properties. This study allows to a number of conclusions to be drawn, which may direct the path of any further investigation. These measurements, such as overall emission lifetime and quantum yield determination (*Table 2.2*) were carried out in aqueous (deuterated where applicable) media, in order to determine the effectiveness of sensitized emission and the inner sphere hydration number. Incorporation of the chosen 2-methyl-azathioxanthone chromophore into the target Eu-complex significantly altered its photophysical properties. Irrespective of the nature of the chelating framework, a bathochromic (red) shift was observed both in absorption (380 nm) and emission (440 nm) maximum. As a result of the heavy metal effect, a noticable increase was observed in the molar extinction coefficient, from 4,070 cm^{-1} to 5,130 cm^{-1} (in H_2O for Eu(MS)DAdP2), whilst a 200 cm^{-1} increase in the triplet energy (22,800 cm^{-1} for GdDPP2) was also measured upon pyridine nitrogen ligation to the metal centre.

Luminescence titrations were carried out with each complex incorporating a pH dependent binding moiety in order to determine the apparent protonation constant (pK_a) (detailed information in *Section 3.2*). These measurements provide vital information regarding the limiting structures of the studied Eu-complex, signaling whether in the given pH region the sulfonamide group is bound or unbound to the metal centre. For both Eu(MS)DCP2 and Eu(MS)DAdP2, the pK_a fell in the range 6.1 - 6.2. Behaviour at pH 4.5 and pH 8 was therefore assessed. For Eu(MS)DGP2, as a result of competitive glutarate binding, the sulfonamide binding constant shifted to 7.6. Three pH régimes therefore were considered; pH = 3 for the aqua bound species, pH = 5.5 for the glutarate bound species, and pH = 8 for the sulfonamide nitrogen bound species. Measuring the radiative lifetimes in water and deuterium oxide, using these specified pH values[21], the inner sphere hydration value (q) may be calculated[22] for each individual species. Quantum yield determinations were carried out for each Eu complexes with the same speciation and pH values in mind.

Complex	pH[a]	k_{H2O}	k_{D2O}	Δk_{corr}[b]	q'_{corr}[c]	Φ_{Eu}[d]
EuDCP2	6.0	4.15[g]	0.81	3.02[g]	2[f]	—[e]
Eu(MS)DCP2	4.5	2.08	1.32	0.51	1	0.9 %
Eu(MS)DCP2	8.0	2.43	2.10	0.08	0	1 %
EuDGP2	*3.0*	*3.45*	*1.59*	*1.85*	*2*[f]	*1.2 %*
EuDGP2	*7.5*	*2.97*	*1.58*	*1.28*	*1*[f]	*1.2 %*
Eu(MS)DGP2	3.0	1.70	0.92	0.53	1	1.7 %
Eu(MS)DGP2	5.5	1.41	1.00	0.16	0	2 %
Eu(MS)DGP2	8.0	2.13	1.87	0.01	0	1.8 %
Eu(MS)DAdP2	4.5	1.36	1.21	0	0	6.1 %
Eu(MS)DAdP2	8.0	2.38	2.12	0.02	0	5.4 %

[a] ΔpH = ±0.1 [b] For the Eu complexes a correction to Δk of 0.25 ms^{-1} has been applied for the outer sphere water contribution. [c] The values of q'_{corr} have been obtained by multiplying Δk_{corr} by 1.2 (are corrected to ±0.5). [d] Quantum yield measurements were carried out in H_2O. [e] Very weak Eu emission was detected as

described previously. [f] Analysis was made with the assumption of fast NH → ND exchange in D_2O, and $\Delta k'$ of 0.07 ms^{-1} has been applied for every exchangeable NH oscillator. [g] Low lifetime value may be attributed to pO_2 sensitivity of the chrmophores T_1 state or high outer sphere OH contribution.

Table 2.2. Quantum yields and rate constants (ms^{-1}) for depopulation of the excited states in H_2O and D_2O for each individually coordinated Eu species (293K).

The above summarised values confirm the importance of direct sensitiser binding, making sensitization more efficient. The incorporation of the pH switch sterically shields the Eu centre even further, increasing the radiative lifetime values, replacing the local water molecule(s) and causing significant changes in the Eu emission spectra (*Fig. 2.10*).

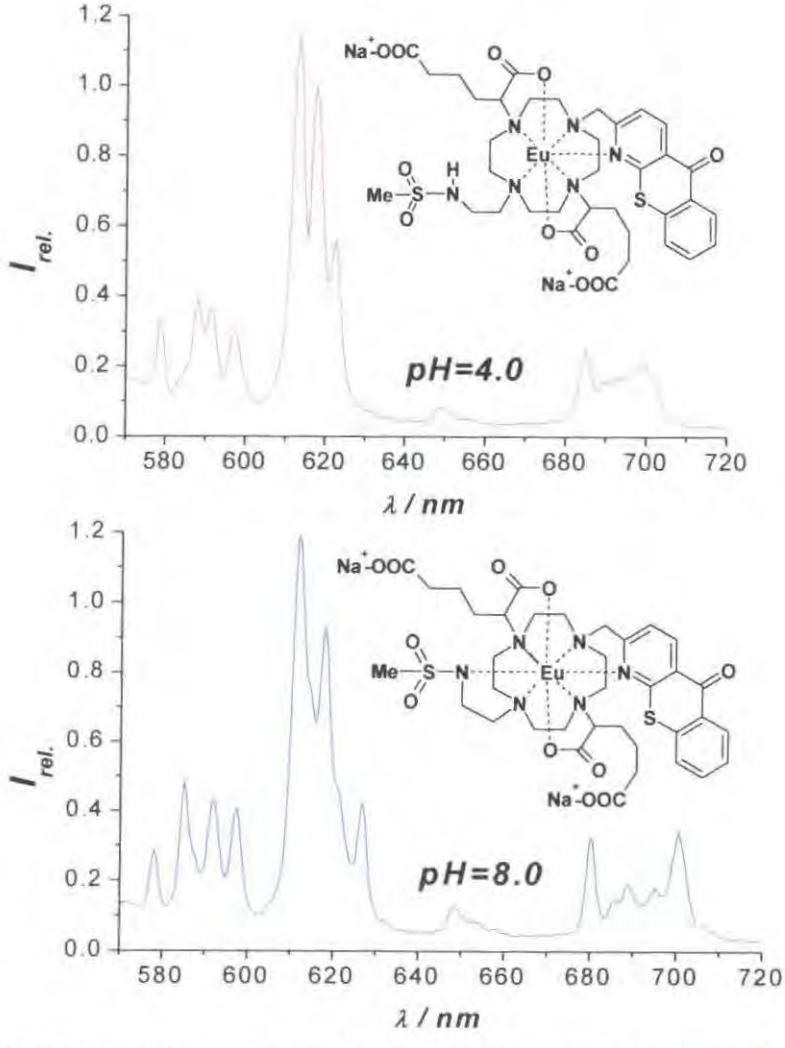

Fig. 2.10. Eu(III) emission spectrum for ***Eu(MS)DAdP2*** in water at pH 4 and 8 highlighting the structural changes upon pH dependent sulfonamide nitrogen ligation ([complex] = 20 μM, 295 K, I = 0.1 M NaCl, *details on structural changes in Section 3.2.3*).

Another important observation was that by changing the nature of the pendant arm a significant increase was observed in the quantum yield. This advantageous change may be attributed to an increase in the steric bulk around the Eu complex, resulting in more effective shielding of the lanthanide centre. Surprisingly, when calculating the *q*-values for Eu(MS)DAdP2, no water was found to be present in the inner sphere regardless of the ligation of the sulfonamide moiety. This interesting observation may be a consequence of the 'wrapping effect' of the pendant adipate arm. Such a premise is consistent with the 0.1 unit increase in the pK_a of the sulfonamide group. The lower quantum yield value of the sulfonamide bound species may be attributed to distortion in the packed 'adipate-wrapped' geometry by intramolecular sulfonamide ligation, exposing the emissive Eu(III) state to outer sphere OH quenching.

2.4.2 Complexes Incorporating Amide Pendant Arms

The second major group of ligands synthesised incorporated amide pendant arms. These complexes have been synthesized in an attempt to measure intracellular carbonate (*Chapter 4.*) and intra/extracellular citrate (*Chapter 5.*) concentrations using ratiometric Eu emission analysis. The choice of pendant arms may also determine the uptake and localization profile inside a living cell, as detailed in previous publications,[3, 9, 10, 23, 24] along with their effect on anion binding and the shielding of the lanthanide centre. In order to understand the differences provided by the nature and charge of the pendant arms a series of complexes was synthesized, based on alanine and phenylalanine chelators (*Fig. 2.11*). Complexes based on phenylalanine pendant arms were synthesized in a hope that the overall bulkiness provided by the introduction of the phenyl group might also suppress the binding affinity of some hydrophilic endogenous anions.

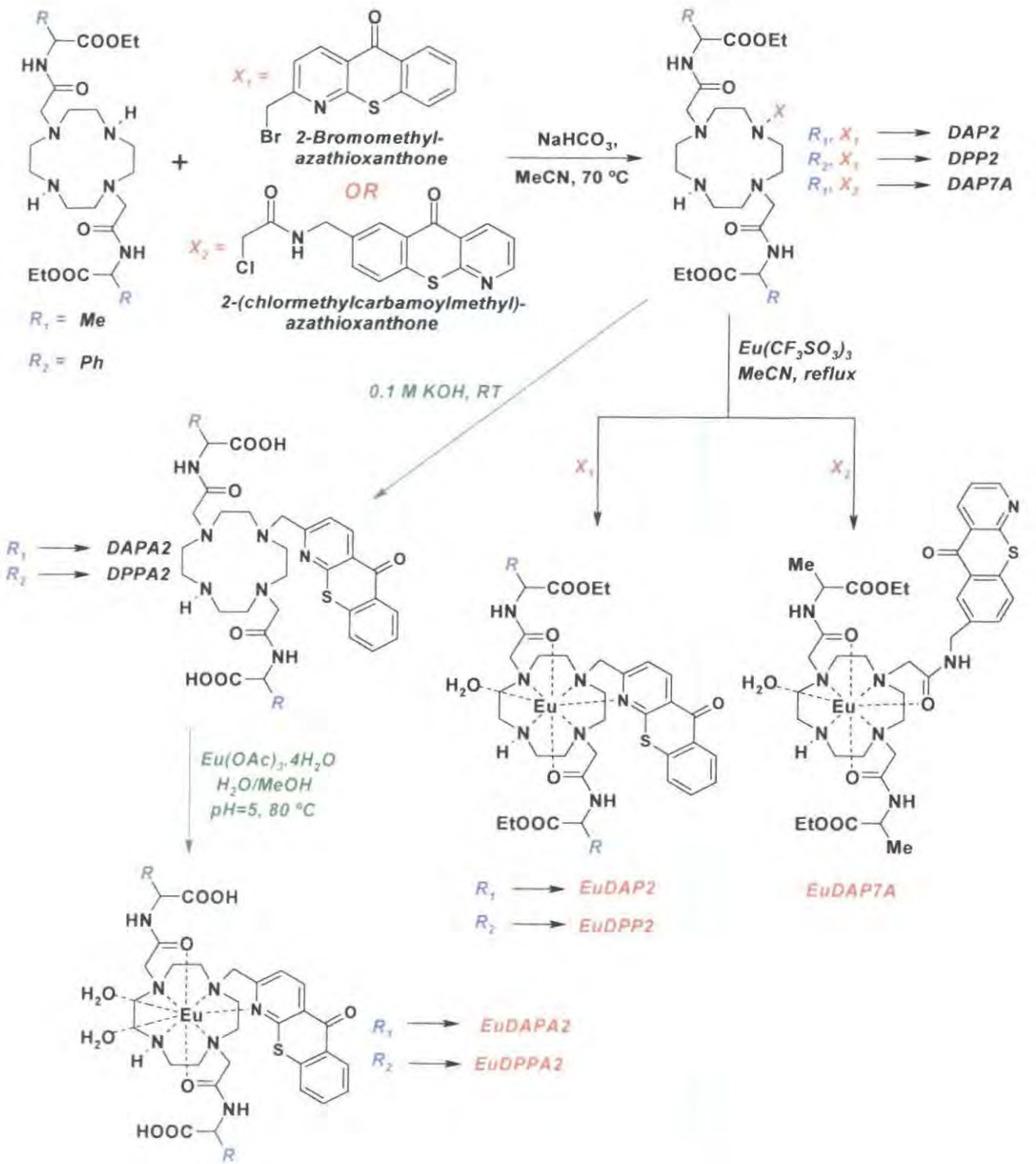

Fig. 2.11. Synthesis and applied synthetic procedures for Eu(III) complexes incorporating amide pendant arms.

The N-bromoethanoyl-(*S*)-alanine and (*S*)-phenylalanine precursors, were reacted with 1,7-diCBZ-tetraazacyclododecane in acetonitrile followed by hydrogenolysis ($Pd(OH)_2$/(C)/EtOH). The chosen sensitizing moiety for the series of sensors was 2-methyl-azathioxanthone, or 2-(methylcarbamoylmethyl)-azathioxanthone. Each sensitizing moiety was added to the chelating framework, using the improved alkylation conditions with $NaHCO_3$ as the base, in hot acetonitrile.

Complexation reactions were undertaken using the appropriate ligand, with the lanthanide added as the anhydrous triflate salt. In the case of ligands incorporating alanine pendant arms, the good water solubility of the final complex possessing triflate as counterion obviated the time consuming anion exchange process. For complexes with more hydrophobic phenylalanine arms the triflate anion, e.g on ***EuDPP2***$^{2-4}$ was subsequently replaced by chloride using anion exchange chromatography to enhance water solublility.

In an attempt to gain more kinetic stability towards endogenous anion binding, and to allow a study of the effect of complex charge on cellular localization and uptake, complexes with less overall positive charge were also synthesized. This was effected by hydrolysis of the ester groups in the pendant arms using KOD in D_2O, monitoring the reaction by ^1H NMR. The europium(III) ion was introduced as its acetate salt led to good yield and good complex solubility in water. It is important to note that the synthesis of analogous Gd(III) complexes was also undertaken by following the synthetic procedure of the Eu analogue. Proof of complexation and purity were observed by the previously mentioned methods (*Fig. 2.12*).

Having successfully synthesized these europium complexes, a wide range of experiments, with regard to their purpose of design has been carried out, which will be detailed in full extent in the individual chapter dedicated to their study as anion sensors. (*EuDAP7A as carbonate sensor (Chapter 4.) and EuDAP2, EuDPP2, EuDAPA2, EuDPPA2 as citrate citrate sensors (Chapter 5.)*).

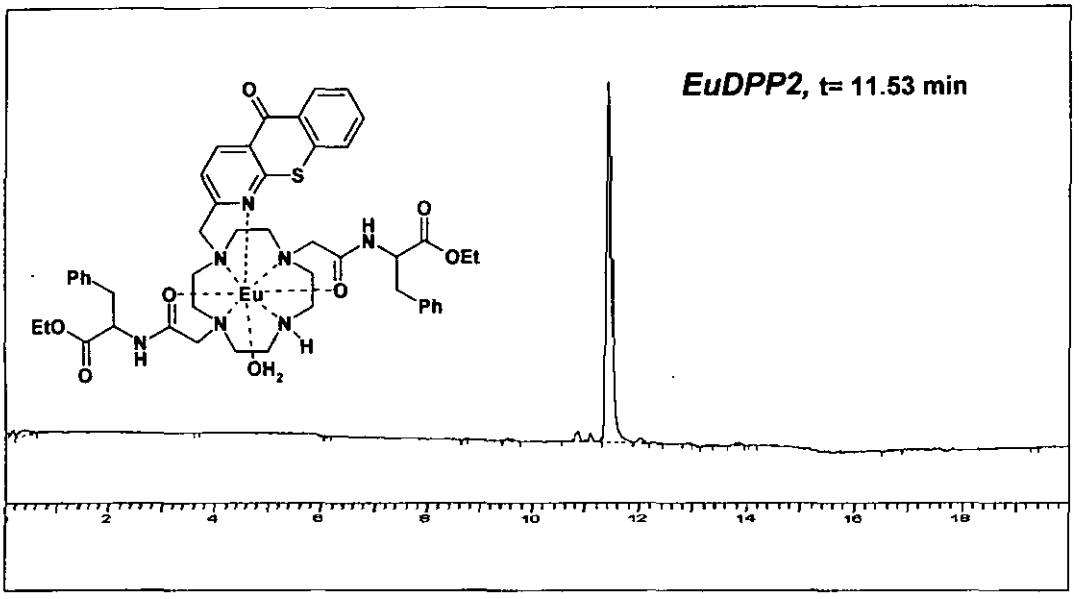

For details of the HPLC purification/analysis see Chapter 6.

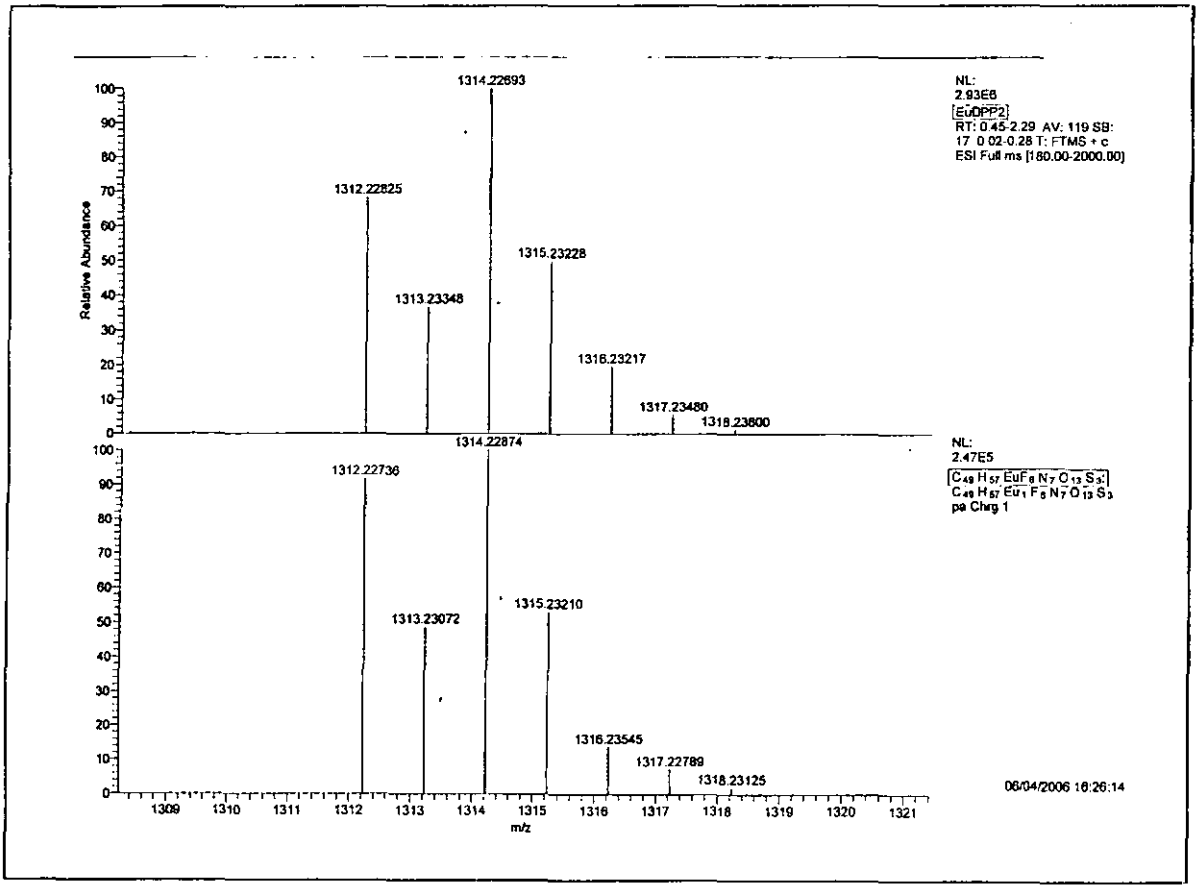

Fig. 2.12. (*upper*) HPLC characterisation for EuDPP2 (*lower*) $HRMS^+$ spectra and the corresponding calculated isotope pattern for its triflate salt $[EuDPP2(CF_3SO_3)_2]^+$.

2.4.2.1 Complex Data

Following their successful synthesis, lifetime and quantum yield measurements were carried out for these Eu complexes possessing amide pendant arms. (*Table 2.3*), Regarding changes in chromophore photophysical properties upon incorporation into the chelating framework, similar observations were found as before using 2-methyl-azathioxanthone as the sensitizing moiety. The luminescent properties of ***EuDAP7A***[25] bearing the 7-(methylcarbamoylmethyl)-azathioxanthone moiety were examined. The absorption and emission maxima were both red-shifted by 4 nm compared to the ligand ($\lambda_{abs.}$= 384 nm, and $\lambda_{em.}$= 440 nm), while the triplet energy was measured to be 22,200 cm^{-1} for GdDAP7A (20,500 cm^{-1} for the '*7-amide*' chromophore), with the low temperature phosphorescence emission spectrum resembling a dominant $n\pi^*$ character of the T_1 state. (*Similar observation was made for GdDPP2 incorporating a 2-methyl-azathioxanthone sensitiser, with E_{T1}= 22,800 cm^{-1}.*) The molar extinction coefficient also increased from 9,590 cm^{-1} to 12,710 cm^{-1} (in H_2O). This 3,000 cm^{-1} increase in the light absorbing property renders EuDAP7A the most efficient Eu complex synthesised to date that incorporates an azathioxanthone sensitiser moiety.

Complex[a]	k_{H2O}	k_{D2O}	Δk_{corr} [b]	q'_{corr} [c]	Φ_{Eu} [d]
EuDAP2	3.84	1.79	1.65	2	4.4 %
EuDPP2	3.13	2.08	0.65	1	3.8 %
EuDAPA2	4.11	1.43	2.28	2	1.2 %
EuDPPA2	3.99	1.62	1.97	2	0.9 %
EuDAP7A	2.27	1.11	0.76	1	5.1 %

[a] All measurments were carried out at pH = 7.4. [b] For the Eu complexes a correction to Δk of 0.25 ms^{-1} has been applied for outer sphere water contribution, and $\Delta k'$ of 0.075 ms^{-1} for every exchangeable NH oscillator assuming fast NH → ND exchange in D_2O, [c] The values of q'_{corr} have been obtained by multiplying Δk_{corr} by 1.2 (are corrected to ±0.5). [d] Quantum yield measurements were carried out in H_2O.

Table 2.3. Quantum yields and rate constants (ms^{-1}) for depopulation of the excited states in H_2O and D_2O for synthesized Eu complexes incorporating amide type pendant arms (293K).

The radiative lifetimes in water and deuterium oxide for each Eu complexes studied in this section were measured allowing inner sphere hydration value (q) to be calculated[22]. These complexes only show one major solution species in the observed biological pH régime (5 – 8). As a result, each quantum yield and radiative lifetime measurement was carried out at a constant pH value (7.4 ±0.1). It must be noted here that below pH = 3 each complex incorporating the 2-methyl-azathioxanthone chromophore displayed a significant decrease in Eu luminescence intensity. This is probably a consequence of pyridyl nitrogen protonation, eliminating the direct bond and short distance between the antenna and the metal centre, lowering the desired energy transfer and making it accessible towards quenching by proximate OH oscillators, therefore significantly lowering the luminescence quantum yield.

Comparing the measured radiative lifetimes and the q-values calculated from them, it is evident that changing the nature of the pendant arm significantly alters the overall complex geometry therefore the accessibility of the Eu centre. The introduction of bulky phenyl groups on the pendant arms results in a decrease in the number of inner sphere water molecules; ***EuDAP2*** possesses two water molecules bound to the Eu centre, while ***EuDPP2*** binds only one as a result of more effiective shielding by the esterified phenylalanine arms. As a result of incorporating a chromophore which binds in a different manner to the Eu centre, therefore making the overall complex geometry more 'packed' and the Eu centre less accessible, the complex ***EuDAP7A*** only possesses one inner sphere water molecule. Hydrolyzing the pendant arm ester groups generally makes shielding of the lanthanide centre less effective, resulting in an increase in the inner sphere hydration number, and a decrease in the measured quantum yield values.

The highest quantum yield among the complexes of this class was observed in case of EuDAP7A, which is a combination of its 'tighter' complex geometry and more efficient sensitization of Eu emission by the chromophore.

It is important to note, that each numerical value obtained and every (binding) constant is reported as an average of at least three separate measurements. The given error values were calculated incorporating the experimental error of the corresponding measurement. For demonstration purpose, luminescence spectras giving the best fit or smallest standard deviancy are used.

2.5 References

1 P. Atkinson, K. S. Findlay, F. Kielar, R. Pal, D. Parker, R. A. Poole, H. Puschmann, S. L. Richardson, P. A. Stenson, A. L. Thompson, and J. Yu, *Org. Biomol. Chem.*, 2006, **4**, 1707.

2 J. Yu and D. Parker, *Eur. J. Org. Chem.*, 2005, 4249.

3 J. Yu, D. Parker, R. Pal, R. A. Poole, and M. J. Cann, *J. Am. Chem. Soc.*, 2006, **128**, 2294.

4 D. Parker and J. Yu, *Chem. Commun.*, 2005, 3141.

5 M. P. Lowe and D. Parker, *Chem Commun.*, 2000, 707.

6 M. P. Lowe and D. Parker, *Inorg, Chim. Acta*, 2001, **317**, 163.

7 M. P. Lowe, D. Parker, O. Reanay, S. Aime, M. Botta, G. Castellano, E. Gianolio, and R. Pagliarini, *J. Am. Chem. Soc.*, 2001, **123**, 7601.

8 R. Pal and D. Parker, *Chem Commun.*, 2007, 474.

9 R. A. Poole, G. Bobba, M. J. Cann, J.-C. Frias, D. Parker, and R. D. Peacock, *Org. Biomol. Chem.*, 2005, **3**, 1013.

10 R. A. Poole, C. P. Montgomery, E. J. New, A. Congreve, D. Parker, and M. Botta, *Org. Biomol. Chem.*, 2007, **5**, 2055

11 Y. Bretonniere, M. J. Cann, D. Parker, and R. Slater, *Org. Biomol. Chem.*, 2004, **2**, 1624.

12 H. Fujiwara and K. Kitagawa, *Heterocycles*, 2000, **53**, 409.

13 F. J. Villani, T. A. Mann, E. A. Wefer, J. Hannon, L. L. Larca, M. J. Landon, W. Spivak, and D. Vashi, *J. Med. Chem.*, 1975, **18**, 1

14 J. A. Bristol, E. H. Gold, and R. G. Lovely, *J. Med. Chem.*, 1981, **24**, 927.

15 H. Staudinger and J. Meyer, *Helv. Cim. Acta.*, 1919, **2**, 635.

16 J. L. Wolfe, T. Kawate, A. Belenky, and V. Stanton, *Nuc. Acids Res.*, 1998, **30**, 3739.

17 M. G. N. Russel, R. W. Carling, J. R. Atack, F. A. Bromidge, S. M. Cook, P. Hunt, C. Isted, M. Lucas, R. M. Mckernana, A. Mitchinson, K. W. Moore, R. Narguizian, A. J. Macaulay, D. Thompson, K. A. Wafford, and L. J. Castro, *J. Med. Chem.*, 2005, **48**, 1367.

18 J. C. Scaiano, D. Weldon, C. N. Pliva, and L. J. Martinez, *J. Phys. Chem.*, 1998, **102**, 6898.

19 J. C. Scaiano and L. J. Martinez, *J. Phys. Chem.*, 1999, **103**, 203.

20 A. E. Martin, T. M. Ford, and J. E. Bulkowski, *J. Org. Chem.*, 1982, **47**, 412.

21 A. K. Covington, M. Paabo, R. A. Robinson, and R. G. Bates, *Anal. Chem.*, 1960, **40**, 700.

22 A. Beeby, I. M. Clarkson, R. S. Dickens, S. Faulkner, D. Parker, L. Royle, A. S. de Sousa, J. A. G. Williams, and M. Woods, *J. Chem. Soc. Perkin Trans. 2*, 1999, 493.

23 C. P. Montgomery, D. Parker, and L. Lamarque, *Chem Commun.*, 2007, 3841.

24 Y. Bretonniére, M. J. Cann, D. Parker, and R. Slater, *Org. Biomol. Chem.*, 2004, **2**, 1624.

25 L.-O. Palsson, R. Pal, B. Murray, D. Parker, and A. Beeby, *Dalton Trans*, 2007. 5726.

CHAPTER 3

pH Probes

3 pH Probes

3.1 Introduction

The acidity or alkalinity of a given biological system is often the driving force for the chemical and biological changes occurring within them. Therefore, measuring pH is a vital issue in order to fully understand these processes.

A well established method for assigning the pH in a given medium uses an appropriate ***pH indicator*** compound, such as phenolphthalein, methyl orange, phenol red, bromothymol blue, bromocresol green, bromocresol purple and numerous other compounds. A pH indicator is a halochromic chemical detector compound that is added in small amounts to a solution so that the pH of the solution can be determined easily. The indicator colour varies depending on the pH of the solution as a result of its pH sensitive functional group(s) which alter its photophysical properties. Using indicators, qualitative determinations can be made with universal indicators that have broad colour variability over a wide pH range, such as thymol blue which has two transition in colour red to yellow when pH = 1.2 - 2.8, and yellow to blue when pH = 8.0 - 9.6.[1a] Quantitative determinations can be made using indicators that have strong colour variability over a small pH range, such as methyl orange (yellow to orange when pH = 3.1 - 4.4) or bromothymol blue (yellow to blue when pH = 6.0 - 7.6) (*Fig. 3.1*).[1a] Precise measurements can be made over a wide pH range using indicators that have multiple equilibria in conjunction with spectrophotometric methods to determine the relative abundance of each pH-dependent component that make up the colour of the solution.[1b] These precise measurements require the matching of several important criteria, such as aqueous solution phase, and an appropriate indicator compound signaling in a suitable pH range. Being an invasive method, using these indicators possess several drawbacks, such as introduction of a chemical species into the observed environment; or if the indicator is incorporated onto a solid surface, significant amount of sample is sacrificed in order to determine its pH. Therefore, these methods are only used when significant amount of sample is present or the introduction of the indicator compound does not cause disturbing chemical changes.

Fig. 3.1. (*left to right*) Structures of commonly used indicators bromothymol blue, methyl orange and thymol blue with its pH dependent colour equilibrium.[1a]

Interestingly, since ancient time some 'indicator plants' have been used to determine the pH of soil samples for agricultural uses, as different culture plants requires different levels in soil acidity or alkalinity. One of these plants is the *Hydrangea macrophylla* which blossoms in pink or blue, depending on soil pH. In acidic soils, the flowers are blue; in alkaline soils, the flowers are pink.[1a]

The most common way to measure pH nowadays is using a pH meter with a ***pH selective electrode***,[1c] such as the universal glass electrode, which is a H^+-selective potentiometric sensor (*Fig. 3.2*). All glass pH electrodes have extremely high electric resistance from 50 to 500 MΩ. Therefore, the glass electrode can be used only with a high impedance measuring device like a pH meter, which allows the translation of this potentiometric information to actual pH values.

1. Sensing part of electrode, a bulb made from a specific glass.
2. Sometimes the electrode contains a small amount of AgCl precipitate inside the glass electrode.
3. Internal solution, 0.1M HCl for pH electrodes.
4. Internal electrode, usually silver chloride electrode or calomel electrode.
5. Body of electrode, made from non-conductive glass or plastics
6. Reference electrode, usually the same type as 4.
7. Junction with studied solution, usually made from ceramics or capillary with asbestos or quartz fiber.

Fig. 3.2. Detailed structure of the combination electrode.[1a]

The use of such electrodes allows the sample to be stay chemically inert and undisturbed. Drawbacks associated with this method include the significant sample volume that is needed for these measurements. However, the introduction of new micro

pH-electrodes allows pH measurements in solution volumes as small as 5 µL. As an invasive method, obtaining the sample is a crucial part of these measurements, making them unsuitable for observing living organisms. Also, for precise application daily calibration is required and between measurements any glass and membrane electrodes should be kept in the solution of its own ion to prevent the glass membrane from drying out.

3.1.1 Measuring pH with Optical Sensors

Biochemical processes frequently involve protonation and deprotonation of biomolecules, with concomitant changes in the pH of the milieu. A common strategy to monitor the pH of biochemical events relies on colour changes of pH indicators at visible wavelengths. However, in heterogeneous media where indicator concentration or visual observation is limited, highly sensitive pH indicators and methods to precisely measure their photoactivity are needed. This is especially true when monitoring tissue or intracellular pH using common pH indicators. To overcome these problems, a limited number of fluorescent pH probes have been developed to monitor diverse physiological and pathological processes. Such sensors to visualize biological processes *in vivo* have been designed with the emergence of fluorescence imaging techniques using fluorescent probes. Acidic environments are known to be associated with solid tumours[2a], cystic fibrosis[2b], asthma[3] and several conditions associated with renal disease. For example, intratumoural pH was recently reported to range from pH = 6.3 - 7.0,[2a,4] and lung airway pH values as low as 5.2 have been recorded in asthmatics.[3] Acid responsive probes may also find application for cellular imaging of acidic intracellular vesicles, such as endosomes, lysosomes and phagosomes, where the pH can range from 4.5 to 6.5.[5]

For efficient *in vivo* imaging, dyes that absorb and emit in the visible or NIR region are necessary due to the increased optical transparency and lower tissue autofluorescence in this regime[6]. Up to date a wide variety of probes for studying proton concentrations[7-10] in biological environments have been reported. Two main methods are emerging in the pursuit of probes for imaging local pH; nano-crystals[10,11] relying on FRET applications (*Fig. 3.3*) or small organic fluorophore molecules[8,12]. (*Fig. 3.4*)

Several generations of organic fluorphores have been prepared and show increases in emission as the pH of their local environment changes. This is due to their pH dependent photophysiscal properties; upon protonation of their functional group(s) significant conjugation changes occur within them. Their pK_a values can be modulated by variation of the heteroatom substituent in the conjugated system.

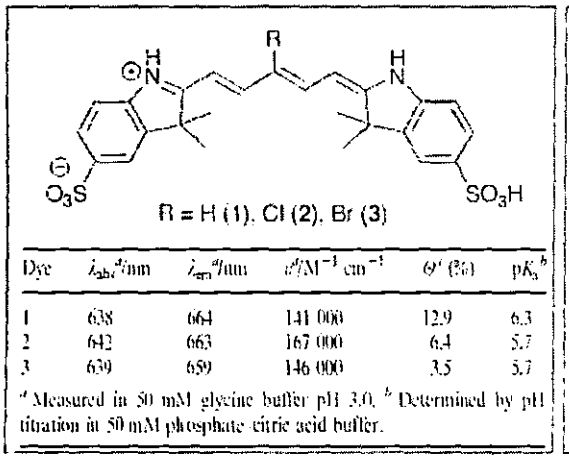

Dye	λ_{abs}[a]/nm	λ_{em}[a]/nm	ε[a]/M^{-1} cm^{-1}	Φ[a] (%)	pK_a[b]
1	638	664	141 000	12.9	6.3
2	642	663	167 000	6.4	5.7
3	639	659	146 000	3.5	5.7

[a] Measured in 50 mM glycine buffer pH 3.0. [b] Determined by pH titration in 50 mM phosphate–citric acid buffer.

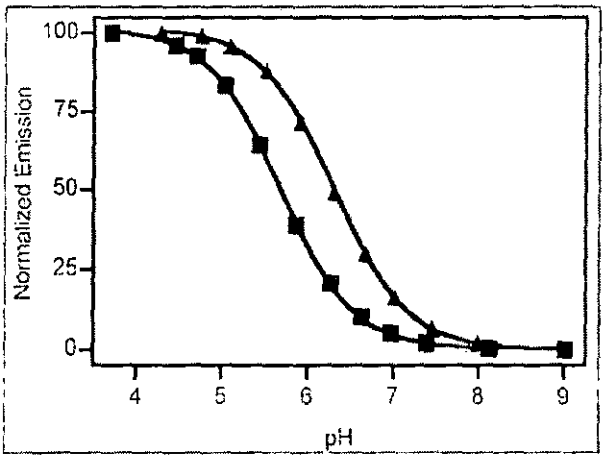

Fig. 3.3. (*left*) Structure and optical properties of a typical pH responsive cyanine fluorochrome. (*right*) Fluorescence-based pH titrations of **1** (▲) and **2** (■) at various pH values in 50 mM phosphate–citric acid buffer. Excitation is at 590 nm and the fluorescence intensity is integrated from 620 to 850 nm.[12]

Most of these sensors are limited by one or more of the following disadvantageous properties: high concentration requirements, the need of co-solvent, insufficient quantum yield, complex chemical structure, sub optimal pK_a values, insufficiently small Stokes' shift, low sensitivity because their photoactivity is in the spectral window where endogenous chromophores either absorb or autofluoresce. Most importantly, they do not possess the property of ratiometric analysis, as the pH is signalled by intensity changes; hence their use is highly concentration dependent, with relatively low accuracy.

The other commonly used fluorescent pH sensors are based on semiconductor nano-crystals (NCs) owing to their photostability, continuous absorption spectra, and efficient, narrow, and tunable emission.[13, 14] These properties of NCs have been exploited for applications in biological imaging and in single particle tracking studies.[15] Whereas NCs are useful in identifying position in a microenvironment, their intrinsic insensitivity

to the presence of most biological or chemical agents renders them of limited utility as sensing probes of that microenvironment. An important recent advance has been the development of water-soluble CdSe NCs with the ability to sense target analytes irreversibly using fluorescence resonant energy transfer (FRET) as a signal transduction mechanism.[8]

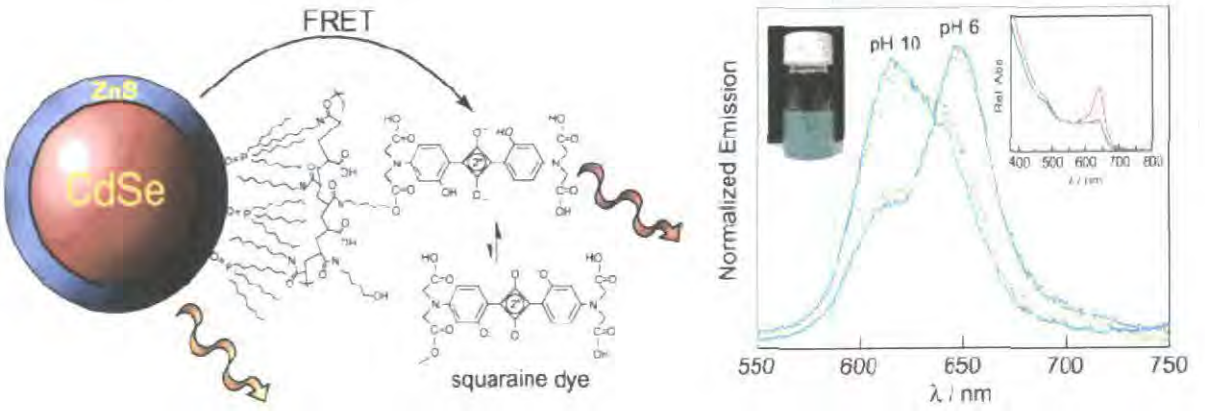

Fig. 3.4. (*left*) A sensor constructed from colloidal CdSe NC with ZnS coating. The native phosphine arms are encapsulated with amphiphilic polymer upon which pH sensitive squaranine dye in conjugated. Upon excitation the NC can either fluoresce or transfer energy to the dye. The FRET efficiency is modulated by environment as the dye's absorption profile is a function of the pH. (*right*) Sensing of the local pH by NC/dye construct. Peak at 600 nm is consistent with NC emission, whilst the peak at 650 nm is consistent with dye emission (Φ = 7 %, λ_{em}= 380 nm, 3.5 : 1 (dye : NC). Insert shows how the absorbance of the dye is suppressed at basic pH (blue).[8]

These constructs thus remove several difficulties encountered with dye-only-based ratiometric nanoscopic sensing systems. As expected from their complex structure, most of these studies do not demonstrate reversible and ratiometric chemical sensing and the probes possess low water solubility. However, the most important requirement towards their application is the proper control of the energy transfer between the NC and dye in order to detect analytes with high precision, irrespective of changes in excitation intensity, wavelength, or collection efficiency.

Each of the highlighted drawbacks of such pH sensors may be overcome by the application of probes based on (luminescent) lanthanide(III) complexes.

3.1.1.1 Advantages of a Europium-based pH probe

The use of fluorescent sensors for detection and monitoring of a variety of chemical species, ranging from simple ions to complex biomolecules, is now widely applied. Although this field is still dominated by organic molecules or nano-crystals, research effort in the development of new measuring methods is turning increasingly towards luminescent metal complexes, including transition metal ions[16] and lanthanide(III) ions[17]. It is appropriate to recall some of the (*Chapter 1.*) advantages of metal complexes over other type of sensors: They possess a more extensive excited state chemistry, owing to the presence of metal-centered (*e.g. dd* and *ff*) and charge-transfer states involving the metal, in addition to the 'organic' excited states associated with the ligand. Hence, they offer more opportunities for perturbing the emission characteristics and may give rise to longer-lived luminescence. Such long lived emission is a very attractive feature of these complexes, as it allows time resolved detection to discriminate between sensor and background emission.

Due to the previous comparison of transition metal and lanthanide complexes (*Chapter 1.*) this section is dedicated only to give a detailed review of previously used lanthanide based luminescent pH sensors. However, it is important to note that several pH-responsive gadolinium based MRI contrast agents have been developed over the past years[18,19] that seek to measure local pH by modulation of relaxivity. Over the past 10 years numerous pH responsive Eu(III) and Tb(III) complexes have been successfully synthesised and studied in Durham[20] This section highlights and compares some of them in order to emphasise why single-component, chemically robust, responsive Eu(III) based chemosensors could be the ultimate target for the analysis of bioactive molecules and ions in solution.

It is well known that the first excited singlet states of many aromatic fluorophores may be quenched by photoinduced electron transfer (PET) from oxidisable groups such as amines. Inhibition of this process through amine protonation or binding to the metal ion may lead to a large increase in the fluorescence intensity, an effect which is highly beneficial in the development of fluorescent sensors.[21] If the fluorophore is able to act as a sensitiser to populate the lanthanide excited state, subsequent changes in the lanthanide

emission may occur. Therefore, protonation of the pendant amine group inhibits PET quenching, significantly increasing the quantum yield of the emission. Control of the pH range where this change takes place can be achieved by varying the basicity of the pendant amine.

In some lanthanide complexes with aryl sensitisers, this 'PET sensor principle' may not affect the lanthanide excited state directly. Upon protonation of the heterocyclic ring nitrogen, complexes incorporating a phenanthridine sensitizing moiety[22,23] (*Fig. 3.5*) display a significant increase in the quantum yield of emission, due to the suppression of such quenching pathways. Moreover, the effect of protonation, results in dramatic changes in the chromophore's photophysical properties, *e.g.* a significant red shift (30 nm) in the absorption maximum, allowing selective excitation of the protonated species in the presence of unprotonated complex, with an excited state pK_a = 4.4. This protonation constant, along with the excitation wavelength can be modified by varying the substituent in α-position to the aryl nitrogen or by direct substitution on the nitrogen itself, causing changes in the conjugation of the N lone pair.[24,25]

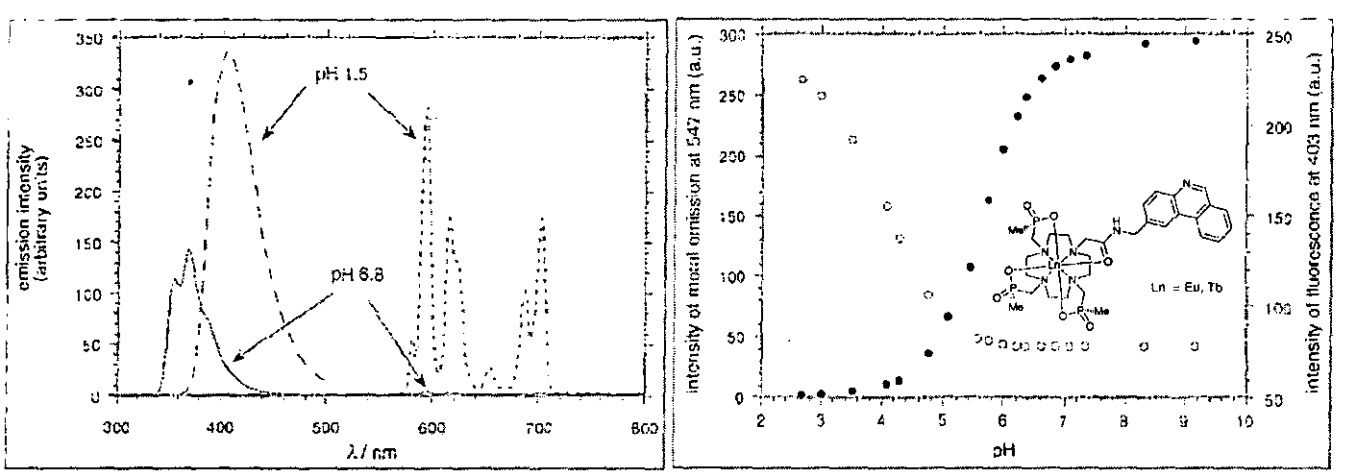

Fig. 3.5. (*left*)) Effect of pH on phenanthridinium fluorescence (λ_{ex} = 320, λ_{em} = 405 nm) and on the europium luminescence (λ_{ex} = 370, λ_{em} = 594 nm, delay 0.1 ms) in the Eu complex at pH 1.5 and 6.8. (*right*) Effect of pH on phenanthridinium fluorescence (o, λ_{ex} = 304, λ_{em} = 403 nm) and on terbium luminescence (•, λ_{ex} = 304, λ_{em} = 547 nm) in the Tb complex as a function of the pH, highlighting the pK_a of the singlet (4.2) and triplet (5.7) excited states respectively.[25]

As a selectively excited, non-ratiometric, pH dependent 'on-off' emission detection process, there is no change in the lanthanide lifetime or the form of the

observed emission spectrum. The response of the metal ion is determined exclusively by the perturbation of the singlet excited state of the chromophore upon protonation. However, using terbium as the lanthanide(III) ion the lifetime of emission was also affected, as a result of an additional deactivation pathway. Upon nitrogen protonation, there is a significant decrease in the triplet energy level of the sensitiser, consequently lowering the energy gap between the chromophore's T_1 state and the terbium emissive state. This reduction permits back energy transfer from the emissive $^5D_4$ state of the metal to the triplet state of the phenanthridine. Not only does this undesired effect lower the lifetime of the emissive state, but also these phenanthridyl chromophores were found to be sensitive towards singlet state quenching by halide ions, with a quenching sequence of $I^->Br^->Cl^-$, consistent with the ease of oxidation of the halide ion. Also, it has been established that the N-methylphenathridinium ion is likely to be attacked by hydroxide ion in a reversible reaction. This occurs on the α-position to the nitrogen, leading to disappearance of the longest wavelength absorption band. Despite the fact that the T_1 energy of this hydroxyl species is higher, so that in the former case, competitive back energy transfer does not occur, the lanthanide luminescence was 'switched-off' completely in an alkaline environment. Due to these effects, complexes bearing phenanthridyl sensitizing moieties allow the possibility of ratiometric *p[halide⁻]* or pO_2 measurements in solution. However, due to the complex nature of their photophysical properties their use as ratiometric pH sensors in solution or when incorporated in mobile sol-gel matrices[26] is rather problematic.

A range of lanthanide complexes incorporating a pendant dansyl or quinolyl sensitisers (*Fig. 3.6*) has also been examined.[27,28]

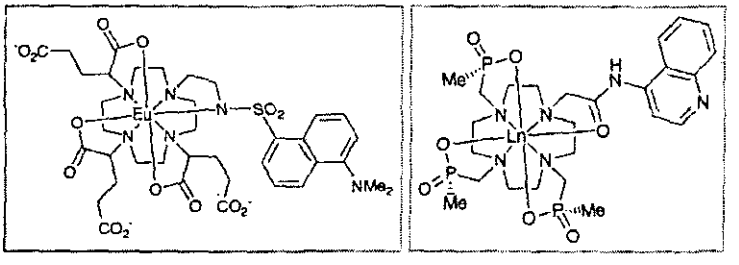

Fig. 3.6. Structure of lanthanide complexes bearing a dansyl[27] (*left*) and quinolyl[28] (*right*) sensitisers.

Protonation of the singlet or triplet excited states in these systems, also gives rise to pH-sensitive emission. Using a 5-(dimethylamino)-naphthalene-1-sulfonyl (dansyl)

group (λ_{ex}= 330 nm, ε = 5,000 $M^{-1}cm^{-1}$) under neutral conditions fluorescence is very efficient (λ_{em}= 500-550 nm), whereas inter-system crossing (ISC) to the triplet state is not, as a result of its highly emissive charge transfer (CT) state. However, protonation of the dimethylamino group, which occurs at pH < 5, removes the CT state and favours the population of the triplet state. This T_1 state lies at 20,600 cm^{-1} which is appropriate for promoting Eu(III) emission, and indeed metal-based luminescence is significantly increased under acidic conditions. [27]

In the quinolyl complex, although protonation of the pendant quinoline moiety does not affect the fluorescence of this group, as a result of increase in the efficiency of energy transfer to the metal, it does lead to a large increase in the europium intensity.[28]

Despite the fact that these complexes each fulfil the requirements of a pH responsive system, their application is also problematic due to a number of downfalls. They possess high ligand fluorescence and their excitation wavelength is not sufficiently long for biological applications. Most importantly, changes in the observed luminescence are not sensitive enough for precise pH determination.

Considering the fact that metal-bound water molecules are able to quench the lanthanide(III) excited states, pH dependent controlling of the hydration state of a suitable lanthanide complex offers an attractive means of modulating emission. Any pH-induced change in the structure of the complex which leads to a change in the number of coordinated water molecules should be signalled by changes in both emission intensity and lifetime. This distinctly different strategy has been employed in a family of pH responsive macrocyclic complexes incorporating a sulfonamide binding moiety[19,26,29], where deprotonation of the sulfonamide group allows the nitrogen to coordinate directly to the metal ion, displacing two bound water molecules, resulting in an increase in the lifetime of the metal based emission (*Fig. 3.7*).

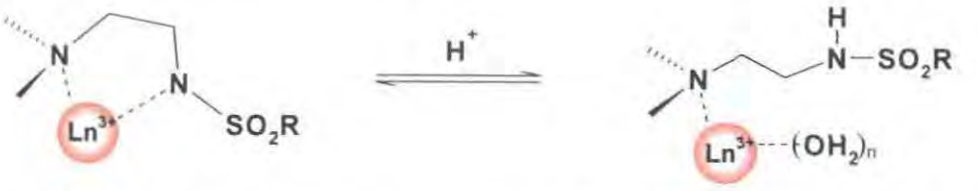

Fig. 3.7. Appending a sulfonamide nitrogen β to a ligand nitrogen allows variation in the coordination environment of the Ln centre as a function of pH.

There is also a large increase in the intensity, due not only to displacement of the quenching inner-sphere water molecules but also to the fact that due to direct binding of the chromophore, the aryl sensitiser in brought closer to the metal ion, promoting the distance dependent energy transfer step. For europium complexes, the form of the emission spectrum in principle is also affected, particularly the relative intensities of the bands, owing to the hypersensitivity of the $\Delta J = 2$ and $\Delta J = 4$ bands to the coordination environment (*Fig. 3.8*). The pK_a of these aryl sulfonamide groups lies typically between 10 and 11[30], but upon binding to Eu or Tb it is lowered by 5 or 6 units, and can be controlled through the basicity of the sulfonyl nitrogen which is, in turn, dependent on the nature of the *para* substituent on the aryl ring.

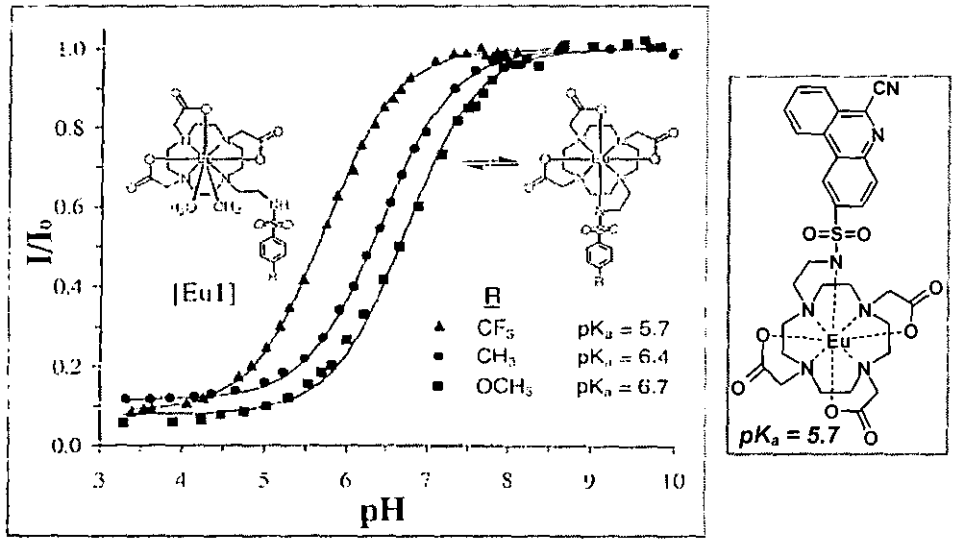

Fig. 3.8. (left) Structures and pH-dependance of the Eu(III) luminescence of complexes incorporating a 'simple' aryl sulfonamide sensitiser;[29] (*right*) structure of the Eu(III) incorporating a (6-cyanophenanthridine)-sulfonamide chromophore.[19]

One of the biggest disadvantages of using a simple aryl sulfonamide sensitiser[29] is the requirement for short wavelength excitation ($\lambda_{ex} < 275$ nm).. The introduction of 6-cyanophenathridine into the sulfonamide, allows sufficient Eu(III) sensitization with a longer wavelength ($\lambda_{ex} = 385$ nm), whilst retaining the pH-induced 'on/off' intramolecular ligation of the sulfonamide nitrogen, with its consequent effect on the metal hydration state and Eu-aryl distance.[26] As for the phenanthridine systems described

earlier, these sulfonamide complexes have been incorporated into sol-gel matrices, where the effect of the microenvironment shifted their pK_a values upwards.[26,31]

These complexes also suffer from some disadvantages. They possess the ability of ratiometric pH sensing due to changes in the hypersensitive Eu(III) emission bands upon sulfonamide nitrogen ligation; however, the bifunctional pH switch also acts as the sensitising moiety. Therefore, this ratiometric aspect could not be used effectively, as the observed luminescence intensity is both concentration and pH dependent: in the protonated form, due to the longer metal-sensitiser distance, the sensitizer is much less effective at sensitizing Eu(III).

3.1.2 Choice of pH-dependent Binding Moiety

Considering the limitations of the previously synthesised pH-responsive lanthanide complexes, a new concept was defined in order to create an efficient single-component, ratiometric pH-probe with controllable modulation of lanthanide luminescence. The implementation of such a probe for use *in vivo* requires that several criteria are satisfied. These include: non-toxicity; stability with regard to the biological half-life; outstanding water solubility and a relatively simple construct. The problem of the concentration dependence and pH-linked fluctuations in the luminescence intensity may be overcome by the incorporation of an integral chromophore that remains directly bound to the metal ion over the observed pH region. At the same time a pH-responsive, intramolecular binding group is required, such that significant changes in the lifetime and most importantly the structure of the Eu emission occur, as a result of reversible displacement of inner-sphere water molecule(s). Furthermore, by varying the structure of the macrocyclic ligand, competitive binding by endogenous anions and proteins may be suppressed, thereby paving the way for the development of complexes which operate directly in 'biological' samples.

By introducing a chromophore with long wavelength excitation into the ligand that remains coordinated to the Eu^{3+} ion (2-methyl-azathioxanthone), a non-UV absorbing sulphonamide moiety is then required in order to avoid any undesirable sensitization by the 'switch' itself. Therefore, the use of an aryl group containing pendant

arms as a pH-dependent intramolecular ligating group was discounted. Bearing in mind the above mentioned criteria, a methylsulfonamidoethyl moiety (*Fig. 3.9*) was selected for use as the pendant arm. This was to be appended β to the ligand nitrogen donor in the expectation that the switch itself will coordinate to the lanthanide centre as a function of pH. The pH-dependent ligation was estimated to occur within the desired pH region of 5 - 8. Therefore, in solution with increasing alkalinity, at pH 5 the protonated Eu(III) complex, with the sulfonamide moiety unbound to the metal centre should dominate, whilst towards pH 8 this species would be replaced by the sulfonamide bound Eu(III) complex. This requires a target pK_{MLH} value of around 6.5 to be achieved. The pK_a values of sulfonamides are usually in the region of 10 – 11.[30] However, early work from *Kimura* established that the protonation constant associated with the binding of a sulfonamide nitrogen to a zinc centre falls in the pH range 5 - 7.5.[32,33] Control over the facility of complex protonation is provided by the nature of the N substituent.

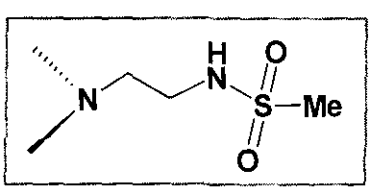

Fig 3.9. *The structure of methylsulfonamidoethyl moiety.*

Complexes incorporating this pH dependent binding moiety will be described in this chapter.

3.2 Luminescent Titrations and pK_a Determinations

Having syntesised (*Chapter 2.*) some pH-responsive Eu(III) complexes (and Gd(III) analogues where applicable) incorporating a methylsulfonamidoethyl moiety, luminescence titrations were carried out to determine the apparent protonation constants (pK_a). These measurements not only confirm whether the pH dependent sulfonamide ligation to the Eu(III) centre occurs in the desired pH region, but also help to identify the limiting structures of the Eu(III) emission spectrum and the dominant species in solution. These luminescence titrations were carried out monitoring the Eu(III) emission spectrum as a function of pH. Complex concentration was obtained from adjusting the samples absorbance to 0.1 ±0.01. Titrations were carried out using a constant 0.1 M salt

background (NaCl), whilst the pH was adjusted using concentrated sodium hydroxide and HCl solutions. It is important to note, that the outline of this work was different from the way it will be presented in this section. Preparing the target Eu(III) complex, luminescence titrations to determine the pK_a value and studying the effect of some biologically common anions were carried out before synthesizing the next target pH-responsive Eu(III)complex. This was done as the observations and conclusions of each study directed the structural modifications of the complex to overcome the problems regarding its biological applications. In this section, these measurements will be detailed parallel for this series of Eu(III)complex, to give detailed information about the effect of structural modification on the luminescent properties.

3.2.1 pK_a Determination of Eu(MS)DCP2

The first system to be examined was the 'Eu-DO2A' derivative (*Fig. 3.10*), Eu(MS)DCP2. The structure of each complex is also given on the accompanying laminated sheet, *Appendix 1.*

By studying the pH dependence of the Eu(III) luminescence over the pH range 3 to 9, profound changes in the form and intensity of the emission spectra were observed. Substantial and reversible changes were particularly evident in the splitting of the $\Delta J = 1$ and the form of the $\Delta J = 2$ and $\Delta J = 4$ manifolds. A plot of the emission intensity ratio (612/618 nm) *versus* pH revealed a significant change and an apparent protonation constant, $\boldsymbol{pK_{HEu(MS)DCP2} = 6.08}$ (±0.05) was determined, by differentiation of the curve. Similar pK_a values were obtained (±5 %) by examining changes in the ratio of other pairs of emission bands, *e.g.* 618/615 or 680/587 nm.

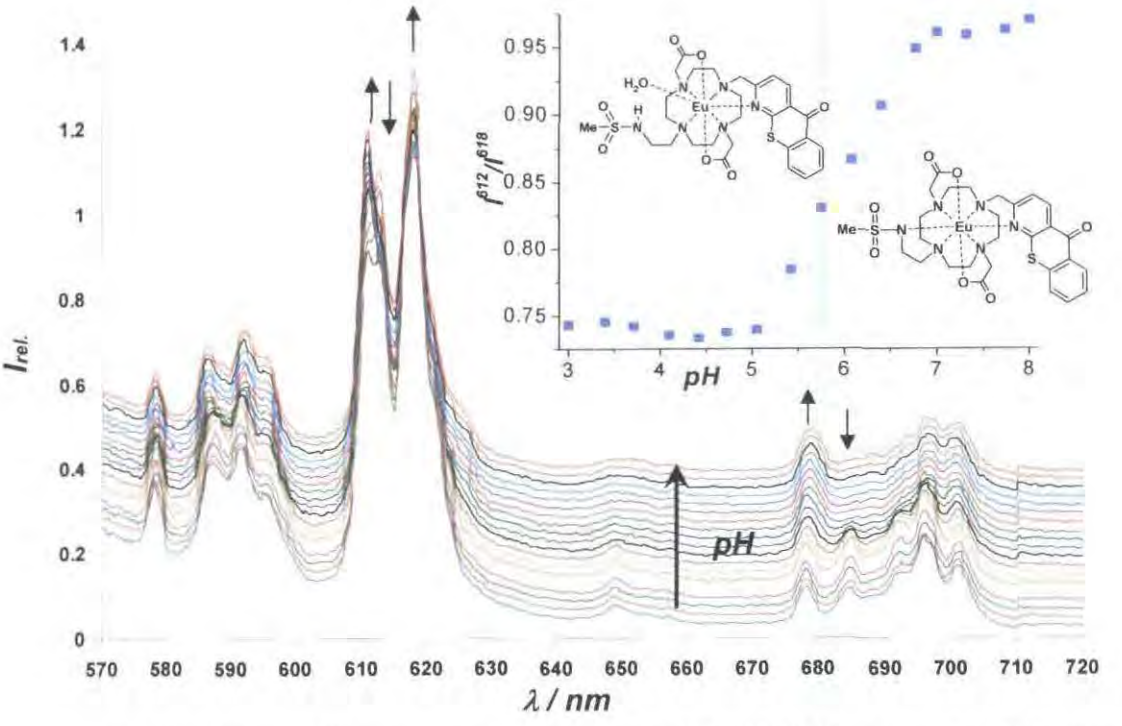

Fig. 3.10. Variation of the europium emission spectrum of ***Eu(MS)DCP2*** as a function of pH over the range 3 to 9 ([complex] = 20 μM, λ_{exc} = 380 nm, 298 K, I = 0.1 M NaCl). (*insert*) Intensity ratio *vs.* pH plot, highlighting the dominant Eu(III) species at the limiting ratios. (Please note that baseline is increasing as a function of the pH, only to ensure better visibility of the changes in the Eu(III) emission. This was achieved by adding a systematically increasing constant to the numerical intensity values. Arrows and their direction refer to the increase or decrease of the highlighted peak. This form of presentation will be applied in the future.)

3.2.2 pK_a Determination of Eu(MS)DGP2

By studying the effect of added biologically common anions, such as citrate, lactate and carbonate, on the emission profile of Eu(MS)DCP2, the complex showed a pronounced sensitivity towards intermolecular anion ligation. This eliminated its pH mapping function by suppressing the desired intramolecular sulfonamide ligation.

This undesired effect may be overcome by introducing negatively charged bulky pendant carboxylic side chains (*i.e.* α-glutarate pendant arms) onto the chelating framework, as detailed previously (*Chapter 2.*). The complex ***Eu(MS)DGP2*** was therefore synthesized and a pH titration carried out in order to assess the apparent protonation constant (*Fig. 3.11*)

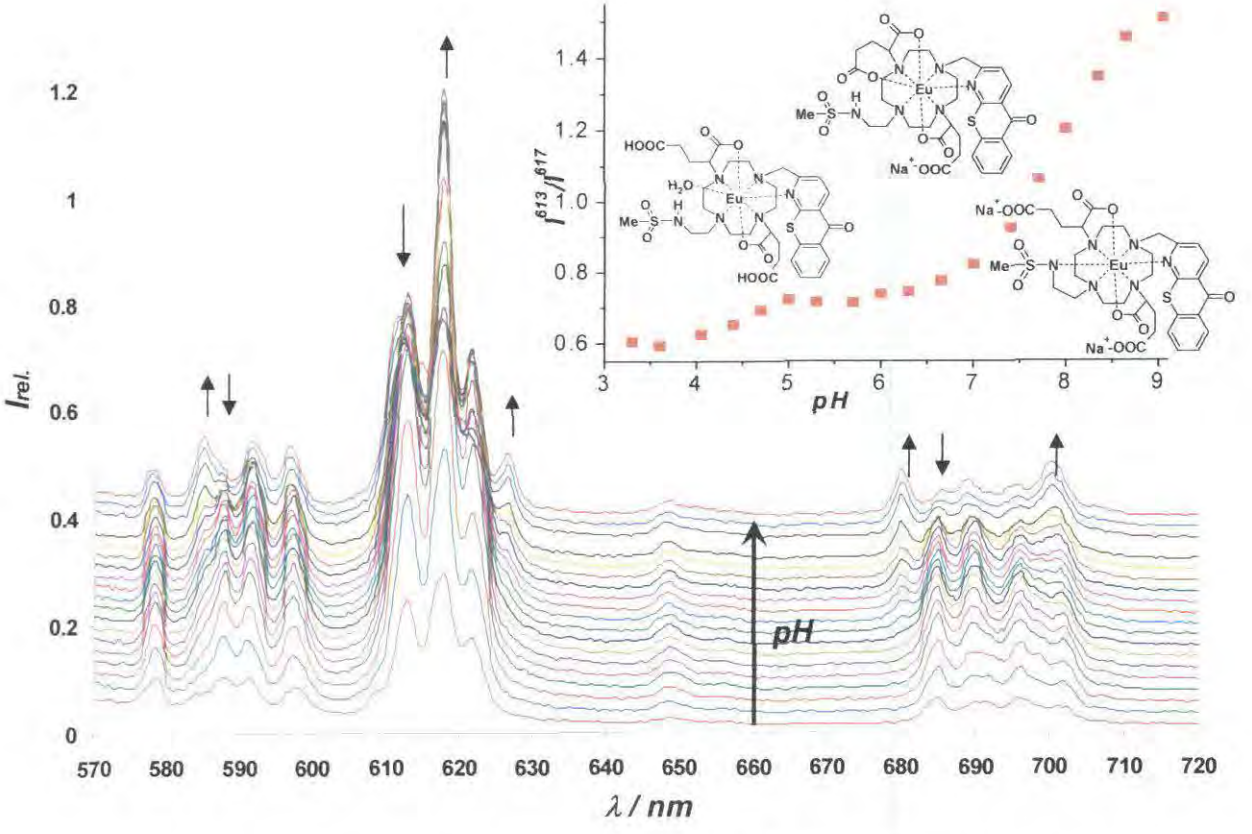

Fig. 3.11. Variation of the europium emission spectrum of ***Eu(MS)DGP2*** as a function of pH over the range 3 to 9 ([complex] = 20 μM, λ_{exc} = 380 nm, 298 K, I = 0.1 M NaCl). (*insert*) Intensity ratio (613/617 nm) *vs.* pH plot, highlighting the dominant Eu(III)species at the limiting ratios.

For ***Eu(MS)DGP2***, each of the previously studied intensity ratios were more or less invariant over the pH range of 3 to 7, only above pH 7 was the appearance of the 627 and 680nm bands more evident. Such behaviour accords with earlier observations[19, 29] with analogues complexes incorporating glutarate pendant arms, in which intramolecular (7-ring) carboxylate ligation competed with sulphonamide chelation. This intramolecular competition shifted the apparent protonation constant, $pK_{HEu(MS)DGP2}$ to ~ ***7.6***.

By starting the titration in the acidic region, the coordinated water molecule was displaced as a result of glutarate ligation. The $pK_{H2Eu(MS)DGP2}$ of this ligation mode was determined to be 4.4 (±0.05). A further increase in pH led to the onset of sulphonamide binding which competes with glutarate arm binding. Around pH 8, the 'sulfonamide N' binds to the Eu(III) centre and becomes the dominant species in solution.

3.2.3 pK_a Determination of Eu(MS)DAdP2

The intramoleclaur ligation of the glutarate pendant arm can be obviated, with consequently gained more kinetic stability towards anion binding, by introducing a methylene spacer into the pendant carboxylate arm. This is due to the unfavourable 8-ring chelate formation associated with an α-adipate pendant arm.

Confirmation of this theory was sought by examining the pH titration of ***Eu(MS)DAdP2*** (*Fig. 3.12*). No evidence for carboxylate binding was observed and the apparent $pK_{HEu(MS)DAdP2}$, associated with protonation of the N-bound sulphonamide, reverted to ***6.17*** (±0.05) (*Fig. 3.13*).

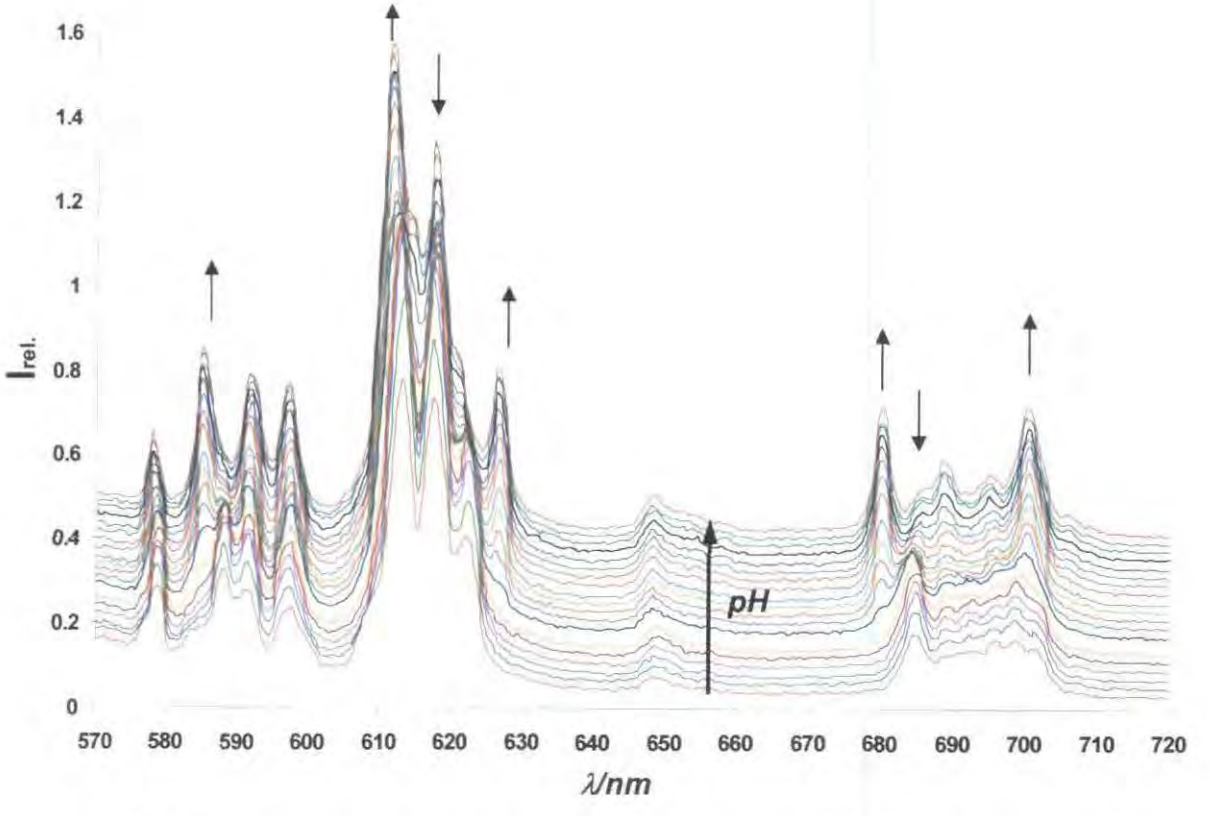

Fig. 3.12. Variation of the europium emission spectrum of ***Eu(MS)DAdP2*** as a function of pH over the range 3 to 9 ([complex] = 20 μM, λ_{exc} = 380 nm, 298 K, I = 0.1 M NaCl).

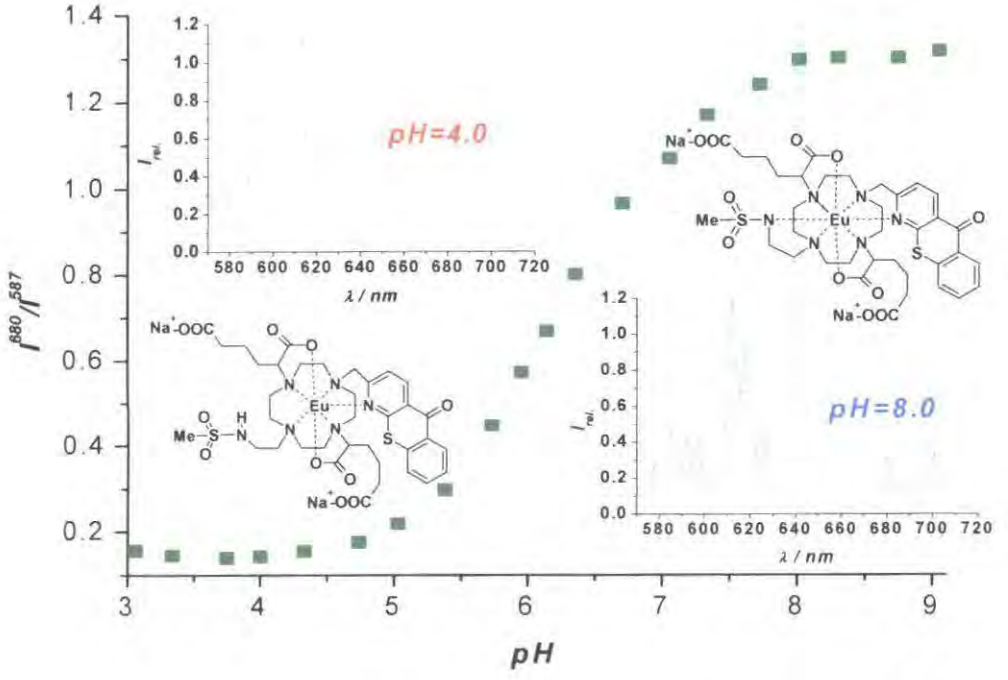

Fig. 3.13. Intensity ratio *vs.* pH plot, highlighting the dominant Eu(III)species at the limiting ratios and their Eu(III) emission spectrums.

The plot of the change in emission intensity ratio (680/587 nm) *versus* pH revealed an 80% change in this ratio over the pH range 4.5 to 8, and the apparent protonation constant was calculated to be 6.17 (±0.05). This was confirmed by examining changes in the ratio of other pairs of emission bands. However, the cited intensity ratio provided the biggest change as a function of the pH.

By comparing these luminescence titrations, it was noted that the bands evolving at 627 nm and 680 nm with increasing pH, are consistent with the onset of sulfonamide ligation to the Eu(III) centre.

Changes in the complex hydration state, q, as a function of pH were assessed (*see Section 2.4.1.1*) by measuring the radiative rate constants for excited state depopulation in H_2O and D_2O and using an established relation to deduce the number of water molecules bound to the Eu.[34, 35] In each case at pH 8, a q value of zero was obtained, with partial hydration only in more acidic media (q = 1 for Eu(MS)DCP2 at pH 4.5 and for Eu(MS)DGP2 at pH 3). However, with Eu(MS)DAdP2 the hydration state apparently remained zero over the observed pH range, with a slightly higher overall quantum yield

(ca. 6 %). This presumably is a result of efficient shielding of the Eu(III) centre from water by the α-adipate pendant arms.

3.2.3.1 Variation of Ralaxivity with pH of Gd(MS)DAdP2

Confirmation of the constancy in the hydration sate of Eu(MS)DAdP2 was sought by examining the pH dependence of the relaxivity of the Gd(III) analogue (*Fig.3.14*). The measured relaxivity for Gd(MS)DAdP2 was 3.1 (±0.2) $mM^{-1}s^{-1}$ over the pH range 3 to 5.5 and was reduced to 1.9 (±0.15) $mM^{-1}s^{-1}$, by pH 8.5 with an apparent binding constant of 6.2 (±0.15). Such low relaxivity values and the minor change in them are consistent with changes only in the extent of the second sphere of hydration for a $q = 0$ system.[19]

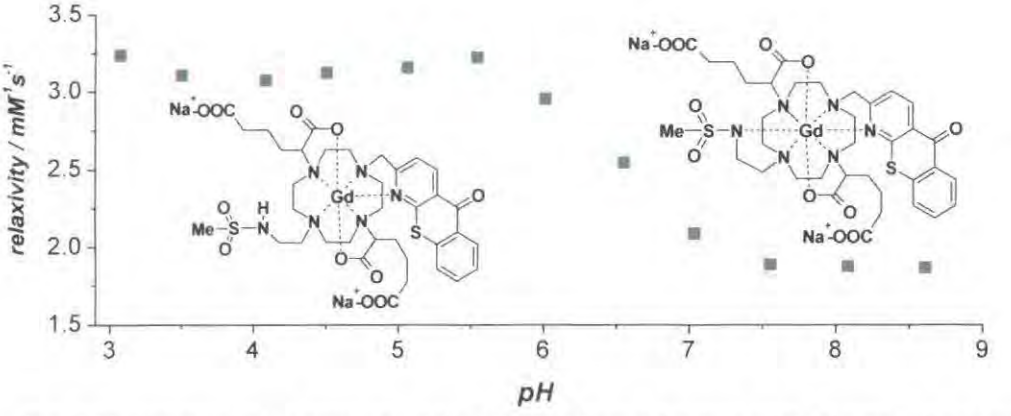

Fig. 3.14. Variation of the relaxivity of Gd(MS)DAdP2 as a function of pH ([complex] = 90 μM, 310 K, I = 0.1 M NaCl).

3.3 Effect of Added Anions on the Emission Profiles

In order to judge whether the synthesised pH-responsive complex is suitable for biological applications, the emission behaviour was examined in the presence of common biological anions. Preliminary studies involved pH titration of a given Eu(III) complex, in a stimulated extracellular ionic background ('anion-stew' = 0.9 mM hydrogenphosphate; 0.13 mM citrate; 2.3 mM lactate; 30 mM bicarbonate and 0.1 M chloride, each as sodium salts). Each complex exhibited some anion sensitivity in the observed pH regime (3 to 9). Titrations were carried out from basic solutions with acidification in order to avoid the undesirable evolution of carbon dioxide (*equation 3.1*)

$$HCO_3^- + H^+ \rightleftharpoons H_2O + CO_2\uparrow \qquad (3.1)$$

In order to understand the complexity of these titrations and to determine the nature of the predominant $EuL(anion)_x$ ternary species in solution over a given pH range, pH titrations were carried out using individual anion solutions. To avoid a significant change in the ionic strength of the sample, each titration used a common background of 0.1 M NaCl. For the Eu(MS)DAdP2 complex, titrations were also carried out using 0.3 mM ascorbate (sodium salt) as a background medium, in order to study its quenching/binding effect on the Eu emission spectra.

If a particular anion revealed an affinity towards the given complex, titrations were undertaken increasing the anion concentration up to its limiting extracellular concentration value, maintaining a constant pH (initial complex solutions also contained 0.1 M NaCl). These measurements were carried out by volumetric addition of the studied anion, using stock solutions of its sodium salt, to minimize the increase in sample volume and consequent decrease in complex concentration. Each titration point has been corrected by the decrease in the recorded sample absorbance following the volumetric change.

3.3.1 Effect of Added Anions on the EuDCP2 Emission Spectrum

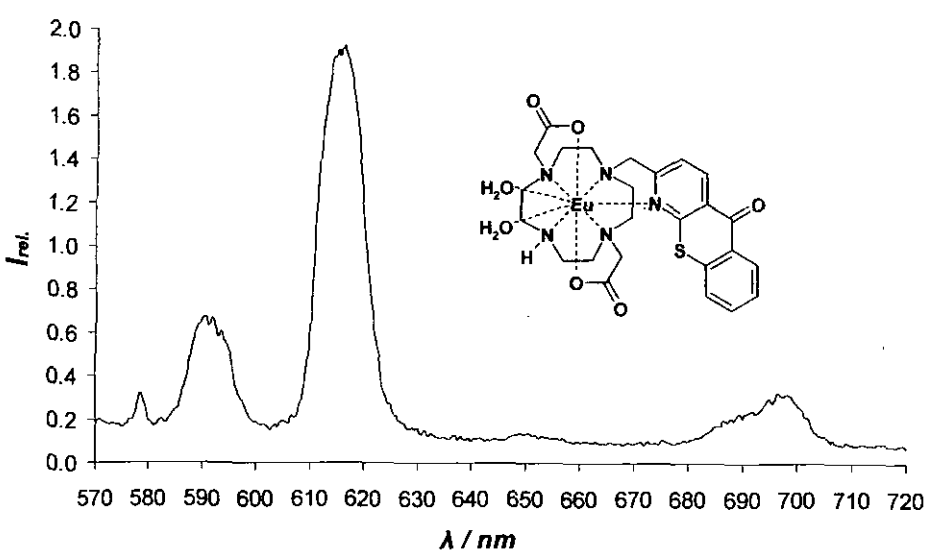

Fig. 3.15. Structure and emission spectrum of EuDCP2 ([complex] = 20 μM, 298 K, λ_{ex} = 380 nm, I = 0.1 M NaCl) in D_2O, pD = 7.0. (pD = pH (meter reading) + 0.41)[36]

The synthesis of EuDCP2 was carried out in order to compare its behaviour and luminescence properties to Eu(MS)DCP2, thereby undertanding the benefit and role of the sulfonamide moiety. The Eu(III) emission spectrum of EuDCP2 was very weak in H_2O as a result of the quenching OH oscillators of the bound water molecules ($q = 2$). By repeating the measurement in D_2O a more intense Eu emission was observed (*Fig. 3.15*).

In the presence of simulated extracellular salt solution (termed 'anion-stew' hereafter) significant changes were observed, in both the intensity and structure of the Eu emission spectrum (*Fig. 3.16*). This can be explained by the replacement of bound water molecules associated with the formation of a ternary complex, [EuDCP2(anion)$_x$] of differing relative stability and differing emission profiles.

To understand these changes in detail, further titrations were required, examining the influence of each anion separately. As this complex was found to be extremely sensitive towards anion binding and was only synthesised to confirm the importance of the pH switch, detailed information on these studies will not be presented.

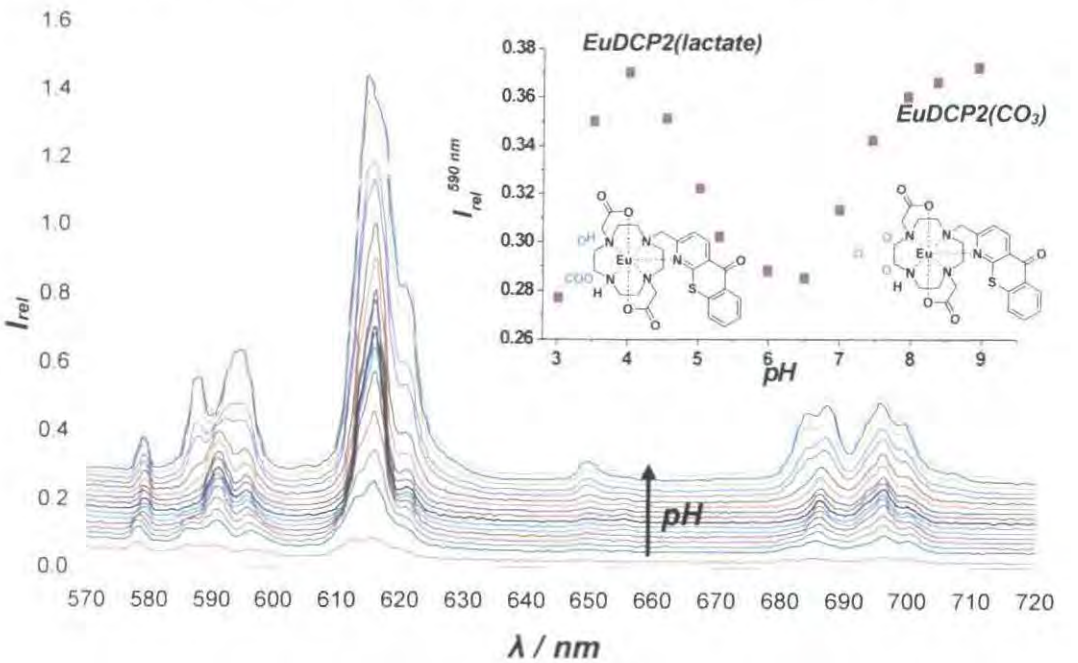

Fig. 3.16. Luminescence titration of EuDCP2 using 'anion stew' as background medium ([complex] = 20 μM, 298 K, λ_{ex} = 380 nm, I = 0.1 M NaCl). (*insert*) Intensity (590 nm) *vs.* pH plot, highlighting the dominant EuDCP2(anion) species of the limiting spectrum (1 : 1 binding was assumed, *see 3.3.2.1*).

To summarise the observed changes; using a 2.3 mM lactate anion solution modest Eu intensity and significant structural changes were observed in the Eu emission spectra. Similar observations were made, with larger intensity change in the Eu emission when using 30 mM carbonate solution as the background. The explanation for this higher intensity change may be attributed to the bidentate nature of carbonate binding to the Eu centre displacing both water molecules from the inner sphere, in contrast to lactate binding that leaves one proximate OH oscillator following chelation.[37] This conclusion were supported by radiative lifetime measurements for the system (τ_{H_2O}= 0.24 ms in 0.1 M NaCl), which showed a 46% increase at pH 4 (lactate binding) and a significant 87% increase at pH 9 (carbonate binding).

No Eu emission could be observed when using a 0.9 mM phosphate or a 0.13 mM citrate solution as the background medium. This may be a result of a spontaneous ligand exchange reaction. This theory was confirmed by measuring the radiative lifetimes of the sample in each case in D_2O (λ_{ex} = 380 nm). Upon chromophore excitation no Eu emission was observed in both the phosphate and citrate background, as a result of the displacement of the Eu from the complex.

Having defined the observed spectral changes in the case of added carbonate and lactate, it was possible to rationalise the overall spectral changes when using the mixed anion background. Over the pH range 9 to 6.5 the binding of carbonate to the lanthanide centre causes significant changes in the structure of the Eu emission, whilst in the more acidic régime (4 to 6.5) lactate binding can be observed. As the pH was lowered even further the observed Eu(III) intensity decreased significantly, probably due to the onset of pH catalysed complex dissociation.

3.3.2 Effect of Added Anions on the Eu(MS)DCP2 Emission Spectrum

Significant spectral changes were observed using 'anion-stew' as the background medium in the emission spectrum of Eu(MS)DCP2 (*Fig. 3.17*). Changes in the intensity were not as dramatic as with EuDCP2. This is due to the increase in shielding of the Eu(III) centre by the introduction of the pH switch. Measurements of radiative lifetimes in H_2O and D_2O at acidic pH, were consistent with a q =1 complex (k_{H_2O} =2.08 ms^{-1} and

k_{D_2O} =1.32 ms^{-1}). However, significant changes in the structure of the Eu emission were also observed, as the pH decreased from 9 to 3.

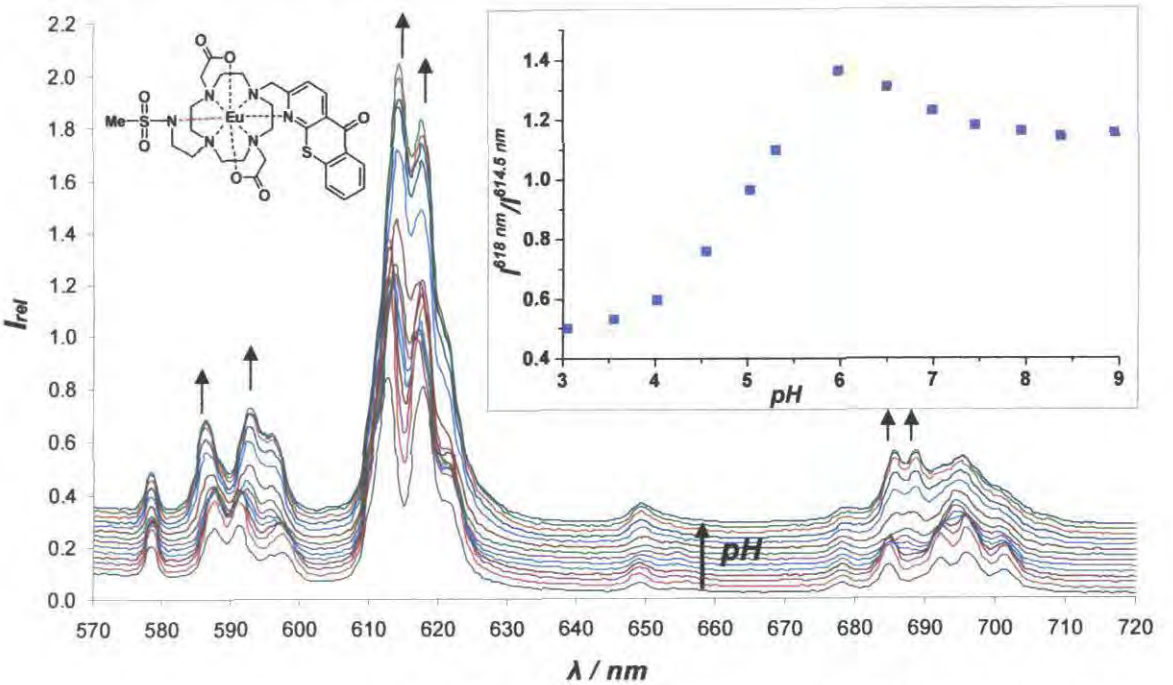

Fig. 3.17. Luminescence titration of Eu(MS)DCP2 using 'anion-stew' as the background medium ([complex] = 20 μM, 298 K, λ_{ex} = 380 nm, I = 0.1 M NaCl). (*insert*) Intensity ratio (618/614.5 nm) *vs.* pH plot indicating the presence of different dominant Eu(MS)DCP2(anion)$_x$ species at the limiting ratios.

The nature of the overall spectral changes can be displayed by selecting a suitable pair of emission wavelengths, with well pronounced intensity changes over the observed pH region, then plotting this intensity ratio as a function of pH (*Fig. 3.17 insert*). The observed changes in the Eu emission spectra were attributed to a competition between the intramolecular sulfonamide ligation and intermolecular anion binding. Over the acidic region, phosphate, lactate and citrate competition is more likely, whilst towards basic pH carbonate binding could be expected. In this case this ratio was obtained by selecting peaks 614.5 and 618 nm, but similar changes can be plotted using 590/593 nm and 700.5/689 nm.

To understand these changes in the Eu emission profile, further luminescence titrations were required using individual anion solutions at their appropriate extracellular concentration. Using a 0.9 mM phosphate anion solution, no changes were observed in

spectral properties (intensity and structure) compared to the luminescent titration carried out to determine the pK_a of the sulfonamide group.

Dramatic spectral changes were observed, however, when using 30 mM carbonate solution as background medium (*Fig. 3.18*). The most significant change in the europium emission was observed by studying the changes in the $\Delta J = 1$, $\Delta J = 2$ and $\Delta J = 4$ manifolds over the pH range 6 to 9. Plotting an intensity ratio (585.5/590 nm, or 614.5/611 nm) *versus* pH, these structural changes can be most effectively illustrated, and can be attributed to bidentate binding of carbonate to the lanthanide centre. This intermolecular binding suppresses the desired intramolecular ligation of the sulfonamide group.

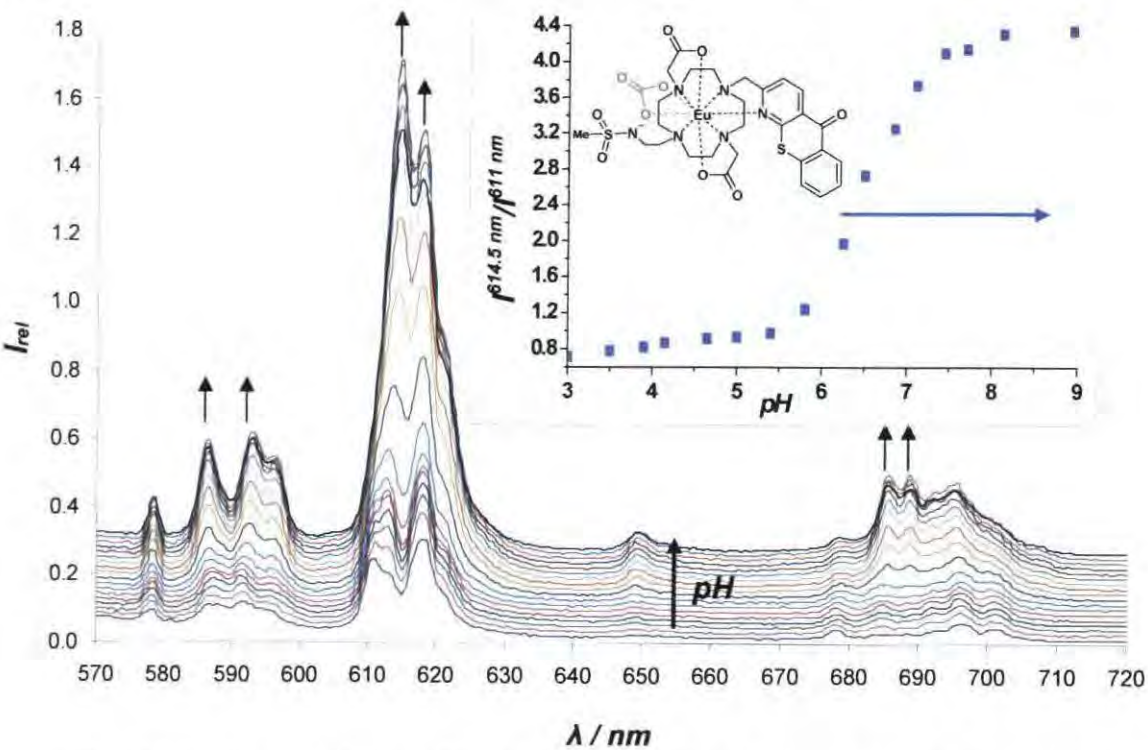

Fig. 3.18. Luminescence titration of Eu(MS)DCP2 using 30 mM sodium carbonate as background medium ([complex] = 20 μM, 298 K, λ_{ex} = 380 nm, I = 0.1 M NaCl). (*insert*) Intensity ratio (614.5/611 nm) *vs.* pH plot, highlighting the dominant Eu(MS)DCP2(CO_3) species in the basic region.

On changing the background to 2.3 mM lactate solution (*Fig. 3.19*), pronounced changes were also observed in the structure and intensity of the Eu emission. In this case, intermolecular anion binding was observed over the pH range 3 to 7, with a significant

increase in the intensity of the metal based emission in acidic region. Plotting the 615.5/613 nm intensity ratio as a function of pH, lactate binding was observed to Eu(MS)DCP2 in this acidic régime (similar plots were obtained using 685/700 nm and 588/594 nm). This binding competes with the intramolecular process and consequently shifts the apparent protonation constant associated with the sulfonamide group from 6.1 to 7.5.

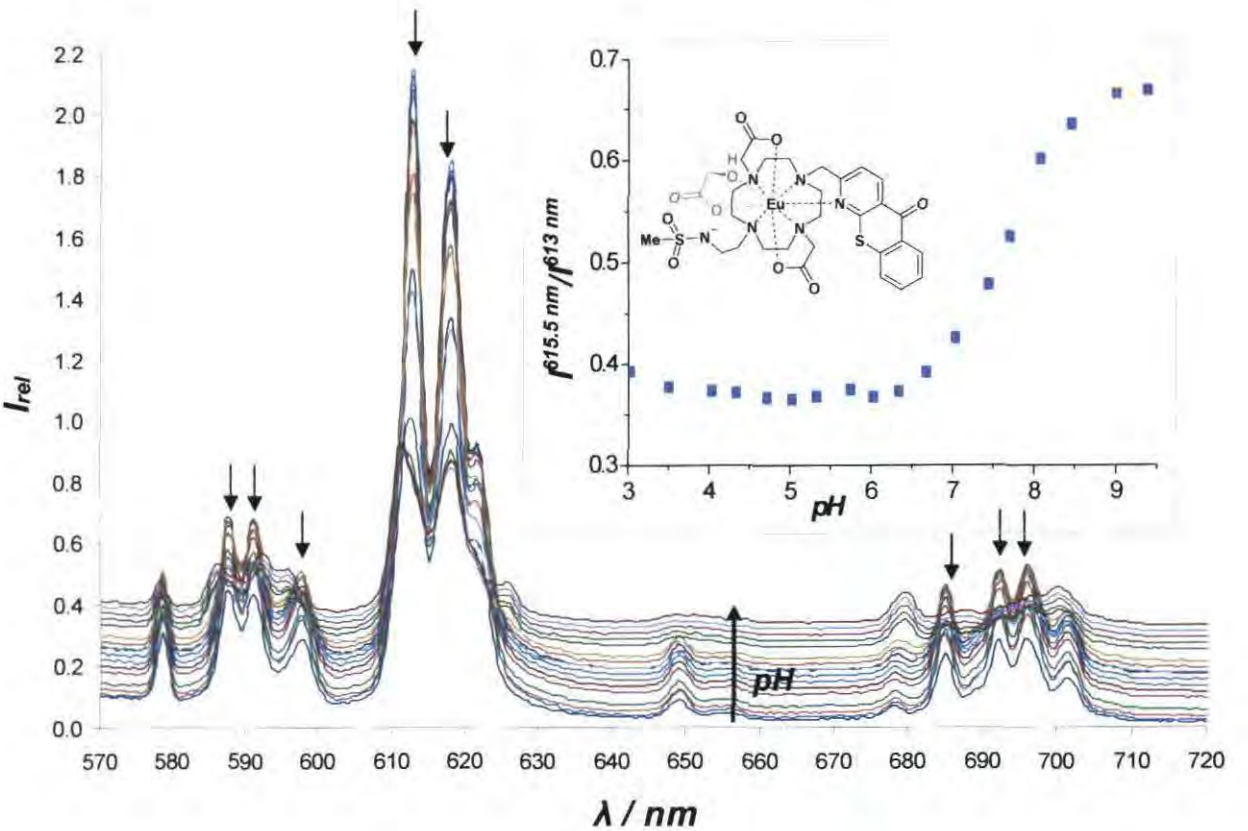

Fig. 3.19. Luminescence titration of Eu(MS)DCP2 using 2.3 mM lactate as the background medium ([complex] = 20 μM, 298 K, λ_{ex} = 380 nm, I = 0.1 M NaCl). (*insert*) Intensity ratio (615.5/613 nm) *vs.* pH plot, highlighting the dominant Eu(MS)DCP2(lactate) species in the acidic region.

In the presence of an 0.13 mM citrate solution, significant changes were observed both in intensity and structure of the emission profile (*Fig. 3.20*) due to strong citrate binding (which also confirms the suggestion for strong citrate binding studying EuDCP2). The biggest structural change was observed in the $\Delta J = 2$ manifold, where an intense band was observed at 614 nm over a certain pH region. Plotting the 614/612 nm

intensity ratio (or 694/700 nm) as a function of pH, strong citrate binding was suggested, and the Eu(MS)DCP2(citrate) adduct is the dominant species from pH 4.5 till pH 7.5. Above pH 7.5, the bound citrate is displaced following intramolecular sulfonamide ligation. This competitive intermolecular anion binding also shifts the pK_a associated with protonation of the pH dependant binding moiety to 7.6.

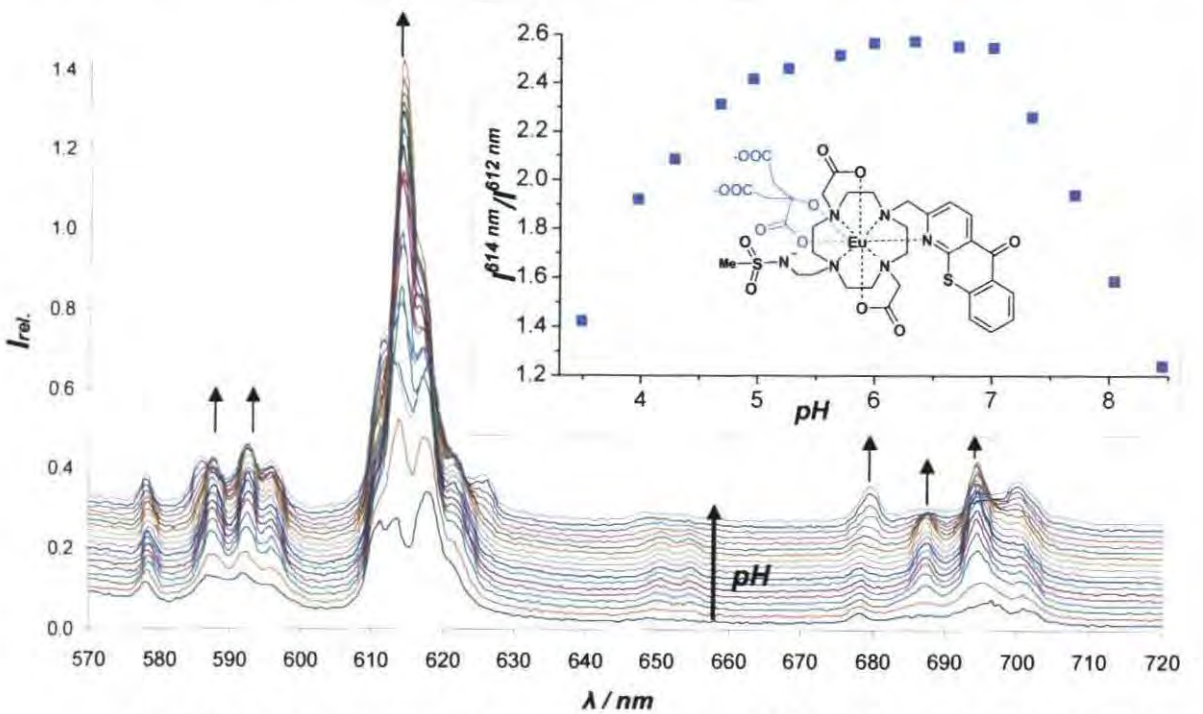

Fig. 3.20. Luminescence titration of Eu(MS)DCP2 using 0.13 mM citrate as the background medium ([complex] = 20 μM, 298 K, λ_{ex} = 380 nm, I = 0.1 M NaCl). (*insert*) Intensity ratio (614/612 nm) *vs.* pH plot, highlighting the dominant, hypothetical Eu(MS)DCP2(citrate) species at pH 4.5 to 7.

The formation of the intense 614 band in the $\Delta J = 2$ manifold upon citrate ligation, was previously observed when studying the first ratiometric citrate sensor (EuDPP2)[38] (*see 1.3.3.1*). The proposed bidentate binding of the citrate, via the OH and α-carboxylate forming a 5-ring chelate, has been confirmed by X-ray crystallography (*Fig. 3.21 left*) analysis of a related triamide complex.[37]

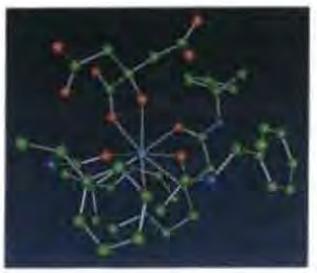

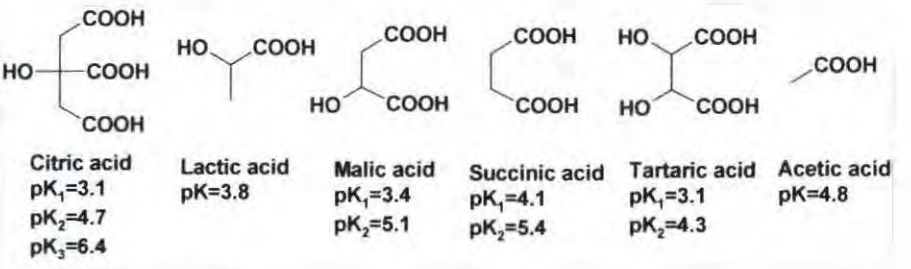

Fig. 3.21. (*left*) X-ray structure of a Eu related triamide(citrate) complex;[37] (*right*) structure and protonation constants of the studied anions (298 K I = 0.1 M NaCl).

However, to confirm this hypothesis, further studies were carried out using structurally related anions. A suitable pH was chosen (pH = 6.0 (±0.05)), and a 2.5 mM solution of sodium acetate, succinate, tartarate, and malate was used as the background medium (*Fig. 3.21 right & 3.22*).

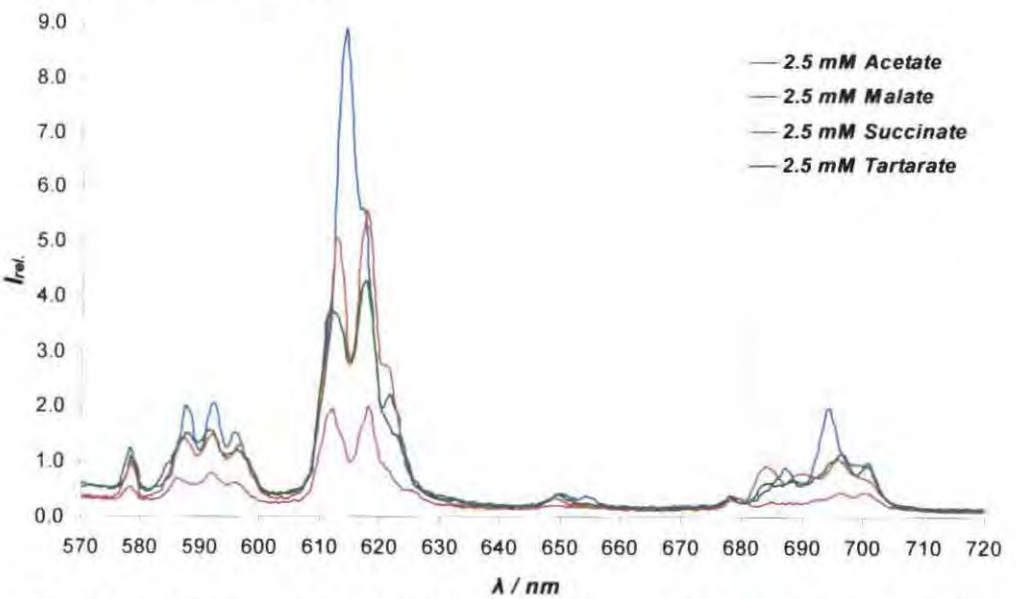

Fig. 3.22. Emission spectra of Eu(MS)DCP2 using various 2.5 mM anion solutions as background medium (pH = 6.0, [complex] = 20μM, 298 K, λ_{ex} = 380 nm, I = 0.1M NaCl).

The structural homology of the studied anions is evident. Only upon addition of malate, was a single major band observed at 614 nm in the $\Delta J = 2$ manifold. This is consistent with the proposed structure of the putative ternary adducts with malate and citrate, incorporating a 5-ring α-hydroxycarboxylate chelate to the Eu(III) centre.

Moreover, these measurements were consistent with a similar binding profile for lactate, acetate, succinate and tartarate possibly binding via the carboxylate.

With this background in mind, it is now possible to interpret the complexity of the spectral changes in Eu emission using 'anion-stew' as the background medium (*Fig. 3.17*), by examining the changes in the $\Delta J = 1$, $\Delta J = 2$ and $\Delta J = 4$ manifolds. As found previously with EuDCP2, over the basic pH region carbonate binding causes significant spectral changes in the Eu emission, suppressing the desired intramolecular sulfonamide ligation. From around pH 6 (where $[HCO_3^-] \approx [CO_2.aq]$) the onset of lactate anion binding is evident until pH 4. At pH values below 4, due to the protonation of lactate, an aqua Eu(MS)DCP2 species emerges, which results in a significant drop in emission intensity. Due to its 20 times higher concentration, the lactate anion suppresses the influence of added citrate. To summarise this, these intermolecular processes suppress the desired intramolecular binding, thus the sulfonamide nitrogen remains uncoordinated over the studied pH range.

3.3.2.1 Photophysical Response to Endogenous Anions

Significant changes were observed in the Eu(MS)DCP2 emission spectrum, in the presence of different anions. Hence, separate titrations were carried out in order to determine apparent binding constants. These measurements were executed by monitoring changes in the Eu emission spectrum anion concentration up to the limiting extracellular concentration value. In each of these studies, the pH of the solution was maintained (±0.05) at a constant value, selecting a pH where the added anion showed maximum effect on the Eu emission, within the biological pH region of 5 to 7.5. Apparent binding/affinity constants were obtained from these luminescent titrations by fitting a selected intensity ratio *versus* added anion concentration using *equation 3.2*, and Origin 6.0™ mathematical software. For each study 1:1 (complex : anion) binding was assumed. This has been confirmed by ESMS identification of the appropriate ternary adduct, such as Eu(MS)DAdP2(CO_3). (ESMS$^+$ spectrum of Eu(MS)DAdP2 in the presence of Na_2CO_3 shown peaks consistent with $[Eu(MS)DAdP2(CO_3)Na_3]^+$ (*m/z 1089*), possessing the corresponding isotope pattern)

$$[X] = \frac{\frac{(F-F_0)}{(F_1-F_0)}/K + [EuL]*\frac{(F-F_0)}{(F_1-F_0)} - [EuL]*\left(\frac{(F-F_0)}{(F_1-F_0)}\right)^2}{1-\frac{(F-F_0)}{(F_1-F_0)}}$$

[X]: the total concentration of studied anion
[EuL]: the total concentration of the complex
K: the binding constant
F is the ratio of selected peaks
F_0 is the ratio at the beginning
F_1 is the final ratio
[EuLX]: the concentration of the ternary adduct
$[X_f]$: the concentration of free anion
$[EuL_f]$: the concentration of the free complex.

$$EuL + X \rightarrow EuLX$$

$$K = \frac{[EuLX]}{[X_f][EuL_f]}$$

Eq. 3.2. The analysis used and its explanation for calculating the binding constant (K) of an applied anion. (*Binding constants will be presented as logK values [M^{-1}]*)

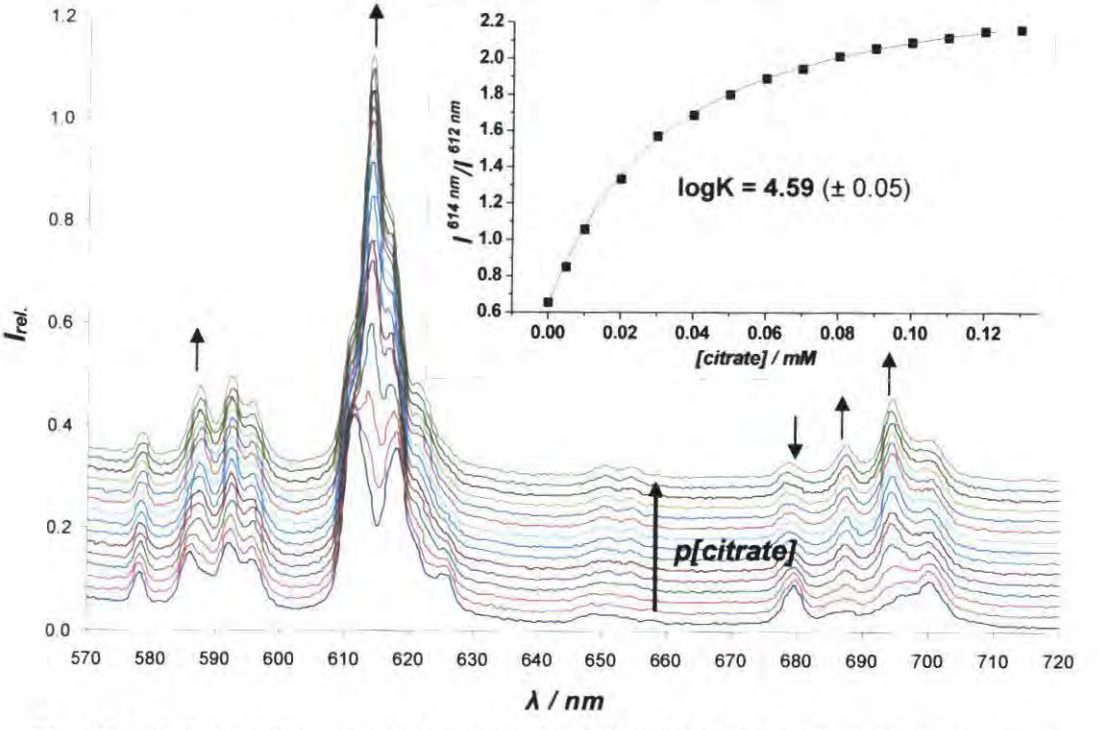

Fig. 3.23. Variation of Eu emission spectrum for Eu(MS)DCP2 following addition of sodium citrate solution (pH = 7.4 (±0.05), [complex] = 20μM, 298 K, λ_{ex} = 380 nm, I = 0.1M NaCl). (*insert*) Intensity ratio (614/612 nm) *vs.* added [citrate] plot (*squares and line refer to measured values and fitted curve respectively*) for determining the apparent binding constant of citrate. (Limiting values: LV_{min}= 0.65 and LV_{max}= 2.4)

Determination of the apparent binding constant for citrate was carried out by varying the concentration of the added anion from 0 – 130 μM, maintaining a constant

pH = 7.4 (±0.1) (*Fig. 3.23*). The chosen intensity ratio (614/612 nm) as a function of added citrate concentration revealed a strong citrate dependence of the Eu emission. Calculation of the apparent binding constant confirmed this strong binding with a value of logK= 4.59 ± 0.05 M^{-1}. Similar value was obtained (±0.2) using the 680/694 nm ratio.

For the calculation of the apparent binding constant for bicarbonate, a pH of 7.4 was found to be appropriate. The bicarbonate concentration was varied from 0 to 30 mM by addition of sodium bicarbonate (0.1 and 1 M) solution. Variation of the Eu emission spectrum (*Fig. 3.24*) revealed bicarbonate binding, for which the binding constant was found to be logK = 1.97 ±0.03 M^{-1} using the intensity ratio 614.5/611 nm. A similar value (±0.1) was obtained using the 680/689.5 nm ratio.

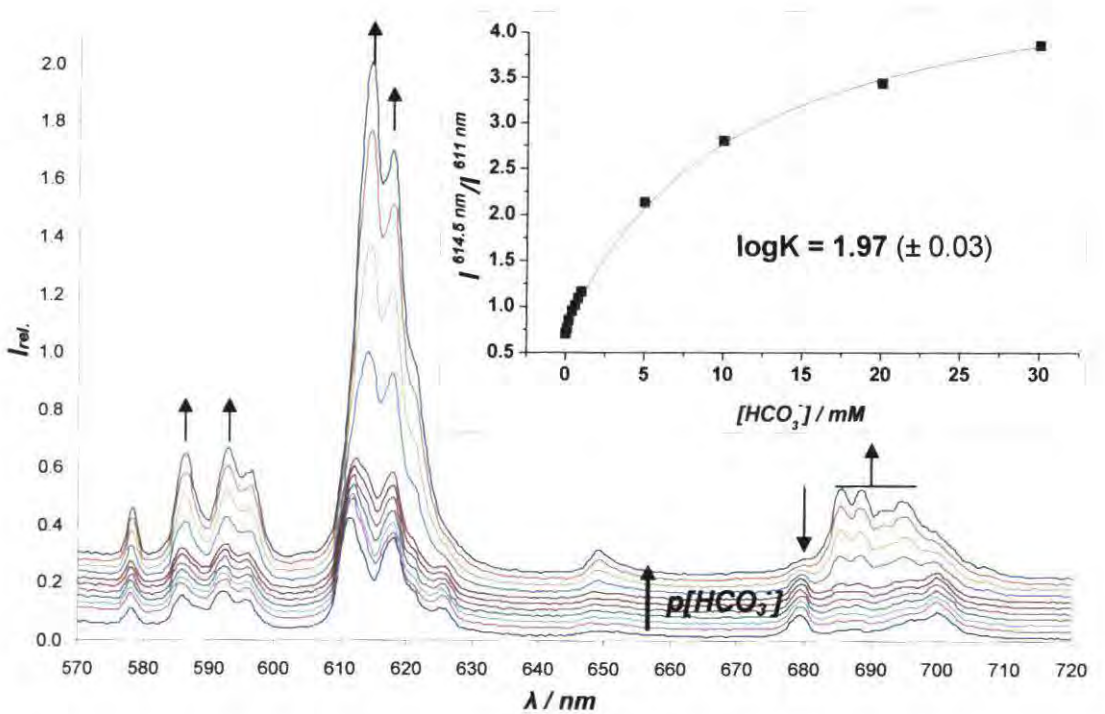

Fig. 3.24. Variation of Eu emission spectrum for Eu(MS)DCP2 following addition of sodium bicarbonate solution (pH = 7.4 (±0.05), [complex] = 20 μM, 298 K, λ_{ex} = 380 nm, I = 0.1 M NaCl). (*insert*) Intensity ratio (614.5/611 nm) *vs.* added [HCO_3^-] for determining the apparent binding constant of bicarbonate. (LV_{min}= 0.70 and LV_{max}= 4.85)

For examining the variation of Eu emission with lactate (*Fig. 3.25*), a pH of 5.5 was chosen as the influence of lactate was pronounced in acidic environment. The lactate

concentration was varied from 0 to 2.3 mM by addition of 0.1 M sodium lactate stock solution. An apparent affinity constant of logK = 3.50 ±0.06 M^{-1} was calculated using the 612.5/615 nm intensity ratio (or 680/696.5 nm (±0.2)).

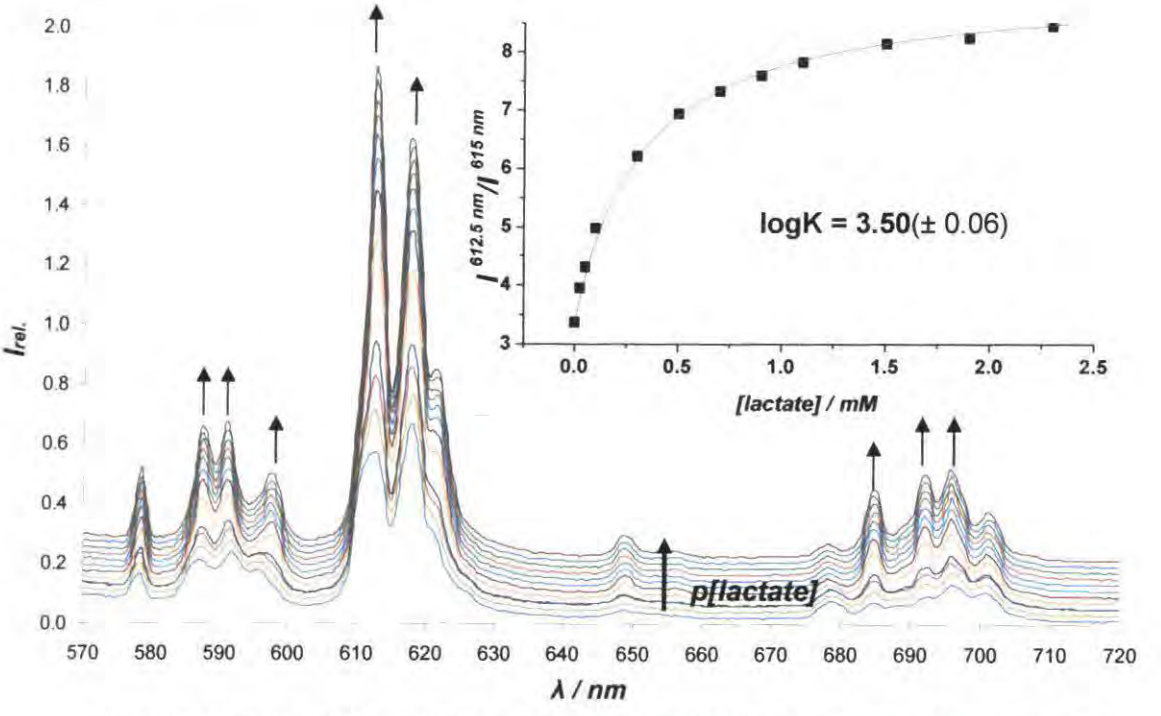

Fig. 3.25. Variation of Eu emission spectrum for Eu(MS)DCP2 following addition of sodium lactate solution (pH = 5.5 (±0.05), $C_{complex}$ = 20 μM, 298 K, λ_{ex} = 380 nm, I = 0.1 M NaCl). (*insert*) Intensity ratio (612.5/615 nm) *vs.* added [lactate] for determining the apparent binding constant of lactate. (LV_{min}= 3.37 and LV_{max}= 9.20)

As a result of high anion affinity and consequent suppression of sulfonamide ligation to the Eu(III) centre, the complex Eu(MS)DCP2 was considered to be unsuitable for the desired applications.

3.3.3 Effect of Added Anions on the Eu(MS)DGP2 Emission Spectrum

Having found that Eu(MS)DCP2 was highly sensitive towards endogenous anion binding over the desired biological pH range, bulky, negatively charged carboxylate side arms were incorporated into the structure. Using α-glutarate pendant arms, competitive intramolecular competition between α-glutarate and N-sulfonamide ligation occurred,

consequently shifting the sulfonamide pK_a to a higher value. The effect of added anions was also examined with this complex, in order to understand the effect of structural modifications on anion affinity.

Using 'anion-stew' as a background medium (*Fig. 3.26*), significant changes were observed in both intensity and structure of the Eu emission spectra as the pH was varied from 9 to 3. Here again, to understand the complex nature of these competing intermolecular (anion binding) and intramolecular (glutarate or sulfonamide ligation) processes, which determine the properties of Eu emission, luminescent pH titrations were also required using individual anion solutions.

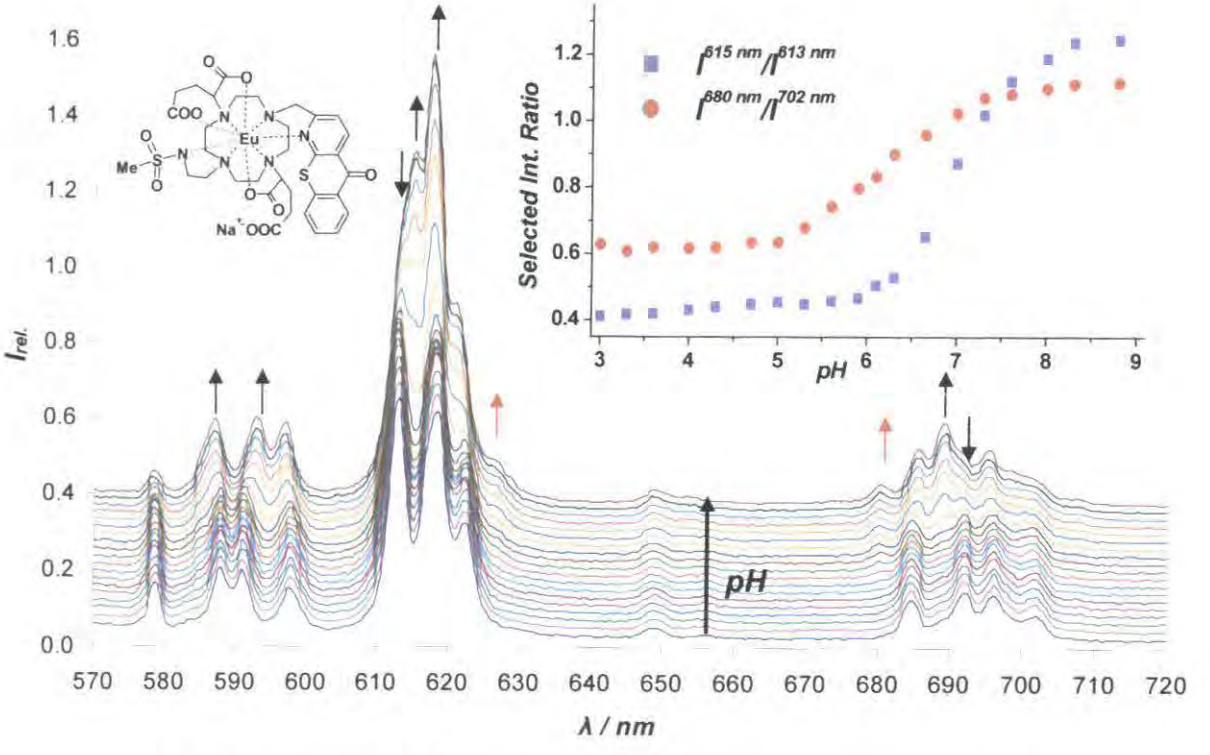

Fig. 3.26. Variation of Eu emission of Eu(MS)DGP2 with pH, using 'anion-stew' as the background medium ([complex] = 20 μM, 298 K, λ_{ex} = 380 nm, I = 0.1 M NaCl). (*insert*) Intensity ratio (■ 615/613 nm and ● 680/702nm) *vs.* pH plots, indicating the presence of different dominant Eu(MS)DCP2(anion) species at the limiting ratio.

Examining the spectral data in *Fig. 3.26,* a significant observation is the emergence of bands at 680 and 627 nm which, as previously established, are consistent with sulfonamide binding. The intensity of these peaks is not as high as in the absence of added anions (*Fig.3.11*), but their presence indicates that over the basic pH region there is a competition between sulfonamide ligation and carbonate binding. Comparing the plotted changes in the $\Delta J = 2$ (615/613 nm) and $\Delta J = 4$ (680/702 nm) manifold, it was established that an protonation constant for the N-sulfonamide bound species is shifted back to 6.3, whilst the apparent pK_a of 7.2 was estimated for the carbonate bound species. Therefore, in an attempt to interpret the selected intensity ratio (613/615 nm and 680/702 nm) *versus* pH plots, especially the different pK_a values obtained from them, it was neccessary to study each individual anion's influence on the Eu emission, to interpret this complex emission profile and hence establish the pH-dependent solution state speciation of Eu(MS)DGP2.

Using a phosphate anion solution (0.9 mM) as the background, no significant changes were observed in emission intensity and structure compared to the titration in the absence of added phosphate.

Using a 0.13 mM citrate solution as the background medium, no significant changes were observed to those observed in assessing the pH dependence of Eu emission. This may either be a result of either steric or electrostatic repulsion. Due to the relatively large size of the citrate anion, compared to other anions studied, it may not be able to coordinate to the Eu centre as a result of unfavourable steric interactions involving the carboxylic acid side-chains. On the other hand, as the pH increases citrate become multiply negatively charged, which leads to electrostatic repulsion between the anion and the negatively charged complex $[Eu(MS)DGP2]^{2-}$.

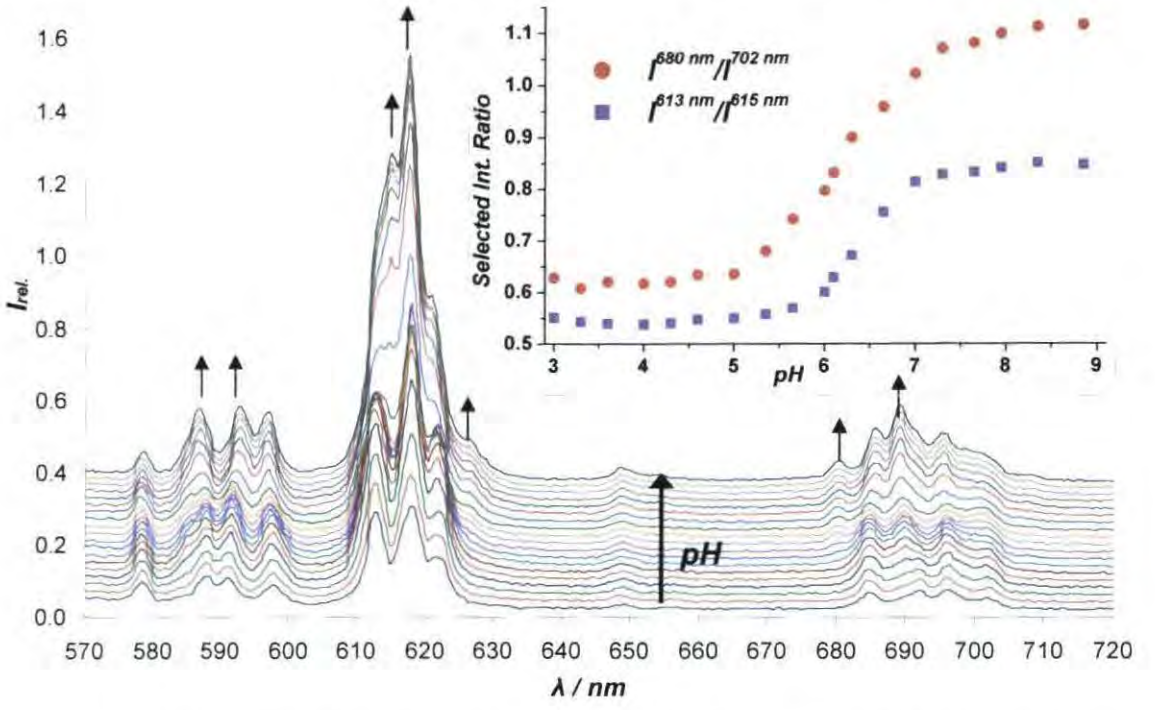

Fig. 3.27. Variation of Eu emission of Eu(MS)DGP2 with pH, using 30 mM carbonate as the background medium ([complex] = 20μM, 298 K, λ_{ex} = 380 nm, I = 0.1M NaCl). (*insert*) Intensity ratio (■ 615/613 nm and • 680/702nm) *vs.* pH plot, indicating the competition between intramolecular and intermolecular binding.

Using 30 mM $[CO_3^{2-}]_{tot}$ solution as the background, dramatic spectral changes were observed. The most significant change in the structure of the Eu emission spectra (*Fig. 3.27*) was observed above pH 6. Plotting either of the stated intensity ratios with pH gave a similar pK_a value of 6.3. As the pH rises from the acidic region (pH 3) to 4.5, the glutarate bound complex is likely to be the dominant species. As the pH is raised further, with the introduction of an excess of bicarbonate in the solution, this intramolecular chelation mode suffers competition from bicarbonate ligation. Above pH 6, the carbonate bound species begin to form and sulfonamide ligation competes with it. As a result, the previously found pK_a = 7.6 associated with intramolecular ligation was lowered to 6.3. Similar values were found when using 680/704 nm or 615/617 intensity ratios although, the numeric difference between the limiting values was not as well pronounced.

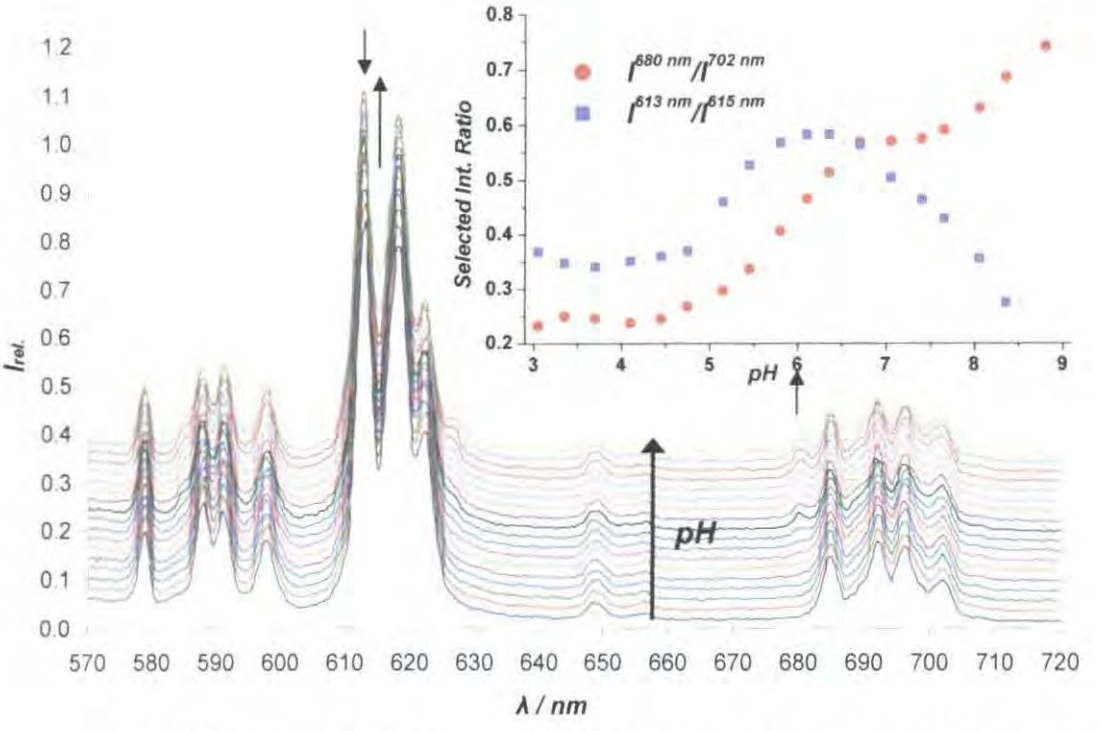

Fig. 3.28. Variation of Eu emission of Eu(MS)DGP2 with pH, using 2.3 mM lactate as the background medium ([complex] = 20 μM, 298 K, λ_{ex} = 380 nm, I = 0.1 M NaCl). (*insert*) Intensity ratio (■ 615/613 nm and • 680/702nm) *vs.* pH plot, indicating the competition between intramolecular and intermolecular binding.

Using a 2.3 mM lactate background solution very informative changes were observed (*Fig. 3.28*). Studying the intensity ratios 613/615 nm and 680/702 nm *versus* pH plots, the following conclusion can be drawn: above pH 3.5, lactate replaces the bound water molecule from the inner coordination sphere and this anion bound species dominates in solution till pH 4.5. A further increase in pH results in competition between the lactate bound species and two intramolecular ligation processes, glutarate- and sulfonamide-N binding. Above pH 6.5, the glutarate bound species starts to disappear and only the N-sulfonamide bound species competes with intermolecular lactate interference.

Having associated the complex speciation profiles in solution over the observed pH range, it is now possible to interpret the pH-dependent profiles obtained, using 'anion-stew' as the background medium (*Fig. 3.29*). The competition between intra and/or intermolecular processes complicates the speciation profile. For easier understanding the

pH-dependent speciation is presented in a tabular summary, defining the intra or/and intermolecular bound species of Eu(MS)DGP2, within the stated pH range.

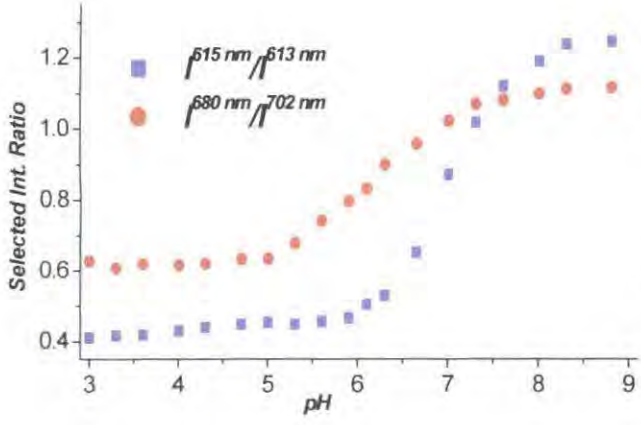

pH	H_2O	lactate	glutarate	MS[a]	HCO_3^-
3 - 3.5	X				
3.5 - 4.0	X	X			
4.0 – 5.2		X	X		
5.2 – 6.0		X	X	X	
6.0 – 7.2			X[b]	X	X
7.2 – 9.2				X[c]	X

[a] sulfonamide group; [b] possible binding; [c] reached constant concentration in solution.

Fig. 3.29. (*left*) Intensity ratio (■ 615/613 nm and ● 680/702nm) *vs.* pH plots for Eu(MS)DGP2 using 'anion-stew' as background medium. (*right*) Interpretation of the suggested binding profile, highlighting the different *inter* and *intra*molecular bound species as a function of the pH.

These studies and their consequent interpretation certainly prove that, by introducing Eu(MS)DGP2 into the mixed endogenous anion background, the protonation constant associated with sulfonamide ligation shifted back to 6.3. However, the complex nature of the Eu emission spectrum and the complex intensity ratio *versus* pH plots makes this complex unsuitable as pH probe.

In order to calculate the apparent affinity constant values for bicarbonate and lactate binding to Eu(MS)DGP2, titrations were carried out at constant pH, studying the changes in the structure of Eu emission as a function of added anion concentration.

3.3.3.1 Photophysical Response to Endogenous Anions

Luminescence titrations to determine these binding constants were carried out under the same circumstances as detailed previously (*see 3.3.2.1*). Lactate interference was studied at pH 5.5, while the effect of added bicarbonate was monitored at pH 7.5. The error of pH maintenance was established to be ±0.05.

The binding constant of lactate was determined by monitoring the Eu emission spectrum following increase in lactate concentration of the solution (*Fig. 3.30*) at a constant pH 5.5 (±0.05). The lactate range was limited to 2.3 mM. A binding constant, logK = 3.86 ±0.01 M^{-1} was calculated using changes in the intensity ratio 612.5/618 nm. Similar values were obtained (±0.3) using 612/685 nm or 612.5/621.5 nm ratios.

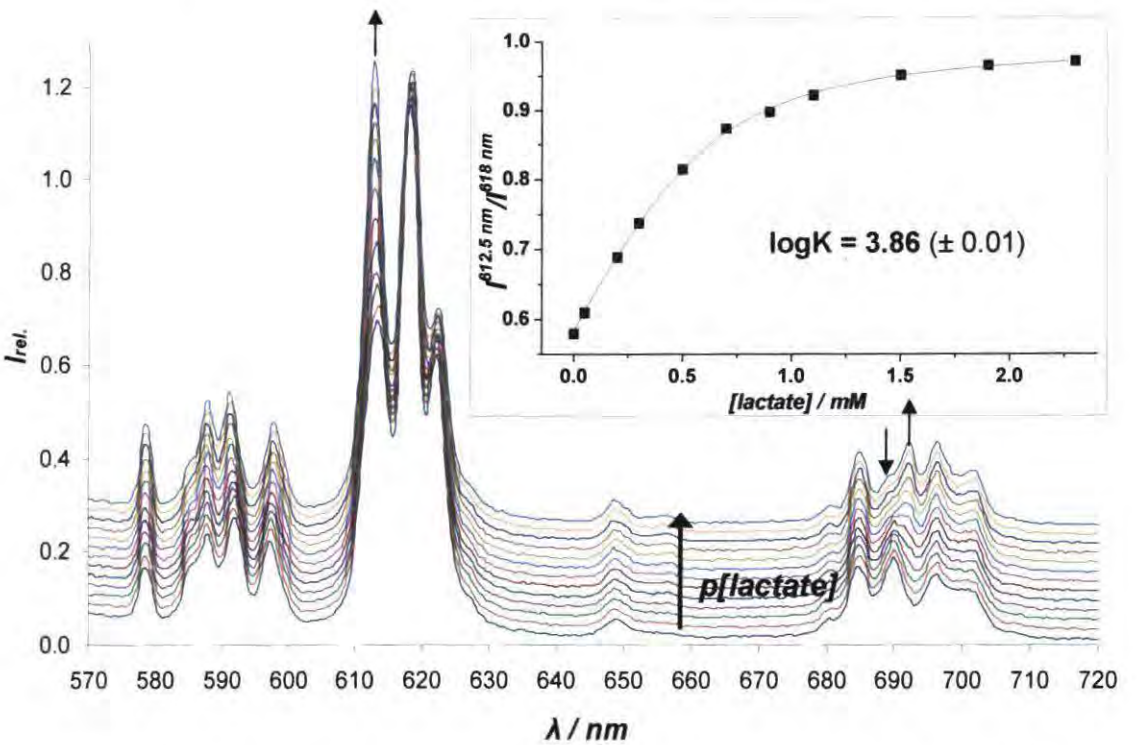

Fig. 3.30. Variation of Eu emission spectrum for Eu(MS)DGP2 following addition of sodium lactate solution (pH = 5.5 (±0.05), [complex] = 20 μM, 298 K, λ_{ex} = 380 nm, I = 0.1 M NaCl). (*insert*) Intensity ratio (612.5/618 nm) *vs.* added lactate plot, for determining the apparent binding constant. (LV_{min}= 0.58 and LV_{max}= 0.98)

A similar study was carried out to determine the apparent binding constant for bicarbonate. The bicarbonate concentration was varied from 0 to 30 mM by addition of sodium bicarbonate (0.1 and 1 M) solutions, whilst the pH was kept constant at pH 7.5 (±0.05). Variation of the Eu emission spectrum (*Fig. 3.31*) revealed carbonate binding, of similar affininty to that found with Eu(MS)DCP2. The binding constant was established to be logK = 2.15 ±0.02 M^{-1}, using the intensity ratio 615/617.5 nm. Similar values (±0.4) were calculated using 615/627.5 nm or 702/689.5 nm ratios.

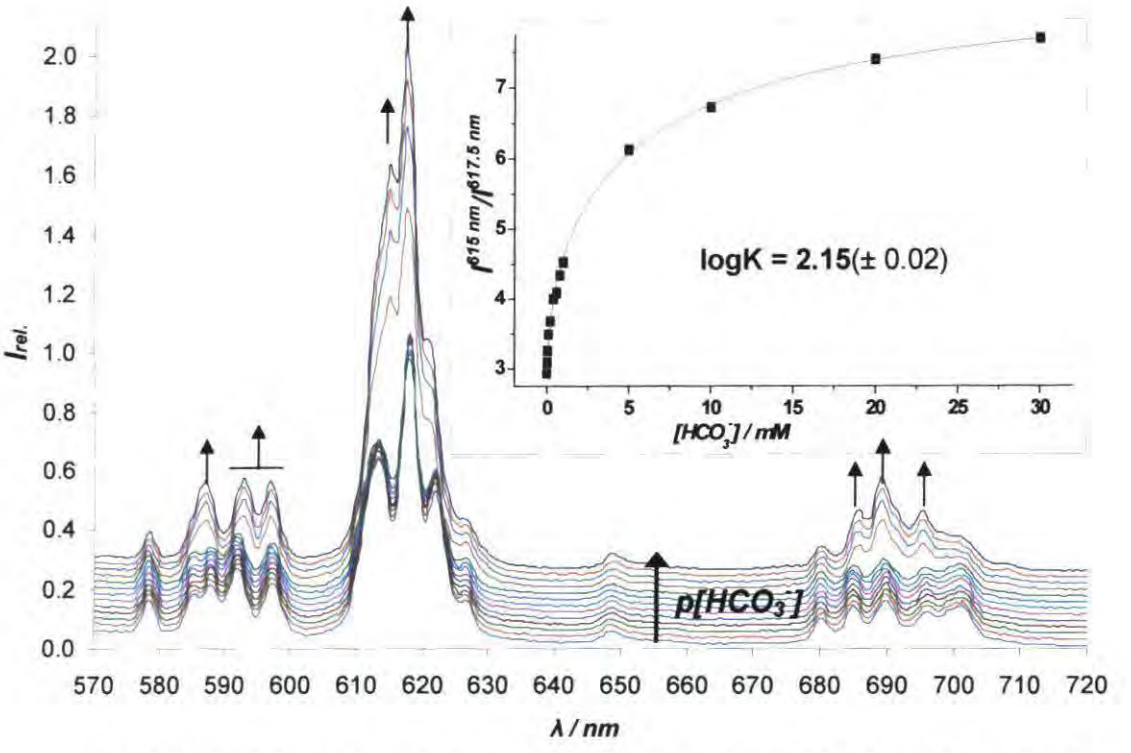

Fig. 3.31. Variation of Eu emission spectrum for Eu(MS)DGP2 following addition of sodium bicarbonate solution (pH = 7.5 (±0.05), [complex] = 20 μM, 298 K, λ_{ex} = 380 nm, I = 0.1 M NaCl). (*insert*) Intensity ratio (615/617.5 nm) *vs.* added bicarbonate plot, for determining the apparent binding constant. (LV_{min}= 2.94 and LV_{max}= 8.50)

The apparent binding constant revealed that the affinity of the given anion for Eu(MS)DGP2 is of the same order as was found for Eu(MS)DCP2. This shows that the attempt to suppress intermolecular anion binding, by introducing bulky negatively pendant arms, was only successful in obviating citrate binding. Moreover, this structural modification introduced intramolecular glutarate binding, which complicated the emission profile even further.

3.3.4 Effect of Added Anions on the Eu(MS)DAdP2 Emission Spectrum

The complex Eu(MS)DGP2 is sensitive towards endogenous anion binding over the desired biological pH range, and more importantly confirmed competitive glutarate ligation occurs to the Eu centre. Therefore, a methylene spacer was introduced to the

carboxylic side-chain and the corresponding adipate complex examined. The absence of intramolecular carboxylate ligation shifted the sulfonamide pK_a back to 6.2.

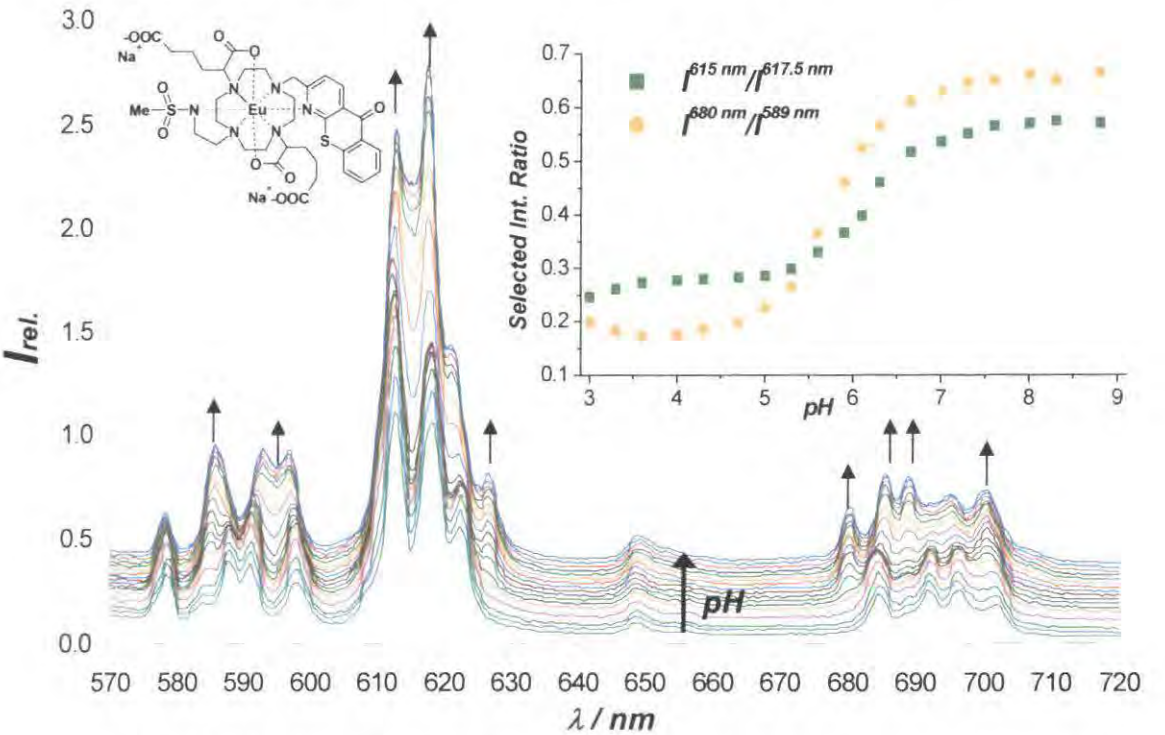

Fig. 3.32. Variation of Eu emission of Eu(MS)DAdP2 with pH, using 'anion stew' as the background medium ([complex] = 20μM, 298 K, λ_{ex} = 380 nm, I = 0.1M NaCl). (*insert*) Intensity ratio (■ 615/617.5 nm and • 680/598 nm) *vs.* pH plots, indicating the presence of differing Eu(MS)DAdP2(anion) species at the limiting ratios.

However, following introduction of Eu(MS)DAdP2 into the 'anion-stew' (*Fig. 3.32*), changes were observed in both intensity and structure of the Eu emission as the pH was varied from 9 to 3. Studying the intensity ratio 615/617.5 nm or 680/587.5 nm *versus* pH plots, it was evident that the lack of intramolecular competition from the carboxylate pendant arm tuned the pK_a for sulfonamide ligation back to 6.0 (±0.1). This value was obtained regardless of the nature of the intensity bands examined, i.e. whether using ratios involving bands associated with sulfonamide ligation (628 or 680 nm) or bands related to intermolecular anion competition. The changes observed in the $\Delta J = 2$ manifold were much more pronounced, and were used to monitor intensity ratio changes. Consequently, from the protonation constant calculation, using 'anion-stew' as background medium, and notwithstanding intermolecular binding of endogenous anions,

the complex Eu(MS)DAdP2 meets the criteria for use in measuring pH. But, in order to understand the changes thet occurred in the emission profile in detail, the influence of individual anions needed to be assessed.

Using a phosphate anion solution (0.9 mM) as the background medium, no significant changes were observed in the Eu emission spectrum, as before. Using a 0.13 mM citrate solution as the background medium, again no significant changes were observed in the Eu emission profile.

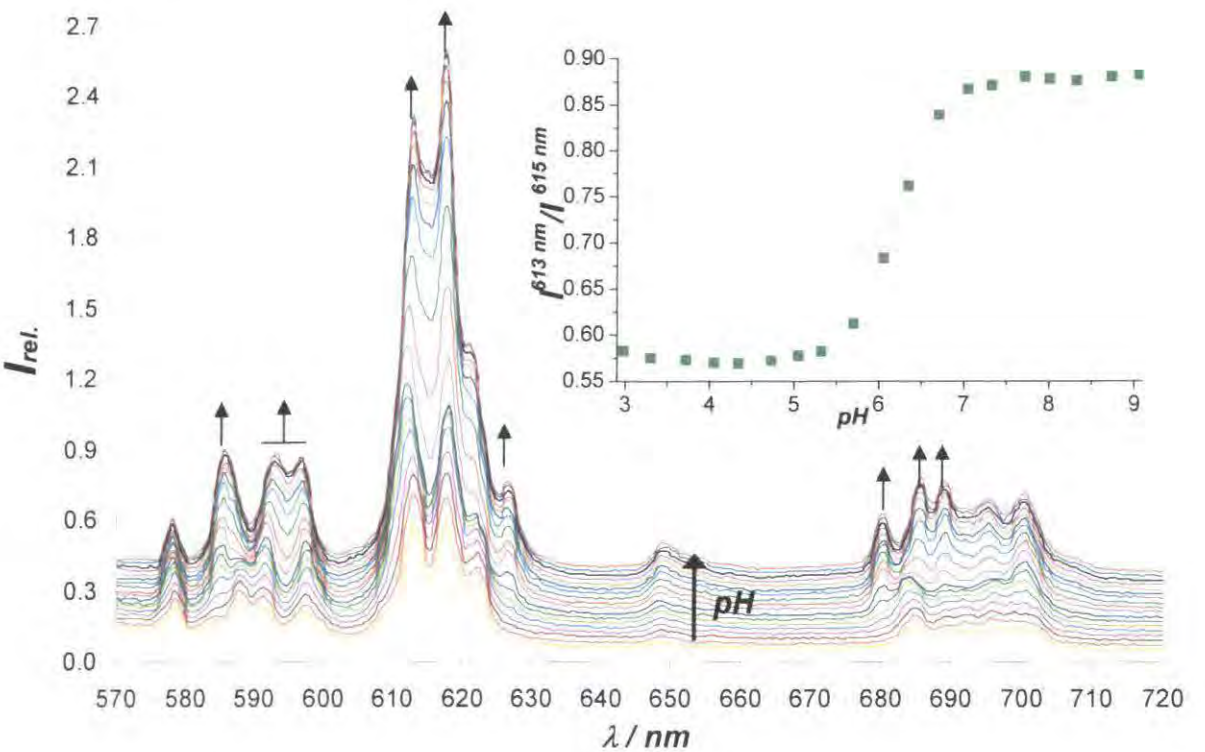

Fig. 3.33. Variation of Eu emission of Eu(MS)DAdP2 with pH, using 30 mM carbonate as the background medium ([complex] = 20 μM, 298 K, λ_{ex} = 380 nm, I = 0.1 M NaCl). (*insert*) Intensity ratio (613/615 nm) *vs.* pH plot, indicating the competition between intramolecular sulfonamide and intermolecular carbonate binding.

Using 30 mM $[CO_3^{2-}]_{tot}$ solution as the background medium, similar spectral changes were observed to those found with 'anion stew'. The most significant change in the structure of the Eu emission spectra (*Fig. 3.33*) was observed above pH 6. Plotting the intensity ratio (613/615 nm) *versus* pH, a pK_a = 6.3 was estimated. This value is similar to that determined in similar studies with Eu(MS)DGP3, based on intensity ratio changes

linked to sulfonamide ligation. This suggests that, as the pH is raised above 6, competitive bicarbonate binding occurs. Similar observations were found when using 680/589 nm or 615/617 nm intensity ratio *versus* pH plots.

Using a 2.3 mM lactate background solution very informative changes were also observed (*Fig. 3.34*). Examining the variation of the intensity ratio 612.5/622.5 nm as a function of pH, it was evident that from pH 3.5 the species Eu(MS)DAdP2(lactate) was dominant. Increasing the pH further resulted in the appearance of the sulfonamide arm bound complex, confirming a competition between intermolecular lactate and intramolecular N-sulfonamide ligation, increasing the 'sulfonamide nitrogen' pK_a to 6.3. Similar values were calculated (±0.1) using different intensity ratios selected from the $\Delta J = 2$ and $\Delta J = 4$ manifold.

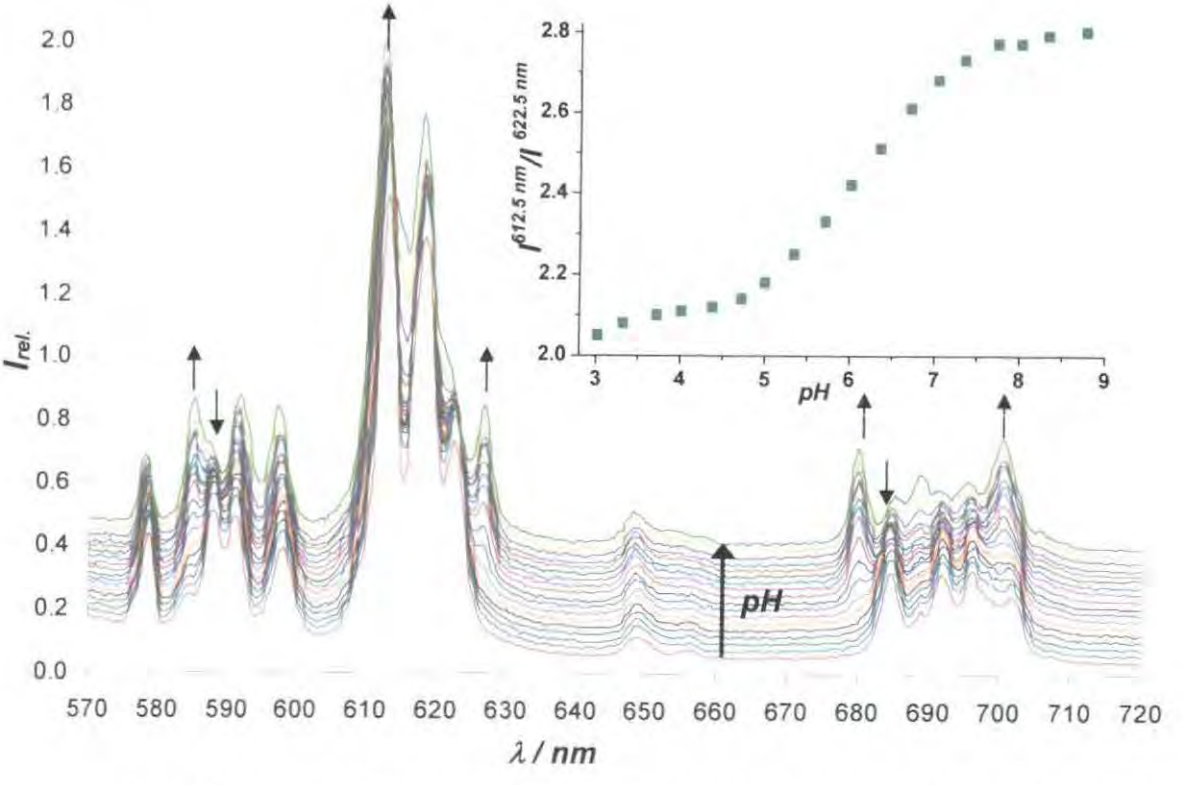

Fig. 3.34. Variation of Eu emission of Eu(MS)DAdP2 with pH, using 2.3 mM sodium lactate as the background medium ([complex] = 20 μM, 298 K, λ_{ex} = 380 nm, I = 0.1 M NaCl). (*insert*) Intensity ratio 612.5/622.5 nm *vs.* pH plot, indicating the competition between intramolecular and intermolecular binding.

Having assigned the pH ranges over which competition of a given anion takes place, it was possible to interpret the intensity ratio *versus* pH plots using 'anion-stew' as the background medium (*Fig. 3.32*). In the acidic pH régime above pH 3.5, lactate binds to the Eu centre. As the pH reaches 5.5 reversible intramolecular sulfonamide ligation competes with this lactate bound species. However, as the pH was increased from 6 to 8, intermolecular carbonate binding also occur. As a consequence of the competition between these three species in solution, the apparent protonation constant of the sulfonamide nitrogen species was established to be 6.1. Such a value is highly satisfactory for measuring pH over the desired 5.5 to 7.5 pH region.

3.3.4.1 Photophysical Response to Endogenous Anions

In order to calculate the apparent affinity constants for binding bicarbonate and lactate to Eu(MS)DAdP2, titrations were carried out again at constant pH. Titrations to determine these binding constants were carried out under the same conditions as detailed previously. Lactate interference was studied at pH 5.5, while the effect of added bicarbonate was monitored at pH 7.5 (±0.05).

An apparent binding constant of logK = 4.09 ±0.03 M^{-1} was calculated observing the variation of the intensity ratio 612.5/618.5 nm with added lactate concentration (*Fig. 3.35 top*). Similar values can be obtained (±0.4) using 612.5/680 nm or 612.5/622.5 nm intensity ratios.

A similar study was carried out to estimate the apparent binding constant for bicarbonate binding. Bicarbonate concentration was varied from 0 to 30 mM maintaining the pH at 7.5 (±0.05). Changes in the Eu emission spectrum (*Fig. 3.35 bottom*) revealed the same degree of carbonate affinity, as was found previously for Eu(MS)DCP2 and Eu(MS)DGP2. The biding constant was found to be logK = 2.15 ±0.02 M^{-1}, using the intensity ratio 612/617.5 nm.

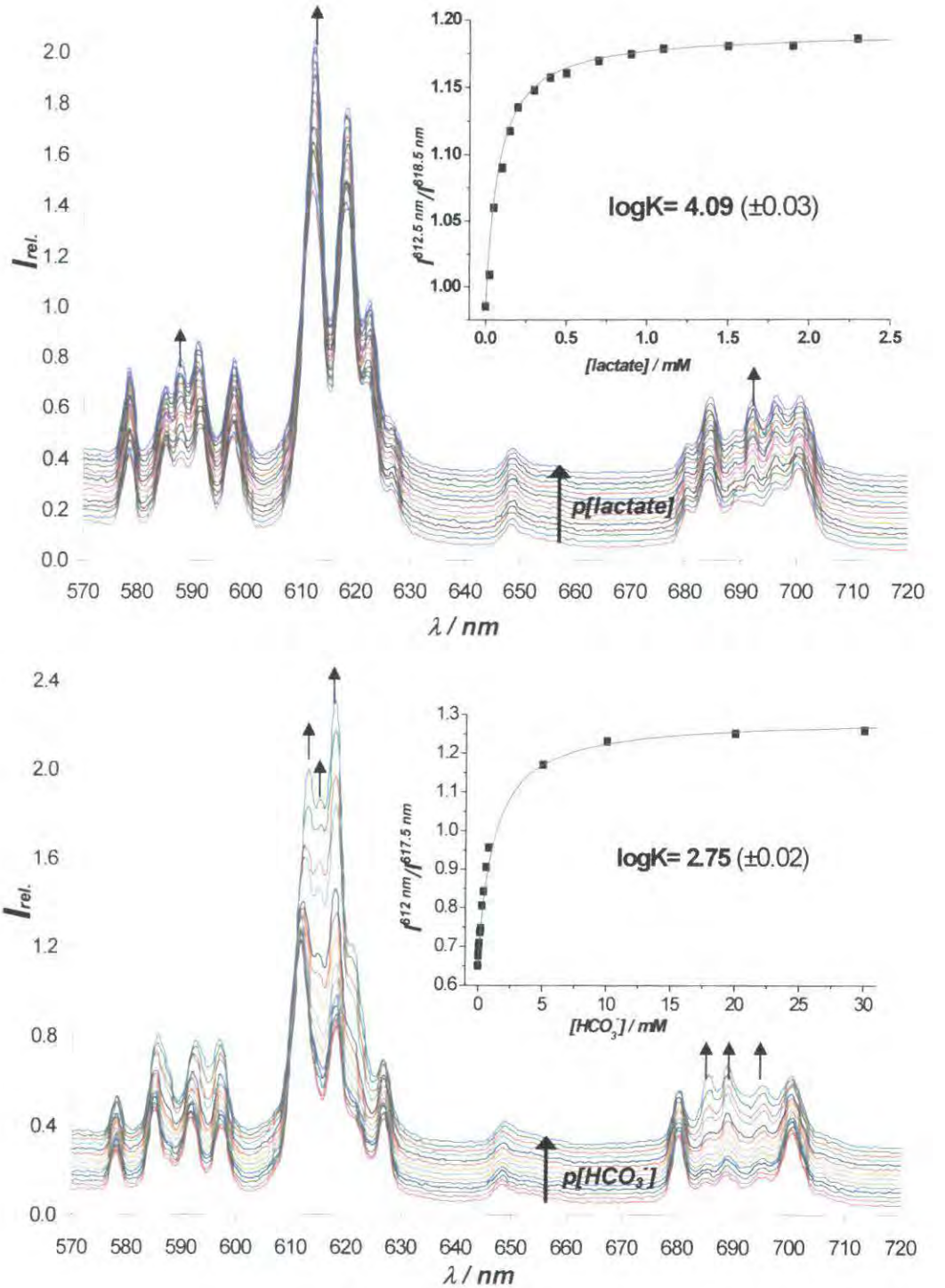

Fig. 3.35. Change in the form of Eu emission spectrum for Eu(MS)DAdP2 (*top*) as a function of added sodium lactate solution (pH = 5.5 (±0.05)), with intensity ratio (612.5/618.5 nm) vs. added lactate plot, for determining the apparent binding constant; (*bottom*) as a function of added sodium bicarbonate solution (pH = 7.5 (±0.05)), with intensity ratio (612/617.5 nm) *vs.* added bicarbonate plot, for determining the apparent binding constant ([complex] = 20 μM, 298 K, λ_{ex} = 380 nm, I = 0.1 M NaCl, LV_{min}= 0.98 and LV_{max}= 1.18 (*top*), LV_{min}= 0.65 and LV_{max}= 1.26 (*bottom*)).

A summary of anion binding constants and the protonation constants for the 3 complexes examined in given below (*Fig. 3.36*). Despite the fact that the complex Eu(MS)DAdP2 still exhibits some sensitivity towards anion binding, this thorough examination proved that it can be used for the desired application as a ratiometric pH probe measuring pH over the desired biological region.

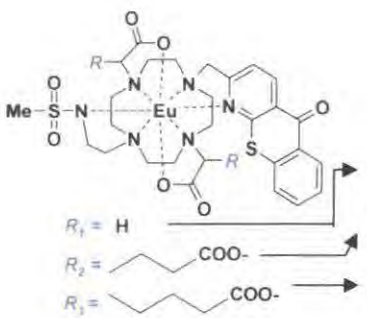

$\log K_{EuLX}$	lactate (pH = 5.5)	bicarbonate (pH = 7.4)	citrate[a] (pH = 7.4)	sulfonamide pK_a (±0.1)
Eu(MS)DCP2	3.50 (±0.06)	1.97 (±0.03)	4.59 (±0.05)[b]	6.1
Eu(MS)DGP2	3.86 (±0.01)	2.15 (±0.02)	<1	7.6
Eu(MS)DAdP2	4.09 (±0.08)	2.75 (±0.02)	<1	6.2

Fig. 3.36. (*left*) Sturcture of studied pH-probes. (*right*) Summary of $\log K_{EuLX}$ [M^{-1}] and pK_a values (298 K, I = 0.1 M NaCl). [a]Over the pH range 3.3 to 8.0 in the presence of 2 mM sodium citrate, no evidence for citrate binding was found for Eu(MS)DGP2 and Eu(MS)DAdP2, and only spectral changes associated with the sulphonamide N-ligation or (for Eu(MS)DGP2) intramolecular coordination of the terminal glutarate carboxylate group was observed. [b]$\log K_{pH=6.5}$ = 4.73 (±0.03).

3.4 Quenching Studies with Eu(MS)DAdP2

The complex Eu(MS)DAdP2 was found to be appropriate as a pH probe, in mixed endogenous anion solution. Therefore it was essential to study its susceptibility to quenching of the Eu(III) excited state by biologically common electron rich donors, such as urate and ascrorbate. As found previously with several complexes bearing azaxanthone and tetraazatriphenylene chromophores,[39] the introduction of these low molecular weight reductants may cause a significant decrease in both emission intensity and lifetime. The driving force for this charge transfer process is the free energy of the excited state of the lanthanide ion (ΔG_{Eu} = 2.06 eV).

Prior to any potentiometric studies, a titration was undertaken to see whether the introduction of urate and/or ascorbate had any effect on the complex emission properties. This was executed by the method applied to determine the apparent binding constants for common oxy-anions. A constant pH = 7.4 (±0.05) was maintained and changes in the Eu

emission were monitored following addition of a 0.1 M sodium ascorbate stock solution. The addition of sodium urate was carried out by addition of solid uric acid prior to pH adjustment of the solution, as a result of its low water solubility.

Addition up to 1 mM concentrations of ascorbate and urate neither perturbed the intensity of the emission spectrum nor changed the measured radiative lifetimes. Consequently, this complex and its chromophore do not suffer from excited state quenching, which is an advantage for their applications. Further quenching studies were not carried out.

3.5 Effect of Added Protein on the Eu(MS)DAdP2 Emission Profile

The complex Eu(MS)DAdP2 was synthesised to measure intra or extracellular pH. It showed sensitivity towards some endogenous anion binding. Despite this, intensity ratio *versus* pH plots showed it can be used for the desired purpose. However, biological fluids and living organisms are complex environments; major components are protein of different molecular weight. Therefore, it was essential to study the effect of added protein onto the Eu emission spectrum. Such a study was carried out using Human Serum Albumin (HSA).

Human serum albumin is a 66.6 kDa weight monomeric protein (*Fig. 3.37 insert*); it possesses a complex conformation with a sequence containing 585 amino acids. It is the most abundant protein in human blood plasma (30 – 50 g/L), comprising more than half of the blood serum protein. It is produced in the liver and is associated with several important transport functions (e.g. thyroid hormones, fatty acids, bilirubin and a vast number of drugs), as well as pH buffer and reversible Ca^{2+} binding functions. An important feature of its structure is a well defined binding pocket, or 'cleft' with five binding sites of different affinities (IB, IIA, IIA-IIB, IIIA, IIIB), comprising different amino acid sequences.[40] This cleft is suitable for binding or interacting with the aromatic moiety in complexes, such as the 2-methyl-azathioxnahtone chromophore in Eu(MS)DAdP2.

Luminescence titrations were carried out in order to study the effect of protein using the simulated extracellular anion mixture, with 0.7 mM human serum albumin added (*Fig. 3.37*) to the background medium.

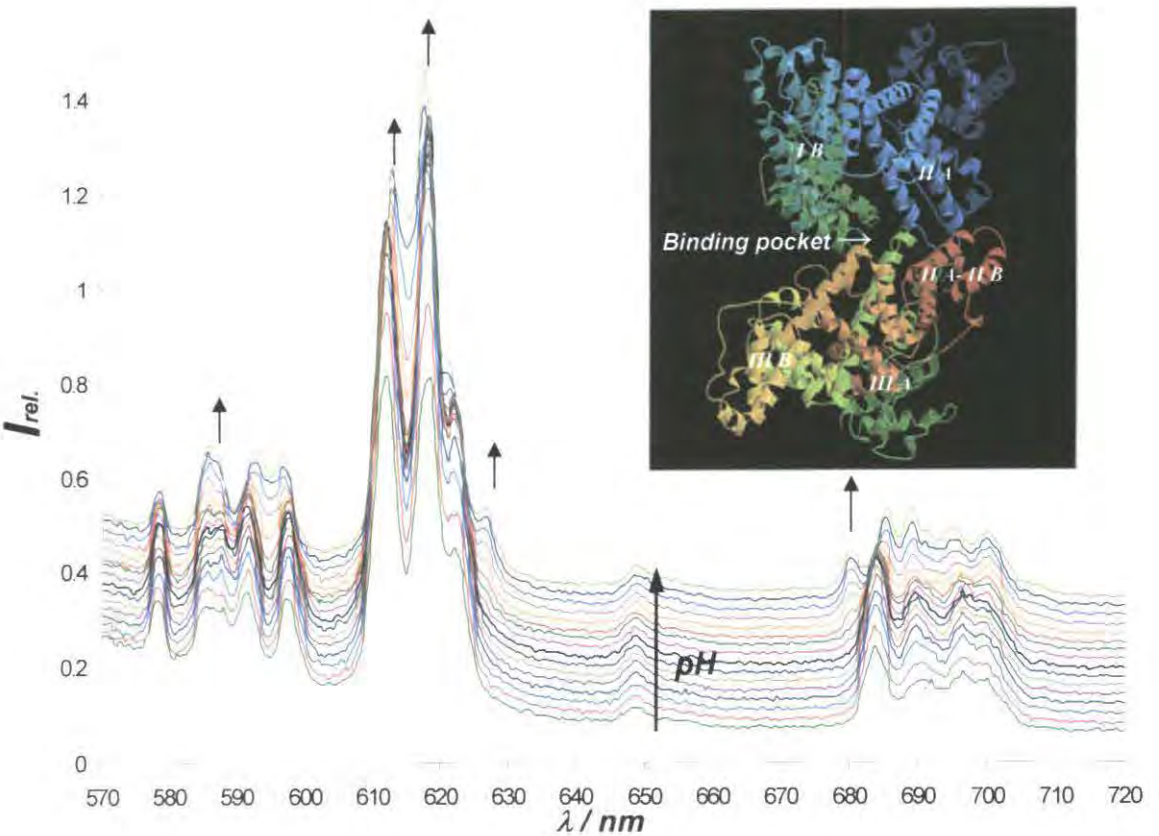

Fig. 3.37. Variation of Eu emission of Eu(MS)DAdP2 with pH, using a simulated extracellular anion mixture, with 0.7 mM HSA added ([complex] = 20μM, 298 K, λ_{ex} = 380 nm, I = 0.1M NaCl). (*insert*) Schematic structure, and conformation of HSA showing the highest affinity dinging sites for aromatic substrates.[40]

The same spectral changes were observed as the pH was decreased from 8.5 to 3, as was found, using purely 'anion-stew' as background. The titration was repeated using modified 'anion-stew', containing 5 mM bicarbonate with 0.7 mM HSA added, and simply 0.7 mM HSA as the background medium, with a similar outcome. The pK_a of the sulfonamide group was estimated to be 7.2 (±0.1) in each case (*Fig. 3.38*). Evidently, the value is raised, presumably a result of a protein-complex interaction. A similar pH dependent sulfonamide ligation profile was apparent in the pH range of 6 to 8 using reconstituted 100% human serum solution as the background medium, or using different intensity ratios to analyse the data, such as 615/618nm, 615/622 nm or 627.5/589 nm.

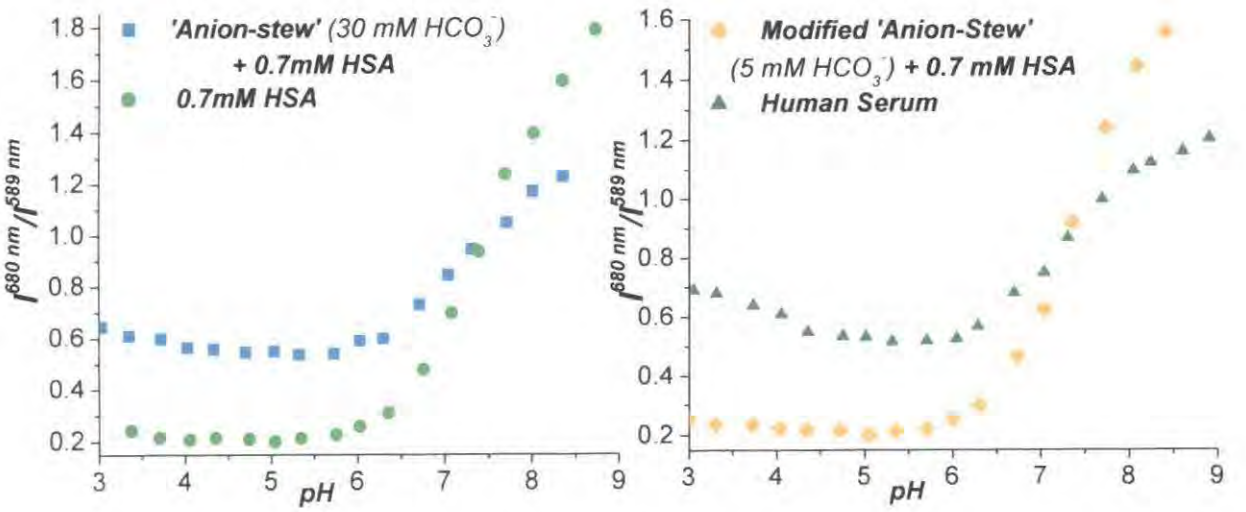

Fig. 3.38. Intensity ratio (680/684 nm) *versus* pH plot for Eu(MS)DAdP2 using different media each containing 0.7 mM HSA ([complex] = 20 μM, 298 K, λ_{ex} = 380 nm, I = 0.1 M NaCl).

Not only the protonation constant was altered upon protein binding, but also a significant 50 % increase was observed in the radiative lifetime at pH 7.4. A large 14 % (100%) increase in quantum yield was recorded. This may be attributed to the fact that upon complex binding in the protein cleft, the aryl chromophomre and Eu centre are more shielded from vibrational deactivation. As a result, the energy transfer between chromophore and the lanthanide excited state may also become more efficient.

An attempt was made to demonstrate the applicability of Eu(MS)DAdP2 for pH measurement. Spectroscopic analysis can be used when an extracellular pH determination is required, simply by obtaining a small volume of such fluid and measuring the selected emission intensity ratio of the sample. This analysis requires a high resolution spectrofluorimeter and an appropriate pH calibration curve for the complex in the relevant medium. However, for *in cellulo* applications a different approach is required. One such application, involves the use of a powerful fluorescence microscope, with suitable excitation wavelength and emission filters for observing the total Eu emission and the ligand fluorescence. More importantly, for pH measurements, filters dedicated to individual ΔJ manifolds are required. Therefore with the incorporation of a fibre optic into the microscope setup, measuring different 'areas' of the Eu emission can be achieved for a selected cell or cell compartment, where the complex localises. Consequently,

instead of measuring selected peak intensity ratios, selected 'area' ratios of the Eu emission can be plotted as a function of pH. This analysis requires that the ratio of the integrated changes in a selected manifold will be proportionate to the changes of its consistent bands. The calibration curve obtained (*Fig. 3.38 insert*) used the selected area ratio ($1/\Delta J = 2$) / ($\Delta J = 4$) manifolds (i.e. [1/618-628nm]/678-689nm) (*Fig. 3.39*). With this in mind, the application of Eu(MS)DAdP2 as a luminescence pH probe using fluorescence microscopy seems to be promising.

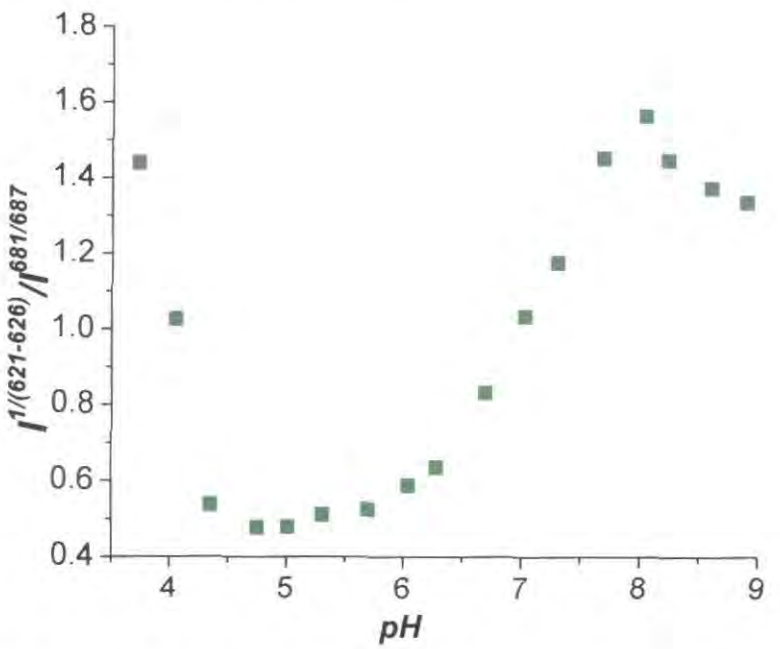

Fig. 3.39. 'Area' ratio (1/618-628nm)/678-689nm *versus* pH plot for Eu(MS)DAdP2 using reconstituted human serum solution ([complex] = 20 μM, 298 K, λ_{ex} = 380 nm, I = 0.1 M NaCl).

3.5.1 Photophysical Response to Protein (HSA)

Further studies of the effect of added protein on complex luminescence needed to be investigated. Therefore, titrations were carried out using either 'anion-stew' or water as the background medium at a constant pH 7.4 (±0.05), monitoring the changes in both ligand fluorescence (440 nm) and Eu emission (570 – 720 nm) (*Fig. 3.40*) as a function of added protein concentration. These titrations were carried out by adding HSA as a lyophilised solid to the complex solution.

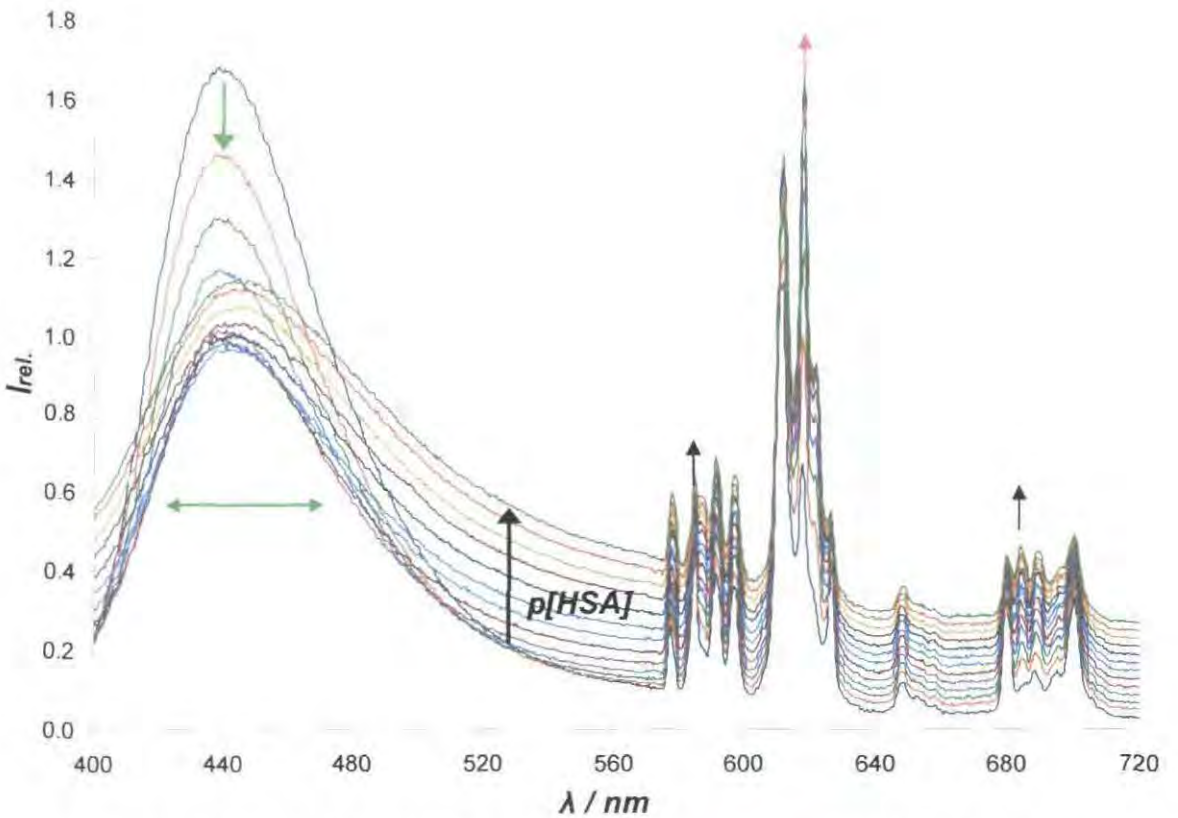

Fig. 3.40. Changes in the form of ligand fluorescence (400 - 570 nm) and Eu emission (570 - 720 nm) for Eu(MS)DAdP2 *as a function of* [HSA] *in* water (pH = 7.4 (±0.05), [complex] = 20 μM, 298 K, λ_{ex} = 380 nm, I = 0.1 M NaCl), varying the protein concentration form 0 to 0.75 mM.

During each of these titrations, significant structural changes in the Eu emission were not observed. Therefore, the concept of direct binding of any of the proteins functional groups to the Eu centre can be eliminated. Interestingly, with increasing protein concentration *in solution the ratio of ligand fluorescence versus* Eu emission intensity, did change significantly. This change involved a significant decrease in the ligand fluorescence at 440 nm following addition of HSA. This may be attributed to quenching of the chromophore fluorescence (S_1 state) by electron transfer involving the aromatic groups in HSA. However, the protein affinity of Eu(MS)DAdP2 can be described by an apparent binding constant. Values for logK = 4.46 ±0.03 M^{-1} and 4.21 ±0.02 M^{-1} were calculated from the selected intensity ratio 440/612 nm *versus* [HSA] plot, for 'anion-stew' and water (*Fig. 3.41*) as background, respectively. Although

changes in the Eu emission spectra were not well defined, a similar value (±0.05) was calculated from the minor changes that occured in the $\Delta J = 2$ manifold.

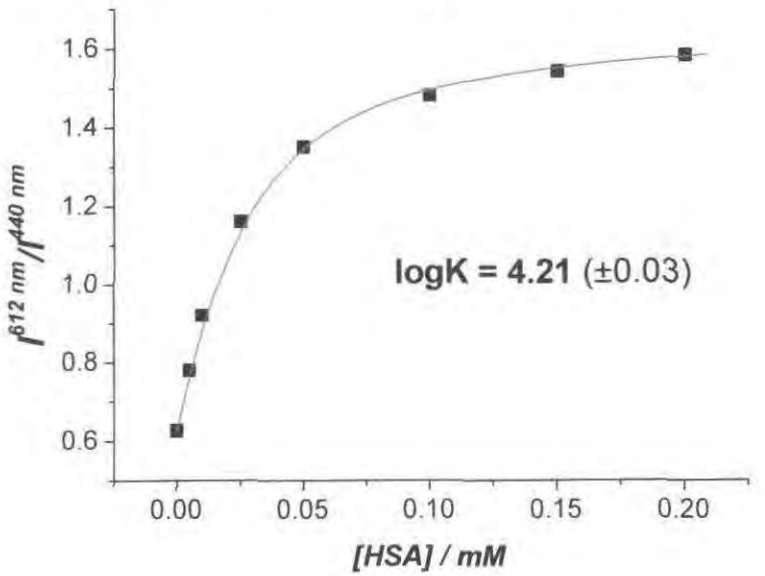

Fig. 3.41. Determination of the apparent binding constant for interaction of Eu(MS)DAdP2 with HSA in water, from selected intensity ratio (612/440 nm) *versus* added HSA plot for a 1:1 binding model (pH = 7.4 (±0.05), [complex] = 20 μM, 298 K, λ_{ex} = 380 nm, I = 0.1 M NaCl, LV_{min} = 0.60 and LV_{max} = 1.60).

3.5.1.1 Analysis of Protein Binding Using Gd(MS)DAdP2

To confirm the reversible protein binding interaction, relaxivity titrations were carried out, monitoring the relaxivity change as a function of pH for Gd(MS)DAdP2 with constant 0.7 mM HSA, in water (*Fig. 3.42. left*) or in 'anion-stew'. The apparent protein binding constant was estimated by titration with [HSA] at constant pH 7.4 (±0.05) both in water, and in 'anion-stew' (*Fig. 3.42. right*).

The relaxivity of Gd(MS)DAdP2 in the presence of 0.7 mM HSA in water, was measured to be 3.1 $mM^{-1}s^{-1}$ at pH 3 (37 °C, 60 mHz). Increasing the pH to 7.5 caused the relaxivity to rise to 14.2 $mM^{-1}s^{-1}$. Further increases in pH caused no significant relaxivity change. The inverse experiment (pH 9 to 3) gave the same result with ±5 % fluctuation of the observed relaxivity vaules. Repetition of this study, using mixed extracellular anion solution as background, did not alter the values obtained significantly (±7 %). Taken together, this behaviour is consistent with reversible binding of the complex to the protein

as suggested by the luminescence experiments. The relaxivity titration at constant pH (7.4), monitoring the change as a function of added HSA gave a similar value, logK = 4.14 ±0.07 M^{-1} (logK = 4.22 ±0.05 M^{-1} using 'anion-stew' as background) for the protein binding constant (logK = 4.21 ±0.03 M^{-1} by luminescence titration).

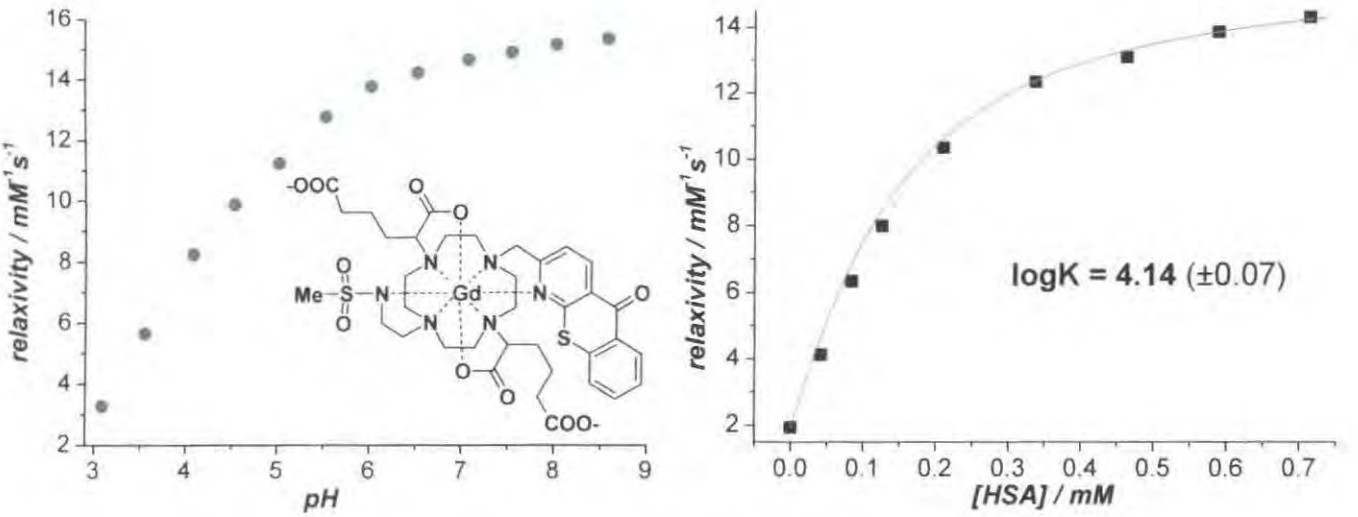

Fig. 3.42. (*left*) Variation of the relaxivity of Gd(MS)DAdP2 with pH in the presence of 0.7mM HSA in water. (*right*) Plot of the change in relaxivity with added protein concentration showing a fit for a 1:1 binding model at pH 7.4 ([complex] = 90 μM, 310 K, 60 mHz, I = 0.1 M NaCl, LV_{min} = 1.93 and LV_{max} = 16.00).

These studies prove that whilst the complex Eu(MS)DAdP2 does exhibit sensitivity towards anion and protein binding, it can be used for the desired application as a ratiometric pH probe, within the desired biological pH range 6 to 8.[41]

3.6 'In cellulo' Studies

The cellular uptake profile of the complex Eu(MS)DAdP2 was examined in mouse embryonic fibroblast (NIH 3T3) cells, which were grown in a monolayer on 0.1 mm thick glass cover slips. Incubation times varied from 1 to 24 h, while two different complex concentrations were loaded onto the cells (50 and 100 μM) by dissolving lyophilised complex in Dulbecco's Modified Eagle Medium (DMEM) containing 10% NCS (Newborn Calf Serum) and 1% Penicillin-streptomycin. Prior to mounting of the cells without any additional treatment, incubation was carried out for each individual time

point in a copper jacketed incubator using 5% CO_2 and about 10% relative humidity. Cover slips were mounted, by withdrawal of the growth medium, subsequent washing with phosphate buffered saline (PBS) solution (x3) followed by sealing them around the edge onto the 1 mm thick microscope slide. The uptake and distribution of the complex within the cell was observed by fluorescence microscopy, following excitation of the chromophore.

Epifluorescence images were taken on a Zeiss Axiovert 200M epifluorescence microscope with objectives 63x/1.40 oil DIC and 40x/1.40 oil DIC respectively, equipped with an Axiocam CCD camera. For excitation a 340 - 390 nm (90% transmission) band-pass (BP) filter was used. Ligand fluorescence were observed using a 445 - 465 nm band-pass filter (80% transmission), while Eu emission was observed using a 570 nm long-pass (LP) filter (85% transmission).

Confocal microscopy images were taken on a Zeiss LSM 500 META confocal microscope using a BIORad 405 nm diode laser for excitation. An LP 590 nm emission filter was used for observing europium luminescence and a BP 505 - 550 filter to allow ligand fluorescence to be observed.

3.6.1 Cellular Uptake Study

As shown on *Fig. 3.43*, incubation of NIH 3T3 cells with Eu(MS)DAdP2 resulted in fluorescence that could be readily detected. For each time point (2, 4, 6, 8, 10, 12, 24 h), epifluorescence and confocal images were recorded; the former images were taken immediately, whilst confocal images were recorded in each case after the 24 h time point. When optical sections through the cells were taken, the fluorescence could be detected in each layer. This confirms that the complex has been successfully taken up into the cells, and was not merely associating with the cell membrane. As a control, untreated cells were mounted and they showed no fluorescence in each of the observed wavelength regions. While only one set of images for each time point is shown here, images were taken at a number of points across the slide, with a similar localisation profile observed at each position. Epifluorescence images will not be presented here, as they revealed a similar localisation profile, but due to the instrumental differentiation, these images possess lower resolution.

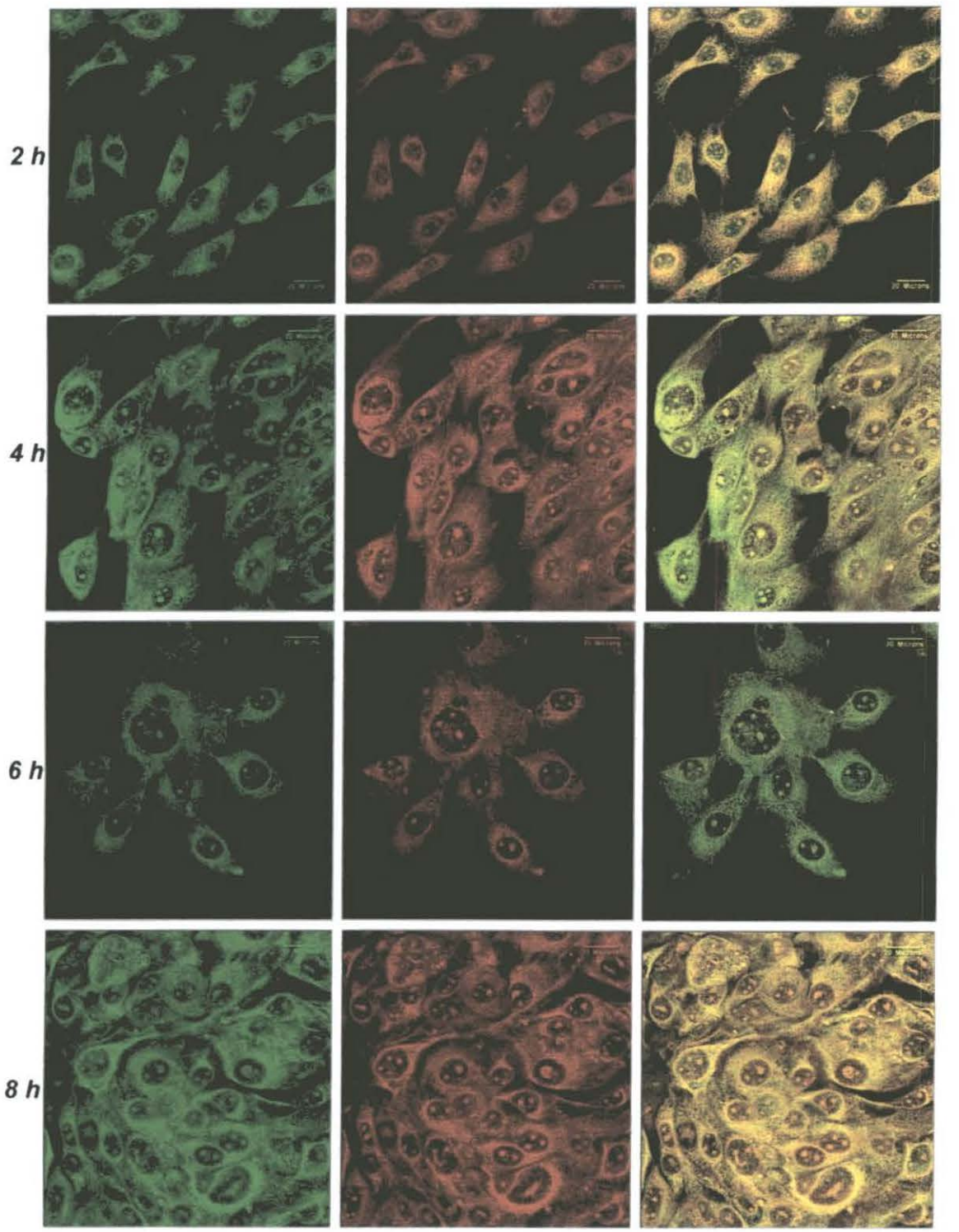

Fig. 3.43. Confocal microscopy images at different loading time points, showing the localisation and cellular uptake of Eu(MS)DAdP2 ([complex] = 100 μM, 405 nm diode laser excitation) (*left*) Ligand fluorescence was observed using a BP 505 - 550 filter, (*centre*) Eu emission was observed using LP 590 nm filter; (*right*) merged images (using ImageJ™ software).

Two different loading concentrations were applied 50 μM and 100 μM. Each provided bright images, with no significant concentration dependence in image quality and more importantly, localisation profile. Images recorded at 30 min and 1 h showed similar localisation profiles, with less overall fluorescence intensity. Therefore, long acquisition times were required, which led to some image distortion. No time dependence for both ligand and Eu emission intensity was observed in the 2 to 12 h loading period, and neither were significant changes observed in complex localisation. This effect was studied, by comparing the acquisition time of constant overall brightness of each recorded image containing a constant number of cells and as a function of complex loading time. The colour consistency of the merged images proves that the complex remains inert and no evidence for complex dissociation was apparent within the cells; i.e. separate ligand fluorescence was not observed.

By analysing each image recorded, there appears to be complex localisation in the nucleolus, with possible localisation in other organelles in the cytoplasm. The appearance of these organelles is most consistent with the size and distribution of ribosomes. As the images revealed a more intense fluorescence around the nuclear membrane, it is also possible that there is some degree of perinuclear localisation. However, the light intensity of the nucleoli was found to be 2.8 times higher (using AXInt™ intensity analysing software) than that in the cytoplasm and 1.5 times higher than in the nuclear membrane (*Fig. 3.44*). This intensity differentiation permits the acquisition of an exclusive image of the nucleolus by adjusting the excitation intensity or the gain of the microscope (acquisition time).

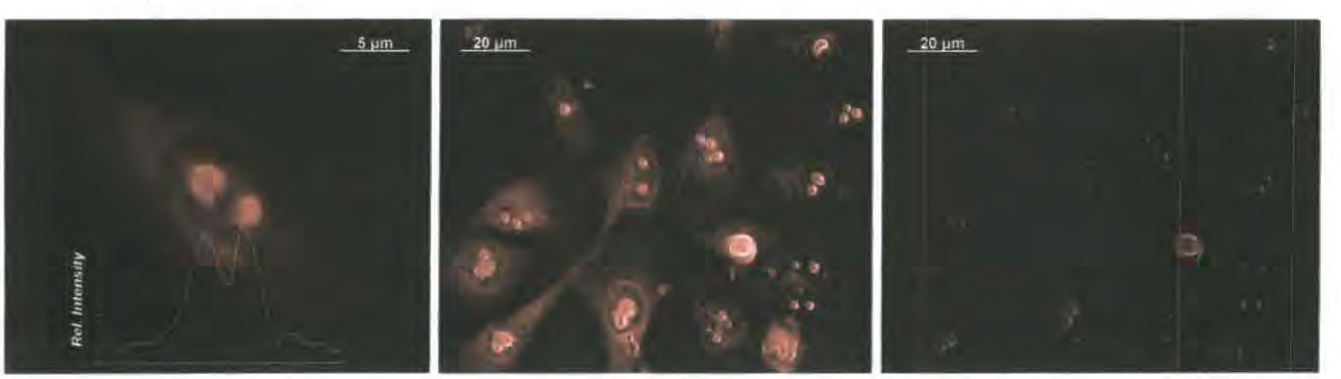

Fig. 3.44. Fluorescent microscopy images of Eu(MS)DAdP2 ([complex] = 100 μM, λ_{ex}= BP 340 - 390 nm, λ_{em} = LP 570 nm) in NIH 3T3 cells. (*left*) Eu emission of a cell with light intensity integration (*middle*) Image of a population using 710 ms and (*right*) 54 ms acquisition time.

The number of nucleoli in the cell depends on its mitotic stage and its health status. The nucleolus is visible before mitosis (interphase), dissolves at prophase, and then becomes discernible again at telophase.[42] As is evident from the images, almost every cell examined has more than two nucleoli. This is consistent with the fact that NIH 3T3 cells, like more malignant cells, possess a higher nucleolus number, a feature which is related to their cell proliferative activity[43]

This hypothesis for localisation was based on similar observations, with EuDPP2, another europium complex that possesses this particular coordinating sensitising moiety (*Fig. 3.45*).[44] Further information on this localisation profile can be obtained via co-localisation experiments, involving staining with a probe for ribosomal localisation, such as Syto-RNASelect®. Application of this dye using fluorescence and confocal microscopy was successfully achieved, using 488 argon laser to excite the dye. Fluorescence microscopy observations were undertaken using suitable emission filters to detect its narrow emission at 528 nm.

Fig. 3.45. Confocal microscopy images of EuDPP2[44] (λ_{ex} = BP 340 - 390 nm, λ_{em} = LP 505 nm) incorporating 2-methyl-azathioxnathone sensitising moiety, co-localised with Syto-RNASelect® (λ_{ex} = 488 nm, λ_{em} = BP 505 - 550 nm) in NIH 3T3 cells. Orange regions of the merged images correspond to areas where both stain and complex are localized confirming ***ribosomal localization***, (highlighting strong localization in the nucleus).

Cell viability was found to be concentration and time dependent, and was monitored by visual counting of the number of cells in a selected population as a function of time. From bright field measurements, more than 95% of the cells looked healthy over the 24 h period. More accurate determination of cell viability can be undertaken, by co-

loading with calcein-AM, a dye used to assess cell viability in most eukaryotic cells. In live cells, the non-fluorescent calcein-AM is converted to green fluorescent calcein, following acetoxymethyl ester hydrolysis catalyzed by intracellular esterases. Cells should be examined by microscopy using appropriate excitation and emission filters so that the red europium and green calcein emission could be examined separately. However, it is difficult to select an appropriate filter set up for this dye, as the very small separation between excitation (490 nm) and emission (515 nm) wavelengths meant that spectral overlap occured consequently sabotaging the experiment. This problem could be overcome by using a system involving narrower band excitation wavelengths, *e.g.* by excitation with an argon laser (488 nm).

3.6.1.1 'In cellulo' pH Determination

At present, an appropriate fluorescence microscope with high optical magnification, in order to focus on cell compartments is not available. This would be highly beneficial as, using the appropriate emission band-pass filter to measure the selected intensity band ratio, it would allow the determination of the the local pH of a given organelle. For more accurate pH measurements, incorporation of a fluorimeter into the microscope set up, e.g. via optical fibre would be required.

In an attempt to utilise the pH-mapping function of the complex, NIH 3T3 cells loaded with 50 μM complex were used in a trial experiment. Fast egress of Eu(III) complexes designed for '*in cellulo*' applications has been observed. Withdrawal of the medium containing the complex leads to fast migration and subsequent release of the complex from the cells.[45] Therefore, cells were removed from their growth medium containing the complex, and quickly washed three times with PBS. Cells were suspended in PBS following scraping them into a fluorescence cuvette (detaching them from the surface using trypsin takes 5 min, with addition washes using PBS) and measuring the emission spectrum (*Fig. 3.46. left*). This process was completed within a minute, to ensure minimal release of complex from the cells. In the absence of an appropriate calibration curve in simulated intracellular mouse skin fibroblasts, the intensity ratio *vs.* pH plot for Eu(MS)DAdP2 in reconstituted 100% human serum was used (*Fig. 3.46. right*). Due to the descending baseline of the spectrum caused by ligand fluorescence and

light scattering, subtraction of the ligand fluorescence from the Eu emission spectrum was used, prior to analysis of the 680/617.5 nm intensity ratio.

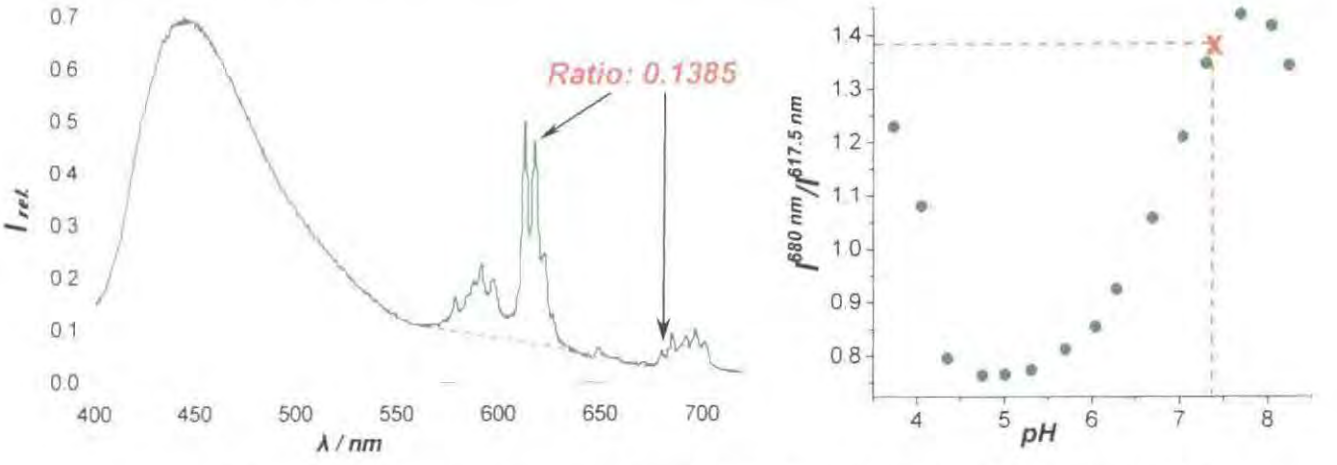

Fig. 3.46. (*left*) Luminescence spectrum of NIH 3T3 cells loaded with 50 μM Eu(MS)DAdP2 for 6h. (*right*) Intensity ratio (680/617.5 nm) vs. pH plot using reconstituted 100% human serum as the background medium ([complex] = 20 μM, 298 K, λ_{ex} = 380 nm, I = 0.1 M NaCl).

Determination of the pH, using the selected intensity ratio of 0.1385, gave a global pH within the cell of 7.4. However, evidently the error of this measurement is relatively high (est. ±0.2). In order to confirm this, a large number of cells (ca. 20,000) with same loading concentration and time were removed mechanically from their cover slips, washed with PBS (x3), and subsequent sonicated to achieve a homogenous cell lysate solution (50μL). The emission spectrum of this sample was recorded with low resolution due to the small sample volume. A pH of 7.6 (±0.1) was obtained using the usual intensity ratio. In comparison, the pH of the solution was also measured using a narrow, accurately calibrated electrode. A pH value of 7.47 (±0.05) was measured.

These trial experiments carry a number of assumptions. They do, however, support the application of Eu(MS)DAdP2 as a ratiometric pH probe, capable of estimating intracellular pH.

3.6.2 Determination of the Intracellular Europium Concentration

The images obtained by fluorescence microscopy allow identification of the localisation and uptake profile of the complex at a given time point. However, this does

not provide quantitative information about how effectively the complex is taken up. This issue can be addressed by focusing on a constant number of cells at each time point and plotting the image acquisition time for a constant brightness as a function of the incubation time. The exact concentration of the complex per cell can be determined through a combination of flow-cytometry, to determine the number of cells in a population, and ICP-MS (inductively coupled plasma – mass spectrometry), to determine the total lanthanide (europium) concentration. Determination of this value can also be achieved for a known population of cells, by measuring the absorbance of the complex in the growth medium, prior to and after loading into the cells.

The counting of the number of cells for a given population was undertaken by flow cytometry. This is a fluorescence based technique that allows the counting and sorting of a population of cells. These measurements were carried out by scraping the cells off their cover slips and re-suspending them in PBS. Following introduction of the sample into the instrument, hydrodynamic focusing allowed the diameter of the flow to be narrowed to such an extent that single cells were forced down the centre of the stream. The cells were interrogated by a laser, using an appropriate excitation wavelength for the chromophore. Emitted light was directed to a series of detectors, usually focussed onto a PMT (photomultipler) tube, by application of the confocal principal for accuracy. The range of wavelengths that are permitted to reach each of the detectors is controlled through the use of band-pass filters, allowing multi-detection of different stains. The chosen wavelengths for counting cells loaded with Eu(MS)DAdP2 were 355 nm and 440 nm, for excitation and ligand fluorescence detection respectively.

For determination of the complex concentration in the counted cells, ICP-MS was used. This technique allows an accurate determination of the concentration of an element in a given sample, with typical detection limits of the order of ppt to ppb. In this method, the sample is injected into an argon plasma, where the elements in the sample are atomised and ionised; these ions are then passed through a quadrupole mass spectrometer. Through calibration with elemental standards, accurate concentrations can be calculated since the observed ion signal is proportionate to the concentration. Prior to injection of the sample, quantitative dilution and digestion using 5% nitric acid solution was undertaken. Nitric acid addition not only dissociates the europium in the complex and

ensures a uniform distribution within the sample, but also prevents complex adherence to the sample vial.

For determination of $[Eu(MS)DAdP2]_{TOT}$ concentration in the cells, an 8 h loading time point with a 100 μM loading concentration was chosen. Not only the sorted (201,794) cells were submitted for ICP-MS, but also the combination of PBS used to wash them after growth medium withdrawal. The number of Eu(MS)DAdP2 complexes inside a single cell was determined to be 2.9×10^7. This value gives a $[Eu]_{total}$ of 12.5 μM inside a single cell (assuming 4,000 μm^3 mean cell volume), which means that 12.5% of the original loading concentration had been taken up by the cells. This measurement was confirmed by comparing the absorbance values of the complex containing growth medium prior to and after incubation, gaving a 14% (±2%) decrease in complex concentration. Surprisingly, 31% of the complex concentration measured by ICP-MS was measured from the submitted PBS solution. This not only confirms the observed relatively fast influx of the complex, but warns about rapid egress, upon withdrawal of complex from the growth medium. Although time dependent egress experiments were not carried out in this work, this behaviour is consistent with a diffusion-driven transport mechanism across the cell membrane. The driving force of this hypothetical mechanism is the complex concentration gradient between the intracellular and extracellular space. This also supports the observed time independent complex uptake profile, noted in the fluorescence microscopy studies.

This hypothesis for complex uptake/egress can be confirmed by loading the complex onto the cells at 4 °C. If europium luminescence can still be clearly observed with the same localization profile, this would suggest that the complex does not enter the cells by endocytosis. The relatively even distribution of the complex in the cytoplasm also supports this premise. Molecules and conjugates entering cells via endocytosis are believed to be initially trapped in endocytotic vesicles and then transferred into endosomes. Only molecules and conjugates escaping from the endocytosis pathway can survive to act as probes.[46]

3.7 Conclusions and Future Work

A series of pH-responsive ratiometric Eu(III)complexes has been synthesised incorporating an efficient sensitiser and a pH dependent binding moiety. Their luminescence properties were thoroughly studied to find the best candidate for intra- and extracellular pH measurements, and to assess changes in the photophysical properties and sensitivity towards anion binding as a function of complex structural modifications. The complex, Eu(MS)DAdP2 exhibited sensitivity towards endogenous anions and protein. Despite this, even using reconstituted 100% human serum, a suitable calibration curve was obtained and can be applied to determine the local pH using selected intensity ratio *vs.* pH plots for spectroscopic applications. Selected emission band ratio versus pH plots allow microscopic applications, measuring pH from 6 to 8 using an appropriate microscope setup.

Cellular uptake images revealed fast uptake of the complex and a well distributed localisation within the cell. However, fast egress was also observed. Ribosomal localisation with higher intensity in the nucleoli was observed, as found previously for complexes bearing the same sensitising moiety. An uptake study proved that a significant amount of complex enters the cell possibly via concentration gradient diffusion. The localised complex stays inert inside the cell, and no evidence of toxicity was found. Images were observed using non-fixed cells, which is beneficial for live cell imaging applications.

Therefore, this complex shows promise for application as a ratiometric pH probe for use in biological samples and living cells.

Further work is required to assess and confirm the localisation profile of the complex and to determine the mechanism of cellular uptake. Images using different cell lines, such as CHO cells, are underway to study changes in the uptake and localisation as a function of cell type. Two photon excitation and time resolved microscopy applications should also be studied to increase the number of possible applications of this pH-responsive Eu(III)complex.

3.8 References

[1a] University Manuscript, (KLTE) University of Debrecen, Hungary, 1987.

[1b] www.chemguide.co.uk/indicators

[1c] www.omega.com

[2a] R. J. Gillies, N. Raghunand, M. L. Garcia-Martin, and R. A. Gatenby, *Med. Biol. Mag.*, 2004, **23**, 57.

[2b] Y. Song, D. Salinas, D. W. Nielson, and A. S. Verkman, *Am. J. Physiol. Cell Physiol.*, 2006, **290**, 741.

[3] F. L. M. Ricciardolo, B. Gatston, and J. Hunt, *J. Allergy Clin. Immunol.*, 2004, **113**, 610.

[4] G. Helmlinger, F. Yuan, M. Dellian, and R. K. Jain, *Nat. Med.*, 1997, **3**, 177.

[5] O. V. Vieira, R. J. Bothelo, and S. Grinstein, *Biochem. J.*, 2002, **366**, 689.

[6] R. Weissleder and V. Ntziachritos, *Nat. Med.*, 2003, **9**, 123.

[7] M. E. Cooper, S. Gegory, E. Aidie, and S. Kalinka, *J. Fluoresce.*, 2002, **12**, 425.

[8] P. T. Snee, R. C. Somers, G. Nair, J. P. Zimmer, M. G. Bawendi, and D. G. Nocera, *J. Am. Chem. Soc.*, 2006, **128**, 13320.

[9] L. Sterowski, J. C. Mason, H. Lee, M. Say, and G. Patonay, *J. Heterocycl. Chem.*, 2004, **41**, 227.

[10] Z. Zhang and S. Achilefu, *Chem Commun.*, 2005, 5887.

[11] T. J. Rink, R. Y. Tsien, and T. Pozzan, *J. Cell Biol.*, 1982, **95**, 189.

[12] R. Weissleder and S. A. Hildebrand, *Chem Commun.*, 2007, 2747.

[13] W. C. W. Chen, D. J. Maxwell, X. H. Gao, R. E. Bailey, and M. Y. Han, *Curr. Opin. Biotechnol.*, 2002, 40.

[14] M. Y. Han, X. H. Gao, J. Z. Su, and S. M. Nie, *Nat. Bioechnol.*, 2001, **19**, 631.

[15] T. Ueno, Y. Urano, K. Setsukinai, H. Takakusa, H. Kojima, K. Kikuchi, K. Ohkubo, F. Fukuzimi, and T. Nagano, *J. Am. Chem. Soc.*, 2004, **126**, 14079.

[16] J. N. Demas and B. A. DeGraff, *Coord. Chem. Rev.*, 2001, 317.

[17a] D. Parker, *Coord. Chem. Rev.*, 2000, **205**, 109.

[17b] T. Gunnlaugson, J . P. Leonard, *Chem. Commun.*, 2005, 3114.

[17c] D. Parker, Y. Bretonniere, 'Luminescent lanthanide complexes as sensors and imaging probes', *Ernst Schering Res. Found Workshop*, 2005, **49**, 123.

[17d] T. Gunnlaugson, J . P. Leonard, *J. Fluoresc.*, 2005, **15**, 585.

[18] S. Aime, A. Barge, M. Botta, J. A. K. Howard, R. Kataky, M. P. Lowe, J. M. Moloney, D. Parker, and A. S. de Sousa, *Chem. Commun.*, 1999, 1047.

[19] M. P. Lowe, D. Parker, O. Reany, S. Aime, M. Botta, G. Castellano, E. Gianolio, and R. Pagliarin, *J. Am. Chem. Soc.*, 2001, **123**, 7601.

[20] D. Parker and J. A. G. Williams, in 'Responsive Luminescent Lanthanide Complexes', Vol. 40, ed. A. Sigel, H. Sigel, J. Wiley, New York, 2003.

[21] A. P. de Silva, H. Q. N. Gunaratne, T. Gunnlaugsson, A. J. M. Huxley, C. P. McCoy, J. T. Rademacher, and T. E. Rice, *Chem. Rev.*, 19997, **97**, 1515.

[22] D. Parker and J. A. G. Williams, *Chem Commun.*, 1998, 245.

[23] D. Parker, K. Senanayake, and J. A. G. Williams, *Chem Commun.*, 1997, 1777.

[24] I. M. Clarkson, A. Beeby, K. Senanayake, M. P. Lowe, E. Mathieu, L. J. Govenlock, and D. Parker, *New. J. Chem*, 2000, **24**, 377.

[25] D. Parker, K. Senanyake, and J. A. G. Williams, *J. Chem Soc. Perkin Trans. 2*, 1998, 2129.

[26] S. Blair, M. P. Lowe, C.E. Mathieu, D. Parker, and K. Senanayake, *Inorg. Chem.*, 2001, **40**, 5860.

[27] M. P. Lowe and D. Parker, *Inorg, Chim. Acta*, 2001, **317**, 163.

[28a] T. Gunnlaugson, D. A. Mac Dónail, D. Parker, *Chem. Commun.*, 2000, 93.

[28b] T. Gunnlaugsson, D. A. MacDonaill, and D. Parker, *J. Am. Chem. Soc.*, 2001, **123**, 12866.

[29] M. P. Lowe and D. Parker, *Chem Commun.*, 2000, 707.

[30] A. E. Martell and R. M. Smith, 'Critical Stability Constants', Vol.2, Plenum press, 1974.

[31a] T. Gunnlaugsson, C. P. McCoy, F. Stomeo, *Tetrahedron Lett.*, 2004, **45**, 8403.

[31b] C. P. McCoy, F. Stomeo, S. E. Plush, and T. Gunnlaugsson, *Chem. Mater.*, 2006, **18**, 4336.

[32] T. Koike, E. Kimura, I. Nakmura, Y. Hashimoto, and M. Shiro, *J. Am. Chem. Soc.*, 1992, 7338.

[33] T. Koike and E. Kimura, *Chem. Soc. Rev.*, 1998, **27**, 179.

[34] R. S. Dickins, D. Parker, A. S. de Sousa, and J. A. G. Williams, *Chem. Commun.*, 1996, 697.

[35] A. Beeby, I. M. Clarkson, R. S. Dickins, S. Faulkner, D. Parker, L. Royle, A. S. de Sousa, J. A. G. Williams, and M. Woods, *J. Chem. Soc.*, 1999, 493.

[36] A. K. Covington, M. Paabo, R. A. Robinson, and R. G. Bates, *Anal. Chem.*, 1960, 700.

[37] R. S. Dickins, S. Aime, A. S. Batsanov, A. Beeby, M. Botta, J. I. Bruce, J. A. K. Howard, C. S. Love, D. Parker, R. D. Peacock, and H. Puschmann, *J. Am. Chem. Soc.*, 2002, **124**, 12697.

[38] J. Yu and D. Parker, *Eur. J. Org. Chem.*, 2005, **1**, 4249.

[39] R. A. Poole, F. Kielar, S. L. Richardson, P. A. Stenson, and D. Parker, *Chem Commun.*, 2006, 4084.

[40] J. Ghuman, P. A. Zunszain, I. Peptitpas, A. A. Bhattacharya, M. Otagiri, and S. Curry, *J. Mol. Biol*, 2005, **353**, 38.

[41] R. Pal and D. Parker, *Chem Commun.*, 2007, 474.

[42] J. Stevens, *J. Cell Biol.*, 1965, **24**, 349.

[43] M. Horky, V. Kotala, M. Anton, and J. Wesierska-Gadek, *Ann. N. Y. Acad. Sci.*, 2002, **973**, 258.

[44] J. Yu, D. Parker, R. Pal, R. A. Poole, and M. J. Cann, *J. Am. Chem. Soc.*, 2006, **128**, 2294.

[45] R. A. Poole, 'Luminescent Lanthanide Complexes for Cellular Applications', PhD, Durham University, Durham, 2006.

[46] F. Osaki, T. Kanamori, S. Sando, T. Sera, and Y. Aoyama, *J. Am. Chem. Soc.*, 2004, **126**, 6520.

CHAPTER 4

Carbonate Sensors

4 Carbonate Sensors

4.1 Introduction

The bicarbonate ion is an essential component of biological systems and it is vital to many cellular processes in mammals, such as intracellular pH homeostasis, kidney function and sperm maturation[1]. High alkalinity of certain parts of the gut (up to pH 12), is necessary for efficient digestion of plant based material, and found to be achieved by enzyme-regulated bicarbonate transport.[2] Several transport proteins have been identified with the 'bicarbonate super-transporter family', in which Na^+ and HCO_3^- are transported together, or HCO_3^- is exchanged for Cl^-. However, very little is known about how bicarbonate concentrations fluctuate within a cell, in response to cell stimuli or stress. Such analyses are currently limited to radiochemical measurement of overall $H^{14}CO_3^-$ uptake and interferences based upon changes in intracellular pH. Information about how HCO_3^- is localised and varies within cell compartments is needed in order to understand the diverse physiological processes it may control, for example in cyclic-AMP regulation, through pH-independent, reversible binding to the soluble adenylyl cyclase enzyme (sAC)[3]. This 48kDa protein is responsible for a number of bicarbonate-induced, cAMP-dependent processes that sperm undergo before they are able to fertilise the egg[4], such as hyperactivated motility, capacitation[5] and the acrosome reaction. A further example for a bicarbonate regulated enzyme involves phosphofructokinase, a glycolytic control enzyme. It is inhibited upon disruption of the CO_2/HCO_3^- equilibrium, hence blocking glycolysis in muscle[6]. The pathological consequences of perturbing some of these physiological processes may be very significant: mis-expression of carbonic anhydrase (CA) in linked to the presence of a variety of tumour types and CA-II deficiency syndrome in humans is characterised by osteoporosis, mental retardation and renal tubular acidosis.

Systematic acid-base homeostasis is the product of complex interactions between metabolism, regulated exhalation of CO_2 by the lungs and acid or base excretion by the kidneys. The kidney employs three major processes in the maintenance of acid-base homeostasis: (i) reabsorption of filtered bicarbonate, (ii) excretion of protons and (iii) the

synthesis of ammonia and the use of ammonia, phosphate and citrate. Disruption in the acid-base transport in the kidneys results in renal tubular acidosis. The mechanism of this disease has been identified as pH dependent down-regulation of several hormonal pathways, which is mostly driven by the local equilibrium and, consequently, concentration of HCO_3^-.[7]

In recent years it has been reported that patients suffering from cystic fibrosis are characterised with impaired duodenal and pancreatic HCO_3^- secretion, which is believed to neutralize acid within the mucus gel. Cells within the acidic regions of the gastric system are protected, as active epithelial secretion of bicarbonate forms a neutralizing barrier in the pre-epithelial mucus, preventing acid penetration into the cells and consequent cell death.[8] In the absence of this protective layer, erosive esophageal disease, pulmonary acid reflux and inactivation of the pancreatic enzyme occur. Despite these marked acid-related abnormalities, cystic fibrosis patients are remarkably resistant to peptic duodenal ulceration, a phenomenon termed the 'CF paradox', which remains unexplained.

The highlighted bicarbonate regulated cellular processes form only a part of all known CO_2/HCO_3^- dependent functions in the living organisms. Therefore, there is a pressing need for a direct method to allow changes in the HCO_3^- concentration to be measured within the cell, and to monitor the changes in different compartments in real time. Although variations of intracellular pH may be measured, it is not possible to assess their importance, as they may be due to a perturbation of proton or HCO_3^- transport.

4.1.1. Measuring [HCO_3^-]

Until recently, the majority of CO_2 sensors were actually pH sensors, in what a carbonate–bicarbonate buffer is separated from the analyte fluid by a CO_2 permeable membrane. The pH of the buffer changes in response to the CO_2 concentration in the analyte fluid. Then, a pH sensitive fluorescent dye is used to track the pH of the buffer and this, in turn, allows the CO_2 concentration to be inferred. An alternative approach is based on energy transfer to a pH sensitive dye in polymer systems. Very fast responding colorimetric CO_2 sensors based on pH sensitive organic dyes have been demonstrated.[9] The method is based on luminescent quenching between water soluble organic

fluorophores. It requires a pH responsive acceptor dye, with a suitable pK_a, which displays significant difference in its absorption spectra depending on its protonation status. When carbon dioxide dissolves and reacts with water, the dye is protonated and its absorption spectrum will overlap with the emission spectrum of an appropriate donor dye, hence producing a 'quenching-based' sensor.

For qualitative carbonate (CO_3^{2-}) detection, several trivial inorganic reactions are used, such as precipitation of insoluble carbonate salts from solution, or CO_2 elevation. The former one is based on addition of water soluble Ca^{2+} salts following heating of the sample, resulting in $CaCO_3$ as a white precipitate, whilst the latter uses acid-base titrations.

Nowadays, almost all commercial available equipment for quantitative carbonate/bicarbonate concentration measurement are based on ion-selective electrodes. This concept can be divided into two major categories: analyte specific potentiometric membranes[10-12], and enzyme electrodes[13]. The former is based on a specific, often photocurable polyurethane, PVC or silicone rubber membrane composition incorporating carbonate sensitive plasticiser, such as hexyl trifluoroacetophenone or hexyl trifluoroacetylbenzoate ionophores. Variation of the Lewis acidity of the plasticiser exhibits higher pH-dependence of the sensor, with consequently a higher carbonate detection limit. Enzyme electrodes are a novel approach for enhancing substrate sensitivity of ion-selective electrode-based enzyme probes. The concept involves the use of two working enzyme electrodes based on asymmetric cellulose acetate membranes in a different potentiometric cell arrangement. One of the enzyme probes is prepared by immobilizing a suitable enzyme at the surface of a cation-selective electrode, while the second working electrode contains the same (or sometimes different) enzyme immobilised on an appropriate anion-selective electrode. Enzymatic conversion at the surface of each electrode yields a detectable cation and anion, respectively. Since each sensor selectively responds to the same substrate, but in opposite directions, the potential difference between the working enzyme electrodes is greater than obtained when each probe is measured alone versus a standard reference electrode.

It is evident from the nature of these devices, that no simple probe exists that is able to measure direct changes in HCO_3^- activity, for use in a biological environment,

such as living organisms. Moreover, they possess several drawbacks, such as pH-dependence, lack of sensitivity with narrow and low detection limits and selectivity issues originating from interference with other anions present (*e.g.* salicylate, lactate, chloride). Despite these limitations, several specific quantitative non-biological carbonate measuring device rely on their application.

For the delicate nature of qualitative intracellular bicarbonate concentration measurements, fluorescent probes may be used following their successful application as probes for intracellular ionic concentrations.[14] For practical applications, they should be non toxic and cell permeable, susceptible to efficient excitation in the near UV/visible region, thereby avoiding biomolecule co-excitation, and undergo spectral changes that allow ratiometric analyses to be performed, so that the concentration dependence of intensity-based systems is obviated. A limiting feature of several conventional fluorescent probes is that they are sometimes prone to interference from scattered light or auto-fluorescence, as they lack large Stokes' shifts in emission. Such problems may be circumvented with longer-lived probes, as time-gating allows the unwanted short-lived emission to decay to zero and the probe emission can be monitored after an appropriate delay (5 – 500 μs).[15-17] Luminescent Eu and Tb complexes offer much scope in this respect, as they possess emission lifetimes in the range of 0.1 – 4 ms. Hence, the interest in their biochemical applications such as complexes for time-resolved immunoassays[18] and long lived donors in FRET analyses[19] are well advanced. However, over the last decade, a mechanistic approach to the development of responsive lanthanide probes has emerged.[20-23]

4.2.1 Advantages and Concept of Lanthanide-based Carbonate Sensors[17]

Considerable interest is targeted on examining complexes in which the analyte binds to the metal centre, with an affinity that is in line with the local ion concentration. Modulation of the luminescence (Eu, Tb, Yb) or relaxivity (Gd), as detailed in *Chapter 1.*, may be a function of a defined biochemical parameter or set of variables, such as pH, pO_2 or anion concentration. Several lanthanide complexes have been reported to display significant changes in luminescence properties[24-26] or in relaxivity,[27-30] following hydrogencarbonate displacement of the bound water molecules of the metal centre. Such

behaviour offers a means of studying both the concentration of HCO_3^- in solution and the pH in the ambient range, via the pH dependent H_2CO_3/ HCO_3^- equilibrium (effective pK_a = 6.16, C = 0.1 M, 298 K). Gadolinium complexes in which changes in relaxivity values can be plotted as a function of added anion, will not be detailed in this work.[31]

Complexes of the lanthanide ions with macrocyclic heptadentate ligands are particularly appropriate for the detection of HCO_3^- for several reasons. First, the 1 : 1 ML complexes are well defined and relatively stable in aqueous solution and likely to be bound to one or two water molecules. The solution hydration state of the aquated and anion bound complex can be estimated for Eu and Tb using established methodology.[32] Reversible displacement of one or both waters in the diaqua complexes by anion ligation to the lanthanide centre[21,29,33] has been studied in great detail. This event is signalled by changes in the intensity and form of the Ln emission (*Fig. 4.1).*

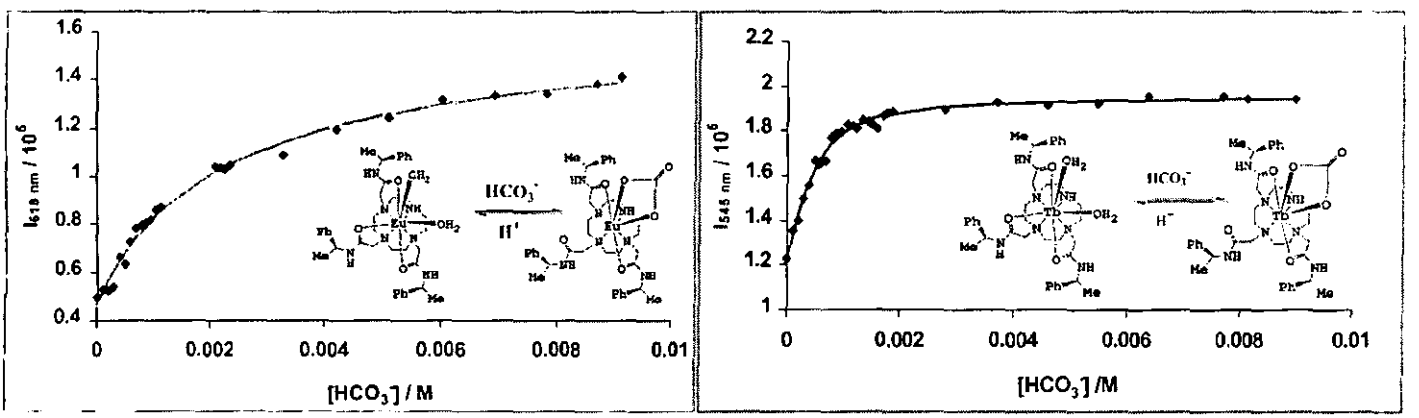

Fig. 4.1. Variation of emission intensity (618 nm) of the given (*left*) Eu(III) and (*right*) Tb(III) complex as a function of added $NaHCO_3$ (1 mM complex, pH 7.4, 0.1 M collidine/HCl buffer).[29]

Proton NMR studies of the Eu analogue have revealed that the di-aqua complex adopts a square-antiprismatic structure while the chelated adduct with HCO_3^- was initially proposed to adopt a twisted square-antiprismatic geometry,[29] but was later shown to adopt a square antiprismatic geometry.[21,33] Pronounced changes were also observed in the intensity of the hypersensitive $\Delta J = 2$ Eu emission band, accompanied by changes in the helicity at the metal centre. The *circular polarisation* of the emission is a sensitive function of complex helicity and pronounced changes in the circularly polarised luminescence from the excited lanthanide have been noted in the presence of different anions (*e.g.* phosphate, HCO_3- and lactate)[24]. Thus, using these chiral lanthanide

complexes, the emission circular polarization (in the $\Delta J = 1$ or 2 bands) may be used to signal the concentration of HCO_3^- (and thereby pH) in solution.

Changes in the form and intensity of the lanthanide emission allow ratiometric analyses to be undertaken. It is most appropriate in analyses of Eu emission spectra as the relative intensity of the magnetic-dipole-allowed $\Delta J = 1$ manifold is usually insensitive to associated change in coordination environment, while the intensity of the electric-dipole-allowed $\Delta J = 2$ and $\Delta J = 4$ transitions change considerably, particularly if the 'hard' axial water molecule is displaced by a more polarisable charged donor. An example of such emission spectra (*Fig. 4.2*) highlights the increase in the relative intensity of the $\Delta J = 2$ manifold for the carbonate-bound species- compared to lactate and citrate – and exemplifies how each bound anion gives a 'fingerprint' emission spectrum, allowing simple identification and ratiometric analysis. This information is required for the application of such a method to intracellular media, where a large variety of anions may compete in binding to the Eu centre.

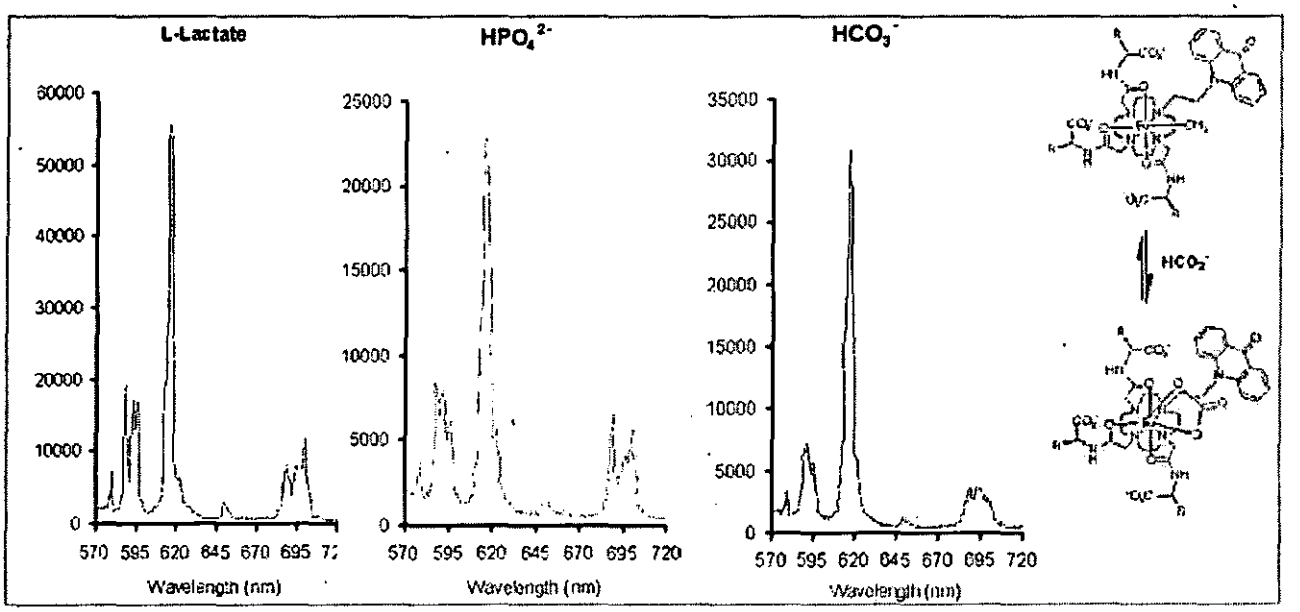

Fig. 4.2. Metal-based emission spectrum for the displayed Eu(III)complex (0.1 mM, 1 mM anion, pH 7.4, λ_{ex} = 410 nm) in the presence of (*left*) (S)-lactate, (*centre*) hydrogenphosphate, (*right*) bicarbonate showing the changes in the form of the emission spectrum signalling reversible anion coordination.[26]

The structure of several of these ternary complexes has been defined by X-ray crystallography and by NMR studies on Eu and Yb analogues[33]. Relative binding affinities have been assessed in simple competitive analyses or in fixed interference studies. They revealed that in the millimolar range, it is the more polarisable (higher energy HOMO) oxygen in HCO_3^- (bound as CO_3^{2-}) and various phosphorylated di-anions (e.g. AMP but not cAMP) which bind most avidly. At ambient pH, it is the bicarbonate anion (range 5 - 25 mM) which wins the competition between endogenous anions. These results are in line with measurements of preferred donor affinity in which the binding order follows the relative polarisibility of the donor[34-37].

In order to develop a suitable reversible, ratiometric Eu(III) sensor for bicarbonate detection, a series of europium complexes (*Fig. 4.3*) was prepared and studied, incorporating an internal acridone sensitiser into the original heptadentate Eu complex (*see Fig.4.1*) used for identification of reversible anion binding.[25,26]

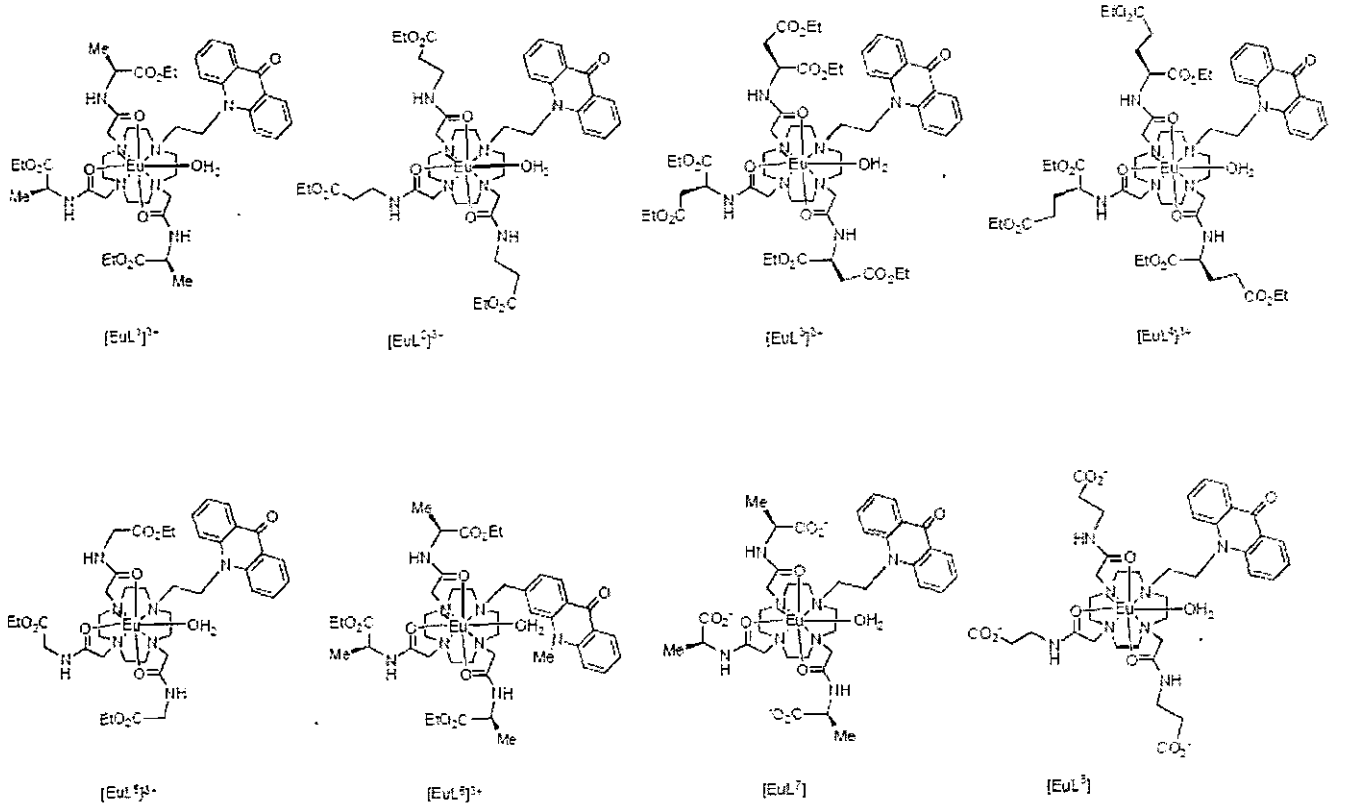

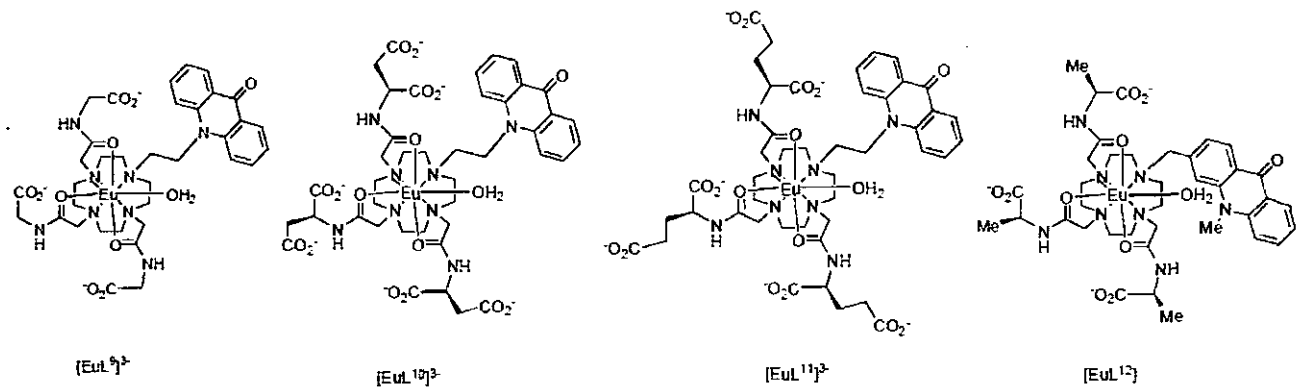

Fig. 4.3. Structure and abbreviation of studied Eu(III) complexes incorporating an acridone sensitiser moiety.[26]

Thorough examination of the Eu emission spectra of these complexes revealed significant intensity and structural changes, as a consequence of a total replacement of the coordinated water molecules. Plotting the intensity ratio of 618/588 nm emission bands in the physiologically relevant bicarbonate range, 2 - 30 mM (*Fig. 4.4*) revealed a threefold change.

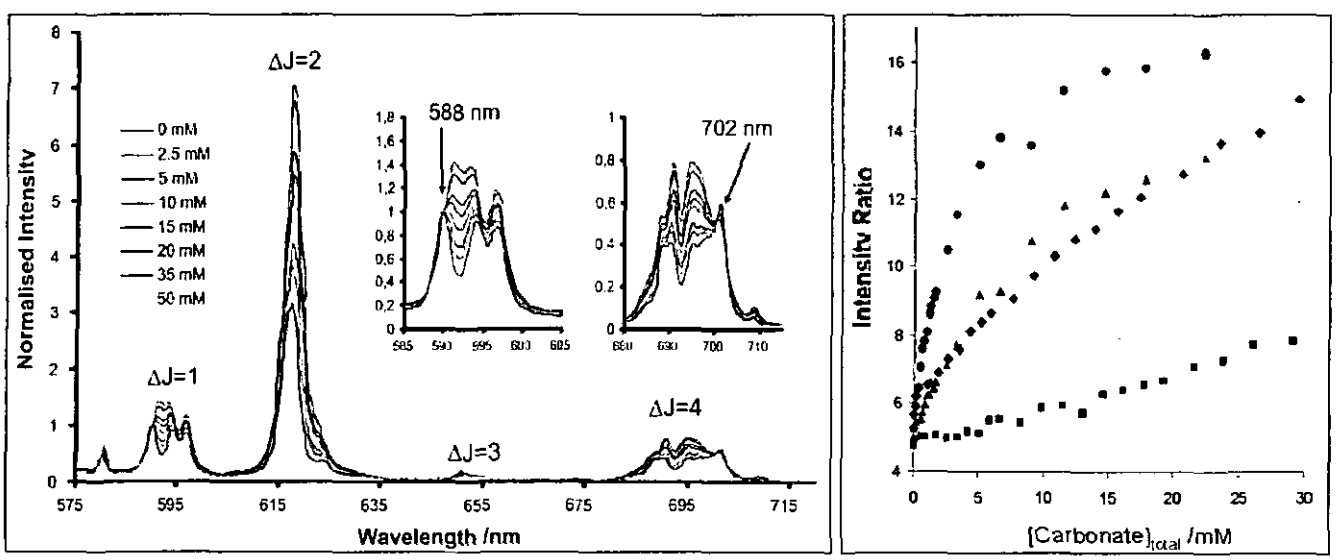

Fig. 4.4. (*left*) Variation of metal based emission in [EuL^7] following incremental addition of $NaHCO_3$, spectrum in the insert reveal the formation on isoemissive points at 588 nm ($\Delta J = 1$) and 702 588 nm ($\Delta J = 4$). (*right*) Variation of Eu emission intensity ratio (618/588 nm) for $[EuL^1]^{3+}$ (•), [EuL^8] (▲), $[EuL^4]^{3+}$ (♦) and $[EuL^{11}]^{3-}$ (■) as a function of added $NaHCO_3$ in a simulated extracellular medium (0.1 mM complex, 0.1 mM MOPS, pH 7.4, 295 K, $\lambda_{ex} = 410$ nm).[26]

The affinity for bicarbonate has been controlled by changing the peripheral electrostatic gradient in the Eu complexes. Thus, anionic, zwitterionic and cationic complexes have been examined (*Fig. 4.5*), revealing some simple trends. Affinity for bicarbonate follows the trend: cationic > neutral > anionic, consistent with Coulombic modulation of the affinity for the anionic species. Within the series of cationic complexes, substitution in the side chain gave rise to complexes of lowered affinity (*e.g.* Gly > β-Ala > Ala > Glu-substittued systems). As cationic complexes were found to be most sensitive, it was established that the zwitterionic and anionic complexes possess the desired affinity and selectivity for bicarbonate. The system has also been calibrated in the presence of protein in a cell (NIH 3T3) lysate.

Europium	Complex	Log K_a
$[EuL^1]^{3+}$	(AlaOEt)	1.95
$[EuL^2]^{3+}$	(β-AlaOEt)	2.09
$[EuL^4]^{3+}$	(GluOEt)	1.69
$[EuL^5]^{3+}$	(GlyOEt)	2.27
$[EuL^7]$	(Ala)	1.49
$[EuL^8]$	(β-Ala)	1.42
$[EuL^9]$	(Gly)	1.28
$[EuL^{12}]$	(C-linked Ala)	1.48
$[EuL^{10}]^{3-}$	(Asp)	0.99
$[EuL^{11}]^{3-}$	(Glu)	0.80

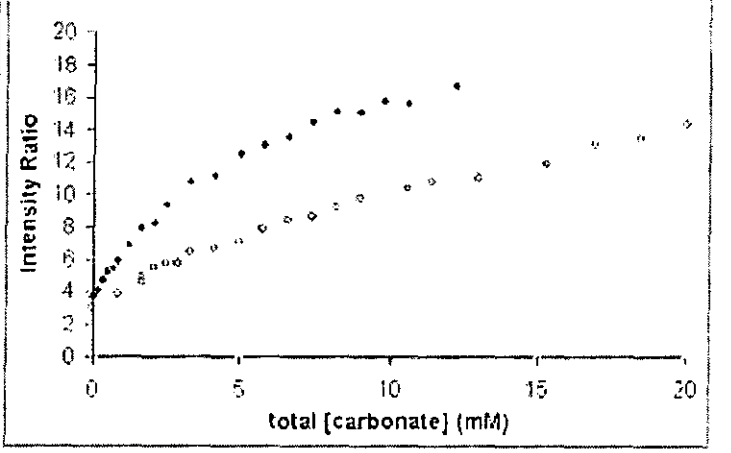

Fig. 4.5. (*left*) Apparent affinity constants for complexation of HCO_3^- (0.1 mM complex, 0.1 mM MOPS, pH 7.4, 295 K, 100 mM NaCl, 2.3 mM lactate, 0.9 mM Na_2HPO_4, 0.13 mM citrate). (*right*) Calibration curves showing the response of $[EuL^7]$ (♦) and $[EuL^{11}]^{3-}$ (◊) to the total added HCO_3^-/CO_3^{2-} in a cell lysate (NIH3T3 cells, 0.1 mM complex, pH 7.4, 295 K, λ_{ex}= 410 nm).[26]

Cellular uptake and toxicity profiles were studied using 50 to 500 μM complex concentration in NIH 3T3 mouse fibroblast cells (*Fig. 4.6*). The charged complexes showed no evidence of cell toxicity (95% live cells after 3h incubation), while the neutral complex showed only slight toxicity over the same period (87%). Imaging of the cells by confocal microscopy revealed uptake and intracellular staining with a similar localization profile for each complex. Indeed, localization and staining appeared to be independent of the period of incubation. Colocalisation studies with Mitotracker Green and Lysotracker Green were consistent with potential localization in the late endosomes/lysosomes.

Fig. 4.6. Confocal fluorescence microscopy images of (*left*) $[EuL^{I}]^{3+}$, (*centre*) $[EuL^{7}]$ and (*right*) $[EuL^{II}]^{3-}$, showing the localization of each complex inside NIH 3T3 cells.[26]

Despite these promising results, the possible applications of these Eu-acridone conjugates as intracellular HCO_3^- sensors may be sabotaged because of several drawbacks in their photophysical properties. The overall quantum yield was limited by radiative deactivation of the chromophore singlet state by competitive fluorescence. N-Alkyl acridones possess low–lying $n\pi^*$ and $\pi\pi^*$ singlet excited states, and the relative energy of the latter is particularly sensitive to solvent polarity. In polar solvents, the $\pi\pi^*$ transition in lowered in energy and the rate of ISC becomes much slower relative to the rate of fluorescence (Φ_{fluor} = 2% in non plar media, Φ_{fluor} = 98% in water). Moreover, as a non-binding chromophore is incorporated, the energy transfer between metal ion and sensitiser is not optimized.

However, this early work was an encouraging milestone in the development of new probes to image intracellular HCO_3^- fluctuations, and hence enhance our understanding of the biological significance of the most important C_1 oxo-anion. Therefore, new and improved Eu-complexes need to be developed with appropriate biological excitation wavelength, sufficiently high luminescent quantum yield and localized cellular uptake. More importantly, they must possess an appropriate bicarbonate affinity in the biological range of 5 - 30 mM HCO_3^- in the presence of other competing biological anions such as citrate and lactate. Hence, the work detailed in this chapter is dedicated to the development of such a Eu complex as a ratiometric carbonate sensor for *in cellulo* applications.

4.2 Concept and Design of a Novel Ratiometric Carbonate Sensor

In order to achieve the target of developing a novel ratiometric carbonate sensor several aspects need to be kept under consideration. Carbonate is present in the body in the range 5 – 30 mM. Therefore, the sensor must possess sufficient affinity within this range, with significantly lower affinity for other biologically common anions, consequently suppressing their competition in binding to the metal centre. Ratiometric sensing can be achieved by Eu-complexes possessing one or two bound water molecules, as upon displacement of these by anion ligation significant intensity and lifetime changes can be observed along with structural changes in the metal based emission spectrum. The previously experienced low overall luminescent quantum yield may be obviated by incorporation of an efficient sensitiser that binds directly to the Eu(III) centre and possesses low competing ligand fluorescence. The direct binding of the chromophore maximizes the energy transfer between the triplet state of the azathioxanthone and the emissive lanthanide state. Axathioxanthones were found to be good candidates to fulfil these requirements.[31,38-40] However, as noted previously, ligation via the sensitiser's pyridyl nitrogen 'opens-up' the geometry of the complex, so that the chromophore sits on top of the complex, consequently distorting the geometry and guiding pendant arm ligation.[39,40] This less shielded Eu centre is more accessible for anion binding, consequently increasing the affinity constant of the analyte and presenting the possibility of decreased sensitivity towards the target anion.

Therefore, as efficient wrapping of the Eu centre by the pendant arms is essential in order to obtain a sufficiently resistant complex towards anion binding, a new breed of azathioxanthone chromophore was required. In designing such a sensitiser, the beneficial photophysical properties of the azathioxanthones must be conserved. Hence, the structure of the parent 2-methyl-axathioxanthone was modified, with the aim of lowering the affinity constant of the target anion, as a result of enhanced steric congestion and more effective lanthanide shielding. The aim was to 'push' the sensitiser out of the lanthanide plane where it was bound via its pyridine nitrogen, with the result of a more compact structure. This may provide more flexibility for 'tighter' pendant arm binding, but preserve the sensitiser's ability to bind directly to the lanthanide centre. This was

achieved by incorporating a 7-(methylcarbamoylmethyl)-azathioxanthone (*Fig. 4.7*) into the chelating framework, allowing amide carbonyl oxygen ligation to the Eu(III) centre.

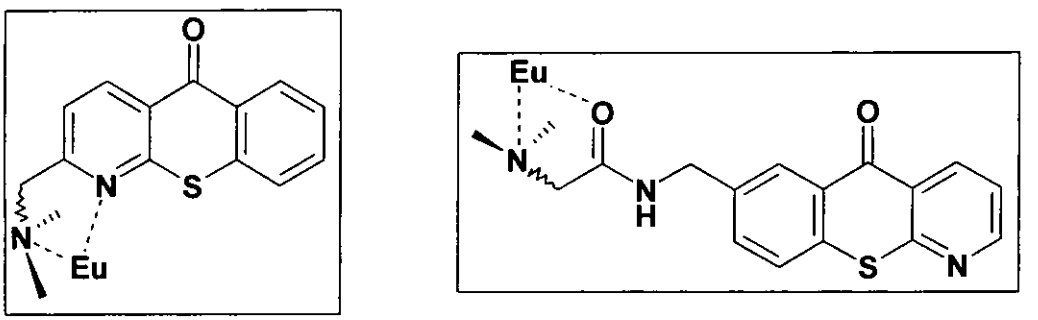

Fig. 4.7. (*left*) 2-Methyl-azathioxnathone (*right*) 7-(methylcarbamoylmethyl)-azathioxanthone and their incorporation into the chelating framework with ligation to the Eu centre.

The choice of pendant arm was another vital part of the design, as they not only bind and shield the Eu centre, thereby modulating anion affinity, but also may determine the cellular uptake and localization profile of the complex.[26,31,41-43] As found by *Bretonniere* with early carbonate sensors[25,26] negatively charged complexes repel anions, consequently lowering their affinity. However, in this case, the aim is to control the target analyte's affinity. The pendant arms were chosen to be (*S*)-alanine ethyl ester moieties. This amide may bind to the Eu centre via the carbonyl oxygen and, as a result of its relatively small aliphatic structure, defines a relatively compact complex geometry. Subsequent hydrolysis allows a neutral complex to be formed with a lower anion affinity. It is important to note that using (*S*)-phenylalanine pendant arms the affinity constant may be lowered even further as a result of steric repulsion. On the other hand, this more bulky pendant arm may also open up the geometry resulting in less effective shielding of the metal centre.

Taking all the previously detailed 'ingredients' into account, our new Eu sensor (*Fig. 4.8*) must incorporate the chosen 7-(methylcarbamoylmethyl)-azathioxanthone sensitiser ($\lambda_{abs.}$= 384 nm, $\lambda_{em.}$= 440 nm, ε_{H_2O} = 12,710 cm^{-1}) and two pendant (*S*)-alanine ethyl ester groups in a non-adjacent configuration (*trans*), consequently leaving one nitrogen unsubstituted on the macrocyclic framework.

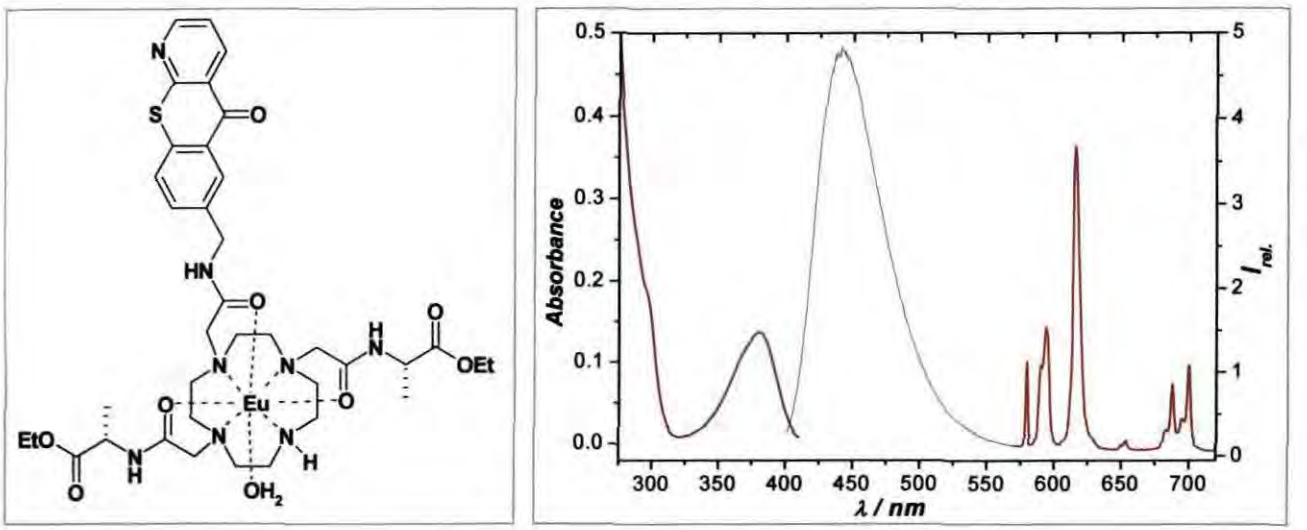

Fig. 4.8. (*left*) Structure of ***EuDAP7A*** for carbonate anion sensing. (*right*) Absorption, chromophore fluorescence and europium emission spectrum for EuDAP7A ([complex] = 10 μM, $\lambda_{max}^{(H2O)}$: 384 nm, $\tau_{Eu(H2O,\ pH=7.4)}$: 0.44 ms, $\tau_{Eu(D2O,\ pD=7.1)}$: 0.90 ms; $\varphi_{Eu\ (pH=7.4)}$: 5%).

Having successfully synthesized and characterized the desired Eu(III)complex (*Chapter 2.4.2*), it was necessary to determine some vital photophysical properties, such as radiative lifetime and quantum yield. The former is of particular interest as it not only determines the detection limit of the sensitised emission, but the solution hydration state of the aquated complex can be estimated using established methodology.[32] Measurements of the radiative lifetime in H_2O ($k = 2.27\ ms^{-1}$) and D_2O ($k = 1.11\ ms^{-1}$) revealed that EuDAP7A possesses only one water molecule bound to the Eu centre. An overall emission quantum yield of 5 % was measured in water (pH 7.4) (*Fig. 4.8*).

In order to reveal, whether the synthesised complex is suitable as a HCO_3^- sensor for biological applications, the emission behaviour was examined in the presence of biologically common anions. To begin these studies, a pH titration was carried out in a stimulated extracellular ionic background ('anion-stew' = 0.9 mM HPO_4^{2-}; 0.13 mM $citrate^{3+}$; 2.3 mM $lactate^-$; 30 mM CO_3^{2-} and 0.1 M Cl^- as sodium salts). Titrations were carried out from basic solution with acidification, in order to avoid the undesirable evolution of carbon dioxide, with each sample containing 0.1 M NaCl to maintain constant ionic strength (*Chapter 3.*).

In order to determine the individual effect of each anion, pH titrations were carried out using various anion solutions. Titrations were also carried out using 0.3 mM ascorbate (as sodium salt) as the background medium, in order to study its effect on the Eu emission spectrum. If a given anion exhibited affinity towards the studied complex, titrations were undertaken varying the anion concentration up to its limiting extracellular concentration value, maintaining a constant pH, over the region where anion binding was most pronounced.

4.3 Effect of Added Anion on the Emission Profile

Using 'anion-stew' as the background medium (*Fig. 4.9*), only minor changes were observed in both the intensity and structure of the Eu emission spectrum as the pH was varied from 9 to 3.

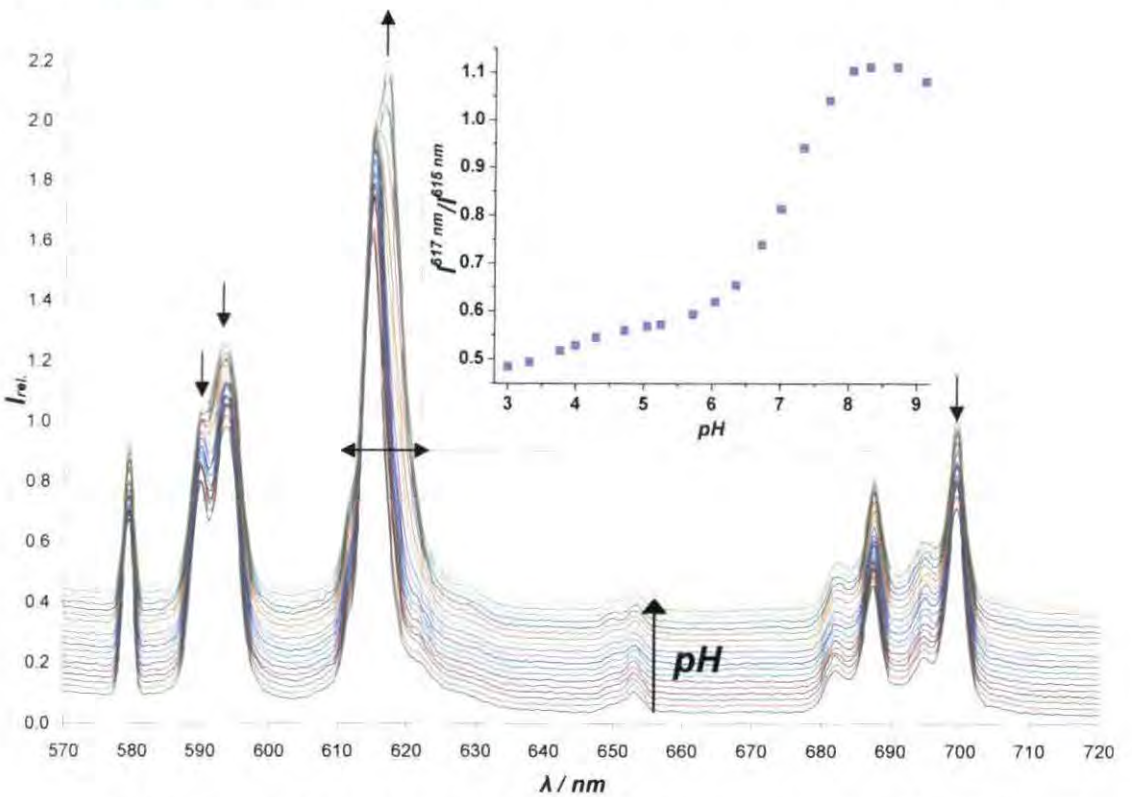

Fig. 4.9. Variation of Eu emission of EuDAP7A with pH, using 'anion stew' as background medium ([complex] = 10 μM, 298 K, λ_{ex} = 384 nm, I = 0.1 M NaCl). (*insert*) Intensity ratio (617/615 nm) *vs.* pH plot, indicating the presence of different dominant EuDAP7A(anion) species at the limiting ratios.

Only small changes were observed in the magetic-dipole-allowed $\Delta J = 1$ and in the electric-dipole-allowed $\Delta J = 2$ and $\Delta J = 4$ manifolds. This may be the result of only a minor change in, or a conservation of the axial donor in the anion adduct.

This theory may be confirmed by ^{1}H NMR or X-ray analyses of the ternary complex. Analysis of the intensity ratio (617/615 nm) *versus* pH plot revealed that in acidic pH, lactate or citrate may compete with the 'aqua' complex. Over the basic pH range, carbonate may be bound to the Eu centre. Two apparent protonation constants characterise this behaviour at 3.8 and 7.1 (±0.1). Similar changes were plotted using the intensity ratios 700/687.5 nm or 594/592 nm.

To understand the nature of the competing intermolecular (anion binding) processes which determine the properties of Eu emission, pH titrations are required using individual anion solutions in the background medium.

Using a 0.9 mM phosphate anion solution as background, (*Fig. 4.10*) no significant changes were observed in the structure of the Eu emission spectrum as the pH was decreased from 9 to 3. Only minor intensity changes were observed in some bands in the $\Delta J = 1$, $\Delta J = 2$ and $\Delta J = 4$ manifold. It is envisaged that the phosphate anion binds to the europium centre in a manner where it does not cause significant distortion of the complex geometry. Indeed, phosphate ligation was observed in the region of pH 5.5 to 7.5, with an apparent protonation constant of 6.7 (±0.1).

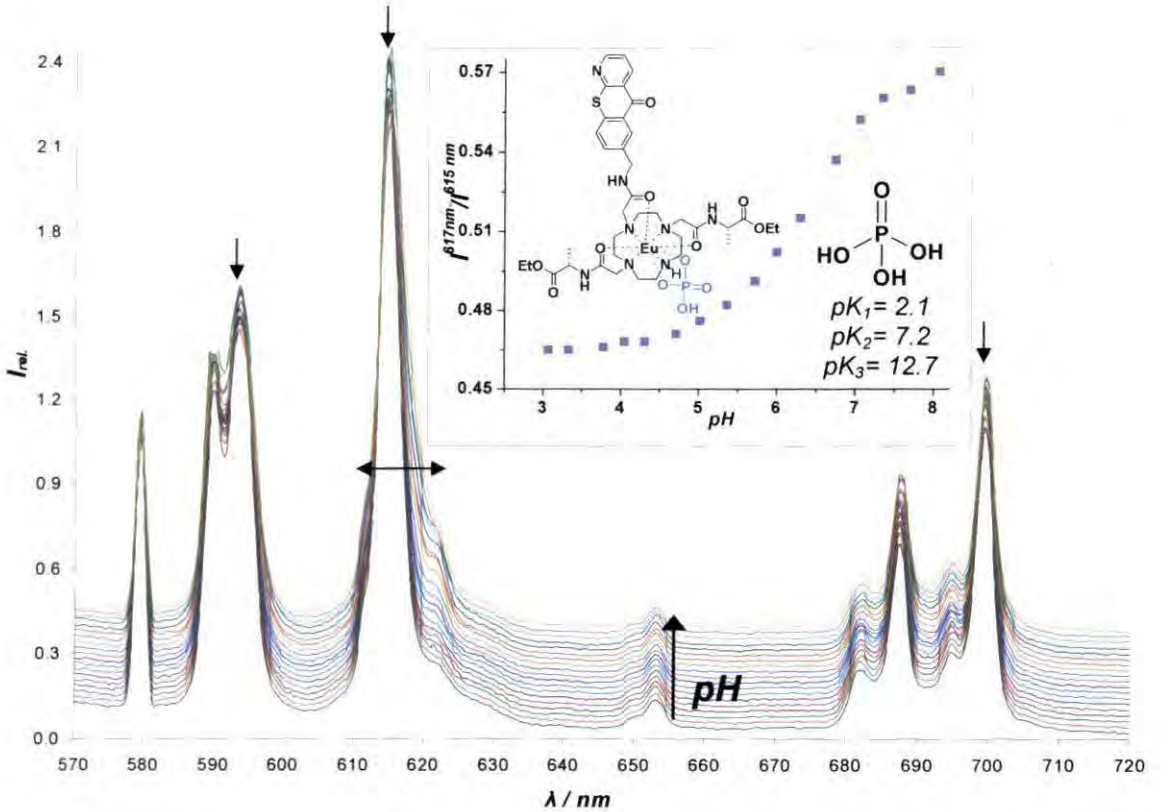

Fig. 4.10. Variation of Eu emission of EuDAP7A with pH, using 0.9 mM sodium mono hydrogen phosphate as background medium ([complex] = 10 μM, 298 K, λ_{ex} = 384 nm, I = 0.1 M NaCl). (*insert*) Intensity ratio (617/615 nm) *vs.* pH plot, highlighting the presence of phosphate ligation to the Eu centre.

Very similar spectral modulation of the Eu emission as a function of the pH were observed, when a 0.13 sodium citrate or a 2.3 mM sodium lactate solution was used as the background medium. By plotting the intensity ratios (617/615 nm or 700/687.5 nm) as a function of pH (*Fig. 4.11. left*), the effect of lactate anion on the Eu emission spectrum was observed from pH 4 ($pK_a = pK_{lactate} = 3.8$). Further increases in pH did not cause any detectable spectral change, confirming the dominancy of EuDAP7A(lactate) in solution between pH 4 to 8. Using 0.13 sodium citrate background(*Fig. 4.11. right*), the formation of EuDAP7A(citrate) began at pH 4 and above pH 6 this citrate-bound species dominates in solution. This binding profile can be represented with a pK_a value of 5.0 (±0.1), equivalent to the second pK_a of citrate.

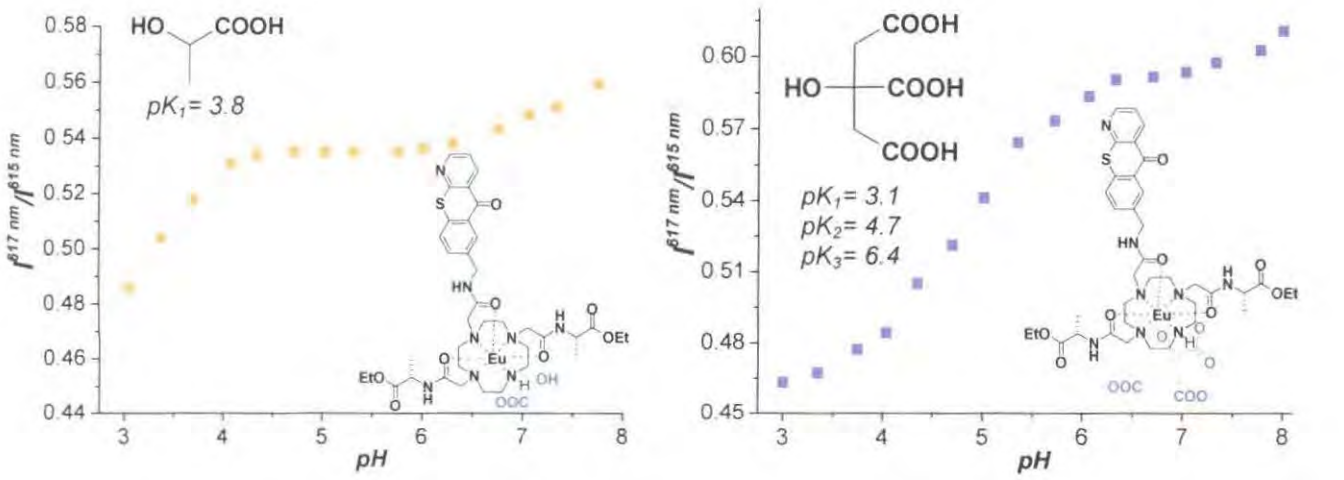

Fig. 4.11. Intensity ratio (617/615 nm) *vs.* pH plots, using (*left*) 2.3 mM sodium lactate and (*right*) 0.13 mM sodium citrate as the background medium, confirming the formation and presence of EuDAP7A(Anion) ternary adducts. ([complex] = 10 μM, 298 K, λ_{ex} = 384 nm, I = 0.1 M NaCl).

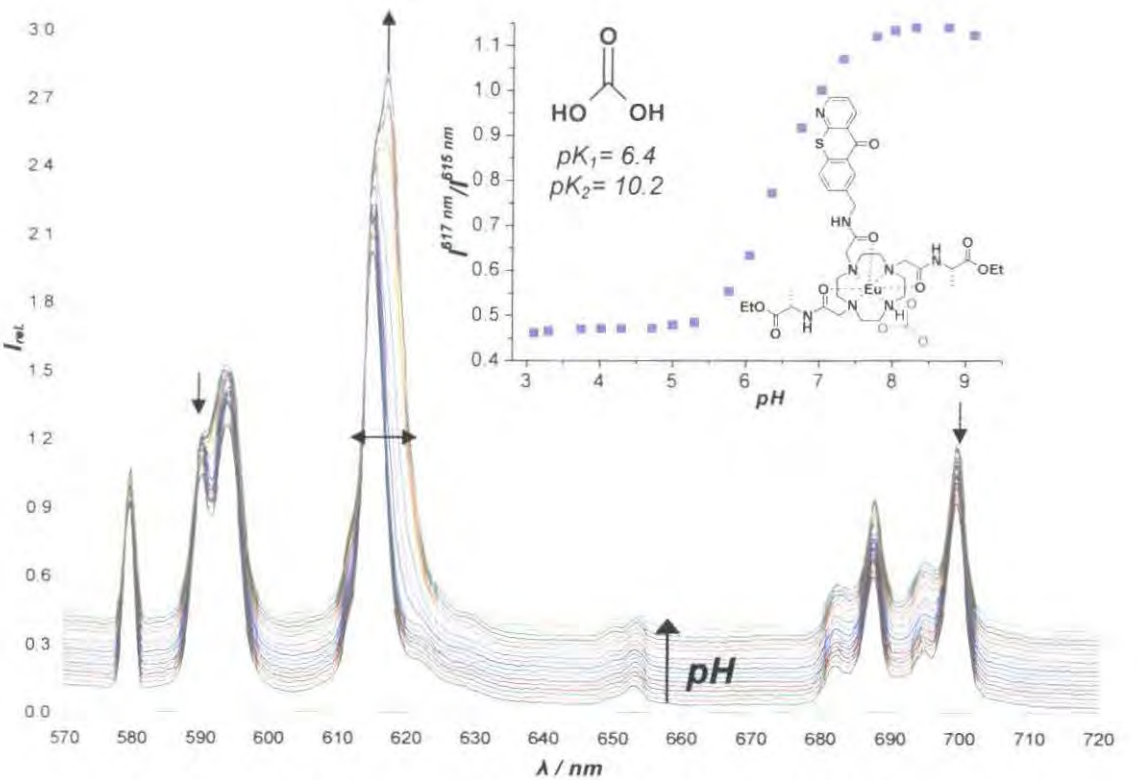

Fig. 4.12. Variation of Eu emission of EuDAP7A with pH, using 30 mM sodium bicarbonate solution as background medium ([complex] = 10 μM, 298 K, λ_{ex} = 384 nm, I = 0.1 M NaCl). (*insert*) Intensity ratio (617/615 nm) *vs.* pH plot, highlighting the presence and possible structure of the carbonate bound species.

Studying the changes in the emission spectrum as a function of the pH, using 30 mM carbonate solution as the background medium (*Fig.4.12*), the most significant change in the Eu(III) emission was observed by studying changes of the $\Delta J = 2$ manifold in basic pH (6 to 9). The appearance of a band at 617 nm was observed, as in the titration using 'anion-stew'. Plotting the intensity ratio (615/617 nm or 688.5/700 nm) *versus* pH above pH 5.5, carbonate ligation to the lanthanide centre was found, with a pK_a value of 6.4 (±0.1). This is in accordance with the first pK_a of carbonate at 6.4. The appearance of the 617 nm peak explains the widening of the $\Delta J = 2$ manifold in each titration, as the pH was raised. Confirmation of 1 : 1 (complex : anion) binding was obtained from $ESMS^+$ spectrum of EuDAP7A in the presence of Na_2CO_3 revealing peaks consistent with $[EuDAP7A(CO_3)]^+$ (*m/z 986*), possessing the correct isotope pattern. Comparing the radiative lifetime measurements in H_2O ($k_{pH=7.4}$ =2.20 ms^{-1}) and D_2O ($k_{pD=7.1}$ =1.94 ms^{-1}), EuDAP7A(CO_3) was revealed to be a $q = 0$ system (*EuDAP7A is q = 1, see 2.4.2.1.*).

Taken together these HCO_3^-/lactate$^-$/citrate^{3-}/HPO_4^{2-} titrations suggest that the anion binds in such a way that the axial donor is *not* perturbed. This may occur, for example, if one of the amide carbonyl groups occupies an axial site, and the anion binds in an equatorial plane.

Having executed these studies, it is possible to interpret the intensity ratio *versus* pH plot when the endogenous anion mixture was used as the background medium (*Fig. 4.13*). In acidic pH, above pH 3.5 lactate binds to the Eu centre, replacing the bound water molecule from the coordination sphere. As a result of its significantly higher concentration, lactate (2.3 mM) suppresses citrate (0.13 mM) binding in this pH regime. As the pH increases further, lactate binding competes with carbonate ligation, shifting the apparent pK_a of the carbonate complex from 6.4 to 7.2 (±0.1).

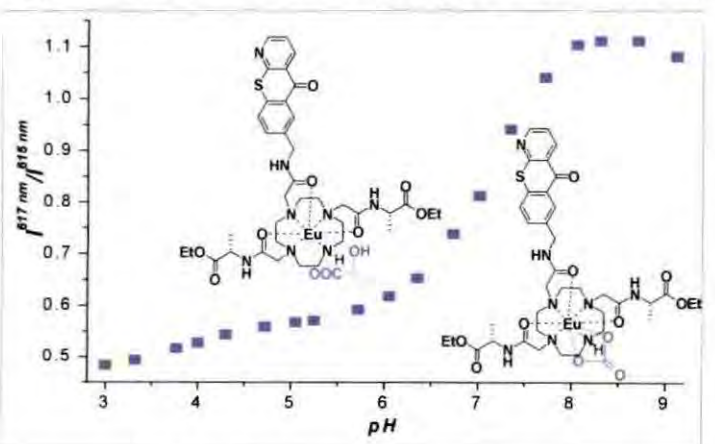

Fig. 4.13. Intensity ratio (617/615 nm) *versus* pH plot for EuDAP7A using 'anion-stew' as the background medium, highlighting the dominant EuDAP7A(anion) species of the limiting ratios in solution. (1 : 1 binding assumed and confirmed by $ESMS^+$ with $[EuDAP7A(CO_3)]^+$)

4.3.1 ^{1}H NMR Studies of Anion Binding

It is widely appreciated that the optical and NMR spectral properties of paramagnetic complexes of the lanthanides are determined by the nature and local symmetry of the coordination environment.[44-46] Europium emission spectra allow information to be obtained concerning the dipolar polarisability of the donor group(s), as the intensities of the electric-dipole allowed transitions are highly sensitive to the nature of the axial donor ligand.[33,47] Analysis of the form and relative intensity of the electric dipole allowed $\Delta J = 2$ transition reveals information on the site symmetry and especially the polarisability of the donor atoms, while by studying C_4-symmetric complexes separation of the two emission bands observed in the magnetic-dipole allowed $\Delta J = 2$ manifold provides direct measurement of the second-order crystal field parameter (B_0^2). Monitoring the changes in the ^{1}H NMR spectra of a given Eu complex, modulation in the polarisibility of the axial donor causes well established changes in the paramagnetically shifted spectrum.[34] Displacement of the bound water molecule occupying the axial site causes significant ^{1}H-NMR shifts for the ligand ring protons, with the biggest change in the 'axial' ring proton resonance.

Studying the effect of introduced anions on the EuDAP7A emission profile as a function of the pH revealed some interesting observations. For example, the europium emission lifetime remained constant ($\tau_{pH=7.4}$ = 0.45 (±0.05) ms) following anion ligation to the europium centre. As noted earlier, irrespective of the nature of anion binding, no significant changes were observed in the form and intensity of the Eu emission spectrum. This behaviour is consistent with the *absence* of change in the polarisiablity and hence, nature of the axial donor group. This theory was confirmed by a comparison of the ^{1}H-NMR spectra of the complex (10 mM EuDAP7A in D_2O, pD 7.1, 295 K) in the presence and absence of 30 mM sodium bicarbonate. Addition of carbonate caused a sharpening of the observed resonances, but no other significant differences were found in the appearance of the paramagnetically shifted spectrum. In contrast, the mean chemical shift of the axial ring proton varied by about 15 ppm between the aqua complex and the carbonate bound species in earlier studies.[29,35]

The spectroscopic observations suggest that EuDAP7A possesses a compact geometry, with an amide carbonyl oxygen coordinated to the Eu centre in the axial position. Therefore, the inner sphere water molecule bounds to the lanthanide in an equatorial site. Following anion binding, insignificant changes in the complex geometry and consequently in the emission or ^{1}H NMR spectra were observed. However, these measurements do not reveal the precise symmetry and geometry of the complex EuDAP7A, and one cannot easily distinguish between pairs $\Lambda(\delta\delta\delta\delta)$ and $\Delta(\lambda\lambda\lambda\lambda)$ for the antiprismatic coordination or even $\Lambda(\lambda\lambda\lambda\lambda)$ and $\Delta(\delta\delta\delta\delta)$ for the putative distorted antiprism. Only by NOE measurements can one assign which is the more stable structure in solution. X-ray crystallography of single crystals of the ternary adduct EuDAP7A(CO_3) could define the structure in solid state.

4.3.2 CPL Studies

Circular polarised luminescence (CPL) is a technique which explores the differential emission of left and right circular polarised light by chiral luminescent complexes.[48] Since the excitation is achieved via the sensitising moiety, the technique overcomes the limitations of low molar absorption coefficients experienced in circular dichroism. Because complexes of opposite helicity will interact differently with circular polarised light, CPL can reveal the helicity about the metal centre, and provide some information about the electronic and magnetic environment of the lanthanide.[37] CPL spectra from EuDAP7A in the absence and presence of 10 mM bicarbonate (*Fig. 4.14*) were obtained at Glasgow University (with Dr. R. D. Peacock).

CPL spectrum of the complex EuDAP7A did not change upon introduction of 10 mM bicarbonate into the solution. This is consistent with the previous suggestion, concluded from luminescence and ^{1}H-NMR studies, that EuDAP7A possesses a compact geometry, with an amide carbonyl oxygen coordinated to the Eu centre in the axial position. This was confirmed by analysis of the splitting of the magnetic dipole allowed $\Delta J = 1$ manifold. Previous work in Durham[34] revealed that change in the nature of axial donor group primary determines the second order crystal field coefficient, B_2^0, that is directly proportional to the splitting of A and E components of the $\Delta J = 1$ manifold. The

splitting was found to be 180 cm^{-1} (6 nm) for water (i.e. in the diaqua complex), and 110 cm^{-1} (3.5 nm) for systems where the amidecarbonyl occupies the axial position.[34] For EuDAP7A, this splitting was 3.5 nm (between bands 593.5 and 587 nm), which did not change upon anion ligation. Therefore, it is very likely to be an amidecarbonyl group which occupies the axial position in the aqua complex and the inner sphere water molecule bounds to the lanthanide in an 'equatorial' site. Therefore, following anion binding, insignificant changes in the complex geometry and consequently in the emission, CPL or ^{1}H-NMR spectra could be observed. This was also confirmed by analysing changes in the emission dis-symmetry factors.

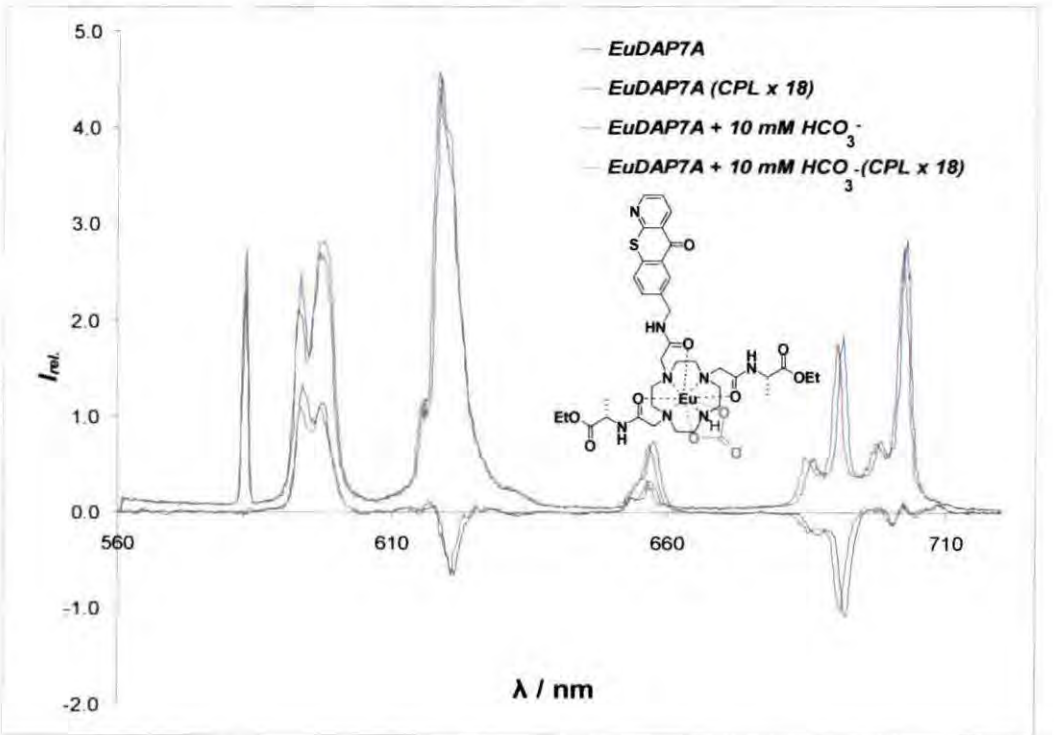

Fig. 4.14. Eu emission and CPL (x 18) spectrum of EuDAP7A in the presence and absence of 10 mM sodium bicarbonate (in D_2O, [complex] = 10 μM, 298 K, λ_{ex} = 384 nm, I = 0.1 M NaCl, pD = 7.2).

Emission dis-symmetry factors, g_{em}, provide a measure of the 'degree of chirality' sensed by an electronic transition and are calculated through application of Equation (5.1) below.[37]

$$g_{em} = 2(I_L - I_R)/(I_L + I_R) \qquad (5.1)$$

($I_{L(R)}$ is the intensity of the left (right) circularly polarised component)

g-Factors were determined (*not shown*) for EuDAP7A in the absence and presence of added bicarbonate and only minor changes occured.

Mirror image CPL spectra have previously been reported for the (*SSS*)-triamide parent complex (*Fig.4.15*).[29,37,49]

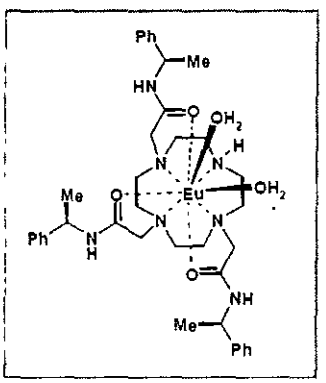

Fig. 4.15. Structure of (*SSS*)-1,4,7-tris(1-phenylethylacetamide)-1,4,7,10-tetraazacyclododecane.

The sign and sequence of the transitions observed for EuDAP7A is the same as for the parent (*SSS*)-tri-amide Eu(III) analogue, whose absolute configuration has been verified by X-ray crystallography.[33] It can be concluded that the lanthanide ion is in the same coordination environment in both the related tri-amide complex and EuDAP7A, and that the helicity of the ligand around the metal centre is the same.[29,34] Each of the (*SSS*)–complexes can therefore be assigned a Δ helicity. Comparison of g_{em} values with the parent tri-amide complex also showed consistency.

4.3.3 Photophysical Response to Endogenous Anions

As this complex has shown sensitivity towards each endogenous anion studied, concentration dependent titrations were carried out in order to determine apparent binding constants. These measurements were executed using the methodology detailed in *Section 3.3.2.1.*

Determination of the apparent binding constant for citrate was carried out by varying the concentration of the added anion from 0 – 130 μM, maintaining a constant pH = 7.4 (±0.05) (*Fig. 4.16*). The intensity ratio (617/615 nm) exhibited a strong citrate dependence. Calculation of the apparent binding constant gave a value of logK= 4.33 ±0.03 M^{-1}. A similar value was obtained (±0.03) using a 688.5/700 nm ratio.

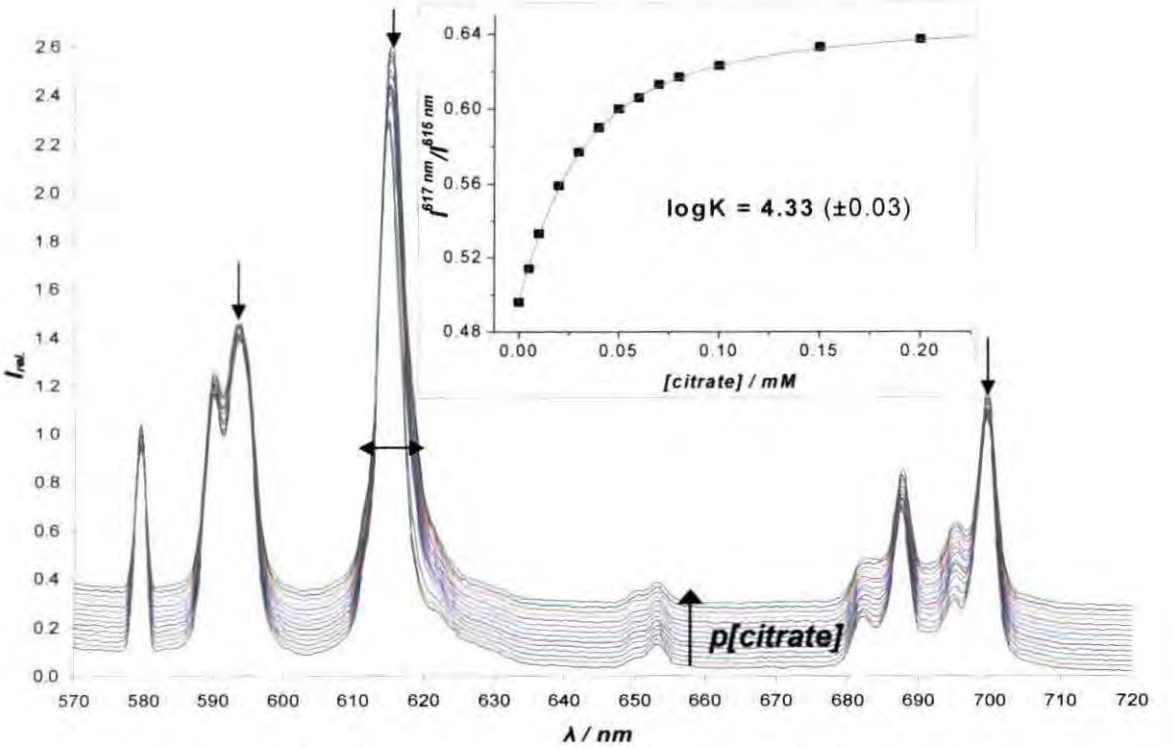

Fig. 4.16. Variation of Eu emission spectrum for EuDAP7A following addition of sodium citrate solution (pH = 7.4 (±0.05), [complex] = 10 μM, 298 K, λ_{ex} = 384 nm, I = 0.1 M NaCl). (*insert*) Intensity ratio (617/615 nm) *vs.* added bicarbonate plot, allowing estimation of the apparent binding constant of citrate. (LV_{min} = 0.496 and LV_{max} = 0.655)

The effect of added lactate on the metal based emission was studied similarly using sodium lactate in the range of 0 – 2.3 mM, maintaining a constant pH = 5.5 (±0.05) (*Fig. 4.17. left*). Using the intensity ratio (617/615 nm or 594/592 nm), a logK value of 2.67 ±0.02 M^{-1} was calculated for lactate binding to the Eu centre. With added monohydrogen phosphate, at a constant pH of 7.4 (±0.05) over the range of 0 - 0.9 mM (*Fig. 4.17. right*), a value of logK 3.14 ±0.03 M^{-1} was calculated. Similar values were obtained by plotting 700/687.5 nm or 594/592 nm ratios.

Determination of the apparent binding constant for bicarbonate was carried out by varying the concentration of the added anion from 0 – 30 mM, maintaining a constant pH = 7.4 (±0.05) (*Fig.4.18*). Upon concentration increase of the analyte, the most notable change was the appearance of a band at 617 nm, as noted above. Calculation of the apparent binding constant gave a value of logK = 3.01 ±0.02 M^{-1}; similar values were obtained (±0.06) using 700/687.5 nm or 594/592 nm ratios.

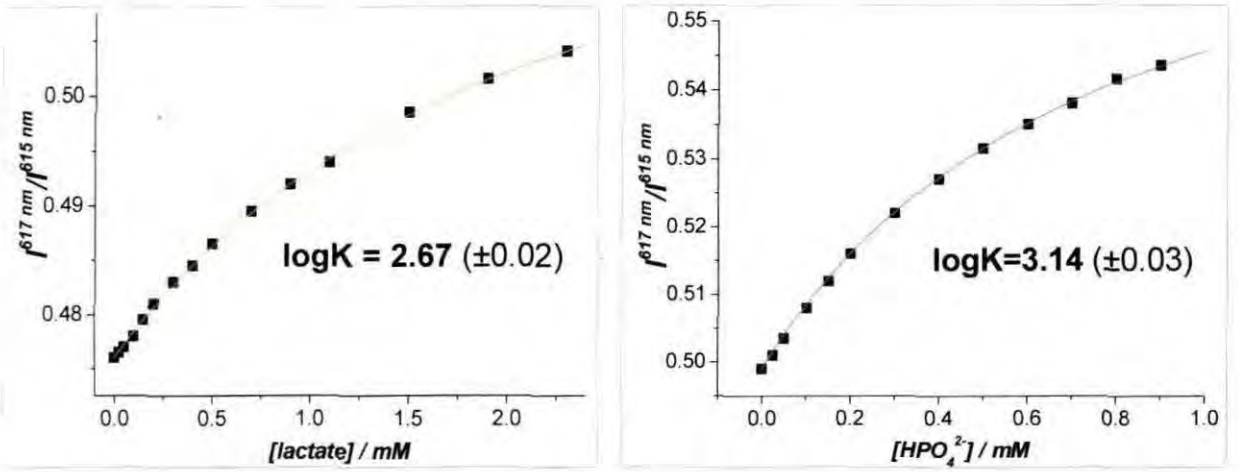

Fig. 4.17. Selected intensity ratio (617/615 nm) *vs.* added anion concentration plot for (*left*) sodium lactate (pH = 5.5 ±0.05) and (*right*) sodium monohydrogen phosphate (pH = 7.4 ±0.05), for determining their apparent binding constant to EuDAP7A. ([complex] = 10 μM, ΔpH= ±0.05, 298 K, λ_{ex} = 384 nm, I = 0.1 M NaCl). (LV_{min}= 0.476 and LV_{max}= 0.523 (*left*), LV_{min}= 0.499 and LV_{max}= 0.580 (*right*))

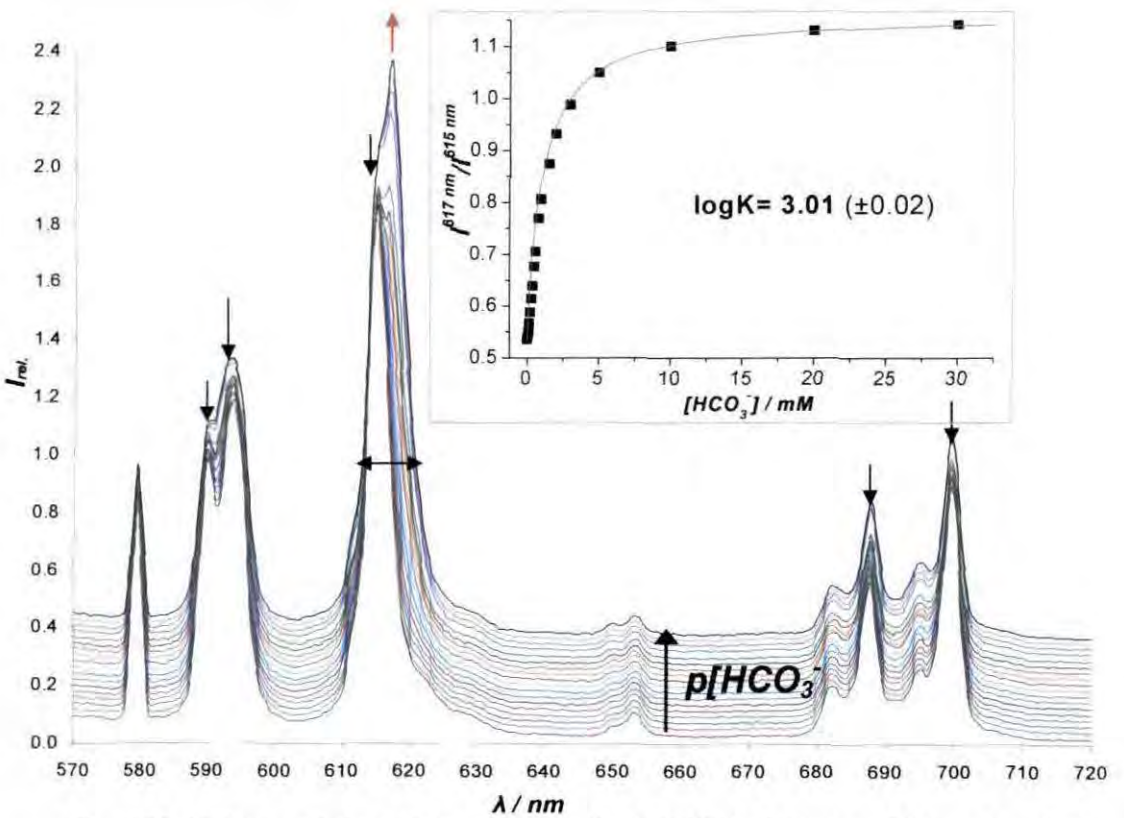

Fig. 4.18. Variation of Eu emission spectrum for EuDAP7A following addition of sodium bicarbonate (pH = 7.4 ±0.05), [complex] = 10μM, 298 K, λ_{ex} = 384 nm, I = 0.1M NaCl). (*insert*) Plot of intensity ratio (617/615 nm) *vs.* added bicarbonate, allowing calculation of the apparent anion binding constant. (LV_{min}= 0.535 and LV_{max}= 0.150)

Titrations were carried out in order to study the effect of added protein on the apparent anion binding constant. Introduction of other extracellular anions to the solution prior to bicarbonate addition, altered the calculated binding constant only slightly, and a ~10% decrease was observed (logK = 2.78 ±0.01 M^{-1}). Repeating the titration with 'carbonate-free anion stew' containing 0.7 mM HSA (or reconstituted 100% Human Serum) as the medium, the calculated affinity remained the same (±0.08). The selectivity for bicarbonate is therefore maintained in the presence of protein (0.7 mM HSA) and endogenous cellular constituents (2.3 mM lactate, 0.9 mM HPO_4^{2-} and 0.13 mM citrate). Measuring the radiative lifetime values in the presence of added anions and/or protein no significant changes were observed with only a 5% decrease in τ_{Eu} with added HSA.

These measurements confirm the possible spectroscopic application of EuDAP7A for measuring bicarbonate concentration in biological samples. However it will be limited in its application, due to the modest structural changes in the emission profile, which can only be monitored with a high resolution emission spectrophotometer.

4.4 Effect of Added Protein on the Emission Profile

The effect of added protein was thoroughly examined. Monitoring the Eu emission spectra of EuDAP7A, as a function of pH, using mixed endogenous anion background with added 0.7 mM HSA, no changes were observed in the spectral properties and consequently in the intensity ratio *versus* pH plot (*Fig. 4.20. left*).

However, interesting observations were made examining the photophysical response of EuDAP7A to added protein. Titrations were carried out at pH 7.4, monitoring changes in both ligand fluorescence (440 nm) and Eu emission (570 – 720 nm) (*Fig. 4.19*), as a function of added protein, using anion-stew or water as background media. Increase of the protein concentration in solution was effected by addition of HSA as a lyophilised solid. Upon increase in added HSA concentration, regardless of the nature of the applied background medium, significant structural changes in the Eu emission were not observed. Therefore, direct binding of functional groups of protein side chains to the Eu centre does not occur.

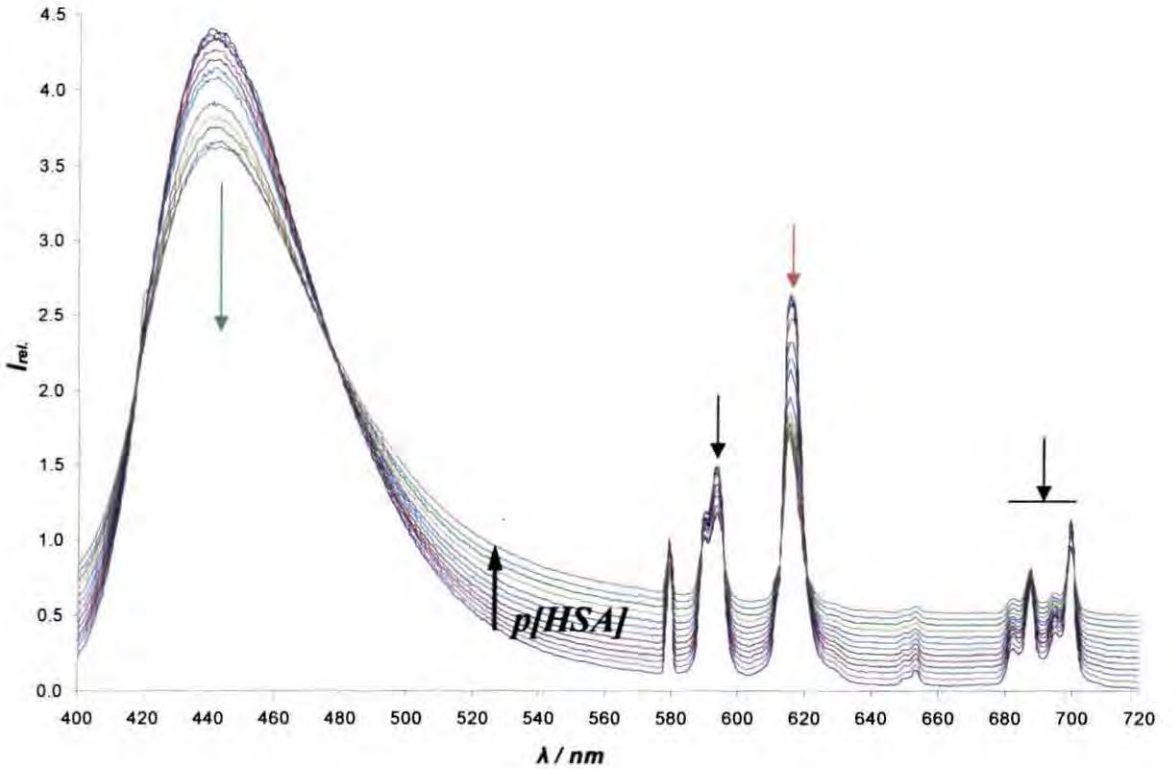

Fig. 4.19. Change in the intensity of ligand fluorescence (400 - 570 nm) and Eu emission spectrum (570 - 720 nm) for EuDAP7A in simulated extracellular anion background as a function of added HSA (pH = 7.4 (±0.05), [complex] = 10 μM, 298 K, λ_{ex} = 380 nm, I = 0.1 M NaCl).

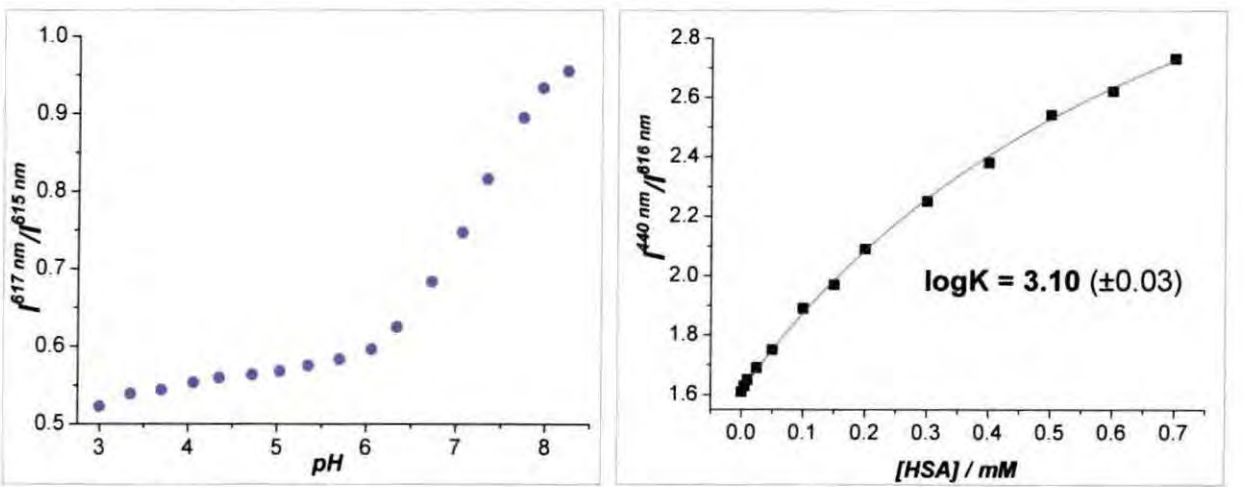

Fig. 4.20. (*left*) Intensity ratio (617/615 nm) *versus* pH plot for EuDAP7A using 'anion stew' containing 0.7 mM HSA as the background medium. (*right*) Determination of the apparent binding constant for HSA in water, from intensity ratio (612/440 nm) *versus* added HSA plot for 1:1 binding model, pH = 7.4 (±0.05). ([complex] = 10 μM, 298 K, λ_{ex} = 384 nm, I = 0.1 M NaCl). (LV_{min}= 1.61 and LV_{max}= 4.00)

With increasing protein concentration, not only the intensity of the ligand fluorescence decreased, but a decrease of the Eu emission was also observed in solution. The change in both ligand fluorescence and Eu emission may be attributed to quenching of the chromophore excited S_1 state by the aromatic groups in HSA. However, as a result of the differential decrease in ligand/Eu intensity, an apparent proton affinity constant could be calculated by examining the ratio of ligand fluorescence (444 nm) to Eu emission intensity (616 nm) *versus* added protein (*Fig. 4.20. right*). The protein affinity of EuDAP7A, regardless of the nature of the medium, was found to be logK = 3.10 ± 0.03 M^{-1}.

No significant changes were observed by studying the change in the radiative lifetime as a function of increasing protein concentration. However, measuring the quantum yield for EuDAP7A in the presence of endogenous anions and protein in their extracellular concentrations, a 40% decrease was observed (φ_{Eu} = 3.3%). This suggests that some quenching of the chromophore T_1 state may also occur, thereby limiting the overall Eu emission.

Notwithstanding these limitations, this complex may still be used for *in vitro* carbonate concentration determination, with the aid of a suitable calibration curve obtained at constant protein concentration.

4.4.1 Analysis of Protein Binding Using GdDAP7A

Measurements of the variation of the relaxivity of Gd complexes as a function of added protein allow an assessment of protein affinity to be made. The complex GdDAP7A was prepared and changes in the relaxivity were monitored as a function of added protein concentration in water in the presence and absence of 30 mM sodium bicarbonate (*Fig. 4.21*). The pH of the solution was maintained at 7.4 (± 0.05).

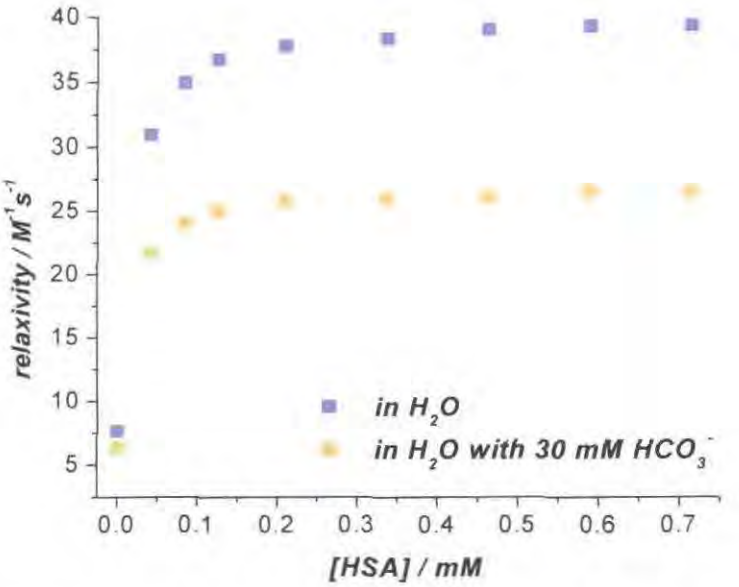

Fig. 4.21. Variation of the relaxivity of GdDAP7A in water (▪) and in the presence of 30 mM added sodium bicarbonate (▪) as a function added protein concentration at pH 7.4 (±0.1). ([complex] = 80 μM, 310 K, 60 mHz, I = 0.1 M NaCl).

The relaxivity was monitored as a function of added HSA in the absence and presence of 30 mM sodium bicarbonate. The relaxivity of GdDAP7A was measured to be 7.6 $mM^{-1}s^{-1}$ as the triflate salt and 6.4 $mM^{-1}s^{-1}$ as the carbonate adduct in water. Incremental addition of protein to the complex solution caused the relaxivity to rise steeply. In the presence of 0.2 mM serum albumin, the relaxivity increased to 39.2 $mM^{-1}s^{-1}$. Further addition of protein caused no significant relaxivity change. When 30 mM bicarbonate was present, this limiting relaxivity value fell to 26.5 $mM^{-1}s^{-1}$, and the inverse addition experiment gave a solution with a similar relaxivity value (±3 $mM^{-1}s^{-1}$). Taken together, this behaviour is consistent with reversible binding of the complex to the protein as suggested in the luminescence experiments. Bicarbonate binds preferentially to the Eu complex in the presence of protein, whilst the bicarbonate adduct itself ($q = 0$) also binds to protein, giving rise to a smaller relaxivity enhancement in the ternary adduct.

Fitting these relaxivity vs. added HSA plots suggested 1 : 1 binding, irrespective of the presence of bicarbonate, and similar apparent binding constant values were obtained with logK = 3.07 ±0.04 M^{-1}. Such a value is in accordance with that calculated from the corresponding luminescence experiment.

4.5 Quenching Studies

Previous studies with the pH probe Eu(MS)DAdP2, incorporating a 2-methyl-azathioxanthone chromophore, revealed its resistance towards quenching by biologically common electron rich donors, such as urate and ascrorbate (*Section 3.4*). Therefore, it was essential to study the susceptibility to quenching of the Eu(III) excited state via charge-transfer interaction by these anions.

In order to examine whether the introduction of urate and/or ascorbate had any effect on the photophisical properties, the Eu emission was monitored at pH 7.4 (±0.05), as a function of added 'quencher'. Sodium ascorbate was added up to a limiting value of 0.5 mM, followed by the incremental addition of up to 1 mM urate.

Addition of ascorbate slightly altered, while urate did not perturb the structure of the Eu emission. However, the intensity of the emission spectrum showed a 35% decrease over the observed ascorbate range, with a further 25% decrease upon addition of 1 mM sodium urate. Monitoring the radiative lifetime values as a function of added 'quencher', only minor changes were observed using ascorbate, but a significant 20% decrease was shown in the measured lifetimes over the observed concentration range of added urate. Consequently, this complex is quenched by these biologically common electron rich donors. However, the effect is not as drastic as found previously for complexes with azaxanthone or tetrazatriphenylene chromophores.[50] The moderate susceptibility towards quenching may be associated with the higher reduction potential of the 7-(methylcarbamoyl-methyl)-azathioxanthone moiety.[43]

4.6 Two Photon Absorption and Photoluminescence[51]

Application of lanthanide complexes usually relies upon a single photon excitation process. Absorbtion of light in the range of 320 - 400 nm by the chromophore ($S_0 \rightarrow S_1$), is followed by an intersystem crossing ($S_1 \rightarrow T_1$) and intramolecular electronic energy transfer to the Ln^{III} ion. For some applications, this approach can be problematic, due to the non-selective nature of the excitation (UV-visible), leading to autofluorescence and photo-damage. It is desirable to avoid the UV-visible range, and target the far

visible/near-IR range (700 - 820 nm) which penetrates biological media more effectively. Multiphoton excitation spectroscopy enables the excitation of chromophores with near-IR optical radiation to generate states that are normally accessed by the absorption of a single UV-quantum of UV light.[52,53]

To date, there have been only limited reports of the observation of the direct excitation of lanthanide ions and of various complexes following multi-photon absorption.[54,55] The high intensities required for two photon absorption necessitate tight focusing of the excitation light, giving the method a high spatial resolution. Two-photon excited (TPE) photoluminescence (PL) can be observed from functionalised Ln^{III} complexes in aqueous solution, following excitation from the output of a cavity dumped mode-locked Ti-sapphire laser, operating at 4 MHz repetition rate. This setup allows a sufficiently long time-gate to be used to efficiently eliminate any undesired short lived emission, such as ligand or auto-fluorescence (τ ~10ns), focusing purely on the long lived Ln emission, (τ ~ms). The procedure provides a high duty cycle with a sufficiently high repetition rate to permit rapid scanning of the sample for microscopic imaging. The cavity dumped laser also allows higher pulse energies than a comparable mode-locked laser. It retains a relatively low pulse energy (<100 nJ/pulse) compared to the use of amplified laser systems, where much higher pulse energies are obtained (>μJ/pulse), with the potential for sample damage.[56]

The complex EuDAP7A in D_2O showed a well resolved fluorescence from both the ligand and long lived emission from the Eu $^5D_0 \rightarrow {}^7F_J$ transitions upon excitation in the near IR range at 758 nmm (*Fig. 4.22 left*). From TPE wavelength *versus* PL emission intensity plots the TPE maximum was determined to be 770 nm. The broad feature centred at 440 nm is fluorescence emission from the ligand and the sharp bands at lower energy are the $^5D_0 \rightarrow {}^7F_{0\text{-}3}$ emission bands of Eu(III). It is important to note that due to the presence of a dichroic mirror in the optical path of the two-photon excitation spectrometer, the $^7F_4$ band cannot be detected. A plot of the log (integrated emission intensity) plotted against log (excitation power) shows a gradient of 2.1 ±0.1, confirming that the emission is due to a two photon absorption

process. Importantly, the spectrum is identical to that obtained by UV excitation (*see Fig.4.8 right*), in contrast to what has been reported previously.[55]

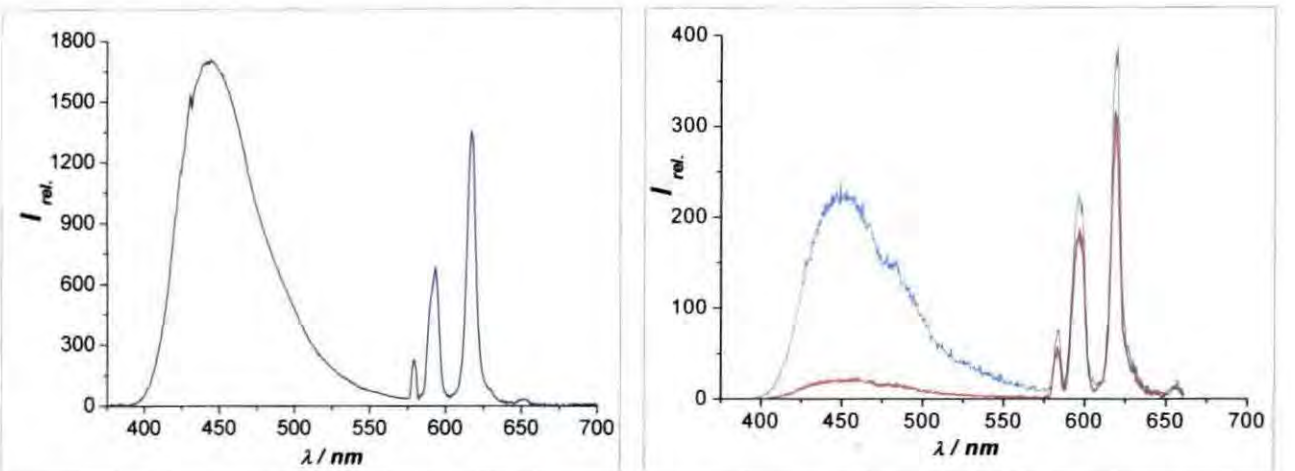

Fig. 4.22. (*left*) Emission spectrum of EuDAP7A excited under two photon absorption conditions at 758 nm. (*right*) Time-gated and total emission of EuDAP7A. The time-gate had a duration of 480 ns and was delayed 75 ns from the laser pulse. (D_2O, [complex]= 30 μM, pD = 7.2).

Due to the instrumental set-up, the time gated emission spectra were also recorded for EuDAP7A (*Fig. 4.22 right*). The broad emission at 450 nm is associated with ligand fluorescence, originated from the sensitiser's S_1 state and significantly reduced in intensity relative to the Eu(III) emission upon time gating. The time gated spectrum does show a relatively small amount of chromophore fluorescence, attributed to the leakage of mode-locked optical pulses, which are not fully suppressed by the cavity dumper of the mode locked laser system.

The results of this study have several important implications:

- EuDAP7A appears to have a sufficiently high TPE cross-section and photoemission to be observed possessing a strong and well-defined signal, despite the fact that this complex was not designed for a high TPE cross-section.
- the technique allows discrimination of any disturbing auto or ligand fluorescence, which can be orders of magnitude stronger then the metal based emission.
- Identical spectra may be obtained for one and two photon excitation, contrary to earlier work.

4.7 'In cellulo' Studies

The cellular uptake profile of the complex EuDAP7A was examined in Chinese hamster ovarian cells (CHO) cells, which were grown in a monolayer on 0.1 mm thick glass cover slips. Incubation times varied from 1 to 12 h, while the complex loading concentration was 100 μM dissolving lyophilised complex in F-12(Ham) media containing 10% NCS (Newborn Calf Serum) and 1% Penicillin-streptomycin. Prior to mounting of the cells without any additional treatment, incubation in a copper jacketed incubator using 5% CO_2 and about 10% relative humidity was carried out for each individual time point. Cover slips were mounted, by withdrawal of the growth medium and subsequently washed three times with phosphate buffered saline (PBS) solution. The uptake and distribution of the complex within the cell was observed by fluorescence microscopy, following excitiation of the chromophore.

Epifluorescence images were taken on a Zeiss Axiovert 200M epifluorescence microscope with 63x/1.40 oil DIC and 40x/1.40 oil DIC objectives. For excitation a band-pass (BP) 340 - 390 nm (90% transmission) filter was used. Ligand fluorescence were observed using a 445 - 465 nm band-pass filter (80% transmission), while Eu emission was observed using a 570 nm long-pass (LP) filter (85% transmission). Confocal microscopy images were taken on a Zeiss LSM 500 META confocal microscope with a BIORad 405 nm diode laser excitation; an LP 590 nm emission filter was used for europium luminescence and a BP 505 - 550 nm filter for the study of ligand fluorescence.

4.7.1 Cellular Uptake Study

2 h

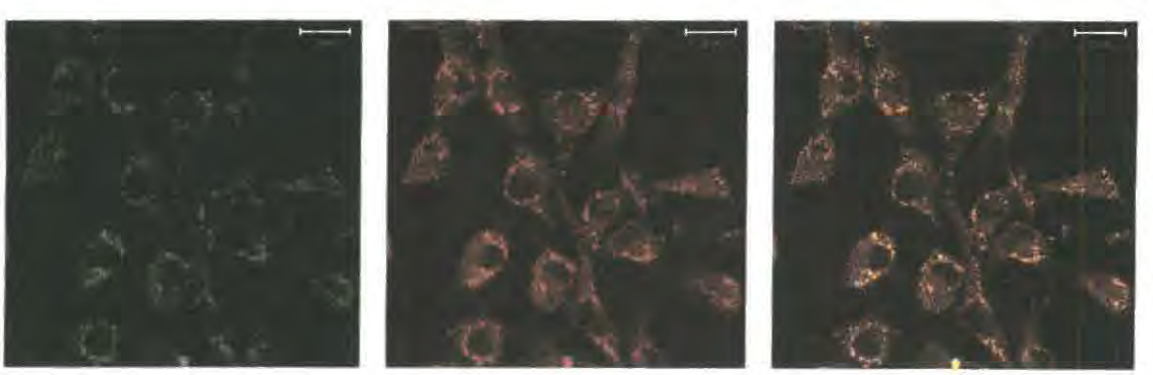

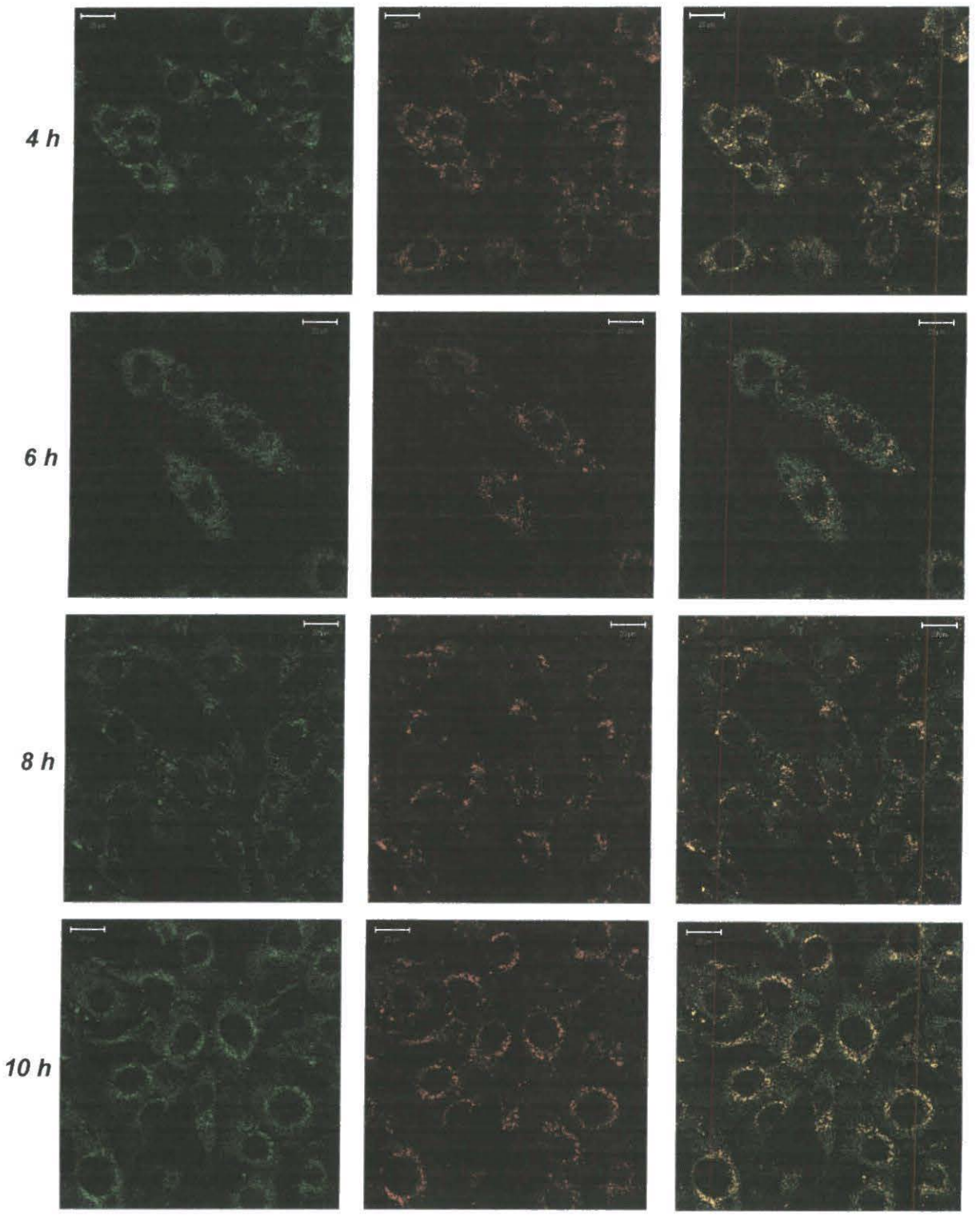

Fig. 4.23. Confocal microscopy images at different loading time points in CHO cells, showing the localisation and cellular uptake of EuDAP7A ([complex] = 100 μM, 405 nm diode laser excitation); (*left*) Ligand fluorescence was observed using a BP 505 - 550 nm filter (*middle*) Eu emission was observed using LP 590 nm filter; (*right*) merged images using ImageJ™ software.

As shown in *Fig. 4.23*, incubation of CHO cells with EuDAP7A resulted in fluorescence that could be readily detected. At each time point (2, 4, 6, 8, 10, 12 h) fluorescence and confocal images were recorded; the former ones immediately, whilst confocal images were recorded for all images after 24h. When optical sections throughout the cells were taken, the fluorescence could be detected in all layers. This confirms that the complex was successfully taken up into the cells, and was not merely associating with the cell membrane. As a control, untreated cells were mounted and they showed no fluorescence in each wavelength region. Images were taken at a number of points across the slide, with a similar localisation profile observed at each position.

Images recorded at 30 min, 1 h and 2 h showed a similar localisation profile, with similar overall fluorescence intensity and acquisition time, with no time dependence of either ligand or Eu emission intensity. This aspect was studied, by comparing the acquisition time for constant overall brightness of each recorded image containing a constant number of cells as a function of complex loading time. The colour consistency of the merged images suggests that the complex remains inert and that no dissociation of Eu has occurred within the cells. There appears to be no fluorescence in the nucleolus, with fluorescence localised in other organelles in the cytoplasm. The appearance of these organelles is most consistent with the size and distribution of late endosomes or lysosomes. This hypothesis for localisation echoes similar observations for the early carbonates sensors synthesised by *Bretonniere*,[26] another europium complex that possesses pendant (S)-alanine ethyl ester arms (*Fig. 4.24*).

Fig. 4.24. Confocal microscopy images of a Eu complex[26] incorporating an N-linked acridone sensitising moiety, co-localised with Lysotracker green® in NIH 3T3 cells. Orange regions of the merged images correspond to areas where both stain and complex are localized confirming ***lysosomal localization***.

In order to confirm this compartmentalisation, it would be necessary to use co-localisation experiments involving staining with a probe for lysosomes, such as Lysotracker™ or Lysosensor™ stains (Invitrogen) with a high specificity for acidic organelles. However, the application of such probes is problematic as Lysotracker Green has maximum excitation and emission wavelength of 504 nm and 511 nm respectively, which overlap with the emission spectrum of the azathioxanthone sensitising moiety. Moreover, it is not possible to select a filter set for this dye as its very small Stokes' shift meant that excitation light could pass through the emission filter. Lysosensor Green overcomes this problem, as it is excited at 443 nm and emits at 505 nm. However, following 405 nm confocal excitation, this emission tends to overlap with the ligand fluorescence of EuDAP7A, or any Eu complex incorporating an azathioxanthone chromophore.

Interesting phenomena occurred when acquiring images from the 4 h time point onwards. As revealed in *Fig. 4.23.*, with the merged image, increasing ligand fluorescence (green) was observed throughout the rest of the cytoplasm. However, based on the image acquisition times, a similar intracellular complex concentration must be present. This green ligand fluorescence may be associated either with slow complex dissociation in the acidic endosomes; or selective quenching of the Eu emission in these organelles, by electron rich bio-molecules, as found in *in-vitro* quenching experiments. A better understanding of this phenomenon requires colocalisation studies with Brefeldin-A®, low temperature (4 °C) cellular uptake studies and egress studies with different complex loading concentrations.

A similar endosomal localization profile has been observed with the C-linked acridone isomer of the Eu complex used above for localization comparison (*Fig. 4.25*), also sythesised by *Bretonniere* as a carbonate sensor.[26]

Brefeldin-A is a lactone antibiotic produced by fungal organisms such as *Eupenicillium brefeldianum* that absorb and emits light at 503 nm and 510 nm respectively. Brefeldin-A interferes with anterograde protein transport from the endoplasmic reticulum (ER) to the Golgi apparatus by inhibiting transport in Golgi, which leads to proteins accumulating inside the ER.[57]

Fig. 4.25. Confocal microscopy images of a Eu complex[25] incorporating a C-linked acridone sensitising moiety, co-localised with Brefeldin-A® in NIH 3T3 cells. Orange regions of the merged images correspond to areas where both stain and complex are localized suggesting ***localization in the endoplasmic reticulum***. However, a more diffuse background is also apparent, corresponding to distribution throughout the cytosol.

Loading the complex onto the cells at 4 °C, if europium luminescence can still be observed with the same localization profile, this would indicate the likehood of the complex entering the cells by endocytosis. The uneven distribution of the complex in the cytoplasm supports this premise. Molecules and conjugates entering cells via endocytosis are believed to be initially trapped in endocytotic vesicles and then transferred into endosomes. Only molecules and conjugates escaping from the endocytosis pathway can survive to act as probes.[58] This may be confirmed by association of the cellular uptake profile. As found with Eu(MS)DAdP2, the relatively fast influx of the complex, and rapid egress, upon withdrawal of the complex from the growth medium suggested complex uptake via a diffusion-driven transport mechanism across the cell membrane. The driving force of this hypothetical mechanism is the complex concentration gradient between the intracellular and extracellular region. This premise is supported by the observed time independent complex uptake, concluded from fluorescence microscopy studies. Relatively rapid cellular uptake was found with EuDAP7A as well; therefore this 'uptake and localisation paradox' needs to be studied further in the future.

The cell viability was found to be concentration and time independent. It was monitored by visual counting of the number of cells in a selected population, as a function of time. From bright field measurements, more than 95% of the cells were judged to be healthy over the studied 12 h period. This observation however, does not

exclude the possibility of complex dissociation; as it might still occur in the late endosomes stabilising the subsequently elevated 'free' europium in a non-toxic form. Further information may be gained by monitoring the egress of the complex from the cell, as upon complex dissociation an increase in ligand fluorescence should be observed in the total emission spectrum.

Another interesting observation was made when the cells were mounted after 4h complex incubation with a subsequent 1h incubation in the absence of complex in F12(Ham) medium (*Fig. 4.26*). As noted previously, after a 4 h incubation with EuDAP7A, lysosomal and/or endosomal localization was observed. The merged ligand fluorescence and Eu emission images showed consistent localization.

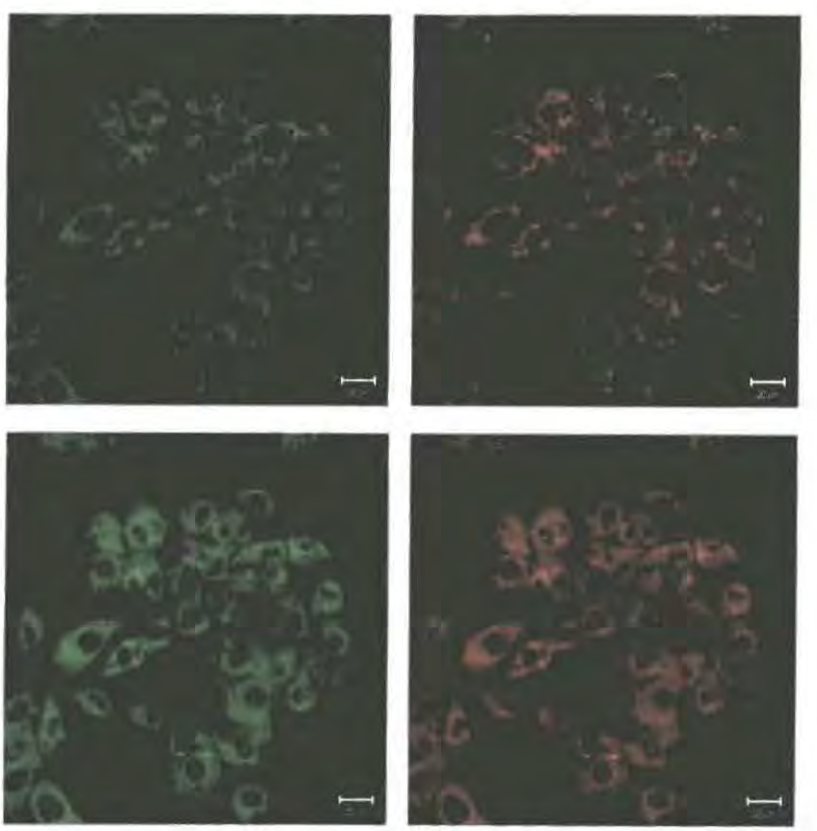

Fig. 4.26. Confocal microscopy images at (*top*) 4 h incubation in the presence (*bottom*) and 1 h subsequent incubation in the absence of EuDAP7A in CHO cells, showing the different localisation of the complex; (*left*) ligand fluorescence; (*right*) Eu emission ([complex] = 100 μM, 405 nm diode laser excitation).

However, after incubation for 1 h following complex withdrawal from the medium, the localization profile has changed. Lysosomal/endosomal localization may still be detected form the images, but a smoother localization is observed throughout the cytoplasm, which may be associated with ribosomal localization or a redirection to regions of high local protein concentration. Such a localization profile was observed when studying the localization and cellular uptake of Eu(MS)DAdP2 and EuDPP2 (*section 3.6.1*), with a more well defined localization in the nucleolus, which is present but is much less evident in this case. The ratio of ligand fluorescence to Eu emission remained constant, with an equal acquisition time (±5%), examining the same cell population. This suggests that, upon withdrawal of EuDAP7A from the growth medium, the complex remains localized in the cell, with egress of less than 10% of the complex to the growth medium; which is consistent with the suggested endocytotic cellular uptake of this Eu-complex. Such an observation is in accordance with the cell viability assessment, and the explanation of time dependent quenching of the Eu emission by bio-molecules, possibly in the endosomes. This agrees with the fact that no significant change in the ligand fluorescence *vs.* Eu emission intensity ratio was measured in the recovered complex solution.

4.7.2 Determination of the Intracellular Europium Concentration

The images obtained by fluorescence microscopy allow identification of the localisation and uptake profile of the complex at a given time point. However, this does not provide quantitative information. Information on this can be gained by focusing on a constant number of cells, at each time point and plotting the image acquisition time for a constant brightness as a function of the incubation time. The exact concentration of the complex in the cell can be determined through a combination of flow-cytometry to determine the number of cells in a population, and ICP-MS to determine the total lanthanide (europium) concentration. Determination of this value can also be made by measuring the absorbance of the complex in the growth medium prior to and after loading it into the cells.

For determination of EuDAP7A concentration in the cells, a 10 h loading time point was chosen. The sorted cells (269,511) were submitted for ICP-MS analysis. The

combined PBS washings, used after growth medium withdrawal, were also analysed. The number of EuDAP7A complexes inside a single cell was determined to be 6.8×10^7. This value gives a $[Eu]_{total}$ of 38 μM inside a single cell (assuming 3,000 μm^3 mean cell volume), *i.e.* 38% of the original loading concentration has been taken up by the cells. This measurement was confirmed by comparing the absorbance values of the complex containing growth medium prior to and after incubation, which gave a 40% (±2%) decrease in complex concentration. The concentration of EuDAP7A in the combined PBS solutions was also measured by ICP-MS, and 7% of the complex concentration was found to be present. This confirms the relatively small decrease in the acquisition times used for the complex withdrawal experiment, detailed above. More importantly, as no significant change in the ratio of ligand fluorescence *versus* Eu emission was found, the observed time dependent localisation profile can be tentatively assigned to quenching of the Eu emissive state or the sensitiser's triplet state in the endocytotic pathway.

The complex EuDAP7A possesses a very interesting uptake and localization profile, with several previously unforeseen features. In order to gain a better understanding of this localization, further investigations of cellular uptake are necessary, including determination of complex concentration as a function of incubation time.

4.8 Conclusions and Future Work

A novel carbonate sensor has been synthesised and studied, incorporating a thoughtfully designed 7-(methylcarbamoylmethyl)-azathioxanthone sensitiser moiety. The luminescence properties have been thoroughly studied, and the changes in the photophysical properties and the sensitivity towards anion binding rationalised. EuDAP7A showed sensitivity towards endogenous anions and protein binding, retaining good selectivity towards the target analyte, bicarbonate. Even in reconstituted 100% human serum, a suitable calibration curve was obtained in the desired 5 – 30 mM HCO_3^- range, using intensity ratio vs. pH plots. The complex exhibits modest resistance towards quenching by biologically common electron rich donors, such as urate and ascorbate. However, due to the small changes in the form and intensity of the Eu emission upon bicarbonate ligation, applications of this complex will be limited. Despite this, two photon excitation and time resolved studies have showed that EuDAP7A or analogues thereof may yet have promising bioimaging application.

Cellular uptake images revealed fast uptake and a well distributed time-dependent localisation within the cell. Uptake studies proved to be complex in nature, with significant amounts of complex entering the cell, possibly via endocytosis. No significant evidence for toxicity was found. Images were observed using unfixed cells, which is beneficial for live cell imaging applications.

Further work is required to assess and confirm the localisation profile of the complex and to determine the mechanism of cellular uptake. Images using different cell lines, such as NIH 3T3, are also required to study changes in the uptake and localisation as a function of cell type.

4.9 References

1 J. H. Zippin, L. R. Levin, and J. Buck, *Trends Endocrinl. Metab.*, 2001, **12**, 366.

2 J. A. T. Dow, *J. Physiology*, 2007, **543**, 633.

3 Y. Chen, M. J. Cann, T. N. Livitin, V. Iourgenko, M. L. Sinclair, L. R. Levin, and J. Buck, *Science*, 2000, **289**, 625.

4 G. S. Kopf, *Adv. De. Biochem*, 1999, **5**, 83.

5 B. U. Kaupp and I. Weyand, *Science*, 2000, **289**, 559.

6 K. C. Ko and R. P. Paradise, *Proc. Soc. Exp. Biol. Med*, 1970, **134**, 469.

7 C. A. Wagner, J. Kovacikova, P. A. Stehbergen, C. Winter, C. Benabbas, and N. Mohebbi, *Nephron Physiology*, 2006, **103**, 1.

8 J. D. Kaunitz and Y. Akiba, *J. Pancreas*, 2001, **2**, 268.

9 A. Mills, Q. Ching, and N. McMurray, *Anal. Chem.*, 1992, **64**, 1383.

10 S. Makarychev-Mikhailov, O. Goryacheva, J. Mortensen, A. Legin, S. Levitchev, and Y. Vlasov, *Electoanalysis*, 2003, **15**, 1291.

11 S. Levitchev, A. L. Smirnova, V. L. Khitrova, L. B. Lvova, A. V. Bratov, and Y. G. Vlasov, *Sensors and Actuators*, 19997, **44**, 397.

12 J. H. Shin, D. S. Sakong, H. Nam, and G. S. Cha, *Anal. Chem.*, 1996, **68**, 221.

13 G. S. Cha and M. E. Meyerhoff, *Electoanalysis*, 2005, **1**, 205.

14 R. P. Haugland, 'Handbook of Fluorescent Probes and Research', 9th ed. Eugene, 2002.

15 J. N. Demas and B. A. DeGraff, *Coord. Chem. Rev.*, 2001, 317.

16 J. L. Lakowicz, 'Principles of Fluorescence Spectroscopy', Academic/Plenum Press., 1999.

17a D. Parker and J. A. G. Williams, in 'Metal Ions in Biological Systems,' New York, Marcel Dekker Inc. 1998, **40**, 233.

17b D. Parker, Y. Bretonniere, 'Luminescent lanthanide complexes as sensors and imaging probes', *Ernst Schering Res. Found Workshop*, 2005, **49**, 123.

17c T. Gunnlaugson, J . P. Leonard, *J. Fluoresc.*, 2005, **15**, 585

17d T. Gunnlaugson, J . P. Leonard, *Chem. Commun.*, 2005, 3114.

18 G. Mathis, *Clin. Chem.*, 1995, 1391.

19 S. G. Jones, D. Y. Lee, J. F. Wright, C. N. Jones, M. E. Lee, S. Y. Gregory, and D. O. Burns, *J. Fluoresc.*, 2001, **11**, 13.

20 D. Parker, *Coord. Chem. Rev.*, 2000, **205**, 109.

21 D. Parker, R. S. Dickins, H. Puschmann, C. Crossland, and J. A. K. Howard, *Chem. Rev.*, 2002, 1977.

22 D. Parker, P.K. Senanyake, and J. A. G. Williams, *J. Chem Soc. Perkin Trans. 2*, 1998, 2129.

23 S. Blair, R. Kataky, and D. Parker, *New. J. Chem*, 2002, 530.

24 R. S. Dickins, T. Gunnlaugsson, D. Parker, and R. D. Peacock, *Chem Commun.*, 1998, 1643.

25 Y. Bretonniere, M. J. Cann, D. Parker, and R. Slater, *Chem. Commun.*, 2002, 1930.

26 Y. Bretonniere, M. J. Cann, D. Parker, and R. Slater, *Org. Biomol. Chem.*, 2004, **2**, 1624.

27 L. Burai, V. Hietopelto, R. Kiraly, E. Toth, and E. Brucher, *Mag. Reson. Imag.*, 1997, **38**, 146.

28 S. Aime, A. Barge, M. Botta, J. A. K. Howard, R. Kataky, M. P. Lowe, J. M. Moloney, D. Parker, and A. S. de Sousa, *Chem. Commun.*, 1999, 1047.

29 J. I. Bruce, R. S. Dickins, L. J. Govenlock, T. Gunnlaugsson, S. Aime, and M. Botta, *J. Am. Chem. Soc.*, 2000, **122**, 9674.

30 M. Botta, S. Aime, A. Barge, G. Bobba, R. S. Dickins, D. Parker, and E. Terreno, *Chem. Eur. J.*, 2003, **9**, 2102.

31 J. Yu, D. Parker, R. Pal, R. A. Poole, and M. J. Cann, *J. Am. Chem. Soc.*, 2006, **128**, 2294.

32 A. Beeby, I. M. Clarkson, R. S. Dickins, S. Faulkner, D. Parker, L. Royle, A. S. de Sousa, J. A. G. Williams, and M. Woods, *J. Chem. Soc.*, 1999, 493.

33 R. S. Dickins, S. Aime, A. S. Batsanov, A. Beeby, M. Botta, J. I. Bruce, J. A. K. Howard, C. S. Love, D. Parker, R. D. Peacock, and H. Puschmann, *J. Am. Chem. Soc.*, 2002, **124**, 12697.

34 J. I. Bruce, D. Parker, R. S. Dickins, and D. J. Tozer, *Dalton Trans*, 2003, 1264.

35 D. Parker, *Chem. Soc. Rev.*, 2004, **2**, 156.

36 L. D. Bari, G. Pintacuda, P. Salvadori, R. S. Dickins, and D. Parker, *J. Am. Chem. Soc.*, 2000, **121**, 5672.

37 J. I. Bruce, D. Parker, S. Lopinski, and R. D. Peacock, *Chirality*, 2002, **14**, 562.

38 P. Atkinson, K. S. Findlay, F. Kielar, R. Pal, D. Parker, R. A. Poole, H. Puschmann, S. L. Richardson, P. A. Stenson, A. L. Thompson, and J. Yu, *Org. Biomol. Chem.*, 2006, **4**, 1707.

39 R. Pal and D. Parker, *Chem Commun.*, 2007, 474.

40 J. Yu and D. Parker, *Eur. J. Org. Chem.*, 2005, 4249.

41 S. Pandya, J. Yu, and D. Parker, *Dalton Trans.*, 2006, 2757.

42 R. A. Poole, G. Bobba, M. J. Cann, J.-C. Frias, D. Parker, and R. D. Peacock, *Org. Biomol. Chem.*, 2005, **3**, 1013.

43 R. A. Poole, C. P. Montgomery, E. J. New, A. Congreve, D. Parker, and M. Botta, *Org. Biomol. Chem.*, 2007, **5**, 2055.

44 B. R. Judd, *Phys. Rev.*, 1962, **127**, 750.

45 G. S. Offelt, *J .Chem. Phys.*, 1962, **37**, 511.

46 S. F. Mason and G. F. Tranter, *Mol. Phys.*, 1983, **50**, 29.

47 J. I. Bruce, D. Parker, and D. J. Tozer, *Chem. Commun.*, 2001, 2250.

48 J. P. Riehl and F. S. Richardson, *Chem. Rev.*, 1986, **86**, 1.

49 R. S. Dickins, J. A. K. Howard, C. L. Maupin, J. M. Moloney, D. Parker, J. P. Riehl, G. Siligardi, and J. A. G. Williams, *Chem. Eur. J.*, 1999, **5**, 1095.

50 R. A. Poole, F. Kielar, S. L. Richardson, P. A. Stenson, and D. Parker, *Chem Commun.*, 2006, 4084.

51 L.-O. Palsson, R. Pal, B. Murray, D. Parker, and A. Beeby, *Dalton Trans*, 2007, 5726.

52 J. R. Lakowiicz, G. Piszczek, B. P. Maliwal, and I. Gryczynski, *Chem. Phys. Chem.*, 2001, **4**, 247.

53 C. Xu and W. W. Webb, *J. Opt. Soc. Am.*, 1996, **13**, 481.

54 M. H. V. Werts, N. Nerambourg, D. Pelegry, Y. LeGrand, and M. Blanchard, *Photochem. Photobiol. Sci.*, 2005, 531.

[55] G. Piszczek, J. R. Lakowicz, J. Dattelbaum, B. P. Maliwal, and I. Gryczynski, *J. Fluoresc.*, 2001, **11**, 101.

[56] G. F. White, K. L. Litvinenko, S. R. Meech, D. L. Andrews, and A. J. Thompson, *Photchem. Photobiol. Sci.*, 2004, **3**, 47.

[57] R. D. Klausner, J. G. Donaldson, and J. Lippincott-Schwartz, *J. Cell Biol.*, 1992, **116**, 1071.

[58] F. Osaki, T. Kanamori, S. Sando, T. Sera, and Y. Aoyama, *J. Am. Chem. Soc.*, 2004, **126**, 6520.

CHAPTER 5

Citrate Sensors

5 Citrate Sensors

5.1 Introduction

The citrate anion exists in all living cells. It is not only an important intermediate in the tricarboxylic acid cycle, but also a key component of fatty acid, cholesterol and hormone synthesis, photorespiration, the glyoxylate cycle and nitrogen metabolism.[1] Due to this metabolic significance, abnormal citrate levels have been linked to the characteristics of several diseases. For example, citrate concentration in urine can reflect renal metabolic imbalance.[2] Decreased urinary citrate excretion has been shown to be important in the pathogenesis of nephrocalcinosis and nephrolithiasis.[3] Recently, citrate has been selected as a marker for the discrimination of prostate cancer.[4,5] Thus, the development of robust citrate assays *in vitro* or *in vivo* is of general significance to the analytical and life sciences.

5.1.1 The Prostate Gland[6-8]

The prostate gland is a male reproductive organ, which is about 3 cm long and weights about 20 g. It is located in the pelvis and sits under the bladder and in front of the rectum (*Fig. 5.1*). The urethra, the narrow tube that runs the length of the penis and is devoted to carry both urine and semen, runs directly through the prostate. Sitting just above the prostate are the two seminal vesicles that secrete about 50 % of the substances that makes up semen. Running alongside and attached to the side of the prostate are the nerves that control erectile function.

The gland is lined with transitional epithelium and fibrous tissue, which gives its soft texture. It can be dividend into four main zones or lobes:

- Peripheral zone, which is the outer layer of the prostate surrounding the distal urethra and is the biggest (70% in volume) portion of the gland from which almost 85% of the prostate cancer originates.[9]
- Central zone, which surrounds the ejaculation ducts, 25% of prostate anomaly can originate in this part of the gland.

- Transition zone, which surrounds the proximal urethra and is very rarely associated with carcinoma. This part is constantly growing and can be associated with benign prostatic enlargement.
- Anterior fibro-muscular zone, which is usually devoid of glandular components, and composed from fibrous tissue and muscle that help expel semen during ejaculation.

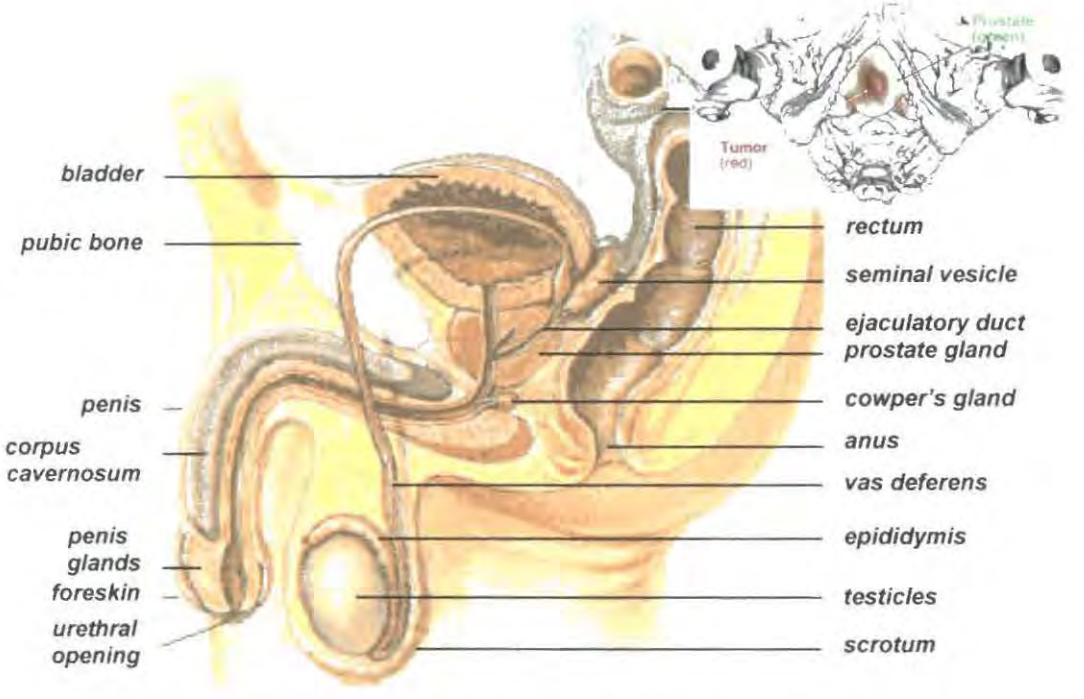

Fig. 5.1. Schematic diagram of male pelvis area, highlighting the prostate gland. (*insert*) Combined scan image of the pelvis area CT ( ), MRI (prostate), and SPECT (tumour) indicating the presence of prostate tumour using 111In-labeled ProstaScint.[10]

The prostate gland is regulated by dihydrotestosterone, which is generated in situ from the male hormone testosterone. The main function of the prostate gland is to store and secrete a clear fluid (pH 7.3) that constitutes about 50% of the volume of the seminal fluid that, along with spermatozoa, constitutes the semen. The rest of the seminal fluid is produced by the seminal vesicles. The prostatic fluid is mainly composed of simple sugars; the protein content is less than 1% and includes proteolytic enzymes, acid phosphatase and importantly, prostate-specific-antigen. The secretion also contains various amounts of zinc and sodium citrate.

5.1.2 Prostate Cancer

Prostate cancer (PCa) is classified as adenocarcinoma, or glandular cancer, that begins when normal semen-secreting prostate gland cells mutate into cancer cells. Initially, in the peripheral lobe a small clump of cancer cells remain confined, a condition known as *prostatic intraepithelial neoplasia*. However, it is not confirmed as a cancer precursor but is closely associated with cancer.[8] Over time, these cancer cells multiply and spread around the surrounding tissue forming a tumour. Eventually, if not recognised, the tumour grow large enough to invade nearby organs, such as the seminal vesicles or the rectum; or the tumour cells may develop the ability to travel in the bloodstream and lymphatic system causing metastasis. Therefore, PCa is considered as a malignant disease.

Prostate cancer is the most common non-skin related male cancer type in the world,[11] affecting one in ten men in the UK.[12] It is an age specific type of cancer and the older the individual is the higher the risk factors associated with prostate adenocarcinoma. More than 65% of all prostate cancer are diagnosed in men over the age of 65.[13] However, the race and family PCa history is also of great importance. According to the *prostate cancer foundation,*[14] African American men are 61% more likely to develop prostate cancer compared with Caucasian men. Men with a first-degree relative, who have a history of PCa, are twice as likely to develop the disease. The risk factor increases further if the affected relative was diagnosed at a young age. Genetics might play a significant role in developing prostate cancer.[15] However, other social and environmental factors, such as diet,[16-18] medication[19] and lifestyle[20] are likely to have an effect as well.[21]

If the cancer is caught at its early stages, most men may not experience any symptoms. Some, however, may experience symptoms that might indicate the presence or progress of prostate cancer. The symptoms are consistent with urinary incontinence and erectile dysfunction as a result of the anatomy of the prostate, Symptoms include the following: frequent urge of urination, urinary dysfunction (bladder control, difficulty starting urination), weak or interrupted urination, painful or burning sensation while urinating, erection problems, and painful ejaculation,

blood in urine or semen and pain or stiffness in the lower back, hips and upper thighs. However, each of these symptoms could indicate the presence of other diseases or disorders.

It is equally important to know that there is no increase in risk of developing prostate cancer if other prostate related non-cancerous conditions are present, such as *benign prostatic hyperplasia* (BHP) or *prostatitis*.[22] However, these conditions may cause similar symptoms to those of prostate cancer.

BHP is a non-cancerous enlargement of the prostate associated with inflammatory in the transition lobe of the prostate. Because the urethra runs directly through the prostate, upon enlargement of the prostate there is narrowing of the urethra, making it difficult and rather painful to urinate. This growth of the prostate is unrelated to prostate cancer however there are number of studies indicating that inflammation of the prostate causes significant non-anatomical changes, which may increase the risk of developing prostate adenocarcinoma. The surgical procedure most commonly used in such cases is called *transurethral resection of the prostate*, where the part of the prostate that presses against the urethra is surgically removed. However in old age *corpora amylacea* may occur, in which a dense accumulation of calcified proteinaceous material in the prostate due to hormonary discunction, can cause similar symptoms.[23]

Prostatitis is an infection in the prostate, and is the most common cause of urinary tract infection in men. Interestingly, some studies[14] have shown that frequent ejaculations may lower the risk of developing prostate cancer, by reducing the carcinogenic deposit which could damage the epithelial cells lining the prostate parallel with frequent increase in testosterone level in the blood.[24] However, it is important to appreciate that sexually transmitted diseases also increase the risk of prostate cancer.

Several genetic and environmental risk factors have been associated with the development of the disease. Unfortunately, despite significant progress in research over the past 20 years, the scientific evidence is not strong enough to be helpful in preventing prostate adenocarcinoma. However, some studies showed delay in the

development and progression of prostate cancer, using finasteride and dutasterine, which are antibiotics typically used for men with non-cancerous BHP.[25]

5.1.3 Current Screening Procedures and Diagnosis

Prostate cancer screening is an attempt to detect unsuspected cancers in their earliest stages. Screening test may lead to more specific follow-up diagonstic tests and if required cancer treatments. As PCa is a slow-growing cancer, the chances to identify the disease in early stage are high. The two most commonly used screening procedure now days are Prostate Specific Antigen (PSA) screening[26-28] or the Digital Rectal Examination (DRE).

The ***PSA blood test*** (*Fig. 5.2*) measures the prostate-specific-antigen level in the blood. PSA is an enzyme produced by the prostate and released in very small amounts into the bloodstream. Specifically, it is a serine protease, and its normal function is to liquifly gelatinous semen after ejaculation, allow spermatozoa to more easily navigate through the uterine cervix. This specific protein can be used as a tumour marker, as upon prostate cancer development or tumor growth, more and more PSA is released. PSA levels under 4 ng/mL are generally considered normal, results over 10 ng/mL are usually considered as abnormal. However, there is no specific normal or abnormal PSA level. The higher the PSA level, the more likely it is that cancer is present. In order to confirm this, other diagnostic procedures are required. However, because various factors, such as medication, race or age, can cause fluctuations in the PSA level, the test does not necessarily indicate the need for other diagnostic tests. These tests often cause inflammation of the prostate or urinary infection and the patient is often exposed to unnecessary radiation This 'overdiagnosis' may even increase the risk of PCa development. In summary, the PSA test carries a wide error range, and it is only used to determine the need of any further diagnostic procedures. More accurate use of the PSA, is the so called PSA monitoring, where increase in the PSA level over time may confirms the presence of PCa. However, this is highly time consuming.

Fig. 5.2. PSA blood test using OxfordScreening Home PSA test showing a negative test result.[26]

The PSA test is often used in conjunction with a ***digital rectal examination***. During DRE, the examiner inserts a gloved, lubricated finger into the rectum and examines the prostate for any irregularities in size, shape and texture. This procedure screens only the back of the prostate; however, 85% of PCa originates from this area. Any hard or lumpy area in the prostate, as they may contain cancer, needs further evaluation. Sadly, PCa which can be felt on DRE is generally more advanced.

If each test results in suspicion of prostate adenocarcinoma, other diagnostic methods, such as prostate biopsy is required. During biopsy the urologist obtains 6-10 small tissue samples with a needle from the prostate via the rectum. After sample acquisition the diagnostic procedure gives rise to the Gleason score or grading system (*Fig. 5.3*), derived by examining the removed tissue under a microscope. This is done to determine whether cancer cells are present, and to evaluate the microscopic feature of any cancer found. Generally speaking after assigning the grade of the studied sample, the Gleason score (sum of two most likely pattern of the observe sample) tends to determine the aggressiveness of the disease, and by obtaining samples from different part of the prostate, the cancer may be localised.

Fig. 5.3. The Gleason grading system showing the five distinctive patterns, that prostate tumor tend to go through as they mutate from normal cells; 1 represents normal prostate epithelial cells, 5 represent cancerous cells that do not look like prostate cells at all.[14]

Localisation of the tumour itself or the location and progress of metastasis can be determined with other staging (determination of how far the cancer has spread) methods. This involves traditional scanning studies, such as CT, MRI and SPECT scans, or through more specialised imaging test such as bone scans. Tissue samples can also be stained for the presence of PSA and other tumour markers.[29] However, this procedure involves a biopsy.

Several other possible markers are currently the focus of attention, such as modified tumor cells (LNCaP models), PCA3 and EPCA-2.[30] PCA3 is exclusively produced by prostate cells and shown to be highly over-expressed in prostate cancer cells. It may be detected in the urine. Early prostate cancer antigene 2 (EPCA-2) is currently being studied as it may signal the presence and level of aggressiveness of PCa.

Most of these diagnostic and screening procedures are highly inaccurate and/or possess the possibility of increasing the risk of developing prostate cancer. Therefore, there is a need for a uniform, well established non-invasive screening procedure. Citrate level tests from prostate- and more preferably seminal fluid samples may overcome the risk and inaccuracy of common screening procedures, such as PSA and biopsy. Once the case of prostate adenocarcinoma has been confirmed, depending on the stage of development of the disease, there are several, mostly invasive, treatment options available.[14] Due to the interest in detection and improved screening these medical methods will not be detailed here.

5.1.4 Citric acid and Zinc Elevation

Prostate secretory epithelial cells have the specialised function and capability of accumulating and secreting extraordinarily high levels of citrate. This is achieved by the existence of a low mitochondrial aconitase (m-Ac) activity that minimises the ability of the cell to oxidise citrate via the Krebs cycle (*Fig. 5.4 left*)[31]. Consequently, citrate synthesised by these cells is accumulated and secreted (often referred as 'net' citrate production), thereby accounting for the extremely high (20 - 200 mM) citrate content of human prostatic fluid. In typical mammalian cell metabolism, the steady-

state citrate/isocitrate ratio is 11/1 which is established by the aconitase equilibrium reaction. In contrast, this ratio is generally 30/1 in prostate cells where the m-Ac enzyme is a regulatory enzyme. Also, the intracellular citrate concentration of prostate cells is estimated to be about 1 - 3 mM as compared with the 0.1 – 0.4 mM for typical mammalian cells. The level of prostate m-Ac enzyme appears to be similar to that associated with other cells, although the levels of m-Ac activity and consequent citrate oxidation are significantly lower in prostate cells. Thus the limiting m-Ac activity is due to unique properties of the enzyme and/or unique mitochondrial conditions that inhibit the enzyme activity.

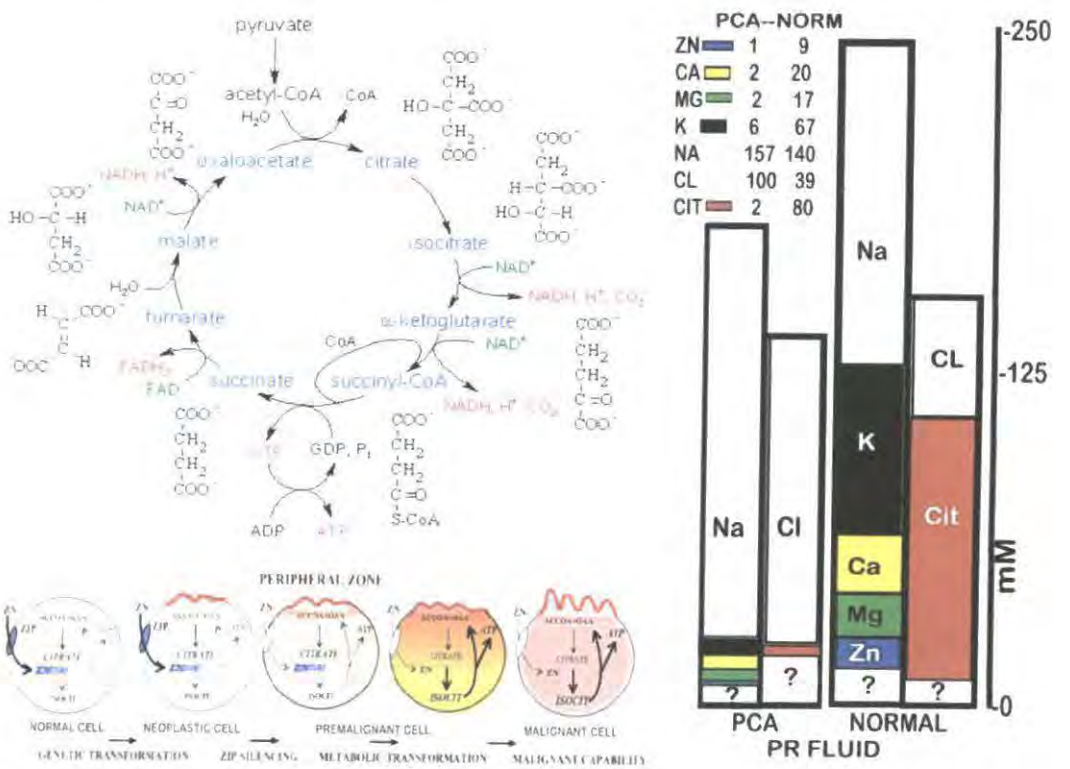

Fig.5.4. (*top left*) Schematic diagram explaining the Krebs cycle and its components.[31] (*right*) Diagram highlighting compositional differences in prostate (PR) fluid most importantly in zinc and citrate, concentrations in normal and prostate cancer patients (PCA). (*bottom left*) The concept of zinc and citrate altered genetic/metabolic development of prostate malignancy.[9]

Prostate epithelial cells normally possess uniquely high cellular and mitochondrial zinc levels. Studies showed that zinc inhibition of the m-aconitase activity accounts for the minimised citrate oxidation and consequently the high citrate

level which characterises prostate cells.[31,32] This is in contrast to the low citrate and zinc levels that prostate cancer cells exhibit.[9] Thus, normal human prostate epithelial cells are citrate-producing cells, whilst malignant prostate epithelial cells are citrate-oxidising cells (*Fig. 5.4 right*). This inhibition only occurs with citrate as the substrate and other divalent cations, such as Ca^{2+}, Mn^{2+} or Cd^{2+} do not inhibit. Whether 'free' zinc or a zinc-citrate complex competes with 'free' citrate for the enzyme active site is yet not fully understood. However, as only m-Ac (and not cis-Ac) is affected by this phenomenon and furthermore, the zinc-citrate complexes affinity to the enzyme is lower than the citrate affinity, the likelihood of the competition of the zinc-chelate with 'free' citrate is minimal. This has been confirmed by X-ray crystallographic studies, identifying a zinc binding site only on the m-Ac enzyme.[33]

The lost ability of the neoplastic epithelial cells, mainly in the peripheral zone of the prostate, to accumulate zinc is a consistent factor in their development of malignancy. Zinc levels are about 80% less in malignant prostate cells.[34] Recent studies have established that the zinc uptaker and transporter, ZIP1, is important in uptake and accumulation of zinc in prostate cells.[35] This study by *Costello* and *Franklin* suggests that the down-regulation of human ZIP1 gene expression and consequent depletion of zinc in the neoplastic prostate cell is an essential step in the development of prostate malignancy.[9] Subsequent studies, therefore, question the possibility of zinc as a tumour suppressor agent,[36] suggesting that ZIP1 may be used as a possible tumour suppressor gene in prostate cancer.[9]

Detection of zinc levels from prostate fluid or biopsy samples may provide a good method for signalling prostate adenocarcinoma[37]. The zinc concentration decreases from 9 to 1 mM as a function of prostate malignancy, although no significant difference in normal prostate cell and BHP zinc levels. The analysis of citrate levels is even more striking, with a reduction from 80 to 2 mM as the disease progresses. The production of 1 mL 'healthy' prostate fluid, on average, requires the production of 100 µmol citrate. To achieve this 50 µmol of glucose and 100 µmol of aspartate are utilised. The extracellular concentrations of glucose and aspartate are 5 mM and 0.03 mM respectively. Therefore the prostate cell, unlike other cells where

aspartate is an essential amino acid, accumulates high aspartate concentrations (1.2 mM). This is achieved by the EAAC1 aspartrate transporter.[38]

It is well established that zinc and consequently citrate levels are markedly decreased in malignant versus normal prostate tissue early in the development of malignancy, as zinc inhibition of m-aconitase truncates the Krebs cycle at the first step of citrate oxidisation (ATP citrate lyase). The Krebs cycle provides the most efficient metabolic alteration for synthesised citrate to be accumulated for secretion (*Fig. 5.5*).

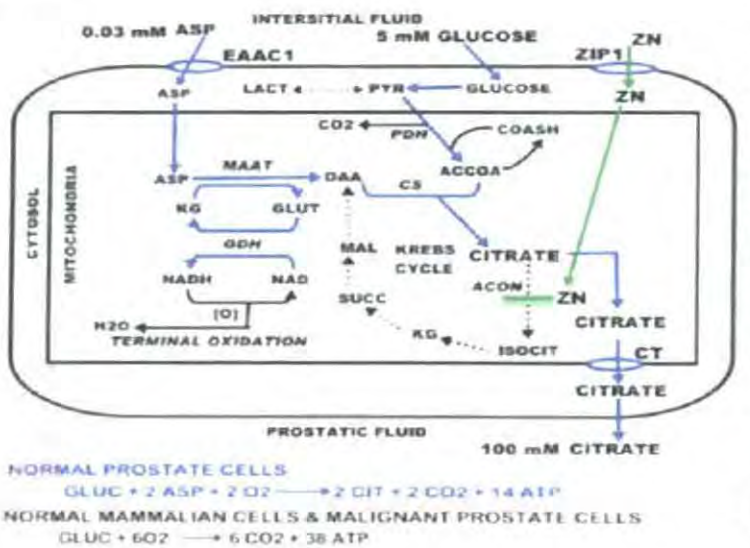

ASP = Aspartate,
GLUT = glutamate,
OAA = oxalacetate,
COASH = coenzyme A,
ACCOA = acetyl coenzyme A
ISOCIT = isocitare,
KG = α-ketoglutarate
SUCC = succinate,
MAL = malate,
PYR = pyruvate,
LACT = lactate,
PDH = pyruvate dehydrognase,
CS = citrate synthase,
ACON = aconitase
MAAT = mitochondrial aspartatic aminotransferase,
DGH glutamis dehydrigenase,
CT = citrate

Fig.5.5. The metabolic pathway and bioenergetics of net citrate production in prostate cells.[9]

To accumulate citrate in the cytosol, the highly specialised prostate cells sacrifice about 60% of the potential energy that could be derived by complete oxidation of glucose. Thus, malignant prostate cells are bioenergetically more efficient. This is in contrast to the general tumour metabolism relationship in which tumour cells are metabolically transformed to high aerobic glycolysis.[39] In contrast, most mammalian cells cannot survive if m-Ac activity and consequently citrate oxidation are inhibited, as is evident from the toxic effect of the m-Ac inhibitor, fluoroacetate (→fluorocitrate). The decrease in citrate levels in prostate cancer cells is an essential metabolic adaptation and may be associated with increase in ATP citrate lyase activity. Therefore, in malignant prostate cells, the cytosol citrate pool is used

'again' via the Krebs cycle. This concept of an increased citrate shuttle, causing rapid export of citrate, has been confirmed in other type of tumour cells as well.[40]

A major problem involved in prostate cancer (PCa) diagnosis is the absence of sensitive, accurate, and preferably non-invasive diagnostic procedures. Moreover, procedures are needed that will permit the early detection, staging, location, and estimated volume of the malignancy; and preferably a mapping of the prostate for follow-up of progression and regression of the malignancy. The unique citrate metabolism relationship of the prostate, coupled with ^{1}H-MRSI (magnetic resonance spectroscopy imaging) provides an excellent diagnostic method.[4,41] Combination of MRI and MRSI results in a metabolic-anatomic visualisation (*i.e.* metabolic map) of the prostate gland, using an endorectal coil. This diagnostic method was found to detect prostate adenocarcinoma with 90% accuracy.[42] In addition to the mapping of the malignant areas of the prostate, it also permits MRSI guided local radiotherapy and chemical seeding.

Clearly, the human prostate (specifically the peripheral zone) has evolved as a highly specialised organ for the primary function of secreting enormously high levels of citrate (20 - 200 mM). One main drawback of citrate level measurement in the prostate fluid is that obtaining the sample requires a biopsy. Prostate fluid, as the main source (about 50%), gives rise to seminal fluid citrate level of about 10 - 55 mM.[43,44] The high citrate content of seminal fluid is consistent with the use as a buffer to maintain the pH of semen (7.2 – 8.0). It may also serve as a chelator for zinc and other divalent cations which are also highly concentrated and involved in liquefaction of semen as well, as an energy source for sperm maturation and viability.[45] Its role might be complex, but importantly, the citrate level in seminal fluid is proportionate to that in the prostate fluid. Therefore, citrate level measurements from seminal fluid samples could aid the detection of prostate malignancy. Despite this, only a few studies involving the NMR detection of citrate in seminal fluid samples have been reported.[46,47]

On a final note, the restoration of high zinc levels in pre-malignant prostate cells may arrest and/or abort prostate malignancy, whilst citrate is found to be an excellent marker for prostatate adenocarcinoma. Therefore, as MRI imaging has its

limitation and expensive instrumental requirements, the design and application of a responsive luminescent citrate sensor to be used in measuring citrate levels in prostate and, more importantly, seminal fluid samples is highly attractive. The current screening methods applied in PCa detection are limited and give questionable results.

5.2 General Luminescence Studies

Based on the methodology established with pH probes (*Chapter 3.*) and carbonate sensors (*Chapter 4.*), a ratiometric optical Eu(III) sensor, with an appropriate citrate affinity is sought for the detection and staging of prostate malignancy.

5.2.1 Design, Concept and Characteristics of a Suitable Citrate Sensor

The complex EuDPP2[48-50] was specifically designed as a sensor for extracellular citrate concentration determination (*Fig. 5.6*).

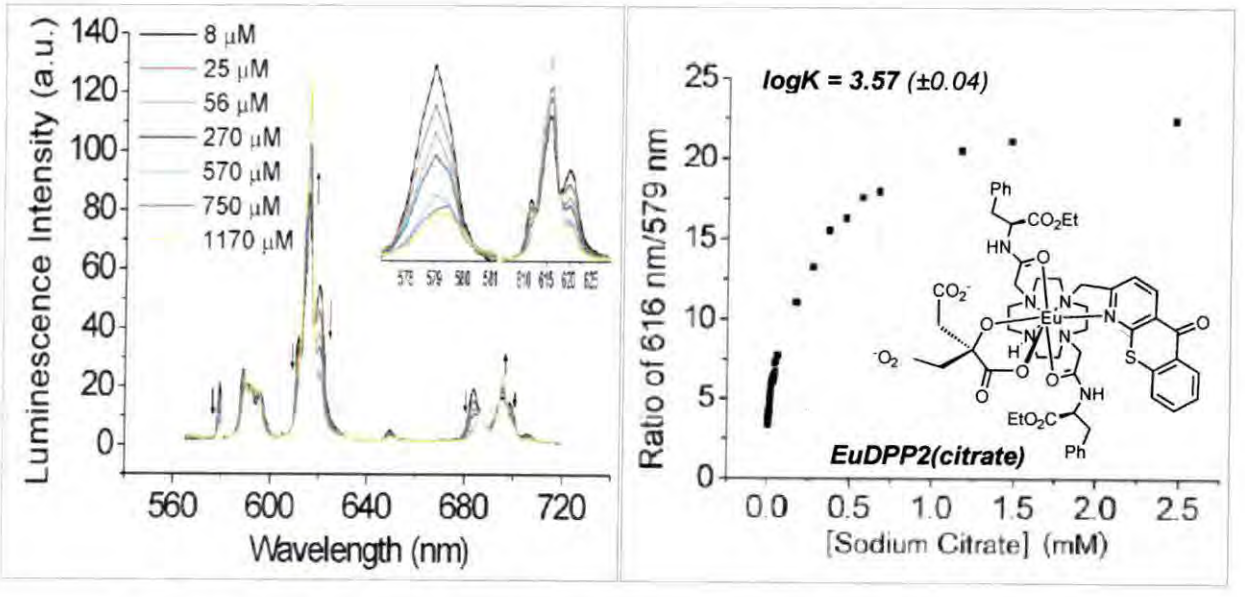

Fig. 5.6. EuDPP2 as a ratiometric europium citrate sensor. (*left*) The luminescence spectra of aqueous EuDPP2 solution (10 μM) upon titration with added sodium citrate (pH = 7.4, λ_{ex}= 380 nm). (*right*) Selected intensity ratio *vs.* added citrate concentration plot for calculating binding constant (logK) for the EuDPP2(citrate) adduct. (LV_{min}= 4.19 and LV_{max}= 24.90)

This complex was successfully used in the presence of other extracellular anions (30 mM bicarbonate, 2.3 mM lactate, 0.1 M chloride and 0.9 mM monohydrogenphosphate), to determine citrate concentration, up to the limiting (0.2 mM) extracellular concentration value. However, as determined by *Kavanagh and Costello*[9,43] (*see Fig. 5.2*), the composition and, more importantly, the limiting ionic concentrations of the prostate fluid is significantly different from the previously used mixed extracellular anion background. The presence of significant concentrations of divalent metal ions, such as Ca^{2+}, Mg^{2+} and Zn^{2+} may perturb the sensitivity towards citrate, as a result of M^{2+}-citrate chelate competition. In order to see how the citrate affinity of EuDPP2 changes upon divalent metal ion introduction, a titration using a 'modified anion-stew' as the background was carried out, monitoring the Eu emission spectrum as a function of added sodium citrate (*Fig. 5.7*). The modified medium was prepared by adding 2 mM zinc chloride, magnesium chloride and calcium chloride, respectively, into the existing 'anion-stew' solution. The citrate concentration was increased in each titration by addition of concentrated sodium citrate solution, possessing the same pH as the studied system. The citrate affinity was found to be dramatically increased (logK >6) in the presence of the divalent metal ions (pH = 7.4 ±0.05).

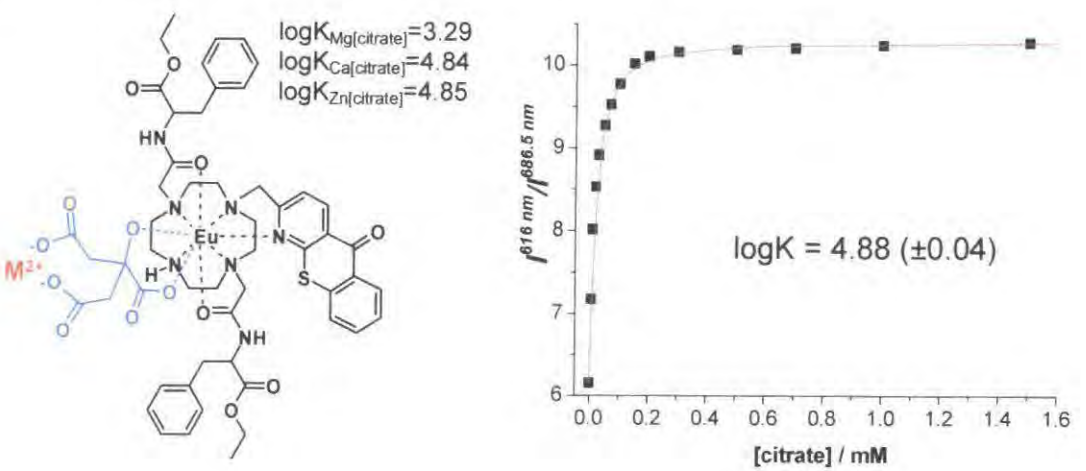

Fig. 5.7. (*left*) Suggested binding mode and structure of EuDPP2(citrate)M (confirmed by ESMS), highlighting the stability constants for citrate with zinc, calcium and magensium.[51] (*right*) Intensity ratio (616/579 nm) *versus* added sodium citrate plot for EuDPP2 in sPFx10D ([complex] = 20 μM, pH = 6.5 ±0.05). (LV_{min}= 6.18 and LV_{max}= 10.24)

This phenomenon must be caused by charge stabilisation of the 'Eu-citrate' adduct. The M^{2+} ion may bind to the two 'free' carboxylate groups, stabilising this adduct (*Fig. 5.7 left*). $ESMS^+$ spectrum of EuDPP2 in the presence of excess amount of sodium citrate and $CaCl_2$ showed peaks consistent with $[EuDPP2(citrate)Ca]^+$, possessing the corresponding isotope pattern (*m/z* ($ESMS^+$) *1243*).

The apparent affinity constant for citrate was found to be extremely high. Nevertheless, a titration was carried out, using simulated prostate fluid as the background medium. This measurement was done in order to see how the different ionic composition of the background, the presence of protein and more importantly the different pH (as $pK_3^{citrate} = 6.3$) affects the apparent binding constant. Due to the high citrate régime in prostate fluid, the simulated prostate fluid (sPF) was used as background in ten times dilution (x10D). This ionic background consists of 0.1 M sodium chloride, 0.04 M potassium chloride, 5 mM magnesium chloride, 4 mM calcium chloride, 2 mM zinc chloride, 3 mM sodium bicarbonate and 0.1 mM protein (HSA). The pH of this background was adjusted to 6.5 (±0.05), to match the pH of prostate fluids samples obtained from PCa patiences. Titration of EuDPP2 in sPFx10D varying the added citrate concentration from 0 to 10 mM revealed strong citrate dependence. However, the intensity ratio *versus* [citrate] plot (*Fig. 5.7. right*) revealed that the binding constant for 'citrate' was 'tuned' back to logK = 4.88 ±0.04 M^{-1}, which is still high for the desired purpose.

As citrate revealed strong affinity towards EuDPP2, it was concluded that new sensors were required, in order to find the best candidate to measure citrate concentration (in the range of 0 – 10 mM) in diluted prostate or seminal fluid samples. Two major systems were examined.

The first system was based on modification of the existing citrate sensors, such as EuDPP2 and EuDAP2. As found previously with the pH probes, modulation of the overall complex charge, led to enhanced charge repulsion and resulted in a significant decrease in citrate affinity. Furthermore, the more bulky phenyl groups in EuDPP2 decreased the affinity of citrate in a simulated extracellular anion background by 50%, compared to EuDAP2 (logK= 3.83 ±0.05 M^{-1}). Taking these

observations into account, the 'hydrolysed' complexes EuDAPA2 and EuDPPA2, with reduced positive charge were synthesized (*Fig. 5.8. top*).

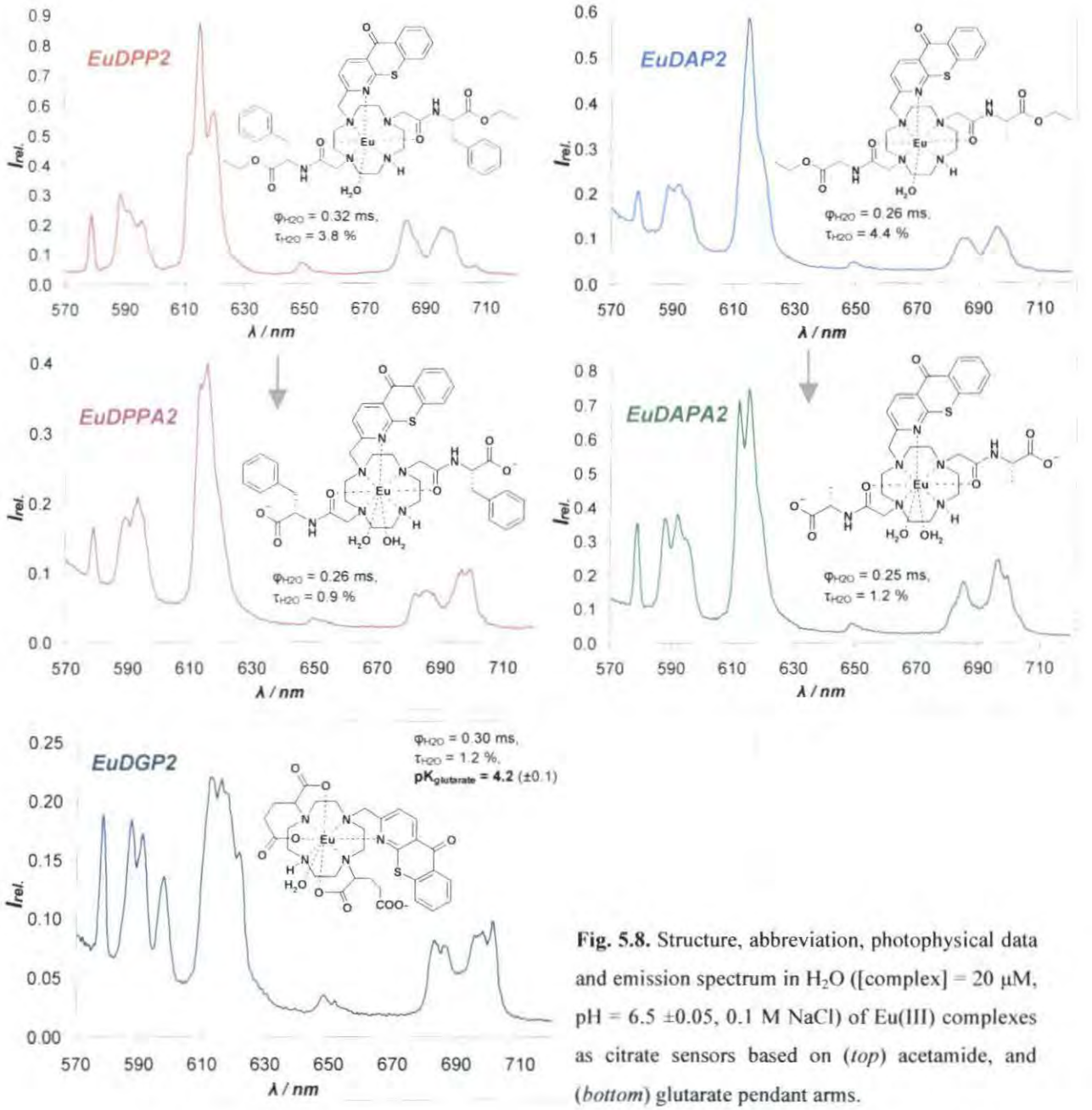

Fig. 5.8. Structure, abbreviation, photophysical data and emission spectrum in H_2O ([complex] = 20 μM, pH = 6.5 ±0.05, 0.1 M NaCl) of Eu(III) complexes as citrate sensors based on (*top*) acetamide, and (*bottom*) glutarate pendant arms.

The other system relied upon competitive intramolecular ligation of the pendant glutarate arm, which had earlier limited the use of Eu(MS)DGP2 as a pH probe. Therefore, the complex EuDGP2 (*Fig. 5.8. bottom*) was synthesised, and its general photophysical properties, such as lifetime and quantum yield, investigated. In

order to determine the pK_a of the pendant glutarate arm, titrations were carried out in 0.1 M sodium chloride solution (*data not shown)*, monitoring the changes in the Eu emission spectrum as a function of pH. From changes in the $\Delta J = 2$ manifold the pK_a was determined to be 4.2 (±0.1), which did not change significantly with the introduction of relevant concentrations of divalent metal ions 4.4 (±0.1).

5.3 Luminescence Studies in Simulated Prostate Fluid

5.3.1 Citrate Dependence Studies

Titrations were carried out, with EuDAP2, EuDPP2, EuDAPA2, EuDPPA2 and EuDGP2, by monitoring changes in the Eu emission spectrum as a function of added citrate. Each titration was executed at pH 6.55 (±0.05).

5.3.1.1 Citrate binding of EuDAP2 and EuDPP2

Monitoring the Eu emission spectrum as a function of added citrate, similar intensity changes were observed for each complex, mainly in the $\Delta J = 2$ and $\Delta J = 4$ manifold (*Fig. 5.9*).

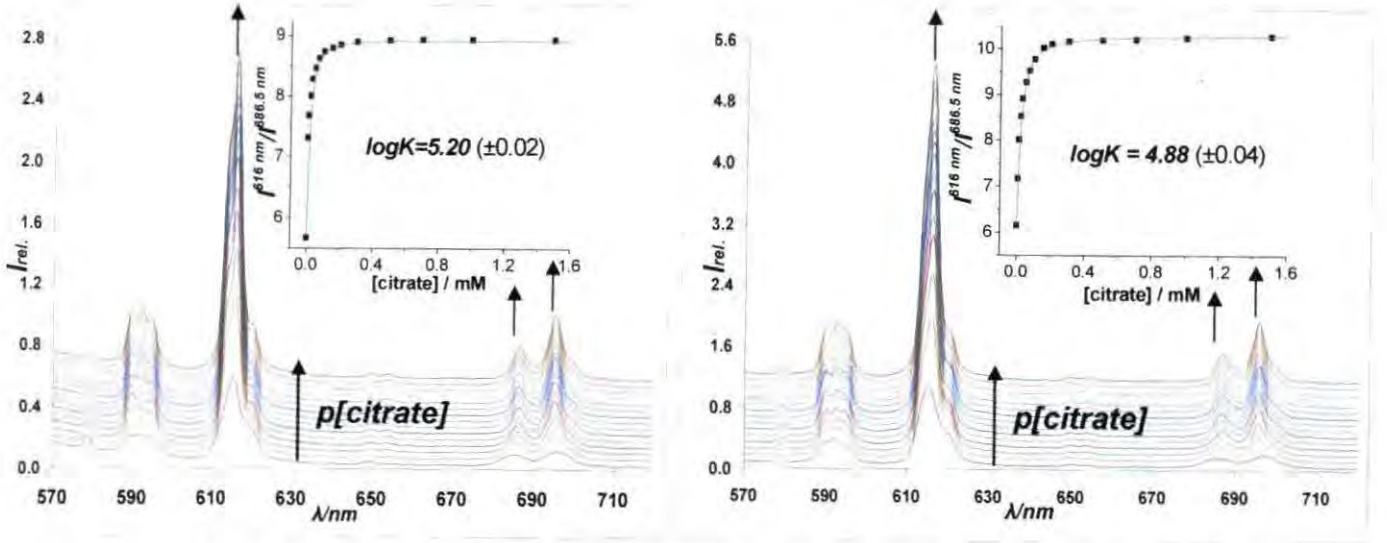

Fig. 5.9. Variation of the Eu emission spectrum as a function of added citrate, showing the intensity ratio (616/686.5) *vs.* [citrate] plot to determine the apparent binding constant of citrate for (*left*) EuDAP2 (*right*) EuDPP2 in sPFx10D ([complex] = 20 μM, pH = 6.55 (±0.05)). (LV_{min}= 5.67 and LV_{max}= 8.94 (*left*), (LV_{min}= 6.16 and LV_{max}= 10.27 (*right*))

The apparent citrate binding constants for EuDPP2 and EuDAP2 were found to be $\log K_{citrate}$ = 4.88 ±0.04 M^{-1} and $\log K_{citrate}$ = 5.20 ±0.02 M^{-1} respectively. These values were initially considered to be higher than required for the desired application. However, as found in the extracellular anion mixture, introduction of the bulkier pendant arms in EuDPP2, led to a 50% decrease in the apparent binding constant. This effect should still be apparent for the 'hydrolysed' systems EuDPPA2 and EuDAPA2. However, in this case, the citrate affinity should be reduced further as result of decreased overall complex charge.

5.3.1.2 Citrate binding of EuDAPA2 and EuDPPA2

Monitoring the structural and intensity changes as a function of added sodium citrate for EuDAPA2 (*Fig. 5.10*), similar spectral changes were observed as for the parent complex. However, calculations using the intensity ratio (615.5/686.5 nm or 615.5/579.5 nm) *versus* added citrate plot, revealed a 5 fold decrease in the citrate affinity compared to EuDAP2, with logK = 4.51 ±0.03 M^{-1}.

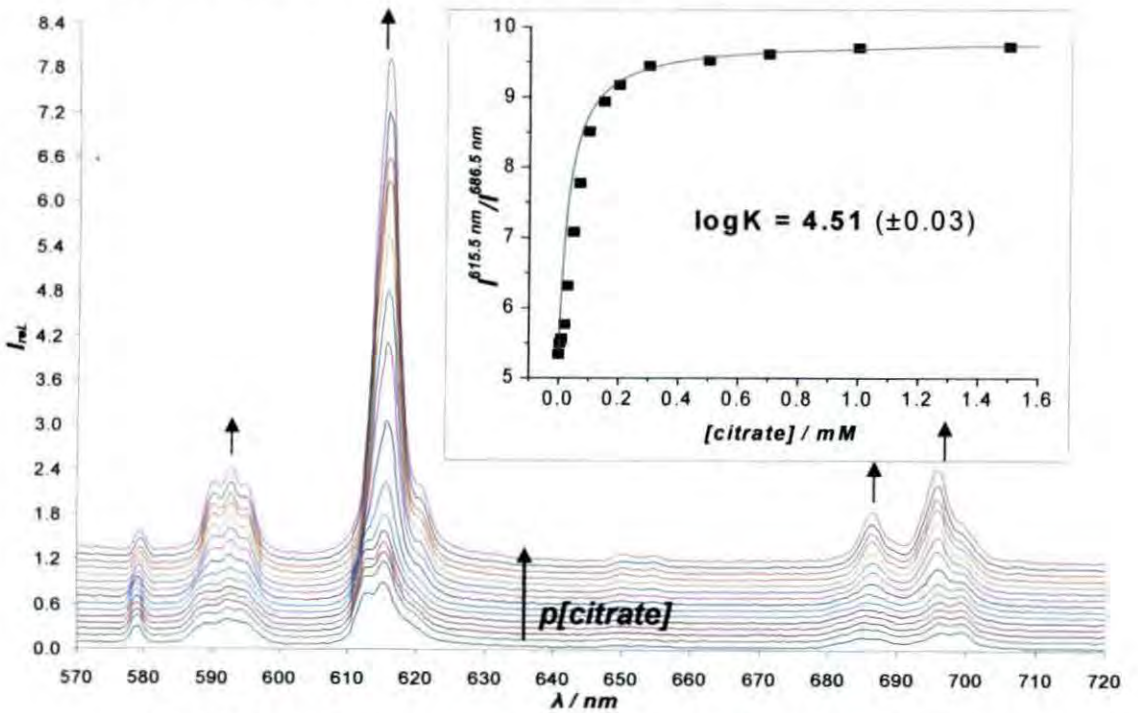

Fig. 5.10. Variation of Eu emission spectrum for EuDAPA2 following addition of sodium citrate solution (pH = 6.55 (±0.05), [complex] = 20 μM, 298 K, λ_{ex} = 380 nm, in sPFx10D). (*insert*) Intensity ratio (615.5/686.5 nm) *vs.* [citrate] plot, for determining the apparent binding constant. (LV_{min}= 5.34 and LV_{max}= 9.70)

A similar titration was carried out with EuDPPA2 (*Fig. 5.11*) and the observed spectral changes were identical as for the parent complex. The intensity ratio (615.5/686.5 nm) *versus* [citrate] plot, also revealed a 5 fold decrease in the citrate affinity compared to EuDPP2, with logK = 4.20 ±0.05 M^{-1}.

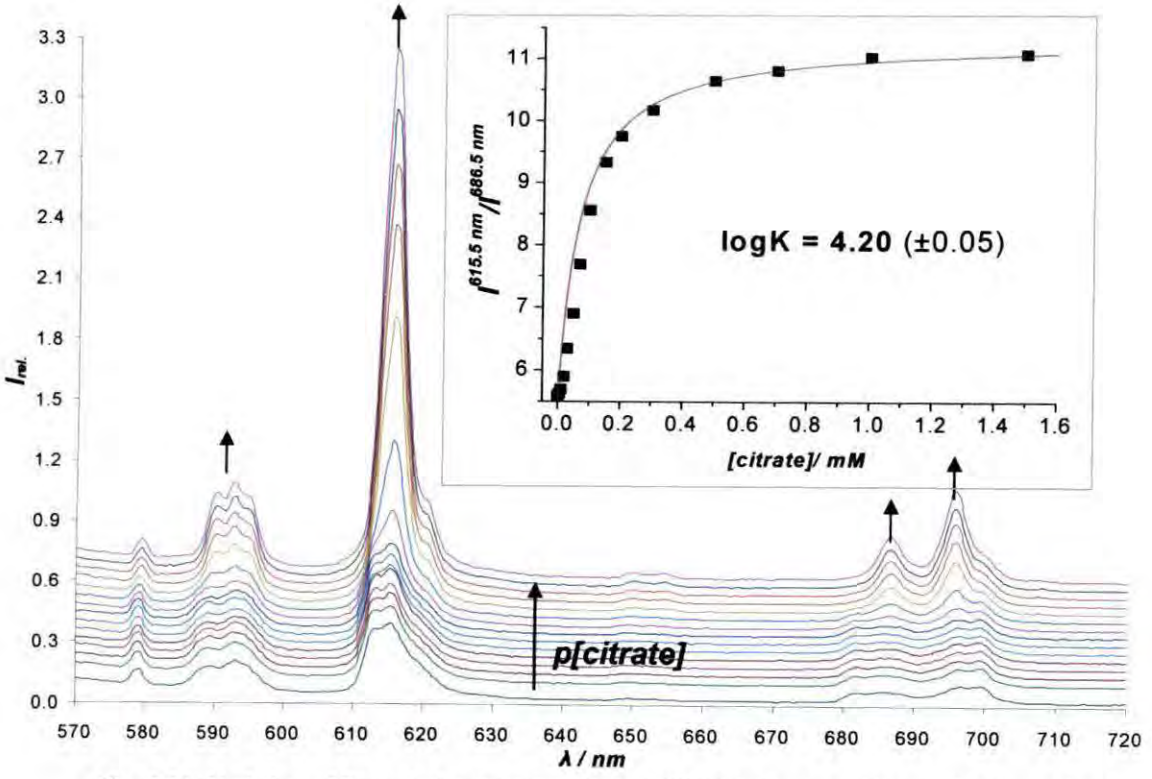

Fig. 5.11. Variation of Eu emission spectrum for EuDPPA2 following addition of sodium citrate solution (pH = 6.55 (±0.05), [complex] = 20 μM, 298 K, λ_{ex} = 380 nm, in sPFx10D). (*insert*) Intensity ratio (615.5/686.5 nm) *vs.* [citrate] plot, for determining the apparent binding constant. (LV_{min}= 5.59 and LV_{max}= 11.07)

Comparing the apparent binding constants for citrate, modulation of complex charge resulted in a 5 fold decrease in citrate affinity, while the 50% decrease in affinity between EuDAPA2 and EuDPP2 was retained. Bidentate citrate ligation was confirmed, by comparing the radiative lifetime values measured in D_2O and H_2O. The number of inner sphere water molecules was calculated from them in the presence of citrate. Both complexes (q = *2* in the absence of citrate, *see 2.4.2.1*) revealed to be q = *0* systems ($k_{H_2O}^{EuDPPA2}$ = 2.26 ms^{-1}, $k_{D_2O}^{EuDPPA2}$ = 1.73 ms^{-1} and $k_{H_2O}^{EuDAPA2}$ = 2.64 ms^{-1}, $k_{D_2O}^{EuDAPA2}$ = 1.80 ms^{-1}). This is only possible upon bidentate ligation of the

target anion. Unfortunately, the calculated apparent binding constant values were still regarded as being higher than the desired affinity for measuring the 0 – 8 mM citrate range. To overcome this problem EuDGP2 was examined.

5.3.1.3 Citrate binding of EuDGP2

The complex EuDGP2 allows intramolecular glutarate ligation to the Eu centre, forming a 7-chelate ring. This $q = 1$ ($k_{H_2O}^{EuDGP2} = 2.97$ ms^{-1}, $k_{D_2O}^{EuDGP2} = 1.58$ ms^{-1}) complex is the dominant species above pH 4.5. Therefore, upon bidentate citrate ligation, not only the inner sphere water molecule must be replaced, but there must be a competition between intramolecular glutarate ligation and intermolecular citrate binding. This competition should significantly decrease the apparent binding constant of citrate, providing a complex with lower citrate affinity.

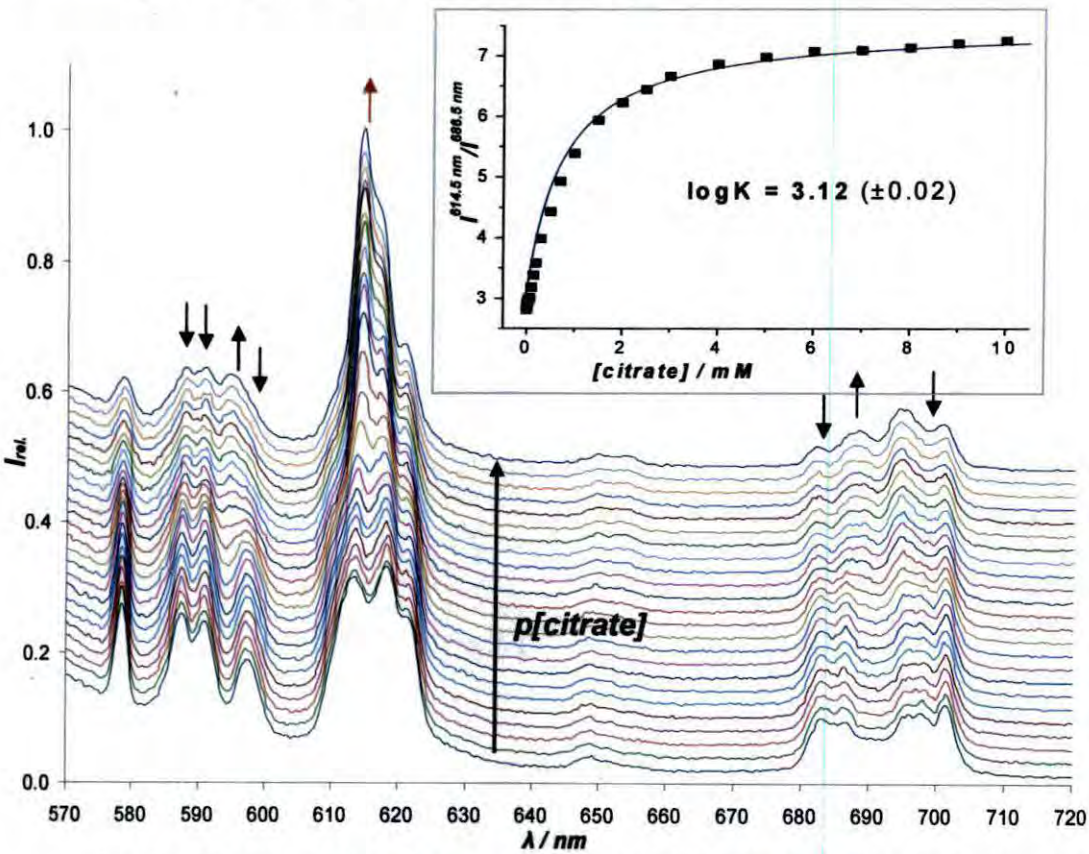

Fig. 5.12. Variation of Eu emission spectrum for EuDGP2 following addition of sodium citrate solution (pH = 6.55 (±0.05), [complex] = 20 μM, 298 K, λ_{ex} = 380 nm, in sPFx10D). (*insert*) Intensity ratio (614.5/686.5 nm) *vs.* added citrate plot, for determining the apparent binding constant. (LV_{min}= 2.81 and LV_{max}= 7.24)

Monitoring the Eu emission spectrum as a function of added sodium citrate (*Fig. 5.12*), well pronounced changes were observed, not only in the intensity, but more importantly, in the structure of the metal based emission. As with Eu(MS)DCP2 (*see 3.3.2.1*), upon citrate ligation to the Eu centre, dramatic changes were manifested in the hypersensitive $\Delta J = 2$ manifold. The increase in intensity of the 614 nm band as a function of added citrate, provides a well defined spectroscopic marker for citrate binding. Examination of the intensity ratio (614.5/686.5 nm) *versus* added citrate plot allowed the apparent binding constant to be estimated. A value of logK = 3.12 ±0.03 M^{-1} was found. Similar values were obtained using other bands from the $\Delta J = 2$ manifold (*e.g.* 614.5/618.5 nm or 614.5/621.5 nm). The complex EuDGP2 seemed to possesses the desired affinity for examination of the target biofluid.

However, as detailed in the section dedicated to prostate cancer, as the disease progresses, significant changes have been defined not only in citrate concentration (from 2 to 80 mM), but proportionately in the divalent metal ion concentration.[9] The concentration of zinc and of other divalent metal ions, such as magnesium and calcium can increase ten fold (*see Fig. 5.2 right*) as the malignancy develops. Magnesium and calcium concentrations vary from 2 to about 20 mM, while zinc may change from 1 to 10 mM. Therefore, as each prostate fluid sample may contain variable concentrations of citrate and M^{2+}, a titration was carried out following the previously applied method, studying changes in the metal based emission in the added citrate region 0 to 10 mM with parallel systematic addition of a 'metal ion stock' (MIS) solution, containing Mg^{2+}, Ca^{2+} and Zn^{2+} in 2 : 2 : 1 ratio. This ratio reflects their relative concentrations in healthy and diseased prostate fluid. The limiting total divalent metal ion concentration was set at 5 mM. Studying intensity ratio *versus* $[citrate]_{total}$ plot, upon increasing divalent metal ion concentration, the apparent citrate binding constant was found to be logK = 2.75 ±0.04 M^{-1}. This 50% decrease in the citrate affinity may be attributed to competition between the M^{2+}-citrate chelate and 'free' citrate. As increase in metal concentration results in a parallel increase in M^{2+}-citrate complex. However, this competition decreases the overall 'citrate affinity' of EuDGP2 even further, resulting in a calibration curve, that should be more accurate over the desired citrate concentration region (*i.e.* 1 to 10 mM).

There is no reported study confirming whether protein concentration remains constant at 0.1 mM as the prostate malignancy develops. A titration, as a control, was undertaken using 'modified' simulated prostate fluid, containing an extracellular level of HSA (0.7 mM) as the background medium. Monitoring the Eu emission as a function of added citrate (with parallel increase in divalent metal ion concentration), no change was observed in the form of the plot and in the calculated apparent citrate binding constant.

The complex EuDGP2 was therefore the lead candidate at this stage, as a citrate probe in diluted prostate fluid samples. Measurements were then carried out in 'real' samples. A series of archived samples of prostate fluid was received, as lyophilised solids impregnated on an absorbent paper disc, from Prof. Les Costello and Dr. R. Franklin (*University of Maryland, USA*). Digestion and subsequent dilution of the samples using 100 mM, pH 6.55 HEPES buffer allowed the soluble components to be extracted. Measurements of the filtered samples were carried out in order to determine their unknown citrate concentration. This was attempted by recording the Eu emission spectrum of the diluted (x10) samples containing 20μM EuDGP2. Our attempt was to use the intensity ratio (614.5/686.5 nm) vs. added citrate concentration plot, obtained with variable metal concentration (*Fig. 5.13 left*), as a calibration curve. However, on recording the Eu emission spectrum, a very distinctive, previously unseen, emission pattern was observed (*Fig. 5.13 right*) with each sample. This could only be attributed to the formation of another EuDGP2(anion) ternary species in solution, with a competitive affinity for the complex. Therefore, the identification of this competing anion was of paramount importance.

The prostate fluid, at pH 6.5, only contains a low concentration of bicarbonate, with an insignificant concentration increase as the disease progresses. Phosphate anion could also be excluded, as it forms insoluble phosphate salts with the divalent metal ions present. From the known metabolic pathway and ionic composition[43] of healthy and prostate fluid, and subsequent introduction of various anions into the simulated prostate fluid, this anion was hypothesised to be lactate.

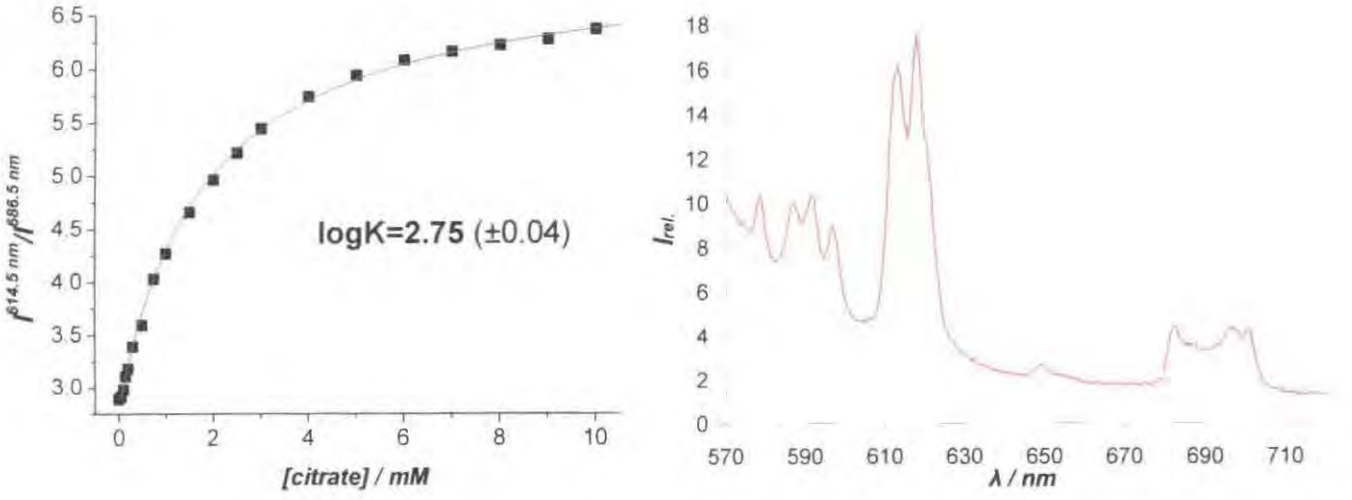

Fig. 5.13. (*left*) Intensity ratio (614.5/686.5 nm) *vs.* added citrate plot, for EuDGP2 determining the apparent binding constant in sPFx10D with added divalent metal ions. (*right*) Eu emission spectrum of EuDGP2 in diluted real prostate fluid sample (the sloping baseline is associated with the small volume, 125 μL and the unfiltered nature of the sample). (pH = 6.55 (±0.05), [complex] = 20 μM, 298 K, λ_{ex} = 380 nm, 0.1 M HEPES). (LV_{min}= 2.89 and LV_{max}= 7.00)

Depending on the concentration and/or the affinity of lactate for the complex, the presence of lactate may sabotage the application of EuDGP2. A literature search suggested that the determination of lactate concentration in the prostate fluid has not been examined in detail. Indeed, there is no scientific evidence of lactate concentration fluctuations, as a function of disease progression. Lactate dehydrogenase (LDH) is a protein found throughout the body. It catalyses the interconversion of pyruvate and lactate, with concomitant interconversion of NADH and NAD^+. At high concentrations of lactate, the enzyme exhibits feedback inhibition and the rate of conversion of pyruvate to lactate is decreased. Nearly every type of cancer, as well as many other diseases, can cause LDH levels to be elevated. Therefore, this protein cannot be used as a marker to diagnose a particular type of cancer. However, LDH levels may be used to monitor treatment of some cancers, including testicular cancer, Ewing's sarcoma, non-Hodgkin's lymphoma, and some types of leukemia. Elevated LDH levels can be caused by a number of noncancerous conditions as well, including heart failure, hypothyroidism, anaemia, and lung or liver disease. An interesting observation is that lactate dehydrogenase-B (LDH-B) is silenced by promoter hypermethylation in human prostate cancer.[52]

Hypermethylation is an increase in the epigenetic methylation of cytosine and adenosine residues in DNA. LDH-B promoter hypermethylation occurred at a higher frequency in prostate cancer (45%), compared to adjacent non-malignant or benign tissue (11%). These studies indicate that there is, in fact, a fluctuation in lactate levels as a function of disease progression.[52] However, questions about the quantity of lactate and the degree of lactate elevation in malignant prostate fluid remain unanswered.

One possible solution to overcome the lactate competition to the europium probe is enzymatic digestion of lactate,[56] prior to citrate concentration determination. An alternative is to redefine a sensor with significantly lower lactate compared to citrate affinity. Interestingly, if there is no fluctuation in lactate concentration as a function of prostate adenocarcinoma development, this competition may lower the apparent citrate binding constant, consequently presenting a more suitable calibration curve.

5.3.2 Lactate Interference in Citrate Analysis

In order to determine the lactate affinity and the likely level of interference in citrate analysis, titrations were executed studying changes in the Eu(III) emission spectrum as the function of added sodium lactate solution. The lactate concentration in the prostate fluid was arbitrarily set at 23 mM, which is ten times higher than its normal extracellular concentration, and slightly higher that the average 15.5 mM lactate concentration measured by *Sharama et al.* in healthy seminal fluid samples.[44]

Titrations were carried out in 10 times diluted simulated prostate fluid at pH 6.55 (±0.05), monitoring changes in the metal based emission as a function of added sodium lactate. Each emission spectrum showed intensity and structural changes, mainly in the hypersensitive $\Delta J = 2$ manifold, as the concentration of lactate anion was increased. The most pronounced structural changes were observed with EuDAPA2 (*Fig. 5.14*), while the intensity ratio (613/686.5 nm) *versus* lactate plot revealed a modest lactate affinity with an apparent binding constant of logK = 3.20 ±0.02 M^{-1}.

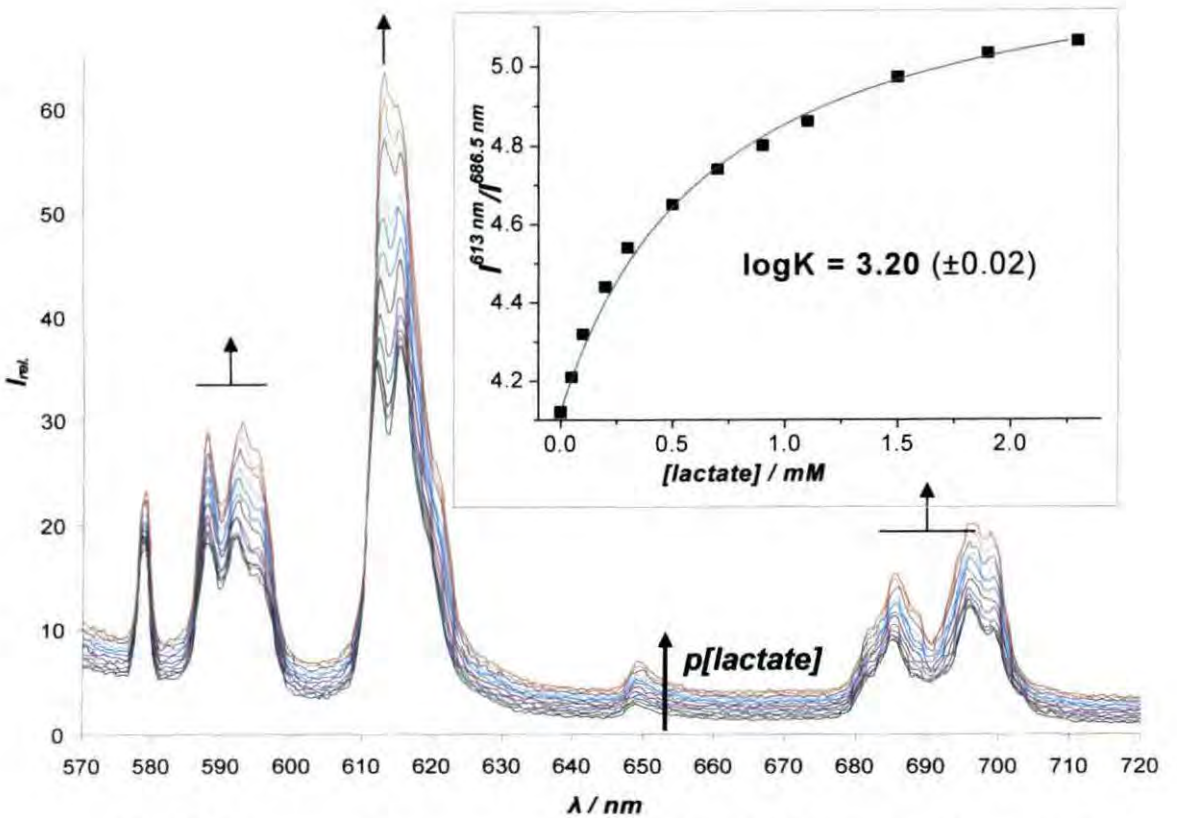

Fig. 5.14. Variation of Eu emission spectrum for EuDAPA2 following addition of sodium lactate solution (pH = 6.55 (±0.05), [complex] = 20 μM, 298 K, λ_{ex} = 380 nm, in sPFx10D). (*insert*) Intensity ratio (613/686.5 nm) *vs.* added lactate plot, determining the apparent binding constant. (LV_{min}= 4.12 and LV_{max}= 5.33)

The lactate affinity of each citrate sensor was measured in diluted prostate fluid and the stated background medium. The apparent binding constants were calculated by the existing method and are presented in *Table 5.1*, along with the corresponding binding constants for citrate.

Complex	$logK_{lactate}$	$logK_{citrate}$	$logK_{lactate}$	$logK_{citrate}$	
	in 'citrate free' anion-stew[a]		in sPFx10D[b]		
EuDAP2	—	**3.83** (±0.05)	**3.41** (±0.03)	**5.20** (±0.02)	
EuDPP2	—	**3.57** (±0.04)	**2.97** (±0.03)	**4.88** (±0.04)	
	in water (0.1 M NaCl)[b]				*Variable M^{2+}*
EuDAPA2	**2.47** (±0.02)	**4.42** (±0.03)	**3.20** (±0.02)	**4.51** (±0.03)	**4.34** (±0.06)
EuDPPA2	**2.32** (±0.03)	**4.11** (±0.02)	**2.82** (±0.03)	**4.20** (±0.05)	—
EuDGP2	**2.46** (±0.02)	**2.52** (±0.02)	**2.90** (±0.01)	**3.12** (±0.02)	**2.75** (±0.04)

Table. 5.1. Comparison of the apparent binding constants [M^{-1}] of lactate and citrate for the studied citrate sensors in various solvents ([complex] = 20 μM, 298 K, λ_{ex} = 380 nm). [a] pH = 7.4 and [b] pH = 6.55 (±0.05).

Examining the apparent binding constant values, the following observations can be made:

- The presence of divalent metal ions, in simulated prostate fluid, increases the apparent binding constant values for both lactate and citrate
- The complex EuDAPA2 and EuDPPA2 exhibit a marked selectivity for citrate (around 20 : 1) in diluted prostate fluid, ascribed to an enhanced electrostatic interaction even in the presence of added divalent metal ions.
- The citrate affinity for both EuDAPA2 and EuDGP2 decreased slightly with an increase in divalent metal ion concentration (*variable M^{2+}*).
- EuDGP2 displays more or less the same affinity for citrate and lactate, making its biological application questionable if lactate is in similar concentration to citrate in solution, or more importantly, if there is a modulation in lactate concentration as a function of disease development.

It is important to note that EuDPPA2 possesses slightly better anion affinity properties, but the better water solubility of EuDAPA2 renders this complex more suitable for biological applications.

The final conclusion of the comparison of citrate *versus* lactate affinity measurements is that, if there is a low constant amount of lactate in the prostate fluid sample, or if the lactate content has been eliminated *via* enzymatic digestion,[56] EuDGP2 may be used successfully. However, if there is significant amount of lactate present in the sample and a low citrate value is likely, EuDAPA2 is required.

To support this proposal, titrations were carried out in diluted simulated prostate fluid containing 2.3 mM sodium lactate as the background (MsPFx10D). Changes in the Eu emission spectrum were manifested as a function of added sodium citrate, up to a limiting concentration of 10 mM. As before, the divalent metal ion concentration was increased in parallel, up to 5 mM [M^{2+}], using a 'metal ion stock solution' (Ca^{2+} : Mg^{2+} : Zn^{2+}, 2 : 2 : 1). Using EuDAPA2 (*Fig. 5.15. top*), similar spectroscopic changes were observed as in the absence of lactate. The apparent citrate binding constant, using the intensity ratio 615.5/686.5 nm was found to be logK = 3.20 ±0.02 M^{-1}. The corresponding K_d value (0.5 mM) for this analysis and the form of the response curve between 0 → 1 mM citrate (equivalent to 0 to 10 mM citrate, as diluted x10), are appropriate for the measurement of citrate in this range in the presence of high lactate background (equivalent to 23 mM). The 220% variation in the 615.5/686.5 nm intensity ratio should ensure reasonable precision in assessing unknown samples.

Studying the changes in the emission spectrum of EuDGP2 (*Fig. 5.15. bottom*) as a function of added citrate, similar spectroscopic changes were observed as in the absence of lactate from the prostate fluid. However, these changes were not as well pronounced. For example, evolution of the 614.5 nm band is much less obvious. These modest intensity and structural changes are associated with lactate/citrate competition. As detailed in *Table 5.1* these two anions have a very similar affinity to EuDGP2, with a $\log K_{citrate}$: $\log K_{lactate}$ ratio of 1.6 : 1. Consequently the apparent binding constant value, which was obtained using the 614.5/686.5 nm intensity ratio, was decreased significantly. This calculated logK = 2.65 ±0.05 M^{-1} value may be adequate; however, the minor spectral changes make EuDGP2 unsuitable for the desired application. In contrast, EuDAPA2 may be used for citrate level measurement

in diluted prostate fluid samples, as a result of lesser lactate interference. This can be envisaged from its $\log K_{citrate}$: $\log K_{lactate}$ ratio of 21 : 1.

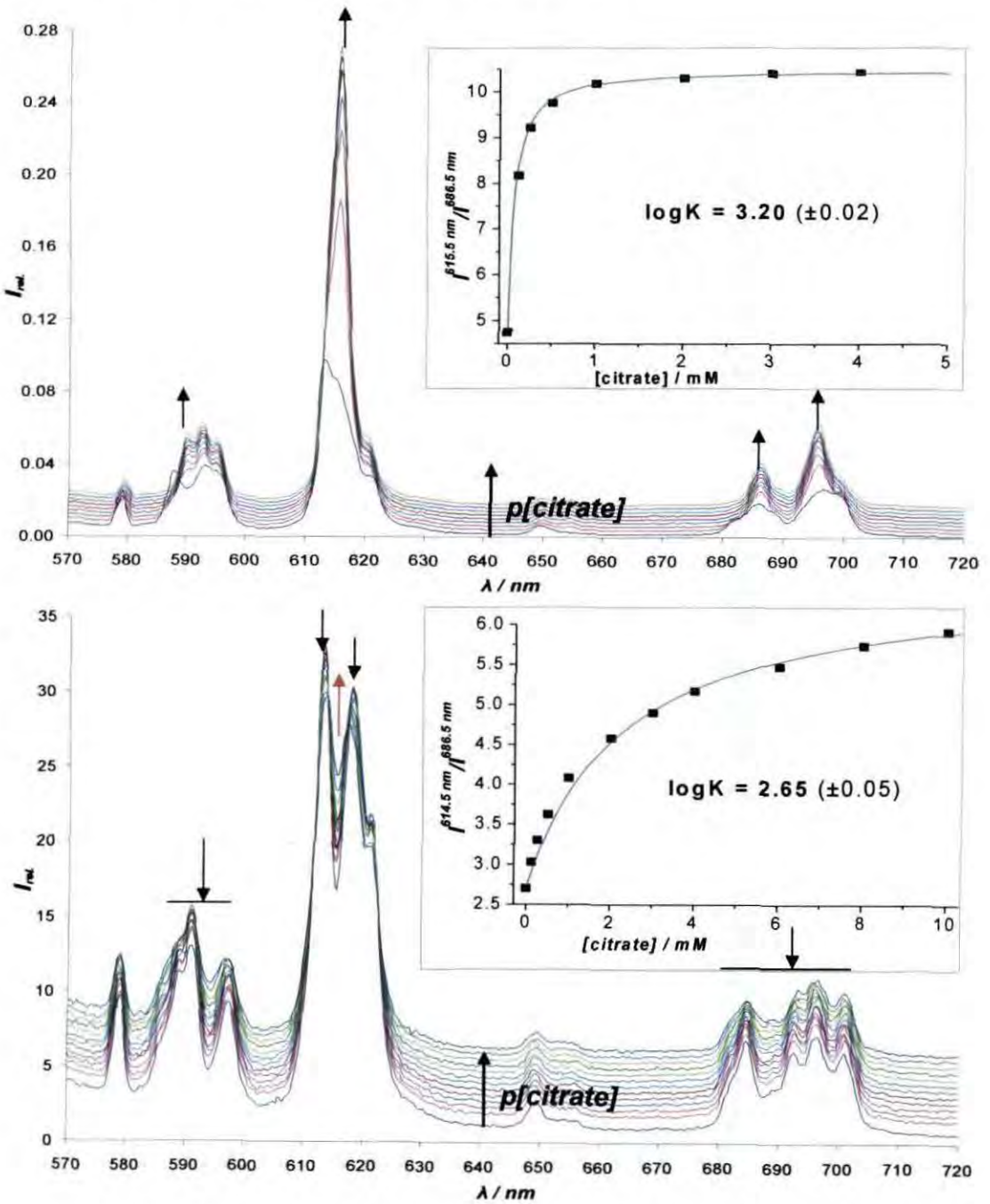

Fig. 5.15. Variation of Eu emission spectrum following addition of sodium citrate and 'metal ion stock' solution for (*top*) EuDAPA2 and (*bottom*) EuDGP2 in MsPFx10D. (*inserts*) Intensity ratio *vs.* added citrate plots, for determining the apparent binding constant. (pH = *6.55 (±0.05)*, *[complex] = 20 μM*, 298 K, λ_{ex} = *380 nm*). (LV_{min}= 4.75 and LV_{max}= 10.45 (*top*), LV_{min}= 2.70 and LV_{max}= 6.60 (*bottom*))

On a final note, until the extent of lactate interference is fully assessed, by the determination of lactate concentration in healthy and cancerous prostate fluid, these two complexes (EuDGP2 and EuDAPA2) possess favourable characteristics for use as citrate sensors in prostate cancer detection and staging. The former may be used in a regime of high citrate / low lactate and the latter when citrate values are lower, or when lactate is elevated. It is worth mentioning as a result of its sufficeint citrate affinity in the 0 to 10 mM range, the complex EuDGP2 may be used to analyse urine samples in the detection of some renal anomaly, such as urolithic kidney dysfunction and nephrolithiasis, whereas the citrate concentration in urine (4 mM in a healthy patient) is significantly increased.[53,54]

5.3.3 Protein Binding Studies

By studying the citrate affinity of EuDGP2, the apparent binding constant did not change as a function of added protein (HSA). However, a significant intensity decrease of the metal based emission was observed as the protein concentration increased in the solution. Therefore, the protein affinity (using human serum albumin as protein) of each complex was studied, using identical conditions, in diluted simulated prostate fluid. The protein was added as a lyophilised solid up to a limiting value of 0.7 mM and the pH was maintained at 6.55 (±0.05).

Monitoring changes in the total emission (440 – 720 nm), significant intensity changes were observed in both ligand fluorescence and europium emission. For example, for EuDAPA3 the behaviour is shown in *Fig. 5.16.* Indeed, no structural changes were observed in the metal based emission following increases in [HSA]. Each complex showed similar spectroscopic changes, and the measured radiative lifetimes did not alter significantly upon protein addition. The change in both ligand fluorescence and Eu emission may be attributed to quenching of the choromophore S_1 and T_1 state possibly involving the Tyr and Trp aromatic groups in HSA. In each case, as a result of non-linear intensity changes in the ligand fluorescence and europium emission, an apparent proton affinity constant may be calculated from the variation of the ligand fluorescence (444 nm) to Eu emission (615 nm) intensity ratio with protein.

The protein affinity was established to be high in each case. The apparent binding constant values were estimated to be in the logK region of 5 to 7, following a trend of EuDPP2 (logK = 7.6) > EuDAP2 (logK = 7.1) > EuDPPA2 (logK = 6.3) > EuDAPA2 (logK = 6.0) > EuDGP2 (logK = 5.2) (±0.07). The complexes bearing aromatic pendant arms and more positive overall complex charge bind to protein more avidly.

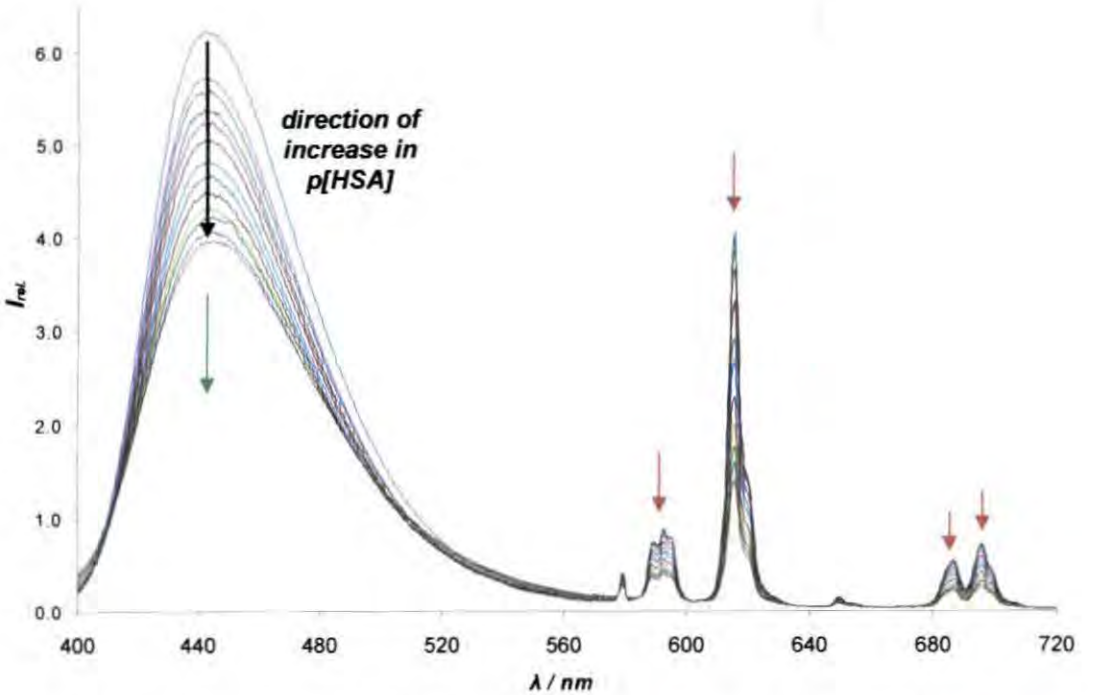

Fig. 5.16. Variation of ligand fluorescence (440 - 570 nm) and Eu emission (570 - 720 nm) following addition of HSA for EuDAPA2 in sPFx10D. (pH = 6.55 (±0.05), [complex] = 20 μM, 298 K, λ_{ex} = 380 nm)

Despite this high protein affinity, the form of the Eu emission spectrum remains unperturbed by added protein. Therefore both EuDAPA2 and EuDGP2 may still be used to analyse citrate in fluids of varying protein concentration.

5.4 'In vivo' Studies in Seminal Fluid Samples

The prostate gland plays a major part in seminal fluid production, with about 50% volumetric contribution (*see 5.1.2.1*). The rest of the fluid is produced mainly by the seminal vesicles. Hence, in seminal fluid, citrate levels are proportionate to the amount of

citrate in the prostate fluid. Therefore, it may be possible to perform a non-invasive detection of prostate adenocarcinoma, by citrate concentration determination from seminal fluid samples. ^{1}H-NMR examination of several seminal fluid samples, collected from healthy male volunteers, by *Sharma* established the average citrate and lactate concentrations to be 55.8 (±11) mM and 15.5 (±2) mM respectively.[44] Therefore in diluted (x10) samples the limiting citrate value should not exceed 7 mM, whilst a 2 mM competing lactate is also present.

A 'proof of principle' study was undertaken. Seminal fluid sample was obtained from a 26 year old healthy male, with no known prostate anomaly. Prior to any measurement, spermatozoa were removed by centrifugation within 5 minute to avoid their degradation and subsequent contribution to the citrate level of the sample. The viscous supernatant was filtered and used without any further treatment, in ten times dilution. As the pH of the seminal fluid was measured to be 7.35, the dilution was executed with 0.1 M HEPES buffer to maintain the pH at 6.55. The citrate concentration was increased by the previously established method, with a parallel increase in divalent metal ion concentration, using the 'metal ion stock' (MIS) solution.

Monitoring the Eu emission spectrum using EuDGP2 (*Fig. 5.17*), as a function of added total citrate concentration, minor spectral changes were observed, consistent with a healthy high initial citrate level in the sample. Studying the initial structure of the Eu emission, no evidence of lactate interference can be observed in the healthy seminal fluid sample. However, the presence of a significant citrate concentration is indicated. Despite the minor changes in the structure of the emission upon citrate addition, a well established modulation of the intensity of the 614.5 nm band can be observed. Plotting the intensity ratio (614.5/686.5 nm) *versus* added citrate concentration an apparent binding constant of logK = 2.42 ±0.09 M^{-1} was calculated. Using the initial 614.5/686.5 nm intensity ratio value of 3.17, and fitting it onto the calibration curve (*Fig. 5.13. left*), obtained from the corresponding measurement in simulated prostate fluid, the citrate level may be estimated to be 3.5 mM, *i.e.* 35 mM for the unprocessed seminal fluid sample. The interfering effect of lactate was not evident here, but will affect the calibration of the citrate response curve.

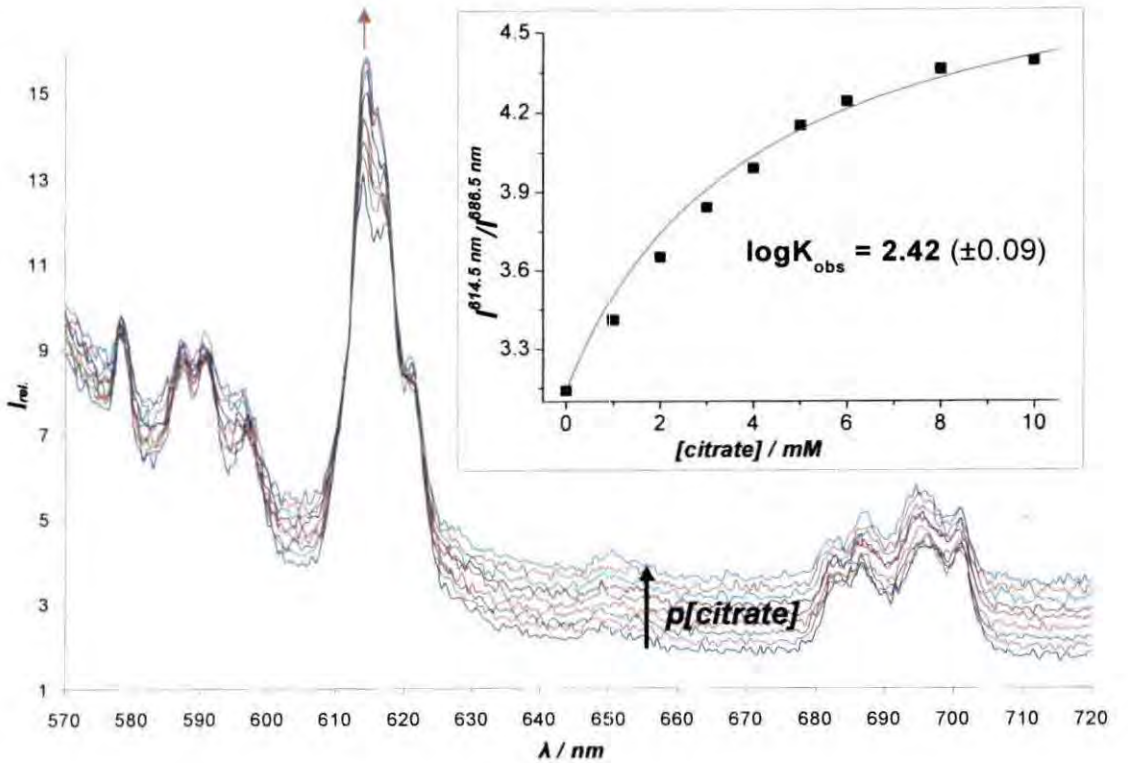

Fig. 5.17. Variation of Eu emission spectrum for EuDGP2 in diluted seminal fluid (x10) following addition of sodium citrate and MIS solution (pH = 6.55 (±0.05), [complex] = 20 μM, 298 K, λ_{ex} = 380 nm, 0.1 M HEPES, while the descending baseline may be attributed to fluorescence from various proteins in the sample). (*insert*) Intensity ratio (614.5/686.5 nm) *vs.* added citrate plot, for determining the apparent binding constant. (LV_{min}= 3.14 and LV_{max}= 4.90)

5.5 Prostate Fluid Analysis

A series of archived samples of prostate fluid was obtained from Prof. Les Costello. Measurements of the regenerated and diluted (x10) samples were undertaken using EuDGP2 (*see 5.3.1.3*). At that stage, the high lactate concentration of the samples and the consequent lactate competition was not assessed. Spectra obtained, even following addition of 10 mM citrate, revealed a profile resembling a lactate-bound species. Evidently [lactate] was high in these samples; therefore the study did not provide quantitative information of the unknown citrate concentrations and consequent detection of PCa. Unfortunately, the small volume of the received samples

did not permit repeat measurements with EuDAPA2. Consequently, two prostate fluid samples were requested with known staging of disease progression. A sample was obtained from a patient with early stage BHP, and one from a patient with highly developed prostate adenocarcinoma. The samples were redigested, and the extracted fluid examined to compare their citrate levels using EuDAPA2 and EuDGP2.

Using EuDGP2 as the designated sensor compound, no conclusive result could be obtained. This was assigned to minor spectroscopic differences between Eu emission spectrum of the BHP and PCa samples, and the insufficiently low citrate affinity of this complex in the desired citrate concentration region.

Monitoring the changes in the Eu emission spectrum with EuDAPA2 significant changes were observed for the PCa fluid sample, in the structure of the metal based emission as a function of added citrate (*Fig. 5.18*).

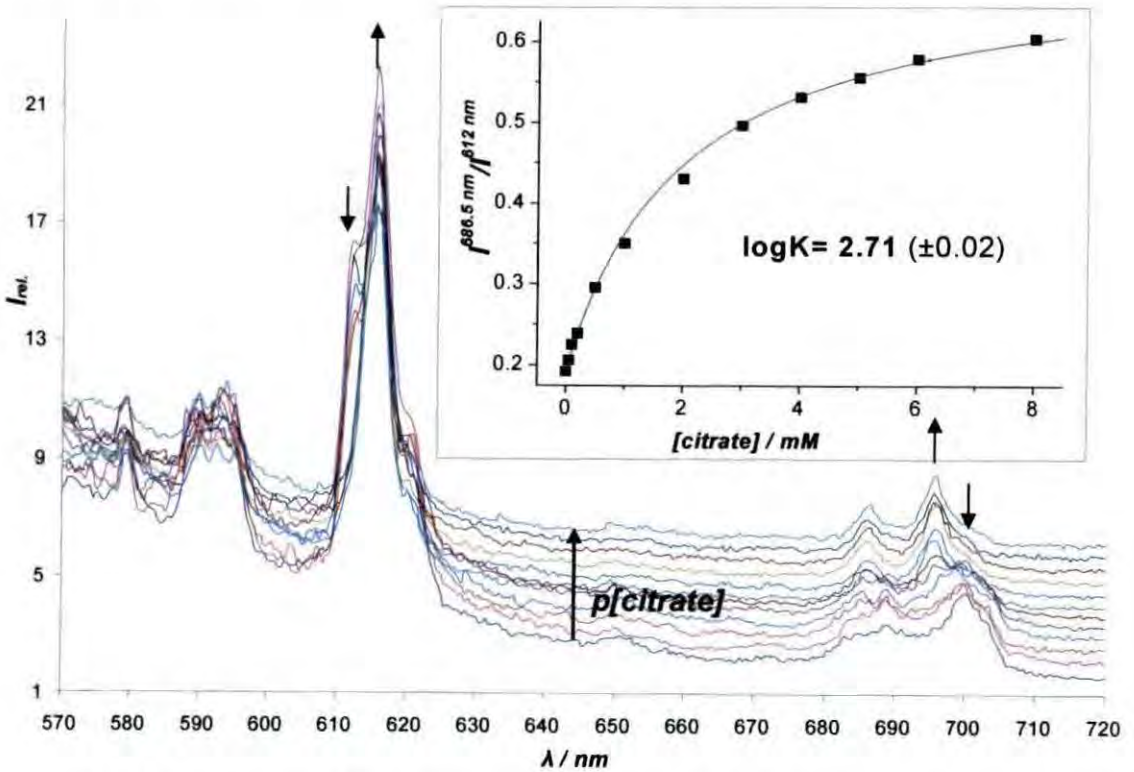

Fig. 5.18. Variation of Eu emission spectrum for EuDAPA2 in diluted PCa prostate fluid (x10) following addition of sodium citrate and MIS solution (pH = 6.55 (±0.05), [complex] = 20μM, 298 K, λ_{ex} = 380 nm, 0.1 M HEPES). (*insert*) Intensity ratio (686.5/612 nm) *vs.* added citrate plot, for determining the apparent binding constant. (LV_{min}= 0.19 and LV_{max}= 0.70)

Indeed well defined changes were observed in the $\Delta J = 2$ and $\Delta J = 4$ manifold. Using the intensity ratio (686.5/612 nm) *versus* added citrate plot, an apparent binding constant value of logK = 2.71 ±0.02 M^{-1} was calculated. Similar values were obtained using 615.5/686.5 nm and 612/615.5 nm ratios. This value is sufficient for citrate concentration determination and may be related to the competition between citrate and lactate. This conclusion was confirmed by examining the structure of the Eu emission for the initial system, as the presence of the 612 nm band was previously assigned (*see Fig. 5.14*) to lactate ligation to the Eu centre.

An interesting observation was made in a control experiment repeating the titration using a background solution obtained by the established method using a blank paper disc. These discs are being used to blot and lyophilise clinical samples for transportation. The initial Eu emission spectrum resembled that obtained for the lactate species! Hence, these discs may contain an unknown amount of lactate or a related α-hydroxyacid, which may be a residue of the paper manufacture procedure. The additional lactate contribution from the paper itself alters the lactate/citrate competition, and consequently perturbs the outcome of the study. On the other hand, as all our samples have been received using the same method transport, this additional lactate contribution could be systematically eliminated in the differentiation of citrate concentration between the two samples. However, as the initial citrate concentration of the PCa sample was sufficiently low to detect the presence of lactate, the lactate concentration of the sample could be determined using EuDAPA2. In the future, this could be achieved using EuDGP2 to determine the citrate content of the healthy seminal fluid, executing and comparing the lactate titration of the PCa sample prior to and after enzymatic digestion of its lactate content.

Using the BHP sample as the background medium (*Fig. 5.19*), similar spectroscopic changes were observed as with the PCa sample. However, the structural changes were less pronounced due to the higher initial citrate content of the sample. Consequently, the obtained apparent citrate binding constant was lowered to logK = 2.04 ±0.03 M^{-1}. Similar values were obtained using 615.5/686.5 nm and 612/615.5 nm ratios.

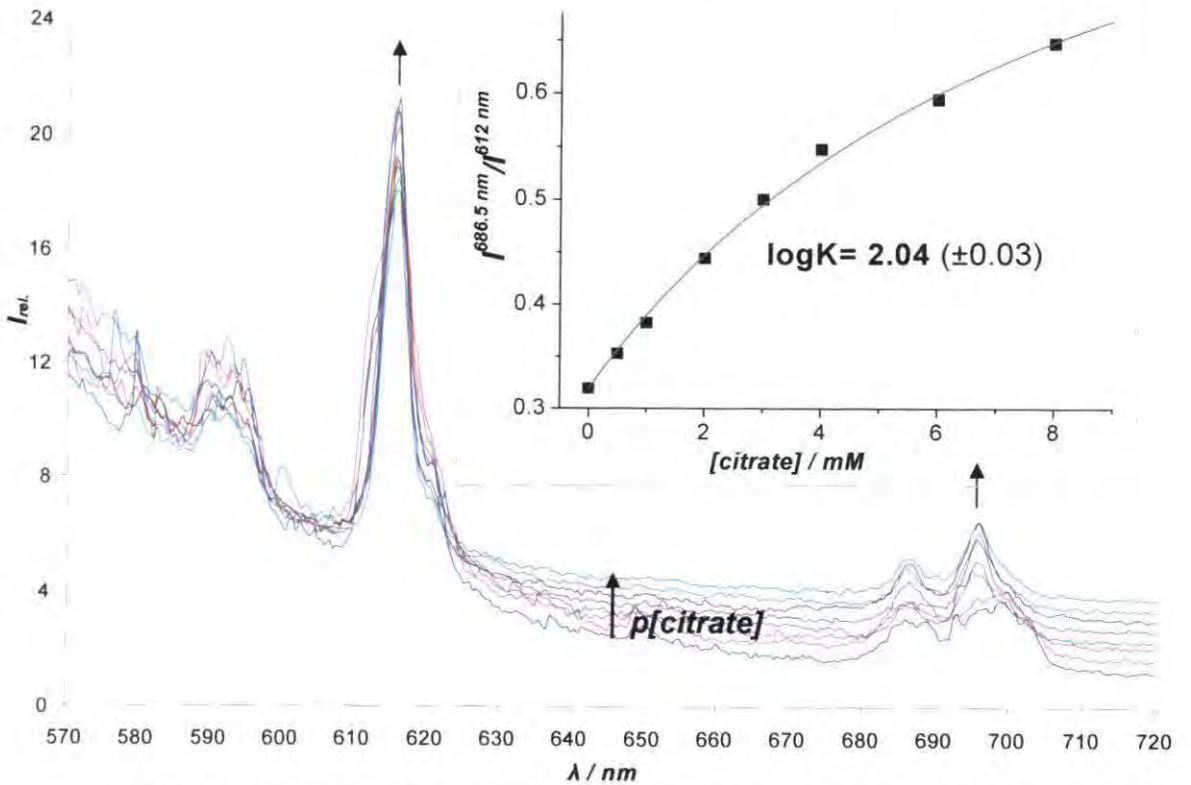

Fig. 5.19. Variation of Eu emission spectrum for EuDAPA2 in diluted BHP prostate fluid (x10) following addition of sodium citrate and MIS solution (pH = 6.55 (±0.05), [complex] = 20 μM, 298 K, λ_{ex} = 380 nm, 0.1 M HEPES). (*insert*) Intensity ratio (686.5/612 nm) *vs.* added citrate plot, for determining the apparent binding constant. (LV_{min}= 0.32 and LV_{max}= 1.00)

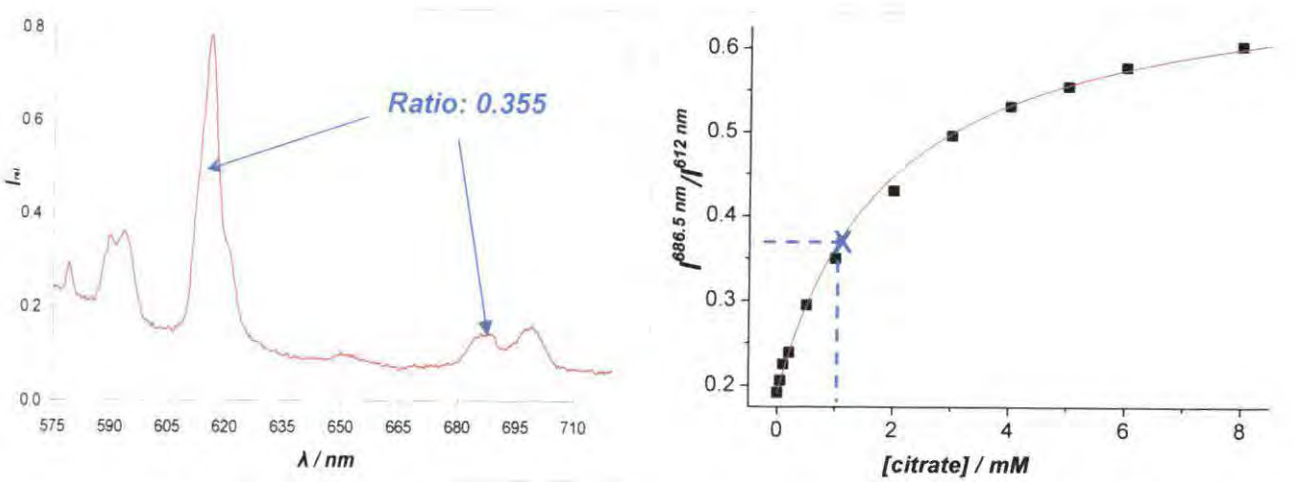

Fig. 5.20. (*left*) Eu emission spectrum of EuDAPA2 in diluted BHP prostate fluid (x10). (*right*) Intensity ratio (686.5/612 nm) *vs.* added citrate plot, for EuDAPA2 in diluted PCa prostate fluid sample determining the apparent binding constant. (pH = 6.55 (±0.05), [complex] = 20 μM, 298 K, λ_{ex} = 380 nm, 0.1 M HEPES) (*for LV values see Fig. 5.18)*

Using the initial 686.5/612 nm intensity ratio of the BHP sample and fitting it onto the calibration curve obtained with the citrate titration of the diluted PCa sample (*Fig. 5.20*), the difference in citrate concentration may be established. This analysis requires the assumption that there is no significant difference in lactate concentration between the two samples, to modulate the lactate-citrate competition.

Fitting the ratio of 0.355 of the BHP sample onto the calibration curve, the difference in citrate concentration was established to be 10 mM for the undiluted sample. This is a promising result in support of the application of EuDAPA2 as a marker for prostate cancer. However, this is only a comparative study of citrate levels in BHP and PCa prostate fluid samples. Further analysis is required of prostate fluid samples obtained from a much larger number of patients with known stage of prostate malignancy. Parallel analysis of healthy prostate fluid samples is also required. Moreover, these samples should be examined in conjunction with analysis of seminal fluid samples, in order to validate the presence of proportionate citrate levels as a function of prostate malignancy. In preference, samples of lyophilised fluid should be transported in plastic Eppendorf vials, rather than the paper-blotting technique.

5.6 'In cellulo' Studies

The cellular uptake profile of complexes EuDPPA2, EuDAPA2 and EuDGP2 was examined in Chinese hamster ovarian cells (CHO) cells, as no prostate cancer cell lines (PC-3 or LNCaP) were available. Cells were grown in a monolayer on 0.1 mm thick glass cover slips. Incubation times varied from 1 to 12 h, while the complex loading concentrations was 100 μM by dissolving lyophilised complex in F-12(Ham) media containing 10% NCS (Newborn Calf Serum) and 1% penicillin-streptomycin. Prior to mounting of the cells without any additional treatment, incubation was carried out for each individual time point in a copper jacketed incubator using 5% CO_2 and about 10% relative humidity. Cover slips were mounted, by withdrawal of the growth medium, and subsequently washed with phosphate buffered saline (PBS) solution (x3). The uptake and distribution of the complex within the cell was observed by fluorescence microscopy, following excitation of the chromophore.

Epifluorescence images were taken on a Zeiss Axiovert 200M epifluorescence microscope with 63x/1.40 oil DIC and 40x/1.40 oil DIC objectives. For excitation a 340 - 390 nm (90% transmission) band-pass (BP) filter was used. Ligand fluorescence was observed using a BP 445 - 465 nm filter (80% transmission), while Eu emission was observed using a 570 nm long-pass (LP) filter (85% transmission). Confocal microscopy images were taken on a Zeiss LSM 500 META confocal microscope using a BIORad 405 nm diode laser for excitation. An LP 590 nm emission filter was used for observing europium luminescence and a BP 505 - 550 nm filter to allow ligand fluorescence to be observed.

5.6.1 Cellular Uptake Study of EuDPPA2

Previous studies in Durham had examined the uptake/localisation behaviour of EuDPP2 in various cell types.[49] In order to study how the pendant arm hydrolysis affects the cellular uptake and localisation profile, EuDPPA2 was incubated with CHO cells, using 50 μM loading concentration and a 1 to 10 h loading period. For each time point, a similar localisation profile was observed, echoing the behaviour of EuDPP2 (*Fig. 5.21*).

Fig. 5.21 Confocal microscopy images of EuDPP2 (λ_{ex}= BP 340-390 nm, λ_{em} = LP 505 nm) incorporating 2-methyl-azathioxnathone sensitising moiety, co-localised with Syto-RNASelect® (λ_{ex}=488 nm, λ_{em} = BP 505-550 nm) in NIH 3T3 cells. Orange regions of the merged images correspond to areas where both stain and complex are localized confirming ***ribosomal localization,*** (highlighting strong localization in the nucleus).[49]

Very weak emission was detected for all images, regardless of the microscope technique (*Fig. 5.22*). Each image required a long acquisition time and displayed high background fluorescence in both observed channels. Ligand fuorescence was found to be of similar intensity to Eu emission throughout the cytosol. However, almost no intranuclear localisation was observed. This may be attributed to the low loading concentration used. The high background noise of the images may tentatively be assigned to rapid egress of the complex, from the cell, which may be related to EuDPPA2's 100 times lower (*see 5.3.3*) protein affinity (and consequently higher resistance towards protein quenching), compared to the parent complex (EuDPP2).

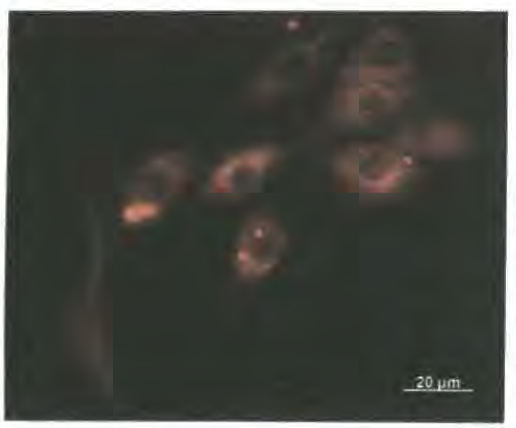

Fig. 5.22 Epifluorescence image of EuDPPA2 (λ_{ex}= BP 340 - 390 nm, λ_{em} = LP 570 nm) in CHO cells, 8h loading time, 50 µM loading concentration. (The image was digitally modified to give a less intense background fluorescence.)

Despite the low image quality, cell viability was found to be time independent. It was monitored by visual counting of the number of cells in a selected population as a function of time. From bright field measurements, more than 95% of the cells were considered to be healthy over the 10 h period. Due to the extensive auto-fluorescence and low image resolution no further studies were carried out with this complex.

5.6.2 Cellular Uptake Study of EuDGP2

The localisation and cellular uptake profile of EuDGP2 was also studied in CHO cells, using a 50 µM loading concentration and a 1 to 8 h incubation period (*Fig. 5.23*). For each time point, a similar localisation profile was observed with parallel metal and ligand based emission. When optical sections through the cells were taken, the fluorescence could be detected in each layer. No time dependence for both ligand and Eu emission intensity was observed over the 1 to 8 h loading period; and neither

were significant changes observed in complex localisation. Furthermore, no evidence was found to indicate complex dissociation. The localisation profile resembled ribosomal distribution and compartmentalisation as was found for EuDPP2 and Eu(MS)DAdP2. This strongly suggests that it is the nature of the chromophore that directs the cellular localisation and compartmentalisation in this series.

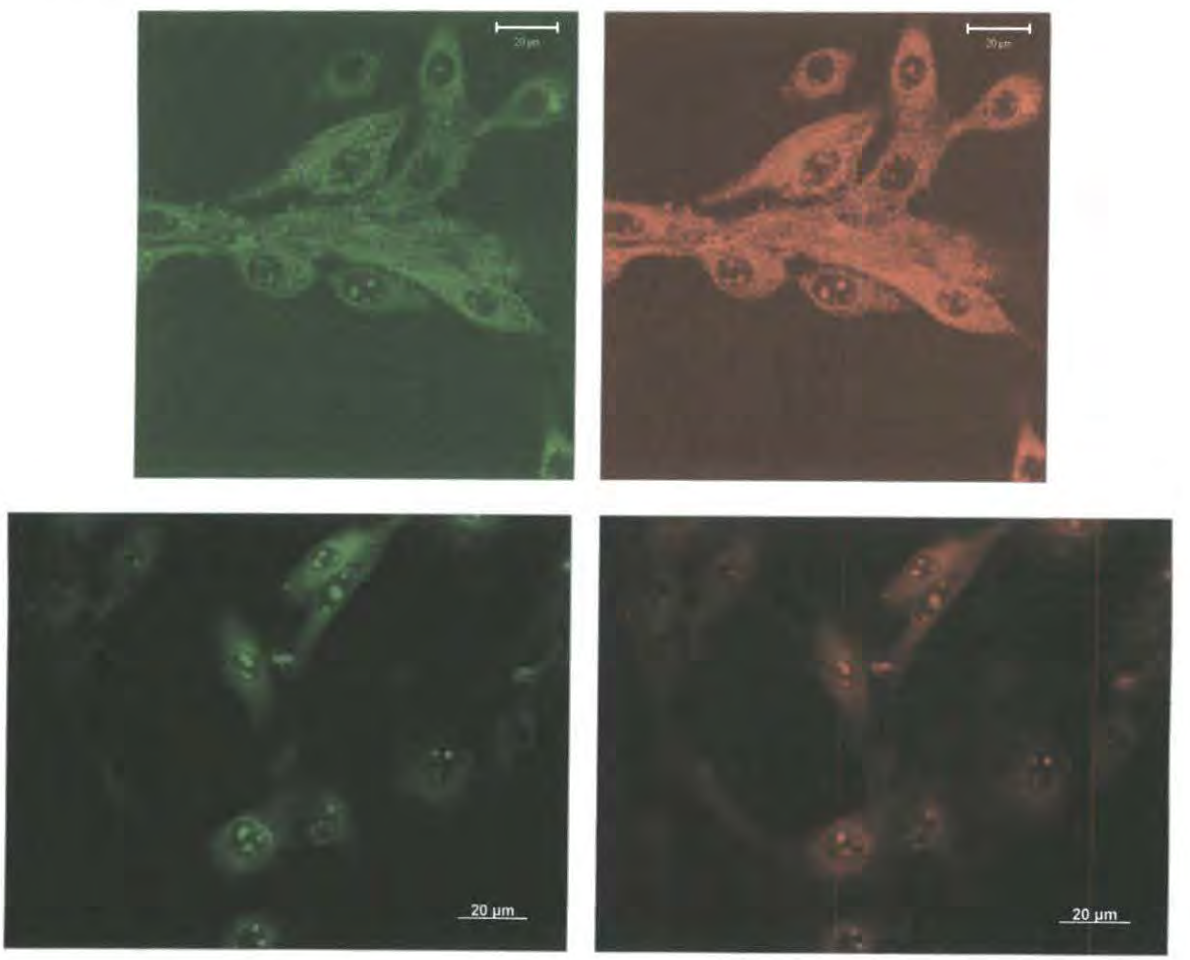

Fig. 5.23. (*top*) Confocal (405 nm diode laser excitation) and (*bottom*) digitally enhanced epifluorescence (BP 340 - 390 nm excitation) microscopy images of EuDAPA2 (50 µM, 8 h) in CHO cells. (*left*) Ligand fluorescence (BP 445 - 465 nm) (*right*) Eu emission (LP 570 nm).

As with Eu(MS)DAdP2, the variation of emitted light intensity throughout the cell was studied. The complex EuDGP2 displayed only a minor (average 20%) increase of image brightness in the nucleoli, compared to a 280% change for Eu(MS)DAdP2.

Cell viability was also found to be time independent and was monitored by the previously established method. From bright field measurements, more than 95% of the cells were found to be healthy over the 8h period.

5.6.3 Cellular Uptake Study of EuDAPA2

The cellular uptake profile EuDAPA2 was examined using CHO cells, using a 100 μM complex concentration in the growth medium (*Fig. 5.24*). Images recorded using the related complex EuDPPA2 had indicated the possibility of rapid cellular uptake and subsequent egress upon complex withdrawal. Accordingly, images were recorded at 5 min, 15 min, 30 min and subsequently at every hour up till 12 h. Indeed, rapid complex uptake was observed, at each time point with similar localisation profile and no significant intensity modulation over the observed 5 min – 8 h time régime. Cell viability was monitored by the established method and was found to be time independent. Bright field microscopy measurements indeed confirmed that more than 90% of the cells looked healthy over the studied 8 h period. Optical sections thorough the cells were taken and luminescence could be detected in each layer. While only one set of images for each time point is shown here, images were taken at a number of points across the slide, with a similar localisation profile observed at each position. The colour consistency of merged images (*not shown*) suggests that the Eu does not dissociate from the complex within the cell. However, as a result of high background fluorescence, every image recorded required relatively long acquisition times. Each image was consistent with complex localisation in the high protein regions of the ribosomes within the cytosol. This behaviour is consistent with that displayed by every complex incorporating a bound 2-methyl-azathioxanthone chromophore.

In contrast to earlier studies with related complexes, little or very weak localisation was observed in the nucleoli.

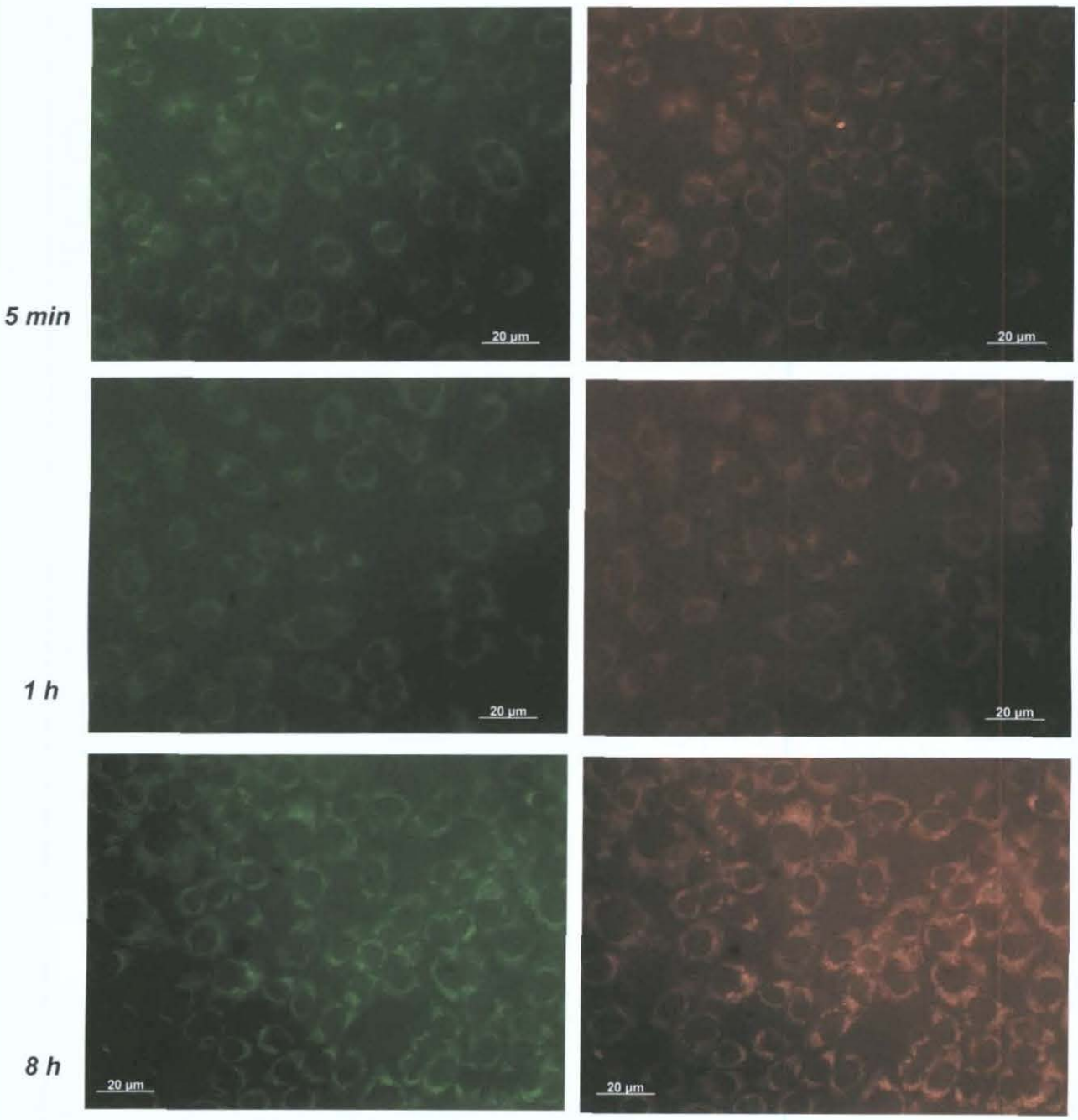

Fig. 5.24. Epifluorescence microscopy images at different loading time points in CHO cells, showing the localisation and cellular uptake of EuDAPA2 ([complex] = 100 µM, BP 340-390 nm excitation) (*left*) Ligand fluorescence was observed using a BP 445 - 465 nm filter (*right*) Eu emission was observed using LP 590 nm filter.

5.6.3.1 Time Resolved Microscopy with EuDAPA2

Time gated microscopy (*see 1.5.4*) images were recorded on a modified Zeiss Axiovert 135 epifluorescence microscope equipped with a Q-switch 355 nm Nd:YAG laser excitation (supplied by EL^{4}Light), 63x/1.40 oil DIC objective, and an Imagex NanoB&W CCD camera. For acquisition and image transformation Imagex Direct v1.21 and Laser Power v2.0 softwares were used. Eu emission was observed using a LP 590 nm filter, while the use of LP 420 nm filter allowed the total fluorescence to be observed.

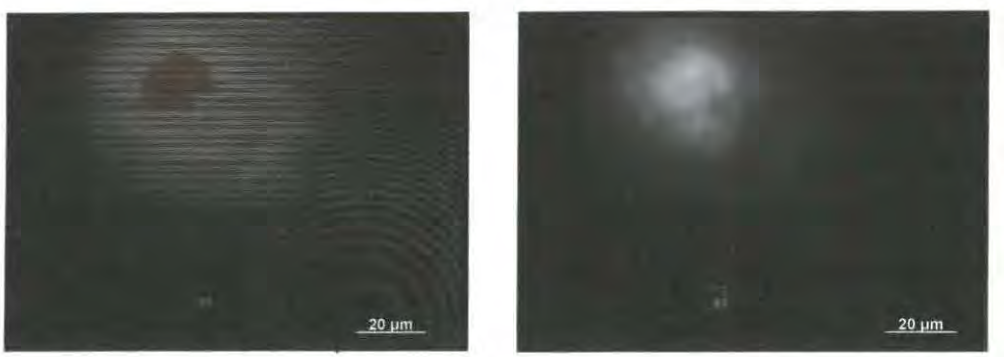

Fig. 5.25. Non-gated microscopy images of EuDAPA2 in a single CHO cell ([complex] = 50 µM, 8 h loading point, 355 nm laser excitation). (*left*) Total emission using a LP 420 nm filter (*right*) Eu emission was observed using LP 590 nm filter. (Red part of the images shows acquisition overload due to high emitted light intensity.)

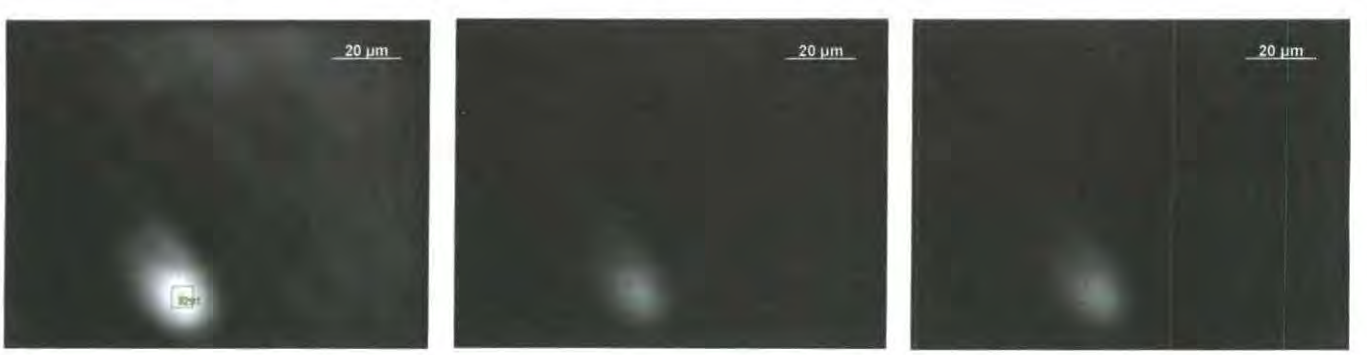

Fig. 5.26. Low resolution time gated microscopy images of EuDAPA2 in a single CHO cell ([complex] = 50 µM, 8 h loading, 355 nm laser excitation) using (*left*) 0.6 µs delay and 90 µs gate (*centre*) 0.8 µs delay and 90 µs gate for Eu emission to be detected using a LP 420 nm filter. (*right*) 0.8 µs delay and 90 µs gate for total emission to be detected using a LP 590 nm filter. (Green numbers on each image determine the maximum relative intensity of the brightest point.)

Time resolved microscopy images (*Fig. 5.25 and 26*) were of low resolution, losing the ability to define compartmentalisation. Europium emission could be readily detected, following a 1 μs delay. Non-gated images showed similar resolution with significant difference in image intensity as a function of the filter selected. This difference was significantly lowered using time gated measurement, due to elimination of the ligand fluorescence. Despite the image quality, these preliminary results suggests that EuDAPA2, and consequently each Eu complex detailed in this thesis, may be used in time gated studies and applications.

5.6.3.2 Determination of the Intracellular Europium Concentration

The images obtained by fluorescence microscopy allow identification of the localisation and uptake profile of the complex. However, this does not provide quantitative information about how effectively the complex is taken up or being released. The exact concentration of the EuDAPA2 per cell, for a given time point was determined through a combination of flow-cytometry, and ICP-MS (inductively coupled plasma – mass spectrometry). Determination of this value can also be estimated, for a known population of cells, by measuring the absorbance of the complex in the growth medium prior to and after incubating the cells.

For determination of EuDAPA2 concentration in the cells, an 8h loading time point was chosen, with a 100 μM loading concentration. The counted and sorted (122,668) cells were analysed using ICP-MS. The PBS used to wash them after growth medium withdrawal was also analysed. The number of EuDAPA2 complexes inside a single cell was determined to be 8.3×10^7. This value gives a $[Eu]_{total}$ of 46 μM inside a single cell (assuming 3,000 μm^3 mean cell volume). This means that 46 % of the original loading concentration had been taken up by the cells. This measurement was confirmed by comparing the absorbance values of the complex containing growth medium prior to and after incubation. A 50% (±5%) decrease in complex concentration was found. Surprisingly, 54% of the total complex concentration was found in the submitted PBS solution. This not only confirms the relatively fast influx of the complex, but explains the high background fluorescence observed. This could be linked to rapid egress upon withdrawal of complex to the surrounding (PBS) medium. This behaviour also suggests

that the complex EuDAPA2 is ta ken up via a diffusion-driven transport mechanism across the cell membrane.

This uptake/egress hypothesis for the complex(es) can be confirmed by loading the complex onto the cells at 4 °C. If europium luminescence can still be clearly observed with the same localization profile, this would suggest that the complex does not enter the cells by endocytosis. The relatively even distribution of the complex in the cytoplasm also supports this premise. Molecules and conjugates entering cells via endocytosis are believed to be initially trapped in endocytotic vesicles and then transferred into endosomes. Only molecules and conjugates escaping from the endocytosis pathway can survive to act as probes.[55]

5.7 Conclusions, Future Work and Comparison of Results

A series of ratiometric Eu(III)complexes has been synthesised, incorporating an efficient sensitiser, for measuring citrate concentrations in seminal and prostate fluid samples. Their luminescence properties were thoroughly studied in a variety of fluids of varying ionic composition, to find the best candidate for prostate adenocarcinoma detection. Divalent metal ion interference in the samples was established and its effect defined for EuDAPA2 and EuDGPA2. However, lactate interference was also established and suggesting the preferred use of EuDAPA2 in future measurement, as it exhibits high citrate/lactate selectivity. Studies in both diluted seminal and prostate fluid samples indicated, that the complex EuDAPA2 might be used successfully for the detection and staging of prostate malignancy using citrate as a tumour marker. The few preliminary results obtained, raised the interest of several groups throughout the world, resulting in a collaboration with Prof. Les Costello, University of Maryland. Hence, collection of seminal and prostate fluid samples from a number of patients has been initiated, which may allow the validation of the application of EuDAPA2.

Cellular uptake images revealed fast complex uptake and a well distributed localisation within the cell, using complexes incorporating the 2-methyl-azathioxathone sensitiser moiety. A significant amount of complex entered the cell and fast egress was also observed. Comparative studies suggested that for complexes incorporating identical

sensitisers, a similar localisation profile was observed. The speed and quantity of complex taken up or released may be a function of the overall charge of the complex. The uptake study with EuDAPA2 also showed that a significant amount of complex enters the cell possibly via concentration gradient diffusion. The complex remains inert once inside the cells, and no evidence for cell toxicity was found. Images were observed using non-fixed cells, which is beneficial for live cell imaging applications. A preliminary time gated microscopy study proved the benefit and possible application of EuDAPA2, and hence related Eu complexes, as long lived luminescent probes.

In summary, complexes EuDAPA2 and EuDGP2 show promise as ratiometric luminescent citrate sensors for the detection of prostate cancer from seminal or prostate fluid samples.

Further work is required to assess and confirm the localisation profile of the complex and to determine the mechanism of cellular uptake. Images using more relevant cell lines, such as PC-3 or LNCaP cells (both human prostate cell lines), are underway to study changes in the uptake and localisation as a function of cell type.

On a final note to summarise the observations and results, made not only with citrate sensors, but each ratiometric Eu complex studied in this thesis, the following conclusions can be established:

- A promising complex, Eu(MS)DAdP2, has been synthesised and assessed as a candidate for measuring extra and intracellular pH in the biological pH region of 5.5 to 8.
- Complex EuDAP7A not only proved to be successful for spectroscopic determination of extracellular bicarbonate concentration, but also its azathioxanthone chromophore was found to possess good photophyisical properties, making it an efficient sensitiser.
- Two possible candidates, EuDGP2 and EuDAPA2, were found to possess suitable kinetic and spectrophysical properties, allowing their use as sensors for citrate anion, e.g. to analyse seminal and/or prostate fluid samples.

- Thorough cellular uptake studies of the complexes of key importance were undertaken and led to important observations regarding localisation and possible uptake mechanisms. These observations not only validate their intracellular applications, but also provide significant milestones toward further complex/sensor design.
- Preliminary time gated microscopy and two photon spectroscopy studies confirmed the application of selected complexes as long lived luminescent probes.

5.8 References

1 T. N. Popova and A. A. Pinheirode de Carvalho, *Biochim. Biophys. Acta*, 1998, **1364**, 307.

2 D. P. Simpson, *Am. J. Physiol.*, 1983, **244**, F223.

3 D. A. Weinstein, M. J. G. Sommers, and J. I. Wolfsdorf, *J. Pediatr.*, 2001, **138**, 378.

4 L. C. Costello, R. B. Franklin, and P. Narayan, *Prostate*, 1999, **38**, 237.

5 J. Kurhanewicz, J. M. MacDonald, D. B. Vigneron, B. Konety, S. J. Nelson, P. Narayan, and H. Hricak, *Urology*, 1995, **45**, 459.

6 *Gray's Anatomy*, **s263**, 1251.

7 'Prostate Cancer FAQ', State University of New York School of Medicine and Urology, 2006.

8 K. Moore and A. Dalley, 'Clinically Oriented Anatomy', Lippincott Williams & Wilkins, 1999.

9 L. C. Costello and R. B. Franklin, *Molecular Cancer*, 2006, **5**, 17.

10 *Courtesy of CASE Western Reserve University and University Hospital MIR.*

11 www.cancer.gov (*UK*)

12 'IARC Worldwide Cancer Incidence Statistics', Oxford Univesity Press., 2001.

13 B. F. Hankey, E. J. Feuer, L. X. Clegg, R. B. Hayes, J. M. Legler, P. C. Prorok, L. A. Reis, R. M. Merrill, and R. S. Kaplan, *J. Natl. Cancer Inst.*, 1999, **91**, 1017.

14 www.prostatecancerfoundation.org

15 A. Potosky, B. Miller, P. Albertsen, and B. Kramer, *J. Am. Med. Assoc.*, 1995, **273**, 548.

16 X. Chavarro, *Proc. Am. Assoc. Cancer Res.*, 2006, **47**, 1.

17 American Association for Cancer Research, 'Magic Tomato, Lycopin prevents Cancer?' 2007.

18 P. H. Gann and E. L. Giovannucci, 'Nutrition and Prostate Cancer ', Prostate Cancer Foundation, 2005.

19 J. Shannon, S. Tewoderos, M. Garzotto, T. M. Beer, R. Derenick, A. Palma, and P. E. Farris, *Am. J. Epdemiol.*, 2005, **162**, 318.

20 E. E. Calle, C. Rodriguez, K. Walker-Thrumond, and M. J. Thun, *N. Engl. J. Med.*, 2003, **248**, 1625.

21 American Cancer Society, 'Overview: Prostate Cancer', 2006.

22 www.cancer.org (*USA*)

23 National Institute of Health, *Web Overview:* 'Prostate Cancer', 2006.

24 M. F. Leitzman, *J. Am. Med. Assoc.*, 2004, **291**, 1578.

25 G. L. Andriole, C. Roehrborn, C. Schulman, K. M. Slawin, M. Somerville, and R. S. Rittmaster, *Urology*, 2004, **64**, 537.

26 www.oxfordscreening.co.uk

27 M. J. Roobol, R. Kranse, H. J. de Koning, and F. H. Schroder, *Urology*, 2004, **63**, 309.

28 W. J. Catalona, J. P. Richie, J. P. De Kernion, F. R. Ahmann, T. L. Ratliff, B. L. Dalkin, L. R. Kavoussi, M. T. MacFarlane, and P. C. Southwick, *J. Urology*, 1994, **152**, 2031.

29 M. Iyer, F. B. Salazar, X. Lewis, L. Zhang, L. Wu, M. Carey, and S. S. Gambhir, *Transg. Res.*, 2005, **14**, 47.

30 D. E. Hansel, A. M. DeMarzo, and E. A. Platz, *J. Urology*, 2007, **177**, 1736.

31 L. C. Costello and R. B. Franklin, *Prostate*, 1991, **19**, 181.

32 L. C. Costello, L. Yiyan, R. B. Franklin, and M. C. Kennedy, *J. Biol. Chem.*, 1997, **272**, 28875.

33 H. Laube, M. C. Kennedy, M. H. Emptage, H. Breinert, and C. D. Stout, *Proc. Natl. Acad. Sci. U.S.A.*, 1996, **93**, 13699.

34 F. K. Habib, M. K. Mason, P. H. Smith, and S. R. Stitch, *J. Cancer*, 1979, **39**, 700.

35 L. C. Costello, R. B. Franklin, P. Feng, B. Milon, M. M. Desouki, K. K. Singh, A. Kajdacsy-Balla, and O. Bagasra, *Mol. Cancer*, 2005, **4**, 32.

36 L. C. Costello, R. B. Franklin, P. Feng, M. Tan, and O. Bagasra, *Cancer Causes Control*, 2005, **16**, 901.

37 V. Y. and S. V. Zaichick, and T. V. Sviridova, *Int. Urol. Nephrol.*, 1997, **29**, 565.

38 L. C. Costello, R. B. Franklin, Y. Liu, and M. C. Kennedy, *J. Inorg. Biochem.*, 2001, **78**, 161.

39 P. L. Pedersen, *Prog. Exp. Tumor Res.*, 1978, **22**, 190.

40 R. A. Parlo and P. S. Coleman, *J. Biol. Chem,*, 1984, **259**, 997.

41 J. Kurhanewicz, M. G. Swanson, S. J. Nelson, and D. B. Vigneron, *J. Mag. Res. Imag.*, 2002, **16**, 451.

42 J. Kurhanewicz, D. B. Vigneron, R. G. Males, M. G. Swanson, K. Y. Yu, and H. Hricak, *Radiol. Clin. North. Am.*, 2000, **38**, 115.

43 J. P. Kavanagh, *J. Reprod.*, 1985, **75**, 35.

44 U. Sharma, K. Chaudhury, N. R. Jagannathan, and S. K. Guha, *Reproduction*, 2001, **122**, 431.

45 L. C. Costello and R. B. Franklin, *Oncology*, 2000, **59**, 269.

46 E. E. Kline, E. G. Treat, T. A. Averna, M. S. Davis, A. Y. Smith, and L. O. Silleurd, *J. Urology*, 2006, **176**, 2274.

47 T. A. Averna, E. E. Kline, A. Y. Smith, and L. O. Sillerud, *J. Urology*, 2005, **173**, 433.

48 J. Yu and D. Parker, *Eur. J. Org. Chem.*, 2005, 4249.

49 J. Yu, D. Parker, R. Pal, R. A. Poole, and M. J. Cann, *J. Am. Chem. Soc.*, 2006, **128**, 2294.

50 D. Parker and J. Yu, *Chem. Commun.*, 2005, 3141.

51 A. E. Martell and R. M. Smith, 'Critical Stability Constants', Plenum Press, Vol.2, 1974.

52 J. W. F. Catto, S. Cross, J. Phillips, A. Leiblich, H. Leung, F. C. Hamdy, and I. Rehman, *British J. Urology Int.*, 2006, **97**, 6.

53 J. H. Parks and F. L. Coe, *Kidney Int.*, 1986, **30**, 85.

54 M. H. Khaskhali, M. I. Bhanger, and F. D. Khand, *J. Chromatography B: Biomed. Sci. Appl.*, 1996, **675**, 147.

55 F. Osaki, T. Kanamori, S. Sando, T. Sera, and Y. Aoyama, *J. Am. Chem. Soc.*, 2004, **126**, 6520.

56 K. Newell, A. Franchi, J. Pouysségur, I. Tannock, *Proc. Natl. Acad. Sci. USA*, 1993, **90**, 1127.

CHAPTER 6

Experimental and Synthetic Procedures

6 Experimental and Synthetic Procedures

6.1 General Experimental

6.1.1 Reagents and Solvents

All commercially available reagents were used as received, from their respective suppliers. Solvents were dried using an appropriate drying agent when required (CH_3CN over CaH_2, CH_3OH over $Mg(OMe)_2$ and THF over Na/benzophenone). Water and air sensitive reactions were carried out under argon atmosphere. Water and H_2O refer to high purity water with conductivity ≤ 0.04 μS cm^{-1} obtained from the 'Purite$_{STILL}$ Plus' purification system.

6.1.2 Chromatography

Thin-layer chromatography was carried out on neutral aluminium oxide plates (Merck Art 5550) or silica plates (Merck 5554), both visualised under UV irradiation (254 nm) or iodine staining. Preparative column chromatography was carried out using neutral aluminium oxide (Merck Aluminium Oxide 90, activity II-III, 70 - 230 mesh), pre-soaked in ethyl acetate, or silica (Merck Silica Gel 60, 230 - 400 mesh).

6.1.3 Spectroscopy

^1H and ^{13}C NMR spectra were recorded on a Varian Mercury 200 (^1H at 199.975 MHz, ^{13}C at 50.289 MHz), Varian Unity 300 (^1H at 299.908 MHz, ^{13}C at 75.412 MHz), Varian VXR 400 (^1H at 399.97 MHz, ^{13}C at 100.57 MHz), on a Bruker Avance spectrometer (^1H at 400.13 MHz, ^{13}C at 100.61 MHz), on a Varian Inova-500 (^1H at 499.78 MHz, ^{13}C at 125.67 MHz), on a 1.53 T magnet connected to a Varian VXR400 console (^1H at 65.6 MHz), or a Bruker AMX 500 spectrometer. All spectra were referenced internally to the solvent residual proton signals, except for complexes in D_2O, where tert-butanol was added as an internal reference ($\delta = 0$ ppm). All chemical shifts are given in ppm and coupling constants in Hz. Splitting patterns are described as singlet (s),

doublet (d), double-doublet (dd), triplet (t), quartet (q), pentet (p), heptet (h) or multiplet (m).

Electrospray mass spectra were recorded on a VG Platform II (Fisons Instrument), operating in positive or negative ion mode as stated, with methanol as the carrier solvent. Accurate masses were measured on a Thermo Finnigan LQT.

UV/Vis absorbance spectra were recorded either on a Perkin Elmer Lambda 900 UV/Vis/NIR spectrometer (using FL Winlab software) or a Unicam UV/Vis UV2 spectrometer (using Vision v3.33 software).

Emission spectra were measured on a ISA Joblin-Yvon Spex Fluorolog-3 luminescent spectrometer (using DataMax v2.20 software), while lifetimes were measured on a Perkin Elmer LS55 luminescence spectrometer (using FL Winlab software). All samples were contained in quartz cuvettes with a path length of 1 cm and polished base. Measurements were obtained relative to a reference of pure solvent contained in a matched cell.

Two-photon excited emission spectrum and time gated photoluminescence were recorded using a two photon excitation source consisted of a mode-locked cavity dumped (APE™ Pulse switch) Ti:Sapphire laser (MIRA™, Coherent) producing near infra red optical pulses with a temporal width of ~150 fs (FWHM) in the wavelength range 740 – 810 nm, and a repetition rate of 4 MHz. The excitation light was focused into the sample solution using an Olympus LWD C A20 (20x) objective. The emission was subsequently collected using a dichroic mirror (Semrock FF735) and detected using a fiber coupled CCD spectrograph (Avantes Avaspec 2048FT) with a 100μm core fibre. The laser power was monitored using a photodiode with a known response curve, calibrated against a free standing power meter. The intensity of the excitation light was varied using a variable ND filter (Edmund Optics) mounted on a translation stage. Typical average excitation power was 5-50 mW corresponding to pulse energies of 1.25 – 12.5 nJ/pulse. Spectra from the CCD spectrograph were corrected for background and spectral response. Validation of the spectrometer was performed using Rhodamine B in methanol and Fluorescein in 0.1 M aqueous NaOH.

Luminescent titrations were carried out by normalising the emission spectra with the absorption spectra in each point in order to revise the decreasement in the sample concentration caused by pH adjustment or addition of an anion/cation stock solution where appropriate. All measurements were carried out using I = 0.1 M NaCl ionic background.

Relaxivity measurements were carried out at 37 °C and 60 MHz on a Bruker Minispec mq60 instrument. The mean value of three separate measurements was recorder and averaged.

Circular Polarised Luminescence (CPL) measurements were made using a home-built (Glasgow University, UK) CPL spectrophotometer based on a Spex Fluopomax-2 spectrofluorimeter with the assistance of Dr R. D. Peacock.

Melting points were measured using a Reichart-Köfler block and are uncorrected

6.1.4 pH Measurements

Monitoring the pH during the procedure of those reaction needed pH adjustment or maintenance was carried out using a "Checker by Hannah" battery operated pH meter (one point calibration using pH = 7.00±0.01 (t = 20 °C) buffer solution supplied by Aldrich). pH metric titrations were monitored using a Jenway 3020 or a Jenway 3320 pH meter attached to an Aldrich Chemical Company micro-pH combination electrode (three point calibration using pH = 4.01 ±0.01, pH = 7.00 ±0.01 and pH = 10.03 ±0.01 (t = 20 °C) buffer solution supplied by Aldrich, error range ΔpH = ±0.02). The adjustment of pH were carried out using conc. NaOH and conc. HCl (or NaOD and DCl if required) solution to avoid any significant increase in sample volume. For measurements carried out in D_2O the pD was calculated using the actual pH meter reading and the equation pD = pH (meter reading) + 0.41 [1, 2]

6.1.5 Lifetime Measurements

Lifetimes of europium complexes were measured by excitation of the sample using a short pulse of light (380 nm or 384 nm depending on the nature of the complex) followed by monitoring the integrated intensity of light (for europium 612 - 618 nm

depended on the measured species and the pH) emitted during a fixed gate time, t_g, after a delay time, t_d. At least 20 delay times were used covering 3 or more lifetimes. A gate time of 0.1 ms was used, and the excitation and emission slits were set to 10 nm and 2.5 nm bandpass respectively. The obtained exponential decay curves were fitted to equation (7.1) below, using Origin 6.0 software (Data Analysis & Technical Graphics)

$$I = A_0 + A_1\exp(-kt) \tag{6.1}$$

Where: I = intensity at time t after the flash

A_0 = intensity after the decay has finished

A_1 = pre-exponential factor

k = rate constant for decay of the excited state.

The excited state lifetime, τ, is the inverse of the radiative rate constant, k.

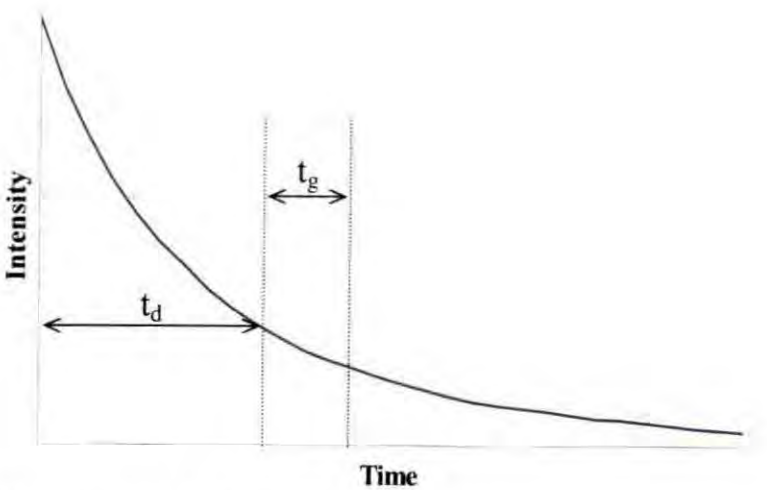

Fig. 6.1. Measured parameters for lifetime measurements.

6.1.6 Inner Sphere Hydration Number (q') Determination[3]

The rate constant for the depopulation of the lanthanide excited state in water ($k_{H_2O} = 1/\tau$) may be split into the sum of a number of different quenching contributions (where k_{rad} is the natural radiative rate constant, k_{nr} is the rate constant for non-radiative

de-excitation, and $\sum k_{XH} / \sum k_{c=O}$ are the sums for the energy transfer to nearby XH and CO matched oscillators) equation (6.2).

$$k_{H_2O} = k_{nat} + k_{nr} + \sum k_{XH} + \sum k_{C=O} \tag{6.2}$$

It is then assumed that in D_2O, all exchangeable XH oscillators do not contribute to the quenching so the equation can be simplified, equation (6.3).

$$k_{D_2O} = k_{nat} + k_{nr} + \sum k_{C=O} \tag{6.3}$$

Therefore the change in the rate constant is given by, equation (6.4).

$$\Delta k = k_{H_2O} - k_{D_2O} = \sum k_{XH} \tag{6.4}$$

Finally an expression was derived, due to the predominance of OH quenching in aqueous media and ignoring other contributions, that related the number of water molecules in the inner coordination sphere to the difference in the rate of quenching in H_2O and D_2O, equation (6.5).

$$q = A(k_{H_2O} - k_{D_2O} + corr_{Ln}) \tag{6.5}$$

In the above equation A is a proportionality constant giving the sensitivity of the lanthanide ion to vibronic quenching by OH oscillators and the $corr_{Ln}$ term allows for the effect of closely diffusing OH oscillators. The incorporation of values for Eu and Tb based complexes leads to the following, equations (6.6) and (6.7).[1]

$$q'_{Eu} = 1.2\left[(k_{H_2O} - k_{D_2O} - 0.25)\right] \tag{6.6}$$

$$q'_{Tb} = 5\left[(k_{H_2O} - k_{D_2O} - 0.06)\right] \tag{6.7}$$

In the likely case of NH oscillators present in close proximity to the lanthanide ion another correction is need to be made in order to obtain the correct q' value (6.8 and 6.9), where n refers to the number of NH oscillators.

$$q'_{Eu} = 1.2\left[(k_{H_2O} - k_{D_2O} - 0.25) - 0{,}075n\right] \quad (6.8)$$

$$q'_{Tb} = 5\left[(k_{H_2O} - k_{D_2O} - 0.06) - 0.01n\right] \quad (6.9)$$

6.1.7 Extinction Coefficient Measurement

The extinction coefficients (ε) (or molar absorption coefficient) of each of the chromophores synthesized were determined by first weighing out accurately (using a 5 decimal place balance) 5 mg of the compound and then dissolving the solid in water to a known volume in a volumetric flask (100 cm^3 of water). Five solutions of known concentration were then made up by dilution for each compound, with absorbances ranging between 0.03 and 0.15. The extinction coefficient of the solution was then calculated using equation (6.10).

$$A = \varepsilon c l \quad (6.10)$$

Where: A = absorbance at λ_{ex}

c = concentration of chromophore in sample

l = pathlength of the cell (a constant value of 1 cm)

A plot of absorption against the concentration of chromophore in solution gives a straight-line graph and the extinction coefficient is the gradient of the line.

6.1.8 Triplet Energy Measurements

Low temperature phosphorescence spectra measurements were carried out on the chromophores to enable the determination of their triplet state involved in sensitisation. An Oxford Instruments optical cryostat operating at 77 K was used with the samples dissolved in EPA (Et$_2$O – isopentane – EtOH [2 : 5 : 5 by volume])and contained in 10 mm cuvettes. The triplet energy was obtained from the extrapolation of the highest energy (shortest wavelength) phosphorescence band, corresponding to the 0-0 transition, using time-gated detection.

6.1.9 Quantum Yield Determination

The quantum yield for a given process is defined as the total number of photons emitted by that process divided by the total number of photons absorbed. The techniques and equipment necessary to make an absolute determination of quantum yields are not generally available. Therefore the usual method is to determine a relative quantum yield where the compound of unknown yield is compared to a compound of known yield. The unknown quantum yield can then be calculated using Equation (6.11).

$$\Phi_x = \Phi_r \cdot \frac{A_r}{A_x} \cdot \frac{E_x}{E_r} \cdot \frac{I_r}{I_x} \cdot \frac{n_x^2}{n_r^2} \qquad (6.11)$$

Where: *r* and *x* refer to reference and unknown respectively

A = absorbance at λ_{ex}

E = corrected integrated emission intensity

I = corrected intensity of excitation light

(as all of the measurements were taken using identical excitation conditions this term can be ignored)

n = refractive index of solution.

The measurements were made relative to a standard (*$EuPh_3dpqC$, previously synthesized and characterized by R. Poole; φ = 16.7%*)[4]. For the standard and each of the unknowns, five solutions with absorbances between 0.02 and 0.1 were used. For each of these solutions the absorbance at the excitation wavelength and the total integrated emission was determined. A plot of total integrated emission against absorbance gives a straight line with slope Em./Abs. The unknown quantum yield can thus be calculated using Equation (6.12).

$$\Phi_x = \Phi_r \cdot \frac{slope_x}{slope_r} \cdot \left(\frac{n_x}{n_r}\right)^2 \qquad (6.12)$$

Since values for both the sample and reference compounds were recorded in water the refractive index term cancels out. Errors in quantum yield determinations can arise due

to the inner filter effect or errors in the amount of absorbed light. This effect can be minimised by only using samples with an absorbance below 0.2. Errors in the amount of light absorbed by each sample can be minimised by choosing the excitation wavelength to be on a relatively flat area of the absorption curve and by using a small bandpass for excitation.

6.1.10 Anion and Protein Influence Measurement in Aqueous Salt and Simulated Extracellular and Prostatic Fluid

To examine the influence of some biologically common anions on synthesised complexes, luminescent titrations were carried out by using an 'Anion stew', containing 30 mM Na_2CO_3, 2.3 mM Na(lactate), 0.9 mM NaH_2PO_4 and 0.13 mM Na_3(citrate) to assess the overall influence of these anions. Luminescence titrations were also carried out by using the above-mentioned anions separately along with [ascorbate] = 0.3 mM and [HSA] = 0.7 mM, in order to study their individual effect on the Eu emission spectra. All measurements was carried out using a constant I = 0.1 M NaCl ionic strength. Titrations were carried out from basic solutions with acidification in order to avoid the undesirable evolution of carbon dioxide (equation 6.13)

$$HCO_3^- + H^+ \rightleftharpoons H_2O + CO_2\uparrow \qquad (6.13)$$

As the studied Eu-complexes showed major changes in their Eu emission spectrum in the presence of some biologically common anions, the concentration dependece of the Eu emission was examined. A series of measurements was carried out with the Eu-complexes presented in this work by applying the appropriate anions that caused significant spectral changes in the Eu emission at a chosen pH where the anion influence was maximised within the relevant pH-range. All of these measurements were carried out by adding the selected anion as liquid concentrated stock solution where the addition at each point was aprox. 0.1 - 0.5% in volume of the original solution observed to avoid significant increase in sample volume. HSA was added as solid. Still all Eu emission spectras were corrected for dilution. Detailed interpretation of these measurements can be found at the discussion of each complex. The apparent binding

constant of the selected anion was calculated according to equation 6.14, using Origin™ software and least squares regression.

$$[X] = \frac{\frac{(F-F_0)/(F_1-F_0)}{K} + [Eu]*(F-F_0)/(F_1-F_0) - [Eu]*\left((F-F_0)/(F_1-F_0)\right)^2}{1-(F-F_0)/(F_1-F_0)}$$

$$\text{Eu} + \text{X} \leftrightarrow \text{EuX} \qquad K = \frac{[EuX]}{[X_f][Eu_f]}$$

[X]: the total concentration of anion in the solution

[Eu]: the total concentration of the complex

K: the binding constant

F: the ratio of selected peaks

F_0: the ratio at the beginning (6.14)

F_1: the final ratio

[EuX]: the concentration of the anion-coordinated complex

$[X_f]$: the concentration of free anion in the mixture

$[Eu_f]$: the concentration of the free complex

Simulated prostatic fluid is the ionic background used in the studies to find an appropriate *citrate sensor* to detect prostate adenocarcinoma, and is consistent of 0.1 M sodium chloride, 0.04 M potassium chloride, 5 mM magnesium chloride, 4 mM calcium chloride, 2 mM zinc chloride, 3 mM sodium bicarbonate and 0.1 mM protein (HSA). The pH of this background was maintained at 6.5 (±0.05). Determination of citrate and lactate affinity using this background was undertaken as detailed above.

6.1.11 Biological Samples: Seminal and Prostatic Fluid

Seminal fluid from a healthy 26 year old male with no known prostate anomaly was used. Samples were used fresh with the spermatozoa removed by centrifugation within 3 min to avid sample degradation. Prostate fluid samples were received from Prof. L. Costello (University of Maryland, USA) as a volume of 25 µL freeze-dried fluid on a 0.5 cm^2 blotting paper, which were suspended in 1mL 0.1 M HEPES buffer (pH = 6.55),

digested for 24 h followed by 30 min sonication (this procedure was carried out twice with each sample disc). These biological fluids were than used as a x10 dilution as stated.

6.1.12 Microscopy

Epifluorescence images were taken on a Zeiss Axiovert 200M epifluorescence microscope with objectives 63x/1.40 oil DIC and 40x/1.40 oil DIC respectively, equipped with an Axiocam CCD camera. For excitation a 340 - 390 nm (90% transmission) band-pass (BP) filter was used. Ligand fluorescence were observed using a BP 445 - 465 nm filter (80% transmission), while Eu emission was observed using a 570 nm long-pass (LP) filter (85% transmission).

Confocal images were taken on a Zeiss LSM 500 META confocal microscope with a BIORad 405 diode laser excitation and an LP 590 nm emission filter were used for europium luminescence and a BP 505 - 550 filter for study of ligand fluorescence.

Time gated microscopy images were recored on a modified Zeiss Axiovert 135 epifluorescence microscope equipped with a Q-switch 355 nm Nd:YAG laser excitation (supplied by EL^4Light, E = 1 W), 63x/1.40 oil DIC objective, and an Imagex Nano CCD camera. For acquisition and image transformation Imagex Direct v1.21 and Laser Power v2.0 softwares were used. Eu emission was observed using a LP 550 nm filter.

6.1.13 Cell Culture Work

Two cell lines were selected for cell cultural studies CHO (Chinese Hamster Ovary) cells and NIH 3T3, mouse skin fibroblast (connective tissue) cells. Both lines are transformed, and compromise adherent cells, which grow in a monolayer. These cell lines were cultured in a copper jacket incubator at 37 °C, average 20% humidity and 5% (v/v) CO_2 in 50 mL volume plastic grow plates. Cells for microscopy were grown in a 24 well-plate using d = 13mm glass cover slips (average thickness l = 0.1 mm). DMEM (Dulbecco's Modified Eagle Media) and F-12(Ham) medias were used for NIH 3T3 and CHO cells respectively. Each containing 10% (v/v) NCS (Newborn Calf Serum) and 1% (v/v) Penicillin-Streptomycin. Complexes were loaded onto cells using the appropriate

growth media. For flow cytometry measurements cells were detached from the glass surface using 1% (v/v) trypsin solution at 37 °C for 5 min. The applied solutions were always submitted for separate ICP-MS measurements to measure any possible europuim complex egress.

6.1.14 Flow Cytometry and Induced Coupled Plasma Mass Sectrometry

Flow cytometric analysis and sorting was conducted using a DakoCytomation Inc. MoFlo multi-laser flow cytometer (Fort Collins, CO, USA) operating at 60 psi, 70 micron nozzle, with the assistance of Dr. A. Congreve. Samples were interrogated with a 100 mW 488 nm solid state laser: (FSC, SSC). Fluorescence signals were detected through interference filters FL1 530/40, FL2 580/30, FL3 630/30 and FL4 670/30). Fluorescence signals were collected in logarithmic mode. The data were analyzed using Summit v4.0 (DakoCytomation) software.

ICP-MS determination of europium concentrations from cells and growth media were carried out by Dr. Chris Otely in the Department of Earth Sciences at Durham University using a Thermo Finningan ELEMENT^2 High Resolution Select Field ICP-MS.

6.1.15 HPLC Analysis/Purification

Reverse phase HPLC analysis were performed at 298 K on a Perkin Elmer System using a 4.6 x 20 mm 4μ Phenomenex Synergi Fusion RP 80i analytical column. In each case an H_2O + 0.1% HCOOH / MeCN + 0.1% HCOOH solvent system was used (gradient elution) with a run time of 20 minutes (Fig.7.2). In each case, a single major roduct was observed in >95% purity using a diode array UV-Vis detector operating at 380 nm, which corresponds to the absorption band of the appropriate azathioxanthone sensitizing moiety (analysis was also undertaken at 280 nm). Such behaviour indicated that each of the species that were eluted bear this chromophore. A fluorescence detector was also connected to the HPLC, monitoring eluent from the column at a wavelength corresponding to the Eu centered emission (616 nm); again emission was seen for each of these peaks, suggesting that each peak corresponding to a chromophore bound species

also was coordinated to Eu in such way that it was efficiently sensitized. For each of Gd-complexes a UV-Vis detector was used, operating with a LP 250 nm detection filter.

Time (min)	Flow (mL/min)	H_2O (%)	MeCN (%)	Gradient
0.5	1	100	0	0
1.0	1	100	0	0
1.0	1	0	100	1
1.0	1	0	100	0
2.0	1	100	0	2

Fig. 6.2. Gradient elution programme for HPLC analysis.

6.1.16 Single Crystal X-ray Diffraction

Crystal structures were determined by data collection using graphite monochromated Mo Kα radiation (λ = 0.71073 Å) on a Bruker area detector diffractometer (Bruker SMART CCD 1K or Bruker ProteumM with Bede Microsource), equipped with Cryostream N_2 open-flow cooling device.[5] In each case, series of narrow ω-scans (0.3°) at several φ-settings were carried out to cover a approximately a sphere of data to a maximum resolution between 0.70 and 0.77 Å. Cell parameters were determined and refined using the SMART software[6], and raw frame data were integrated using the SAINT program.[7] Structures were solved by direct methods and refined by full-matrix least squares on F^2 using SHELXTL software[8] and full-matrix least squares on F using CRYSTALS[9]. Reflection intensities were corrected by numerical integration using SHELXTL software, based on crystal measurements and indexing of the faces[8] or by the multi-scan method, based on multiple scans of identical and Laue equivalent reflections (using the SADABS software)[10]. Non-hydrogen atoms were refined with anisotropic displacement parameters and the hydrogen atoms were positioned geometrically and refined using a riding model. Crystallographic data (excluding structure factors) for the structures included herein have been deposited with the Cambridge Crystallographic Data Centre as supplementary publications Nos.[11]

6.2 Synthetic Procedures and Characterization[12-14]

2-Methanesulfonate-N-methanesulfonylethylamine[15]

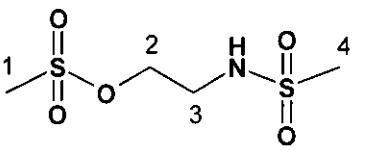

A cold solution of ethanolamine (2.39 g, 39.05 mmol) in dry pyridine (20 ml) was carefully added to a vigorously stirred solution of methanesulfonyl chloride (9.39 g, 82 mmol) in pyridine (20 ml) at – 40 °C. After stirring for 1 h. the mixture was placed into an ice-salt bath and stirred for further 5 h. followed by cooling at 4 °C in the fridge for 12 h. The brown syrup solution was then poured onto crushed ice containing $Cu(OAc)_2$ and the aqueous phase was extracted with $CHCl_3$ (3 x 50 ml). The organic phase was dried (K_2CO_3), filtered and the solvent removed under reduced pressure to give the title compound as a colourless viscous oil which slowly recrystallised in the fridge (2.06 g, 24%); δ_H ($CDCl_3$) 5.18 (NH, br.s, 1H), 4.36 (H^2, t, J = 5.1 Hz, 2H), 3.51 (H^3, t, J = 5.1 Hz, 2H), 3.10 (H^4, s, 3H), 3.03 (H^1, s, 3H); δ_c ($CDCl_3$) 69.1 (C^2), 42.6 (C^3), 41.1 (C^1), 37.8 (C^4) (C *m/z* ($ESMS^+$) 218 $(M + H)^+$; m.p. 24-25 °C. Found C, 21.91; H, 5.07; N, 6.45; S, 29.49% $C_4H_{11}NO_5S_2$ requires C, 22.12; H, 5.17; N, 6.48; S, 29.64 %

N-Methanesulfonyl-aziridine[16]

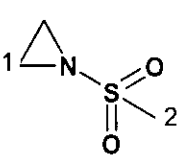

A suspension of 2-Methanesulfonate-N-methanesulfonylethylamine (1.24 g, 5.71 mmol) in DCM (25 ml) was stirred vigorously. Aqueous KOH solution (3.5 M, 1.65 ml) was added after 30 min, and the mixture stirred for 4 h. at room temperature. The organic solvent was removed under reduced pressure and the aqueous phase was extracted with DCM (3 x 25 ml). The combined organic phases was dried (K_2CO_3), filtered and the solvent removed under reduced pressure to give the title compound as white solid (462 mg, 67%) δ_H ($CDCl_3$) 3.07 (H^1, s, 2H), 2.38 (H^2, s, 3H); δ_c ($CDCl_3$) 43.3, 43,4 (C^1), 26.8 .

(C^2); *m/z* (ESMS$^+$) 122 $(M + H)^+$, 144 $(M + Na)^+$; m.p. 31-32 °C; R_f 0.24 (DCM, silica plate). Found C, 29.50; H, 6.56; N, 11.48; S, 26.22% $C_3H_8NO_2S$ requires C, 29.75; H, 6.61; N, 11.57; S, 26.44 %

(±) Dimethyl-2-Bromoglutarate[17]

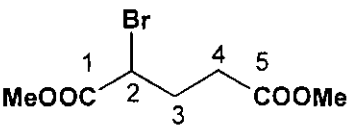

Glutaric acid monomethyl ester (43.8 g, 300 mmol) was added to thionyl chloride (90 ml, 1.24 mol) and the mixture was refluxed for 2 h. Molecular bromine (17 ml, 330 mmol) was added slowly over a 2-3 h. period maintaining reflux conditions. The reaction mixture was allowed to cool followed by further stirring at room temperature for 14 h. The mixture then carefully poured onto MeOH (140 ml) cooled on crushed ice and stirred for 3 h. followed by careful addition of H_2O (150 ml). The aqueous phase was extracted with diethyl ether (3 x 150 ml) and the organic phase was washed with H_2O (150 ml) followed by diluted aqueous $NaHCO_3$ solution (120 ml) and H_2O (120 ml). The organic phase was dried, filtered and the solvent removed under reduced pressure to give a brown oil. The crude mixture then placed into a micro distillation apparatus equipped with a Vigreux column (bath temperature 130 °C) and the desired product was distilled at 70 °C/0.1 mm Hg (43.2 g, 59%) δ_H ($CDCl_3$) 4.32 (H^2, t, *J* 8.0 Hz, 1H), 3.72 (CH_3^5, s, 3H), 3.62 (CH_3^1, s, 3H), 2.44 (H^4, m, 2H), 2.37 (H^3, m, 2H); δ_c ($CDCl_3$) 172.8 (C^5), 170.1 (C^1), 53.3 (CH_3^1), 52.1 (CH_3^5), 44.8 (C^2), 31.4 (C^4), 29.8 (C^3)

(±) Dimethyl-2-Bromoadipate[17]

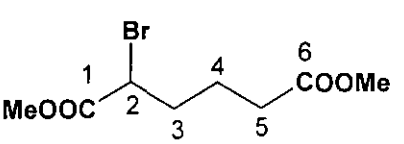

Adipic acid monomethyl ester (23.4 g, 146 mmol) was added to thionyl chloride (46 ml, 636 mmol) and the mixture was boiled under reflux for 2 h. Molecular bromine (8.1 ml, 157 mmol) was added slowly over a 2-3 h. period maintaining reflux conditions. The

reaction mixture was allowed to cool followed by further stirring at room temperature for 12 h. The mixture then carefully poured onto MeOH (80 ml) cooled on crushed ice and stirred for 3h. followed by careful addition of H_2O (100 ml). The aqueous phase was extracted with diethyl ether (3 x 100 ml) and the organic phase washed with H_2O (100 ml) diluted aqueous $NaHCO_3$ solution (100 ml) and H_2O (100 ml). The organic phase was dried, filtered and the solvent removed under reduced pressure to give a brown oil. The crude mixture then placed into a micro distillation apparatus equipped with a Vigreux column at 130 °C and the desired product was distilled at 60 °C/0.1 mmHg (16.11 g, 43%) δ_H ($CDCl_3$) 4.23 (H^2, dd, *J* 8.0 Hz, 1H), 3.78 (CH_3^6, s, 3H), 3.70 (CH_3^1, s, 3H), 2.37 (H^5, m, 2H), 2.08 (H^3, m, 2H), 1.76 (H^4, m, 2H); δ_c ($CDCl_3$) 173.5 (C^1), 170.3 (C^6), 53.3 (CH_3^1), 51.9 (CH_3^6), 45.2 (C^2), 34.3 (C^3), 33.3 (C^5), 22.8 (C^4)

6-Methyl-2-phenylsulfonyl-nicotinic acid

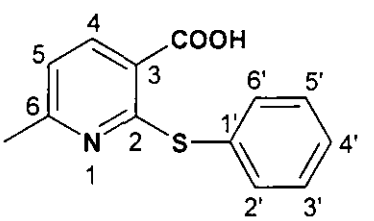

2-Chloro-6-methylnicotinic acid (5.00 g, 29.2 mmol), thiophenol (3.80 g, 34.5 mmol), were dissolved in DMF (30 cm^3) with stirring, followed by CuBr (0.25 g, 17.5 mmol), and K_2CO_3 (6.00 g, 43.5 mmol). The reaction mixture was heated for 15 min. at 130 °C followed by 18 h at 150 °C, generating a light yellow solution. The mixture was cooled down and treated with water (170 cm^3) to give a yellow suspension, which was washed with ether (3 x 80 cm^3). The aqueous solution was acidified with acetic acid yielding a very light yellow precipitate upon cooling, which was filtered, washed with water and dried thoroughly to yield the title compound as a pale yellow microcrystalline solid (5.90 g, 83%), m.p. 170-2 °C; δ_H ($CDCl_3$) 13.40 (1H, br s, -OH), 8.13 (1H, d, *J* 8 Hz, H^4), 7.42-7.52 (5H, m, $H^{2'-6'}$), 7.09 (1H, d, *J* 8 Hz, H^5), 2.23 (3H, s, CH_3); δ_c ($CDCl_3$) 24.8 (CH_3), 119.8 (C^5), 121.4 (C^4), 129.6 (C^3), 130.1 ($C^{3',5'}$), 131.8 ($C^{1'}$), 136.1 ($C^{2',6'}$), 139.9 ($C^{4'}$), 160.4 (C^2), 160.8 (C^6), 167.4 (COOH); *m/z* (ESMS$^+$) 246 $(M + H)^+$, 268 $(M + Na)^+$.

Found C, 63.68; H, 4.44; N, 5.60; S, 12.98% $C_{13}H_{11}NO_2S$ requires C, 63.67; H, 4.49; N, 5.73; S, 13.06%.

2-Methyl-1-azathioxanthone[11, 13]

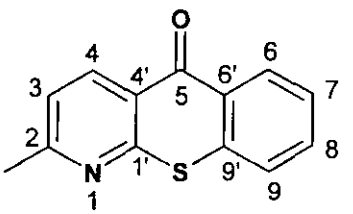

Polyphosphoric acid (60 cm^3) was added to 6-methyl-2-phenylsulfonyl-nicotinic acid (5.50g 22.4 mmol) and the mixture heated at 120 °C for 4 hours under argon with stirring. The resulting brown liquid was cooled to room temperature and then slowly poured onto cold concentrated aqueous sodium hydroxide solution (300 cm^3) with vigorous stirring. The light yellow precipitate that formed was collected via filtration. The product was recrystallised from warm EtOH. The crystals that formed upon standing were filtered and dried thoroughly to yield the *title compound* as a yellow crystalline solid (4.61 g, 90%) %); m.p. 145-7 °C; δ_H ($CDCl_3$) 8.73 (1H, d, *J* 8.2 Hz, H^4), 8.60 (1H, m, H^6), 7.65 (2H, m, $H^{8,9}$), 7.48 (1H, m, H^7), 7.31 (1H, d, *J* 8.2 Hz, H^3), 2.70 (3H, s, CH_3); δ_c ($CDCl_3$) 25.2 (CH_3), 121.7 (C^3), 124.8 (C^7), 127.3 (C^9), 127.5 (C^6), 129.6 ($C^{9'}$), 130.4 (C^4), 133.5 (C^8), 137.5 ($C^{6'}$), 138.5 ($C^{4'}$), 158.0 ($C^{1'}$), 162.1 (C^2), 181.0 (C^5); *m/z* ($ESMS^+$) 228 $(M + H)^+$, 250 $(M + Na)^+$, R_f 0.34 (DCM, silica plate). Found C, 68.43; H, 3.95; N, 6.17; S, 13.99% $C_{13}H_9NOS$ requires C, 68.72; H, 3.89; N, 6.10; S, 13.99%.

X-Ray structure:

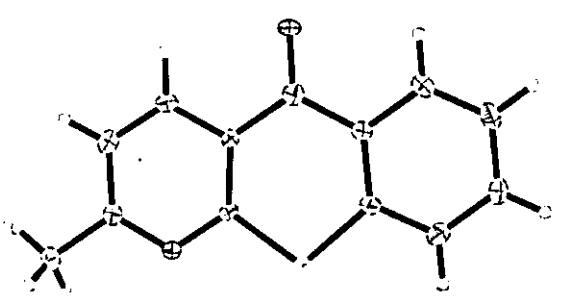

† C_{13} H_9 N O S, M_r = 227.27, Monoclinic ($P2_1$), *a* = 3.8693(5) Å, *b* = 12.3848(16) Å, *c* = 10.4698(13) Å, β = 95.015(2)°, Z = 2, μ = 0.296 mm^{-1} D_{calc} = 1.510 Mg/m^3, T = 120(2) K, 2632 independent reflections [R(int) = 0.0551], R_1 = 0.0634, wR_2 = 0.1510 [I>2sigma(I)].

2-p-Tolylsulfonyl-nicotinic acid

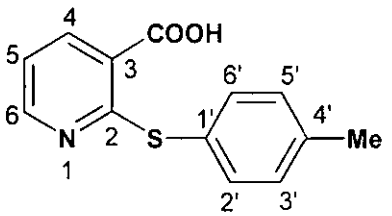

6-Methylnicotinic acid (4.57 g, 29.2 mmol), 4-methyl-thiophenol (4.22 g, 34.5 mmol), were dissolved in DMF (30 cm^3) with stirring, followed by CuBr (0.25 g, 17.5 mmol), and K_2CO_3 (6.00 g, 43.5 mmol). The reaction was heated for 15 minutes at 130 °C followed by 18 hour at 150 °C to form a light yellow solution. The mixture was cooled and treated with water (170 cm^3) to give a yellow suspension, which was washed with ether (3 x 80 cm^3). The aqueous solution was acidified with acetic acid yielding a very light yellow precipitate upon cooling. This material was filtered, washed with water and dried thoroughly to yielding the *title compound* as a white crystalline solid (6.14 g, 87%), m.p. 190-2 °C; δ_H ($CDCl_3$) 13.60 (1H, br s, -OH), 8.41 (1H, d, *J* 7.5 Hz, H^6), 8.20 (1H, d, *J* 7.5 Hz, H^5), 7.38 (2H, m, $H^{3',5'}$), 7.20 (3H, m, $H^{4,2',6'}$), 2.31 (3H, s, CH_3); δ_c ($CDCl_3$) 20.2 (CH_3), 120.2 ($C^{4'}$), 123.2 (C^5), 127.7 (C^3), 130.5 ($C^{3',5'}$), 136.3 ($C^{2',6'}$), 139.6 ($C^{1'}$), 140.0 (C^4), 152.9 (C^6), 162.1 (C^2), 167.4 (COOH); *m/z* (ESMS$^+$) 246 (M + H)$^+$, 268 (M + Na)$^+$. Found C, 63.49; H, 4.50; N, 5.64; S, 13.09% $C_{13}H_{11}NO_2S$ requires C, 63.67; H, 4.49; N, 5.73; S, 13.06%.

7-Methyl-1-azathioxanthone

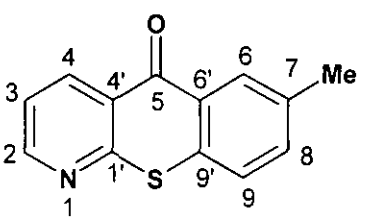

Polyphosphoric acid (60 cm^3) was added to 2-p-tolylsulfonyl-nicotinic acid (5.50g 22.4 mmol) and the mixture heated at 120 °C for 4 hours under argon with stirring. The resulting a brown liquid was cooled to room temperature and then slowly poured onto cold concentrated aqueous sodium hydroxide solution (300 cm^3) with vigorous stirring.

The light green/yellow precipitates that formed were removed via filtration. The product was recrystallised from warm EtOH to yield the *title compound* as a yellow microcrystalline solid (4.32 g, 87%) %); m.p. 139-41 °C; δ_H ($CDCl_3$) 8.85 (1H, d, *J* 7.9 Hz, H^2), 8.72 (1H, d, *J* 7.9 Hz, H^4), 8.50 (1H, s, H^6), 7.78 (1H, d, *J* 8.2 Hz, H^9), 7.63 (2H, m, $H^{3,8}$), 3.29 (3H, s, CH_3); δ_c ($CDCl_3$) 22.9 (CH_3), 123.1 (C^3), 127.5 ($C^{9'}$), 128.2 (C^7), 129.5 ($C^{6'}$), 129.6 (C^9), 130.0 (C^8), 136.3 (C^6), 138.7 (C^4), 139.4 ($C^{4'}$), 156.9 ($C^{1'}$), 159.7 (C^2), 179.8 (C^5); *m/z* (ESMS$^+$) 228 $(M + H)^+$, 250 $(M + Na)^+$; R_f 0.42 (DCM, silica plate). Found C, 68.58; H, 4.57; N, 5.69.; S, 13.09% $C_{13}H_9NOS$ requires C, 68.72; H, 3.95; N, 6.17; S, 14.10%

2-o-Tolylsulfonyl-nicotinic acid

This was prepared as described above for the para isomer yield the *title compound* as a pale yellow crystalline solid (6.02 g, 85%); m.p. 166-8 °C; δ_H ($CDCl_3$) 13.55 (1H, br s, -OH), 8.36 (1H, d, *J* 7.2 Hz, H^6), 8.22 (1H, d, *J* 7.2 Hz, H^5), 7.45 (1H, d, *J* 7.6 Hz, $H^{6'}$), 7.34 (2H, m, $H^{3',5'}$), 7.20 (2H, m, $H^{4,4'}$) 2.20 (3H, s, CH_3); δ_c ($CDCl_3$) 21.5 (CH_3), 120.3 ($C^{2'}$), 127.2 (C^5), 131.1 (C^3), 131.6 ($C^{4',5'}$), 137.0 ($C^{6'}$), 137.2 ($C^{3'}$), 143.2 ($C^{1'}$), 143.7 (C^4), 153.6 (C^6), 162.0 (C^2), 167.4 (COOH); *m/z* (ESMS$^+$) 246 $(M + H)^+$, 268 $(M + Na)^+$. Found C, 64.08; H, 4.29; N, 5.39; S, 12.84% $C_{13}H_{11}NO_2S$ requires C, 63.67; H, 4.49; N, 5.73; S, 13.06%

9-Methyl-1-azathioxanthone

This was prepared as described for the 7-Me isomer above to yield the *title compound* as a light yellow crystalline solid (4.73 g, 95%): m.p. 135-7 °C; δ_H ($CDCl_3$) 8.92 (1H, dd, *J* 8, 1.8 Hz, H^2), 8.74 (1H, dd, *J* 8, 1.8 Hz, H^4), 8.34 (1H, dd, *J* 8, 2 Hz, H^6), 7.76 (1H, dd, *J* 8, 2 Hz, H^8), 7.67 (1H, t, *J* 8 Hz, H^3), 7.54 (1H, t, *J* 8 Hz, H^7), 2.52 (3H, s, CH_3); δ_c ($CDCl_3$) 20.1 (CH_3), 123.8 (C^3), 126.0 ($C^{4'}$), 127.3 (C^7), 127.8 (C^6), 129.1 ($C^{6'}$), 135.0 (C^8), 135.2 (C^9), 136.6 ($C^{9'}$), 138.1 (C^4), 157.2 (C^2), 158.9 ($C^{1'}$), 181.4 (C^5); *m/z* (ESMS$^+$) 228 $(M + H)^+$, 250 $(M + Na)_+$, R_f 0.29 (DCM, silica plate). Found C, 68.80; H, 3.97; N, 6.24.; S, 13.41% $C_{13}H_9NOS$ requires C, 68.72; H, 3.95; N, 6.17; S, 14.10%

2-m-Tolylsulfonyl-nicotinic acid

This was prepared as described above for the para isomer to yield the *title compound* as a pale yellow crystalline solid (6.02 g, 85%); m.p. 160-2 °C; δ_H ($CDCl_3$) 13.60 (1H, br s, -OH), 8.41 (1H, d, *J* 7.9 Hz, H^6), 8.20 (1H, d, *J* 7.9 Hz, H^4), 7.28 (5H, m, $H^{5,2',3',4',6'}$) 2.23 (3H, s, CH_3); δ_c ($CDCl_3$) 21.7 (CH_3), 120.1 ($C^{5'}$), 122.0 (C^5), 129.7 ($C^{3'}$), 130.2 ($C^{3,4'}$), 134.0 ($C^{6'}$), 137.3 ($C^{2'}$), 138.7 ($C^{1'}$), 139.8 (C^4), 153.2 (C^6), 158.1 (C^2), 167.4 (COOH); *m/z* (ESMS$^+$) 246 $(M + H)^+$, 268 $(M + Na)^+$. Found C, 63.96; H, 4.45; N, 5.26; S, 13.33% $C_{13}H_{11}NO_2S$ requires C, 63.67; H, 4.49; N, 5.73; S, 13.06%

6-Methyl-1-azathioxanthone and 8-Methyl-1-azathioxanthone

Polyphosphoric acid (60 cm^3) was added to 2-m-tolylsulfonyl-nicotinic acid (5.50g 22.4 mmol) and the mixture heated at 120 °C for 4 hours under argon with stirring. The resulting a brown liquid was cooled to room temperature and slowly poured onto cold concentrated aqueous sodium hydroxide solution (300 cm^3) with vigorous stirring. The light grey precipitate that formed was removed via filtration. The product was washed with water and dried thoroughly to yield a 1 : 1 mixture (obtained from ^{1}H-NMR) of the *title compounds* as a light yellow powder. Products were separated by column chromatography (silica, toluene-CH_2Cl_2-EtOAc 45:45:10). Pure fractions were combined together and the solvents removed by reduced pressure. Each product was recrystallised from warm EtOH. The crystals that formed upon standing were filtered and dried thoroughly to yield the *given compound* as a pale yellow crystalline solid.

6-Methyl-1-azathioxanthone

Yield 0.41g (8%); m.p. 184-6 °C; δ_H ($CDCl_3$) 8.81 (1H, dd, *J* 8 Hz, H^2), 8.79 (1H, d, *J* 8 Hz, H^4), 8.34 (1H, m, H^9), 7.42 (2H, m, $H^{2,7}$), 7.31 (2H, m, $H^{3,8}$), 2.23 (3H, s, CH_3); δ_c ($CDCl_3$) 22.3 (CH_3), 122.5 (C^3), 126.2 (C^8), 127.1 ($C^{4'}$), 128.7 (C^7), 129.8 (C^9), 138.8 ($C^{1'}$), 139.1 (C^2), 142.3 ($C^{6'}$), 152.7 (C^4), 159.2 ($C^{4'}$), 180.8 (C^5); *m/z* (ESMS$^+$) 228 $(M + H)^+$, 250 $(M + Na)^+$; R_f 0.31 (DCM, silica plate). Found C, 69.13; H, 4.04; N, 6.02.; S, 13.84% $C_{13}H_9NOS$ requires C, 68.72; H, 3.95; N, 6.17; S, 14.10%.

8-Methyl-1-azathioxanthone

Yield 0.56g (11%); m.p. 126-8 °C; δ_H ($CDCl_3$) 8.72 (1H, d, *J* 8 Hz, H^2), 8.66 (1H, d, *J* 8 Hz, H^4), 7.52 (1H, s, H^9), 7.50 (1H, d, *J* 7.9 Hz, H^6), 7.41 (1H, t, *J* 8 Hz, H^3), 7.30 (1H, d, *J* 7.9 Hz, H^7) 2.88 (3H, s, CH_3); δ_c ($CDCl_3$) 24.5 (CH_3), 121.8 (C^3), 125.5 (C^6), 128.3 ($C^{1'}$), 130.7 (C^7), 131.6 (C^9), 131.8 ($C^{9'}$), 138.3 (C^4), 138.8 ($C^{6'}$), 142.4 (C^8), 153.3 (C^2), 157.8 ($C^{4'}$) 182.1 (C^5); *m/z* (ESMS$^+$) 228 (M + H)$^+$, 250 (M + Na)$^+$, R_f 0.36 (DCM, silica plate). Found C, 68.73; H, 3.99; N, 5.81.; S, 14.13% $C_{13}H_9NOS$ requires C, 68.72; H, 3.95; N, 6.17; S, 14.10%.

2-Bromomethyl-1-azathioxanthone

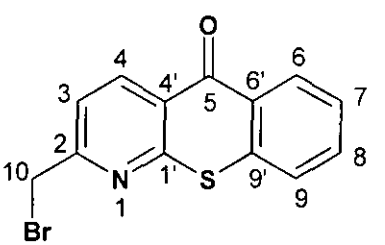

2-Methyl-1-azathioxanthone (1.00 g, 4.41 mmol) was dissolved in CCl_4 (30 mL) and the reaction was heated to 80 °C under argon. N-Bromosuccinimide (392 mg, 0.5 eq.) was added along with benzoyl peroxide (10 mg) and the stirred reaction was monitored using TLC (SiO_2, toluene : DCM : MeOH, 49:49:2) and ^{1}H-NMR. After 15 h and the addition of 2.5 equivalents of NBS the crude reaction mixture was allowed to cool to room temperature and then filtered. The solvent was removed under reduced pressure and the residue purified by column chromatography on silica gel (toluene : DCM, 90 : 10), to yield the *title compound* as bright yellow crystalline solid, (0.57 g, 42%). m.p.: 190-2 °C; δ_H ($CDCl_3$) 8.84 (1H, d, *J* 8.1 Hz, H^4), 8.58 (1H, dd, *J* 8.0 Hz, H^6), 7.65 (2H, m, $H^{8,9}$), 7.57 (1H, d, *J* 8.1 Hz, H^3), 7.52 (1H, m, H^7), 4.61 (2H, s, H^{10}); δ_c ($CDCl_3$) 32.6 (CH_2), 121.8 (C^3), 125.8 (C^4), 126.7 (C^9), 127.2 (C^7), 129.1 ($C^{9'}$), 130.2 (C^6), 133.3 (C^8), 137.5 ($C^{6'}$), 139.2 ($C^{4'}$), 158.6 ($C^{1'}$), 161.1 (C^2), 180.6 (C^5); *m/z* (ESMS$^+$) 307, 309 (M + H)$^+$, 329, 331 (M + Na)$^+$; R_f 0.40 (Toluene:DCM:MeOH 49:49:2, silica plate). Found C, 52.13; H, 3.08; N, 5.01; S, 9.78% $C_{13}H_8NOSBr$ requires C, 50.99; H, 2.62; N, 4.58; S, 10.46%

2-Dibromomethyl-1-azathioxanthone

During the above-mentioned procedure 2-dibromomethyl-1-azathioxanthone was also isolated as a yellow powder, (0.89g, 2.313 mmol, 52%). δ_H ($CDCl_3$) 8.71 (H^4, d, *J* 8.1 Hz), 8.58 (H^6, d, *J* 8.0 Hz), 7.65 ($H^{8,9}$, m), 7.50 (H^7, m), 7.28 (H^3, d, *J* 8.1 Hz), 6.60 (H^{10}, s);); δ_c ($CDCl_3$) 37.8 (CH_2), 122.0 (C^3), 126.4 (C^4), 126.7 (C^9), 127.1 (C^7), 129.6 ($C^{9'}$), 130.3 (C^6), 133.1 (C^8), 137.8 ($C^{6'}$), 139.5 ($C^{4'}$), 160.2 ($C^{1'}$), 164.3 (C^2), 180.2 (C^5); *m/z* *m/z* (ESMS$^+$) 388, 390 $(M + 1)^+$, 410, 412 $(M + Na)^+$; R_f 0.42 (Toluene:DCM:MeOH 49:49:2, silica plate)

7-Bromomethyl-1-azathioxanthone

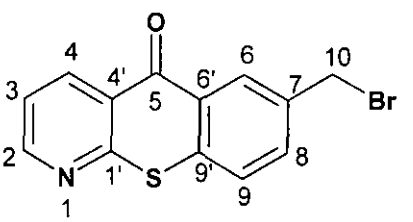

7-Methyl-1-azathioxanthone (1g, 4.41 mmol) was dissolved in CCl_4 (30 mL) and the mixture was boiled under argon using a 100W tungsten lamp. N-Bromosuccinimide (1g, 5.61 mmol) was added along with benzoyl peroxide (10 mg) and the mixture was vigorously stirred for 24 h. After confirming by TLC (silica, DCM – 2.5% MeOH) that the 7-methyl-1-azathioxanthone had been consumed the crude mixture was allowed to cool to room temperature and filtered. The solvent was removed under reduced pressure and the residue purified by column chromatography (silica, toluene : DCM, 90 : 10), to yield the *title compound* as bright yellow crystalline solid, (1.09 g, 81%). m.p. 160-2 °C; δ_H ($CDCl_3$) 8.83 (1H, dd, *J* 7.8 Hz, H^4), 8.80 (1H, dd, *J* 7.8 Hz, H^2), 8.58 (1H, s, H^6), 7.76 (1H, d, *J* 7.9 Hz H^8), 7.70 (1H, d *J* 7.9 Hz, H^9), 7.53 (1H, q, *J* 7.8 Hz, H^3), 4.62 (2H, s, H^{10}); δ_c ($CDCl_3$) 32.4 (C^{10}), 122.1 (C^3), 126.8 ($C^{1'}$), 127.5 (C^9), 129.1 (C^6), 130.1 ($C^{6'}$), 133.9 (C^8), 137.0 (C^7), 137.8 (C^2), 138.1 ($C^{9'}$), 153.7 (C^4), 158.7 ($C^{4'}$), 180.5 (C^5); *m/z* (ESMS$^+$) 307, 309 $(M + H)^+$, R_f=0.51 (silica, DCM – 2.5% MeOH). Found C, 51.34; H, 2.98; N, 4.19; S, 10.02% $C_{13}H_8NOSBr$ requires C, 50.99; H, 2.62; N, 4.58; S, 10.46%

7-Dibromomethyl-1-azathioxanthone

During the above-mentioned procedure 7-dibromomethyl-1-azathioxanthone was also isolated as a yellow powder, (203 mg, 529 μmol, 12%). δ_H ($CDCl_3$) 8.84 (2H, m, $H^{2,4}$), 8.62 (1H, s, H^6), 8.03 (1H, d, *J* 8.5 Hz H^8), 7.73 (1H, d *J* 8.5 Hz, H^9), 7.50 (1H, q, *J* 8.0 Hz, H^3), 6.79 (2H, s, H^{10}); δ_c ($CDCl_3$) 39.5 (C^{10}), 122.3 (C^3), 126.5 ($C^{1'}$), 126.6 (C^9), 127.9 ($C^{6'}$), 128.5 (C^6), 132.7 (C^8), 138.2 ($C^{9'}$), 139.4 (C^2), 140.9 (C^7), 153.9 (C^4), 158.6 ($C^{4'}$), 180.2 (C^5); *m/z* (ESMS$^+$) 388, 390 $(M + 1)^+$, 410, 412 $(M + Na)^+$; R_f 0.51 (silica, DCM – 2.5% MeOH)

7-Azidomethyl-1-azathioxanthone

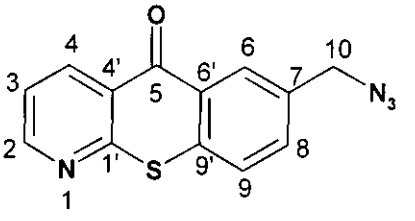

7-Bromomethyl-1-azathioxanthone (120mg, 39.3 μmol) and NaN_3 (51 mg, 78 μmol) were dissolved in DMF (3 mL) and the mixture was stirred under argon at 80°C for 12 hrs. The reaction was monitored by TLC (DCM – 2.5 % MeOH) and a further 2 eqs. of NaN_3 was added in 3 h. intervals until TLC showed that the 7-bromomethyl-1-azathioxanthone starting material had been consumed. The mixture was allowed to cool down to room temperature and filtered. The solvent was removed under reduced pressure and the remaining yellow solid was dissolved in DCM (20 ml) and washed with H_2O (3 x 20 ml). The organic solvent was removed under reduced pressure and the residue purified by column chromatography (silica, toluene : DCM, 90 : 10), to yield the title compound as bright yellow crystalline solid, (55 mg, 20.6 μmol, 53%). m.p. 136-38 °C; δ_H ($CDCl_3$) 8.81 (1H, dd, *J* 7.8 Hz, $H^{2,4}$), 8.51 (1H, s, H^6), 7.65 (1H, m, $H^{8,9}$), 7.45 (1H, q, *J* 7.8 Hz, H^3), 4.50 (2H, s, H^{10}); δ_c ($CDCl_3$) 54.3 (C^{10}), 122.1 (C^3), 126.5 ($C^{1'}$), 127.4 (C^9), 129.2 ($C^{6'}$), 129.4 (C^6), 132.8 (C^8), 134.7 (C^7), 137.7 (C^2), 138.1 ($C^{9'}$), 153.7 (C^4), 158.7 ($C^{4'}$), 180.5 (C^5); *m/z* (ESMS$^+$) 226 $(M - N_3)^+$, $IR_{(CDCl3)}[cm^{-1}]$: 807, 889 (tri.sub.benzol), 1073, 1156 (frame C=O), 1129 (νC-N), 1261, 1322 (νC-N), 1345 (δ_sAr-CH_2), 1396 (νC-S),

1442 (δ_sCO-CH_2), 1467 (δ_{as}Ar-CH_2), 1578 (frame Ar(C-C)), 1639 (νC=O in conjugated aromatic ring system), 1995 (ν aliphatic–CH_2), 2097 (νN=N=N), R_f=0.52 (silica, DCM – 2.5% MeOH). Found C, 58.39; H, 3.11; N, 20.67; S, 12.01% $C_{13}H_8N_4OS$ requires C, 58.21; H, 2.98; N, 20.89; S, 11.94%

7-Phthalimidomethyl-1-azathioxanthone

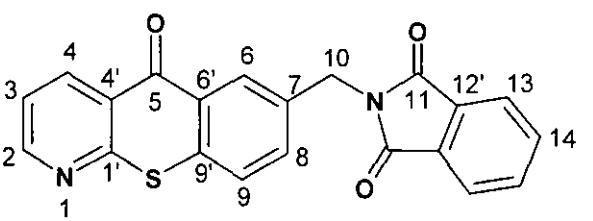

7-Bromomethyl-1-azathioxanthone (200mg, 885 μmol) and potassium phthalimide (655mg, 3.54 mmol) in DMF (20 ml) were stirred, under argon, for 16 h. at room temperature. The solution was poured into ice/water (300 ml) and a white/pale yellow precipitate was formed, the mixture was cooled in the fridge for 2 h. The mixture was extracted with DCM (3 x 300 ml) and the organic phase was dried and the solvent removed under reduced pressure to give a pale yellow powder which was dissolved in DCM (100 ml) and washed with water (pH 10, 2 x 100 ml). The organic phase evaporated and the remaining pale yellow powder was recrystallised from DCM:EtOH to yield the title product as a pale yellow solid. (310 mg, 831 μmol, 94%) m.p. >240 °C; δ_H ($CDCl_3$) 8.82 (1H, dd, *J* 8.1 Hz, H^4), 8.80 (1H, dd, *J* 8.1 Hz, H^2), 8.61 (1H, s, H^6), 7.88 (1H, m, H^{13}), 7.75 (2H, m, $H^{8,14}$), 7.62 (1H, d *J* 8.0 Hz, H^9), 7.45 (1H, q, *J* 8.1 Hz, H^3), 5.00 (2H, s, H^{10}); δ_c ($CDCl_3$) 41.3 (C^{10}), 122.2 (C^3), 123.8, 123.9 (C^{13}), 126.6 ($C^{1'}$), 127.3 (C^9), 129.2 ($C^{6'}$), 129.6 (C^6), 132.9 ($C^{12'}$), 133.3 (C^8), 134.5, 134.6 (C^{14}), 135.6 (C^7), 137.2 ($C^{9'}$), 138.1 (C^2), 153.6 (C^4), 158.8 ($C^{4'}$), 168.1 (C^{11}), 180.5 (C^5); *m/z* (ESMS$^+$) 373 (M + H), 395 $(M + Na)^+$, 411 $(M + K)^+$, R_f=0.8 (silica, DCM – 2.5% MeOH). Found C, 67.53; H, 3.29; N, 7.87; S, 8.71% $C_{21}H_{12}N_2O_3S$ requires C, 67.74; H, 3.23; N, 7.53; S, 8.60%

7-Aminomethyl-1-azathioxanthone

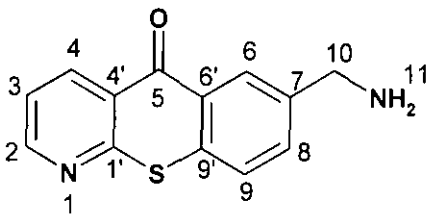

A solution of 7-phthalimidomethyl-1-azathioxanthone (300 mg, 807 μmol) in DCM (20 ml) was mixed with $NH_2NH_2.H_2O$ (117 μl, 2.42 mmol) and MeOH (5 ml). The mixture was heated at 50°C followed by further additions of $NH_2NH_2.H_2O$ (80 μl, 1.6 mmol) at 3h. intervals, until TLC analysis (silica, DCM – 2.5% MeOH) showed that the 7-phthalimidomethyl-1-azathioxanthone had been consumed. The white/pale yellow cloudy mixture was allowed to cool followed by the addition of 6M $HCl_{(aq.)}$ until a pH of 2 was reached. The resultant solution containing a white precipitate was heated for 1 h. then allowed to cool to room temperature and further cooled in the fridge for 1 h. The solution was filtered, followed by drying of the filtrate under vacuum to yield title compound as a yellow hydrochloride salt (confirmed by ^{1}H-NMR). This was dissolved in H_2O (25 ml containing 1.5 eqs. NaOMe then extracted with $CHCl_3$ (3 x 50 ml). The organic phase was dried under reduced pressure to leave the title product as a bright yellow solid. (58 mg, 240 μmol, 37%); m.p. 114-115 °C; δ_H ($CDCl_3$) 8.83 (1H, dd, *J* 7.8 Hz, H^4), 8.80 (1H, dd, *J* 7.8 Hz, H^2), 8.51 (1H, s, H^6), 7.68 (1H, d, *J* 8.0 Hz H^8), 7.62 (1H, d *J* 8.0 Hz, H^9), 7.45 (1H, q, *J* 7.8 Hz, H^3), 4.03 (2H, s, H^{10}), 1.67 (2H, br.s, H^{11}); δ_c ($CDCl_3$) 46.2 (C^{10}), 121.8 (C^3), 126.6 ($C^{1'}$), 127.0 (C^9), 128.0 (C^6), 129.6 ($C^{6'}$), 132.6 (C^8), 136.0 (C^7), 138.1 (C^2), 142.5 ($C^{9'}$), 153.5 (C^4), 159.0 ($C^{4'}$), 180.9 (C^5); *m/z* (ESMS$^+$) 243 $(M + H)^+$, 265 $(M + Na)^+$; $IR_{(CDCl3)}[cm^{-1}]$: 808 (tri.sub.benzol), 826 (νNH_2), 1076 (frame C=O), 1159 (νC-N), (δ_sAr-CH_2), 1400 (νC-S), 1448 (δ_sCO-CH_2), 1474 (δ_{as}Ar-CH_2), 1580 (νNH_2), 1602 (frame Ar(C-C), 1641 (νC=O in conjugated aromatic ring system), 2930 (ν aliphatic–CH_2), 3048 (ν aromatic-CH_2), 3384 (νNH_2) R_f=0.06 (silica, DCM – 2.5% MeOH). Found C, 64.21; H, 4.60; N, 11.86; S, 13.10% $C_{13}H_{10}N_2OS$ requires C, 64.46; H, 4.13; N, 11.57; S, 13.22%

Chloro-acetic acid 2,5-dioxo-pyrrolidin-1-yl ester[18,19]

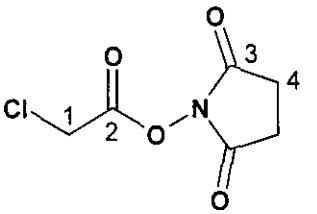

Chloro acetic acid (2.0g, 21 mmol), EDC (4.05g, 21 mmol) and N-hydroxy succinimide (2.43g, 21 mmol) were stirred in dry Et_2O and DCM (10%) (10 mL) for 14h. The solvents were removed under reduced pressure and the remaining residue was purified by column cromatography (silica, EtOAc) (1.53 g, 8 mmol, 38%); m.p. 102-4 °C; δ_H ($CDCl_3$) 4.39 (2H, s, H^1), 2.89 (4H, s, H^4); δ_c ($CDCl_3$) 25.8 (C^4), 38.1 (C^1), 163.4 (C^2), 168.7 (C^3) R_f=0.51 (silica, EtOAc). Found C, 37.47; H, 3.28; N, 7.26% $C_6H_6NO_4Cl$ requires C, 37.60; H, 3.13; N, 7.31%

7-(Chloromethylcarbonoylmethyl)-1-azathioxanthone

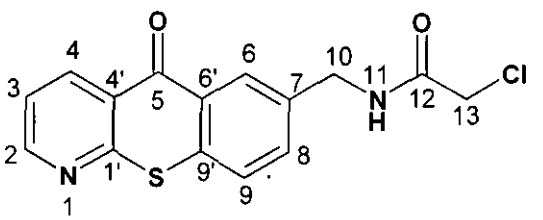

7-Aminomethyl-1-azathioxanthone (40mg, 165μmol) and Chloro-acetic acid 2,5-dioxo-pyrrolidin-1-yl ester (60mg, 248 μmol)) in DMF (3 ml) were stirred, under argon, for 2 h. at room temperature, until TLC analysis (silica, DCM – 3.5% MeOH) showed that all starting 7-aminomethyl-1-azathioxanthone had been consumed. The solvent was evaporated under reduced pressure and the remaining bright yellow solid was sonicated in H_2O (pH = 5, trace amount of LiCl). The mixture was extracted with DCM (3 x 100 ml) and the organic phase was dried and the solvent removed under reduced pressure to give the as pale yellow powder which was purified by column chromatography (silica, DCM – 3% MeOH) to yield the title compound as pale yellow crystalline solid. (45 mg, 141 μmol, 85%) m.p. 188-190 °C; δ_H ($CDCl_3$) 8.86 (1H, dd, *J* 8.0 Hz, H^4), 8.83 (1H, dd, *J* 8.0 Hz, H^2), 8.51 (1H, s, H^6), 7.67 (2H, d, $H^{8,9}$), 7.50 (1H, q *J* 8.0 Hz, H^3), 7.06 (1H, s, H^{11}), 4.66 (2H, d, *J* 6.1 Hz H^{10}), 4.17 (2H, s, H^{13}); δ_c ($CDCl_3$) 42.8 (C^{13}), 43.5 (C^{10}),

122.1 (C^3), 126.6 ($C^{1'}$), 127.4 (C^9), 128.8 (C^6), 129.1 ($C^{6'}$), 133.0 (C^8), 136.7 ($C^{9'}$), 137.2 (C^7), 138.3 (C^2), 153.7 (C^4), 158.8 ($C^{4'}$), 166.6 (C^{12}), 180.7 (C^5); *m/z* (ESMS$^+$) 341, 343 (1:3) (M + Na); $IR_{(CDCl3)}[cm^{-1}]$: 762 (νC-Cl), 807 (tri.sub.benzol), 1077, 1160 (frame C=O), 1136 (νC-N), 1400, 1200 (νC-C(=O)), 1263, 1309 (νC-N), 1385 (δ_sAr-CH_2), 1448 (δ_sCO-CH_2), 1474 (δ_{as}Ar-CH_2), 1581 (AMID-II), 1605 (frame Ar(C-C)), 1643 (νC=O in conjugated aromatic ring system), 1676 (νC=O_{amid}), 2889 (ν aliphatic–CH_2), 3049 (νAr-CH_2), 3134 (AMID-II), 3278 (νNH_{amid}), 3423 (ν$NH_{Sec.amid}$) R_f=0.61 (silica, DCM – 3% MeOH). Found C, 56.68; H, 3.51; N, 8.70; S, 10.01% $C_{15}H_{11}N_2O_2SCl$ requires C, 56.52; H, 3.45; N, 8.79; S, 10.04%

1,7-Bis(benzyloxycarbonyl)-1,4,7,10-tetraazacyclododecane[20]

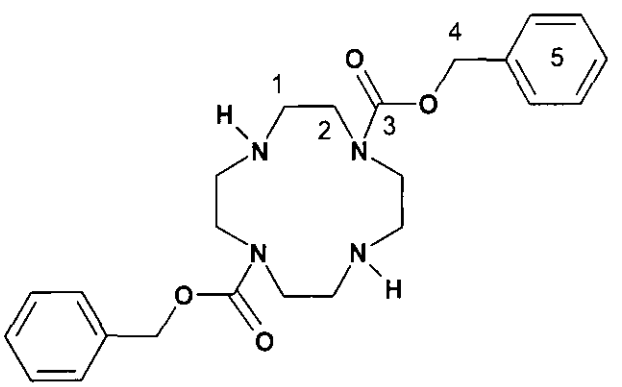

Tetraazacyclododecane (1.25 g, 7.25 mmol) was dissolved in H_2O (9 mL) and the pH was adjusted to 3 by addition of aqueous HCl (6 M, 2.5 mL), followed by the addition of dioxane (7.5 mL). Benzyl chloroformate (3.2 g, 16 mmol) was dissolved in dioxane (7.5 mL) and the solution was added droppwise to the mixture through a syringe in 9 h, while the pH was kept between 2-3 by the addition of aqueous NaOH (2 M) solution. After the addition was complete, the solvents were removed under reduced pressure, yielding a solid residue was extracted with Et_2O (4 × 25 mL) to give an oil that proved to be 1,4,7,10-tetrakis(benzyloxycarbonyl)-1,4,7,10-tetraazacyclododecane [δ_H ($CDCl_3$) 7.27 (m. 20 H, H^5), 5.02 (s, 4 H, H^4), 3.28 (s, 16 H, $H^{1,2}$); δ_H ($CDCl_3$) 156.6 (C^3), 136.1, 128.3, 128.7, 128.0 (C^5), 67.0 (C^4), 49.9 ($C^{1=2}$), R_f = 0.84 (DCM, silica plate)]

Aqueous NaOH (20 % w/v, 20 mL) was added to the remaining residue and the mixture was extracted with Et_2O (4 × 25 mL). The organic phases were combined, washed with aqueous NaOH (5 % w/v, 2 × 20 mL) and dried over Na_2SO_4. The solvent was removed by rotary evaporation and the residue was dried under reduced pressure for 10 h to give the title product as a viscous colourless oil 2.8 g (6.36 mmol, 88%). δ_H ($CDCl_3$) 7.35 (m, 10 H, H^5), 5.15 (s, 4 H, H^4), 3.42 (br.m, 8 H, H^2), 2.85 (br.m, 16 H, H^1); δ_H ($CDCl_3$) 156.6 (C^3), 136.1, 128.3, 128.7, 127.8 (C^5), 66.9 (C^4), 50.6, 48.9 ($C^{1,2}$), *m/z* (ESMS$^+$) 441 $(M + 1)^+$, 463 $(M + Na)^+$, $R_f = 0.51$ (DCM, silica plate)

1,7-Bis(benzyloxycarbonyl)-4,10-bis(tert-butoxycarbonylmethyl)-1,4,7,10-tetraazacyclododecane[20]

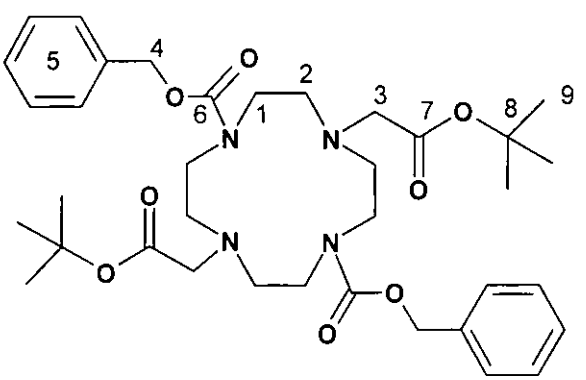

1,7-Bis(benzyloxycarbonyl)-1,4,7,10-tetraazacyclododecane (3.69 g, 8.37 mmol) and tert-butyl bromoacetate (3.37 g, 17.30 mmol, 2eq., 3 % excess) were dissolved in dry MeCN (30 mL) followed by the addition of Cs_2CO_3 (7.40 g, 22.70 mmol, 2,5 eq.). The mixture was stirred at reflux for 20 h. The caesium salts were filtered off and MeCN was removed by rotary evaporation to give a dark yellow oil as a crude product (5.40 g). This was dissolved in CH_2Cl_2 and loaded onto a silica gel column (90 g). The column was eluted with $CH_2Cl_2 \rightarrow$2% MeOH and the fractions containing the product were combined. Removal of the solvent under reduced pressure gave the *title compound* as a pale yellow oil (5.11 g, 7.65 mmol, 91 %). δ_H ($CDCl_3$) 7.33 (br.s, 10 H, H^5), 5.12 (s, 4 H, H^4), 3.42 (br.m, 8 H, H^1), 3.31 (br.s, 4 H, H^3), 2.86 (br.m, 8H, H^2), 1.46 (s 18 H, H^9); δ_c ($CDCl_3$) 170.4 (C^7), 156.3 (C^6), 136.8, 128.3, 127.8, 127.7 (C^5), 80.7 (C^8), 66.8 (C^4), 55.9 (C^3),

54.2, 46.7 ($C^{1,2}$), 28.0 (C^9), *m/z* (ESMS$^+$) 669 $(M + 1)^+$, 691 $(M + Na)^+$, R_f 0.74 (DCM - 2.5% MeOH, silica plate)

1,7-Bis(tert-butoxycarbonylmethyl)-1,4,7,10-tetraazacyclododecane[20]

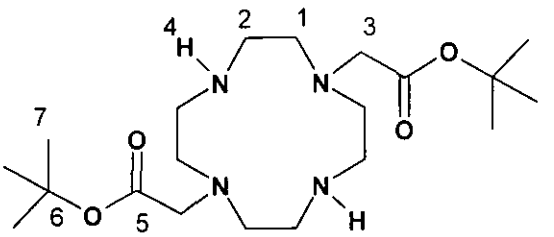

1,7-Bis(benzyloxycarbonyl)-4,10-bis(tert-butoxycarbonylmethyl)-1,4,7,10-tetraaza-cyclododecane (3 g, 44.91 mmol) was dissolved in absolute EtOH (50 mL) and $Pd(OH)_2/C$ (Pd content 10 %, 100 mg) was added. The mixture was hydrogenated in a Parr hydrogenation apparatus (25 psi) for 48h. The catalyst was filtered off and EtOH was removed under reduced pressure. The resulting oil was dissolved in Et_2O (50 mL) and the solution was extracted with cold aq. NaOH solution (20 % (w/v), 3 mL). The ethereal solution was dried (Na_2SO_4) and the Et_2O was removed under vacuum to give a slightly yellow oil which slowly crystallised to reveal a pale yellow solid (1.61 g, 40.41 mmol, 90%). δ_H ($CDCl_3$) 3.33 (s, 4 H, H^3), 2.84 (t^a, 8 H, H^2, ^3J = 5.1 Hz), 2.65 (t^a, 8 H, $H^{1'}$, ^3J = 5.1 Hz), 1.46 (s 18 H, H^7); δ_c ($CDCl_3$) 170.9 (C^5), 80.8 (C^6), 57.0 (C^3), 51.9, 45.8 ($C^{1,2}$), 28.3 (C^7), *m/z* (HRMS$^+$) 401.3122 $(M + H)^+$ ($C_{20}H_{41}O_4N_4$ requires 401.3132), m.p. 90 °C, R_f 0.87 (DCM - 2.5% MeOH, alumina plate).

1,7-Bis(tert-butoxycarbonylmethyl)-4-[(1-azathioxanthone)-2-methyl]- 1,4,7,10-tetraazacyclododecane

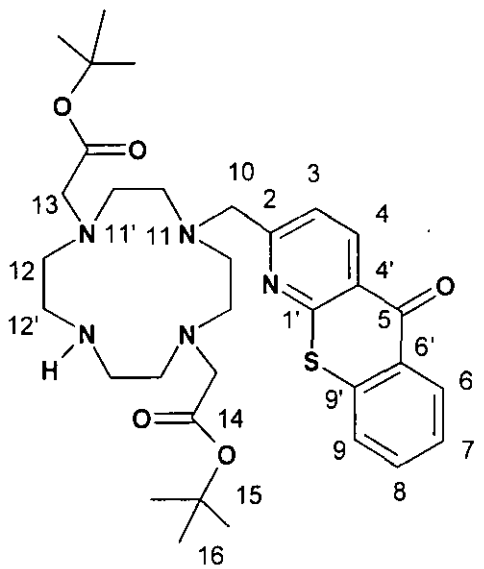

1,7-Bis(tert-butoxycarbonylmethyl)-1,4,7,10-tetraazacyclododecane (250 mg, 0.62 mmol) was combined with 2-bromomethyl-1-azathiaxanthone (1.1 eq., 190 mg) and K_2CO_3 (1 eq., 86 mg) and the mixture stirred in dry MeCN (12 mL) at reflux under argon for 18 h. The reaction was monitored by TLC (DCM : MeOH, 97 : 3) and $ESMS^+$ to confirm that the brominated starting material had been consumed. The solvent was removed under reduced pressure. The resulting solid was dissolved in a small volume of DCM (5 mL) and the KBr/K_2CO_3 was filtered out. The crude mixture was purified by column chromatography (DCM→2% MeOH) to yield the title compound as a yellow oil (161 mg, 0.26 mmol, 42%) δ_H ($CDCl_3$) 8.71 (1H, H^4, d, *J* 8.1 Hz), 8.60 (1H, H^6, d, *J* 8.0 Hz), 7.68 (2H, $H^{8,9}$, m), 7.49 (1H, H^7, m), 7.30 (1H, H^3, d, *J* 8.1 Hz), 3.87 (2H, H^{10}, s), 3.13-2.78 (20H, $H^{11,11',12,12',13}$, m), 1.42 (18H, H^{16}, s); δ_c ($CDCl_3$) 180.7 (C^5), 170.2 (C^{14}), 161.3 (C^2), 158.6 ($C^{1'}$), 139.2 ($C^{4'}$), 137.5 ($C^{6'}$), 133.3 (C^9), 130.2 (C^6), 129.3 ($C^{9'}$), 127.5 (C^7), 127.1 (C^8), 124.8 (C^4), 122.2 (C^3), 80.9 (C^{15}), 52.4 (C^{10}), 57.9 (C^{13}), 50.1, 47.8 ($C^{11,11',12,12'}$), 27.8 (C^{16}); *m/z* ($HRMS^+$) 626.3402 $(M + H)^+$ ($C_{33}H_{48}O_5N_5S$ requires 626.3371), R_f 0.18 (DCM – 3% MeOH, alumina).

1,7-Bis(carboxylmethyl)-4-[(1-azathioxanthone)-2-methyl]-1,4,7,10-tetra-azacyclododecane

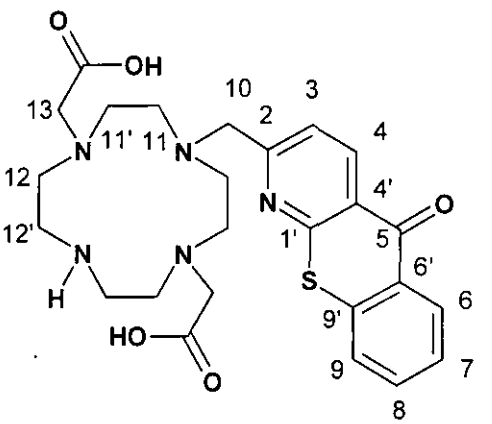

A mixture of trifluoroacetic acid (0.7 mL) and DCM (0.3 mL) was added to 1,7-bis(tert-butoxycarbonylmethyl)-4-[(1-azathioxanthone)-2-methyl]-1,4,7,10-tetra-azacyclo-dodecane (20 mg, 32 μmol) and the reaction left under argon at room temperature for 36 h. The solvents were removed under reduced pressure and a small volume of DCM (3 x 3 mL) was added and removed again under reduced pressure. The crude mixture was dissolved in water (3 mL) and extracted with DCM (3 mL) thrice, and lyophilised to yield the title compound as a pale-orange oil as the bis(trifluoroacetate) salt (14 mg, 27 μmol, 86%) which used in a complexation reaction immediately. δ_H (D_2O) 8.69 (1H, H^4, d, *J* 8.0 Hz), 8.40 (1H, H^6, d, *J* 8.0 Hz), 7.75 (2H, $H^{8,9}$, m), 7.55 (1H, $H^{3,7}$, m), 6.91 (3H, br.m, 2xCOOH + NH), 3.76 (2H, s, H^{10}), 3.07 (20H, $H^{11,11',12,12',13}$, m), *m/z* (ESMS$^+$) 672 (M + 2Na + CF_3CO_2)$^+$

[EuDCP2]

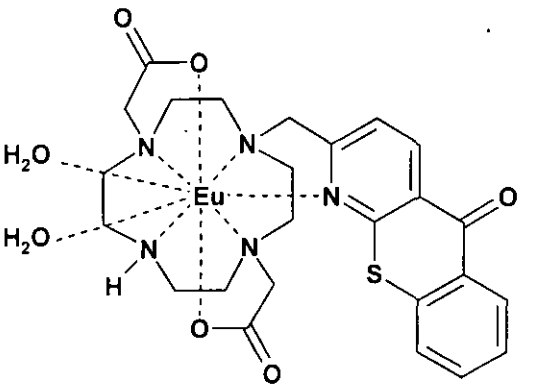

1,7-bis(carboxylmethyl)-4-[(1-azathioxanthone)-2-methyl]-1,4,7,10-tetra-azacyclo-dodecane (14 mg, 27 μmol) was added to $EuCl_3 .6H_2O$ (1.2 eq., 11 mg) and the solids dissolved in a aqueous MeOH (5 : 2 mL). The pH was carefully adjusted to 5 by addition of aqueous HCL and and the reaction stirred at 80 °C for 60 h. After the reaction was cooled to room temperature the pH was then adjusted carefully to 10 by addition of conc. aqueous NaOH solution (in order to get rid of excess Eu as $Eu(OH)_3$) resulting in a white precipitate that was removed via a fine syringe filter. The pH was adjusted back to neutral and the solid lyophilised to give the Eu-complex as a light brown powder containing aprox. 2% NaCl as a result of pH adjustment. *m/z* (HRMS$^+$) 728.1178 $(M + Na + Cl)^+$ ($C_{25}H_{34}O_5N_5SEuNaCl$ requires 728.1152), $\lambda_{max}(H_2O)$ 380 (4070 $dm^3mol^{-1}cm^{-1}$); $\tau^{Eu}_{(H2O,\ pH=6.0)}$: 0.23 ms, $\tau^{Eu}_{(D2O,\ pD=5.6)}$: 1.41 ms; $\phi^{Eu}_{(pH=6.0)}$= 0.6%

1,7-Bis(tert-butoxycarbonylmethyl)-4-[(1-azathioxanthone)-2-methyl]-10-[methyl-sulfonylamino)ethyl]- -1,4,7,10-tetraazacyclododecane

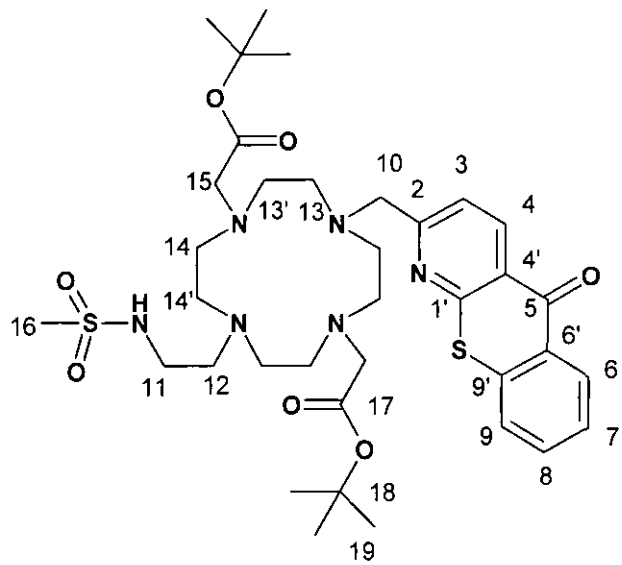

1,7-bis(tert-butoxycarbonylmethyl)-4-[(1-azathioxanthone)-2-methyl]- 1,4,7,10-tetraaza-cyclododecane (87 mg, 0.14 mmol) was combined with N-methanesulfonyl-aziridine (1.1 eq., 17.3 mg) and K_2CO_3 (1 eq., 19 mg) and the mixture stirred in dry MeCN (8 mL) at reflux under argon for 24 h. The reaction was monitored by TLC (DCM : MeOH, 97 : 3) and $ESMS^+$ to confirm that the starting secondary amine had been consumed. The solvent was removed under reduced pressure. The resulting solid was dissolved in a small volume of DCM (3 mL) and the K_2CO_3 was filtered out. The crude mixture was purified by column chromatography on neutral alumina (DCM→2% MeOH) to yield the title compound as a light brown oil (72 mg, 97 μmol, 69%). δ_H ($CDCl_3$) 8.71 (1H, H^4, d, *J* 8.0 Hz), 8.60 (1H, H^6, d, *J* 8.0 Hz), 7.68 (2H, $H^{8,9}$, m), 7.49 (1H, H^7, m), 7.31 (1H, H^3, d, *J* 8.0 Hz), 3.90 (2H, H^{10}, s), 3.13-2.78 (24H, $H^{11,12,13,13',14,14',15}$ m),), 2.01 (3H, H^{16}), 1.41 (18H, H^{19}, s); δ_c ($CDCl_3$) 180.7 (C^5), 170.2 (C^{17}), 161.3 (C^2), 158.6 ($C^{1'}$), 139.2 ($C^{4'}$), 137.5 ($C^{6'}$), 133.3 (C^9), 130.2 (C^6), 129.3 ($C^{9'}$), 127.5 (C^7), 127.1 (C^8), 124.8 (C^4), 122.2 (C^3), 81.1 (C^{18}), 67.0, 67.8 ($C^{11,12}$), 52.4 (C^{10}), 57.9 (C^{15}), 50.1, 47.8 ($C^{13,13',14,14'}$), 38.5 (C^{16}), 27.8 (C^{19}), *m/z* ($HRMS^+$) 747.3560 $(M + H)^+$ ($C_{36}H_{55}O_7N_6S_2$ requires 747.3568), R_f 0.44 (DCM – 3% MeOH, alumina).

1,7-Bis(carboxymethyl)-4-[(1-azathioxanthone)-2-methyl]-10[methylsulfonylamino)-ethyl]- 1,4,7,10-tetraazacyclododecane

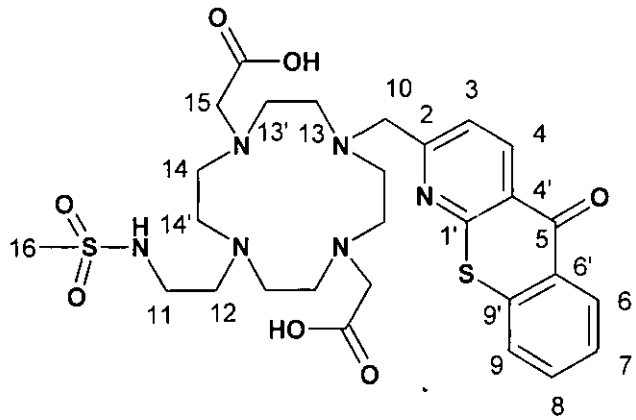

A mixture of trifluoroacetic acid (1.5 mL) and DCM (0.5 mL) was added to 1,7-bis(tert-butoxycarbonylmethyl)-4-[(1-azathioxanthone)-2-methyl]-10-[methylsulfonyl-amino)ethyl]- 1,4,7,10-tetraazacyclododecane (72 mg (97 μmol) and the mixture stirred under argon at room temperature for 28 h. The solvents were removed under reduced pressure and a small volume of DCM (3 x 3 mL) was added and removed again under reduced pressure. The crude mixture was dissolved in water (5 mL) and extracted with DCM (5 mL) thrice, and lyophilised to yield the *title compound* as a dark orange oil which slowly crystallised (55 mg, 87 μmol, 90%). This compound was used for complexation immediately. δ_H (D_2O) 8.69 (1H, H^4, d, *J* 8.0 Hz), 8.40 (1H, H^6, d, *J* 8.0 Hz), 7.75 (2H, $H^{8,9}$, m), 7.55 (1H, $H^{3,7}$, m), 6.91 (3H, br.m, 2xCOOH + NH), 3.76 (2H, s, H^{10}), 3.07 (24H, $H^{11,12,13,13',14,14',15}$, m) 2.00 (3H, H^{16}, s), *m/z* (ESMS$^+$) 658 (M - H+ 2Na)$^+$; m.p. 120-1 °C

[Eu(MS)DCP2]

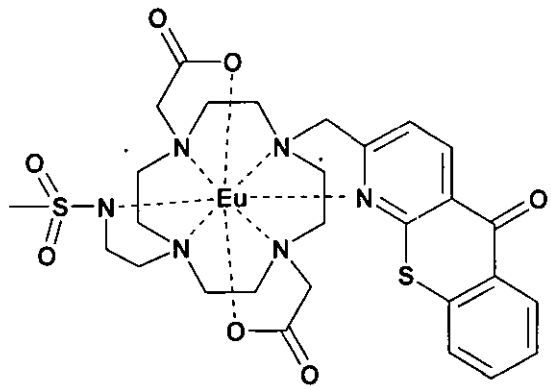

1,7-Bis(carboxy-methyl)-4-[(1-Azathioxanthone)-2-methyl]-10-[methylsulfonylamino)-ethyl]- 1,4,7,10-tetraazacyclododecane (28 mg, 44 μmol) was added to $Eu(CF_3SO_3)_3$ (1.1 eq., 26 mg) and the solids dissolved in MeCN (2 mL) and the reaction stirred at reflux temperature for 30 h. After the reaction was cooled to room temperature the solvents were removed under reduced pressure, the remaining residue was dissolved in aqueous MeOH (5 :1, 5 mL). The pH was then adjusted carefully to 10 by addition of conc. aqueous NaOH solution (in order to get rid of the excess Eu as $Eu(OH)_3$) resulting in a white precipitate that was removed via a fine syringe filter). The pH was adjusted back to neutral and lyophilised to give a light brown solid, which was loaded onto a DOWEX 1-X8(Cl) anion exchange resin. The column was eluted with water → 10% NH_4OH and the fractions were analysed by $ESMS^+$. The fractions were combined and lyophilised to yield the Eu-complex as a light brown powder. *m/z* ($HRMS^+$) 819.0914 $(M + H + Cl)^+$ ($C_{28}H_{35}O_7N_6S_2EuCl$ requires 819.0915), $\lambda_{max}(H_2O)$ 380 (4070 $dm^3mol^{-1}cm^{-1}$); $\tau^{Eu}_{(H2O, pH=4.5)}$: 0.48 ms, $\tau^{Eu}_{(H2O, pH=8.0)}$: 0.41 ms; $\tau^{Eu}_{(D2O, pD=4.1)}$: 0.76 ms, $\tau^{Eu}_{(D2O, pD=7.6)}$: 0.48 ms; $\phi^{Eu}_{(pH=3.0)}$= 1 %, $\phi^{Eu}_{(pH=8.0)}$= 0.9%

1,7-Bis(α-dimethylglutarate)-1,4,7,10-tetraazacyclododecane[21] (as a stereoisomeric mixture)

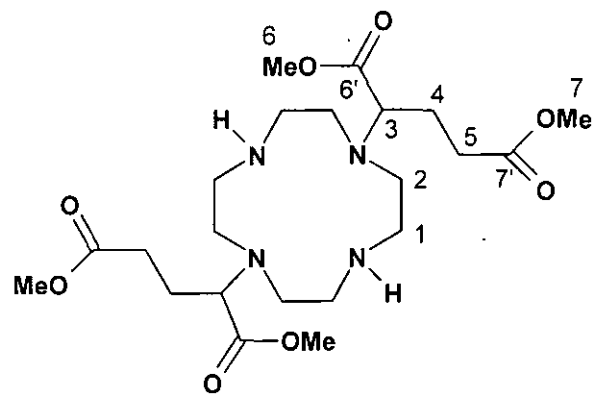

Tetraazacyclododecane (2.00 g, 11.61 mmol), and racemic dimethyl-2-bromoglutarate (6.10 g, 25.54 mmol) was dissolved in dry MeCN (20 mL) followed by addition of $NaHCO_3$ (2.14 g, 2.2 eq.). The mixture was stirred at 55 °C under argon. The reaction was monitored by TLC (DCM : MeOH : NH_4OH, 89 : 10 : 1) and $ESMS^+$. After 7 days dimethyl-2-bromoglutarate had been consumed, and the solvent was removed under reduced pressure. The remaining residue was dissolved in DCM (20 mL), the organic layer was washed with HCl (pH 3), dried over K_2CO_3 and the solvents removed under reduced pressure. The residue was purified by column chromatography over silica (DCM : THF : MeOH : NH_4OH, 25 : 65 : 5 : 5). The fractions containing the *title product* were combined and the solvents were removed under reduced pressure to yield a pale brown oil (1.23 g, 2.52 mmol, 21%) δ_H ($CDCl_3$) 7.68 (2H, br.s, NH), 3.63 (6H, s, H^7), 3.57 (6H, s, H^6), 3.26 (2H, m, H^3), 2.78 (16H, m, $H^{1,2}$), 2.36 (4H, m, H^5), 1.92 (4H, m, H^4) δ_c ($CDCl_3$) 173.4 ($C^{7'}$), 172.9 ($C^{6'}$), 64.1 (C^3), 51.9 ($CH_3{}^6$), 51.8 ($CH_3{}^7$), 48.7, 46.5 ($C^{1,2}$), 30.0 (C^5), 22.6 (C^4), *m/z* ($HRMS^+$) 489.2923 $(M + H)^+$ ($C_{22}H_{41}O_8N_4$ requires 489.2919),R_f 0.32 (DCM : MeOH : NH_4OH, 89 : 10 : 1, silica).

1,7-Bis(α-dimethylglutarate)-4-[(1-azathioxanthone)-2-methyl]- 1,4,7,10-tetraaza-cyclododecane

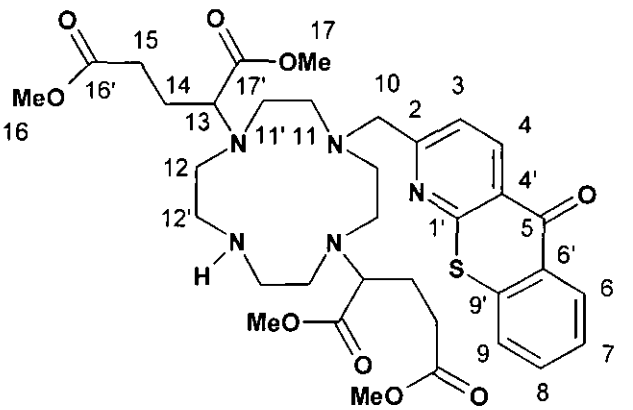

1,7-Bis(α-dimethylglutarate)-1,4,7,10-tetraazacyclododecane (160 mg, 327 μmol) was combined with 2-bromomethyl-1-azathiaxanthone (1 eq., 100 mg) and $NaHCO_3$ (1.1 eq., 28 mg) and the mixture stirred in dry MeCN (4 mL) at 60 °C under argon for 48 h. The reaction was monitored by TLC (DCM : MeOH, 97 : 3) and $ESMS^+$ to confirm that the brominated starting material had been consumed. The solvent was removed under reduced pressure and the resulting solid was dissolved in a small volume of DCM (5 mL) and the Na-salts filtered out. The crude mixture was purified by column chromatography (DCM→0.2% MeOH) to yield the *title compound* as a yellow oil (127 mg, 178 μmol, 54%); δ_H ($CDCl_3$) 8.78 (1H, d, *J* 8.0 Hz, H^4), 8.58 (1H, m, H^6), 7.69 (2H, m , $H^{8,9}$), 7.52 (1H, m, H^7), 7,34 (1H, d, *J* 8.0 Hz, H^3), 3.91 (2H, s, H^{10}), 3.73 (6H, s, H^{16}), 3.66 (6H, s, H^{17}), 3.19 (2H, m, H^{13}), 3.06 (16H, m, $H^{11,11',12,12'}$), 2.42 (4H, m, H^{15}), 1.90 (4H, m, H^{14}); δ_c ($CDCl_3$) 180.5 (C^5) 173.4 ($C^{16'}$), 172.9 ($C^{17'}$), 161.4 (C^2), 158.6 ($C^{1'}$), 138.4 ($C^{4'}$), 137.5 ($C^{6'}$), 133.3 (C^8), 130.0 (C^6), 129.0 ($C^{9'}$), 127.1 (C^7), 126.6 (C^9), 125.3 (C^4), 122.2 (C^3), 65.1 (C^{13}), 51.9 (C^{17}), 51.8 (C^{16}), 51.3, 50.4, 49.2, 46.5 ($C^{11,11',12,12'}$), 46.1 (C^{10}), 30.9 (C^{15}), 25.7 (C^{14}); R_f 0.16 (DCM – 3% MeOH, alumina); *m/z* (HRMS$^+$) 714.3163 $(M + H)^+$ ($C_{35}H_{48}O_9N_5S$ requires 714.3173).

1,7-Bis(α-dimethylglutarate)-4-[(1-azathioxanthone)-2-methyl]-10-[methylsulfonyl-amino)ethyl]- 1,4,7,10-tetraazacyclododecane

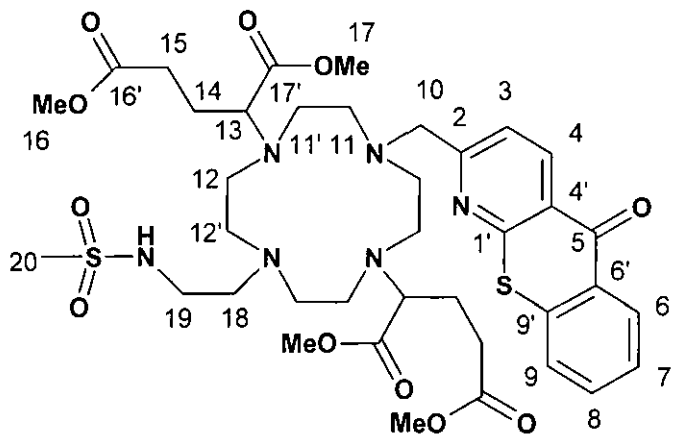

4-[(1-Azathioxanthone)-2-methyl]-1,7-bis(α-dimethylglutarate)-1,4,7,10-tetraaza-cyclo-dodecane (110 mg, 150 μmol) was combined with N-methanesulfonyl-aziridine (1.1 eq., 19.4 mg) and K_2CO_3 (1 eq., 22 mg) stirred in dry MeCN (5 mL) at reflux temperature (85 °C) under argon for 46 hrs. The reaction was monitored by TLC (DCM : MeOH, 97 : 3) and $ESMS^+$ to confirm that the starting material had been consumed. The solvent was removed under reduced pressure and the resulting solid was dissolved in a small volume of DCM (3 mL) and the K_2CO_3 removed by filtration. The crude mixture was purified by column chromatography (DCM→2% MeOH) to yield the title compound as a light brown oil which slowly crystallized from the melt (50 mg, 60 μmol, 41%). δ_H ($CDCl_3$) 8.70 (1H, d, *J* 8.0 Hz, H^4), 8.48 (1H, m, H^6), 7.63 (2H, m , $H^{8,9}$), 7.44 (2H, d+dd, $H^{3,7}$), 3.83 (2H, s, H^{10}), 3.63 (6H, s, H^{16}), 3.60 (6H, s, H^{17}), 3.26 (2H, m, H^{13}), 3.02 (3H, s, H^{20}), 2.93 (16H, m, $H^{11,11',12,12'}$), 2.50 (6H, m, $H^{15,18}$), 1.90 (4H, m, H^{14}), 1.56 (2H, t, *J* 7.8 Hz, H^{19}); δ_c ($CDCl_3$) 180.5 (C^5) 173.3 ($C^{16'}$), 173.0 ($C^{17'}$), 162.1 (C^2), 158.8 ($C^{1'}$), 138.5 ($C^{4'}$), 137.5 ($C^{6'}$), 133.7 (C^9), 130.0 (C^6), 128.9 ($C^{9'}$), 127.2 (C^7), 126.6 (C^8), 125.5 (C^4), 122.7 (C^3), 65.9 (C^{13}), 51.7 (C^{17}), 51.4 (C^{16}), 54.2, 51.3, 49.2, 46.6 ($C^{11,11',12,12'}$), 46.1 (C^{10}), 38.1 (C^{20}), 33.4 (C^{18}), 30.9 (C^{15}), 25.7 (C^{14}), 22.9 (C^{19}), R_f 0.39 (DCM – 3% MeOH, alumina), m.p. 137-9 °C, *m/z* ($HRMS^+$) 835.3358 $(M + H)^+$ ($C_{38}H_{55}O_{11}N_6S_2$ requires 835.3370).

1,7-Bis(α-glutarate)-4-[(1-azathioxanthone)-2-methyl]-10-[methylsulfonyl-amino)ethyl]- 1,4,7,10-tetraazacyclododecane

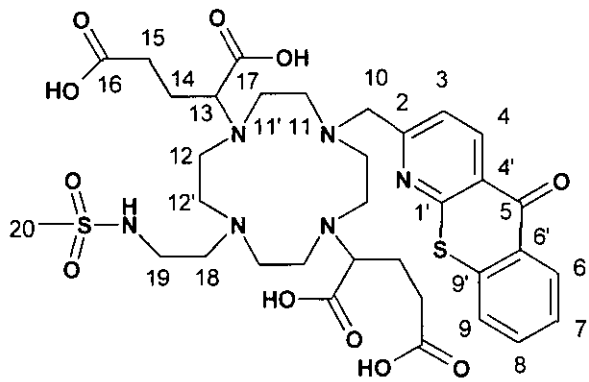

Freshly made aqueous KOD solution (2.5 mL, 0.1 M) was added to 1,7-bis(α-dimethylglutarate)-4-[(1-azathioxanthone)-2-methyl]-10-[methylsulfonylamino)ethyl]-1,4,7,10-tetraaza-cyclododecane (50 mg, 60 μmol). The reaction mixture was kept under argon at room temperature and progress was monitored by NMR. After 3 h no ester methyl group signals were observed in the ^{1}H-NMR spectrum (δ_H 3.8 ppm), the pH of the mixture was increased (pH ≈ 6) with conc. HCl and the solution loaded onto a DOWEX 50X4-100 strong cation exchange resin. The column was eluted with water → 10% NH_4OH and the fractions were analysed by $ESMS^+$. The fractions were combined and lyophilised to yield the *title compound* as a dark orange oil (26 mg, 33 μmol, 55%), which was used in a complexation reaction immediately. δ_H (D_2O): mainly broad overlapping signals, but no sign of ester Me groups in ^{1}H-NMR, δ_H (D_2O) 8.46 (1H, d, *J* 8.0 Hz, H^4), 8.18 (1H, m, H^6), 7.44 (4H, m , $H^{8,9,3,7}$), 3.83 (2H, s, H^{10}), 3.26 (2H, m, H^{13}), 3.02 (3H, s, H^{20}), 3.09 (22H, br.m, $H^{11,11',12,12',15,18}$), 2.05 (6H, m, $H^{14,19}$); *m/z* ($ESMS^-$) 779 $(M-H)^-$.

[$Na_2Eu(MS)DGP2$]

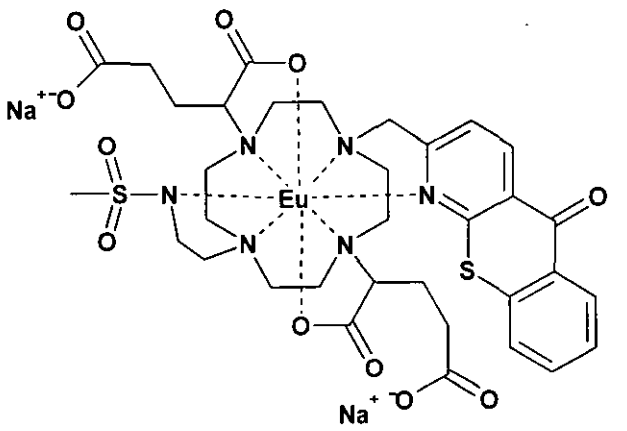

1,7-Bis(α-glutarate)-4-[(1-azathioxanthone)-2-methyl]-10-[methylsulfonylamino)ethyl]-1,4,7,10-tetraazacyclododecane (25 mg, 32 μmol) was added to $Eu(CH_3CO_2)_3 .4H_2O$ (1.1 eq., 15 mg) and the solids dissolved in a H_2O (2 mL). The pH was carefully adjusted to 5 by addition of acetic acid and the reaction left to stir at 70 ° C for 72 hrs. After the reaction was cooled to room temperature, the solvents were removed under reduced pressure and the remaining residue was dissolved in H_2O (5 mL). The pH was then adjusted carefully to 10 by addition of conc. NaOH solution (in order to remove the excess Eu as $Eu(OH)_3$) resulting in a white precipitate that was removed via a fine syringe filter. The pH was adjusted back to neutral with acetic acid and the mixture lyophilised to yield the sodium salt of the Eu-complex as a bright yellow solid contained aprox. 2% NaOAc as a result of pH adjustment (26 mg, 28 μmol). *m/z* (HRMS$^-$) 927.1562 $(M - H)^-$ ($C_{34}H_{42}O_{11}N_6S_2Eu$ requires 927.1565); $\lambda_{max}(H_2O)$ 380 (4070 $dm^3mol^{-1}cm^{-1}$); $\tau^{Eu}_{(H2O,\ pH=3.0)}$: 0.59 ms, $\tau^{Eu}_{(H2O,\ pH=5.5)}$: 0.71 ms, $\tau^{Eu}_{(H2O,\ pH=8.0)}$: 0.47 ms; $\tau^{Eu}_{(D2O,\ pD=2.6)}$: 1.10 ms, $\tau^{Eu}_{(D2O,\ pD=5.1)}$: 1.00 ms, $\tau^{Eu}_{(D2O,\ pD=7.6)}$: 0.53 ms; $\phi^{Eu}_{(pH=3.0)}$= 1.8 %, $\phi^{Eu}_{(pH=5.5)}$= 2.0 %, $\phi^{Eu}_{(pH=8.0)}$= 1.7 %

1,7-Bis(α-dimethyladipate)-1,4,7,10- tetraazacyclododecane[21] (as a stereoisomeric mixture)

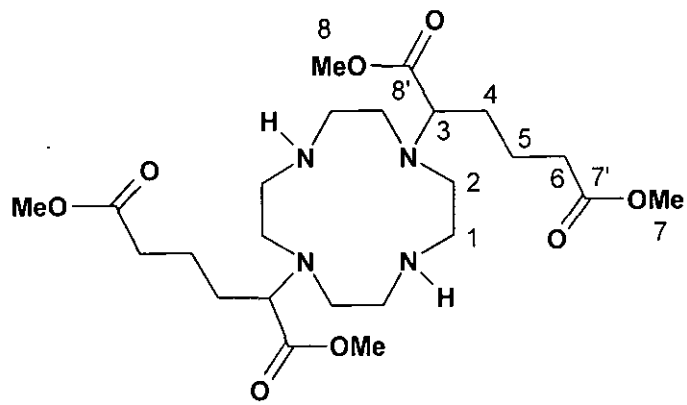

Tetraazacyclododecane (1.20 g, 6.98 mmol), racemic dimethyl-2-bromoadipate (3.88 g, 15.35 mmol) was dissolved in dry MeCN (20 mL) followed by addition of $NaHCO_3$ (1.29 g, 2.2 eq.). The mixture was stirred at 55 °C under argon. The reaction was monitored by TLC (DCM : THF : MeOH, 50 : 50 : 5) and $ESMS^+$. After 4 days of reaction the dimethyl-2-bromoadipate had been consumed, and the solvent was removed under reduced pressure. The remaining residue was dissolved in DCM (10 mL). The organic layer was washed with HCl (pH 3), dried over K_2CO_3 and the solvents removed under reduced pressure. The residue was purified by column chromatography over silica (DCM : THF : MeOH, 50 : 50 : 3). The fractions containing the *title product* were combined and the solvents were removed under reduced pressure to yield a transparent viscous oil which slowly crystallised to reveal a white solid (760 mg, 1.47 mmol, 21%) δ_H ($CDCl_3$) 4.18 (1H,m, H^3) 3.77 (6H, s, H^7), 3.73 (6H, s, H^8), 3.29 (16H, m, $H^{1,2}$), 2.36 (4H, m, H^6), 1.78 (8H, m, $H^{4,5}$) δ_c ($CDCl_3$) 174.0 ($C^{7'}$), 173.9 ($C^{8'}$), 70.3 (C^3), 53.0 (C^8), 52.7 (C^7), 52.6, 52.1, 51.8, 46.6 ($C^{1,2}$), 33.7 (C^4), 33.6 (C^6), 31.0 (C^5), *m/z* ($HRMS^+$) 517.3245 (M + H)$^+$ ($C_{24}H_{45}O_8N_4$ requires 517.3232), R_f 0.42 (THF : DCM : MeOH, 50 : 50 : 5, silica); m.p.: <10 °C.

1,7-Bis(α-dimethyladipate)-4-[(1-azathioxanthone)-2-methyl]-1,4,7,10-tetraazacyclododecane

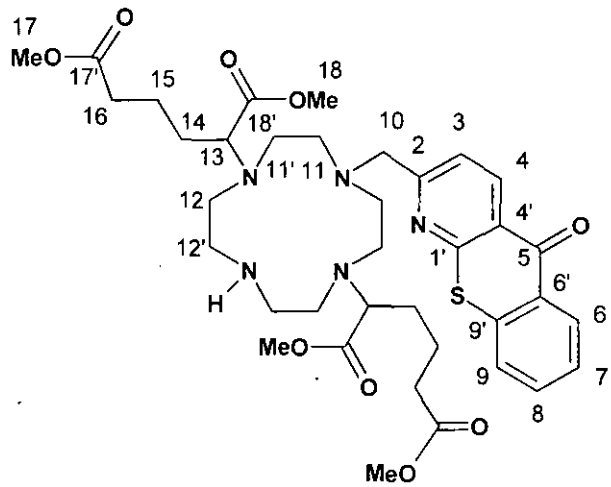

1,7-Bis(α-dimethyladipate)-1,4,7,10-tetraazacyclododecane (310 mg, 600 μmol) was combined with 2-bromomethyl-1-azathiaxanthone (1 eq., 183 mg) and $NaHCO_3$ (1 eq., 50 mg) and the mixture stirred in dry MeCN (10 mL), the mixture was heated initially at 60 °C for 4 h followed by 70 °C for 20 h under argon. The reaction was monitored by TLC (DCM : THF : MeOH : Et_3N, 80 : 20 : 3.5 : 3.5, silica) and $ESMS^+$ to confirm that the brominated starting material had been consumed. The solvent was removed under reduced pressure and the resulting solid was dissolved in a small volume of DCM (5 mL) and the sodium salts removed by filtration. The crude mixture was purified by column chromatography (DCM : THF 80 : 20 → 3% MeOH : Et_3N (1 : 1)); fractions containing clean product were combined and the solvents were removed under reduced pressure. The remaining residue was dissolved in DCM (5 mL) and washed with water (3x15 mL). The organic layer was evaporated dry to yield the *title compound* as a pale yellow oil (165 mg, 170 μmol, 28%) δ_H ($CDCl_3$) 8.80 (1H, d, *J* 8.0 Hz, H^4), 8.60 (1H, br.d, *J* 7.9 Hz, H^6), 7.67 (2H, m , $H^{8,9}$), 7.55 (1H, dt, *J* 7.9 Hz, H^7), 7,34 (1H, d, *J* 8.0 Hz, H^3), 4.19 (1H,m, H^{13}), 3.81 (2H, s, H^{10}), 3.73 (6H, s, H^{17}), 3.69 (6H, s, H^{18}), 3.17 (16H, m, $H^{11,11',12,12'}$), 2.38 (4H, m, H^{16}), 1.78 (8H, m, $H^{14,15}$) δ_c ($CDCl_3$) 181.2 (C^5) 173.4 ($C^{16'}$), 172.9 ($C^{17'}$), 162.1 (C^2), 158.8 ($C^{1'}$), 138.4 ($C^{4'}$), 137.5 ($C^{6'}$), 133.4 (C^9), 130.2 (C^6), 129.1 ($C^{9'}$), 127.1 (C^7), 126.7 (C^8), 125.8 (C^4), 122.5 (C^3), 70.3 (C^{13}), 52.0 (C^{18}), 51.8 (C^{17}), 51.9, 51.8, 51.7, 49.2 ($C^{11,11',12,12'}$), 48.1 (C^{10}), 33.8 (C^{14}), 33.7 (C^{16}), 29.9 (C^{15}), R_f

0.33 (DCM : THF : MeOH : Et_3N, 80 : 20 : 3.5 : 3.5, silica plate), *m/z* (HRMS$^+$) 742.3489 $(M + H)^+$ ($C_{37}H_{52}O_9N_5S$ requires 742.3486).

1,7-bis(α-dimethyladipate)-4-[(1-azathioxanthone)-2-methyl]-10-[methylsulfonyl-amino)ethyl]- 1,4,7,10-tetraazacyclododecane

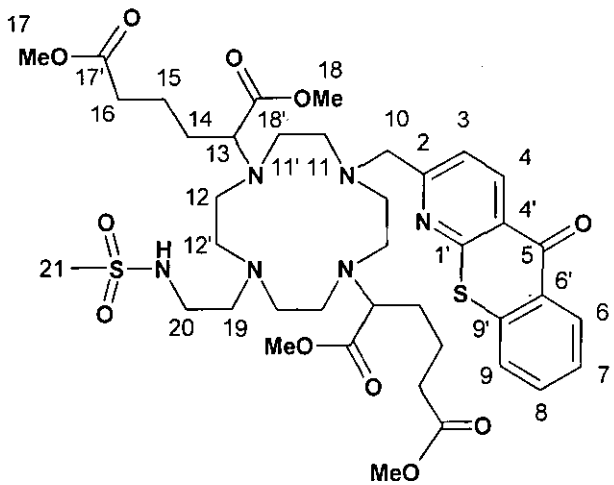

1,7-Bis(α-dimethyladipate)-4-[(1-Azathioxanthone)-2-methyl]-1,4,7,10-tetraaza-cyclododecane (190 mg, 256 μmol) was combined with 2-methanesulfonato-N-methanesulfonylethylamine (1.2 eq., 67.2 mg) and Na_2CO_3 (1.5 eq., 42 mg) and the mixture stirred in dry MeCN (10 mL) was reflux for 30 h under argon. The reaction was monitored by TLC (DCM : THF : MeOH : Et_3N, 80 : 20 : 2.5 : 2.5, silica) and ESMS$^+$ to confirm that the starting material had been consumed. The solvent was removed under reduced pressure. The resulting solid was dissolved in a small volume of DCM (5 mL) and the sodium salts were filtered out. The crude mixture was purified by column chromatography (DCM : THF 80 : 20 → 3% MeOH : Et_3N (1 : 1)). The fractions containing product only were combined and the solvents were removed under reduced pressure. The remaining residue was dissolved in DCM (5 mL) and washed with water (3x10 mL). The organic layer was evaporated to yield the *title compound* as a pale brown oil (170 mg, 197 μmol, 77%): δ_H ($CDCl_3$) 8.80 (1H, d, *J* 8.0 Hz, H^4), 8.66 (1H, br.d, *J* 7.9 Hz, H^6), 7.76 (2H, dd, *J* 7.9 Hz, $H^{8,9}$), 7.65 (1H, dt, *J* 7.9 Hz, H^7), 7,53 (1H, d, *J* 8.0 Hz, H^3), 4.19 (1H,m, H^{13}), 3.84 (2H, s, H^{10}), 3.66 (6H, s, H^{17}), 3.64 (6H, s, H^{18}), 3.06 (16H,

m, $H^{11,11',12,12'}$), 2.98 (3H, dd, H^{21}), 2.33 (6H, m, $H^{16,19}$), 1.68 (10H, m, $H^{14,15,20}$), δ_c ($CDCl_3$) 180.8 (C^5) 174.9 ($C^{18'}$), 173.5 ($C^{17'}$), 165.4 (C^2), 158.1 ($C^{1'}$), 138.1 ($C^{4'}$), 137.7 ($C^{6'}$), 133.1 (C^9), 130.1 (C^6), 129.2 ($C^{9'}$), 126.9 (C^7), 126.7 (C^8), 125.8 (C^4), 121.7 (C^3), 65.7 (C^{13}), 51.8 (C^{18}), 51.4 (C^{17}), 54.3, 54.1, 50.2, 50.1 ($C^{11,11',12,12'}$), 50.0 (C^{10}), 40.1 (C^{21}), 34.4 (C^{14}), 33.8 (C^{16}), 30.6 (C^{19}) 29.6 (C^{15}), 22.3 (C^{20}) , R_f 0.61 (DCM : THF : MeOH : Et_3N, 80 : 20 : 2.5 : 2.5, silica), *m/z* (HRMS$^+$) 863.3686 $(M + H)^+$ ($C_{40}H_{58}O_{11}N_6S_2$ requires 863.3679).

1,7-bis(α-adipate)-4-[(1-azathioxanthone)-2-methyl]-10-[methylsulfonyl-amino)ethyl]- 1,4,7,10-tetraazacyclododecane

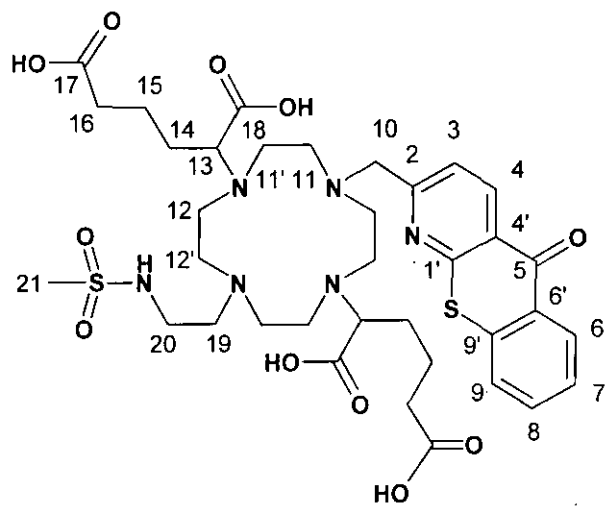

Freshly made aqueous KOD solution (5 mL, 0.1 M) was added to 4-[(1-azathioxanthone)-2-methyl]-10-[methylsulfonylamino)ethyl]-1,7-bis(α-dimethyladipate)-1,4,7,10-tetraaza-cyclododecane (57 mg, 66 μmol) and the mixture was stirred under argon at room temperature; the reaction was monitored by ^{1}H-NMR. After 3 h, no methyl group signals were observed in the ^{1}H-NMR spectrum; the pH of the mixture was adjusted (pH ≈ 6) with conc. HCl, washed with DCM (3x5 mL) and loaded onto a DOWEX 50X4-100 strong cation exchange resin. The column was eluted with water → 10% NH_4OH and the fractions were analysed by ESMS$^+$. The appropriate fractions were combined and lyophilised to yield the *title compound* as a dark orange oil (25 mg, 33 μmol, 47%), which was used in a complexation reaction immediately. δ_H (D_2O): mainly

broad overlapping signals, but no sing of ester Me groups in ^{1}H-NMR, δ_H (D_2O) 8.55 (1H, d, *J* 8.0 Hz, H^4), 8.24 (1H, m, H^6), 7.49 (4H, m , $H^{8,9,3,7}$), 3.16 (27H, br.m, $H^{10,11,11',12,12',16,19,21}$), 1.67 (10H, m, $H^{14,15,20}$); *m/z* (ESMS$^-$) 805 $(M - H)^+$.

[Na_2Eu(MS)DAdP2]

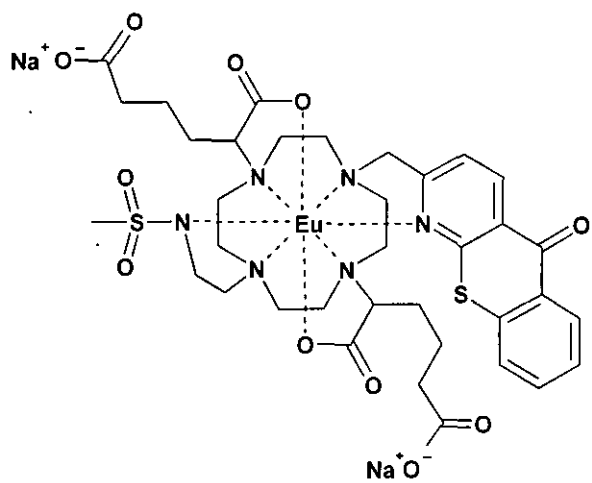

1,7-Bis(α-adipate)-4-[(1-azathioxanthone)-2-methyl]-10-[methylsulfonylamino)ethyl]-1,4,7,10-tetraazacyclododecane (25 mg, 31 μmol) was added to $Eu(OAc)_3$.$4H_2O$ (1.1 eq., 13 mg) and the solids dissolved in 2.5 mL H_2O : MeOH (5 : 1). The pH was carefully adjusted to 5 by addition of acetic acid and the reaction left to stir at 75 ° C for 72 h. After the reaction was cooled to room temperature, the pH was then adjusted carefully to 10 by addition of conc. NaOH solution (in order to remove excess Eu as $Eu(OH)_3$) resulting in a white precipitate removed via centrifugation. The pH was adjusted back to neutral and the sample lyophilised to give a bright yellow solid solid contained aprox. 2% NaOAc as a result of pH adjustment (30 mg, 30 μmol). *m/z* (HRMS$^+$) 979.1816 $(M + H + Na)^+$ ($C_{36}H_{47}O_{11}N_6S_2EuNa$ requires 979.1849); $\lambda_{max}(H_2O)$ 380 (4070 $dm^3mol^{-1}cm^{-1}$); $\tau^{Eu}_{(H2O,\ pH=4.5)}$: 0.83 ms, $\tau^{Eu}_{(H2O,\ pH=8.0)}$: 0.43 ms; $\tau^{Eu}_{(D2O,\ pD=4.1)}$: 0.83 ms, $\tau^{Eu}_{(D2O,\ pD=7.6)}$: 0.47 ms; $\phi^{Eu}_{(pH=4.5)}$= 6.1 %, $\phi^{Eu}_{(pH=8.0)}$= 5.3 %

[Na_2Gd(MS)DAdP2]

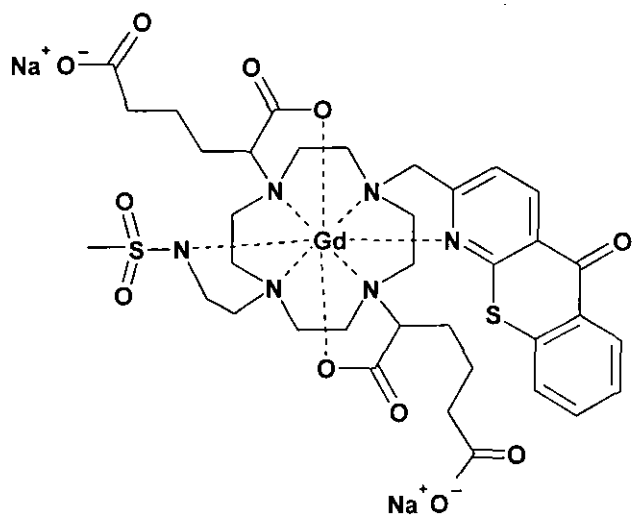

The Gd-complex was prepared as described for the europium analogue. *m/z* ($HRMS^+$) 999.2178 $(M + Me + Na)^+$ ($C_{36}H_{46}O_{11}N_6S_2GdNa$ mono Me-ester requires: 999.2111) $r_{1p}^{(pH=4.5)}$: 3.12 $mM^{-1}s^{-1}$ $r_{1p}^{(pH=8.5)}$: 1.87 $mM^{-1}s^{-1}$.

(S)-Ethyl-N-bromoethanoyl-alanate[22]

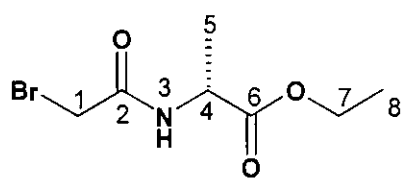

S-Alanine ethyl ester hydrochloride (7.70 g, 50 mmol) was stirred in $CHCl_3$ (40 ml) at -30 °C (acetone/dry ice) along with Et_3N (15 ml, 100 mmol) and bromoacetylbromine (4.5 ml, 51 mmol) for 3h. followed by further 7 h. of stirring at room temperature. The mixture was washed with aqueous HCl (6 M, 40 ml) followed by H_2O (4 x 25 ml). The organic phase was dried and the solvent removed under reduced pressure and the crude product was recrystalised from DCM/pet. ether to give the title product as a pale yellow crystalline solid (8.17 g, 68%) m.p.: 30-31 °C; δ_H ($CDCl_3$) 7.16 (H^3, br.s, 1H), 4.56 (H^4, q, 1H, J = 7.2 Hz), 4.23 (H^7, q, 2H, J = 7.1 Hz), 4.07 (H^1, s, 2H), 1.45 (H^5, d, 3H, J = 7.2 Hz), 1.30 (H^8, t, 3H, J = 7.1 Hz) δ_c ($CDCl_3$) 172.6 (C^6), 165.8 (C^2), 62.0 (C^7), 49.0 (C^4),

42.7 (C^1), 18.5 (C^5), 14.4 (C^8), *m/z* (ESMS$^+$) 260.9; 262.9 $(M + H)^+$. Found C, 35.82; H, 5.08; N, 5.68% $C_7H_{12}NO_3Br$ requires C, 35.31; H, 5.04; N, 5.88%.

(SS)-1,7-Bis(benzyloxycarbonyl)-4,10-bis(ethoxycarbonyl-2-ethylcarbamoylmethyl)-1,4,7,10-tetraazacyclododecane

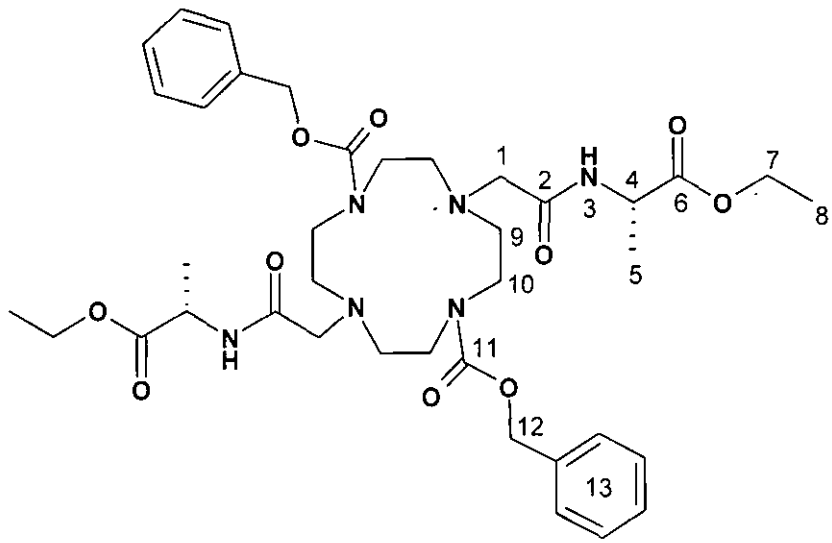

1,7-Bis(benzyloxycarbonyl)-1,4,7,10-tetraazacyclododecane (2.40 g, 5.45 mmol) and (S)-ethyl-N-bromoethanoyl-alanate (2.74 g, 11.5 mmol) were dissolved in dry MeCN (50 mL) followed by the addition of K_2CO_3 (4.50 g, 32.61 mmol). The mixture was stirred at 60 °C for 5 days under argon and the reaction was monitored by ESMS and TLC (DCM 3% MeOH, alumina) to confirm that the (S)-ethyl-N-bromoethanoyl-alanate starting material had been consumed. The potassium salts were filtered off and MeCN was removed by rotary evaporation to give a dark yellow oil as a crude product, which was purified by column chromatography (alumina, DCM – 5 % MeOH), to yield the *title compound* as pale yellow oil, (3.62 g, 88%). δ_H ($CDCl_3$) 7.60 (H^3, d, 2H, *J* 6.0 Hz), 7.33 (H^{13} br.s, 10 H), 5.12 (H^{12}, s, 4H), 4.60 (H^4, p, 2H, *J* = 7.2 Hz), 4.17 (H^7, h, 4H, *J* = 7.2 Hz), 3.74 (H^1, m, 4H), 2.89 ($H^{9,10}$, br.m, 18H) 1.41 (H^5, d, 6H, *J* = 7.2 Hz), 1.28 (H^8, t, 6H, *J* = 7.1 Hz); δ_c ($CDCl_3$) 173.9 (C^6), 170.4 (C^2), 136.8; 128.4; 127.9; 127.8 (C^{13}), 61.9 (C^7), 61.5 (C^1), 54.1, 48.2 ($C^{9,10}$), 48.2 (C^4), 18.6 (C^5), 14.4 (C^8), *m/z* (ESMS$^+$) 755 $(M + H)^+$, 777 $(M + Na)^+$; R_f 0.62 (alumina, DCM - 3% MeOH).

(SS)-1,7-Bis(ethoxycarbonyl-2-ethylcarbamoylmethyl)-1,4,7,10-tetraaza-cyclododecane

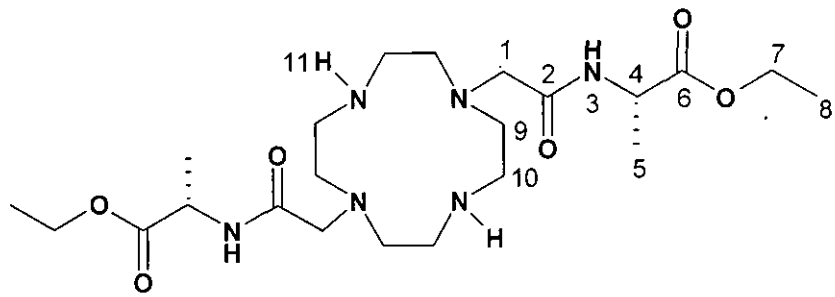

(SS)-1,7-Bis(benzoyloxycarbonyl)-4,10-bis(ethoxycarbonyl-2-ethylcarbamoylmethyl)-1,4,7,10-tetraazacyclododecane (3.60 g, 47.52 *mmol*) was dissolved in absolute EtOH (100 mL) and $Pd(OH)_2/C$ (Pd content 10 %, 170 mg) was added. The mixture was hydrogenated in a Parr hydrogenation apparatus (40 psi) for 5 days. The catalyst was filtered off and EtOH was removed under reduced pressure. The resulting oil was dissolved in DCM (50 mL) and the solution was extracted with cold aq. NaOH solution (20 % (w/v), 5 mL) followed by extraction with H_2O (3 x 30 ml). The organic phase was dried and the solvent removed under vacuum to give the title compound as a pale yellow oil (2.11 g, 91%). %). δ_H ($CDCl_3$) 8.15 (H^{11}, d, 2H, J = 6.0 Hz), 7.60 (H^3, d, 2H, J 6.0 Hz), 4.61 (H^4, p, 2H, J = 7.2 Hz), 4.17 (H^7, h, 4H, J = 7.2 Hz), 3.75 (H^1, m, 4H), 2.91 ($H^{9,10}$, m, 18H) 1.41 (H^5, d, 6H, J = 7.2 Hz), 1.28 (H^8, t, 6H, J = 7.1 Hz); δ_c ($CDCl_3$) 173.9 (C^6), 170.6 (C^2), 61.9 (C^7), 61.6 (C^1), 53.0, 47.4 ($C^{9,10}$), 48.1 (C^4), 18.6 (C^5), 14.4 (C^8), *m/z* (HRMS$^+$) 487.3240 ($M^+ + H)^+$ ($C_{22}H_{42}O_6N_6$ requires 487.3239); R_f 0.26 (alumina, DCM - 7% MeOH)

(SS)-1,7-Bis(ethoxycarbonyl-2-ethylcarbamoylmethyl)-4-[7-(Chloromethyl-carbonoylmethyl)-1-azathioxanthone]- 1,4,7,10-tetraazacyclododecane

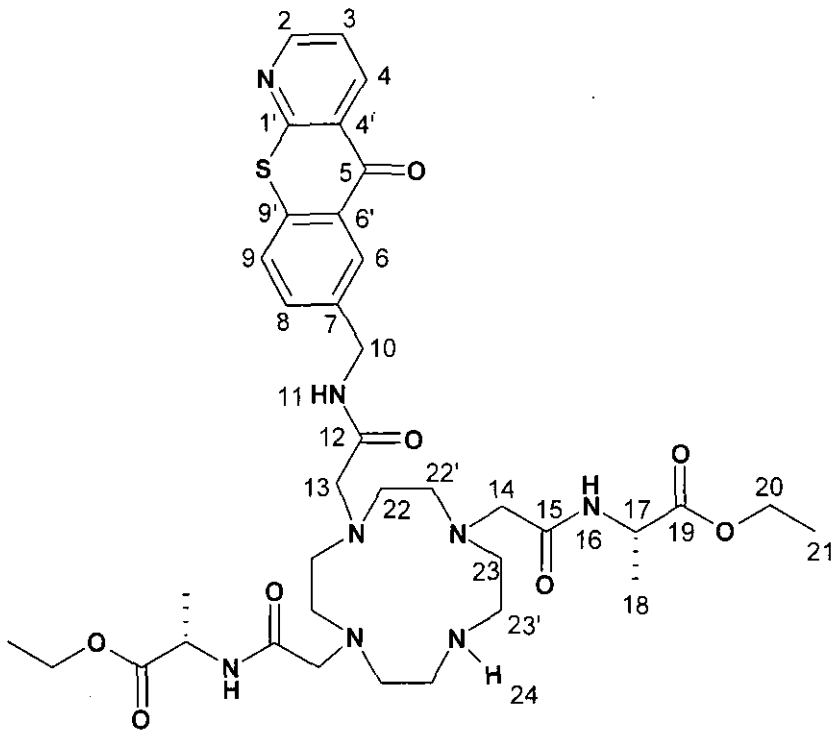

(SS)-1,7-Bis(ethoxycarbonyl-2-ethylcarbamoylmethyl)-1,4,7,10-tetraazacyclododecane (200 mg, 411μmol) was combined with 7-(Chloromethylcarbonoylmethyl)-1-azathioxanthone (100 mg, 314 μmol) and $KHCO_3$ (1 eq., 32 mg) and the mixture stirred in dry MeCN (10 mL), was heated initially at 50 °C for 2 h followed by 70 °C for 22 h under argon. The reaction was monitored by TLC (DCM, 5% MeOH, alumina) and $ESMS^+$ to confirm that the brominated starting material had been consumed. The solvent was removed under reduced pressure and the resulting solid was dissolved in a small volume of DCM (5 mL) and the potassium salts removed by filtration. The crude mixture was purified by column chromatography (DCM → 3% MeOH, alumina); fractions containing clean product were combined and the solvents were removed under reduced pressure to yield the *title compound* as a pale yellow solid (80 mg, 104 μmol, 33%) m.p.: 138-140°C; δ_H ($CDCl_3$) 8.76 ($H^{2,4}$, m, 2H), 8.35 (H^6, s, 1H), 8.11 (H^{16}, d, 2H, J = 6.2 Hz), 7.72 ($H^{8,24}$, m, 3H), 7.56 (H^9, q, 1H, J = 8.1 Hz), 7.43 (H^3, m, 1H), 7.35 (H^{11}, d, 1H, J = 6.2 Hz) 4.48 (H^{17}, 2H, m), 4.10 ($H^{10,20}$, m, 6H), 3.63 (H^{14}, m, 4H), 3.10 ($H^{13,22,22',23,23'}$, m,

18H) 1.39 (H^{18}, m, 6H), 1.24 (H^{21}, t, 6H, J = 7.2 Hz); δ_c ($CDCl_3$) 180.5 (C^5), 173.0 (C^{19}), 171.7 (C^{15}), 171.1 (C^{12}), 158.9 ($C^{4'}$), 153.6 (C^4), 138.8 (C^2), 138.0 (C^7), 136.3 ($C^{9'}$), 133.0 (C^8), 128.8 ($C^{6'}$), 128.2 (C^6), 127.0 (C^9), 126.4 (C^{11}), 121.9 (C^3) 61.7 (C^{20}), 55.9, 53.7, 53.1, 47.3 ($C^{22,22',23'23'}$), 46.1 (C^{13}), 42,7 (C^{10}), 17.6 (C^{18}), 14.4 (C^{21}) *m/z* ($HRMS^+$) 769.3690 ($C_{37}H_{52}O_8N_8S$ requires 769.3702); R_f 0.15 (alumina, DCM - 5% MeOH).

[EuDAP7A(CF_3SO_3)$_3$]

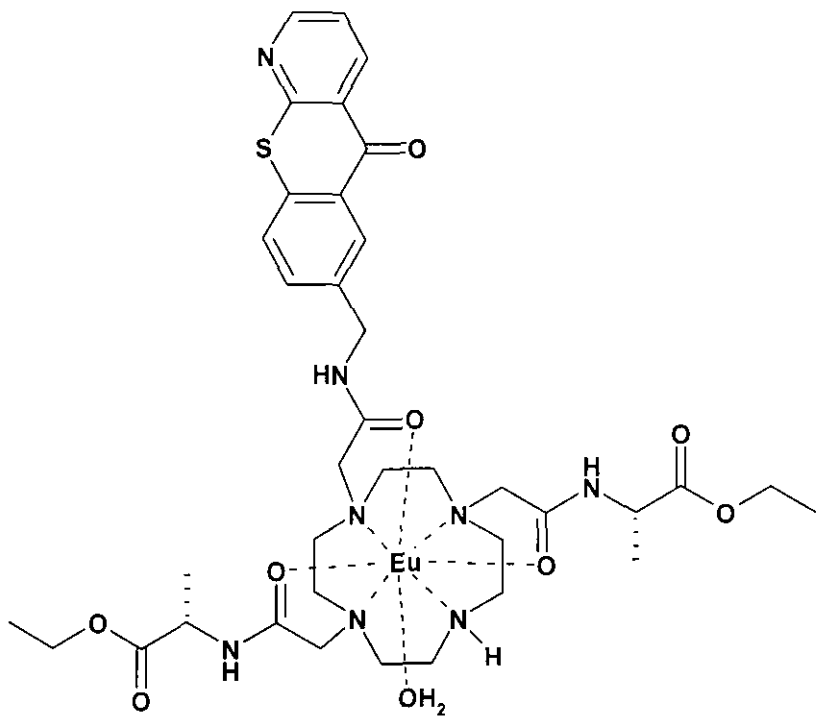

(SS)-1,7-Bis(ethoxycarbonyl-2-ethylcarbamoylmethyl)-4-[7-(Chloromethylcarbonoyl-methyl)-1-azathioxanthone]-1,4,7,10-tetraazacyclododecane (25 mg, 55 μmol) was added to $Eu(CF_3SO_3)_3$ (1 eq., 33 mg) and the mixture was dissolved in dry MeCN (2 mL). The reaction left to stir at 70 ° C for 72 hrs. After cooling to room temperature, the solvents were removed under reduced pressure and the remaining residue was dissolved in dry MeCN (0.1 mL) and the mixture was dropped onto anhydrous Et_2O which resulted in precipitation of the title compound as a triflate salt. The precipitate was separated by centrifugation and dissolved in H_2O (5 ml). The pH was then adjusted carefully to 10 by

addition of conc. NaOH solution (in order to remove the excess Eu as $Eu(OH)_3$) resulting in a white precipitate, removed via a fine syringe filter. The pH was adjusted back to neutral with conc. HCl and the mixture lyophilised to give a bright yellow solid solid contained aprox 2% NaCl as a result of pH adjustment (60 mg, 49 μmol). *m/z* ($HRMS^+$) 1221.2056 $(M + 2CF_3SO_3)^+$ ($C_{37}H_{53}O_8N_8S_2Eu(CF_3SO_3)_2$ requires 1221.2033); $\lambda_{max}(H_2O)$ 384 (12790 $dm^3mol^{-1}cm^{-1}$); $\tau^{Eu}_{(H2O,\ pH=7.4)}$: 0.44 ms, $\tau^{Eu}_{(D2O,\ pD=7.1)}$: 0.90 ms; $\phi^{Eu}_{(pH=7.4)}$= 5.1 %

[GdDAP7A(CF_3SO_3)$_3$]

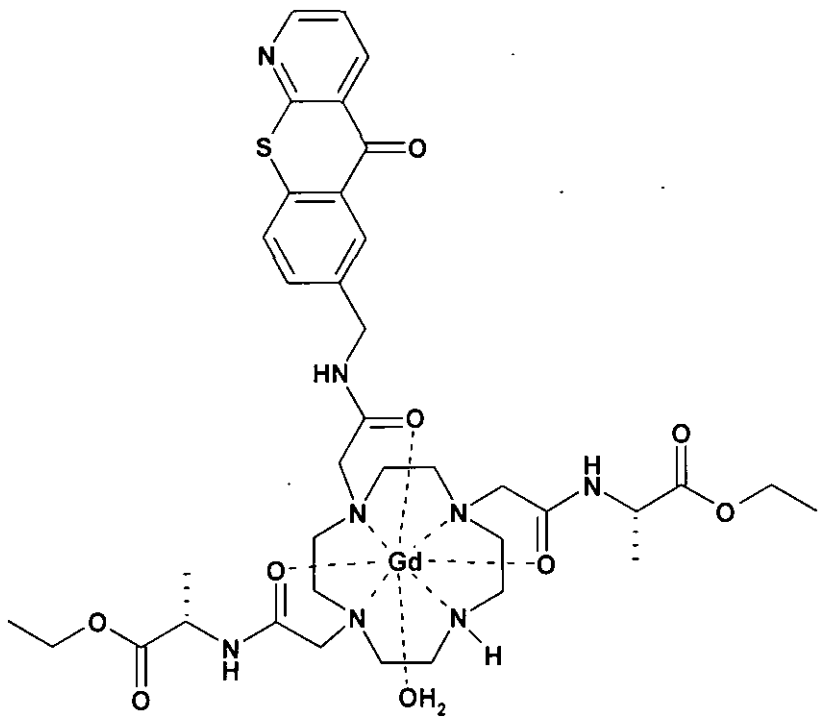

The Gd-complex was prepared as described for the europium analogue. *m/z* ($HRMS^+$) 1259.1270 $(M + 2CF_3SO_3)^+$ ($C_{37}H_{54}O_8N_8S_2Gd(CF_3SO_3)_2$ requires 1259,1859); $\lambda_{max}(H_2O)$ 384 (12790 $dm^3mol^{-1}cm^{-1}$); r_1=7.658 $M^{-1}s^{-1}$

(SS)-1,7-Bis(ethoxycarbonyl-2-ethylcarbamoylmethyl)-4-[(1-azathioxanthone)-2-methyl]- 1,4,7,10-tetraazacyclododecane

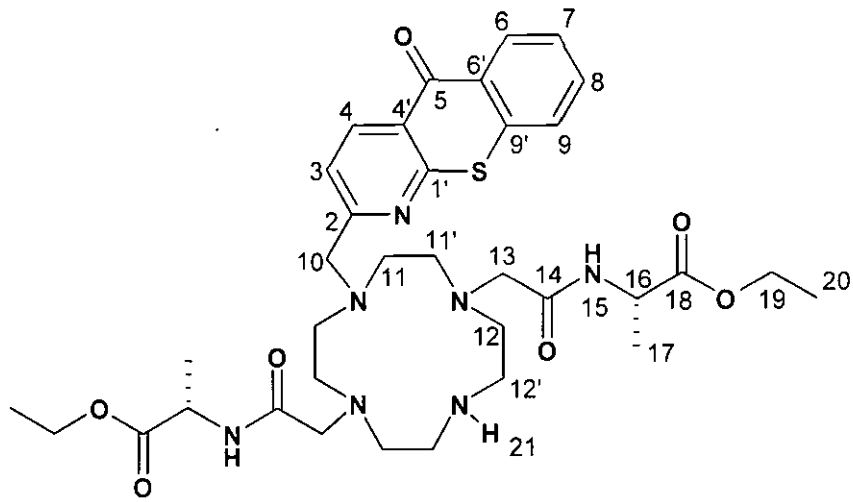

(SS)-1,7-Bis(ethoxycarbonyl-2-ethylcarbamoylmethyl)-1,4,7,10-tetraazacyclododecane (200 mg, 411μmol) was combined with 2-bromomethyl-1-azathiaxanthone (1 eq., 126 mg) and $KHCO_3$ (1 eq., 41 mg) and the mixture stirred in dry MeCN (10 mL), was heated at 70 °C for 36 h under argon. The reaction was monitored by TLC (DCM, 5% MeOH, alumina) and $ESMS^+$ to confirm that the brominated starting material had been consumed. The solvent was removed under reduced pressure and the resulting solid was dissolved in a small volume of DCM (5 mL) and the potassium salts removed by filtration. The crude mixture was purified by column chromatography (DCM → 3% MeOH, alumina); fractions containing clean product were combined and the solvents were removed under reduced pressure to yield the *title compound* as a pale yellow oil (130 mg, 182 μmol, 45%); δ_H ($CDCl_3$): 8.74 (H^4, d, 1H, J = 8.1 Hz), 8.57 (H^6, d, 1H, J = 8.2 Hz), 7.66 ($H^{8,9,21}$, m, 3H), 7.53 (H^7, t, 1H, *J* = 8.2 Hz), 7.39 (H^3, d, 1H, J = 8.1 Hz), 7.33 (H^{15}, br.s, 2H), 4.51 (H^{16}, 2H, p, J = 7.1 Hz), 4.13 (H^{19}, q, 4H, J = 7.1 Hz), 3.93 (H^{10}, m, 2H), 3.15 ($H^{11,11',12,12',13}$, m, 20H) 1.41 (H^{17}, t, 4H, J = 7.1 Hz), 1.24 (H^{20}, q, 6H, J = 7.1 Hz); δ_c ($CDCl_3$) 180.5 (C^5), 173.3 (C^{18}), 170.4 (C^{14}), 162.4 (C^2), 158.6 ($C^{1'}$), 138.7 (C^4), 137.0 ($C^{4'}$), 133.4 (C^9), 130.2 (C^6), 129.1 ($C^{6'}$), 127.3 (C^7), 126.8 (C^8), 125.5 ($C^{9'}$), 122.4 (C^3), 61.7 (C^{19}), 60.6 (C^{10}), 56.0 (C^{13}), 54.2, 53.7, 53.0, 47.0 ($C^{11,11',12,12'}$),

48.4 (C^{16}), 18.2 (C^{18}), 14.4 (C^{20}), *m/z* (HRMS$^+$) 712.34843 $(M + H)^+$ ($C_{35}H_{50}O_7N_7S$ requires 712.34869) R_f 0.36 (alumina, DCM - 5% MeOH).

[EuDAP2(CF_3SO_3)$_3$]

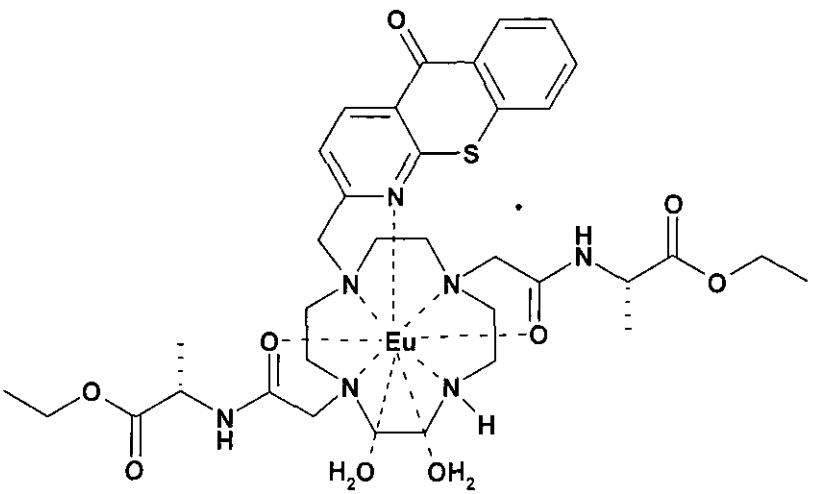

(SS)-1,7-Bis(ethoxycarbonyl-2-ethylcarbamoylmethyl)-4-[(1-Azathioxanthone)-2-methyl]- 1,4,7,10-tetraazacyclododecane (18 mg, 25 μmol) was added to Eu(CF_3SO_3)$_3$ (1 eq., 16 mg) and the solids dissolved in dry MeCN (3 mL) and the reaction left to stir at 80 ° C for 74 hrs. After the reaction was cooled to room temperature, the solvents were removed under reduced pressure and the remaining residue was dissolved in 0.1 mL dry MeCN and the mixture was dropped onto anhydrous Et_2O which resulted in precipitation of the title compound as a triflate salt. The precipitate was spinned out and dissolved in 5 ml H_2O : MeOH (3 : 1) The pH was then adjusted carefully to 10 by addition of conc. NaOH solution (in order to remove the excess Eu as Eu(OH)$_3$) resulting in a white precipitate, whish was removed by centrifugation. The pH was adjusted back to neutral with aqueous HCL and the mixture lyophilised to give a bright yellow solid contained aprox 2% NaCl as a result of pH adjustment (16 mg, 11.5 μmol). *m/z* (HRMS$^+$) 1162.1618 $(M + 2CF_3SO_3)^+$ ($C_{35}H_{49}O_7N_7SEu(CF_3SO_3)_2$ requires 1162.1667); $\lambda_{max}(H_2O)$ 380 (4070 $dm^3mol^{-1}cm^{-1}$); $\tau^{Eu}_{(H2O,\ pH=7.4)}$: 0.24 ms, $\tau^{Eu}_{(D2O,\ pD=7.1)}$: 0.56 ms; $\phi^{Eu}_{(pH=7.4)}$= 4.4 %

(SS)-1,7-Bis(carboxy-2-ethylcarbamoylmethyl)-4-[(1-azathioxanthone)-2-methyl]-1,4,7,10-tetraazacyclododecane

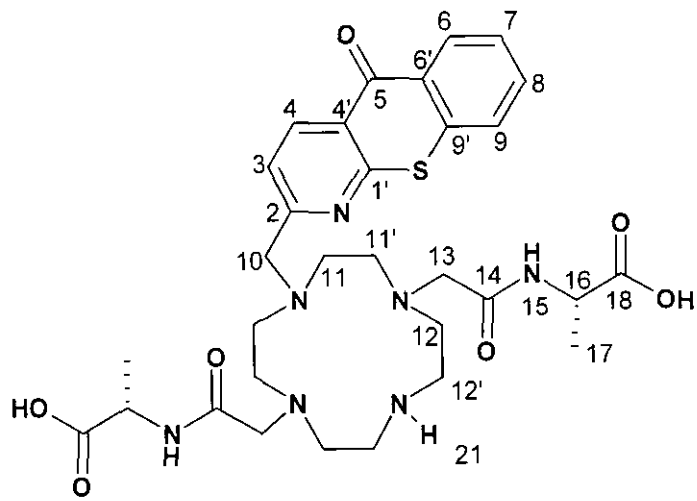

Freshly made aqueous KOD solution (2.5 mL, 0.1 M) was added to (SS)-1,7-bis(ethoxycarbonyl-2-ethylcarbamoylmethyl)-4-[(1-azathioxanthone)-2-methyl]-1,4,7,10-tetraazacyclo-dodecane (61 mg, 86 μmol). The reaction mixture was kept under argon at room temperature and progress was monitored by NMR. After 6 h no ethyl group signals were observed in the ^{1}H-NMR spectrum. The pH of the mixture was increased (pH ≈ 6) with conc. HCl and the solution loaded onto a DOWEX 50X4-100 strong cation exchange resin. The column was eluted with water → 10% NH_4OH and the fractions were analysed by ^{1}H-NMR. The fractions were combined and lyophilised to yield the *title compound* as a pale orange oil (43 mg, 66 μmol, 77%), which was used for complexation reaction immediately. δ_H ($CDCl_3$): 8.17 (H^4, br.d, 1H), 7.98 (H^6, br.d, 1H), 7.47 (H^7,br.t, 1H), 7.25 ($H^{8,9,3,15,21}$, m, 7H), 4.02 (H^{16}, m, 2H, J = 8.1 Hz), 3.73 (H^{10}, br.s, 2H), 3.10 ($H^{11,11',12,12',13}$, m, 20H), 1.14 (H^{17}, d, 6H, J = 7.3 Hz)

[Na_2EuDAPA2(OAc)]

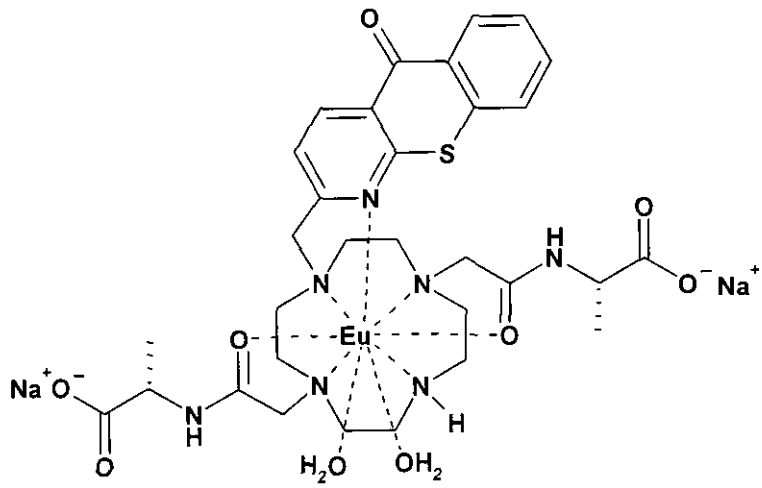

(SS)-1,7-Bis(carboxy-2-ethylcarbamoylmethyl)-4-[(1-azathioxanthone)-2-methyl]-1,4,7,10-tetraazacyclododecane (43 mg, 66 μmol) was added to $Eu(OAc)_3 .4H_2O$ (1.2 eq., 33 mg) and the solids dissolved in 2.5 mL H_2O : MeOH (5 : 1). The pH was carefully adjusted to 5 by addition of acetic acid and the reaction left to stir at 75 ° C for 60 h. After the reaction was cooled to room temperature, The pH was then adjusted carefully to 10 by addition of conc. NaOH solution (in order to remove excess Eu as $Eu(OH)_3$) resulting in a white precipitate removed via centrifugation. The pH was adjusted back to neutral with acetic acid and the sample lyophilised to give a bright yellow solid contained aprox. 2% NaOAc as a result of pH adjustment (20 mg, 22 μmol). *m/z* ($HRMS^+$) 890.2004 (M + Na + OAc) ($C_{31}H_{41}O_7N_7SEuNaCH_3COO$ requires 890.2031); $\lambda_{max}(H_2O)$ 380 (4070 $dm^3mol^{-1}cm^{-1}$); $\tau^{Eu}_{(H2O,\ pH=7.2)}$: 0.24 ms, $\tau^{Eu}_{(D2O,\ pD=7.0)}$: 0.70 ms; $\phi^{Eu}_{(pH=7.4)}$= 1.2 %,

(S)-(Ethyl-N-bromoethanoyl)-phenyl-alanate[22]

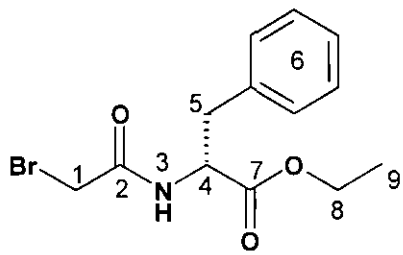

(S)-phenyl-alanine ethyl ester hydrochloride (2.30 g, 10 mmol) was stirred in dry THF (40 ml) at -30 °C (acetone/dry ice) along with Et_3N (3 ml, 20 mmol) and bromoacetyl-bromine (0.89 ml, 11 mmol) for 2h. followed by further 7 h. of stirring at room temperature. The mixture then was dilute with DCM (120 mL) and washed successfully with aqueous HCl (6 M, 40 ml) followed by H_2O (4 x 25 ml). The organic phase was dried and solvent removed under reduced pressure. The crude product was washed with Et_2O to give the title product as a white crystalline solid (2.50 g, 79%) m.p.: 32-33°C; δ_H ($CDCl_3$) 7.28 (H^6, m, 5H), 6.93 (H^3, br.s, 1H), 4.83 (H^4, q, 1H, J = 7.0 Hz), 4.18 (H^8, q, 2H, J = 7.2 Hz), 3.84 (H^1, s, 2H), 3.15 (H^5, 2H, m) 1.26 (H^9, t, 3H, J = 7.2 Hz), δ_c ($CDCl_3$) 171.1 (C^7), 165.5 (C^2), 135.6, 129.6, 128.9, 127.5 (C^6), 62.0 (C^8), 54.0 (C^4), 38.0 (C^5), 28.9 (C^1), 14.3 (C^9), *m/z* (ESMS$^+$) 313.9; 315.9 $(M + H)^+$. Found C, 49.79; H, 5.13; N, 4.40% $C_{13}H_{16}NO_3Br$ requires C, 49.70; H, 5.10; N, 4.46%

(SS)-1,7-Bis(benzyloxycarbonyl)-4,10-bis(ethoxycarbonyl-2-ethylcarbamoylphenyl)-1,4,7,10-tetraazacyclododecane

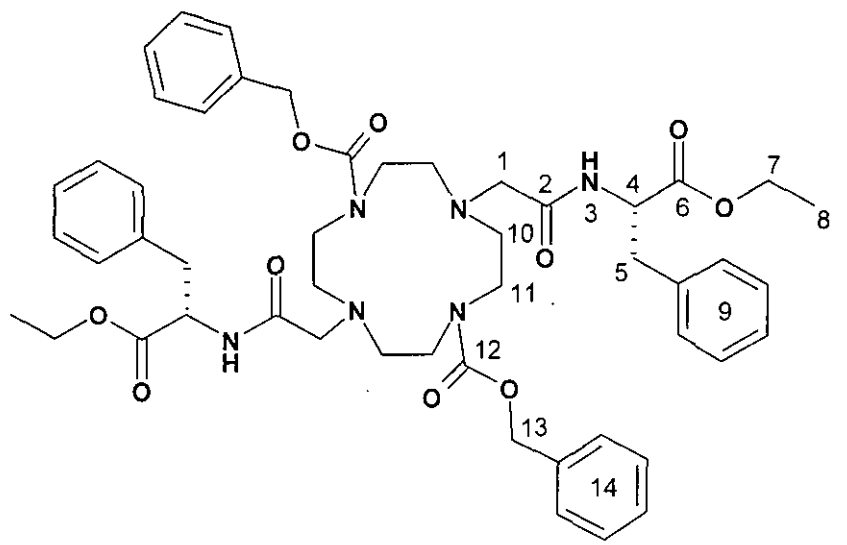

1,7-Bis(benzyloxycarbonyl)-1,4,7,10-tetraazacyclododecane (2.40 g, 5.45 mmol) and (S)-(Ethyl-N-bromoethanoyl)-phenyl-alanate (3.63 g, 11.5 mmol) were dissolved in dry MeCN (40 mL) followed by the addition of K_2CO_3 (4.00 g, 29 mol). The mixture was stirred at 65 °C for 4 days under argon and the reaction was monitored by ESMS and TLC (DCM 3% MeOH, alumina) to confirm that the (S)-(Ethyl-N-bromoethanoyl)-phenyl-alanate starting material had been consumed. The potassium salts were filtered off and MeCN was removed under reduced pressure to give a dark yellow oil as a crude product, which was purified by column chromatography (alumina, DCM – 4 % MeOH), to yield the *title compound* as pale yellow oil, (3.87 g, 78%); δ_H ($CDCl_3$) 7.51 (H^3, d, 2H, *J* 6.0 Hz), 7.27 (H^{6+14}, m, 20H), 5.13 (H^{12}, 4H, s), 4.70 (H^4, m, 2H), 4.04 (H^8, q, 4H, *J* = 7.2 Hz), 3.13 (H^1, s, 4H), 3.09 (H^{10}, m, 8H), 2.66 (H^{11}, m, 8H), 1.18 (H^9, t, 6H, *J* = 7.2 Hz); δ_c ($CDCl_3$) 172.1 (C^6), 162.7 (C^2), 137.1, 137.0, 129.6, 128.8 ,128.5, 127.4, 127.3 (C^{9+14}), 61.8 (C^8), 61.6 (C^1), 53.5 (C^4), 53.7 (C^{11}), 48.3 (C^{10}), 38.0 (C^5), 14.3 (C^9), *m/z* ($ESMS^+$) 907 $(M + H)^+$, 930 $(M + Na)^+$; R_f 0.69 (alumina, DCM - 3% MeOH)

(SS)-1,7-Bis(ethoxycarbonyl-2-ethylcarbamoylphenyl)-1,4,7,10-tetraazacyclododecane

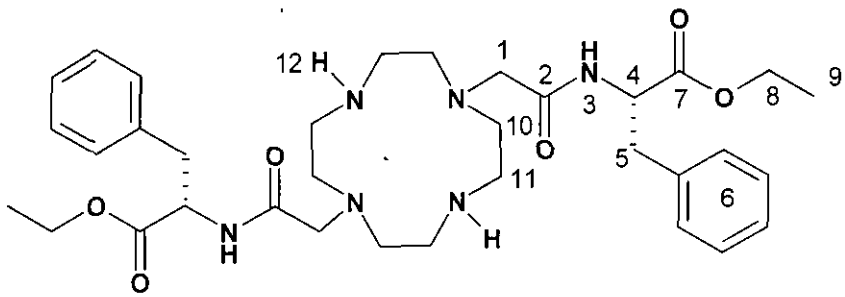

(SS)-1,7-Bis(benzyloxycarbonyl)-4,10-bis(ethoxycarbonyl-2-ethylcarbamoylphenyl)-1,4,7,10-tetraazacyclododecane (3.60 g, 47.52 mmol) was dissolved in absolute EtOH (100 mL) and $Pd(OH)_2/C$ (Pd content 10 %, 170 mg) was added. The mixture was hydrogenated in a Parr hydrogenation apparatus (40 psi) for 5 days. The catalyst was filtered off and EtOH was removed under reduced pressure. The resulting oil was dissolved in DCM (50 mL) and the solution was extracted with cold aq. NaOH solution (20 % (w/v), 5 mL) followed by extraction with H_2O (3 x 30 ml). The organic phase was dried and the solvent removed under vacuum to give the title compound as a pale yellow oil (2.11 g, 91%). %). δ_H ($CDCl_3$) 7.55 (H^{12}, br.s, 2H), 7.51 (H^3, d, 2H, *J* 6.0 Hz), 7.13 (H^6, 10H, m), 4.72 (H^4, m, 2H), 4.03 (H^8, q, 4H, *J* = 7.1 Hz), 3.13 (H^1, s, 4H), 3.08 ($H^{5,10}$, m, 12H), 2.63 ($H^{10'}$, m, 8H), 1.18 (H^9, t, 6H, *J* = 7.1 Hz); δ_c ($CDCl_3$) 172.1 (C^6), 162.8 (C^2), 137.0, 129.6, 128.6, 127.1 (C^6), 61.8 (C^8), 61.5 (C^1), 53.5 (C^4), 52.7 (C^{10}), 47.1 (C^{11}), 38.0 (C^5), 14.3 (C^9)), *m/z* (HRMS$^+$) 639.38639 $(M + H)^+$ ($C_{34}H_{50}O_6N_6$ requires 639.38649), R_f 0.34 (alumina, DCM - 7% MeOH)

(SS)-1,7-Bis(ethoxycarbonyl-2-ethylcarbamoylphenyl)-4-[(1-azathioxanthone)-2-methyl]- 1,4,7,10-tetraazacyclododecane

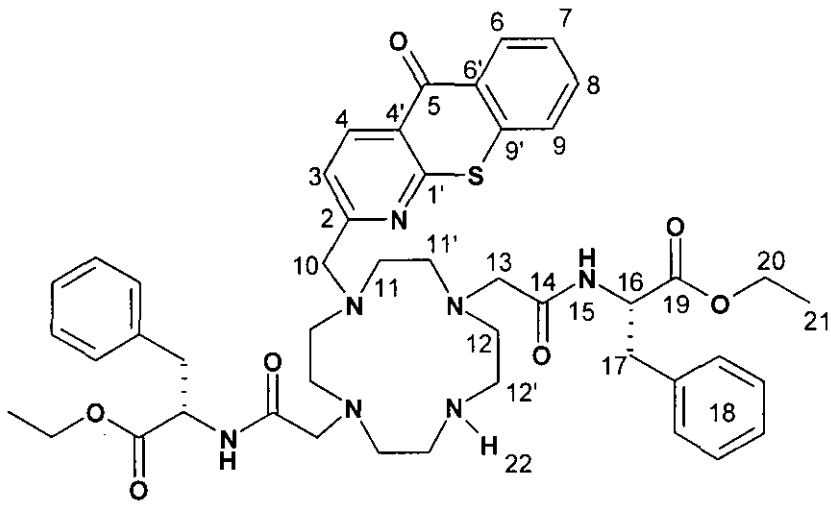

(SS)-1,7-Bis(ethoxycarbonyl-2-ethylcarbamoylphenyl)-1,4,7,10-tetraazacyclododecane (250 mg, 391μmol) was combined with 2-bromomethyl-1-azathiaxanthone (1 eq., 120 mg) and $KHCO_3$ (1 eq., 39 mg) and the mixture stirred in dry MeCN (10 mL), was heated at 70 °C for 40 h under argon. The reaction was monitored by TLC (DCM, 5% MeOH, alumina) and $ESMS^+$ to confirm that the brominated starting material had been consumed. The solvent was removed under reduced pressure and the resulting solid was dissolved in a small volume of DCM (5 mL) and the potassium salts removed by filtration. The crude mixture was purified by column chromatography (DCM → 3% MeOH, alumina); fractions containing clean product were combined and the solvents were removed under reduced pressure to yield the *title compound* as a pale yellow oil (168 mg, 194 μmol, 50%). δ_H ($CDCl_3$) 8.76 (H^4, d, 1H, J = 8.1 Hz), 8.58 (H^6, d, 1H, J = 8.2 Hz), 7.67 ($H^{8,9,22}$, m, 3H), 7.54 (H^7, t, 1H, *J* = 8.2 Hz), 7.20 ($H^{3,15,18}$, m, 13H), 4.81 (H^{16}, t, 2H, J = 8.2 Hz), 4.13 (H^{20}, q, 4H, J = 7.0 Hz), 3.81 (H^{10}, m, 2Hz), 3.02 ($H^{11,11',12,12',13,17}$, 24H, m), 1.23 (H^{21}, t, 6H, J = 7.0Hz); δ_c ($CDCl_3$) 180.5 (C^5), 172.0 (C^{19}), 170.5 (C^{14}), 162.2 (C^2), 158.6 ($C^{1'}$), 138.5 (C^4), 137.1 ($C^{4'}$), 136.6, 129.6, 128.7, 127.2 (C^{18}), 133.4 (C^9), 130.2 (C^6), 129.1 ($C^{6'}$), 127.3 (C^7), 126.8 (C^8), 125.4 ($C^{9'}$), 122.4 (C^3) 61.8 (C^{20}), 60.7 (C^{10}), 53.8, 53.0, 51.5, 47.3 ($C^{11,11',12'12'}$), 53.6 (C^{16}), 37,7 (C^{17}), 14.3

(C^{21}), *m/z* (HRMS$^+$) 864.41018 $(M + H)^+$ ($C_{47}H_{58}O_7N_7S$ requires 864.4113), R_f 0.38 (alumina, DCM - 5% MeOH).

[EuDPP2(CF_3SO_3)$_3$][13]

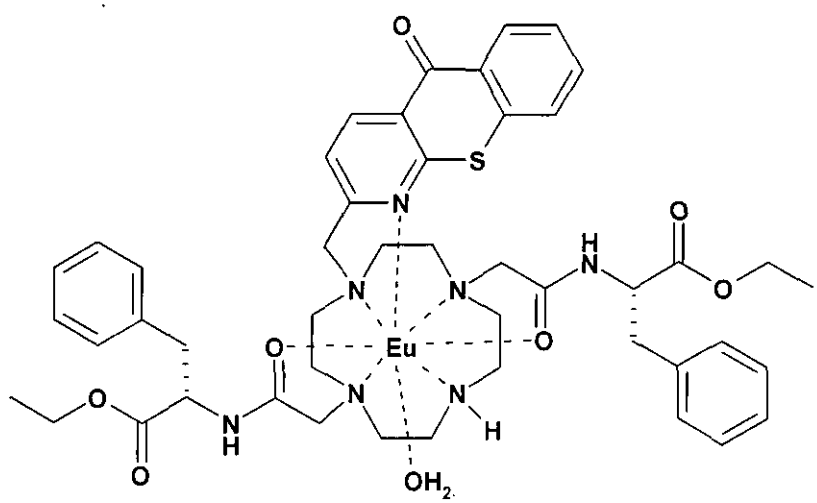

(SS)-1,7-Bis(ethoxycarbonyl-2-ethylcarbamoylphenyl)-4-[(1-azathioxanthone)-2-methyl]- 1,4,7,10-tetraazacyclododecane tetraazacyclododecane (21 mg, 24 μmol) was added to Eu(CF_3SO_3)$_3$ (1 eq., 16 mg) and the solids dissolved in dry MeCN (3 mL) and the reaction left to stir at 80 ° C for 76 hrs. After the reaction was cooled to room temperature, the solvents were removed under reduced pressure and the remaining residue was dissolved in dry MeCN (0.1 mL) and the mixture was dropped onto anhydrous Et_2O (5 mL) which resulted in precipitation of the title compound as a triflate salt. The precipitate was spinned out and dissolved in aqueous MeOH (3 : 1, 5 ml) The pH was then adjusted carefully to 10 by addition of conc. NaOH solution (in order to remove the excess Eu as Eu$(OH)_3$) resulting in a white precipitate, whish was removed by centrifugation. The pH was adjusted back to neutral and the mixture lyophilised to give a bright yellow solid, which was loaded onto a DOWEX 1-X8(Cl) anion exchange resin. The column was eluted with water → 10% NH_4OH and the fractions were analysed by ESMS$^+$. The fractions were combined and lyophilised to yield the Eu-complex as a bright yellow powder. (16 mg, 11.5 μmol). *m/z* (HRMS$^+$) 1314.2271 $(M + 2CF_3SO_3)^+$

($C_{47}H_{57}O_7N_7SEu(CF_3SO_3)_2$ requires 1314.2288); $\lambda_{max}(H_2O)$ 380 (4070 $dm^3mol^{-1}cm^{-1}$); $\tau^{Eu}_{(H2O,\ pH=7.4)}$: 0.32 ms, $\tau^{Eu}_{(D2O,\ pD=7.1)}$: 0.48 ms; $\phi^{Eu}_{(pH=7.4)}$= 3.8 %

[GdDPP2(CF_3SO_3)$_3$][13]

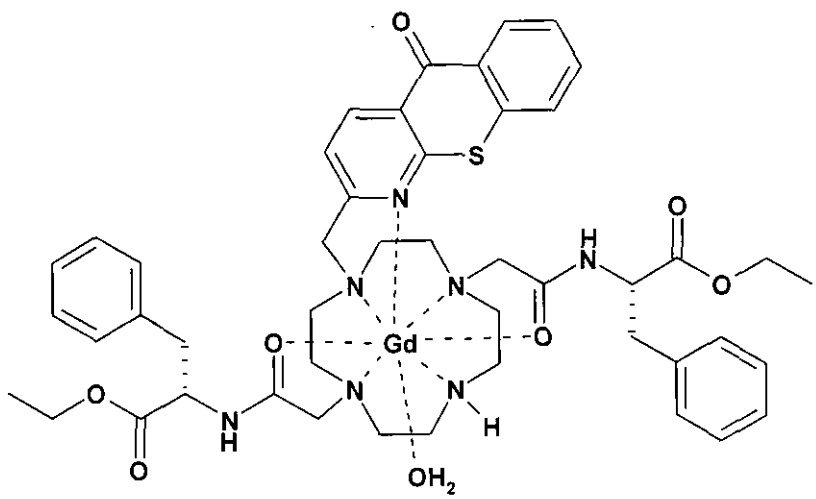

The Gd-complex was prepared as described for the europium analogue *m/z* ($HRMS^+$) 1319.2379 $(M + 2OTf)^+$ ($C_{47}H_{57}O_7N_7SGd(CF_3SO_3)_2$ requires 1319.2321; r_1=7.3 $M^{-1}s^{-1}$

(SS)-1,7-Bis(carboxy-2-ethylcarbamoylphenyl)-4-[(1-azathioxanthone)-2-methyl]-1,4,7,10-tetraazacyclododecane

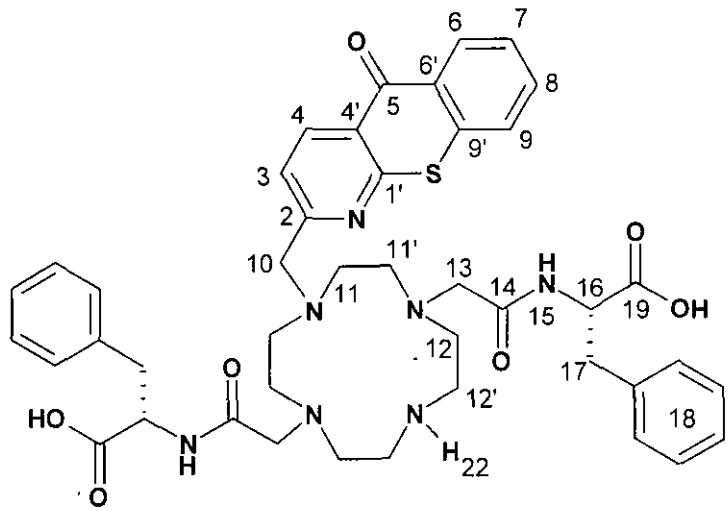

Freshly made aqueous KOD solution (2.5 mL, 0.1 M) was added to (SS)-1,7-bis(ethoxycarbonyl-2-ethylcarbamoylphenyl)-4-[(1-azathioxanthone)-2-methyl]-1,4,7,10-tetraazacyclododecane (51 mg, 59 μmol) with 0.3 mL d^4MeOD. The reaction mixture was kept under argon at room temperature and progress was monitored by NMR. After 10 h ethyl group signals were observed in the ^{1}H-NMR spectrum. The pH of the mixture was increased (pH ≈ 6) with conc. HCl and the solution loaded onto a DOWEX 50X4-100 strong cation exchange resin. The column was eluted with water → 10% NH_4OH and the fractions were analysed by ^{1}H-NMR. The fractions were combined and lyophilised to yield the *title compound* as a pale orange oil (25 mg, 32 μmol, 54%), which was used for complexation reaction immediately. δ_H ($CDCl_3$) 8.22 (H^4, br.s., 1H), 7.94 (H^6, br.s., 1H), 7.00 ($H^{3,7,8,9,15,18,21}$, m, 17H), 4.63 (H^{16}, m, 2H), 4.22 ($H^{10,20}$, m, 6H), 2.76 ($H^{11,11',12,12',13,17}$, m, 24H)

[Na_2EuDPPA2(OAc)]

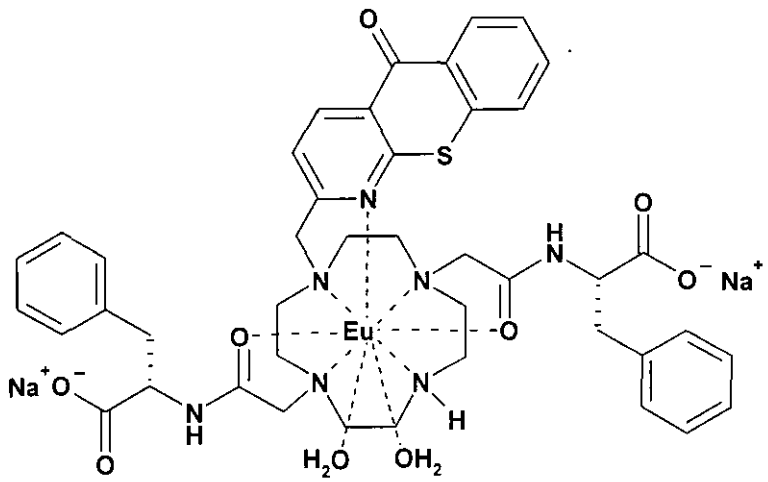

(SS)-1,7-Bis(carboxy-2-ethylcarbamoylphenyl)-4-[(1-azathioxanthone)-2-methyl]-1,4,7,10-tetraazacyclododecane (25 mg, 32 μmol) was added to $Eu(OAc)_3 .4H_2O$ (1.1 eq., 16 mg) and the solids dissolved in 2.5 mL H_2O : MeOH (5 : 1). The pH was carefully adjusted to 5 by addition of acetic acid and the reaction left to stir at 75 ° C for 64 h. After the reaction was cooled to room temperature, The pH was then adjusted carefully to 10 by addition of conc. NaOH solution (in order to remove excess Eu as $Eu(OH)_3$) resulting in a white precipitate removed via centrifugation. The pH was adjusted back to neutral with acetic acid and the sample lyophilised to give a bright yellow solid solid contained aprox. 2% NaOAc as a result of pH adjustment (20 mg, 22 μmol). *m/z* ($HRMS^+$) 1034.2971 (M + Me + OAc) ($C_{43}H_{49}O_7N_7SEuCH_3COO$ (as a mono Me-esther) requires 1034.2994); $\lambda_{max}(H_2O)$ 380 (4070 $dm^3mol^{-1}cm^{-1}$); $\tau^{Eu}_{(H2O,\ pH=7.4)}$: 0.24 ms, $\tau^{Eu}_{(D2O,\ pD=7.0)}$: 0.70 ms; $\phi^{Eu}_{(pH=7.4)}$= 0.8 %,

1,7-Bis(α-glutarate)-4-[(1-azathioxanthone)-2-methyl]-1,4,7,10-tetraaza-cyclododecane

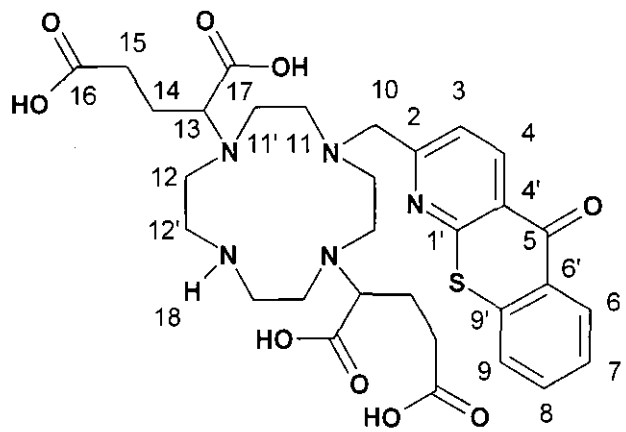

Freshly made aqueous KOD solution (2.5 mL, 0.1 M) was added to 1,7-bis(α-dimethylglutarate)-4-[(1-azathioxanthone)-2-methyl]- 1,4,7,10-tetraaza-cyclododecane (70 mg, 98 μmol). The reaction mixture was kept under argon at room temperature and progress was monitored by NMR. After 8 h no methyl group signals were observed in the ^{1}H-NMR spectrum. The pH of the mixture was decreased (pH ≈ 6) with conc. HCl and the solution loaded onto a DOWEX 50X4-100 strong cation exchange resin. The column was eluted with water → 10% NH_4OH and the fractions were analysed by 1H-NMR. The fractions were combined and lyophilised to yield the *title compound* as a dark yellow solid (38 mg, 57 μmol, 58%), which was used in a complexation reaction immediately. δ_H (D_2O): mainly broad overlapping signals; no Me groups in ^{1}H-NMR, δ_H ($CDCl_3$) 8.33 (1H, d, *J* 8.0 Hz, H^4), 8.11 (1H, d, *J* 8.0 Hz, H^6), 7.41 (5H, m , $H^{8,9,3,7,18}$), 3.53 (2H, s, H^{10}), 3.09 (18H, br.m, $H^{11,11',12,12',13}$), 1.90 (8H, m, $H^{14,15}$); *m/z* (ESMS$^-$) 656 $(M-H)^-$.

[NaEuDGP2]

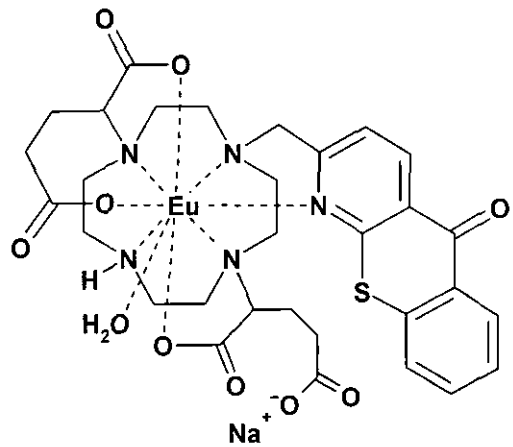

1,7-Bis(α-glutarate)-4-[(1-azathioxanthone)-2-methyl]-1,4,7,10-tetraaza-cyclododecane (33 mg, 50 μmol) was added to $Eu(CH_3CO_2)_3$ (1.1 eq., 23 mg) and the solids dissolved in a H_2O : MeOH (10 :1, 3 mL). The pH was carefully adjusted to 5 by addition of acetic acid and the reaction left to stir at 80 ° C for 72 hrs. After the reaction was cooled to room temperature, the solvents were removed under reduced pressure and the remaining residue was dissolved in 5 mL H_2O. The pH was then adjusted carefully to 10 by addition of conc. NaOH solution (in order to remove the excess Eu as $Eu(OH)_3$) resulting in a white precipitate, removed via centrifugation. The pH was adjusted back to neutral with acetic acid and the mixture lyophilised to give a bright yellow solid contained aprox 2% NaOAc as a result of pH adjustment (33 mg, 37 μmol). *m/z* (HRMS$^-$) 821.1639, $(M + Me)^+$ 889.1474 $(M^- + Na + OAc)^+$ ($C_{31}H_{36}O_9N_5SEu$ mono Me-esther requires 821.1675, $C_{31}H_{36}O_9N_5SEuNaCH_3COO$ requires 889.1471); $\lambda_{max}(H_2O)$ 380 (4070 $dm^3mol^{-1}cm^{-1}$); $\tau^{Eu}_{(H2O,\ pH=3.0)}$: 0.29 ms, $\tau^{Eu}_{(H2O,\ pH=8.0)}$: 0.30 ms; $\tau^{Eu}_{(D2O,\ pD=2.6)}$: 0.59 ms, $\tau^{Eu}_{(D2O,\ pD=7.6)}$: 0.63 ms; $\phi^{Eu}_{(pH=3.0)}$= 1.2 %, $\phi^{Eu}_{(pH=8.0)}$= 1.2 %

6.3 HPLC Data of Complexes

For experimental details on HPLC analysis see section 6.1.15.

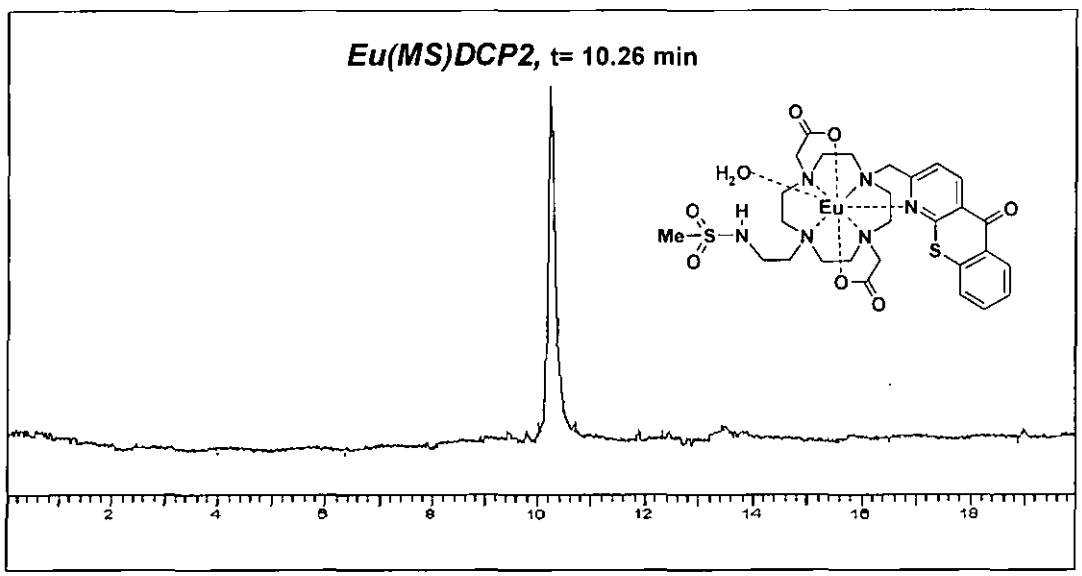

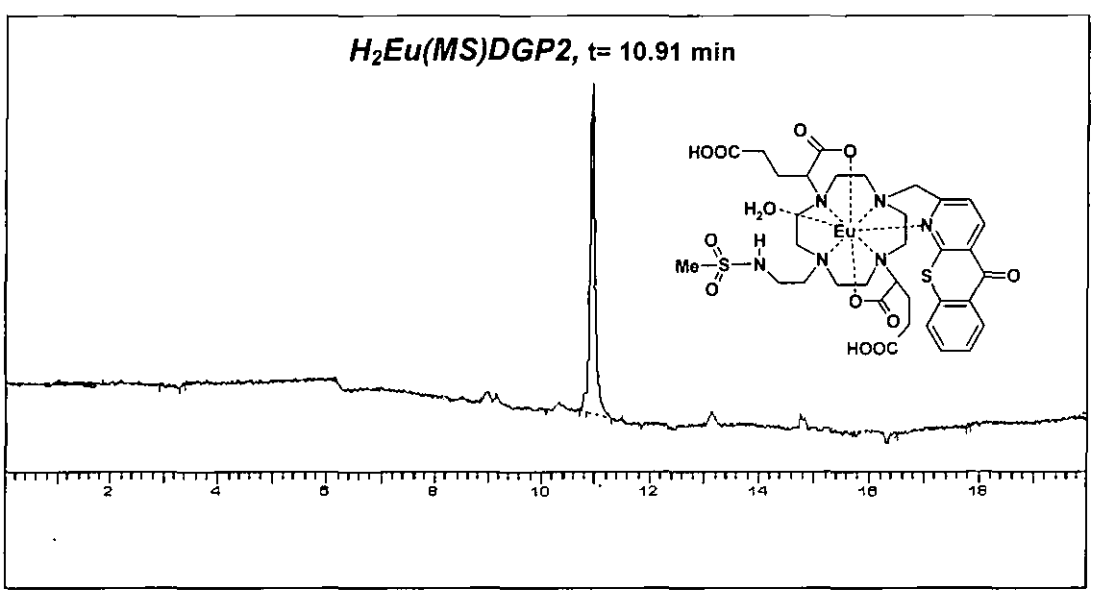

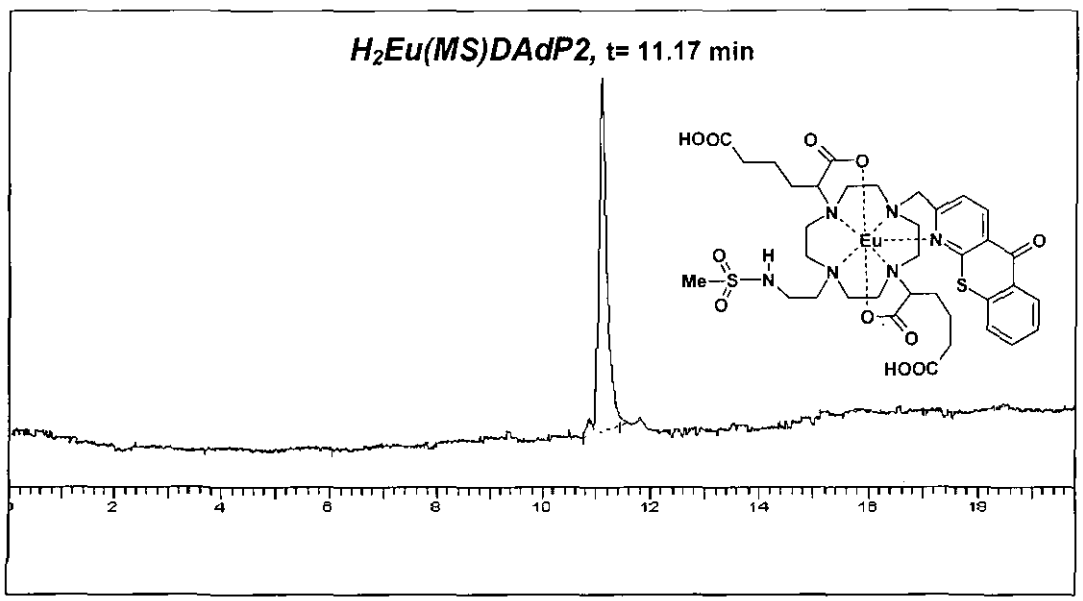
$H_2Eu(MS)DAdP2$, t= 11.17 min
HOOC
O
O
N
N
Eu
N
O
Me
S
H
N
O
O
S
N
N
O
O
HOOC
2
4
6
8
10
12
14
16
18

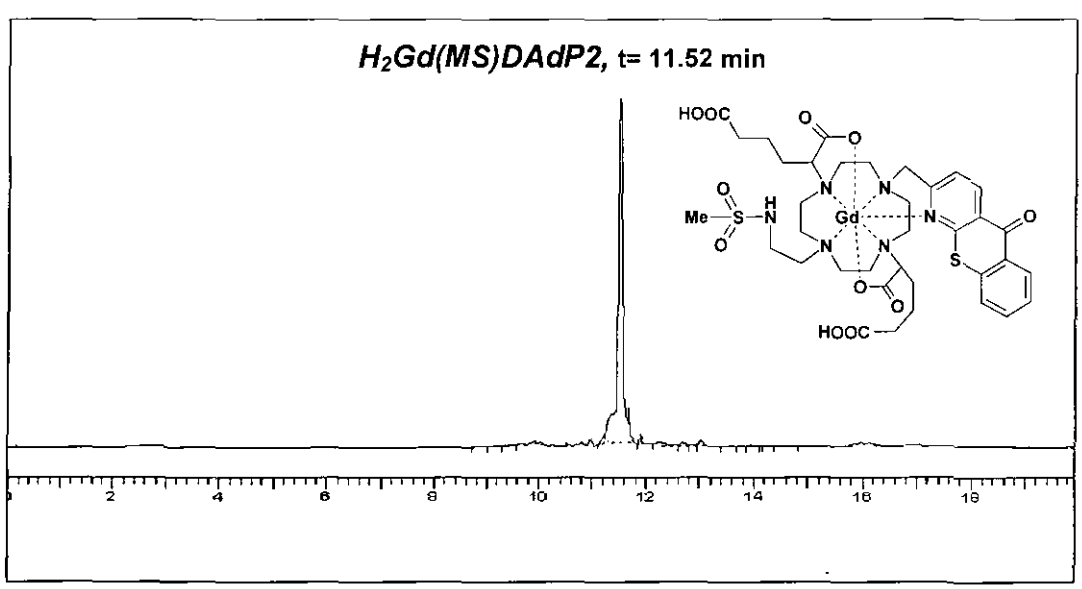
$H_2Gd(MS)DAdP2$, t= 11.52 min
HOOC
O
O
N
N
Gd
N
O
Me
S
H
N
O
O
S
N
N
O
O
HOOC
2
4
6
8
10
12
14
16
18

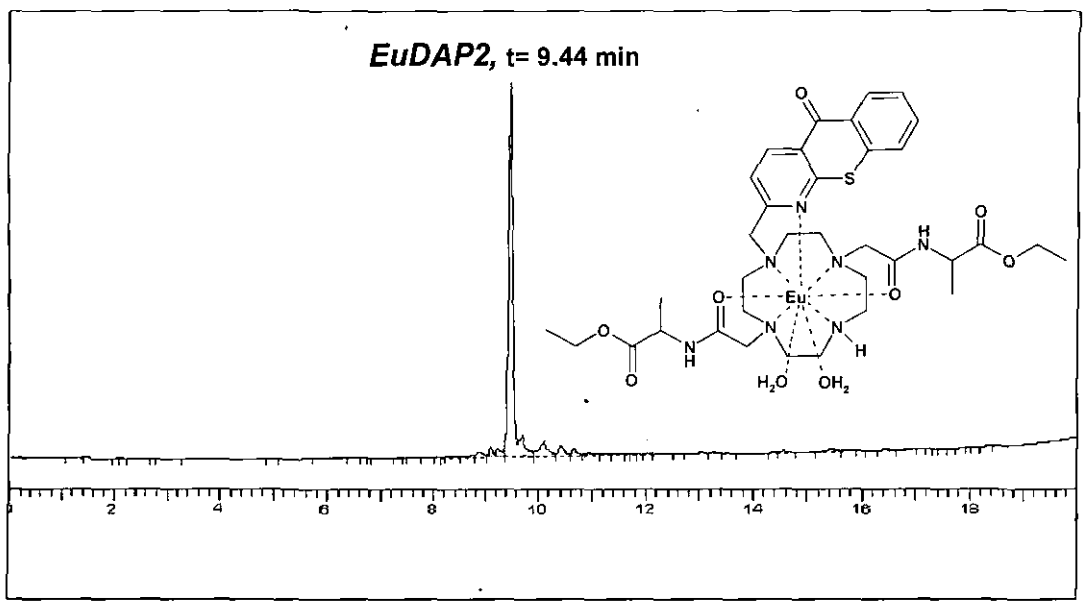
EuDAP2, t= 9.44 min
Eu
H2O
OH2
2
4
6
8
10
12
14
16
18

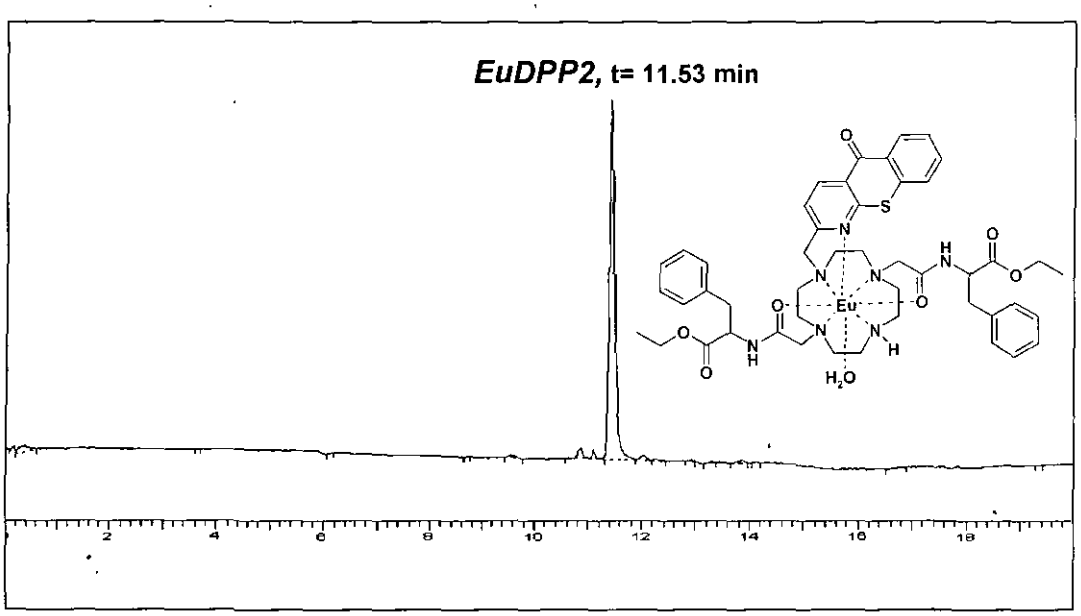
EuDPP2, t= 11.53 min
Eu
H2O
2
4
6
8
10
12
14
16
18

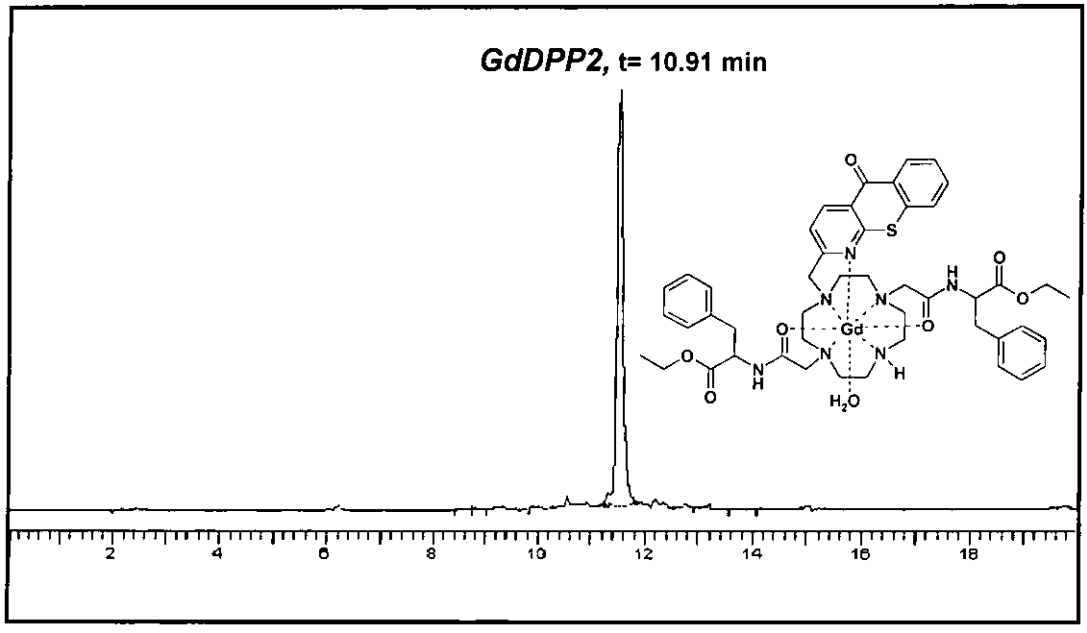
GdDPP2, t= 10.91 min
Gd
H_2O
2
4
6
8
10
12
14
16
18

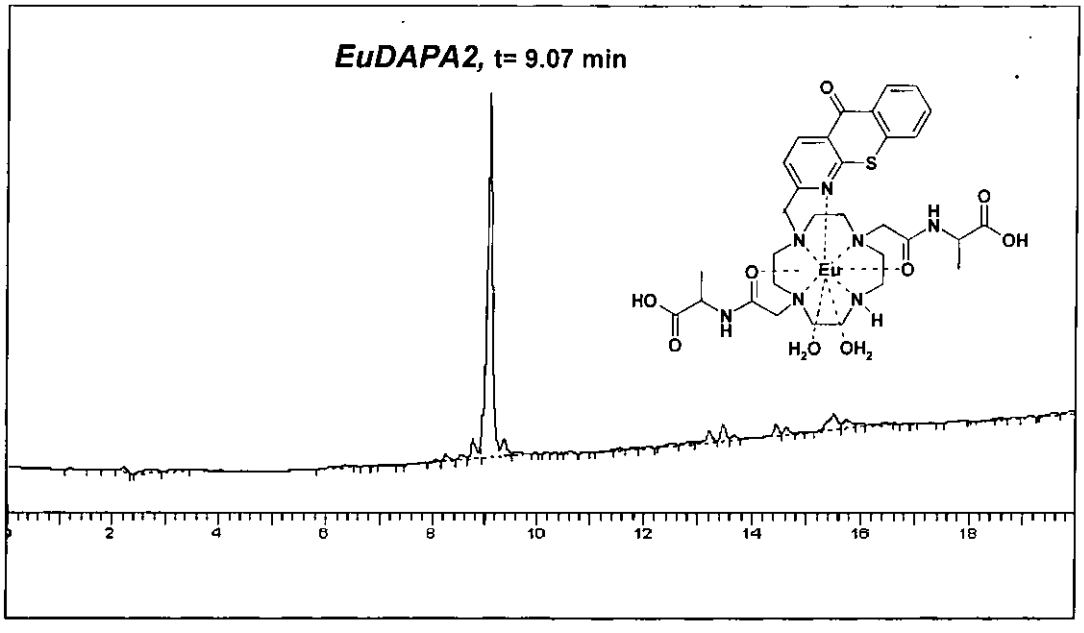
EuDAPA2, t= 9.07 min
Eu
HO
OH
H_2O
OH_2
2
4
6
8
10
12
14
16
18

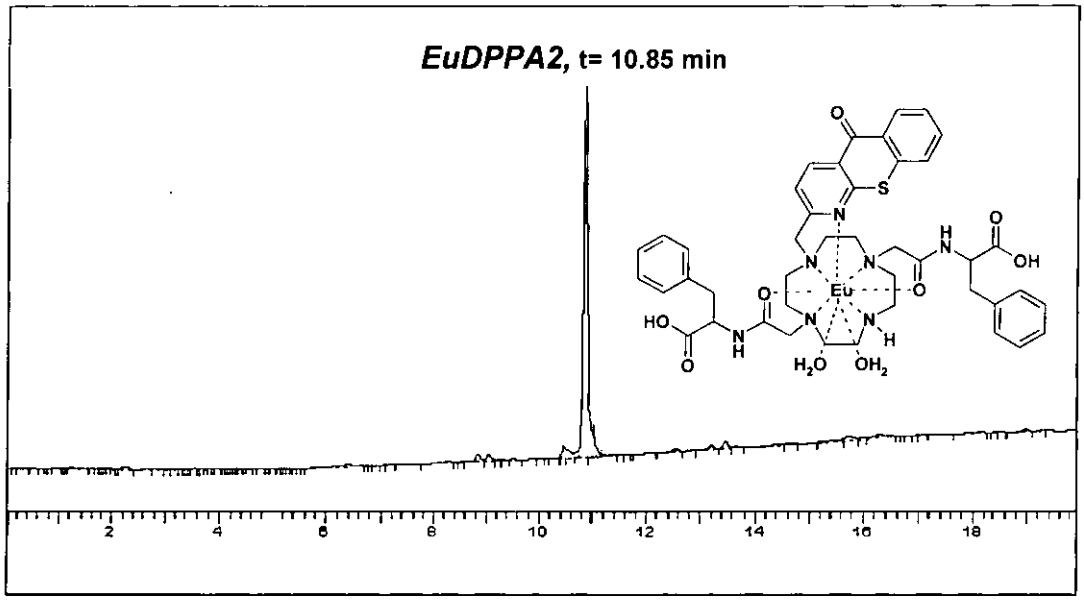
EuDPPA2, t= 10.85 min
2
4
6
8
10
12
14
16
18

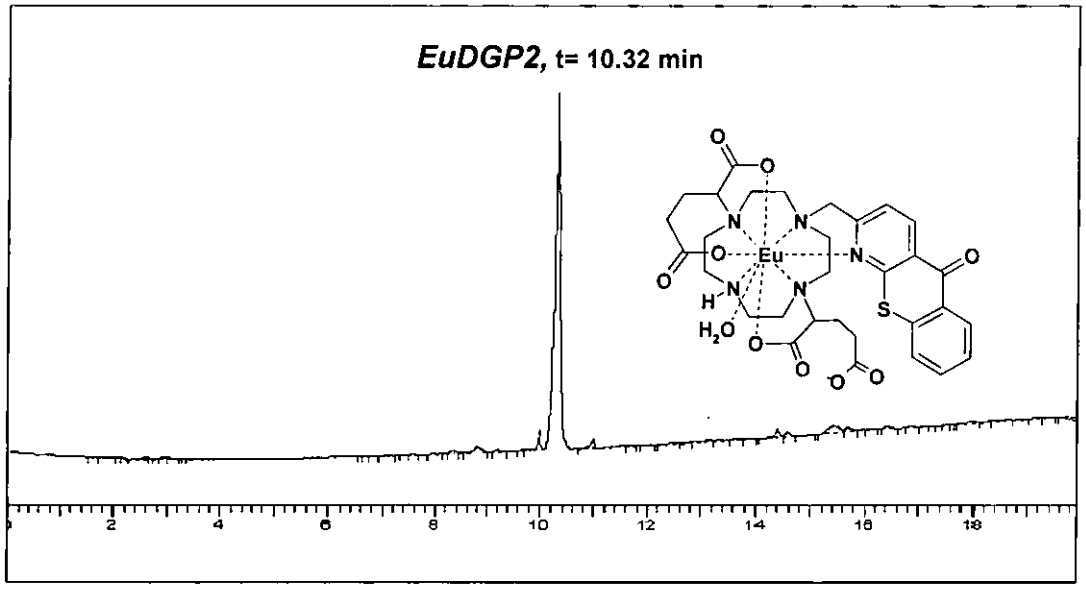
EuDGP2, t= 10.32 min
2
4
6
8
10
12
14
16
18

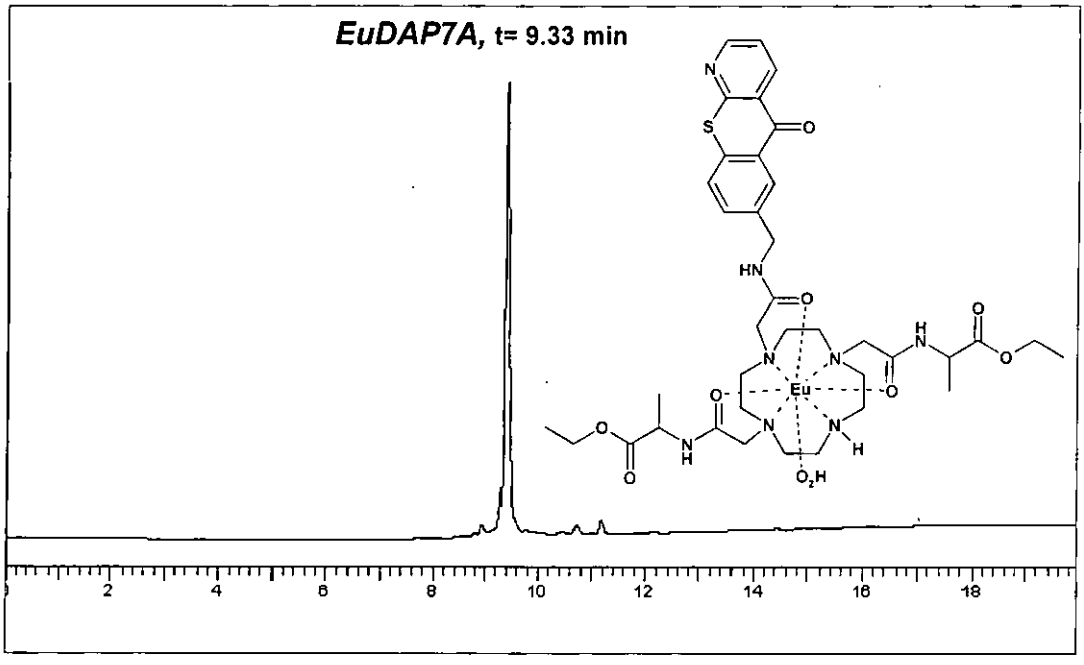
EuDAP7A, t= 9.33 min
2
4
6
8
10
12
14
16
18

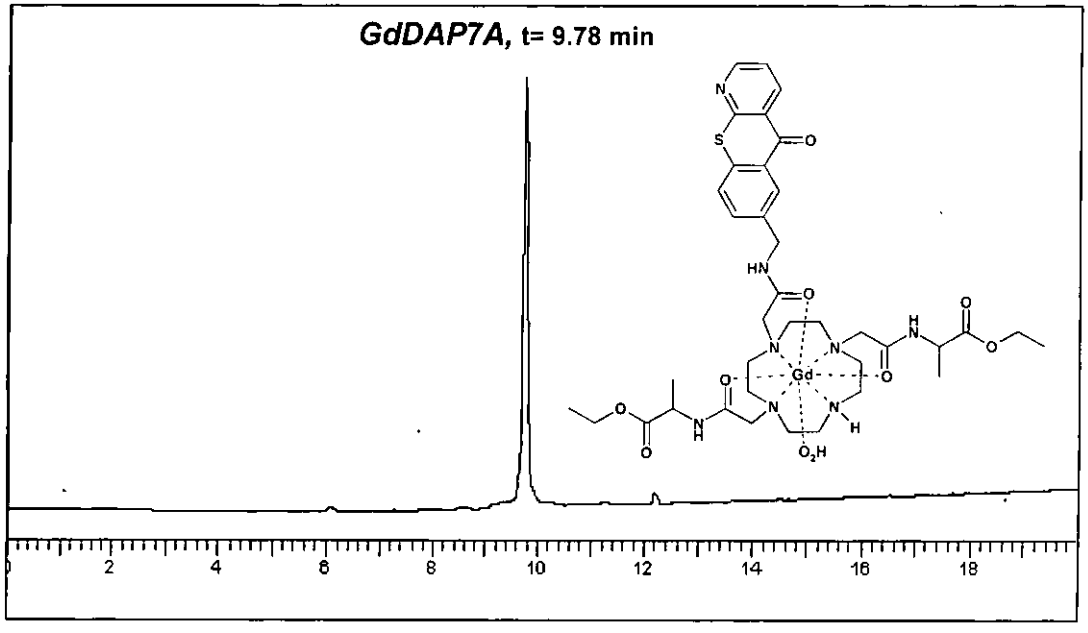
GdDAP7A, t= 9.78 min
2
4
6
8
10
12
14
16
18

6.4 References

1 L. Pentz and E. R. Thornton, *J. Am. Chem. Soc.*, 1967, **Dec**, 6931.

2 A. K. Covington, M. Paabo, R. A. Robinson, and R. G. Bates, *Anal. Chem.*, 1960, **40**, 700.

3 A. Beeby, I. M. Clarkson, R. S. Dickens, S. Faulkner, D. Parker, L. Royle, A. S. de Sousa, J. A. G. Williams, and M. Woods, *J. Chem. Soc., Perkin Trans. 2*, 1999, 493.

4 R. A. Poole, ' Luminescent Lanthanide Complexes for Cellular Applications', PhD Thesis, Durham University, Durham, 2006.

5 J. Cosier and A. M. Glazer, *J. Appl. Cryst.*, 1986, **19**, 105.

6 SMART-NT, 'Data Collection Software, version 5.0', Madison, Wisconsin, U.S.A., 1999.

7 SAINT-NT, 'Data Collection Software, version 5.0', Madison, Wisconsin, U.S.A., 1999.

8 SHELXTL, 'Data Collection Software, version 5.1', Madison, Wisconsin, U.S.A., 1999.

9 P. W. Betteridge, J. R. Carruthers, R. I. Cooper, K. Prout, and D. J. Watkin, *J. Appl. Cryst.*, 2003, **36**, 1487.

10 G. M. Sheldrick, 'Empirical Absorption Correction Program', University of Göttingen, 1998.

11 P. Atkinson, K. S. Findlay, F. Kielar, R. Pal, D. Parker, R. A. Poole, H. Puschmann, S. L. Richardson, P. A. Stenson, A. L. Thompson, and J. Yu, *Org. Biomol. Chem.*, 2006, **4**, 1707.

12 R. Pal and D. Parker, *Chem Commun.*, 2007, 474.

13 J. Yu, R. Pal, R. A. Poole, M. J. Cann, and D. Parker, *J. Am. Chem. Soc.*, 2006, **128**, 2294.

14 D. Parker, R. Pal, and J. Yu, 'Responsive luminescent lanthanide complexes - Int. Pat. Appl.' 2006.

15 I. Stirling, G. Bruton, S. H. Calvert, and B. P. Clarke, *Eur. Pat. Appl.*, 1984.

16 F. Mikovsky, R. Fikentscher, and G. Uhl *Ger. Offen.*, 1975, 13.

17 H. Reinheckel, *Alfa-Bromo esters*, 1965.

18 M. Woods and A. D. Sherry, *Inorg. Chim. Acta*, 2003, **351**, 395.

19 K. Senanyake, A. Kenwright, D. Parker, and S. van der Hoorn, *Chem Commun.*, 2007, 2923.

20 Z. Kovacs and A. D. Sherry, *Synthesis*, 1997, **July**, 759.

21 M. P. Lowe and D. Parker, *Inorg, Chim. Acta*, 2001, **317**, 163.

22 E. Fischer and R. Shultze, *Chem. Ber.*, 1907, **40**, 908.

Appendix 1 – *Abbreviation and structure of complexes*

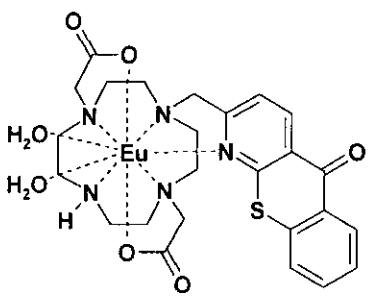

EuDCP2

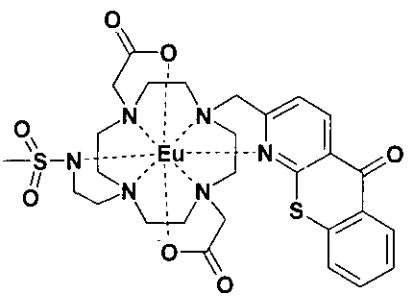

Eu(MS)DCP2

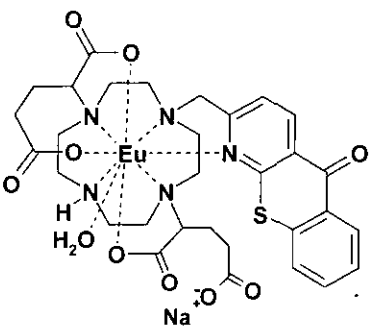

***Na*[EuDGP2]**

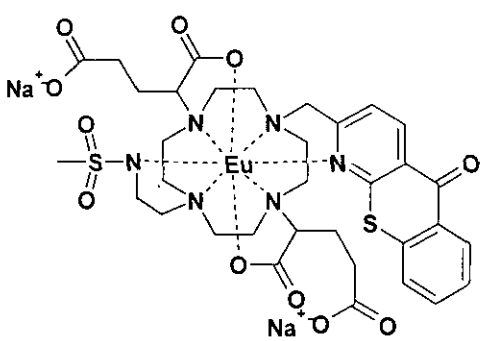

***Na*$_2$[Eu(MS)DGP2]**

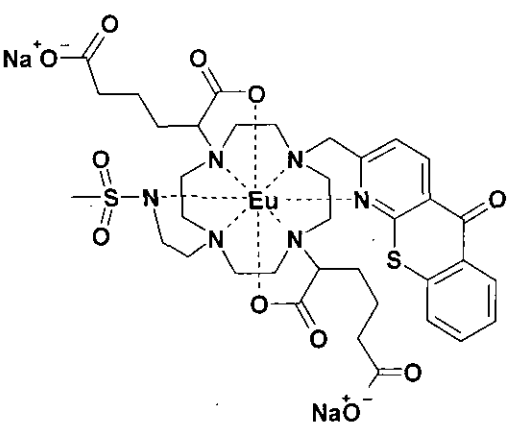

***Na*$_2$[Eu(MS)DAdP2]**

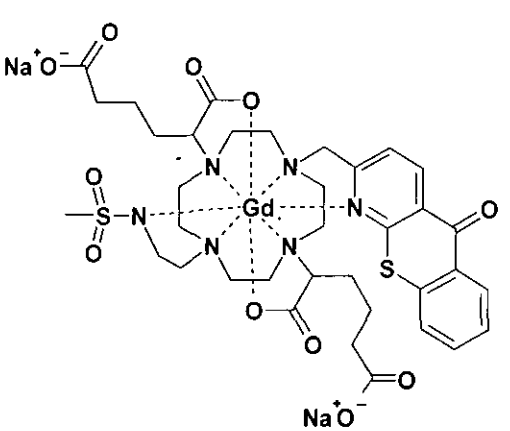

***Na*$_2$[Gd(MS)DAdP2]**

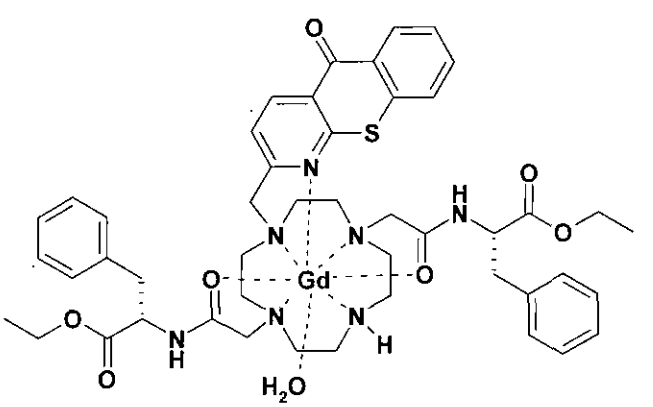

GdDPP2

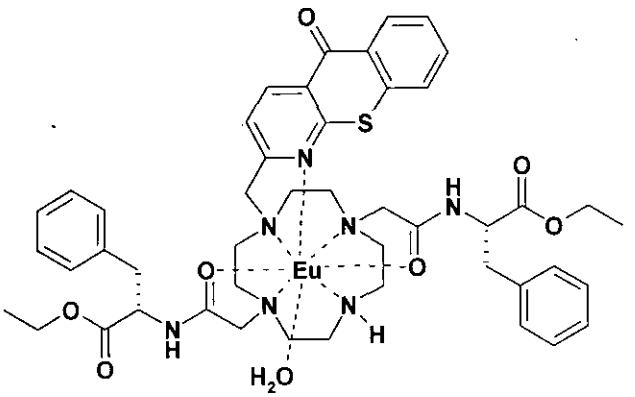

EuDPP2

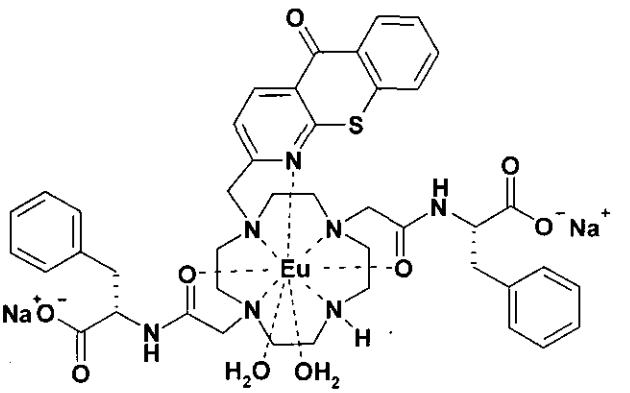

***Na*$_2$[EuDPPA2]**

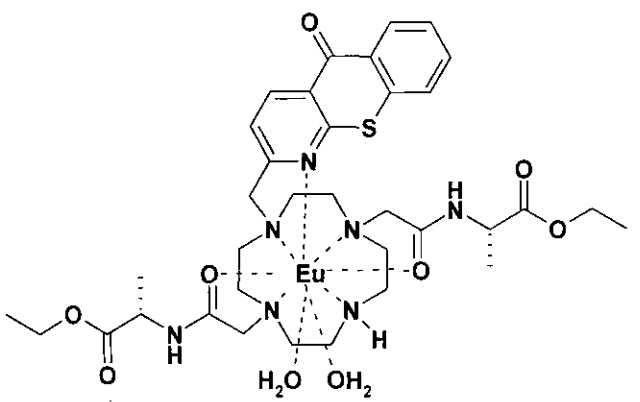

EuDAP2

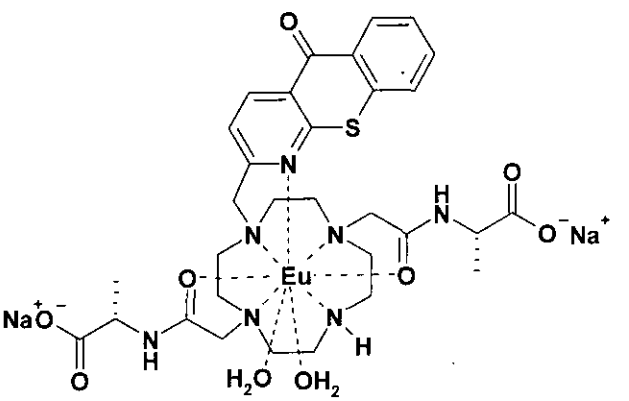

***Na*$_2$[EuDAPA2]**

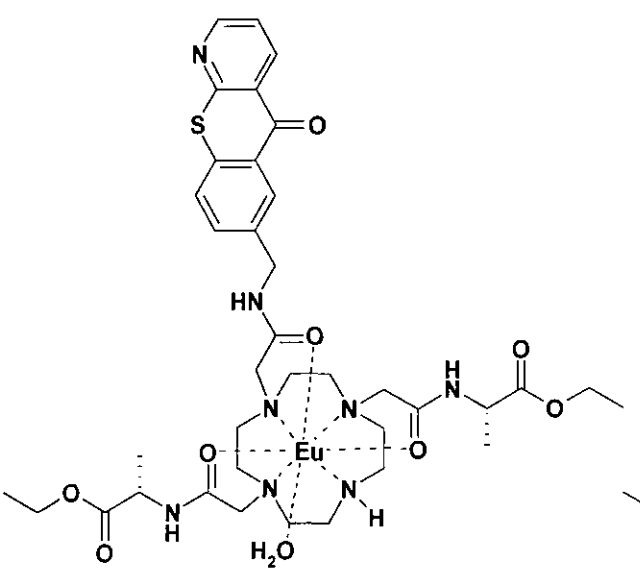

EuDAP7A

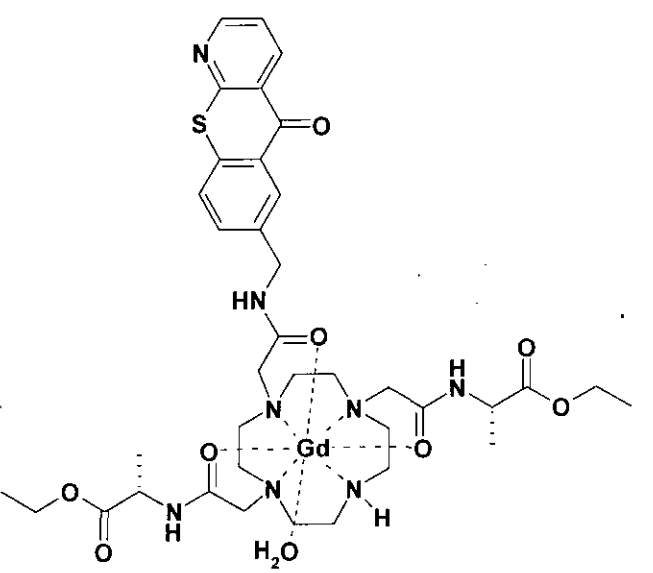

GdDAP7A

Appendix 2 – *Cell Death (IC_{50}) Measurements*[1]

The **IC_{50}**, or the half maximal inhibitory concentration, represents the concentration of an inhibitor that is required for 50% inhibition of its target. In simpler terms, it measures how much of a particular substance/molecule is needed to inhibit some biological process by 50%. IC_{50} values were determined using the MTT assay,[2] which makes use of the conversion of MTT (3-(4,5-dimethylthiazol-2-yl)-2,5-diphenyltetrazolium bromide) to a purple formazan product by the mitochondrial dehydrogenase enzymes of viable cells. This insoluble formazan was quantified spectrophotometrically upon dissolution in DMSO.

Approximately 5 x 10^3 NIH 3T3 cells in 100 μL DMEM were seeded into each well of flat-bottomed 96-well plates and allowed to attach overnight. Complex solutions were added to triplicate wells to give final concentrations over a 0-100 μM range. Following 24 h incubation, MTT (1.0 mM) was added to each well, and the plates incubated for a further 4 h. The culture medium was removed, and DMSO (150 μL) was added. The plates were shaken for 20 seconds and the absorbance measured immediately at 540 nm in a microplate reader. IC_{50} values were determined as the applied complex concentration required to reduce the absorbance to 50% of that in the untreated, control wells, and represent the data as the average of at least three independent experiments. The obtained IC_{50} values in [μM] units are presented in the following tabular summary.

Complex	I.	II.	III.	**IC_{50}**	*st. dev.(±)*
Eu(MS)DAdP2	89.11	60.38	51.47	**55.92**	*19.1*
EuDGP2	>100	86.35	66.09	**>90**	—
EuDAP2	99.24	>100	>100	**>100**	—
EuDAPA2	18.86	24.14	18.04	**20.34**	*3.31*
EuDPP2	81.86	83.17	76.08	**78.97**	*2.68*
EuDPPA2	79.23	100.63	80.42	**89.93**	*10.04*
EuDAPA7A	>100	>100	>100	**>100**	—

These values in some cases, especially with EuDAPA2, are not consistent with the observed cell viability values (higher than 90%) using bright field microscopy. However, cell viability observations were made during the observed individual time regions, which sometimes did not exceed 12h. Furthermore, conversion of the applied MTT could be ceased by selective inhibition of specific cellular metabolitic pathways, or cellular hibernation upon long term complex exposure, which not necessarily concludes in cell death. Therefore, despite the sometimes rather low and contradictory IC_{50} values, as shown by cellular uptake and luminescent studies these complexes can still be successfully used in the studied time domain as cellular probes.

[1] Measured with Elizabeth J. New

[2] J. Carmichael, W. G. DeGraff, A. F. Gazdar, J. D. Minna, J. B. Mitchell, Cancer Res., 1987, **47**, 936.